01 Mar 1983

The influence of local buckling on the structural behavior of singly-symmetric cold-formed steel columns

Gale P. Mulligan

Teoman Peköz

CCFSS LIBRARY
22 1 * 450
c1

Gale P. Mulligan, Teoman Pekoz,
THE INFLUENCE OF LOCAL BUCKLING
ON THE STRUCTURAL BEHAVIOR OF
SINGLY-SYMMETRIC COLD-FORMED
STEEL COLUMNS

DATE	ISSUED TO

Department of Structural Engineering
School of Civil and Environmental Engineering
Cornell University

Report No. 83-1

THE INFLUENCE OF LOCAL BUCKLING ON THE STRUCTURAL BEHAVIOR OF SINGLY-SYMMETRIC COLD-FORMED STEEL COLUMNS

by

Gale P. Mulligan

Teoman Pekőz, Project Director

A Research Project Sponsored by
The American Iron and Steel Institute

Ithaca, N.Y. March 1983

PREFACE

This report is based on a thesis presented to the faculty of the Graduate School of Cornell University for the degree of Doctor of Philosophy.

The sponsorship of the American Iron and Steel Institute and the cooperation of the committees of the Institute are gratefully acknowledged.

TABLE OF CONTENTS

CHAPTER		Page
1.	INTRODUCTION	
1.1	General	1
1.2	Objectives of Research	2
1.3	Scope of Research	3
2.	POST-BUCKLING BEHAVIOR AND EFFECTIVE WIDTH	
2.1	Introduction	5
2.2	Post-Buckling Strength	6
2.2.1	Uniformly Compressed Stiffened Elements	7
2.2.2	Eccentrically Compressed Stiffened Elements	9
2.2.3	Uniformly Compressed Unstiffened Elements	19
2.3	Sub-Ultimate Behavior	21
2.3.1	Thomasson's Approach	23
2.3.2	Present Approach	25
2.4	Summary	28
3.	LOCAL BUCKLING INTERACTION	
3.1	Introduction	41
3.2	Instability Analysis Using the Finite Strip Method	42
3.2.1	Basis of the Finite Strip Method	42
3.2.2	Comparison of the FEM and FSM	43
3.2.3	Literature Survey	44
3.2.4	Linear Instability Formulation	45
3.2.5	Finite Strip Instability Analysis Program	48
3.3	Local Buckling Interaction in Structural Sections	49
3.3.1	Channel Sections	50
3.3.2	Lipped Channels	52
3.4	Edge Stiffeners	56
3.4.1	Effect of Stiffener Radius on Local Buckling	59
3.5	Post-Local Buckling Interaction	61
3.5.1	Effective Section Method	63
3.6	Summary	65
4.	LOCAL AND OVERALL BUCKLING INTERACTION	
4.1	Introduction	81
4.2	Literature Survey	81
4.3	Local and Flexural Buckling Interaction	84
4.4	Post-Local and Overall Buckling Interaction	86
4.4.1	Q-Factor Method	86
4.4.2	Effective Section Method	89
4.5	Post-Local Buckling and Beam-Column Behavior	90
4.5.1	Current Analysis Methods	90
4.5.2	Proposed Analysis Method	92
4.6	Summary	102

5. EXPERIMENTAL INVESTIGATION

5.1 Introduction 112
5.2 Test Specimens 112
5.2.1 Test Specimen Design 114
5.3 Material Properties 115
5.4 Initial Imperfections 116
5.4.1 Local Initial Imperfection of Stub Columns 117
5.4.2 Local and Overall Initial Imperfection of Long Columns 121
5.5 Experimental Procedures, Instrumentation, and Alignment 126
5.5.1 Stub Column Test Procedure 126
5.5.2 Long Column Test Procedure 127
5.5.3 Instrumentation 128
5.5.4 Alignment 129
5.5.4.1 Summary of Column Alignment 132
5.6 Experimental Results 133
5.6.1 Stub Columns 133
5.6.1.1 Local Buckling Stresses 136
5.6.2 Long Columns 139
5.7 Other Experimental Research 143
5.7.1 Stub Columns 143
5.7.2 Long Columns 144
5.8 Summary 146

6. COMPARISON OF EXPERIMENTAL AND THEORETICAL RESULTS

6.1 Introduction 195
6.2 Stub Column Evaluation 195
6.2.1 General 195
6.2.2 Ultimate Strength 197
6.2.3 Sub-Ultimate Response 200
6.3 Long Column Evaluation 204
6.3.1 General 204
6.3.2 Ultimate Strength 206
6.3.3 Sub-Ultimate Response 212
6.4 Evaluation of Other Experimental Research 216
6.4.1 Stub Columns 216
6.4.2 Long Columns 218
6.5 Summary 218

7. CONCLUSION

7.1 Summary and Conclusions of Research 256
7.2 Future Research 262

APPENDIX

A. FINITE STRIP INSTABILITY FORMULATION

A.1 Introduction 264

A.2 Finite Strip Formulation 264
A.3 Global Formulation 271

B. NUMERICAL SOLUTION OF THE INSTABILITY PROBLEM

B.1 Introduction 276
B.2 The Eigenproblem and Its Solution 276
B.2.1 Inverse Iteration, Polynomial Iteration, and the Sturm Sequence Property 278
B.2.2 Determinant Search Algorithm 281
B.3 The Equation Solver 283
B.4 Variable Length and Minimum Buckling Load Analysis 284

C. VERIFICATION OF FINITE STRIP INSTABILITY ANALYSIS PROGRAM

C.1 Introduction 289
C.2 Local Buckling 289
C.3 Overall Buckling 291

D. SUB-ULTIMATE RESPONSE FOR STUB COLUMNS 296

E. SUB-ULTIMATE RESPONSE FOR LONG COLUMNS 323

REFERENCES 348

LIST OF TABLES

TABLE		Page
2.1	Comparison of the Sub-Ultimate Approach of the Present Study and Thomasson's [1978] Approach	29
5.1	Dimensions of Stub Column Specimens	148
5.2	Dimensions of Long Column Specimens	149
5.3	Tensile Material Properties	150
5.4	Maximum Amplitude of Local Initial Imperfections in Stub Columns	151
5.5	Maximum Amplitude of Local and Overall Initial Imperfections in Long Columns	152
5.6	Experimental Results for Stub Columns	153
5.7	Experimental Buckling Coefficients for Stub Columns	154
5.8	Influence of Strain Gage Location on Buckling Coefficient	155
5.9	Experimental Results for Long Columns	156
5.10	Chilver's [1953] Stub Column Tests	157
5.11	Pekoz's [1977] Stub Column Tests	158
5.12	Thomasson's [1978] Long Column Tests	159
5.13	Loughlan's [1979] Long Column Tests	160
6.1	Evaluation of Channel Stub Columns	221
6.2	Evaluation of Lipped Channel Stub Columns	222
6.3	Evaluation of Concentrically Loaded Long Columns	223
6.4	Evaluation of Eccentrically Loaded Long Columns	224
6.5	Evaluation of Chilver's [1953] Stub Columns	226
6.6	Evaluation of Pekoz's [1977] Stub Columns	227
6.7	Evaluation of Thomasson's [1978] Long Columns	228
6.8	Evaluation of Loughlan's [1979] Long Columns	229
A.1	Linear Plane Stress Finite Strip Stiffness Matrix	272
A.2	Second-Order Plate Bending Finite Strip Stiffness Matrix	273
A.3	Consistent Initial Stress Finite Strip Stiffness Matrix for Longitudinal Membrane Loading	274
C.1	Buckling Coefficients K for a Simply Supported Plate Under Uniform Axial Compression	293
C.2	Buckling Coefficients K for the Structure of Table C.1 Using the Finite Element Method	293
C.3	Buckling Coefficients K for a Simply Supported Plate Subjected to Pure In-Plane Bending	294
C.4	Strong Axis Flexural Buckling of a Single Plate	294

LIST OF FIGURES

FIGURE		Page
2.1	Buckling of a Thin Plate	30
2.2	Loading Conditions	31
2.3	Comparison of Experimental and Theoretical Failure Loads for Stiffened Plates Under Eccentric Load	32
2.4	Effective Width for Flange Under Stress Gradient	33
2.5	Comparison of Effective Width Approach of Present Study for Eccentrically Compressed Plates and LaBoube's [1978] Approach for Beam Webs	34
2.6	Effective Width for Unstiffened Compression Elements	35
2.7	Comparison of Effective Width Approaches for Unstiffened Compression Elements	36
2.8	Post-Buckling Stress-Strain Response	37
2.9	Thomasson's [1978] Sub-Ultimate Approach	38
2.10	Deviation of Sub-Ultimate Approach	39
2.11	Sub-Ultimate Approach of Present Study	40
3.1	Local Buckling Interaction in a Uniformly Compressed (Plain) Channel	68
3.2	Local Buckling Interaction in a Uniformly Compressed, Idealized, Lipped Channel	69
3.3	Flange Buckling for Uniformly Compressed Lipped Channels	70
3.4	Web Buckling for Uniformly Compressed Lipped Channels	71
3.5	Local Buckling Modes in Lipped Channels	72
3.6	Effect of Larger Stiffener on Flange Buckling for Uniformly Compressed Lipped Channels	73
3.7	Influence of Stress Gradient Across Flange on Flange Buckling in Lipped Channels	74
3.8	Influence of Stress Gradient Across Flange on Web Buckling in Lipped Channels	75
3.9	Edge Stiffener	76
3.10	Radius Effect for Idealized Flange-Stiffener Model Subjected to Uniform Compression	77
3.11	Theoretical Post-Buckling Behavior of Structural Sections	78
3.12	Comparison of Effective Section Approaches for (Plain) Channels	79
3.13	Comparison of Effective Section Approaches for Lipped Channels	80
4.1	Interaction of Local and Overall Buckling for a Uniformly Compressed Channel	104
4.2	Effective Section	105
4.3	Behavioral Assumptions	106
4.4	Strength of Lipped Channel Beam-Columns	107
4.5	Load-Deflection Response of Lipped Channel Beam-Columns	108
4.6	Load-Strain Response of Lipped Channel Beam-Columns	109
4.7	Strength of Lipped Channel Beam-Columns	110
4.8	Load-Deflection Response and Elastic Failure	111

5.1	Test Specimen Cross Section and Typical Strain Gage Instrumentation	162
5.2	Local Initial Imperfection Measuring Devices for Stub Columns	163
5.3	Variation of Maximum Local Initial Imperfection with Flat Width-to-Thickness Ratio for Lipped Channels	164
5.4	Local Initial Imperfection in Web of Channel Stub Column SC/1 120x60	165
5.5	Local Initial Imperfection in Flanges of Channel Stub Column SC/1 120x60	166
5.6	Local Initial Imperfection in Flanges of Channel Stub Column SC/1 60x60	167
5.7	Local Initial Imperfection in Web and Flanges of Lipped Channel Stub Column SLC/2 120x60	168
5.8	Local Initial Imperfection in Web of Lipped Channel Stub Column SLC/1 180x60	169
5.9	Local Initial Imperfection in Flanges, at Flange-Lip Juncture, in Lipped Channel Stub Column SLC/2 180x60	170
5.10	Local Initial Imperfection in Lip of Lipped Channel Stub Column SLC/2 180x60	171
5.11	Overall Initial Imperfection Measurement and Reduction for Long Columns	172
5.12	Weak Axis Overall Initial Imperfection of Long Column CLC/2.1 180x60	173
5.13	Strong Axis Overall Initial Imperfection of Long Column CLC/2.1 180x60	174
5.14	Overall Initial Imperfection of Long Column CLC/2.1 180x60	175
5.15	Local Initial Imperfection in Flanges, at Flange-Lip Juncture, of Long Column CLC/2.1 180x60	176
5.16	Stub Column Test Setup	177
5.17	Long Column End Fixture	178
5.18	Long Column Test Setup	179
5.19	Typical Dial Gage Instrumentation	180
5.20	Eccentric Alignment of Long Columns - Longitudinal Strain Distributions	180
5.21	Axial Load-Strain Response for Lipped Channel Stub Columns	181
5.22	Strain Gradient in Lipped Channel Stub Columns with Large Web-to-Flange Ratios	183
5.23	Axial Load-Deformation Response for Stub Columns	184
5.24	Stub Column Failure Modes (a) Channels (b) Lipped Channels	185
5.25	Determination of Critical Buckling Stress	187
5.26	Web Local Buckling	188
5.27	Section Local Buckling	189
5.28	Comparison of Experimental and Theoretical Buckling Coefficients for Channels	190
5.29	Comparison of Experimental and Theoretical Buckling Coefficients for Lipped Channels	191
5.30	Failure Modes for Concentrically Loaded Long Columns	192

5.31	Failure Modes for Eccentrically Loaded Long Columns - with and without Braces	193
5.32	Violent Failure Mode for Test CLC/1 90x90	194
6.1	Maximum Flange Out-of-Plane Deformation for Channel Sections	230
6.2	Influence of Local Buckling Interaction on Ultimate Strength for Lipped Channel Sections	231
6.3	Axial Load-Deformation Response For Channel SC/1 90x30	233
6.4	Axial Load-Deformation Response for Channel SC/1 100x60	234
6.5	Axial Load-Deformation Response for Lipped Channel SLC/2 120x60	235
6.6	Axial Load-Deformation Response for Lipped Channel SLC/2 180x60	236
6.7	Axial Load-Deformation Response for Lipped Channel SLC/1 90x90	237
6.8	Axial Load-Deformation Response for Lipped Channel SLC/1 120x30	238
6.9	Axial Load-Deformation Response for Lipped Channel SLC/1 270x90	239
6.10	Sub-Ultimate Response for CLC/2 120x60	240
6.11	Sub-Ultimate Response for CLC/2.3 120x60	242
6.12	Sub-Ultimate Response for CLC/2.4 120x60	244
6.13	Sub-Ultimate Response for CLC/2.1 120x60	246
6.14	Sub-Ultimate Response for CLC/3 120x60	248
6.15	Sub-Ultimate Response for CLC/1 90x90	250
6.16	Sub-Ultimate Response for CLC/2.2 180x90	252
6.17	Sub-Ultimate Response for CLC/2.1 180x90	254
A.1	Membrane and Bending Finite Strip Subjected to a Linearly Varying Longitudinal Edge Load	275
B.1	Determinant Search Algorithm	287
C.1	Plate Buckling Curve for a Simply Supported Plate in Uniform Compression	295
D.1	SC/1 60x30	297
D.2	SC/1 120x30	298
D.3	SC/2 120x30	299
D.4	SC/1 40x60	300
D.5	SC/2 40x60	301
D.6	SC/1 60x60	302
D.7	SC/1 120x60	303
D.8	SC/1 180x60	304
D.9	SC/2 180x60	305
D.10	SLC/1 60x30	306
D.11	SLC/1 90x30	307
D.12	SLC/1 60x60	308
D.13	SLC/2 60x60	309
D.14	SLC/1 120x60	310
D.15	SLC/1 180x60	311

D.16	SLC/1 240x60	312
D.17	SLC/3 240x60	313
D.18	SLC/1 60x90	314
D.19	SLC/2 60x90	315
D.20	SLC/2 90x90	316
D.21	SLC/1 180x90	317
D.22	SLC/2 180x90	318
D.23	SLC/4 180x90	319
D.24	SLC/5 180x90	320
D.25	SLC/2 270x90	321
D.26	SLC/1 360x90	322
E.1	CLC/1 120x60	324
E.2	CLC/4 120x60	326
E.3	CLC/5 120x60	328
E.4	CLC/1 180x60	330
E.5	CLC/2 180x60	332
E.6	CLC/3 180x60	334
E.7	CLC/4 180x60	336
E.8	CLC/1 180x90	338
E.9	CLC/2 180x90	340
E.10	CLC/3 180x90	342
E.11	CLC/1.1 120x30	344
E.12	CLC/2.2 120x60	346

NOTATION

A	Area or constant
$\underset{\sim}{A}$	Global matrix of displacement gradients
B	Constant
$\underset{\sim}{B}_O, \underset{\sim}{B}_L$	Strain matricies
b	Finite strip width
C	Constant (constitutive)
C_w	Torsional constant
c	Stress factor or distance to centroid
D	Plate rigidity or constant
$\underset{\sim}{D}$	Constitutive or diagonal matrix
d_z	Self-weight deflection
E	Young's modulus
e	Eccentricity or elevation
F_y	Yield stress
f	Stress
f'	Reduced stress
G	Shear modulus
$\underset{\sim}{G}$	Discretization matrix for $\underset{\sim}{\varepsilon}_L$
I	Moment of inertia
$\underset{\sim}{I}$	Diagonal identity matrix
J, j	Torsional constants
K	Buckling coefficient or effective length factor
$\underset{\sim}{K}$	Stiffness matrix

$\underset{\sim}{K}_o$	Small displacement stiffness matrix
$\underset{\sim}{K}_\sigma$	Initial stress stiffness matrix
L	Length
$\bar{L}$	Test length or length associated with the eigenvalue $\bar{\lambda}$
$\underset{\sim}{L}$	Lower triangular matrix
M	Moment
m	Harmonic parameter
$\underset{\sim}{N}$	Shape function matrix
OR	Outside radius
P	Axial load
Q	Strength reduction factor
R	Ratio of effective-to-full width
r	Inside radius or radius of gyration
r_o	Polar radius of gyration
S	Stress ratio or section modulus
T	Membrane line load
$\underset{\sim}{T}$	Matrix of membrane loads
t	Thickness
u	In-plane displacement
$\underset{\sim}{u}$	Field variable
V	Volume
v	In-plane displacement
$\underset{\sim}{v}$	Eigenvector
W	Total plate width
w	Plate flat width or out-of-plane displacement
w_o	Location of neutral axis on tensile side of plate

x	Coordinate axis
x_y	Distance between effective and gross centroids under a uniform compressive yield stress
x_o	Location of shear center from centroid
$\bar{x}$	Location of gross centroid from web
$\underset{\sim}{x}, \underset{\sim}{\bar{x}}$	Iteration vectors
Y_m	Harmonic function
y	Coordinate axis
$\underset{\sim}{y}, \underset{\sim}{\bar{y}}$	Iteration vectors
$\underset{\sim}{0}$	Null matrix
z	Coordinate axis
α	Compression eccentricity, aspect ratio, eigenvalue, or dimensionless parameter
β	Stress ratio or torsional constant
β'	Stress reduction factor
Δ	Lateral or local deformation, or local or overall initial imperfection
$\underset{\sim}{\Delta}$	Nodal displacements (parameters)
δ	Variation symbol
ε	Strain
ε_y	Yield strain (F_y/E)
$\underset{\sim}{\varepsilon}$	Green's strain vector
$\underset{\sim}{\varepsilon}_o$	Linear strains
$\underset{\sim}{\varepsilon}_L$	Nonlinear strains
η	Iteration parameter
$\underset{\sim}{\theta}$	Vector of displacement gradients

θ	Rotation
λ	Stress ratio or eigenvalue
μ	Poisson's ratio or eigenvalue
ξ	Dimensionless parameter
Π	Potential energy
ρ	Rayleigh quotient or density
σ	Stress
$\underline{\sigma}$	Stress vector
ω	Eigenvalue

Subscripts, Superscripts, Abbreviations

a	Axial or adequate
act	Actual
av	Average
b	Bending
cr	Critical
c.g.	Center of gravity
e	Edge or effective
exp	Experimental
eff.c.g.	Effective center of gravity
f	Flexural
i,j	Generalized reference axes
l	Limiting
max	Maximum
min	Minimum

1,2	Reference axes or
1,2,3	Reference indicies for the web, flange, and lip, respectively
p	Plane stress
'	Elastic
s	Stiffener or strong axis
s.c.	Shear center
t	Torsional
tf	Torsional-flexural (combined axial and bending)
tfo	Torsional-flexural (axial)
th	Theoretical
u,ult	Ultimate
w	Weak axis
y	Yield

CHAPTER 1

INTRODUCTION

1.1 General

Cold-formed steel sections are formed from thin steel sheets, of typical thickness 0.015-0.25 inches, by either production cold roll forming or by specialized press braking. As a result, it is possible to produce economically a variety of cross-sectional shapes, which have high strength-to-weight ratios. Some structural applications include primary and secondary load-carrying framing members, such as columns, purlins and wall studs; and shear diaphragms, such as floor and roof decks and wall panels (Yu [1973]). Their design is governed by the American Iron and Steel Institute (AISI) Specification [1980], which is unique because of its generality, e.g., no specific shape is presumed.

The philosophy behind cold-formed steel structural members is illustrated with the following example, adopted from Seaburg [1981]. Suppose it is required to design a 10-foot column, of any shape, to support a given axial load. One solution would be to employ a 3/4-inch square mild steel bar. However, a subsequent analysis of this slender column would show that it would fail, by flexural buckling, at a load of only about 500 pounds. Alternately, this same bar could be rolled into a thin strip about 12 inches wide and, in turn, used as the column. In this case, the strip would buckle essentially under its own weight. On the other hand, if this strip is formed, or bent, into the shape, say, of a lipped channel, its load-carrying capacity would be increased by twenty times that of the original bar.

This simple example illustrates, of course, that the structural efficiency of a section is dependent on the manner in which the available material is distributed, which is a basic property utilized in the design of cold-formed steel members. Equally important is that this property leads to the proportioning of very thin structural sections which are prone to local buckling of the individual plate elements, or portions of the section between bends. It is this latter area that the present investigation addresses.

1.2 Objectives of Research

The primary objectives of the research described herein are to study the interaction of local buckling between plate elements in thin-walled structural sections and to study the influence of local buckling on the overall modes of behavior. The research is specialized to column and beam-column applications of singly-symmetric steel shapes, e.g., channels and lipped channels.

The needs for this research became apparent in previous investigations conducted at Cornell University. DeWolf [1973] studied the behavior of doubly-symmetric sections with locally buckled stiffened or unstiffened compression elements. A stiffened element is defined as one which is supported along both unloaded edges by other plate elements, and an unstiffened element is defined as one which is supported along the unloaded supported edge by another plate element and has a free unloaded edge. Later Kalyanaraman [1978] examined, more thoroughly, the behavior of doubly-symmetric sections with locally buckled unstiffened compression elements. Both investigations employed an effective width concept (see Chapter 2) to predict the yield strength, for beams and short columns, and

the flexural buckling strength, for long columns. Also, Desmond [1978] studied edge stiffened elements. In this case, an edge stiffened element is defined as one which is supported along one unloaded edge by a stiffened element and along the other unloaded edge by a stiffener. Edge stiffener requirements were derived which made the strength of the edge stiffened element equivalent to that associated with an identical stiffened element. Again an effective width concept was employed.

All of the above investigations were necessarily limited in scope to the specific areas under study. For example, local buckling interaction with other plate elements was precluded. Thus, the applicability of the approaches which were developed was left open to question when local buckling interaction occurred. Also, because these investigations were limited to doubly-symmetric shapes, analogous procedures for treating the effects of local buckling in singly-symmetric shapes were not defined. Finally, a need was established for work in the area of the sub-ultimate behavior of locally buckled plate elements.

1.3 Scope of Research

The following interrelated areas are within the scope of the present research project.

- Local buckling interaction between stiffened and unstiffened or edge stiffened elements in uniformly compressed short columns.
- Sub-ultimate behavior of uniformly compressed elements, with an emphasis on stiffened elements.
- The influence of local buckling on the overall modes of behavior of singly-symmetric long columns and beam-columns. This area encompasses an investigation of stiffened elements subjected to a stress gradient.

CHAPTER 2 deals with the post-buckling behavior of isolated thin plates. Effective width approaches for eccentrically compressed stiffened elements and for the sub-ultimate behavior of uniformly compressed elements are derived. Uniformly compressed stiffened and unstiffened elements are also treated.

CHAPTER 3 studies local buckling interaction in thin-walled structural sections. The finite strip method is employed to formulate the equations which govern the linear instability of arbitrary plate structures, and the associated numerical solution procedures are discussed. This method is then used to study the local instability of various thin-walled configurations. Edge stiffeners are also addressed. Next effective section methods, which utilize the approaches from Chapter 2, are defined for analyzing local buckling interaction in structural sections.

CHAPTER 4 treats the interaction between local and overall buckling. Existing analysis methods are first reviewed. Then an effective section method and beam-column analysis method is derived for predicting the behavior and strength of singly-symmetric shapes. Again the approaches developed in Chapter 2 are integrated to define the effective section.

CHAPTER 5 presents the experimental investigation. Stub column tests of channel and lipped channel sections, and long column and beam-column tests of lipped channel sections are reported. Information pertaining to initial imperfections and testing procedures is also included.

CHAPTER 6 verifies the methods developed in Chapters 2-4 by comparing the predicted results with the empirical data from Chapter 5.

CHAPTER 7 summarizes the research and discusses areas that warrant further investigation.

CHAPTER 2

POST-BUCKLING BEHAVIOR AND EFFECTIVE WIDTH

2.1 Introduction

Contrary to column behavior, plates exhibit significant strength after the occurrence of buckling. When this "post-buckling" strength is fully utilized, a structurally efficient and economical design can be obtained. In this chapter, methods of utilizing the post-buckling strength of plates are described. Specifically the following areas are treated: stiffened compression elements under both uniform and non-uniform (linear) compression, unstiffened compression elements under uniform compression, and sub-ultimate response.

As an introduction, the simply supported thin flat plate of Figure 2.1 displays in-plane response as long as the applied uniform compressive stress f remains less than some critical value f_{cr}. At this stage, the associated internal longitudinal stress distribution is uniform across the center of the plate. When the applied stress reaches f_{cr}, a slight buckling wave develops in the plate. Then, as the load is increased further, the out-of-plane deformation increases but is restrained by the transverse stresses that are set up. At the same time, a redistribution of internal longitudinal stress occurs, from uniform to non-uniform, where the majority of load resistance is provided by the less deflected portions of the plate. This process continues until the stress level f_e, at the edge of the plate, reaches yield; after which the plate generally fails.

2.2 Post-Buckling Strength

The post-buckling, non-uniform stress distribution shown at the bottom of Figure 2.1 would unnecessarily complicate practical design. Therefore, the concept of an "effective width" was introduced by von Karman, et al. [1932]. In this approach, the non-uniform stress f acting over the plate width w is replaced by an equivalent uniform stress acting over an effective width w_e. Equilibrium is maintained by defining the effective width such that

$$\int_0^w ftdy = f_e w_e t \qquad 2.1$$

where f_e is the edge stress. After integrating Equation 2.1, the following relationship between w_e and w is obtained.

$$w_e/w = f_{av}/f_e \qquad 2.2$$

where f_{av} is the average stress acting over the total width w. The original equation proposed by von Karman for the effective width at failure was

$$w_e = 1.9t\sqrt{E/F_y} \qquad 2.3$$

where E is Young's Modulus, F_y the yield strength, and t the plate thickness.

Equation 2.3 was derived from rather intuitive reasoning and has an empirical basis. Von Karman recognized that a plate had the ability to withstand loads above the critical buckling stress f_{cr}, defined below (for a complete deviation of f_{cr} see, e.g., Timoshenko and Gere [1961]).

$$f_{cr} = K\pi^2 E/12(1 - \mu^2)(w/t)^2 \qquad 2.4$$

where μ is Poisson's ratio and K is the buckling coefficient which depends on the type of loading, boundary conditions, and plate aspect ratio. For a long, or square, uniformly compressed simply supported plate

$K = 4$, and

$$f_{cr} = \pi^2 E/3(1 - \mu^2)(w/t)^2 \qquad 2.5$$

Further, von Karman reasoned that for a plate stressed beyond the critical stress, the central buckled portion of the plate could not be counted on to provide any appreciable load resistance and that the majority of the load must be carried by the two strips adjacent to the edges of the plate. Thus, the width w in Equation 2.5 was interpreted as the effective width w_e, and the stress f_{cr} was set equal to the yield stress F_y for failure. If these substitutions are made in Equation 2.5, with $\mu = 0.3$, the effective width Equation 2.3 follows immediately.

2.2.1 Uniformly Compressed Stiffened Elements

The simply supported plate of Figure 2.1 is a limiting case of a stiffened compression element. Thus, effective width Equation 2.3 should be applicable. However, research performed subsequent to von Karman's original work revealed deficiencies in this equation. First, Equation 2.3 proved inadequate for elements with relatively small width-to-thickness ratios w/t. Also, for design, it was necessary to predict effective widths associated with stress levels less than the yield condition implied by Equation 2.3. As a result, a wealth of research followed.

Gerard [1957] reviewed several theoretical studies and associated effective width equations for predicting the response of uniformly compressed, post-buckled plates. Later, Jombock and Clark [1961] expanded Gerard's survey to include comparisons with additional effective width

2.2 Post-Buckling Strength

The post-buckling, non-uniform stress distribution shown at the bottom of Figure 2.1 would unnecessarily complicate practical design. Therefore, the concept of an "effective width" was introduced by von Karman, et al. [1932]. In this approach, the non-uniform stress f acting over the plate width w is replaced by an equivalent uniform stress acting over an effective width w_e. Equilibrium is maintained by defining the effective width such that

$$\int_0^w f t dy = f_e w_e t \qquad 2.1$$

where f_e is the edge stress. After integrating Equation 2.1, the following relationship between w_e and w is obtained.

$$w_e/w = f_{av}/f_e \qquad 2.2$$

where f_{av} is the average stress acting over the total width w. The original equation proposed by von Karman for the effective width at failure was

$$w_e = 1.9t\sqrt{E/F_y} \qquad 2.3$$

where E is Young's Modulus, F_y the yield strength, and t the plate thickness.

Equation 2.3 was derived from rather intuitive reasoning and has an empirical basis. Von Karman recognized that a plate had the ability to withstand loads above the critical buckling stress f_{cr}, defined below (for a complete deviation of f_{cr} see, e.g., Timoshenko and Gere [1961]).

$$f_{cr} = K\pi^2 E/12(1 - \mu^2)(w/t)^2 \qquad 2.4$$

where μ is Poisson's ratio and K is the buckling coefficient which depends on the type of loading, boundary conditions, and plate aspect ratio. For a long, or square, uniformly compressed simply supported plate

$K = 4$, and

$$f_{cr} = \pi^2 E/3(1 - \mu^2)(w/t)^2 \qquad 2.5$$

Further, von Karman reasoned that for a plate stressed beyond the critical stress, the central buckled portion of the plate could not be counted on to provide any appreciable load resistance and that the majority of the load must be carried by the two strips adjacent to the edges of the plate. Thus, the width w in Equation 2.5 was interpreted as the effective width w_e, and the stress f_{cr} was set equal to the yield stress F_y for failure. If these substitutions are made in Equation 2.5, with $\mu = 0.3$, the effective width Equation 2.3 follows immediately.

2.2.1 Uniformly Compressed Stiffened Elements

The simply supported plate of Figure 2.1 is a limiting case of a stiffened compression element. Thus, effective width Equation 2.3 should be applicable. However, research performed subsequent to von Karman's original work revealed deficiencies in this equation. First, Equation 2.3 proved inadequate for elements with relatively small width-to-thickness ratios w/t. Also, for design, it was necessary to predict effective widths associated with stress levels less than the yield condition implied by Equation 2.3. As a result, a wealth of research followed.

Gerard [1957] reviewed several theoretical studies and associated effective width equations for predicting the response of uniformly compressed, post-buckled plates. Later, Jombock and Clark [1961] expanded Gerard's survey to include comparisons with additional effective width

methods. Most recently, Thomasson [1978] included comparisons of effective width approaches employed in the design specifications of various countries.

The most widely adopted research on stiffened compression elements was by Winter [1947 and 1948]. He provided extensive experimental data from which the following semi-empirical effective width equation was derived.

$$w_e = 1.9t\sqrt{E/f_e}[1.0 - 0.475\sqrt{E/f_e}/(w/t)] \qquad 2.6$$

where f_e is the edge stress. A comparison of the von Karman Equation 2.3 and Equation 2.6 reveals that the latter approaches the former for large plate width-to-thickness ratios w/t. The term in brackets in Equation 2.6 represents an experimental modification necessary to account for the influence of initial imperfections.

The effective width given by Equation 2.6 served as a basis of governing U.S. specifications for over 20 years (Winter [1970]). Nevertheless, it still represented a conservative approach. Thus, to eliminate this degree of convervatism, the coefficient 0.475 of Equation 2.6 was modified to 0.415 (see Winter [1970]), or

$$w_e = 1.9t\sqrt{E/f_e}[1.0 - 0.415\sqrt{E/f_e}/(w/t)] \qquad 2.7$$

This modified equation forms the basis of the effective width approach for stiffened compression elements contained in the present U.S. specification (AISI [1980]), as well as in several European specifications. Equation 2.7 is valid for w/t ratios above the following limiting value.

$$(w/t)_1 = 1.29\sqrt{E/f_e} \qquad 2.8$$

For w/t ratios less than $(w/t)_1$, the compression element is fully effective, i.e., $w_e = w$. For later use, Equation 2.7 is rewritten below in terms of the critical buckling stress f_{cr}, Equation 2.5.

$$w_e/w = \sqrt{f_{cr}/f_e}(1.0 - 0.218\sqrt{f_{cr}/f_e}) \qquad 2.9$$

Similarly, Equation 2.8 is rewritten as a limiting stress ratio.

$$(f_{cr}/f_e)_1 = 2.17 \qquad 2.10$$

The above equation implies that the effects of local buckling become significant when the stress level exceeds about 50 percent of the theoretical buckling stress f_{cr}.

2.2.2 Eccentrically Compressed Stiffened Elements

The previous section reviewed a widely adopted effective width approach for uniformly compressed stiffened elements. However, the approach is obviously inadequate when the element is compressed eccentrically. The present section deals with an effective width approach for this situation.

The critical buckling of eccentrically loaded plates, with various boundary conditions, has been investigated thoroughly. Timoshenko [1961] discussed the critical behavior of plates under in-plane bending, while Bulson [1969], in an extensive text, reviewed studies of plates with a wide variety of loading and boundary conditions.

Still, research on the post-buckling behavior of eccentrically compressed plates progressed rather slowly. Walker [1964] conducted a theoretical investigation of simply supported, or clamped, eccentrically loaded plates using Galerkin's method to solve the governing large deflection plate equations of von Karman (see Chajes [1974]). He also conducted an experimental investigation on discrete steel plates to justify his theoretical predictions. The practicality of Walker's work was limited, however, due to the inability of his theoretical loading condition of a

linearly varying end load to represent the experimental loading condition of a linearly varying end compression (displacement).

Rhodes and Harvey [1971a and b] recognized the limitations of Walker's work and investigated the post-buckling response of plates subjected to either an eccentric loading or an eccentric compression system. The difference between these two loading systems is illustrated in Figure 2.2. The "load" is applied through rigid bars to produce an end displacement u which varies linearly across the plate, e.g., $u = \bar{u}(1 - \alpha y/w)$ where $\bar{u}$ is the maximum displacement along one longitudinal edge of the plate and α is an eccentricity factor which is directly proportional to the plate angle θ. Moreover, two consecutive displaced positions of the bars, under increasing load are represented in Figure 2.2.

An example of constant compression eccentricity is shown in Figure 2.2a. For this case the loading is applied such that after local buckling the compression eccentricity α remains constant. This implies that the position of the stress resultant P must change to maintain equilibrium. Uniform compression ($\alpha = 0$) is a limiting case of the loading condition of Figure 2.2a.

An example of constant load eccentricity is shown in Figure 2.2b. For this case the eccentricity e remains constant throughout the loading history. Thus, after local buckling, the compression eccentricity α varies to maintain equilibrium.

If the plate is supported to an equal degree along both unloaded edges and is loaded concentrically ($e = w/2$); then the post-buckling response predicted using either of the loading conditions of Figure 2.2 is identical. However, if the plate is loaded or compressed eccentrically,

or has unequal support conditions along its unloaded edges; then the post-buckling response is very much dependent on the specific loading condition used in the analysis. In general, the compressive stiffness for a plate is greater if the load eccentricity is maintained at its original value than if the original compression eccentricity is maintained (Rhodes and Harvey [1971b]).

It is noted that the above discussion is limited to the response of a discrete plate, which is less than practical. For example, in a thin-walled construction application, the plate represents only one component of the total section, e.g., the flange of a lipped channel. Since the compressional response is dictated by the total section, rather than by an individual plate element, the actual loading condition lies somewhere between the two cases represented in Figure 2.2.

In the original work of Rhodes and Harvey [1971a and b], an adaptation of the semi-energy method of Marguerre [1937] was used to solve the problem. Several numerical examples were considered and were compared to the experimental results of Walker [1964]. Later, Rhodes et al. [1975], reported additional experimental work on eccentrically loaded, mild steel, discrete plates. In this later paper, an approximate analysis was performed to derive a design expression, which was in agreement with the more rigorously derived solution. The following expression was derived specifically for simply supported plates, at ultimate, under constant load eccentricity (see Figure 2.2b).

$$P_u/F_y wt = (K_y + 11.4)/K_y[6(e/w) + 0.85] \qquad 2.11$$

where P_u is the ultimate load, e the load eccentricity (constant), w the plate width, and

$$K_y = F_y w^2 t/\pi^2 D$$

$$D = Et^3/12(1 - \mu^2)$$

Equation 2.11 is valid for $e/w \geq 0.5$ and

$$K_y > 8[3(e/w) - 1] \qquad 2.12$$

For values of K_y less than those given by Equation 2.12, the plate is unbuckled and fails by yielding.

Figure 2.3 shows a comparison of ultimate loads predicted using Equation 2.11 and the experimental results reported by Walker [1964], with an average F_y = 25.5 ksi, and Rhodes et al. [1975] and [1977], with an average F_y = 37.3 ksi. (The scales used in this figure are such that a single curve based on Equation 2.11, is applicable to both uniform compression and eccentrically loaded plates.) In general, there is good agreement between experimental and predicted loads. The two horizontal dashed lines represent theoretical cut-off points given by Equation 2.12 for e/w ratios of 0.5 and 1. Discussion of the other curves shown in the figure is delayed until later in this section.

The approach discussed above for stiffened elements under eccentric load is not directly applicable when the element in question represents only one part of a structural section. Therefore, a more general approach is adopted which, as will be subsequently shown, is simple yet representative of the actual structural behavior.

An effective width approach is employed in the present study to model the behavior of a stiffened element under constant compression eccentricity. In the approach, which is a modification of original Swedish research by Thomasson [1978], the following assumptions are made. Elementary beam theory assumptions are presumed valid. Secondly, the effective width is assumed to be uniquely determined from the edge membrane stresses, f_i and

f_j (see Figure 2.4). Lastly, failure is presumed when the maximum membrane stress at the edge of the plate reaches yield (Graves Smith [1969], also see Section 2.3.1).

The effective width is "split" into two parts, w_{ei} and w_{ej}, which are subjected to edge stress levels f_i and f_j, respectively, where $f_i > f_j$ (see Figure 2.4). After local buckling, the portion of the plate subjected to the larger stress is expected to be less effective in resisting load than the remaining portion, e.g., $w_{ei} \leq w_{ej}$.

In Case I of Figure 2.4a, the element is subjected entirely to compression, where the edge stresses are such that $f_i > f_j > 0$ (compression is positive). The proposed expression for w_{ei} is

$$w_{ei} = w_e/2 \qquad 2.13$$

where w_e is defined by Winter's stiffened plate effective width equation given by Equation 2.7 with $f_e = f_i$. An empirical formula proposed by Thomasson [1978] is used to determine w_{ej}.

$$w_{ej} = w_{ei}\ (1.5 - 0.5\ f_j/f_i) \qquad 2.14$$

Since this expression is a function of both edge stress levels, the effect of the stress gradient is included directly in the approach. It is noted that Equations 2.13 and 2.14 approach Winter's effective width when the stress state approaches uniform compression, e.g., $f_j/f_i \rightarrow 1.0$. Hence, the present approach is consistent with existing design specifications (AISI [1980]) for this limiting state. Finally, the total effective width is, of course, subjected to the constraint

$$w_{ei} + w_{ej} \leq w \qquad 2.15$$

In the work of Thomasson, a different expression for the effective width w_{ei} was proposed, e.g.,

$$w_{ei} = Ct\sqrt{E/f_i} \qquad 2.16$$

where C is a constant. Originally Thomasson [1978] used C = 0.76, which was based apparently on earlier work on web buckling (Thomasson [1973]). However, the use of Equation 2.16 with C = 0.76 resulted in poor correlation when compared with the approach and experiments of Rhodes et al. [1975]. Therefore, the constant C was modified to 0.95. It is observed that Equation 2.16 with the modified constant of 0.95 is identical to one-half of the von Karman equation, Equation 2.3. Also, a comparison of the present approach, Equation 2.13, and Thomasson's approach, Equation 2.16 with C = 0.95, reveals that the former is more conservative.

In addition to the pure compressive case, the possibility of a tensile edge stress f_j must be considered (see Case II of Figure 2.4). For this case, Equation 2.13 is still used to calculate w_{ei}, but the effective width w_{ej} is determined from

$$w_{ej} = 1.5w_{ei} + w_o \qquad 2.17$$

which is valid for $f_j < 0$. This expression, adopted from Thomasson, is consistent with the effective width w_{ej} of Equation 2.14 in the limiting case of $f_j \to 0$. Again, the total effective width is subjected to the constraint of Equation 2.15.*

*While this dissertation was in the final stages of preparation, a relevant article (Usami [1982]) was published which also examined the post-buckling of plates in combined compression and bending. In this article a theoretical post-buckling analysis was presented, and an effective width approach was developed which was in general agreement with the theoretical results. It is noted that this approach and that of the present study are very similar, except for a small variation in the coefficients of the equations. For example, Usami's expression for wei is identical to Equation 2.13, and his expressions for wej for fj > 0 and fj < 0 are equal to Equations 2.14 and 2.17, respectively, with the coefficient 1.5 changed to 1.44. As a result of this comparison, the approach proposed independently in this section is provided with a theoretical justification.

Although not strictly valid, a comparison is made in Figure 2.3 between the approach of this study, Equations 2.13 through 2.15 and 2.17, and the results and approach of Rhodes et al. [1975]. The inconsistency in this comparison is due to the different loading conditions; the present approach assumes constant compression eccentricity, whereas in the work of Rhodes constant load eccentricity is assumed. Nevertheless, some qualitative judgements can be made from this comparison. The curves based on Equations 2.13 through 2.15 and 2.17 were calculated for several fixed stress ratios f_i/f_j with f_i held constant at 30 ksi, which was slightly larger than the weighted average yield stress for the experiments. The curve labeled (1) corresponds to uniform compression. In general, the approach of the present study yields conservative results, and any difference between the approaches is due to the different loading conditions, as noted earlier. The conservatism noted above for the constant compression eccentricity case agrees qualitatively with that reported by Rhodes and Harvey [1971b] for a simply supported plate. These authors compared the behavior of a plate which was subjected to constant compression and constant load eccentricities. Initially, in the pre-buckled state, both loading conditions were identical, i.e., the compression eccentricity α (see Figure 2.2) was equal to the same value. For the case of constant load eccentricity, it was shown that after buckling the compression eccentricity reduced, from its pre-buckling value, to maintain equilibrium and was less than the value for the constant compression eccentricity case. Also, the most highly compressed edge occurred, at $y = o$ in Figure 2.2, for the constant compression eccentricity case which would lead to earlier failure, relative to that for constant load eccentricity.

Moreover, it is believed that the condition of constant compression eccentricity, on which the present approach is based, is more appropriate for thin-walled structural sections. Typically, an eccentrically loaded section has plate elements which are uniformly and eccentrically compressed. If, as is generally the case, the uniformly compressed elements (or their stiffnesses) have a dominating influence on the axial response of the section, then the loading condition for the eccentrically compressed elements is more closely approximated by the constant compression eccentricity condition. Even if this is not the case, the conservatism noted earlier for the constant compression eccentricity condition makes it an amenable approach for the general design of eccentrically compressed stiffened elements.

At this point it is appropriate to discuss the relationship of the present approach for stiffened elements under eccentric load (stress gradient) to approaches for beam webs. Also, since previous comparisons were restricted to $f_i > f_j > 0$ (see Figure 2.4a), this discussion serves to establish a basis for Equation 2.17, which is valid for $f_j < 0$ (see Figure 2.4b).

As mentioned earlier, the present approach is consistent with existing design methods for the limiting case of uniform compression, i.e., with $f_i = f_j$. It is not, however, consistent with methods for the limiting case of pure bending. For example, LaBoube [1978] proposed a design method for beam webs which was based on a fully effective web and used empirical formulas to reduce the moment resistance of the beam. (It should be noted that LaBoube's approach has been recently adopted by the

U.S. specification, see AISI [1980a].) In contrast to this, an effective width concept is used in the present study. It is felt that such an approach leads to a better physical understanding of the problem.

LaBoube [1978] also investigated an effective width approach for beam webs. In an extensive experimental investigation of steel sections in bending, the following empirical effective width equation was derived

$$w_{ei} = 61.5\, t\sqrt{K/f'} < w \qquad 2.18$$

where w_{ei} is defined in Figure 2.4b. (Actually, LaBoube derived two effective width expressions. One, Equation 2.18, was derived for webs supported by a stiffened element (compression flange), and another was derived for webs supported by an unstiffened element. Since these expressions were nearly identical, Equation 2.18 is assumed valid for both cases.) The buckling coefficient K in Equation 2.18 was defined as

$$K = 4 + 2(1 + \beta)^3 + 2(1 + \beta) \qquad 2.19$$

where $\beta = |f_j/f_i|$. This expression is an approximation to the theoretical elastic buckling coefficient for a simply supported long plate under bending (Thomasson [1973]) and is valid for $f_j/f_i \leq 0$. Also, the stress factor f' is defined by

$$f' = \beta' F_y \qquad 2.20$$

where β' is a reduction factor used apparently to account for the amount of lateral support supplied to the web by the compression flange and the local buckling interaction between the compression flange and the web. Ignoring the effects of interaction, β' is taken as 1.0 and 0.8 for beams with stiffened and unstiffened compression flanges, respectively. Finally, the effective width in the compression zone closest to the neutral axis is ignored (see Figure 2.4b). Therefore,

$$w_{ej} = w_o \qquad 2.21$$

The ultimate loads predicted using LaBoube's approach, Equations 2.18 through 2.20, and those predicted using the approach of the present study, Equations 2.13, 2.15, and 2.17, are compared in Figure 2.5 for a simple plate in bending with $f_j/f_i = -0.5$ and $F_y = 30$ ksi. The vertical scale employed in this figure is analogous to the ratio of average to ultimate stresses. For the moment, discussion is restricted to beam webs with stiffened compression flanges, e.g., $\beta' = 1.0$ in Equation 2.20. In this case, the approach of the present study is more conservative when compared with LaBoube's approach for w/t ratios less than about 135, and it is less conservative for larger w/t ratios. Although LaBoube investigated different values of f_j/f_i and F_y than those employed to construct Figure 2.5, e.g., $2/3 < f_j/f_i < -1$ and $30 < F_y < 50$ ksi; it is interesting to note that his experimental results followed a similar pattern. In the range of approximately $80 < w/t < 100$, his experimental results indicated a fully effective web, and for w/t greater than 200, his approach deteriorated and predicted ultimate loads which were unconservative. Because of the method that LaBoube used to present his results, it was not possible to directly compare his experimental effective widths to the effective width approach of this study; instead it was only possible to extract trends of LaBoube's approach, such as those noted above.

Also, lower ultimate loads are predicted by LaBoube's approach for webs supported by unstiffened compression flanges (see Figure 2.5 curve labeled $\beta' = 0.8$). The lateral support supplied to the flange by an unstiffened compression element is less than that supplied by a stiffened element; consequently the effective width is reduced by using $\beta' < 1.0$, in Equation 2.20, which reduces the load. It is mentioned that LaBoube's beams were fabricated by connecting two channels together, face-to-face,

with braces (ties). However, the support supplied to the flange by these braces must have been inadequate, which necessitated the above reduction. Further discussion of this problem is contained in Chapter 6.

2.2.3 Uniformly Compressed Unstiffened Elements

Uniformly compressed unstiffened elements, or plates with one unloaded edge free, can also sustain additional loading after local buckling. Winter [1947] recognized this post-buckling strength and proposed the following unstiffened plate effective width equation, which was based on empirical work by Miller [1943].

$$w_e = 0.8t\sqrt{E/f_e}[1.0 - 0.202\sqrt{E/f_e}/(w/t)] \qquad 2.22$$

where the effective width w_e is distributed as indicated in Figure 2.6. However, in part due to the novelty of the approach, an effective width concept for unstiffened elements was not as widely accepted as it was for stiffened elements. This precaution still carries over in present day specifications (AISI [1980]) for unstiffened elements which are founded, in part, on elastic and inelastic critical buckling.

Analogous to Equation 2.9, Equation 2.22 is rewritten below in terms of the critical buckling stress, f_{cr} of Equation 2.4, where one unloaded edge is assumed to be simply supported, e.g., K = 0.425 in Equation 2.4.

$$w_e/w = 1.29\sqrt{f_{cr}/f_e}(1.0 - 0.326\sqrt{f_{cr}/f_e}) \qquad 2.23$$

In contrast to this, Kalyanaraman [1977,1978] assumed K = 0.5 in Equation 2.4 to define the critical stress and obtained

$$w_e/w = 1.19\sqrt{f_{cr}/f_e}(1.0 - 0.3\sqrt{f_{cr}/f_e}) \qquad 2.24$$

Also, on the basis of the form of Equation 2.24 (or equivalently on the form of Equation 2.9), test results, and an analytical study of post-buckling behavior of unstiffened elements; Kalyanaraman derived the following semi-empirical relationship for the effective width.

$$w_e/w = 1.19\sqrt{f_{cr}/f_e}(1.0 - 0.298\sqrt{f_{cr}/f_e}) \qquad 2.25$$

It is seen that the above more rigorously derived equation is nearly identical to Equation 2.24.

In addition, Kalyanaraman suggested a general effective width approach wherein one equation, Equation 2.9, was applied to both unstiffened and stiffened compression elements. To justify this approach, he showed that Winter's stiffened plate effective width Equation 2.9 provided a conservative estimate of the unstiffened plate effective width given by Equations 2.25 or 2.24.

Similarly, a comparison is made between Equations 2.9 and 2.23 in Figure 2.7 to test Kalyanaraman's approach with respect to the latter equation which is derived assuming a buckling coefficient K of 0.425. In general, Equation 2.9 provides a conservative estimate of the effective width.

It is interesting to compare the research of Chilver [1953] with Winter's work. Chilver, on a purely empirical basis, derived the following effective width equation which was applicable to both stiffened and unstiffened elements.

$$w_e/w = 0.724(f_{cr}/f_e)^{0.3} \qquad 2.26$$

The above equation is plotted in Figure 2.7 for comparison with Equations 2.9 and 2.23. Overall, Equation 2.9 provides the better agreement with Chilver's empirical equation.

2.3 Sub-Ultimate Behavior

Winter's [1947,1948,1970] effective width equations, discussed above, have proved very successful in predicting ultimate loads, i.e., when the edge stress is at yield, $f_e = F_y$. Also, these equations have been employed for predicting the sub-ultimate response, e.g., service load deflections when $f_e < F_y$. This has some justification since Winter used, in addition to ultimate effective width data, sub-ultimate data in deriving his empirical equations. However, recent research by DeWolf [1973], Desmond [1978], Kalyanaraman [1978], and others showed that employing the same effective width equation for both ultimate and sub-ultimate behavior was inadequate. For example, this approach resulted in adequate predictions of strength but resulted in overly conservative predictions of stiffness.

The intent of the present section is to review the pertinent literature and to propose an approach for predicting the sub-ultimate behavior of locally buckled plates.

Dawson and Walker [1972] addressed the sub-ultimate problem in detail, and the following discussion was abstracted from their work. Consider the post-buckling response of the uniformly compressed, simply

supported, flat plate of Figure 2.1. The longitudinal membrane stress f has an average value f_{av}

$$f_{av} = \frac{1}{w} \int_0^w f dy \qquad 2.27$$

and a maximum value f_e at the edges of the plate. The edge stress varies periodically along the length, L, and has a maximum value f_{emax} and an average value f_{eav}

$$f_{eav} = \frac{1}{L} \int_0^L f_e \, dx \qquad 2.28$$

The specific distribution of the edge stress is governed largely by the boundary constraints along the unloaded sides. For a long plate where the sides are free to wave (no transverse stresses), the maximum edge stress f_{emax} occurs at the crest of a buckle, i.e., $f_{emax} = f_e(x = L/2)$.

Moreover, the end shortening, u, is defined by

$$u = \frac{1}{E} \int_0^L f_e dx \qquad 2.29$$

from which

$$f_{eav} = \frac{Eu}{L} \qquad 2.30$$

Hence, the shortening of the plate is an integrated effect and depends not on peak values of stress, but on average values of the edge stress. If an effective width approach is adopted for this situation, a Levy [1942] type effective width definition must be used, e.g.,

$$w_e/w = f_{av}/f_{eav} \qquad 2.31$$

On the other hand, failure is a local phenomenon and depends on peak values of stress. Failure of the plate occurs when the maximum, edge,

membrane stress reaches yield (Graves Smith [1969]), i.e., when $f_{emax} = F_y$, and the buckling wave develops into a local kink. In actuality, yielding occurs through a combination of longitudinal and shear stresses, but the simplified one-dimensional assumption of failure at $f_{emax} = F_y$ agrees with test results (see later discussions). Finally, von Karman's definition of effective width is appropriate for ultimate conditions. Thus

$$w_e/w = f_{av}/f_{emax} \qquad 2.32$$

It should be noted that Equations 2.2 and 2.32 are identical, i.e., $f_e \equiv f_{emax}$ and that the subscript max was omitted in earlier presentations for convenience only.

The above discussion suggests that two effective width equations based on the definitions of Equations 2.31 and 2.32 are needed to adequately represent the sub-ultimate and ultimate post-buckling response, respectively. Dawson and Walker [1972] pursued this approach and derived semi-empirical expressions for modeling both the stiffness and collapse of post-buckled plates. These expressions, which will not be presented here, form the basis of the "reduced stress" concept used in British specifications for cold-formed steel sections (BS 449 [1974], Walker [1975]).

2.3.1 Thomasson's Approach

Thomasson [1978] also investigated the sub-ultimate response of post-buckled plates and proposed a multi-curve effective width approach which simulated the theoretical behavior as reported by Graves Smith [1969]. Indicative of this behavior, including plasticity effects, is a relatively stiff initial stage which is followed by a gradual loss of stiffness (decreasing tangent stiffness) as the ultimate stress, $f_{ult} = f_{avmax}$, is approached (see Figure 2.8 where strain equals $\varepsilon = Ef$).

Eventually, near the ultimate stress, the stiffness vanishes as indicated by the flat portions of the curves. The effects of plate initial imperfection Δ_o in masking critical buckling and decreasing slightly the ultimate stress are also shown in Figure 2.8. In all cases yielding, which is indicated in the figure by upward pointing arrows, provides a good approximation of the ultimate stress. Also, the stress-strain response predicted from Winter's effective width Equation 2.9 is shown in Figure 2.8 to furnish a reasonable estimate of ultimate conditions. Still the sub-ultimate response predicted by this equation is clearly inadequate.

The stress-strain response based on Thomasson's effective width approach, which is defined subsequently, is shown in Figure 2.9a. For the sub-ultimate range, he used an approximation, curve a, of Yamaki's [1959] theoretical elastic solution for an imperfect plate ($\Delta_o/t = 0.1$). And since Winter's effective width Equation 2.9 agreed with the state of affairs at ultimate (Figure 2.7), Thomasson adopted an approximation, curve b, of Winter's equation. The transition from sub-ultimate to ultimate, or from curve a to b, was handled by defining an empirical curve c.

The associated effective widths are shown in Figure 2.9b. The specific expressions for curves a and b are as follows:

$$\text{curve a,}\quad R = 0.827\lambda^{-0.662} \tag{2.33}$$

$$\text{curve b,}\quad R = 0.780\lambda^{-0.864} \tag{2.34}$$

where $\lambda = (f_e/f_{cr})^{\frac{1}{2}}$ and $R = w_e/w$. These equations are fully effective, i.e., $R = 1.0$, when

$$\lambda \leq 0.75 \tag{2.35}$$

A linear transition curve c is defined from the appropriate intersection points 1 and y, e.g.,

$$\text{curve c,}\quad R = R_1 + (R_y - R_1)(\lambda - \lambda_1)/(\lambda_y - \lambda_1) \qquad 2.36$$

where, at ultimate, $\lambda_y = (F_y/f_{cr})^{\frac{1}{2}}$ and the corresponding ordinate R_y is determined from Equation 2.34 with $\lambda = \lambda_y$. The initial abscissa λ_1 is determined from the following empirical equation

$$\lambda_1 = 0.3 + 0.6\lambda_y \qquad 2.37$$

and the corresponding ordinate R_1 is calculated from Equation 2.33 with $\lambda = \lambda_1$.

One fault of Thomasson's approach is that the maximum stress, f_{avmax}, occurs prior to yielding, i.e., at $f_e < F_y$; thus an elastic failure is predicted. This behavior is, to a small extent, visible in Figure 2.9a which was plotted for a specific λ_y value equal to $\sqrt{10}$. For the larger values of λ_y typically encountered in practical thin-walled steel construction, this behavior becomes much more pronounced. Since the prediction of an elastic failure would only complicate existing design procedures, an alternate approach is needed. One such approach is proposed in the following section.

2.3.2 Present Approach

The sub-ultimate approach of the present study follows Thomasson's work in simulating the theoretical behavior of a post-buckled plate (Figure 2.8); however a single curve representation is adopted which predicts failure by yielding, i.e., at ultimate $f_e = F_y$. Winter's effective width equation (Equation 2.9) is employed in the present approach to define this ultimate condition. Also, the sub-ultimate response predicted

with the approach is dependent on the yield strength and reflects, in an approximate manner, the effects of two-dimensional and surface yielding. This is more in line with the actual behavior (Figure 2.8) than that predicted by Equation 2.9 which is independent of the yield stress, at $f_e < F_y$.

The approach is derived by assuming the following relationship between the average and edge stresses.

$$S = A + B\lambda + C\lambda^2 + D\lambda^3 \qquad 2.38$$

where $S = f_{av}/f_{cr}$, $\lambda = (f_e/f_{cr})^{\frac{1}{2}}$, and A-D are constants. The constants are determined from the four boundary conditions at the transition from fully effective to partially effective, point f, and at the final or ultimate point y (Figure 2.10).

Winter's effective width Equation 2.9 is assumed valid for establishing the boundary conditions. This equation is first rewritten in terms of the parameters S and λ as the linear function

$$S_w = \lambda - 0.218 \qquad 2.39$$

Equation 2.39 is also shown in Figure 2.10. The intercepts of Equations 2.38 and 2.39 follow immediately as

$$S(\lambda_f) = S_w(\lambda_f) \qquad 2.40$$

$$S(\lambda_y) = S_w(\lambda_y) \qquad 2.41$$

where $\lambda_y = (F_y/f_{cr})^{\frac{1}{2}}$ and the initial abscissa λ_f is calculated from Equation 2.10, or $\lambda_f = 0.6789$. The slope at the initial point f is assumed consistent with the fully effective curve ($S = \lambda^2$), or

$$\left.\frac{dS}{d\lambda}\right|_{\lambda_f} = 2\lambda_f \qquad 2.42$$

Lastly, the slope at the final point y is assumed as follows

$$\left.\frac{dS}{d\lambda}\right|_{\lambda_y} = 0 \qquad 2.43$$

which is compatible with the theoretical behavior (Figure 2.8). The above four boundary conditions, Equations 2.40 through 2.43, permit explicit determination of the constants A-D of Equation 2.38.

$$D = 2[(1 - \lambda_f)\lambda_y - 0.218]/(\lambda_f - \lambda_y)^3 \qquad 2.44$$

$$C = \lambda_f/(\lambda_f - \lambda_y) - 1.5D(\lambda_f + \lambda_y) \qquad 2.45$$

$$B = -\lambda_y(2C + 3D\lambda_y) \qquad 2.46$$

$$A = \lambda_f^2(1 - B/\lambda_f - C - \lambda_f D) \qquad 2.47$$

Figure 2.11a illustrates the stress-strain response predicted from Equation 2.38 where a smooth transition into the post-buckling range is indicated. Also, in the sub-ultimate range, good agreement is obtained between Equation 2.38 and Yamaki's [1959] theoretical elastic solution for an imperfect post-buckled plate. Although these characteristics are important, the most important factor is that Equation 2.38 does not suffer from the deficiency noted earlier for Thomasson's approach and that failure is predicted at $f_e = F_y$.

The effective width equation corresponding to Equation 2.38 is

$$R = A/\lambda^2 + B/\lambda + C + D\lambda \qquad 2.48$$

where $R = w_e/w$ and all other parameters are defined previously. This expression is presented in Figure 2.11b, where Winter's effective width Equation 2.9 is also shown for comparison.

Finally, the effective widths predicted with Equation 2.48 and Thomasson's approach of Equations 2.33-2.36 are compared in Table 2.1 for several values of λ_y^2 ($=F_y/f_{cr}$) and f_e/F_y ratios. It is noted

that a value of λ_y^2 equal to 128 corresponds approximately to a flat width-to-thickness ratio, w/t, of 500 for a mild steel (F_y = 30 ksi) plate element. Table 2.1 shows that for moderate values of λ_y^2, less than 16, larger effective widths are predicted with Equation 2.48, relative to Thomasson's approach. This indicates that a stiffer axial response is associated with Equation 2.48 for this range of λ_y^2. On the other hand, larger effective widths are predicted with Thomasson's approach for larger values of λ_y^2. Moreover, the worst disagreement between Equation 2.48 is obtained for intermediate values of the parameter f_e/F_y, but as the limiting value of $f_e/F_y = 1$ is approached, the disagreement between the two approaches diminishes.

2.4 Summary

The post-buckling strength of plates and associated effective width approaches were discussed in this chapter. First, past and current effective width methods for uniformly compressed stiffened elements were reviewed. Then, eccentrically compressed stiffened elements were treated. For this case, an effective width approach was proposed which was consistent with current specification equations for the limiting state of uniform compression. Next, various effective width methods were compared for analyzing uniformly compressed unstiffened elements, and the unified approach of employing a single effective width equation for both unstiffened and stiffened compression elements was verified. Lastly, the sub-ultimate behavior of post-buckled compression elements was investigated, and Swedish research in this area was reviewed. For this case, an effective width approach was derived which was again consistent with existing design specifications.

Generally, the work presented in this chapter was limited to isolated plate elements. The more practical application of this work to structural sections is taken up in the following two chapters.

Table 2.1 COMPARISON OF THE SUB-ULTIMATE APPROACH OF THE PRESENT STUDY AND THOMASSON'S [1978] APPROACH

	w_e(Eq. 2.48)/w_e(Thomasson*)									
f_e/F_y	.1	.2	.3	.4	.5	.6	.7	.8	.9	1.0
λ_y^2										
2	1.	1.	1.010	1.066	1.085	1.079	1.066	1.062	1.051	1.034
4	1.	1.067	1.110	1.109	1.087	1.064	1.057	1.051	1.045	1.039
8	1.064	1.125	1.111	1.078	1.036	1.024	1.018	1.016	1.020	1.027
16	1.125	1.107	1.062	1.012	0.976	0.965	0.963	0.969	0.982	1.004
32	1.112	1.050	0.989	0.933	0.905	0.898	0.902	0.915	0.938	0.974
64	1.058	0.974	0.906	0.849	0.831	0.829	0.838	0.858	0.891	0.940
128	0.985	0.891	0.823	0.770	0.758	0.760	0.774	0.801	0.843	0.904

*Eqs. 2.33-2.36

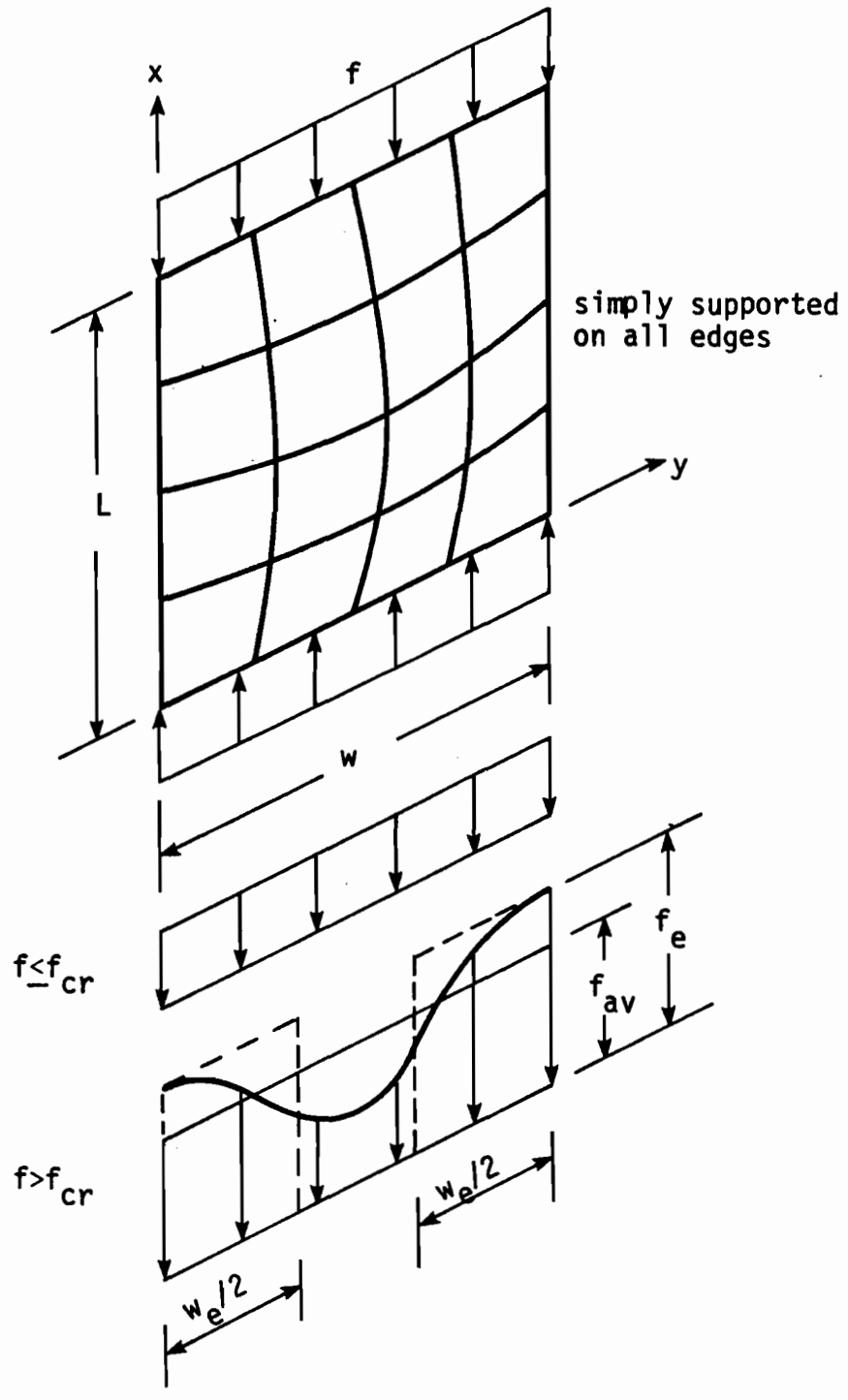

Figure 2.1 BUCKLING OF A THIN PLATE

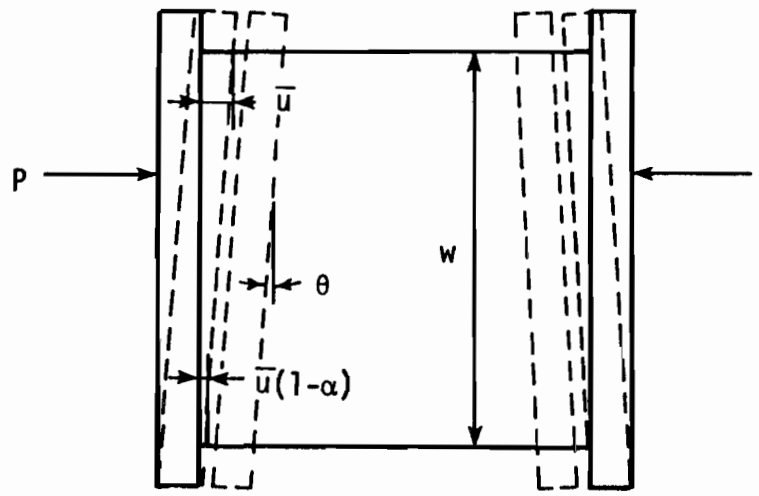

(a) Constant compression eccentricity
(α = constant)

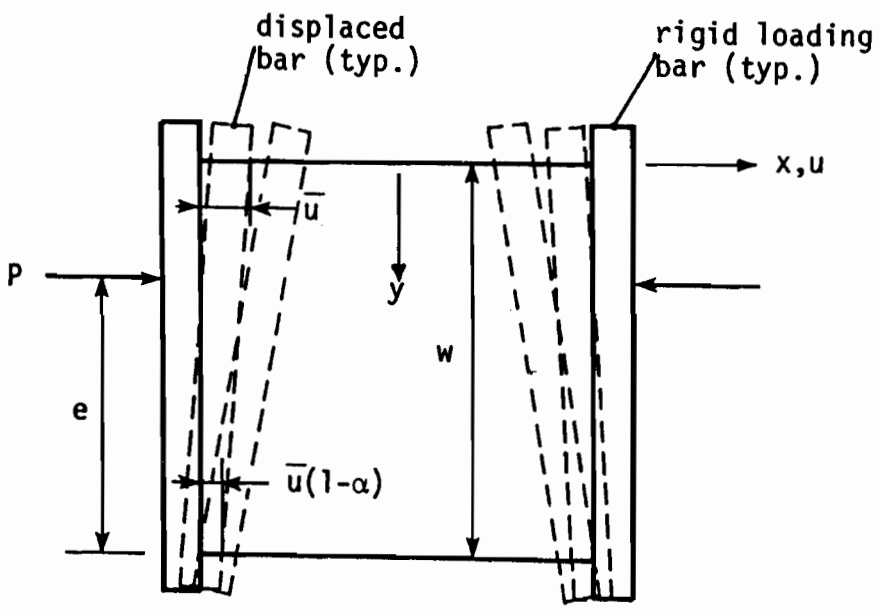

(b) Constant load eccentricity
(e = constant)

Figure 2.2 LOADING CONDITIONS
(After Rhodes and Harvey [1971b])

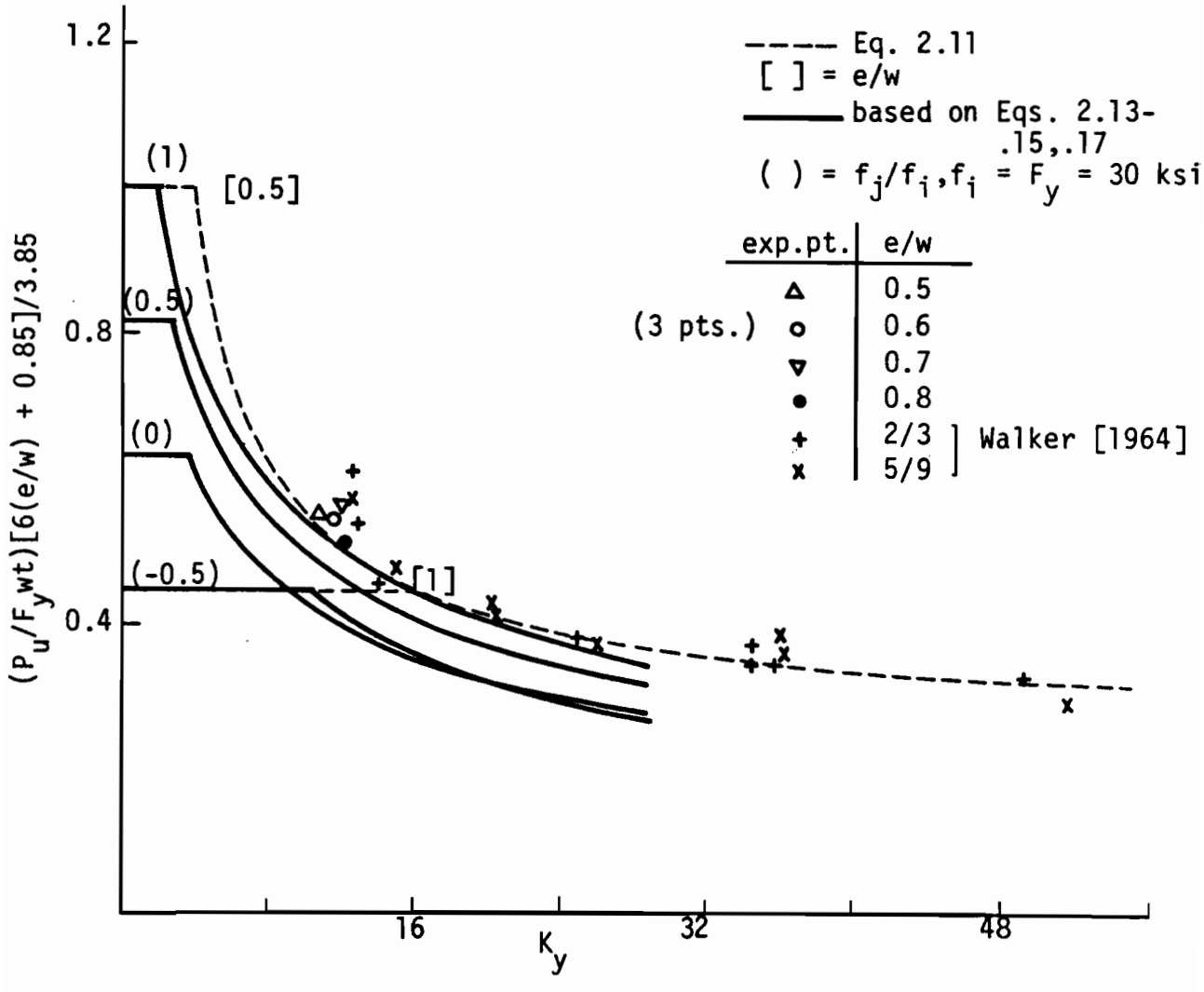

Figure 2.3 COMPARISON OF EXPERIMENTAL AND THEORETICAL FAILURE LOADS FOR STIFFENED PLATES UNDER ECCENTRIC LOAD (After Rhodes et al. [1975])

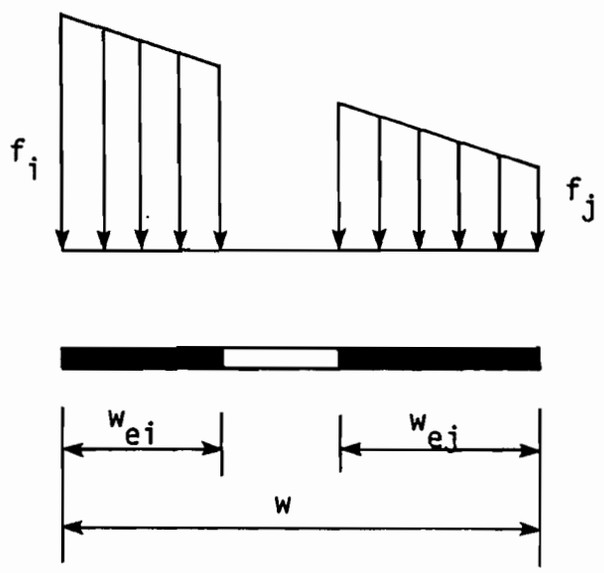

(a) Case I: $f_i > f_j > 0$

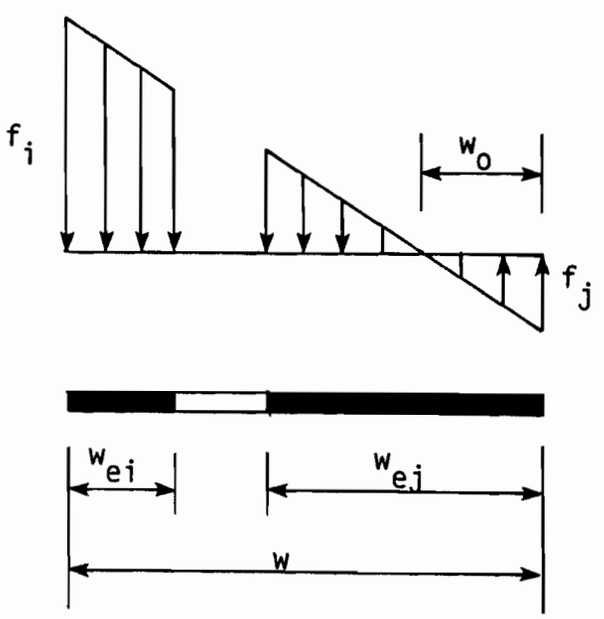

(b) Case II: $f_i > 0 > f_j$

Figure 2.4 EFFECTIVE WIDTH FOR FLANGE UNDER STRESS GRADIENT

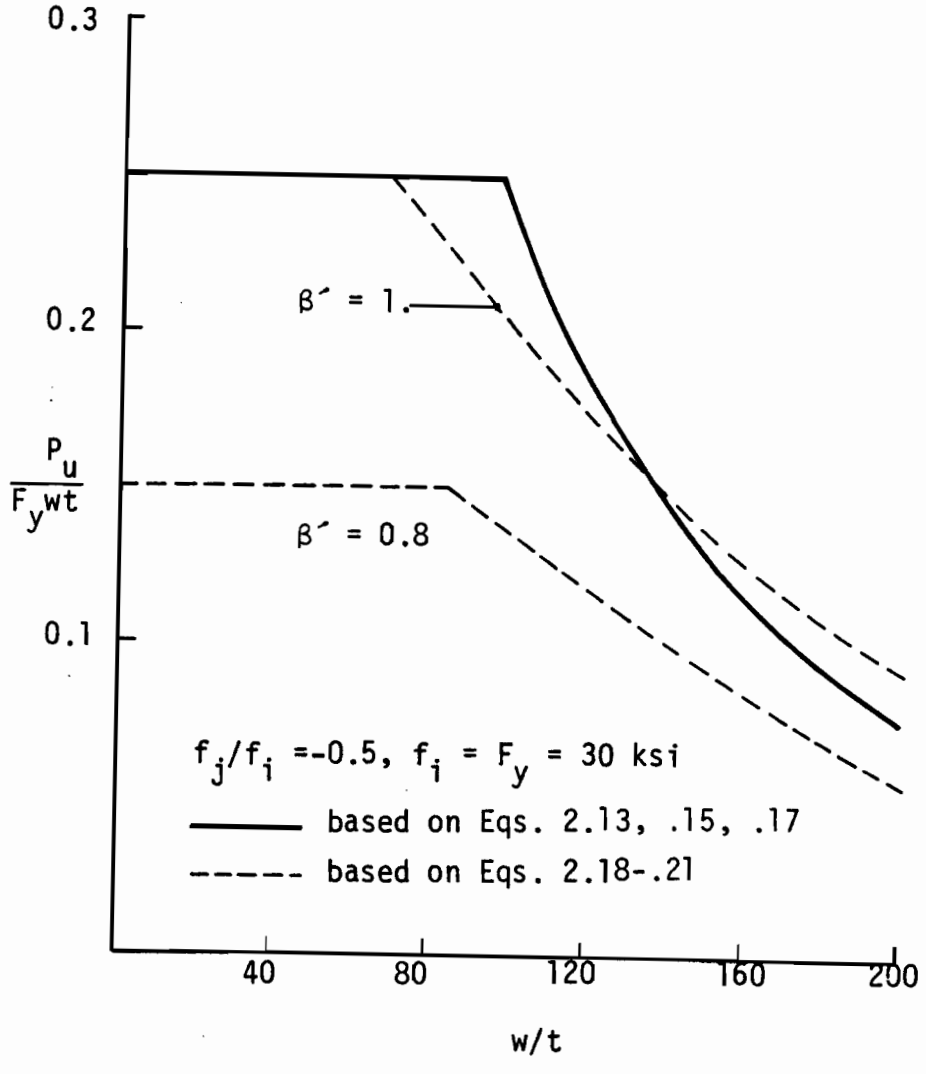

Figure 2.5 COMPARISON OF EFFECTIVE WIDTH APPROACH OF PRESENT STUDY FOR ECCENTRICALLY COMPRESSED PLATES AND LABOUBE'S [1978] APPROACH FOR BEAM WEBS

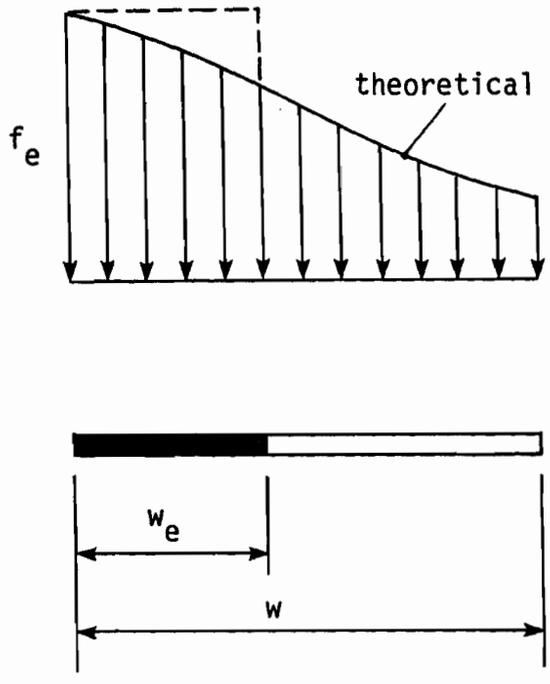

Figure 2.6 EFFECTIVE WIDTH FOR UNSTIFFENED COMPRESSION ELEMENTS

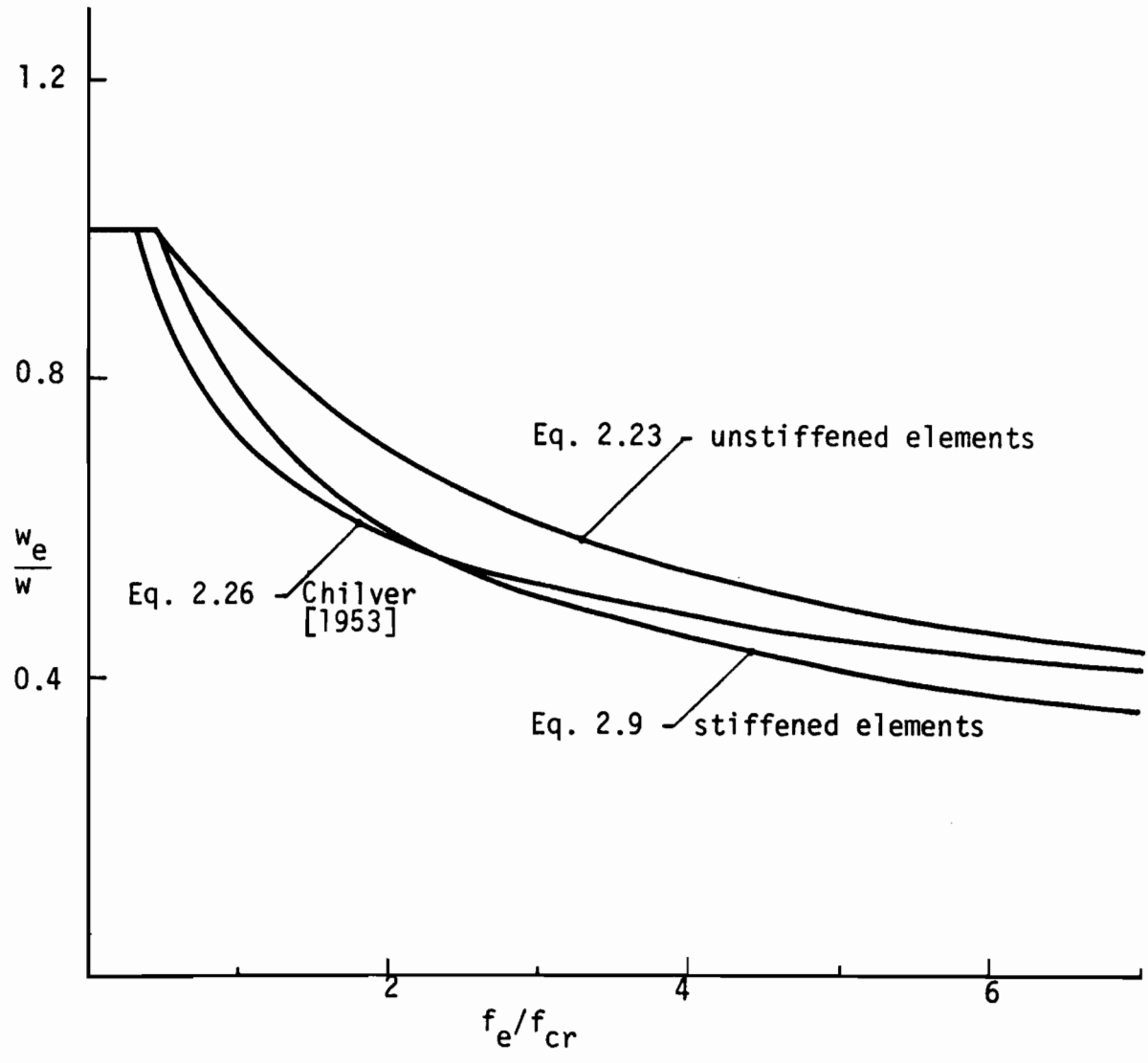

Figure 2.7 COMPARISON OF EFFECTIVE WIDTH APPROACHES FOR UNSTIFFENED COMPRESSION ELEMENTS

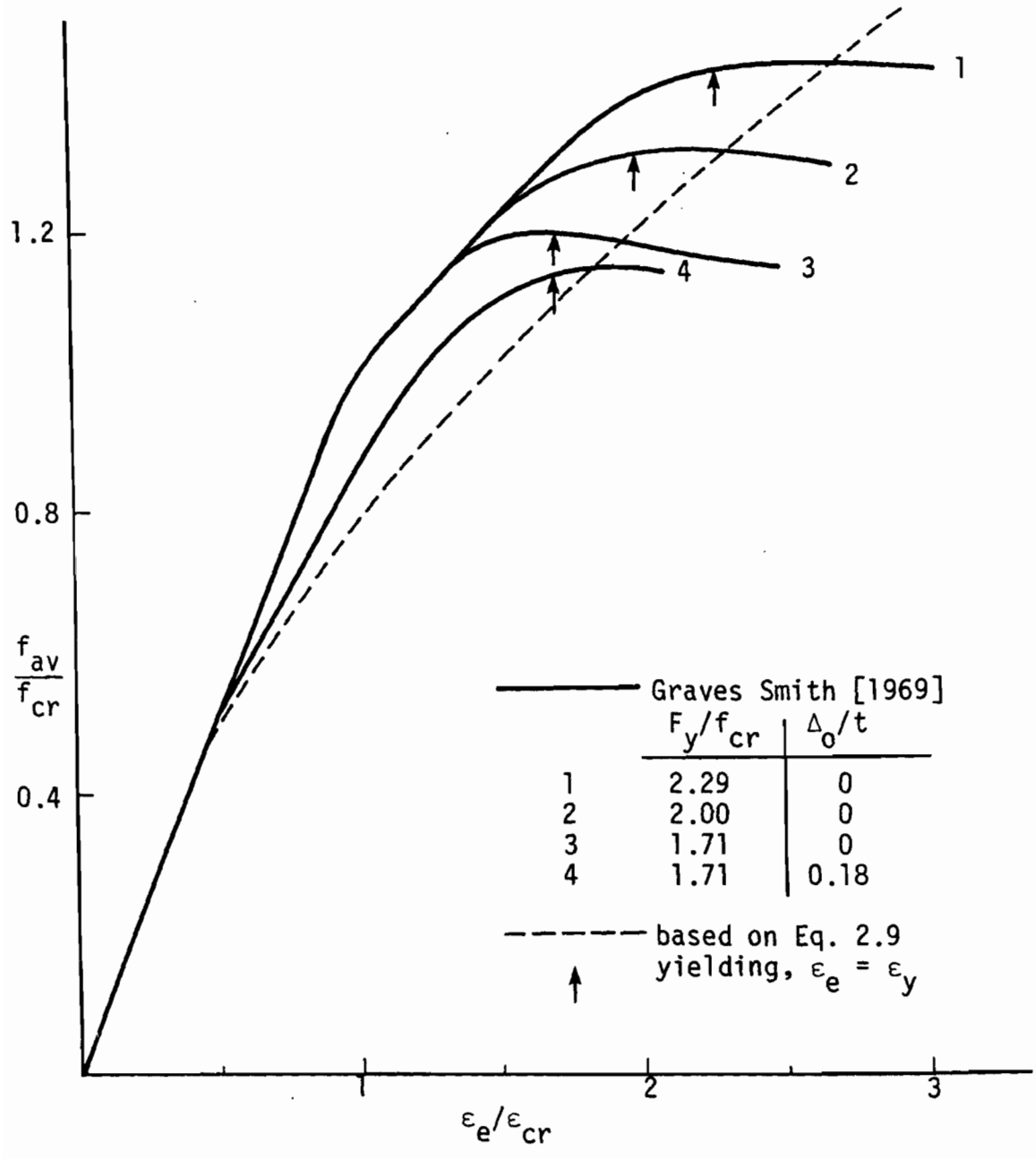

Figure 2.8 POST-BUCKLING STRESS-STRAIN RESPONSE
(After Graves Smith [1969])

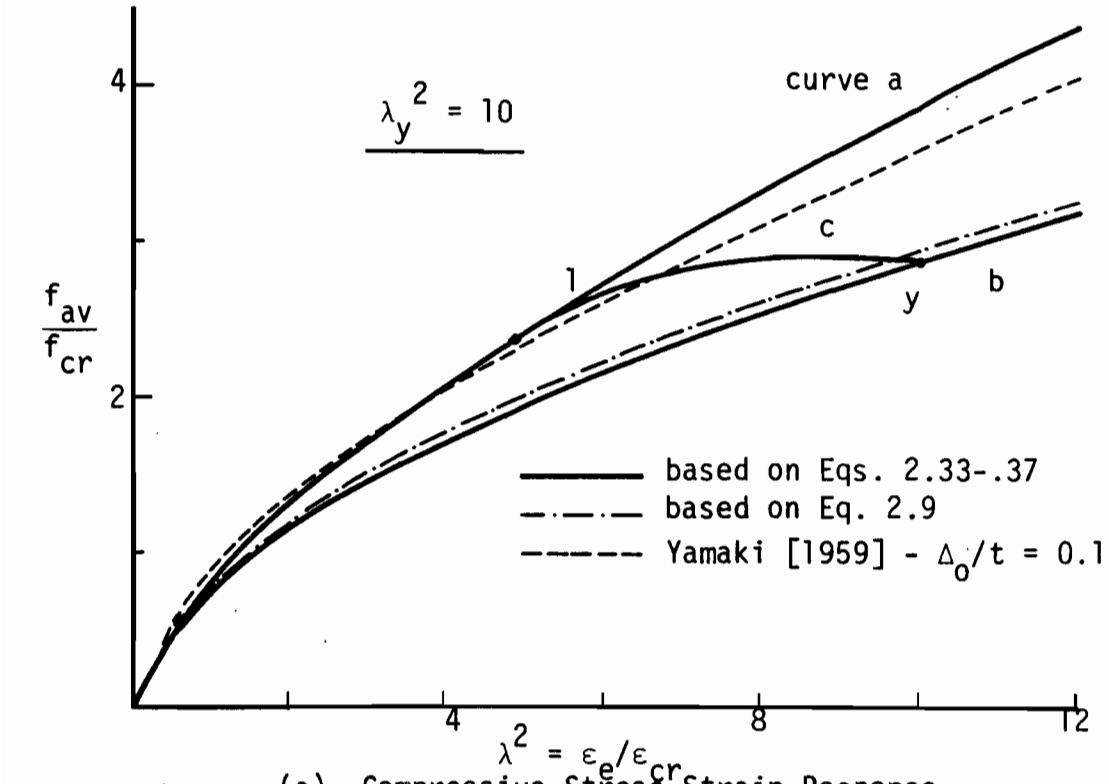

(a) Compressive Stress-Strain Response

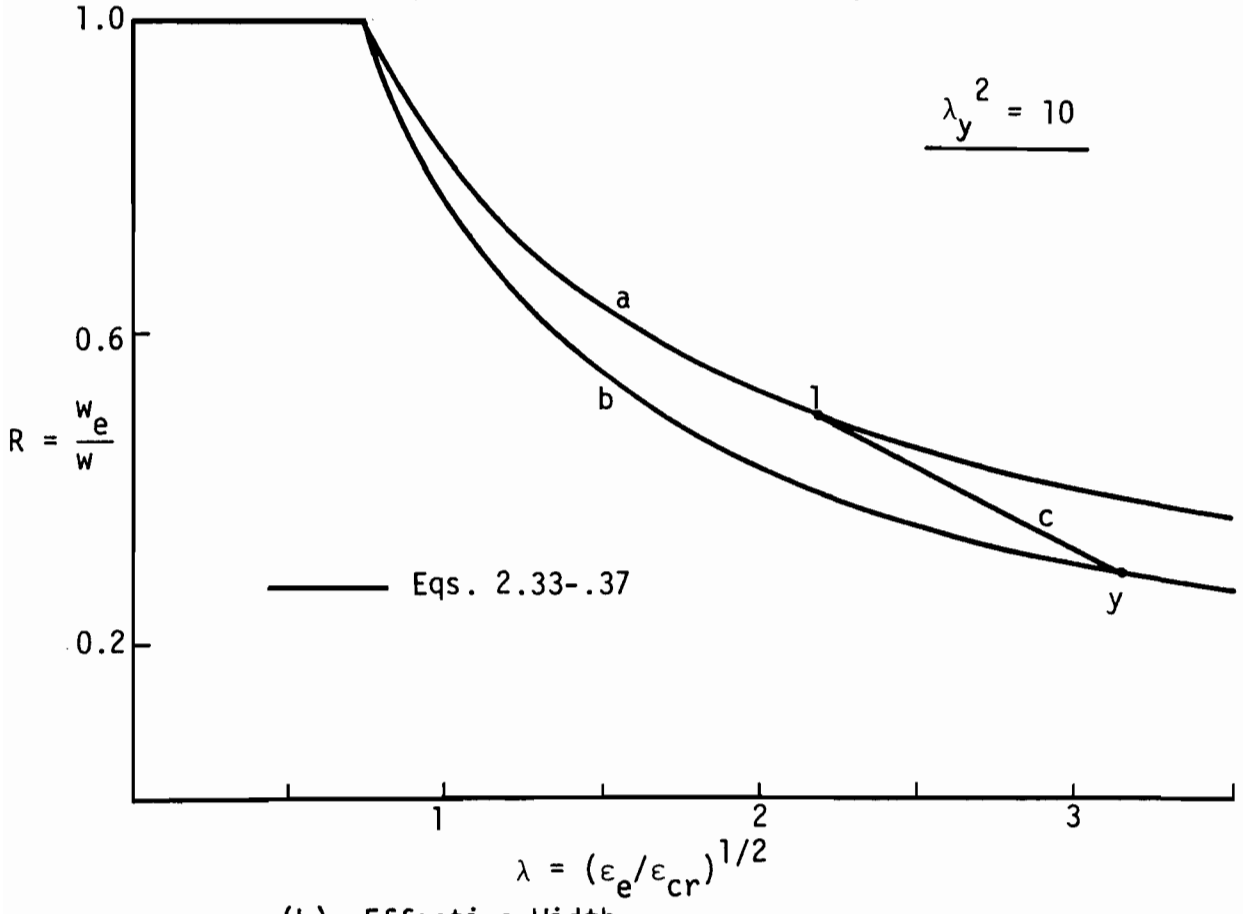

(b) Effective Width

Figure 2.9 THOMASSON'S [1978] SUB-ULTIMATE APPROACH

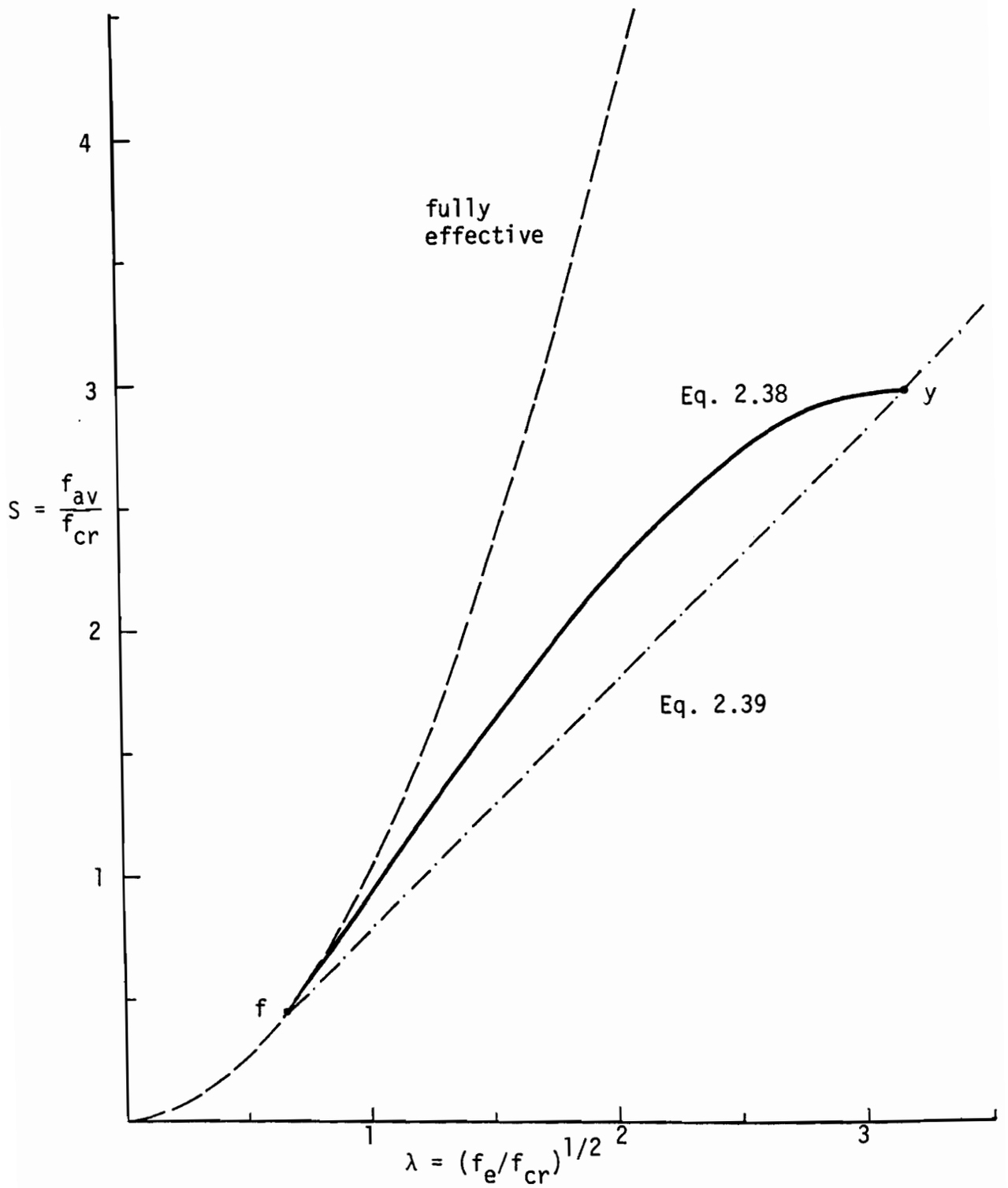

Figure 2.10 DERIVATION OF SUB-ULTIMATE APPROACH

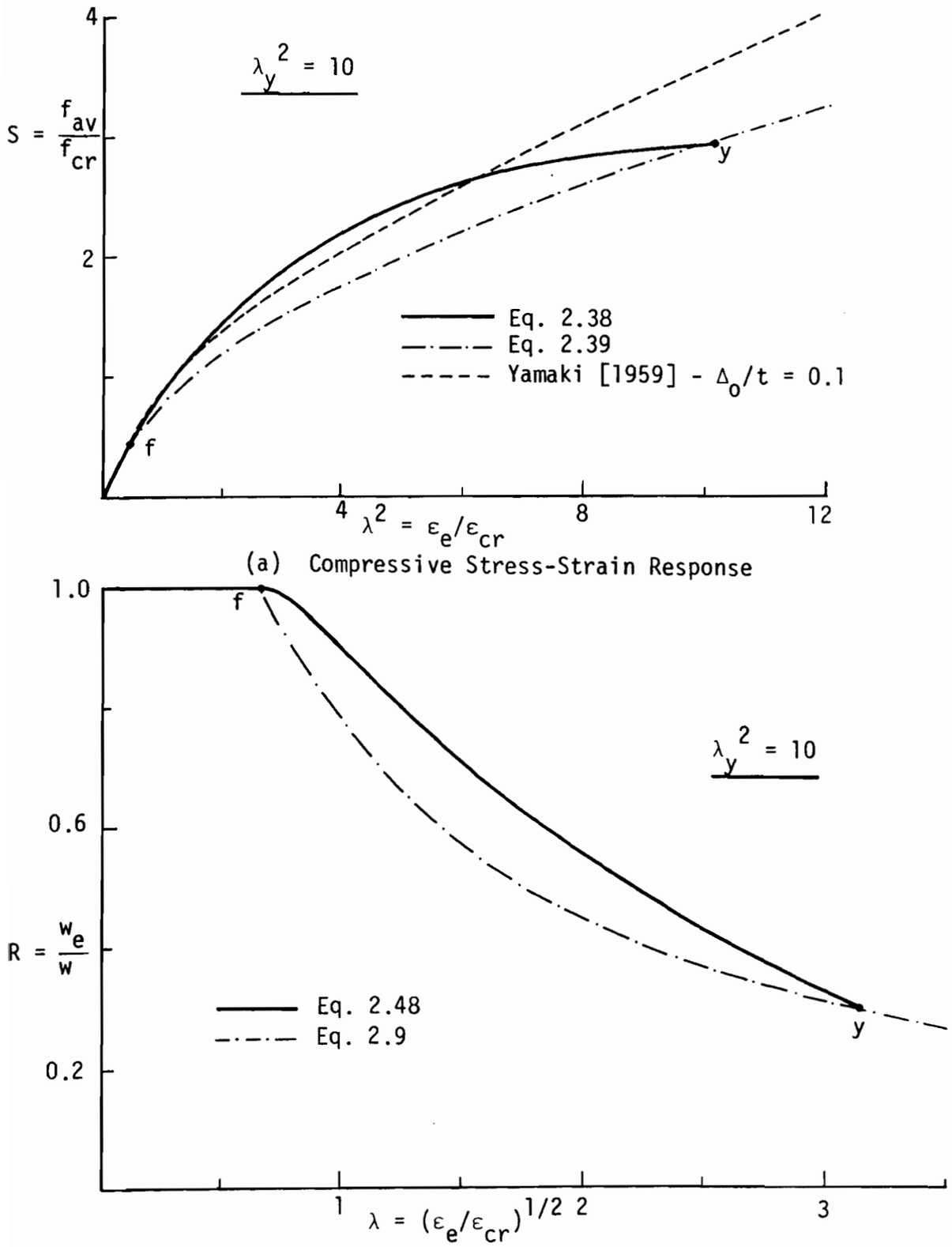

(a) Compressive Stress-Strain Response

(b) Effective Width

Figure 2.11 SUB-ULTIMATE APPROACH OF PRESENT STUDY

CHAPTER 3

LOCAL BUCKLING INTERACTION

3.1 Introduction

The discussions of the previous chapter were generally limited to isolated plates. However, in construction applications the behavior of structural sections, cold-formed out of thin steel sheets, is more important. It is convenient to consider such sections to be composed of a series of interconnected plates, and of primary concern is how buckling of one plate affects the buckling and post-buckling response of the remaining plates that comprise the section. In such an instance, a theoretical local buckling analysis predicts simultaneous buckling of all component plates due to continuity conditions which are enforced at the plate junctures. It is not immediately clear whether this behavior is exhibited in an actual (imperfect) thin-walled section. Also of concern is how the component plates interact in the post-buckling range.

In the present chapter, the numerical method employed to analyze the instability of general thin-walled sections is first discussed. Then the theoretical response for local buckling interaction in thin-walled sections is established by analyzing several common structural shapes under various support and loading conditions. Also, edge stiffener requirements are reviewed and discussed. Finally, the post-buckling response of thin-walled sections is treated using an effective section concept.

3.2 Instability Analysis Using the Finite Strip Method

Typically, the instability of thin plates and thin-walled structures is governed by partial differential equations which, for problems of even moderate complexity, prove extremely difficult to solve. Hence, approximate numerical methods must be adopted. Of these, the energy methods have been the most widely used (Timoshenko and Gere [1961]).

In recent years, the finite element method (FEM), which may be considered an outgrowth of the classical energy methods, has proved to be a powerful tool in instability analysis, as well as in other areas of structural mechanics (Gallagher [1975]). In this method the continuum is discretized as an assemblage of elements that are "joined" together at discrete points with due consideration given to continuity and equilibrium. The formulation yields a set of algebraic equations, in terms of generalized parameters, from which the solution is obtained. In some cases this solution can be very costly, and even prohibitive, which is especially true in an instability analysis. Therefore, it is advantageous to seek methods which reduce the computational effort, but at the same time retain the basic advantages of the finite element method. One such method that satisfies these requirements is the topic of this section — the finite strip method (FSM) (Cheung [1976]).

3.2.1 Basis of the Finite Strip Method

The basis of the finite strip method, which has been alternately described as a semi-analytical finite element method (Zienkiewicz [1977]), lies in the choice of the trial solution of the problem. For example, consider the two-dimensional (2-D) problem of seeking some unknown function $u(x,y)$ which satisfies the following partial differential equation

$$\underset{\sim}{A}(u) = 0 \qquad 3.1$$

over a domain Ω (area) and which satisfies certain boundary conditions. In the FSM, the Kantorovich method (Crandall [1956]) is used for selection of an approximate solution u* of the form

$$u^*(x,y) = \sum_{m}^{M} X_m Y_m \qquad 3.2$$

where $Y_m(y)$ are known independent functions of y alone which satisfy, a priori, the geometric boundary conditions on the y = constant boundaries and $X_m(x)$ are unknown functions of x alone. When the trial solution u* is substituted into the governing equation, Equation 3.1, and when the y integration is performed, a set of M ordinary differential equations are obtained in terms of the X_m. These equations must then be solved with the appropriate boundary conditions on the x = constant boundaries to obtain the X_m. This is usually accomplished by the application of some weighted residual or stationary functional method, depending on the original statement of the problem.

3.2.2 Comparison of the FEM and FSM

Since the finite strip method is basically a special form of the finite element method, it is useful to compare the discretizations used in each method, say for a 2-D problem.

In the FEM the field variable $\underset{\sim}{u}$ is discretized as a product of known shape functions $\underset{\sim}{N}$ and selected nodal parameters which are in general unknown, i.e.,

$$\underset{\sim}{u} = \underset{\sim\sim}{N}\underset{\sim}{\Delta} \qquad 3.3$$

The shape functions $\underset{\sim}{N}$ are dependent on both independent variables, x and y, and are normally derived from a polynomial representation of $\underset{\sim}{u}$.

In the FSM the field variable $\underset{\sim}{u}$ is also discretized as a product of shape functions and nodal parameters

$$\underset{\sim}{u} = \sum_{m} Y_m \underset{\sim}{\sim} N \underset{\sim}{\Delta}_m \qquad 3.4$$

However, the shape functions are now derived from a polynomial representation in one direction, x in this case, and a continuously differentiable series Y_m in the other direction, e.g., a Fourier series. And if the series portion of the shape function is chosen appropriately, the discretization of Equation 3.4 replaces effectively the original 2-D problem with M uncoupled 1-D problems.

Due to the reduction in dimensionality, the FSM possesses certain advantages over the FEM. Usually the formulation results in a smaller number of equations with a small bandwidth which, in turn, reduces the core requirements necessary for solution. This is especially important in an analysis for instability which requires a relatively large computational effort. Also, the amount of input and output is drastically reduced.

The FSM is not without disadvantages. One of which is that the method is limited to structures in which the material properties and geometry are constant in a coordinate direction. Another disadvantage is that for the solution to "uncouple," as discussed above, the discretization must satisfy certain boundary conditions. Nevertheless, for structures that satisfy these requirements, the FSM is a powerful analytical tool.

3.2.3 Literature Survey

The finite strip method was first developed by Cheung [1968] for the analysis of elastic slabs. In this reference, results were presented for slabs with various support conditions, and a comparison was made with

results obtained using the FEM. The FSM was then applied to the analysis of folded plate structures by Cheung [1969] who combined a flat plate bending finite strip with a plane stress strip to model both the bending and membrane actions. Numerical examples were presented and compared with alternate methods of analysis. Other applications and developments related to the FSM may be found in a recently published text by Cheung [1976].

The application of the FSM to instability problems has been a more recent development. Przemieniecki [1973] was one of the first researchers to investigate the instability of plates and thin-walled sections using the FSM. He developed geometric stiffness matricies for a state of uniform biaxial compression and presented several numerical examples. However, his analysis was limited by an assumption which required all plate junctures to remain perfectly straight. This assumption was later relaxed by Plank and Wittrick [1974], thus allowing for an interaction between local and overall buckling modes. Recently, Graves Smith and Sridharan [1978a] extended the FSM for analyzing the buckling of plate structures under arbitrary loading. Also, a method was presented [1978b] for analyzing the post-local buckling of thin-walled structures under end compression. Finally, Hancock [1979] proposed a variant of the FSM for predicting the post-buckling behavior of columns with plate imperfections.

3.2.4 Linear Instability Formulation

The equations governing instability are derived below from the more general large displacement-small strain formulation for a geometrically nonlinear problem (Zienkiewicz [1971,1977]).* A stationary functional

*It is noted that for conciseness the derivation of an explicit finite strip representation is relegated to Appendix A.

method is employed where the functional is defined by the total potential energy of an elastic structure,

$$\Pi = \tfrac{1}{2} \int_V \underset{\sim}{\varepsilon}^T \underset{\sim}{\sigma} dV - \underset{\sim}{\Delta} \underset{\sim}{P} \qquad 3.5$$

where $\underset{\sim}{\varepsilon}^T$ = Green's strain vector (superscript T indicates transpose), $\underset{\sim}{\sigma}$ = vector of Piola-Kirchhoff stresses, and $\underset{\sim}{P}$ = generalized conservative forces associated with the generalized displacements $\underset{\sim}{\Delta}$. A total Lagrangian description of Equation 3.5 is adopted in which the volume, V, is referenced to the undeformed state.

First, the usual finite element discretization of the field variable is made as

$$\underset{\sim}{u} = \underset{\sim\sim}{N} \underset{\sim}{\Delta} \qquad 3.6$$

where the vector $\underset{\sim}{\Delta}$ is chosen as a set of nodal displacements. Further, Green's strain $\underset{\sim}{\varepsilon}$ is expressed conveniently as the sum of linear infinitesimal strains $\underset{\sim}{\varepsilon}_0$ and nonlinear strains $\underset{\sim}{\varepsilon}_L$, e.g.,

$$\underset{\sim}{\varepsilon} = \underset{\sim}{\varepsilon}_0 + \underset{\sim}{\varepsilon}_L \qquad 3.7$$

where the $\underset{\sim}{\varepsilon}_0$ and $\underset{\sim}{\varepsilon}_L$ are linearly and quadratically dependent on the $\underset{\sim}{u}$, respectively. Using the finite element discretization of Equation 3.6 allows the strains to be written as

$$\underset{\sim}{\varepsilon} = \underset{\sim}{B}_0 \underset{\sim}{\Delta} + \underset{\sim}{B}_L \underset{\sim}{\Delta}/2 \qquad 3.8$$

where the strain matricies $\underset{\sim}{B}_0$ and $\underset{\sim}{B}_L$ are independent and linearly dependent on $\underset{\sim}{\Delta}$, respectively (Wood et. al. [1978]). Next, the stresses, which for the case of small strains correspond with the true stresses (Zienkiewicz [1971]), are related to the strains by the following isotropic constitutive law.

$$\underset{\sim}{\sigma} = \underset{\sim\sim}{D} \underset{\sim}{\varepsilon} \qquad 3.9$$

where $\underset{\sim}{D}$ is a matrix of elastic constants. While, with Equations 3.8 and 3.9, it is now possible to discretize the potential energy Π; this representation is not pursued here. Instead, the discussion proceeds directly to the instability formulation.

The stationarity of the total potential energy, Equation 3.5, defined by

$$\delta\Pi = 0 \tag{3.10}$$

where δ is the variation symbol, would lead to the equilibrium requirements for the problem. This criterion is not, however, sufficient to define instability; it only serves to define a stationary point of Π which may represent stable, neutral, or unstable equilibrium (Gallagher [1975]). In order to establish the type of equilibrium, the second variation of the functional must be employed. Therefore, instability is defined by the load (stress) for which $\delta^2\Pi$ ceases to be positive-definite (Dym [1974]), or for neutral equilibrium by

$$\delta^2\Pi = 0 \tag{3.11}$$

Applying this energy criterion to the previous formulation leads to the following linearized instability condition.

$$(\underset{\sim}{K}_0 + \underset{\sim}{K}_\sigma)\delta\underset{\sim}{\Delta} = 0 \tag{3.12}$$

where $\underset{\sim}{K}_0$ is the usual symmetric small displacement stiffness matrix and $\underset{\sim}{K}_\sigma$ is the symmetric initial stress matrix which accounts for the effects of the membrane forces (stresses). Both these matricies are defined below.

$$\underset{\sim}{K}_0 = \int_V \underset{\sim}{B}_0^T \underset{\sim}{D} \underset{\sim}{B}_0 dV \tag{3.13}$$

$$\underset{\sim}{K}_\sigma = \int_V (\partial \underset{\sim}{B}_L^T / \partial \underset{\sim}{\Delta}) \underset{\sim}{\sigma} dV \tag{3.14}$$

Actually, the criterion of Equation 3.11 leads to a more complicated expression than that given by Equation 3.12, e.g., see Zienkiewicz [1977].

However, for the structures and loading to be considered here, Equation 3.12 is sufficient. Furthermore, in the present development it is assumed that the stresses defining $\underset{\sim}{K}_\sigma$ are obtained from an independent, linear (membrane) analysis, that their spacial distribution remains constant during buckling, and that these stresses are related by a common factor λ. This allows Equation 3.12 to be restated as

$$(\underset{\sim}{K}_o + \lambda \underset{\sim}{K}_\sigma)\delta\underset{\sim}{\Delta} = 0 \qquad 3.15$$

The above equation is identified immediately as a standard eigenproblem from which the eigenvalue represents the buckling load and the eigenvector represents the buckling mode. Explicit finite strip forms of the matricies that define Equation 3.15 are derived in Appendix A.

3.2.5 Finite Strip Instability Analysis Program

A special purpose computer program, which was based on the finite strip method (see Appendix A) and on the theory discussed earlier in this section, was developed to analyze the linear elastic instability of thin-walled structures of arbitrary cross section. As a result of the finite strip discretization, the analysis is specialized to structures with constant longitudinal geometry and material properties and to structures with rigid diaphragm, end support conditions. Also, only linearly varying, longitudinal, edge tractions (loading) are considered. Because both in-plane and out-of-plane response are included in the analysis, prediction of local, flexural, torsional, or combination buckling modes is possible.

The instability condition of Equation 3.15 is solved using an in-core determinant search algorithm, after Bathe [1971,1976], which combines several eigensolution techniques in an effective and efficient manner.

This algorithm, its underlying theory, and programming details are discussed in Appendix B.

Because the buckling of any thin-walled structure is very much dependent on its length, two types of analyses are incorporated in the program, a constant length and variable length analysis. The variable length analysis uses a unique storage scheme to eliminate the necessity of reforming the governing stiffness matricies each time the length is changed (see Appendix B.4). Also an option is included in the variable length analysis for a minimum buckling load solution which is automatically determined, if it exists, using polynomial interpolation (see Appendix B.4).

Another feature of the program is that dynamic allocation storage, as described by Bathe [1976], is utilized. In this scheme all essential information is stored, in vector form, in a central one-dimensional array which is updated during different phases of the analysis to minimize storage requirements. This storage scheme proved very effective in the present program where different types of analysis were possible.

Finally, it is noted that automatic data generation schemes are implemented in the program to simplify input requirements.

The program is verified in Appendix C where the results of analyzing several plate problems are compared with known solutions.

3.3 Local Buckling Interaction in Structural Sections

The instability of a thin-walled section may be considered to be controlled by one of the plate elements that comprise the cross section. As, the buckling load for this controlling element is exceeded, it is no longer capable, by itself, of resisting the applied load. Therefore,

it must rely on the restraint provided by the remaining elements until the buckling load of the overall section is reached.

This type of local buckling interaction in thin-walled sections is investigated here. Specifically, channel and lipped channel sections are analyzed for instability, under various support and loading conditions, using the finite strip method discussed in the previous section. All analyses employ a Poisson ratio of 0.3 and a discretization consisting of four finite strips, each, for the web (stiffened element) and flanges (unstiffened or edge stiffened elements), and one strip for the lip (edge stiffener). This discretization was found sufficient to produce satisfactory results. Also, the analyses are restricted to local buckling where the web-flange junctures are assumed to remain straight which precludes overall modes. This restriction is relaxed later, in Chapter 4, to study interaction of local and overall buckling. Moreover, if all plate junctures are presumed to remain straight, it is necessary to model only the flexural action. All results discussed in this section are valid for buckling in a mode with one longitudinal half-wave.

3.3.1 Channel Sections

First, the instability of uniformly compressed channel sections is investigated. Symmetry of the buckling mode is assumed, and only one-half of the channel is analyzed which reduces the computational effort.

The results of the analysis in the form of minimum buckling coefficients, K_{min}, are presented in Figure 3.1 for various flange-to-web width ratios, w_2/w_1. The critical length, L_{cr}; which is also presented in this figure as the web aspect ratio, L_{cr}/w_1; represents the value that is associated with K_{min}. Excellent correlation is observed between the

finite strip results and a known solution (Kroll et. al. [1943]). Also, for w_2/w_1 ratios approaching zero (0), the web buckling coefficient, K_1, approaches the theoretical result for a plate with simply supported longitudinal edges, i.e., $K_1 = 4.0$, and for w_2/w_1 approaching infinity, the flange buckling coefficient, K_2, approaches the result for a plate with fixed and free longitudinal edge supports, i.e., $K_2 = 1.25$.

As mentioned previously, one plate element is usually responsible for buckling of the overall section. This response is indicated in Figure 3.1. For w_2/w_1 ratios less than the limiting value indicated by the vertical dashed line ($w_2/w_1 \approx 0.35$), which was established from Kroll et. al. [1943], the web element initiates buckling and forces the flange element to buckle prematurely and simultaneously. And for w_2/w_1 ratios above this limiting value, the flange element initiates buckling. It is interesting to observe that in this range, $w_2/w_1 > 0.35$, a larger critical length, L_{cr}, is obtained due to the dominating influence of the flange which requires a relatively large half-wavelength. Also, for w_2/w_1 equal to the limiting value, the web and flanges buckle independently at the same stress level. The corresponding buckling coefficients K_1 and K_2 are slightly larger than their simply supported values of 4.0 and 0.425, respectively, because the section is forced to buckle at a half-wavelength which is different from that associated with each isolated (simply supported) element.

Compatibility conditions established at plate element junctures require all elements of the section to buckle simultaneously. Thus, the following general relationship exists between the buckling coefficients for the web and flange.

$$K_2 = K_1(w_2/w_1)^2 \qquad 3.16$$

which is valid for uniformly compressed sections of constant thickness.

3.3.2 Lipped Channels

For lipped channels, the addition of a lip or edge stiffener complicates the behavior. As a result, the findings of several finite strip instability analyses are discussed here. First, an idealized lipped channel is analyzed in uniform compression. Then the response of an actual section, is investigated, and the effect of stiffener (lip) size is examined. Finally, the influence of non-uniform, linear, edge-compression is studied. Symmetry is employed in the analysis of only the idealized lipped channel, and reference is made to the introduction of Section 3.3 for other details of the analyses.

The local buckling response for an idealized lipped channel under uniform longitudinal compression is investigated first. To simplify matters, the lip is assumed to provide sufficient rigidity (out-of-plane) to force the lip-flange juncture to remain straight and is assumed to provide negligible torsional restraint. Consequently, an idealized section is analyzed where the lip is replaced by a simple support.

The results of the analysis are shown in Figure 3.2 which are similar to that obtained for plain channels (see Figure 3.1). For a w_2/w_1 ratio equal to the limiting value of one (1), the web buckles into a square wave, independent of the restraint provided by the flange, and vice-versa. The associated minimum buckling coefficients for the web and flange are the same as that for a simply supported square plate, i.e., $K_1 = K_2 = 4$. Also, for w_2/w_1 ratios less than this limiting value, the restrained web initiates buckling, which is indicated by $K_1 > 4$. Conversely, for $w_2/w_1 > 1$,

the restrained flange initiates buckling and forces premature instability of the web, i.e., $K_1 < 4$. Moreover, the finite strip results approach the theoretical results for plates with fixed-fixed longitudinal edge supports, $K_1 = 6.97$, and with fixed-hinge supports, $K_2 = 5.41$, as the w_2/w_1 ratio approaches zero (0) and infinity, respectively. Finally, Equation 3.16, which relates K_1 to K_2, is equally valid for the case under study and, in fact, is valid for any section under uniform compression.

The assumptions made earlier with respect to the lip are now removed, and the response of an actual lipped channel, including the lip, is investigated. Also, to determine the influence of web buckling, the analysis is conducted for sections with four different w_1/w_2 ratios, all greater than one (1). Uniform compression is assumed, and the width of the lip, w_3, is chosen to satisfy the edge stiffener requirements (Desmond [1978]) defined in Section 3.4. Further, symmetry is not employed, in this and all subsequent analyses, to preclude any artificial constraint on the buckling mode.

The results of the analyses are presented in Figures 3.3 and 3.4 where the numbers in parentheses refer to the w_1/w_2 ratios. These results are valid for buckling with one longitudinal half-wave, i.e., $m = 1$ in Equations A.4 and A.5. Results for higher order buckling modes, i.e., for $m > 1$, are obtained simply from the $m = 1$ curve by keeping the ordinates constant and multiplying the abscissas by m.

The flange buckling coefficient, K_2, is presented, in Figure 3.3, as a function of the flange aspect ratio, L/w_2, where L is the length. Generally, three extremes are observed; see points labeled a, b, and c; and the associated buckling modes are portrayed in Figure 3.5, for the specific w_1/w_2 ratio equal to two (2). A local buckling mode is observed

for the primary minimum, point a, and occurs at relatively small aspect ratios, L/w_2. This buckling mode indicates clearly the restraining effect of the flange on the web. For the secondary minimum, point c, the flange buckles in a local-torsional mode at relatively large aspect ratios. Due to this mode of action, the restraining effect of the flange on the web is now absent. The buckling mode associated with the peak of the curve, point b, is a mixture of the local and local-torsional modes described above. For aspect ratios intermediate to points a through c, buckling modes similar to those in Figure 3.5 are obtained.

As the parameter w_1/w_2 is increased, the buckling response deviates from that described above. This is indicated in Figure 3.3 where the peak of the curves becomes less pronounce as w_1/w_2 is increased. For a web-to-flange ratio of four (4), the peak no longer exists, and only the primary minimum is observed. In this case, the buckling modes are either local (Figure 3.5a) or local-torsional (Figure 3.5c) to the left and right of the minimum, respectively.

The web buckling coefficient, K_1, is presented in Figure 3.4, and because of the similarity of this figure to Figure 3.3, discussion is limited. Again, the response of K_1 is influenced by the w_1/w_2 ratio, but the magnitude associated with the primary minimum is only slightly affected by changes in this parameter.

Instability is governed by the absolute minimum buckling coefficient, K_{min}. For example, in Figures 3.3 and 3.4, the minimum buckling coefficient is associated with the primary minimum point on the curves; consequently the local buckling mode of Figure 3.5a governs the response. In this respect, it is observed that web buckling has a detrimental influence on the minimum flange buckling coefficients of Figure 3.3. Also, good

agreement is obtained between the K_{min} of Figures 3.3 and 3.4, and the results of Figure 3.2 for the idealized lipped channel. These findings are, of course, influenced by the edge stiffener, which is discussed next.

To investigate the influence of the edge stiffener, an analysis is repeated for the section from Figure 3.3 which has $w_1/w_2 = 2$, but the lip size, w_3, is doubled. The results of this analysis ($w_3/w_2 = 0.426$) are compared with those of the original analysis ($w_3/w_2 = 0.213$) in Figure 3.6 where the flange buckling coefficient, K_2, is presented. The corresponding web buckling coefficient, K_1, may be obtained from Equation 3.16. It is seen that doubling the size of the stiffener affects only the secondary minimum, which is raised. And the primary minimum, which governs buckling, remains unaffected.

There is a limit to the response described above. For example, a larger stiffener could initiate buckling which would change the response. Also, a smaller stiffener could lower the secondary minimum to the point where it governs buckling. In effect, these are the reasons why design specifications place requirements on stiffener size (see Section 3.4).

Next, the behavior of a lipped channel compressed by non-uniform, longitudinal, edge compression is examined. There is no known solution to this problem which has practical applications for sections subjected to combined axial and bending action. The longitudinal stress f at a distance x from the web (see insert on Figure 3.7) is defined by the linear relationship

$$f = f_1(1 - cx/w_2) \qquad 3.17$$

where f_1 is the stress level at the web, $x = 0$, and c is a stress factor. A rectangular lipped channel is analyzed for instability under different stress conditions, or various values of c. The results are shown in

Figures 3.7 and 3.8 where the buckling coefficients for the flange, K_2, are based on the maximum stress level and the web buckling coefficients, K_1, are based on the web stress. Note that for c = -0.5, flange buckling is delayed with respect to the results for uniform compression, but that for c = 0.5, it is the same in the region of the primary minimum (see Figure 3.7). Another observation is that the stress distribution defined by c = -0.5 exaggerates web buckling in the local-torsional mode of Figure 3.5c (see Figure 3.8).

3.4 Edge Stiffeners

As discussed above, the size of the lip or edge stiffener affects the local buckling behavior. This is recognized in the current design specification (AISI [1980]) which stipulates the following minimum stiffener moment of inertia, about its own centroidal axis.

$$I_{smin} = 1.83t^4[(w/t)^2 - 4000/F_y]^{\frac{1}{2}} \qquad 3.18$$

where w is the flat-width of the edge stiffened element, e.g., the flange of a lipped channel, and F_y the yield stress in ksi. Equation 3.18 has been verified experimentally and has a theoretical basis (Winter [1970]). If the edge stiffener is proportioned to meet the above requirement, then the edge stiffened element may be considered a stiffened element for design purposes.

More recently, Desmond [1978] proposed edge stiffener requirements which were based on linear instability theory, an ultimate strength criterion, and experiments. Similar to Equation 3.18, Desmond's requirements depend on the width-to-thickness ratio w/t and yield strength, but three different requirements are defined depending on the range of the w/t

ratio. A general limiting width-to-thickness ratio $(w/t)_l$, which follows from Equations 2.10 and 2.4, is employed where

$$(w/t)_l = 110.8(K/F_y)^{\frac{1}{2}} \qquad 3.19$$

The factor K is the buckling coefficient of the compression element. For relatively small w/t ratios the compression element is fully effective without a stiffener. Also ignoring any rotational restraint at the supported longitudinal edge, the other edge being free; the buckling coefficient K in Equation 3.19 is 0.425. Therefore, for

$$w/t < (w/t)_{lu} = 110.8(0.425/F_y)^{\frac{1}{2}} \qquad 3.20a$$

$$I_{sa} = 0 \qquad 3.20b$$

where I_{sa} is the adequate stiffener moment of inertia about its own centroidal axis. For the second or "fully effective" range,

$$(w/t)_{lu} < w/t < (w/t)_{ls} = 110.8(4/F_y)^{\frac{1}{2}} \qquad 3.21a$$

$$\frac{I_{sa}}{t^4} = 120\frac{[(w/t)/(w/t)_{ls} - (w/t)_{lu}/(w/t)_{ls}]^3}{[1.0 - (w/t)_{lu}/(w/t)_{ls}]^3} \qquad 3.21b$$

where $(w/t)_{lu}$ and $(w/t)_{ls}$ are defined in Equations 3.20a and 3.21a, respectively. The stiffener requirement of Equation 3.21b was empirically justified and was derived such that buckling and yielding occurred simultaneously. It is noted that a buckling coefficient of four (4) was employed in defining $(w/t)_{ls}$ from Equation 3.19. Above, $(w/t)_{ls}$ only elastic buckling occurs. In this range, Desmond found that basing a stiffener requirement on that derived from a buckling criterion, defined below, was insufficient to provide the edge stiffened element with the post-buckling strength of a similar stiffened element. (A stiffener requirement based on a buckling criterion is defined as one which forces the local and local-torsional buckling modes to occur simultaneously, see Section 3.3.) Therefore, he employed an ultimate strength criterion where

an adequate stiffener was defined as that which provided the edge stiffened element with a strength equal to that for a fully stiffened element. Based on this criterion, the following requirement was formulated using a statistical correlation between several hypothetical stiffener requirements and experimental data. For the third or "post-buckling" range,

$$w/t > (w/t)_{1s} \qquad 3.22a$$

$$I_{sa}/t^4 = 115(w/t)/(w/t)_{1s} + 5 \qquad 3.22b$$

In addition, a restriction was placed on the overall stiffener depth D_s, defined as the sum of the stiffener depth w_3 and the inner radius r (see Figure 3.9a), to preclude the detrimental effects of stiffener buckling interacting with the edge stiffened element, e.g.,

$$D_s \leq 0.25w \qquad 3.23$$

The calculation of the stiffener property I_{sa} must admit the possibility of a partially effective stiffener depth w_3. Therefore, the effective area distribution of Figure 3.9b is employed. The effective width of the stiffener w_{3e} is determined from the stiffened plate effective width Equation 2.9,

$$w_e/w = \sqrt{f_{cr}/f_e}\,(1.0 - 0.218\sqrt{f_{cr}/f_e}) \qquad 2.9$$

with the critical stress equal to that for an unstiffened element, e.g., K = 0.425 in Equation 2.4, and with f_e equal to the yield stress F_y. Then the effective area $w_{3e}xt$ is distributed as indicated in the figure. It is noted that a straight segment approximation of the actual stiffener radius is used in Figure 3.9. At first, in accordance with Desmond, the actual radius was employed for calculation of the stiffener properties; however, Desmond's original stiffener calculations could not be duplicated using this approach. Instead, the straight segment approximation of Figure 3.9 provided good agreement with Desmond's calculations and, therefore, was

adopted in this study. This approximation is, of course, limited to relatively small radius-to-thickness ratios, r/t.

Some interesting observations follow from the local buckling interaction study of Section 3.3.2 where the edge stiffener size of $w_3 = 0.213w_2$ was established from Equation 3.22 with $F_y = 30$ ksi and $w_2/t = 60$. From Figure 3.3, it is observed that for a square lipped channel ($w_1/w_2 = 1$), where the effects of web buckling are small, this edge stiffener size is just adequate to force the local buckling mode of Figure 3.5a to govern, i.e., the minimum buckling coefficient for the flange is associated with the primary minimum. Another observation follows from Figure 3.6 where the effect of a larger stiffener is investigated, including the influence of web buckling. In this figure it is seen that using a larger stiffener is ineffective in changing the minimum buckling coefficient of the flange due to the dominating influence of the web.

Moreover, local buckling interaction affects the stiffener requirement. For example, if the buckling criterion defined earlier is used to establish a stiffener requirement, then a smaller requirement would result for sections where the web initiates buckling, i.e., for $w_1/w_2 > 1$, as compared to a requirement established for a section where the influence of the web is small, i.e., for $w_1/w_2 = 1$ (refer to Figure 3.3).

3.4.1 Effect of Stiffener Radius on Local Buckling

In the local buckling studies of Section 3.3.2, the edge stiffener was approximated by a sharp right angled lip. Yet actual edge stiffeners include a transitionary radius (see Figure 3.9). Also, curved stiffeners formed entirely from a circular bend are used in practical applications.

Therefore, it is important to establish how this radius influences the local buckling response.

In the present section the effect of the stiffener radius is studied using an idealized flange-stiffener model (see Figure 3.10). This idealized model is chosen to preclude local buckling interaction with other elements, and the longitudinal edge support is treated as simply supported and fixed in order to bound the support that exists in an actual section. Two different edge stiffeners — a sharp right angled lip and one quarter of a hollow cylinder, or arc — are examined and are proportioned to meet Desmond's stiffener requirements for F_y = 30 ksi and w_2/t = 60. This results in dimensions for the right angled lip and arc of w_3/t = 12.8 and r/t = 10.06, respectively (see Figure 3.9). The stiffener moment of inertia I_s for the arc is calculated using the actual cross section. Finally, the finite strip method of Section 3.2 is employed to analyze the model in uniform compression, where four, one, and six straight finite strips are used for the discretizations of the flange, lip, and arc, respectively.

In general, the arc stiffener is less effective than the equivalent right angled lip (see Figure 3.10). For example, a smaller buckling coefficient K_2 is associated with the flange-arc model. Also, the buckling modes corresponding to Figure 3.10 are similar to those indicated for the flange in Figure 3.5. It is interesting to note that for a simply supported edge, the flange-stiffener model does not exhibit a secondary minimum (see Section 3.3.2), and that the buckling coefficient decreases continually for L/w_2 greater than about four (4). This is due to the complete absence of any rotational restraint at the supported, unloaded edge, and the associated buckling mode is torsional about an enforced axis of rotation.

A relatively simple method to account for the reduced buckling strength due to the effect of the stiffener radius would be to include a portion of the radius in the definition of the flat-width w, e.g., $w = w_2 + r$ where w_2 is the flat-width of the edge stiffened element and r the radius of the stiffener. Because of the direct dependence of the stiffener requirements on w (see Section 3.4), this results in a larger required stiffener which, in turn, offsets at least partially the effect of the radius.*

3.5 Post-Local Buckling Interaction

While the problem of local buckling interaction in thin-walled sections has been investigated in the past by numerous researchers, the behavior after the occurrence of local buckling has received relatively little attention. Rhodes and Harvey [1976] investigated the theoretical post-buckling behavior of plain channel struts under compression and bending. Their analysis was an extension of earlier work (Rhodes and Harvey [1971a]) on single plates where the semi-energy method of Marguerre [1937] was utilized to obtain unknown coefficients of an assumed deflected form. The extension involved enforcing compatibility between plate elements of the section. Because the deflected form was assumed to remain unchanged after buckling, with only a different magnitude, a constant post-buckling tangent stiffness was obtained, e.g., curve "a" in Figure 3.11b where P and u represent the axial load and displacement, respectively. This figure is discussed in more detail shortly.

*Note that this method has no quantitative basis.

As in local buckling interaction (see Section 3.3), the restraint provided by one plate element of a section to another could also affect the behavior, i.e., the restraint could change in the post-buckling realm. This aspect was investigated by Rhodes [1978] who included the effects of changing rotational restraints and changing deflected form. These effects were found to lead to significant changes in the post-buckling stiffness at loads only slightly in excess of the buckling load. Therefore, in this same paper, Rhodes studied the effects of changing restraint in more detail, where to simplify the analysis the deflected form was assumed to remain constant after buckling. In brief, some very interesting results were obtained from an analysis of the uniformly compressed square box section of Figure 3.11a, which had unequal thickness, t_1 and t_2. The load-end displacement for the specific case of $t_1/t_2 = 2$ is shown in Figure 3.11b. From the results, the following behavior was postulated. At initial buckling indicated by P_{cr}, the initial reduction in tangent stiffness to curve "a" was primarily due to buckling of the restrained thinner plates, while the thicker plates remained relatively unaffected. Then at a larger load, a form of "secondary local buckling" occurred where the thicker plates developed substantial out-of-plane deflections. The associated end displacement was slightly less than u_s which represented the value at which the thicker plates would buckle if their unloaded edges were simply supported. In this range of end displacement the thicker plates behaved as if simply supported but with initial imperfections induced by the buckled thinner plates. After secondary buckling, the restraint between plates reduced significantly and approached a simple support condition.

Frieze [1978] also investigated the post-buckling behavior of thin-walled sections where there was interaction between the component plates. The governing differential equations were cast into finite difference form and then solved using a dynamic relaxation technique. Plasticity and residual stress effects were included. The theoretical model was correlated with experimental data and was found to yield slightly conservative failure predictions. Frieze also included a comparison between theoretical failure loads for uniformly compressed square box sections, with unequal thicknesses and $(w/t)_{max} \leq 80$, and theoretical failure loads obtained by treating the component plates as if simply supported and isolated. In general, the latter simpler approach predicted failure loads within 3% of those obtained by analyzing the actual section.

3.5.1 Effective Section Method

The above theoretical studies of post-local buckling interaction in thin-walled sections suggest the possibility of a very simplified analysis approach wherein the component plate elements are treated as isolated. This approach is investigated here for singly-symmetric sections using an effective section method defined by the effective widths of the individual, simply supported, plate elements. A method used to account for local buckling interaction between the plate elements is also investigated for comparison with the simply supported plate results.

A loading condition of uniform compression (constant compression eccentricity) is assumed. Further, the length of the section is restricted such that web-flange intersections remain straight, e.g., as in short struts where buckling in overall modes is not critical. From the results of Section 2.2.3, the stiffened plate effective width Equation 2.9 is

employed to calculate the effective widths of all plate elements, both stiffened and unstiffened. This equation is written in the following generalized form.

$$w_e/t = 163.3\sqrt{K/f_e}\,[1 - 35.6\sqrt{K/f_e}/(w/t)] \qquad 3.24$$

where all terms were defined previously. The above equation is valid for w/t ratios greater than the limiting width-to-thickness ratio $(w/t)_1$ of

$$(w/t)_1 = 110.8\sqrt{K/f_e} \qquad 3.25$$

For w/t ratios less than this value the element if fully effective. The effective section is obtained by applying Equation 3.24 to all component elements. The actual manner in which the effective widths are distributed is irrelevant due to the assumption of uniform compression. The axial load P is determined from

$$P = f_e A_e \qquad 3.26$$

where A_e is the area of the effective section. At failure, the ultimate load P_u is determined from Equation 3.26 with $f_e = F_y$.

The effective section method described above is applied to channels and lipped channels with various web-to-flange ratios w_1/w_2, and the results are presented in Figures 3.12 and 3.13. These results are based on ultimate conditions with F_y = 30 ksi; thus the vertical axis is equivalent to the ratio of average-to-ultimate stresses. For the lipped channels, the edge stiffeners are designed to meet Desmond's requirements (see Section 3.4), and are assumed fully effective. Finally, and most importantly, the curves in Figures 3.12 and 3.13 are based on two different assumptions. For the dashed curves it is assumed that there is no interaction between the component elements. Therefore, simply supported boundary conditions are employed where the buckling coefficient K in

Equation 3.24 is taken equal to 0.425 and 4.0 for unstiffened and stiffened elements, respectively. The discontinuity in the dashed curves represents the transition of the web, element 1, from fully to partially effective. For the solid curves, it is assumed that there is full interaction between the component elements, and the elastic local buckling coefficients from Figures 3.1 and 3.2 are assumed valid for the channels and lipped channels, respectively.

As shown in Figure 3.12 for channel sections, when the w_1/w_2 ratios are small, accounting for local buckling interaction yields larger ultimate loads relative to loads that are calculated by treating the component plates as simply supported. However, for larger w_1/w_2 ratios, which are more practical in actual applications, it does not matter whether interaction is accounted for or not; the ultimate loads are nearly identical. In contrast to this, significant differences are obtained for lipped channels with large w_1/w_2 ratios (see Figure 3.13). This time the largest ultimate loads are associated with the simply supported boundary conditions.

3.6 Summary

The problem of local buckling interaction in thin-walled sections was investigated in this chapter. First, the numerical methods employed to solve the instability problem were discussed. The finite strip method was used for the problem discretization. A general formulation for linear instability was reviewed where the details were relegated to Appendix A. The special purpose finite strip instability analysis program, developed in this study, was then addressed. The determinant search algorithm employed for the eigensolution and other special features of the analysis

program were discussed in Appendix B. The program was verified by analyzing several simple plate examples in Appendix C.

Second, local buckling interaction in structural sections, subjected to longitudinal compression, was investigated using the aforementioned program. Channel and lipped channel sections were studied thoroughly. For the latter, the effects of the edge stiffeners and non-uniform compression were included; both of which were found to significantly affect the local buckling response.

Third, edge stiffeners were discussed, and current and proposed design requirements were reviewed. Also, a simple model was analyzed to investigate the effect of stiffener radius on the local buckling behavior. The results showed that a stiffener formed into the shape of an arc was less effective in resisting buckling than an equivalent right angled lip.

Finally, the behavioral aspects of post-local buckling interaction in thin-walled sections were established by reviewing the pertinent literature. This provided, at least, partial justification for a simplified analysis method wherein the component plates were treated as isolated and simply supported. For this purpose, an effective section method was presented where the effective widths of the component elements were determined using the stiffened plate effective width equation. Also, an effective section method was defined to account for local buckling interaction in thin-walled sections where the interactional critical buckling stresses of each element were used to calculate the respective effective widths. The ultimate loads predicted using this method were then compared with those predicted by treating the component plates as simply supported. A discussion of the suitability of these methods for predicting the

response of actual thin-walled sections is postponed until Chapter 6 where experimental justification is provided.

All of the work presented in this chapter was restricted to only local buckling effects. The influence of overall buckling and bending where the cross section displaces in an overall mode is investigated subsequently.

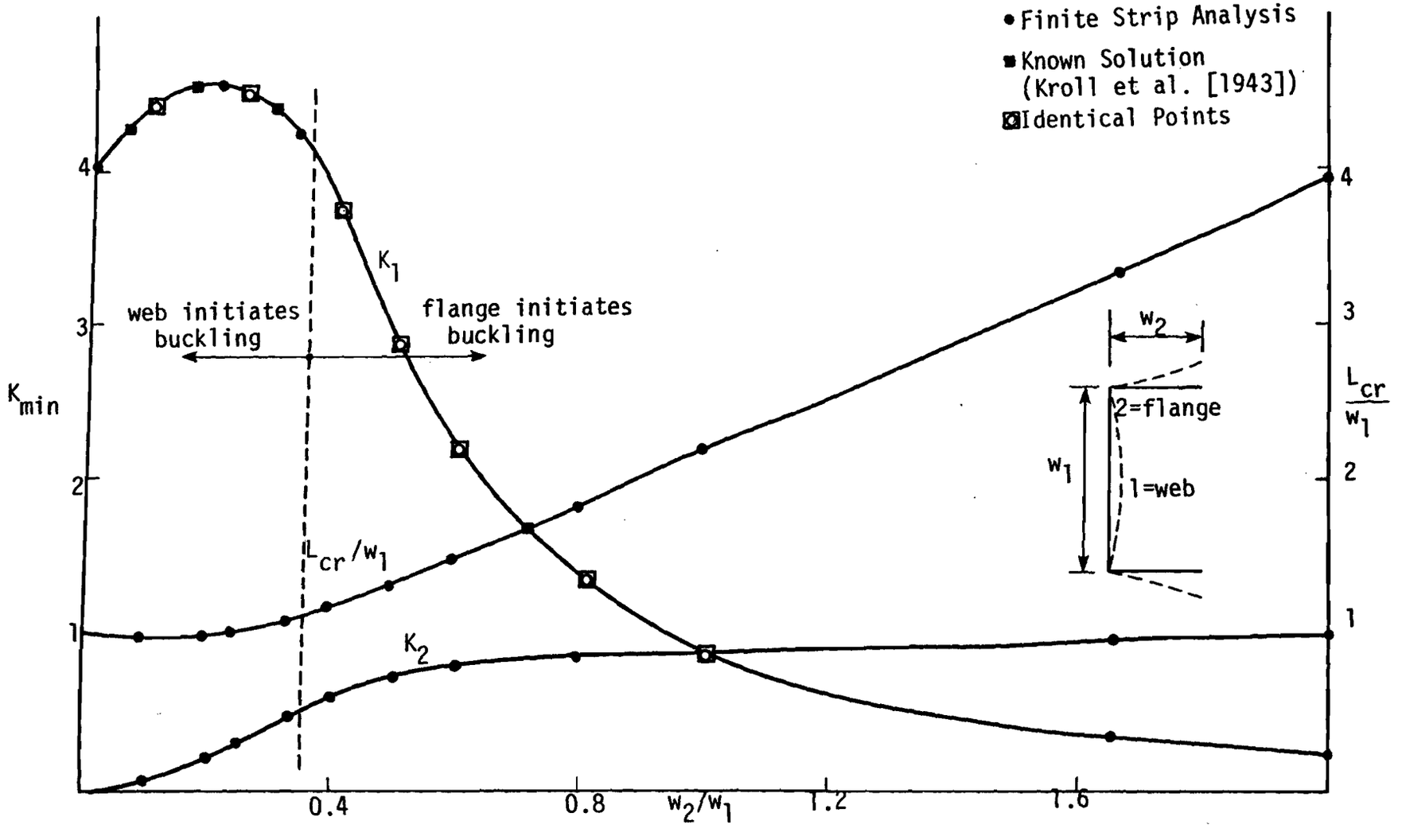

Figure 3.1 LOCAL BUCKLING INTERACTION IN A UNIFORMLY COMPRESSED (PLAIN) CHANNEL

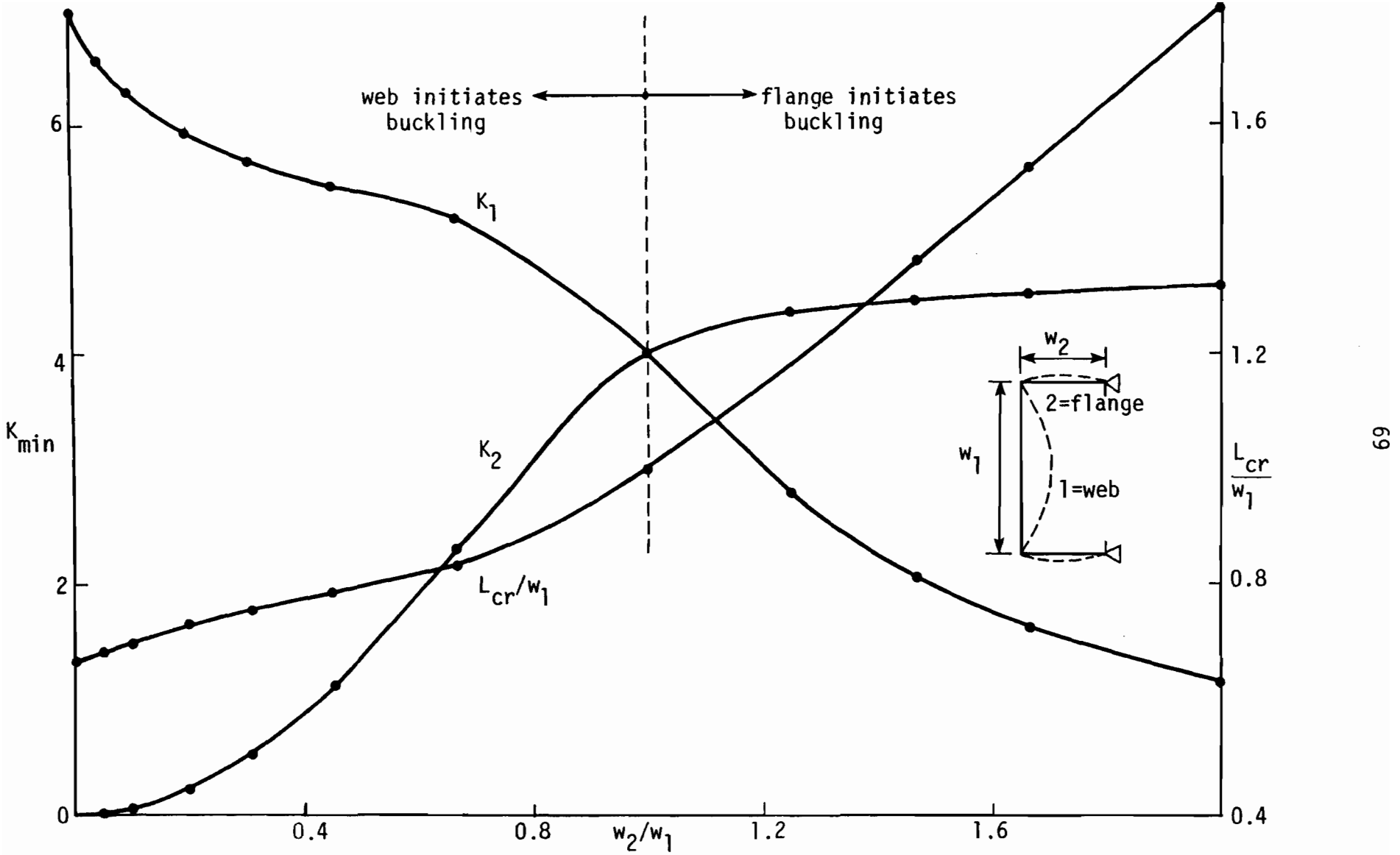

Figure 3.2 LOCAL BUCKLING INTERACTION IN A UNIFORMLY COMPRESSED, IDEALIZED, LIPPED CHANNEL

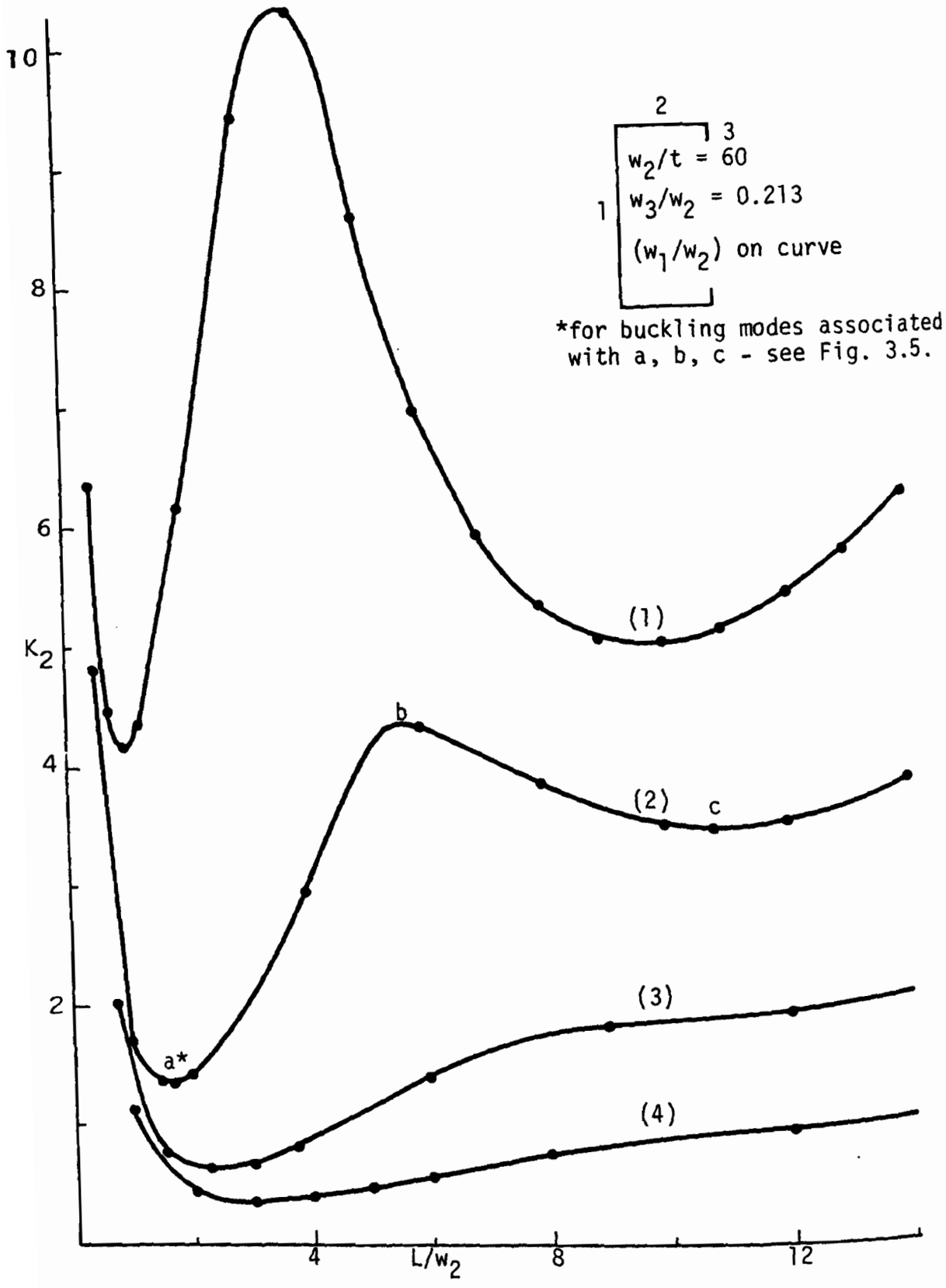

Figure 3.3 FLANGE BUCKLING FOR UNIFORMLY COMPRESSED LIPPED CHANNELS

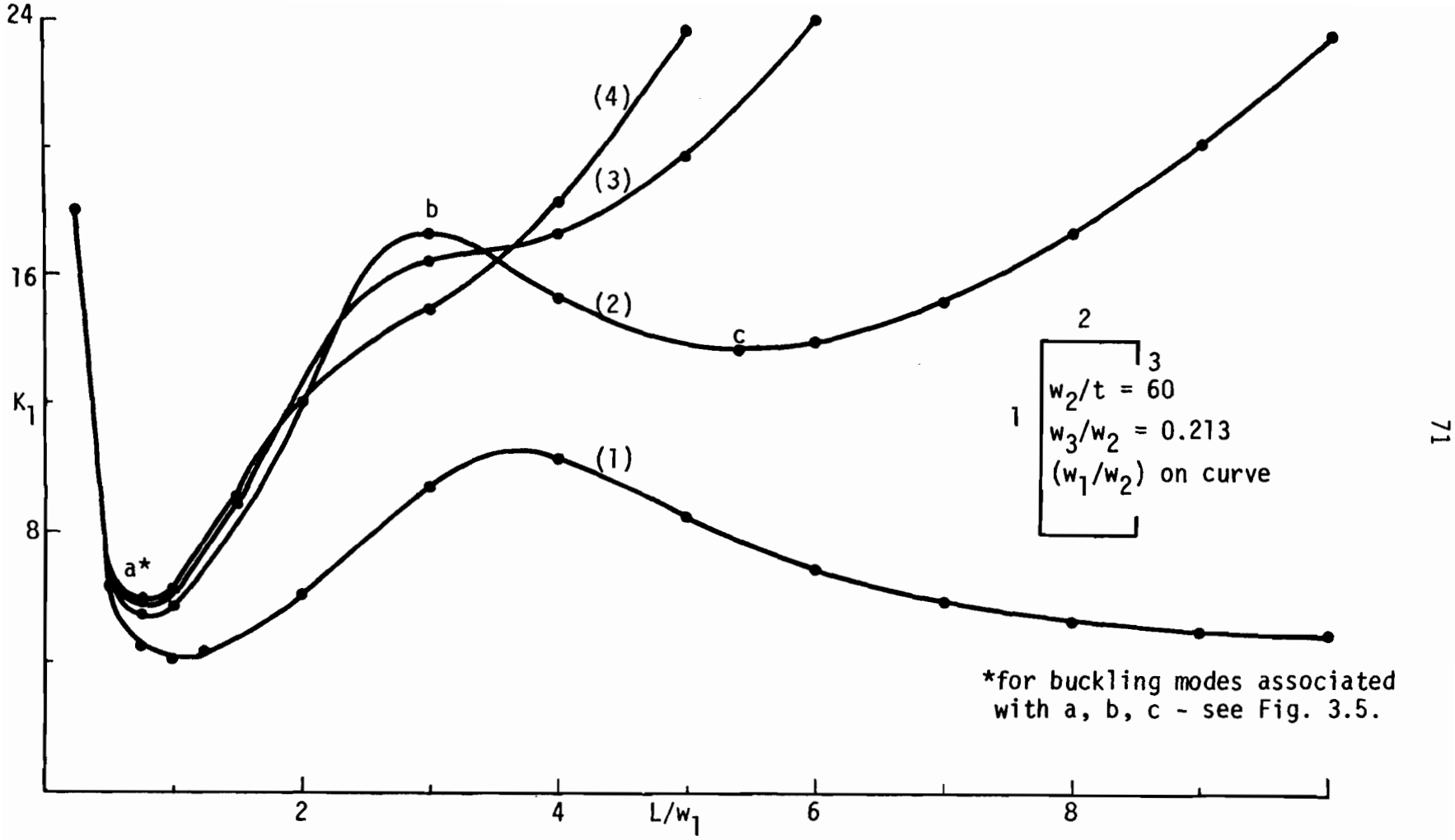

Figure 3.4 WEB BUCKLING FOR UNIFORMLY COMPRESSED LIPPED CHANNELS

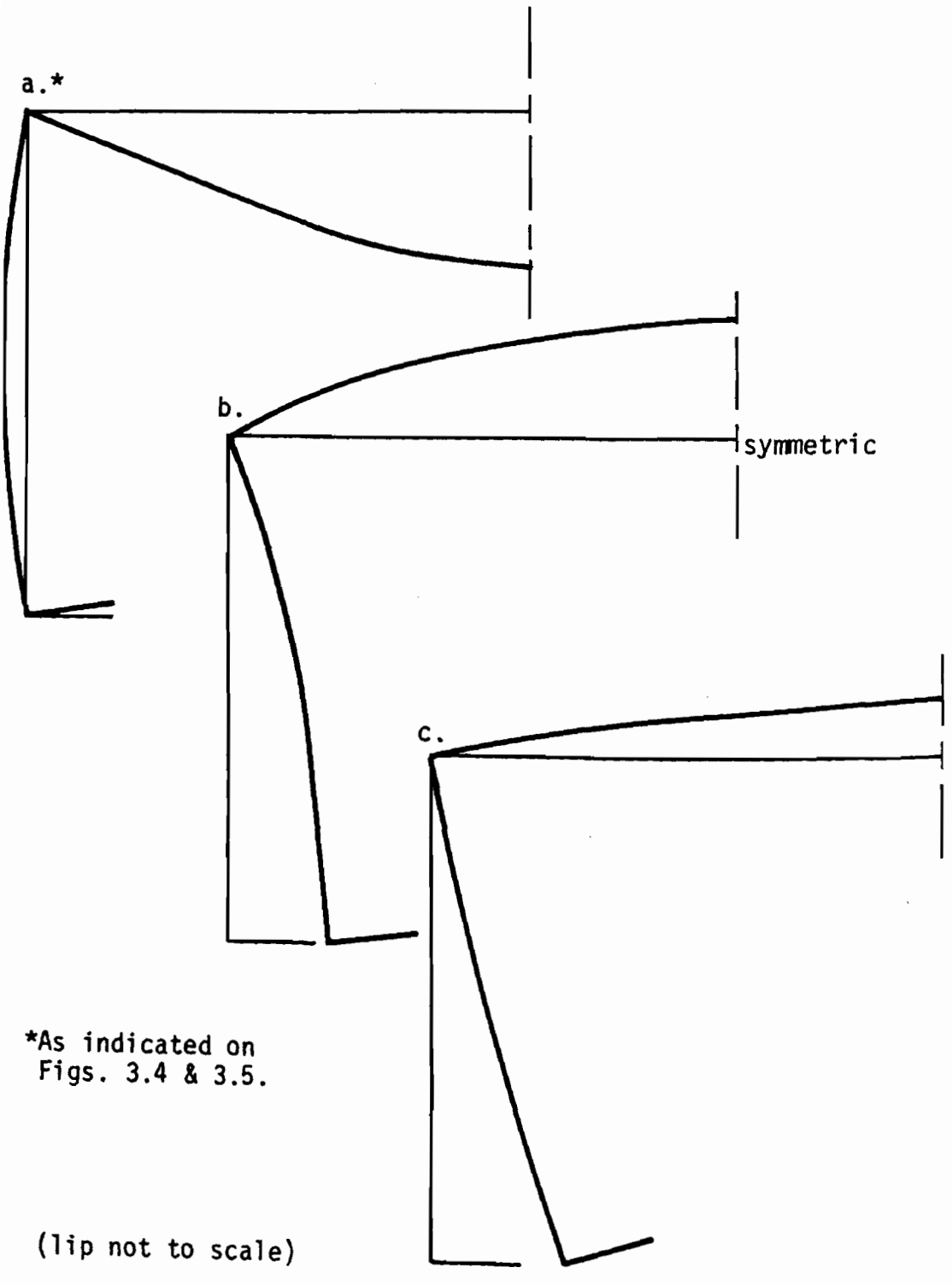

Figure 3.5 LOCAL BUCKLING MODES IN LIPPED CHANNELS

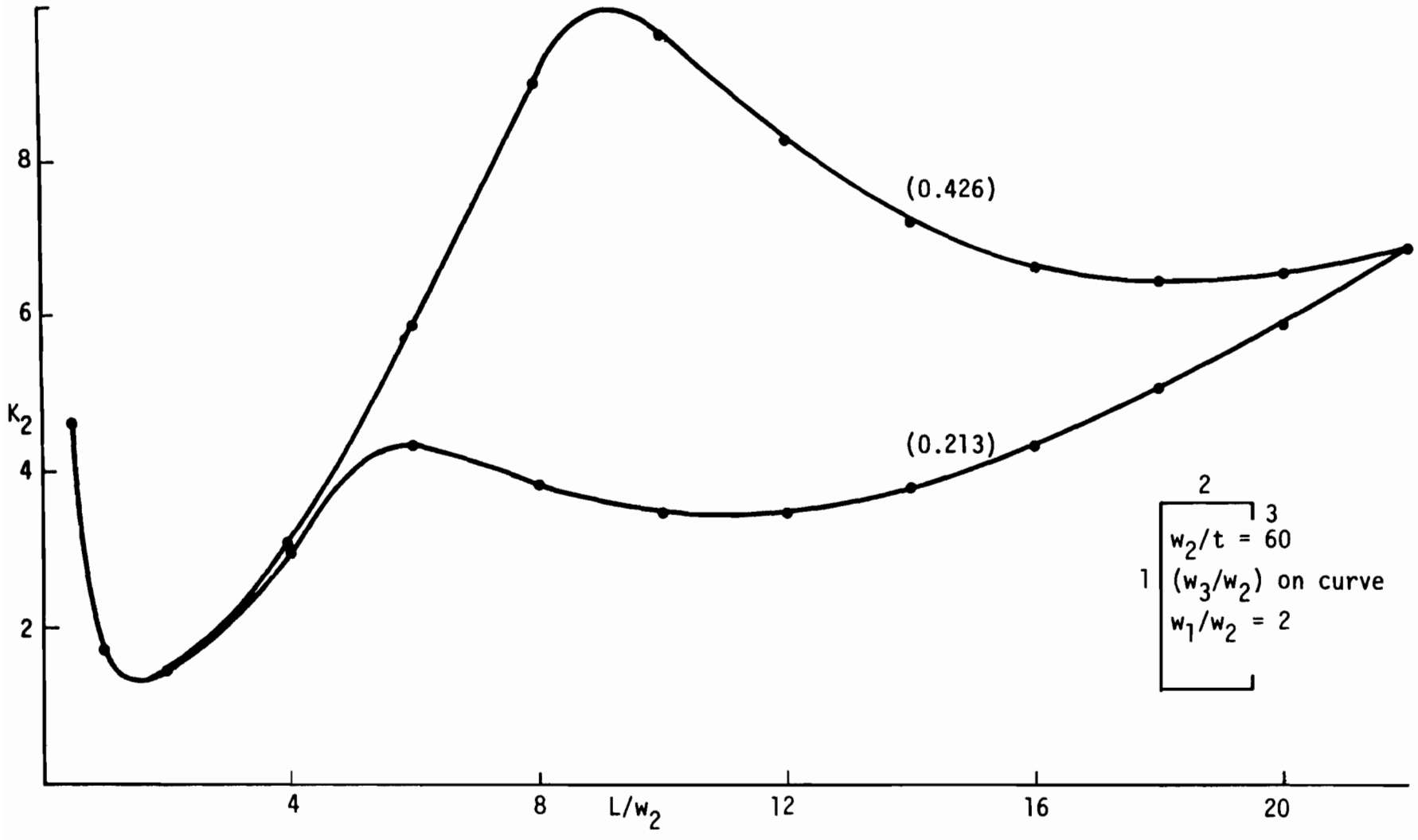

Figure 3.6 EFFECT OF LARGER STIFFENER ON FLANGE BUCKLING FOR UNIFORMLY COMPRESSED LIPPED CHANNELS

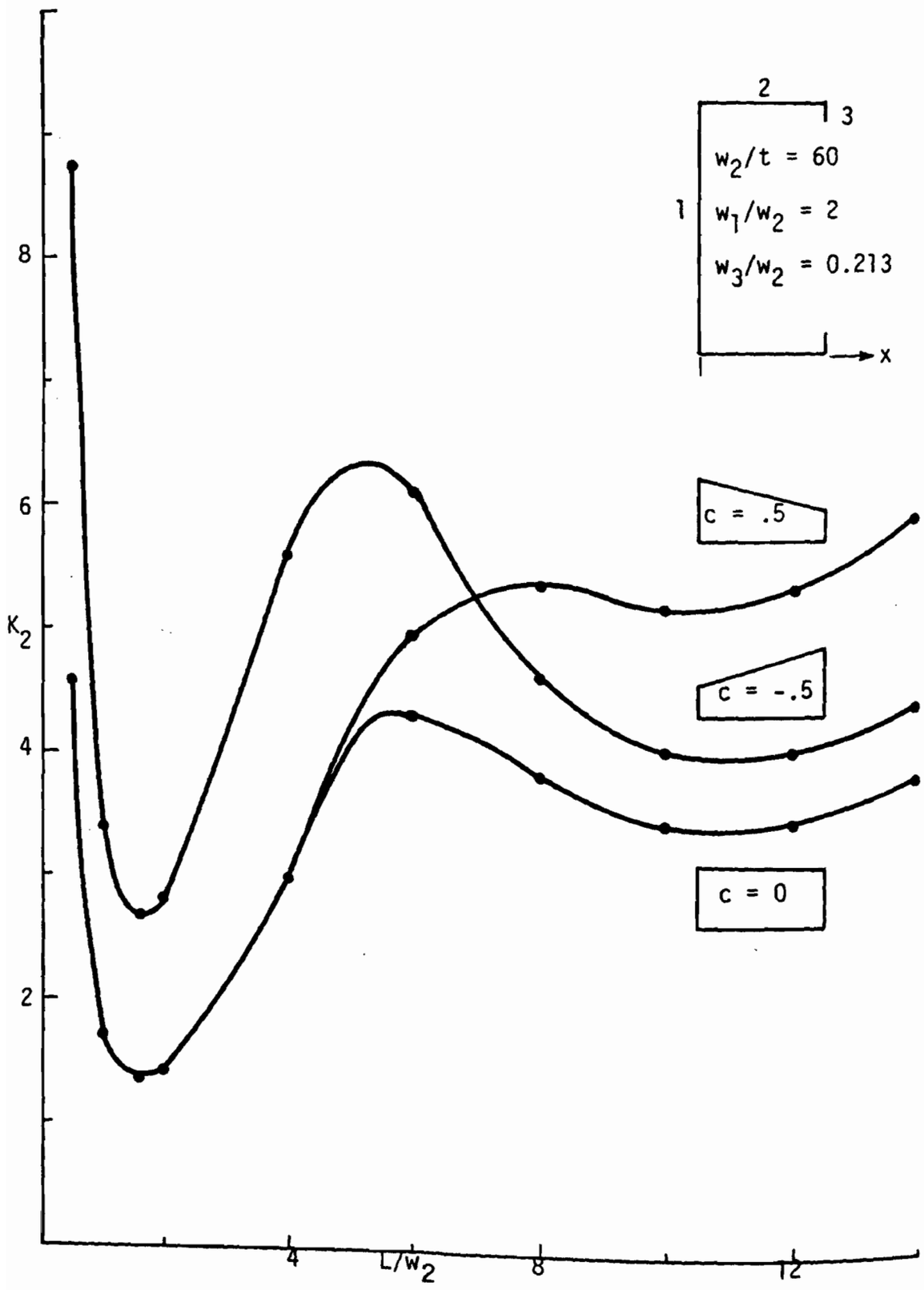

Figure 3.7 INFLUENCE OF STRESS GRADIENT ACROSS FLANGE ON FLANGE BUCKLING IN LIPPED CHANNELS

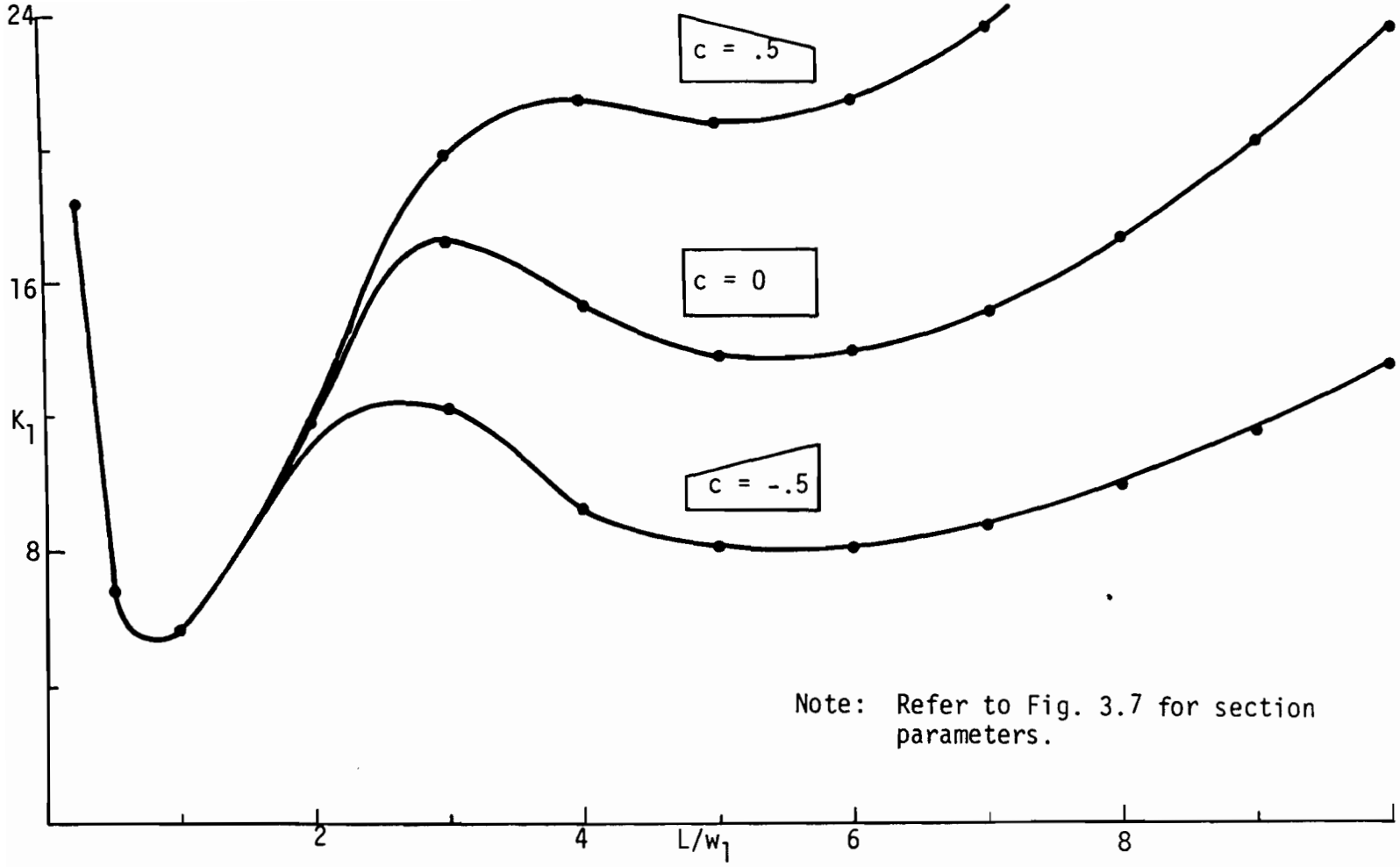

Figure 3.8 INFLUENCE OF STRESS GRADIENT ACROSS FLANGE ON WEB BUCKLING IN LIPPED CHANNELS

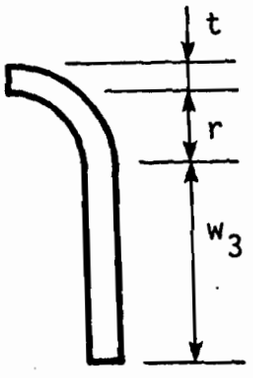

(a) Actual stiffener

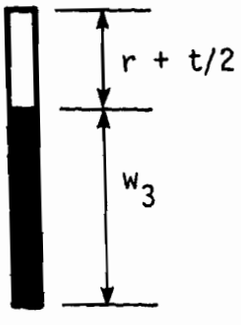

(1) fully effective

(2) $w_{3e}/w_3 \geq 0.5$

(3) $w_{3e}/w_3 < 0.5$

(b) Stiffener approximation and effective area distribution

Figure 3.9 EDGE STIFFENER

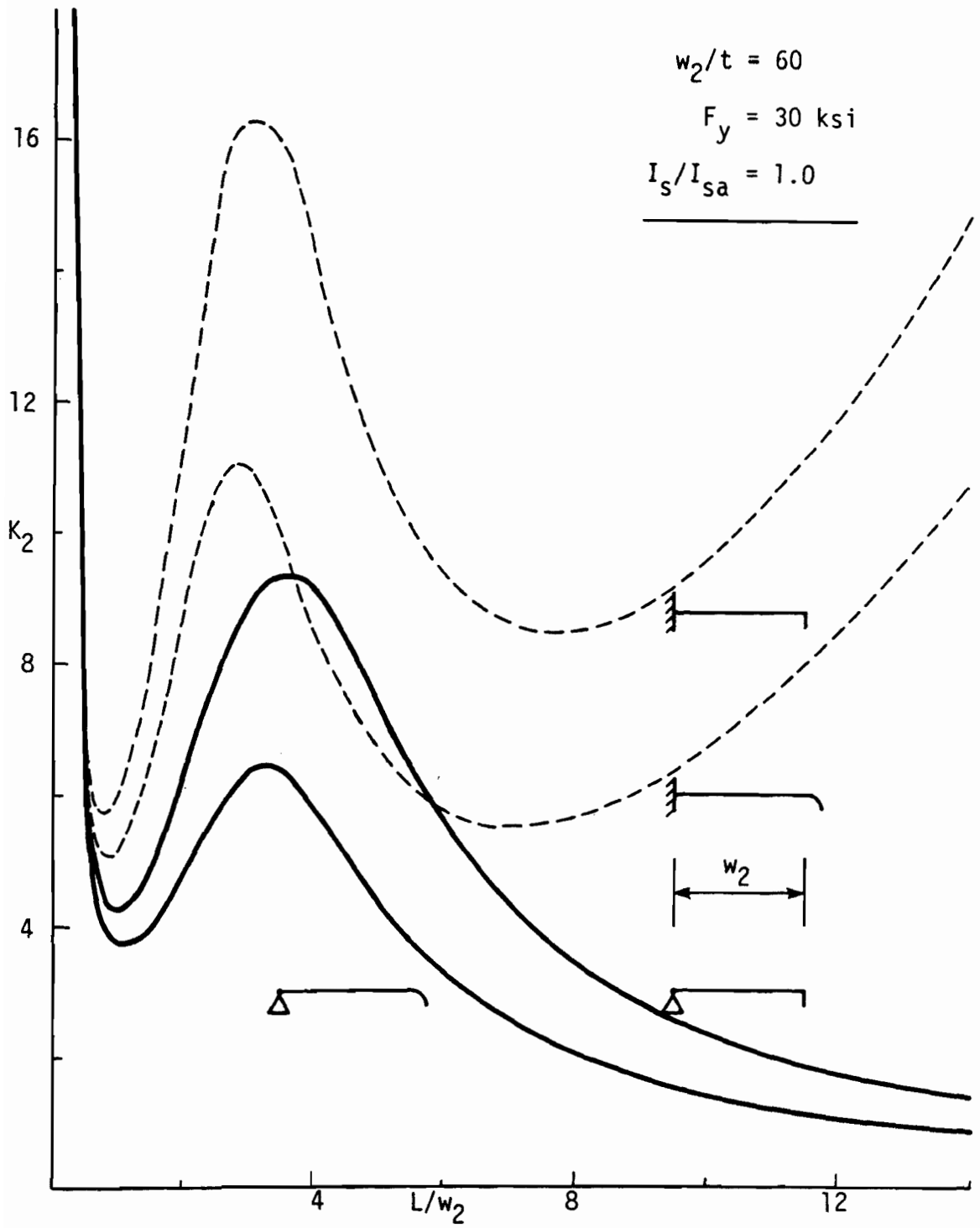

Figure 3.10 RADIUS EFFECT FOR IDEALIZED FLANGE-STIFFENER MODEL SUBJECTED TO UNIFORM COMPRESSION

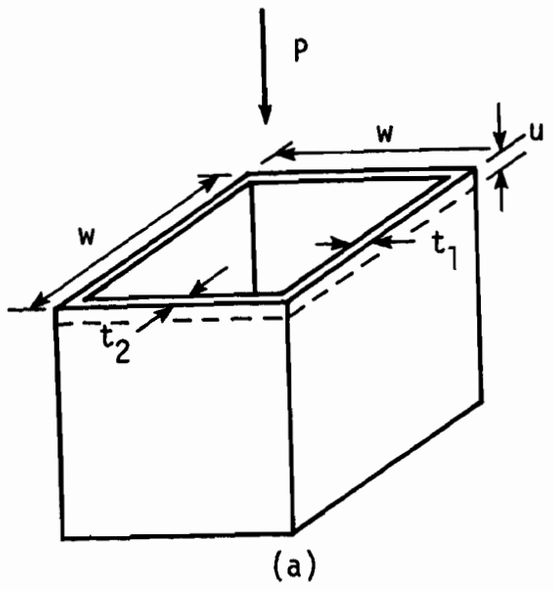

(a)

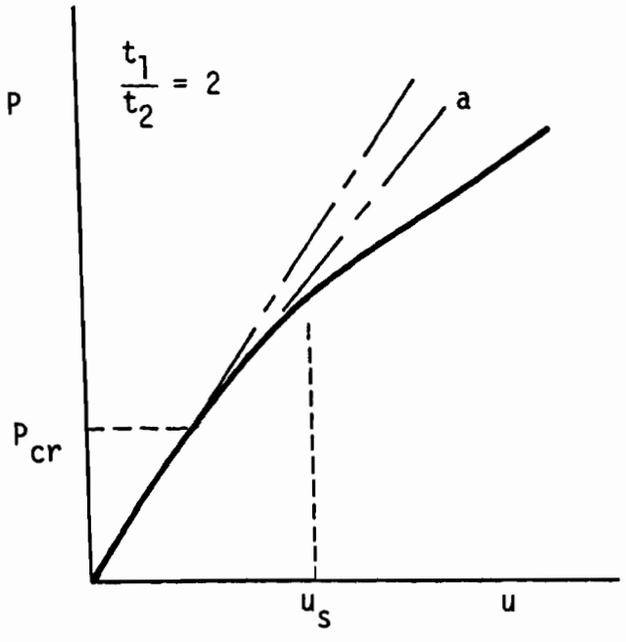

(b) Axial load-displacement response

Figure 3.11 THEORETICAL POST-BUCKLING BEHAVIOR OF STRUCTURAL SECTIONS (after Rhodes [1978])

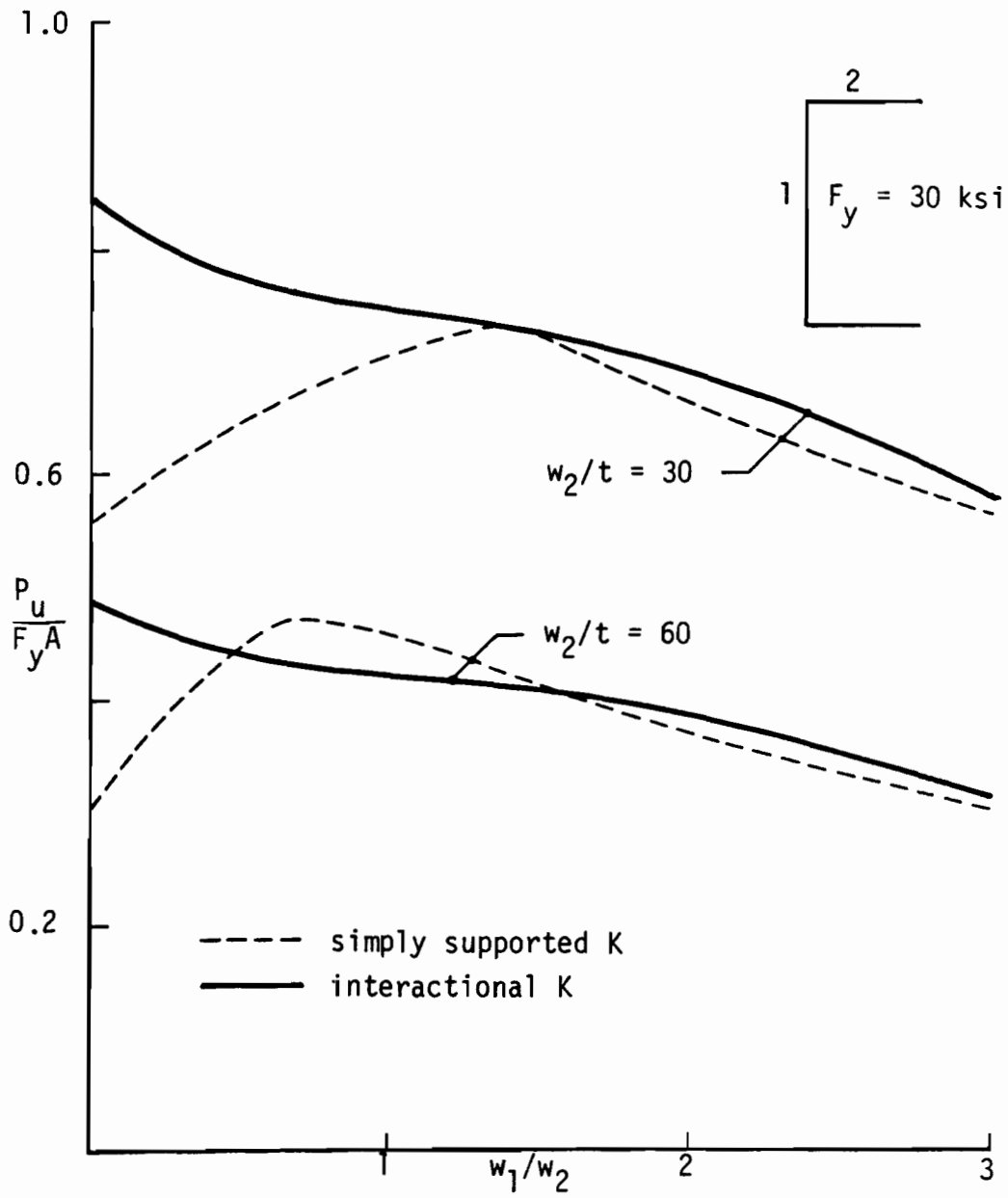

Figure 3.12 COMPARISON OF EFFECTIVE SECTION APPROACHES FOR (PLAIN) CHANNELS

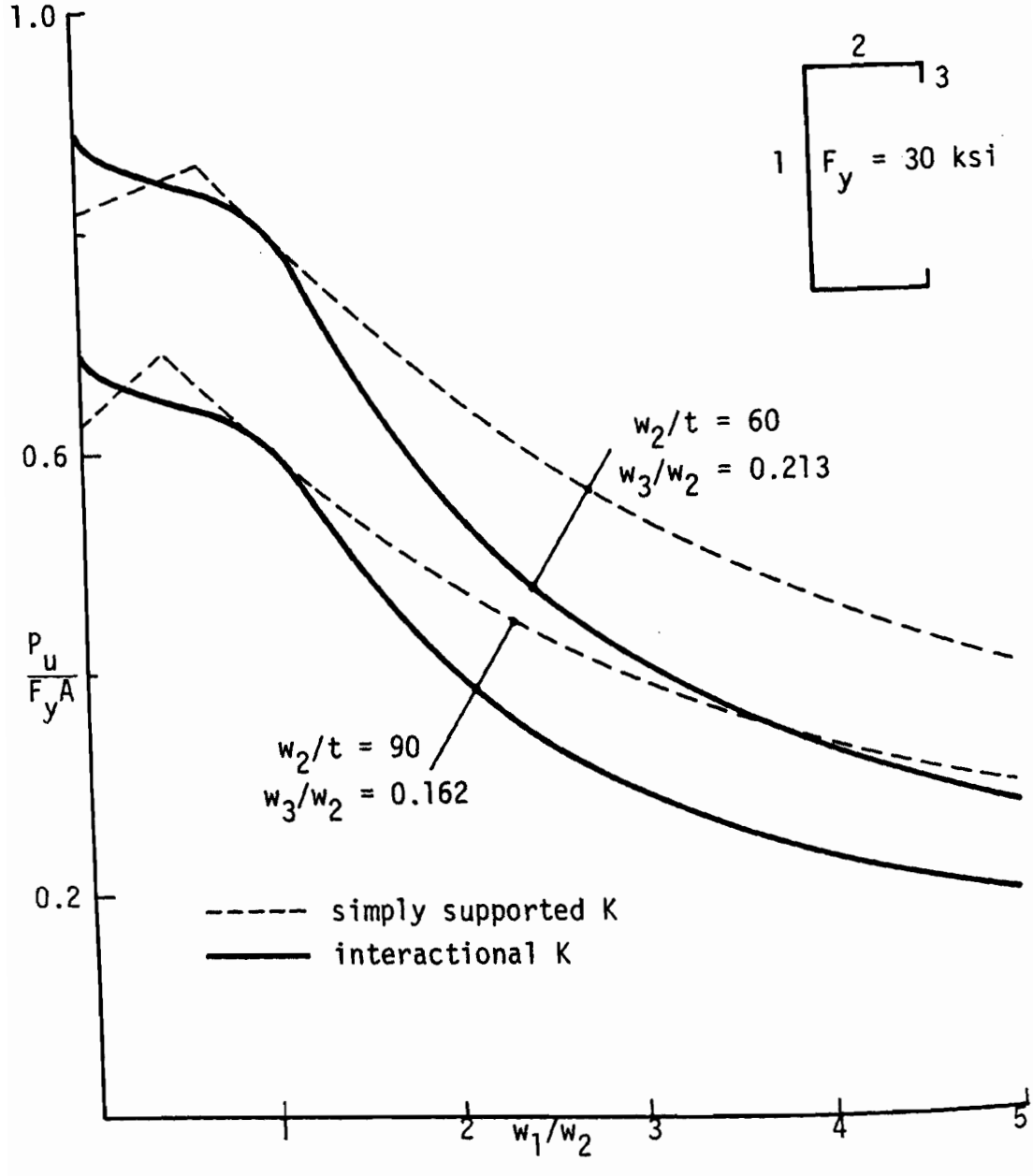

Figure 3.13 COMPARISON OF EFFECTIVE SECTION APPROACHES FOR LIPPED CHANNELS

CHAPTER 4

LOCAL AND OVERALL BUCKLING INTERACTION

4.1 Introduction

The problem of local and overall buckling interaction is addressed in this chapter. Thus, the junctures of component plate elements of a thin-walled section which were previously constrained to remain straight (Chapter 3) are now allowed to deflect. This introduces other modes of behavior which must be considered. In general, these other modes are adversely affected by local buckling of the component plates. For example, due to the effects of local buckling, the flexural buckling strength is weakened when compared to the strength without local buckling effects.

More specifically, the behavior and strength of thin-walled, singly-symmetric columns and beam-columns is studied. An analysis method, utilizing an effective section concept, is derived to predict the sub-ultimate and ultimate response.

4.2 Literature Survey

Early work in the field of interactional buckling was conducted by Bijlaard and Fisher [1952] who investigated the effects of local buckling on flexural and torsional buckling of thin-walled sections. No post-local buckling effects were included. Later, these same authors (Bijlaard and Fisher [1953]) extended their analysis to include post-local buckling effects through the use of an "equivalent post-buckling modulus," E_{eq}. This was used to reduce the Euler buckling stress f_{cr} as follows

$$f_{cr} = \pi^2 E_{eq}/(L/r)^2 \qquad 4.1$$

where L is the column length and r the radius of gyration. In the inelastic range a Johnson parabola was employed. Theoretical strength predictions were in good agreement with reported experimental results for square aluminum box sections. However, post-local buckling effects were insignificant due to the small width-to-thickness ratios studied, e.g., w/t ≈ 30 and 50.

Graves Smith [1969] also researched theoretically the problem of interaction of local and flexural buckling of thin-walled aluminum box sections. An "apparent bending stiffness" was employed to account for local buckling effects. Again, good agreement was obtained between theoretical and experimental ultimate loads for sections with small w/t ratios, w/t = 50.

Investigations into imperfection sensitivity of symmetric thin-walled columns was initiated by van der Neut [1969 and 1973]. A simplified model was utilized to study the effects of two types of imperfection: local plate out-of-flatness and column out-of-straightness. The model consisted of two load carrying flanges connected by webs, which were rigid in shear and laterally, but had no longitudinal stiffness. In the so-called "optimum" range where Euler and local buckling occurred simultaneously, the model was found to be very sensitive to both types of imperfections mentioned above, i.e., the imperfections caused a significant reduction in load carrying capacity. This mode of action was very similar to that observed for shell-type structures. Gilbert and Calladine [1974] extended van der Neut's work and proposed an imperfect column strength approach via a Perry column formula (see Walker [1975]).

The interaction of local and flexural buckling has also been studied in thin-walled stiffened panels, such as bridge decks, by Tvergaard [1973a,b], Tulk and Walker [1976], and Fok, et. al. [1976]. Similar to van der Neut's results, these structures also exhibited imperfection sensitivity.

DeWolf [1973,1974], and later Kalyanaraman [1977,1978], accounted for local buckling effects through the use of an effective width concept. The flexural buckling strength of cold-formed steel, symmetric columns was predicted by both a tangent modulus approach, e.g., Equation 4.1 with E_{eq} replaced by the tangent modulus E_t, and a SSRC (Structural Stability Research Council) column formula (Johnston [1976]). Both methods were iterative and effective section properties were utilized. The load capacities predicted by these methods correlated well with experimental results reported by these authors. The latter method, based on the SSRC formula, is discussed in detail below (Section 4.4). In addition to flexural buckling, the effective width concept has been employed to predict torsional-flexural buckling in locally buckled, thin-walled sections by Wang and Pao [1980].

Interaction of local and flexural buckling in singly-symmetric, thin-walled, steel sections, such as lipped channels, has been investigated by Loughlan [1979,1980]. Concentric and eccentric loading was considered, and sophisticated theoretical predictions were in good agreement with experimental results. In a later paper, Rhodes and Loughlan [1980] presented a simplification of earlier work wherein local buckling effects were accounted for using an effective width method. However, because only one element — the web or stiffened element — was assumed to be partially effective, their analysis method had limited applications.

Similarly, Thomasson [1978] (also see Konig and Thomasson [1980]) derived a method to analyze interactional buckling of singly-symmetric, thin-walled sections. An effective section was employed to account for local buckling; however, in addition, the variation of the effective section along the length of the column was included. To verify his theoretical approach, Thomasson tested lipped channel, steel columns; with and without longitudinal intermediate stiffeners for the web. In general, the theoretical predictions correlated well with the experimental results.

Lastly, interaction of local and overall buckling is recognized in current design specifications. In the U.S., the "Q-factor method" is employed to reflect local buckling effects by reducing the basic yield strength (AISI [1980]). This method is described below in Section 4.4.

4.3 Local and Flexural Buckling Interaction

In this section the interaction between local and flexural buckling is studied for a uniformly compressed channel section. Post-local buckling is not included. In order to restrict the overall response to flexural buckling, the dimensions of the section are chosen as $w_2 = 0.2w_1$, where w_2 and w_1 refer to the widths of the flange and web, respectively (see Figure 4.1). The section is analyzed for instability using the finite strip method of Chapter 3. All component plate junctures are allowed to deflect, and the discretization consists of four finite strips for each flange and the web. Only buckling in a single longitudinal half-wave is considered.

The critical buckling stress f_{cr}, nondimensionalized with respect to Young's modulus E, is presented in Figure 4.1 as a function of the web aspect ratio L/w_1. For small L/w_1 ratios, less than about 2, the buckling

response is predominantly local, and the associated buckling mode is shown in the insert to Figure 3.1. Also, the minimum buckling coefficient K_{min} associated with $w_2/w_1 = 0.2$ in Figure 3.1 is approximately equal to the buckling coefficient associated with the critical stress of Figure 4.1 at $L/w_1 \simeq 1$. This indicates that overall buckling effects are negligible for small aspect ratios which is reinforced by inspection of the buckling mode. For larger aspect ratios $L/w_1 > 4$, the buckling response is predominantly flexural where the section translates about the weak axis with little or no local plate buckling. In this range the flexural buckling strength predicted by the finite strip method is in excellent agreement with that obtained from Euler's Equation 4.2.

$$f_{cr} = \pi^2 E/(L/r)^2 \qquad 4.2$$

where r is the minimum radius of gyration. In the intermediate range of $2 < L/w_1 < 4$, the buckling response is a mixture of local and flexural. However, this interaction is inconsequential because local buckling in a higher number of longitudinal half-waves, which is not considered in the analysis, would govern in this range of L/w_1.

For comparison the theoretical results of Wittrick and Williams [1971] are also shown in Figure 4.1. These results are in good agreement with the finite strip results, and any discrepancies are due to the different values of Poisson's ratio, μ, used in the respective analyses which are noted on the figure.

4.4 Post-Local and Overall Buckling Interaction

4.4.1 Q-Factor Method

The effect of local buckling in reducing column strength is accounted for in the AISI Specification [1980] by the Q-factor method (Winter [1970]).

Short, concentrically loaded, compression members which are not subject to local buckling fail by simple yielding at

$$P_u = AF_y \tag{4.3}$$

where P_u is the ultimate load, A the full cross-sectional area, and F_y the yield strength. However, when the member buckles locally, a reduced ultimate load is obtained, e.g.,

$$P_u = A_e F_y \tag{4.4}$$

where A_e is the effective area of the cross section (see Section 3.5.1). The ultimate load given by Equation 4.4 may be reinterpreted as the result of a reduced strength QF_y. Thus, from Equation 4.3,

$$P_u = A(QF_y) \tag{4.5}$$

where by definition Q is a factor less than unity (1) that accounts for the effects of local buckling. Equating Equations 4.4 and 4.5 yields

$$Q = A_e/A \tag{4.6}$$

From the above discussion it is seen that, for short compression members, the effects of local buckling on simple yielding may be accounted for through the use of a reduced stress QF_y. The effects of local buckling on other failure modes, such as flexural buckling in longer members, are handled similarly by simply replacing the yield stress in equations developed for compact sections (no local buckling) with the reduced stress QF_y.

One failure mode for a concentrically loaded compression member is flexural buckling. For this case the buckling stress f_f is predicted using the SSRC column curve (Johnston [1976], Winter [1970]). Thus

for $f_f > QF_y/2$ 4.7a

$$f_f = QF_y - (QF_y)^2/4f'_f \quad 4.7b$$

for $f_f < QF_y/2$ 4.7c

$$f_f = f'_f = \pi^2 E/(K_f L/r)^2 \quad 4.7d$$

where f'_f is the elastic Euler buckling stress, r the minimum radius of gyration, and K_f the column effective length factor, e.g., $K_f = 1$ for a column with simply supported ends. The buckling stress f_f of Equation 4.7b is for inelastic buckling. Actually, this stress, Equation 4.7b, with $Q = 1$ was derived for hot-rolled members to approximate the effects of residual stresses due to cooling and gradual yielding behavior. These effects are also present in cold-formed members; however the residual stresses are now due to the forming process.

Other failure modes for concentrically loaded compression members are torsional and torsional-flexural. These modes are especially critical for thin-walled sections due to their open cross sections. However, because the present study is concerned with singly-symmetric sections, where the shear center and centroid do not coincide, only torsional-flexural buckling is considered. For this case, the torsional-flexural buckling stress f_{tfo} is predicted by (Chajes et. al. [1966], Winter [1970])

for $f_{tfo} > QF_y/2$ 4.8a

$$f_{tfo} = QF_y - (QF_y)^2/4f'_{tfo} \quad 4.8b$$

for $f_{tfo} < QF_y/2$ 4.8c

$$f_{tfo} = f'_{tfo} \quad 4.8d$$

where f'_{tfo} is the elastic torsional-flexural stress

$$f'_{tfo} = \frac{1}{2\beta}[(f'_{fx} + f'_t) - ((f'_{fx} + f'_t)^2 - 4\beta f'_{fx} f'_t)^{\frac{1}{2}})] \qquad 4.9$$

The elastic torsional buckling stress f'_t is given by

$$f'_t = [GJ + \pi^2 EC_w/(K_t L)^2]/Ar_o^2 \qquad 4.10$$

where G is the shear modulus, J St. Venant's torsion constant, C_w torsional warping constant, K_t effective length factor for torsion, and r_o the polar radius of gyration. Also,

$$\beta = 1 - (x_o/r_o)^2 \qquad 4.11$$

where x_o defines the location of the shear center from the centroid (see Figure 4.2). Finally, the elastic flexural buckling stress f'_{fx}, about the x axis, follows from Equation 4.7d as

$$f'_{fx} = \pi^2 E/(K_{fx} L/r_x) \qquad 4.12$$

where K_{fx} is the x axis effective length factor and r_x the x axis radius of gyration. The definitions of the geometric parameters J, C_w, and etc., are contained in AISI [1971]. It is noted that the inelastic torsional-flexural buckling stress, Equation 4.8b, is approximated by a parabolic law which is identical to that employed for inelastic flexural buckling. Another point worth mentioning is that the Q-factor method for torsional buckling, Equation 4.8, actually results in a double counting of the local buckling effects. For instance, the local and torsional buckling stresses for a simply supported (longitudinal ends) equal leg angle or cruciform are identical (McGuire [1968]). For other shapes this effect is less pronounced, but it is still present (Winter [1970]).

4.4.2 Effective Section Method

DeWolf [1973], and later Kalyanaraman [1978], proposed treating the effects of local buckling in a more direct manner than is presently done in the AISI Specification [1980]. They proposed a modified SSRC method for flexural buckling and employed an effective width concept to account for local buckling. In this method the effective stress f_e is determined from

$$\text{for } f_e > F_y/2 \qquad 4.13a$$

$$f_e = F_y - F_y^2/4f'_e \qquad 4.13b$$

$$\text{for } f_e < F_y/2 \qquad 4.13c$$

$$f_e = f'_e = \pi^2 E/(K_f L/r_e)^2 \qquad 4.13d$$

where r_e is the radius of gyration for the effective section and f'_e the elastic flexural buckling stress. Since the effective stress f_e is dependent on the effective radius of gyration which is, in turn, dependent on the effective stress (see the next paragraph), an iterative procedure must be adopted to solve for the unknown stress f_e. It is noted that these authors also investigated a tangent modulus approach, e.g., Equation 4.13d with E replaced by the tangent modulus E_t. However, the approximation to the tangent modulus implied by Equation 4.13b provided very good correlation with experimental data.

DeWolf studied uniformly-compressed, doubly-symmetric, built-up, box sections and calculated the effective width w_e of the stiffened compression elements from Equation 2.9,

$$w_e/w = \sqrt{f_{cr}/f_e}\ (1.0 - 0.218\sqrt{f_{cr}/f_e}) \qquad 2.9$$

which is dependent on the effective or edge stress level f_e. The effective width was distributed symmetrically as in Figure 2.1.

4.5 Post-Local Buckling and Beam-Column Behavior

Local buckling also affects the strength of eccentrically loaded thin-walled members. For singly-symmetric open shapes, such as lipped channels, which are bent in the plane of symmetry (about the y axis in Figure 4.2), failure may occur by flexural yielding or by torsional-flexural buckling. Methods to treat this special case are discussed below. To simplify matters it is assumed that the member is bent in single curvature by equal end moments.

4.5.1 Current Analysis Methods

In the AISI Specification [1980] yielding, in singly-symmetric shapes, by combined compression and bending is dealt with by the normal interaction formula

$$f_a/f_{ua} + f_b/f_{ub}(1 - f_a/f'_f) \leq 1.0 \qquad 4.14$$

where the axial stress f_a is equal to the axial load P divided by the gross area, P/A; the maximum bending stress f_b equals the bending moment M divided by the section modulus S_e, $f_b = M/S_e$; f_{ua} is the ultimate stress under concentric loading; and f_{ub} is the ultimate stress under bending only. Also the term,

$$1/(1 - f_a/f'_f) \qquad 4.15$$

where f'_f is the Euler stress of Equation 4.7d, represents the approximate magnification factor and accounts for the additional moment resulting from the applied load and the deflection of the beam-column.

The effects of local buckling are included in Equation 4.14 by a "mixed method." For the axial response they are accounted for by the

Q-factor method, and for bending they are accounted for through an effective section. Therefore, the ultimate stress f_{ua} is determined from Equation 4.7 where failure can occur by flexural buckling about either the y or x axes. For lipped channels the ultimate bending stress f_{ub} is taken equal to the yield stress, F_y, where lateral buckling is excluded, and the local buckling effects are treated using an effective section from which the effective section modulus S_e is determined. It is important to note that the present specification (AISI [1980]) only contains methods for determining the effective widths of uniformly compressed elements. Therefore, situations which arise in beam-columns, where the element is subjected to a stress gradient (see Section 2.2.2), can not be handled in a consistent manner.

A singly-symmetric shape with eccentric loading about the y axis (see Figure 4.2) can also fail suddenly by torsional-flexural buckling. Thus, for a given section, both this failure mode and flexural yielding, by Equation 4.14, must be examined to see which is critical. Generally, flexural yielding will govern if the axial load P is applied on the shear center side of the centroid, e.g., e is positive in Figure 4.2. Therefore, this case is not considered here, and reference is made to Pekoz [1969] and Yu [1973].

For loads applied on the side of the centroid opposite the shear center, the torsional-flexural buckling stress f_{tf} is calculated from

for $f_{tf} > QF_y/2$ 4.16a

$$f_{tf} = QF_y - (QF_y)^2/4f'_{tf} \quad 4.16b$$

for $f_{tf} < QF_y/2$ 4.16c

$$f_{tf} = f'_{tf} \quad 4.16d$$

The elastic torsional-flexural buckling stress f'_{tf} is determined from the interaction formula

$$f'_{tf}/f'_{tfo} + f'_{btf}/f'_{bt}(1 - f'_{tf}/f'_{fy}) = 1.0 \qquad 4.17$$

where f'_{tfo} is given by Equation 4.9, f'_{btf} is the maximum compression stress caused by f'_{tf}, f'_{fy} is calculated from Equation 4.7d with $r = r_y$, and f'_{bt} is the maximum compressive stress caused by the elastic critical moment, M'_t.

$$M'_t = -Af'_{fx}[j - (j^2 + r_o^2(f'_t/f'_{fx}))^{\frac{1}{2}}] \qquad 4.18$$

where j is a geometrical parameter defined in AISI [1980] or Yu [1973], and other parameters have been defined previously.

Again, from Equation 4.16b, inelastic buckling is approximated by a parabolic equation, and the Q-factor method is employed to account for local buckling. Also, the moment magnification effects due to the stress (load) f'_{tf} are included in Equation 4.17.

As is evident from the above discussion, the prediction of the torsional-flexural buckling stress is quite complex. Nevertheless the method reviewed has proved successful in representing this phenomenon (Pekoz [1969]). This statement applies mainly to sections when local buckling is not present. When local buckling is present, i.e., when $Q < 1$; very little, if any, experimental data exists to support the method. This deficiency also applies to the Q-factor method for predicting torsional-flexural buckling of concentrically loaded members (Section 4.4.1).

4.5.2 Proposed Analysis Method

In this section an analysis method is proposed for predicting the sub-ultimate behavior and strength of thin-walled, singly-symmetric,

lipped channel columns and beam-columns. Following work by DeWolf [1973] and Thomasson [1978], an effective section is employed to account for local buckling of the plate elements.

The method is based on the following assumptions: (1) elementary beam theory (Timoshenko [1955]) is valid for the locally buckled section; (2) bending is about the y axis only (see Figure 4.2); (3) the lip or edge stiffener is supported against local-torsional buckling (see Section 3.3.2 and Figure 3.5c) by some external constraint, e.g., this constraint could be provided by intermediate lateral (y direction) braces placed between the lips or by connection of the lips to wall sheathing; (4) the effective section is determined from the maximum edge stress levels at the midheight of the column and is assumed constant along the length; and (5) the maximum load resistance is reached when the maximum strain reaches yield or when unstable equilibrium is experienced, i.e., when the load decreases with increasing strain.

Assumption (3) eliminates dependence of the analysis method on requirements associated with edge stiffeners and increases the applicability of the method to other thin-walled shapes such as doubly-symmetric box sections. This assumption is relaxed in Chapter 6 where additional requirements are placed on the method for analyzing lipped channels.

The effective section of Figure 4.2 is used to account for local buckling. Because bending is about the y axis, the web and lips are uniformly compressed at stress levels f_1 and f_2, respectively. The effective width of the lips, w_{3e}, follows from Equation 3.24 as

$$w_{3e}/t = 163.3\sqrt{K_3/f_2}\,[1.0 - 35.6\sqrt{K_3/f_2}/(w_3/t)] \qquad 4.19$$

where the buckling coefficient for the lip, K_3, is taken as its simply supported value of 0.425. The effective width for the web, w_{1e}, follows from the sub-ultimate (and ultimate) approach of Chapter 2, i.e.,

$$w_{1e}/w_1 = A/\lambda^2 + B/\lambda + C + D\lambda \qquad 4.20$$

where $\lambda = (f_1/f_{cr1})^{\frac{1}{2}}$ and the constants A-D are defined by Equations 2.44 through 2.47. Ignoring local buckling interaction, the critical stress f_{cr1} is taken as its simply supported value, e.g., Equation 2.4 with $K_1 = 4$. Equations 2.4 and 2.44 through 2.47 are all referenced to the web element.

The effective widths for the flanges, w_{2e1} and w_{2e2}, are slightly more complicated to define. In general, these are determined from the approach for eccentrically compressed stiffened elements covered in Section 2.2.2. Thus, for the general edge stresses $f_i > f_j > 0$ (Figure 2.4a)

$$w_{2ei} = w_{2e}/2 \qquad 4.21$$

where w_{2e} is defined by Equation 3.24 with f_e, K, and w replaced by f_i, $K_2 = 4$, and w_2, respectively. The expression for the other portion of the effective width w_{2ej} is

$$w_{2ej} = w_{2ei}(1.5 - 0.5f_j/f_i) \qquad 4.22$$

For the case of $f_j < 0$ (Figure 2.4b) the following expression for w_{2ej} is valid

$$w_{2ej} = 1.5w_{2ei} + w_o \qquad 4.23$$

The loading state represented in Figure 4.2 is such that the maximum compressive stress occurs along side one (1). Therefore, the portion of the effective width closer to the web is defined by Equation 4.21 with i = 1, and the other portion is defined from either Equations 4.22 or 4.23 with j = 2, depending on whether the stress level f_2 is compressive ($f_2 > 0$) or tensile.

For a loading state where the maximum compressive stress occurs along side two (2), the effective widths for the flange are calculated as described above, but the reference axes are reversed, e.g., i = 2 and j = 1.

The stresses f_k at the midheight of the beam-column are determined from the usual formulas (Timoshenko [1955]) supplanted with the effective section properties.

$$f_k = P/A_e \pm (Pe_e c_k/I_e) \sec (pL/2) \quad . \; . \; . \quad k = 1,2 \qquad 4.24$$

where k = 1 defines the stress in the web (along reference line 1) and k = 2 defines the stress in the lips; c_k defines the appropriate distance from the effective centroid, eff. c.g., or neutral axis to the web or lips; e_e is the eccentricity of loading with respect to the effective centroid, e_e is positive as shown in Figure 4.2; A_e and I_e are the effective area and moment of inertia, respectively; L is the length of the beam-column; and $p = (P/EI_e)^{\frac{1}{2}}$. In writing Equation 4.24, it is assumed that the effective section is constant along the length as determined from f_k. Because of this dependence and the basic form of Equation 4.24, the two equations generated by Equation 4.24 are inherently nonlinear in the three variables P, f_1, and f_2.

In order to obtain a solution to Equation 4.24, it is necessary to make several behavioral assumptions with respect to the load-strain response. In this discussion it is assumed that the web dominates the local buckling response; therefore the effective centroid is assumed to locate at a position to the right (positive x direction in Figure 4.2) of the gross centroid. Although this assumption is not

strictly necessary, it simplifies matters and covers most practical thin-walled applications. Accordingly the load-strain response is separated into three separate cases depending on the location of the applied load (see Figure 4.3). If the eccentricity e, referenced to the gross centroid, c.g., is positive (negative x direction in Figure 4.2), then the strain ε_1 along reference axis one (1) increases continually with load until failure at $\varepsilon_1 = \varepsilon_y$ as shown in Figure 4.3a. Conversely, if the eccentricity e is negative and has an absolute value greater than the parameter x_y, which is defined below, then the strain ε_2 increases continually with load (see Figure 4.3c). In this case, the strain ε_2 is always greater than ε_1. The characteristic parameter x_y shown in Figure 4.3c is defined as the distance between the gross centroid and the effective centroid for the section under a uniform compressive stress at yield. Because the stress levels are known, e.g., $f_1 = f_2 = F_y$, this latter location may be calculated directly from the corresponding effective section.

The remaining case covers eccentricities in the range of $|e| < x_y$ where e is negative (see Figure 4.3b). For this case, the possibility of a strain reversal for ε_2 is admitted. One possible load-strain curve is shown in the center of Figure 4.3b where a strain reversal occurs before the uniform compressive state, at $\varepsilon_1 = \varepsilon_2 = \bar{\varepsilon}$, is reached. Also, it may occur that ε_2 does not reverse before reaching $\bar{\varepsilon}$ which is not shown in the figure. The ultimate load capacity is reached when either edge strain, ε_1 or ε_2, reaches yield or when elastic unloading is encountered.

An incremental-iterative algorithm is employed to solve Equation 4.24 which allows the complete load-strain history to be traced. The solutions for load eccentricities shown in Figures 4.3a and 4.3c are straightforward and are discussed first. In general, the larger strain is chosen as the incremental strain, which is indicated by arrows in the figures. This strain is increased continuously in strain increments corresponding to a stress of one (1) ksi. It is noted that the possibility of a strain reversal for the smaller strain precludes it from being used as the incremental strain. Then, for a fixed total level for the incremental strain, the remaining unknown strain (stress) is calculated using an iterative procedure based on one of the equations generated from Equation 4.24. The associated load level P is determined from the other equation generated from Equation 4.24 using the secant method (Hornbeck [1975]).

The solution for load eccentricities in the range indicated in Figure 4.3b are obtained in a similar manner. Initially, the larger strain ε_2 is chosen as the incremental strain. Then at $\varepsilon_2 = \bar{\varepsilon}$, which is defined below, the incremental strain is switched to ε_1. The parameter $\bar{\varepsilon}$ defines the strain level that is associated with uniform compression, $\varepsilon_1 = \varepsilon_2 = \bar{\varepsilon}$, and is solved for using a bisection routine (Hornbeck [1975]). The switching of the incremental strain is necessary because of the possibility of a strain reversal for ε_2.

Once convergence is obtained in the iteration loop, for a fixed incremental strain, the associated lateral deflection Δ at the midheight of the beam-column is calculated from

$$\Delta = e_e[1 - \cos(pL/2)]/\cos(pL/2) \qquad 4.25$$

All calculations are performed in double precision due to the sensitivity of the algorithm to small changes in the effective section. Further, a relative error tolerance of 1×10^{-6} is used in the iteration loop.

Typical results predicted from the above analysis method are presented and are discussed in the remainder of this section. The following two lipped channel sections are analyzed (refer to Figure 4.2).

	CLC/AV 120x60	CLC/AV 180x60
w_1/t	123.2	186.1
w_2/t	60.4	60.7
w_3/t	11.5	11.8
OR (in.)	0.163	0.158
t (in.)	0.047	0.047
L (in.)	75.23	95.07
F_y (ksi)	32.06	33.70

where OR refers to the outside radius of the corners.

The variation of the ultimate strength, P_u, with eccentricity, e, is presented in Figure 4.4 for CLC/AV 120x60. In general, the asymmetrical response is due to the asymmetry of the lipped channel. Above a limiting eccentricity of about $e = -0.3^*$, failure is predicted by flexural yielding at reference axis one (1), i.e., $\varepsilon_1 = \varepsilon_y$. A positive lateral deflection Δ is associated with eccentricities in this range. Below the limiting eccentricity, failure is predicted by flexural yielding at axis two (2) and negative lateral deflections Δ are experienced. It is interesting to note that the ultimate load $\overline{P}$, associated with a uniform stress at yield, i.e., with $\varepsilon_1 = \varepsilon_2 = \varepsilon_y$, is never reached due to yielding along side two

*inches.

(2). Also, an extreme sensitivity to eccentricity is experienced near the peak of the response, predicted by Equation 4.24, where small changes in eccentricity produce significant changes in behavior and ultimate load.

As shown in Figure 4.4, it is possible to increase the strength; relative to the strength associated with a concentrically loaded section, i.e., with e = 0; by loading the section within a certain range of negative eccentricities. However, this increased strength also increases the possibility of other failure modes, such as flexural or torsional-flexural buckling, which have to be considered. To investigate this aspect, the flexural buckling load P_e is calculated from Equation 4.13 for buckling about the y axis with simply supported ends, and the torsional-flexural buckling load P_{tf} is calculated from Equation 4.16 for torsionally and flexurally (x axis) fixed end conditions. (The specific end conditions employed here agree with the experimental application considered in Chapter 5. Also the flexural buckling load was determined from the modified SSRC method of Equation 4.13 because of its consistency with the effective section method of Equation 4.24. Comparisons of these and other methods discussed in this chapter with experimental results are included in Chapter 6.) A conservative approach is adopted to calculate the loads P_e and P_{tf}; the effective section properties and the Q-factor are assumed constant at the values computed for a section subjected to a uniform compressive stress at yield. For a certain range of negative eccentricities (Figure 4.4), the torsional-flexural buckling controls over both flexural buckling and flexural yielding and, therefore, limits the strength.

The sub-ultimate response predicted from Equations 4.24 is considered next. In Figure 4.5, the axial load is plotted as a function of the lateral deflection Δ, Equation 4.25, for various eccentricities (e).

Initially, at low stress levels, the concentrically loaded lipped channel (e = 0) behaves as a normal column without out-of-plane deflection. Then, after local buckling, the centroid shifts to an effective location which induces a moment and corresponding out-of-plane deflection. Hence, local buckling transforms the behavior from pure axial to combined bending and axial (beam-column) behavior. This mode of action is not recognized in design specifications that apply the Q-factor method to singly-symmetric sections for predicting flexural buckling, e.g., Equation 4.7.

The behavior for other eccentricities, i.e., for $e \neq 0$, is similar; however it starts out in the beam-column mode. For example, at e = -0.295*, the lipped channel deflects initially in the negative direction (Figure 4.5). Then, at higher load levels, the deflection reverses direction due to the effects of local buckling. This reduces and eventually changes the sign of the effective eccentricity. Torsional-flexural buckling prevents the section from returning to its undeflected position.

The load-edge strain response associated with the various eccentricities considered in Figure 4.5 is presented in Figure 4.6. The response is highly nonlinear and dependent on the position of the axial load. For eccentricities e greater and smaller than about -0.295*, the ultimate load is controlled by yielding at reference axes one (1) and two (2), respectively. At e = -0.295*, the strain ε_2 reverses just prior to yielding, and the ultimate load is controlled by $\varepsilon_1 = \varepsilon_y$, without considering torsional-flexural buckling. However, for slightly smaller eccentricities, i.e., e < -0.295*, the strain ε_2 controls which causes the sensitivity to eccentricity noted earlier. Also, in the range of e < -0.295*, the post-buckling response of the web is important, even though $\varepsilon_1 < \varepsilon_y$, because the web has a relatively large influence on the effective section.

*inches.

The second section, CLC/AV 180x60, which is defined subsequent to Equation 4.25, is analyzed next, and the variation of ultimate strength with eccentricity is presesnted in Figure 4.7. A major difference between the response predicted for this section and that discussed previously for CLC/AV 120x60 (Figure 4.4) is that the former is prone to an elastic failure mode over a certain range of negative eccentricities. The response indicated in Figure 4.8 is representative of this mode of failure; for example, subsequent to reaching ultimate the load decreases to the value P_y which is the load at initiation of yielding. Actually, for the specific eccentricity considered in Figure 4.8, the strength is limited by inelastic flexural buckling at the load P_e, but this is irrelevant to the present discussion.

Extensive calculations, which are not presented here, indicate that the elastic failure noted above is caused by interaction between local and overall buckling. Typically, elastic failure commences when the stress level in the web, reference axis one (1), is within about 20% of yielding. Consequently, a small post-local buckling tangent stiffness is associated with the web, e.g., this is illustrated in the advanced stages of the response predicted from Equation 2.38 in Figure 2.11a. At the same time; overall buckling, or beam-column action, affects the system through its effect on the bending moment. And when elastic failure occurs, typical values for the parameter pL/2 of the moment magnification factor sec(pL/2) of Equation 4.24 range from about $\pi/2.9$ to $\pi/2.6$. Since a value for pL/2 of $\pi/2$ is associated with elastic flexural buckling, the beam-column effect is strongly apparent. Individually these two effects - local buckling and beam-column moment maginfication - produce stable response, but when combined they interact to produce an unstable response of the type shown in Figure 4.8. Finally, it is noted that Thomasson [1978] has

observed analytically a similar elastic failure mode for relatively slender, concentrically loaded, lipped channel, long columns.

4.6 Summary

The problem of local and overall buckling interaction was studied in this chapter. A thorough survey of the available literature revealed that the effects of local buckling on overall buckling were treated by a variety of methods, of which the effective section method was the most widely adopted. Also, the survey revealed that, in certain circumstances, local and overall buckling of thin-walled sections interact to produce an imperfection sensitivity, especially when the local and overall buckling loads are nearly equal. This mode of behavior does not preclude the use of an effective section method to account for local and overall buckling interaction because such methods generally include indirect means which allow for the effects of imperfections in reducing the strength, e.g., through effective width equations and inelastic column curves. However, as discussed later (Chapter 6), the above mode of behavior must be recognized when applying these methods.

Then local and flexural bucking interaction in a uniformly compressed channel section was investigated using the finite strip method of Chapter 3, and good agreement was obtained with a known solution. However, because post-local buckling effects were not considered, such an analysis has limited practicality.

Next the Q-factor method was reviewed for treating post-local buckling interaction with flexural and torsional-flexural buckling. In addition, the modified SSRC method was discussed for predicting flexural buckling in locally buckled sections.

Finally, the effects of post-local buckling on beam-column behavior were studied. Current analysis methods for flexural yielding and torsional-flexural buckling were briefly reviewed. Then an analysis method was derived for predicting the sub-ultimate behavior and strength of singly-symmetric lipped channel columns and beam-columns. In this method, local buckling effects were accounted for through the use of an effective section. Also, an incremental-iterative algorithm was discussed to solve the governing beam column equations. The derived analysis method was then applied to two representative lipped channels in order to illustrate their behavior under concentric and eccentric loading. One of these sections was shown to be prone to an elastic failure due to the interaction between local and overall buckling.

Further evaluations and comparisons of the methods discussed in this chapter are postponed until Chapter 6.

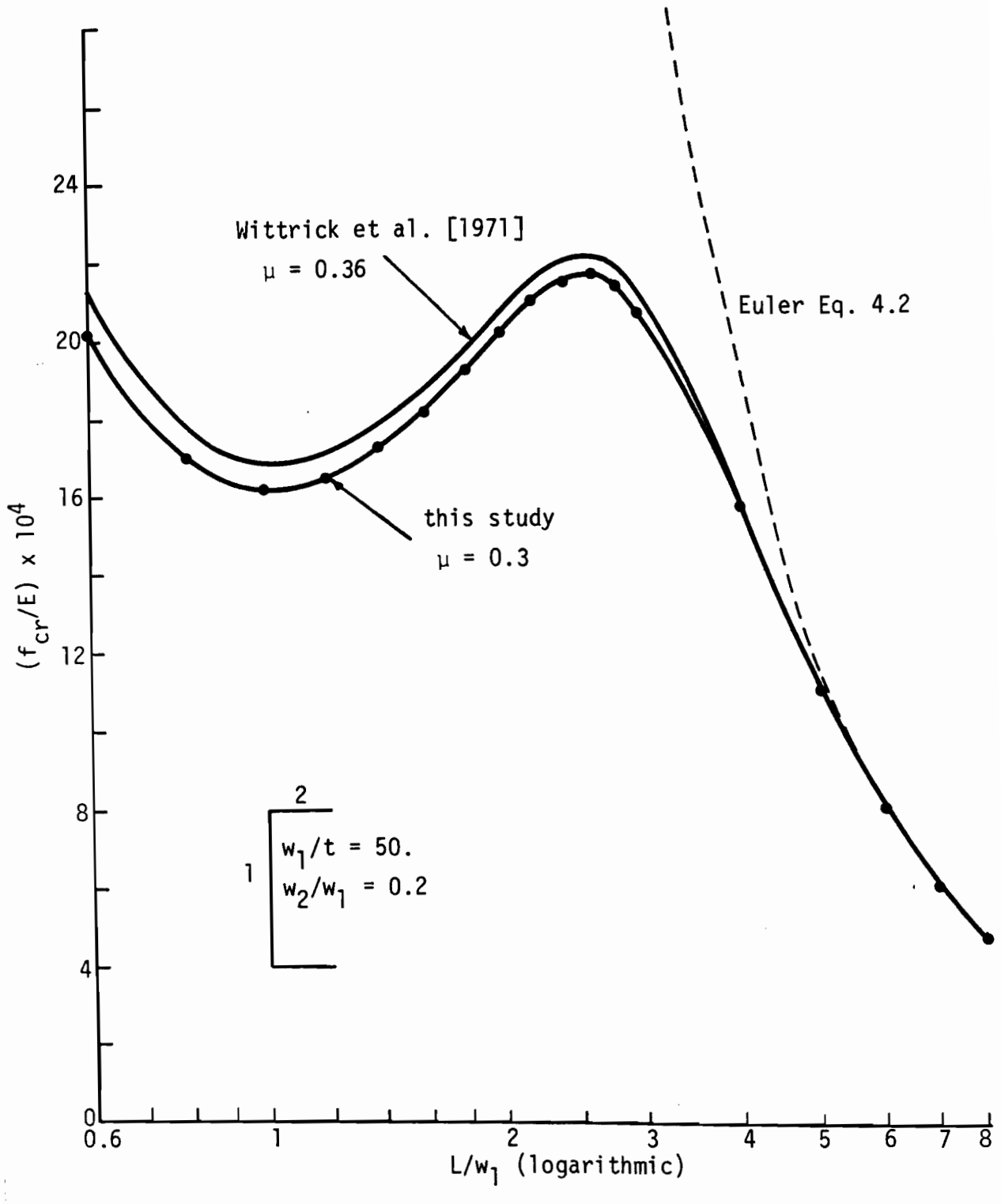

Figure 4.1 INTERACTION OF LOCAL AND OVERALL BUCKLING FOR A UNIFORMLY COMPRESSED CHANNEL

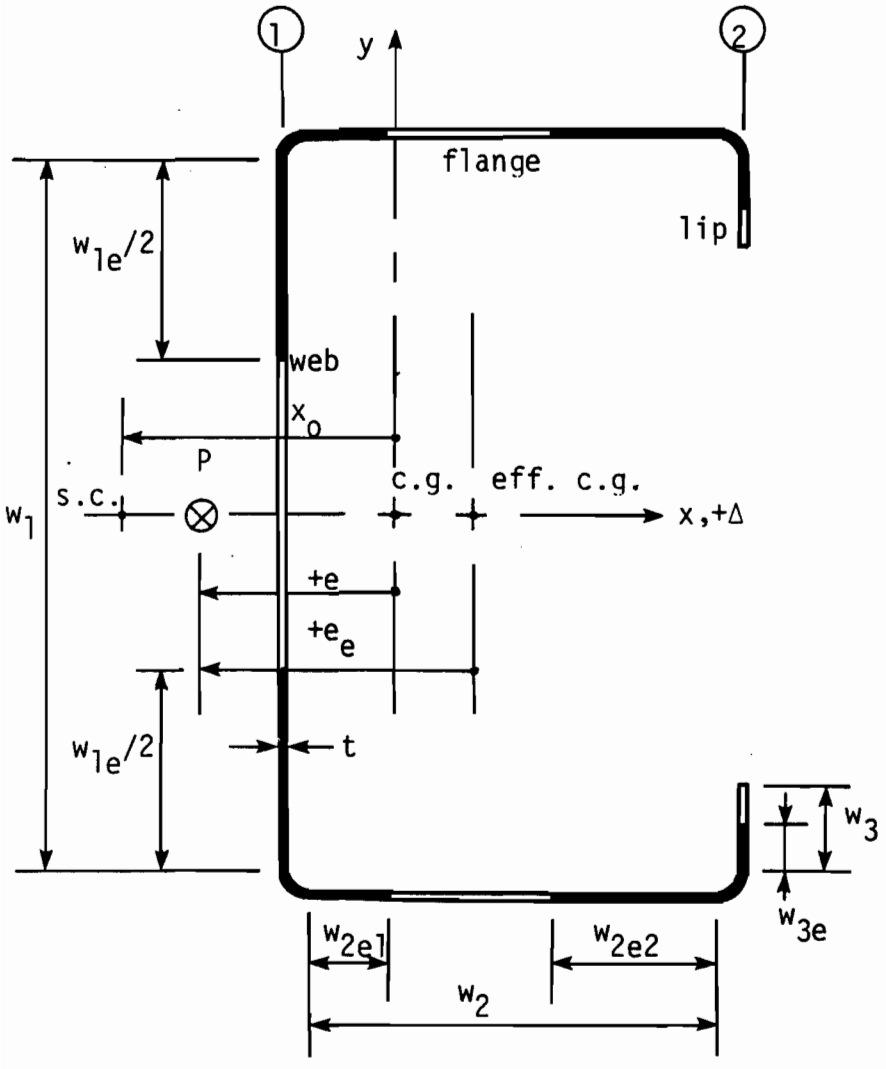

Figure 4.2 EFFECTIVE SECTION

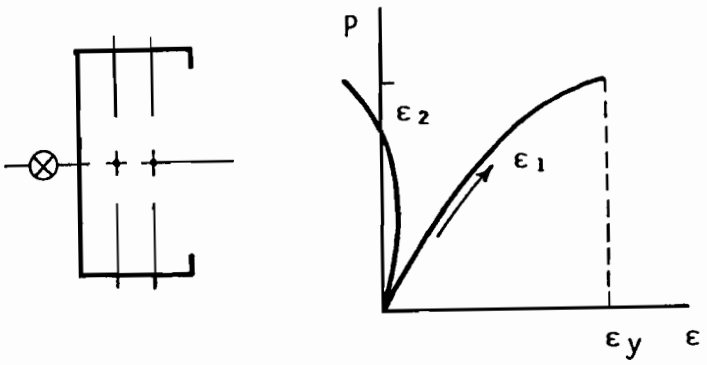

(a) e>o

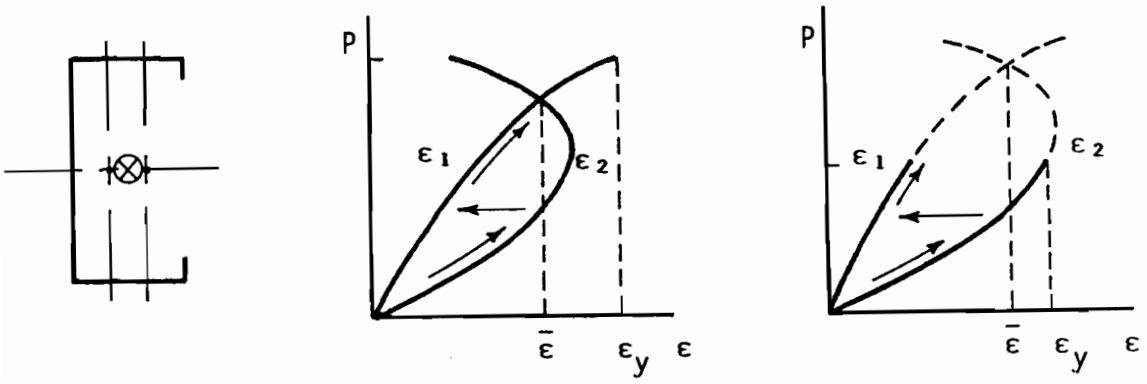

(b) e<o, $|e| < x_y$

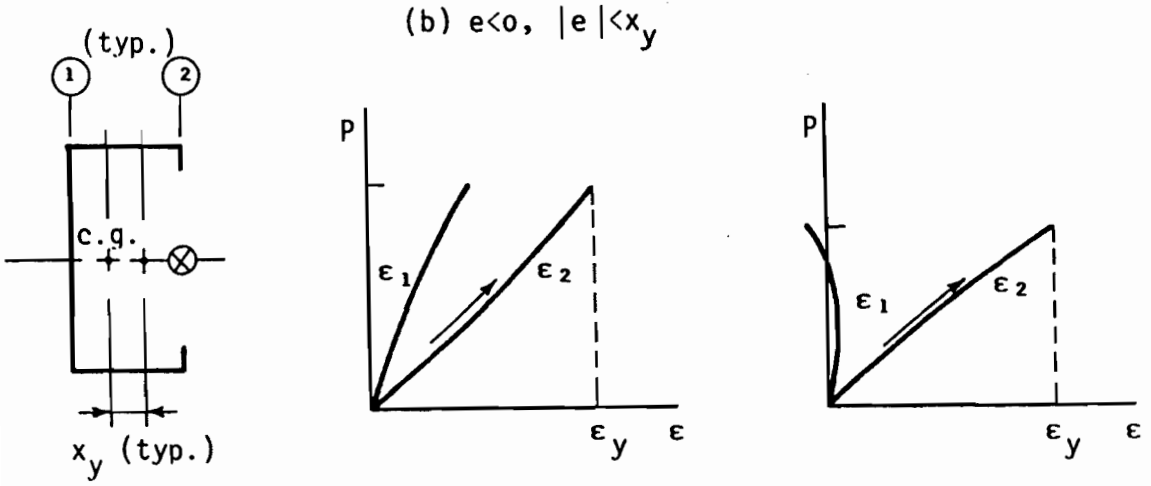

(c) e<o, $|e| > x_y$

Note: Refer to Fig. 4.2 for definition of e

Figure 4.3 BEHAVIORAL ASSUMPTIONS

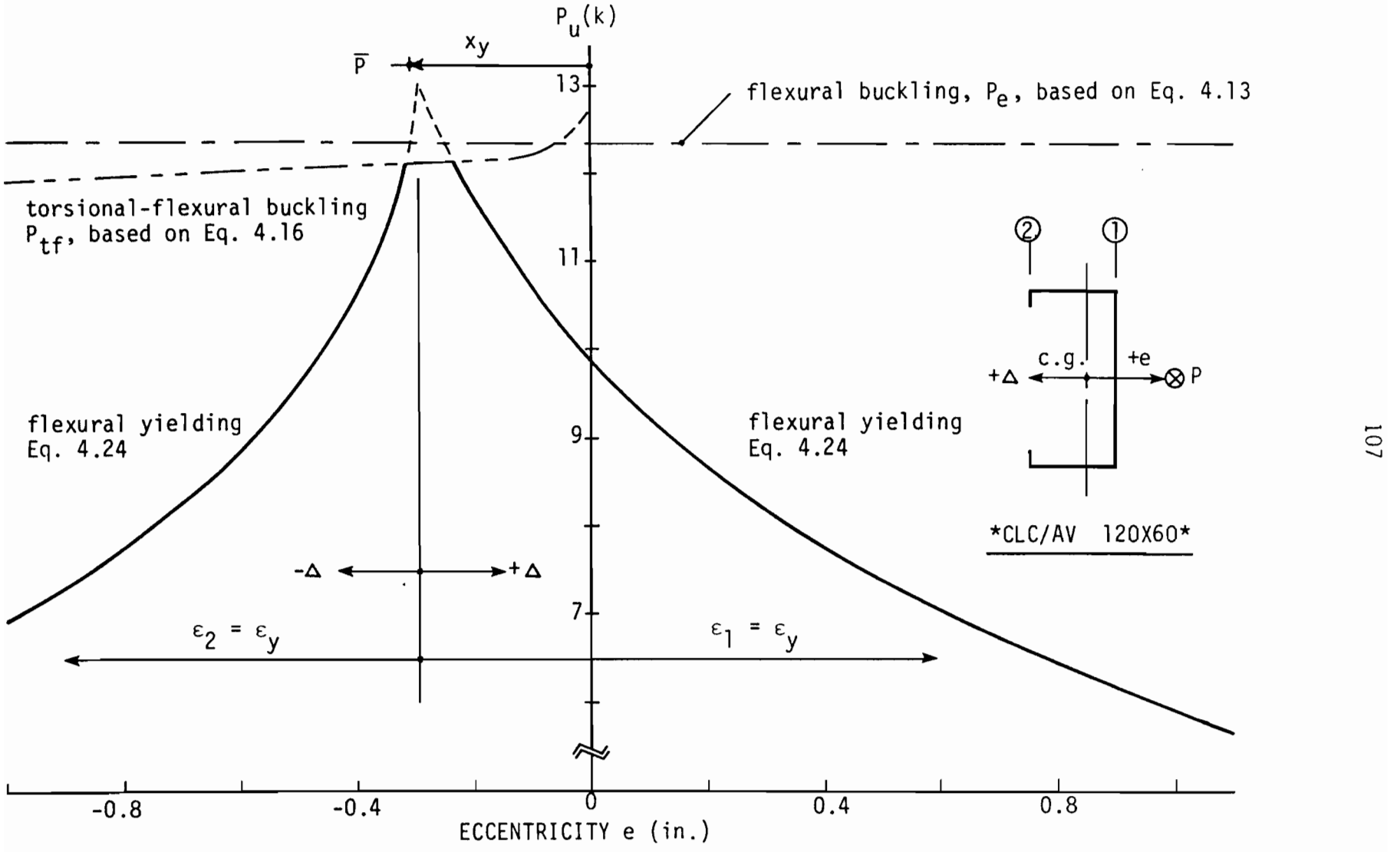

Figure 4.4 STRENGTH OF LIPPED CHANNEL BEAM-COLUMNS

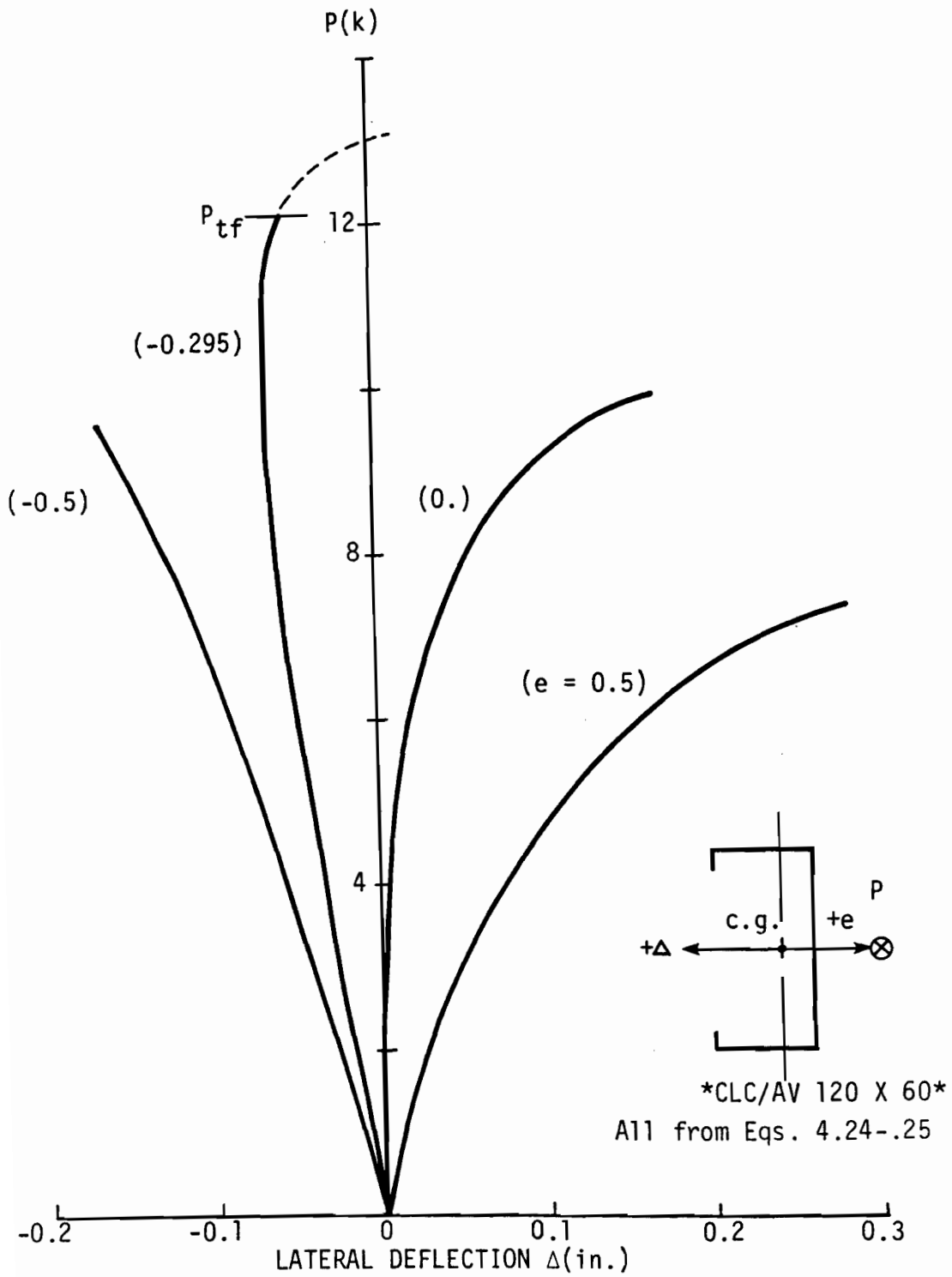

Figure 4.5 LOAD-DEFLECTION RESPONSE OF LIPPED CHANNEL BEAM-COLUMNS

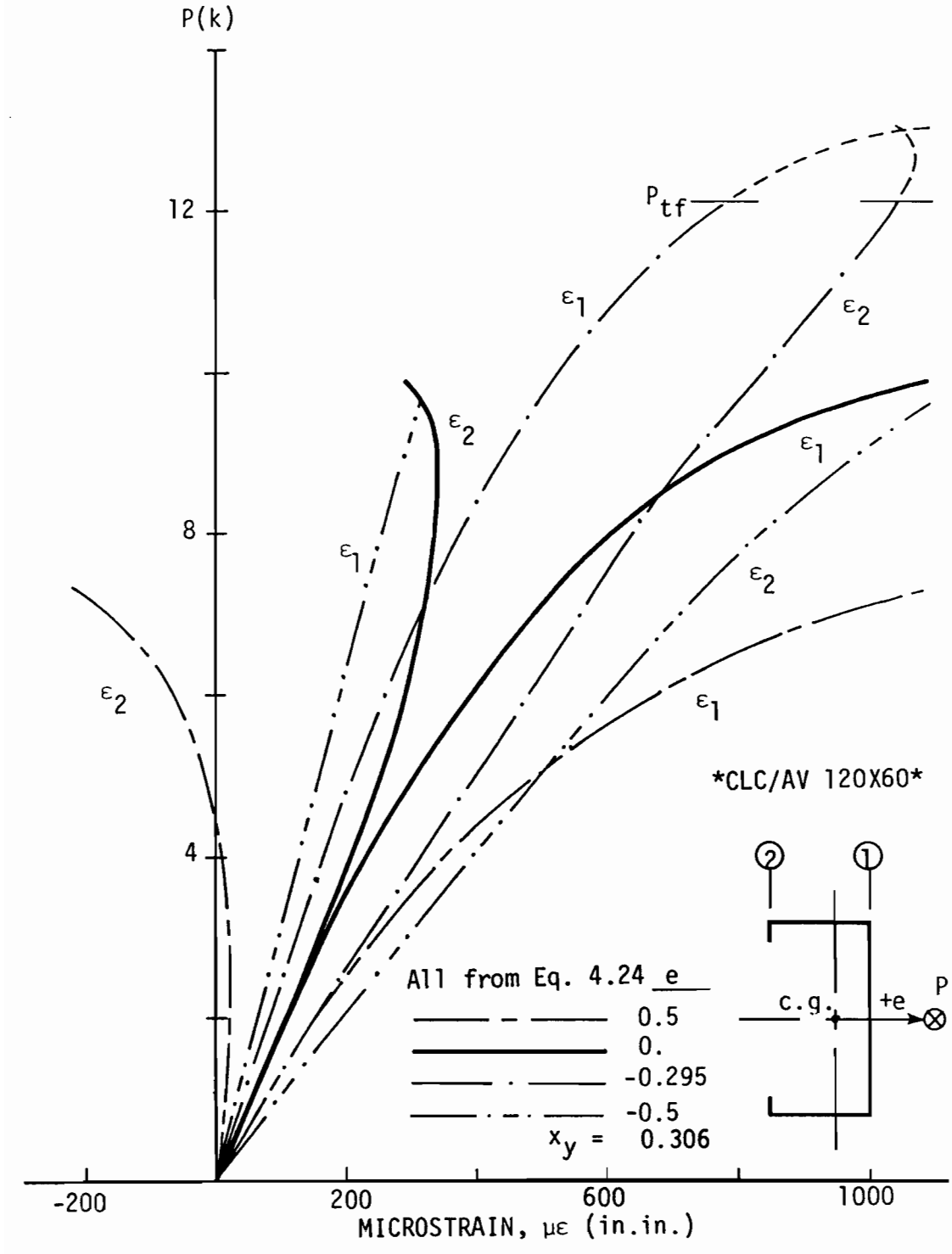

Figure 4.6 LOAD-STRAIN RESPONSE OF LIPPED CHANNEL BEAM-COLUMNS

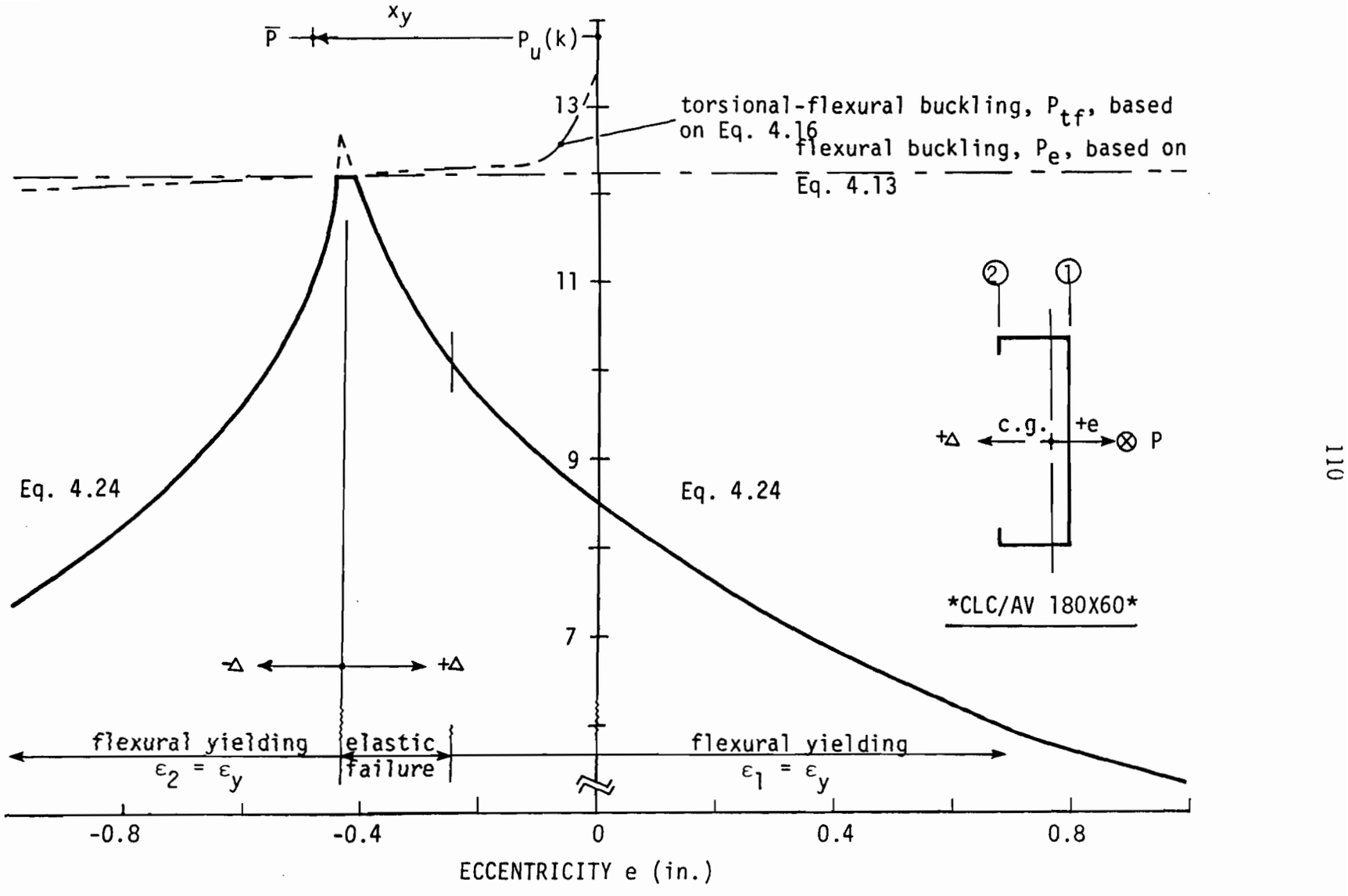

Figure 4.7 STRENGTH OF LIPPED CHANNEL BEAM-COLUMNS

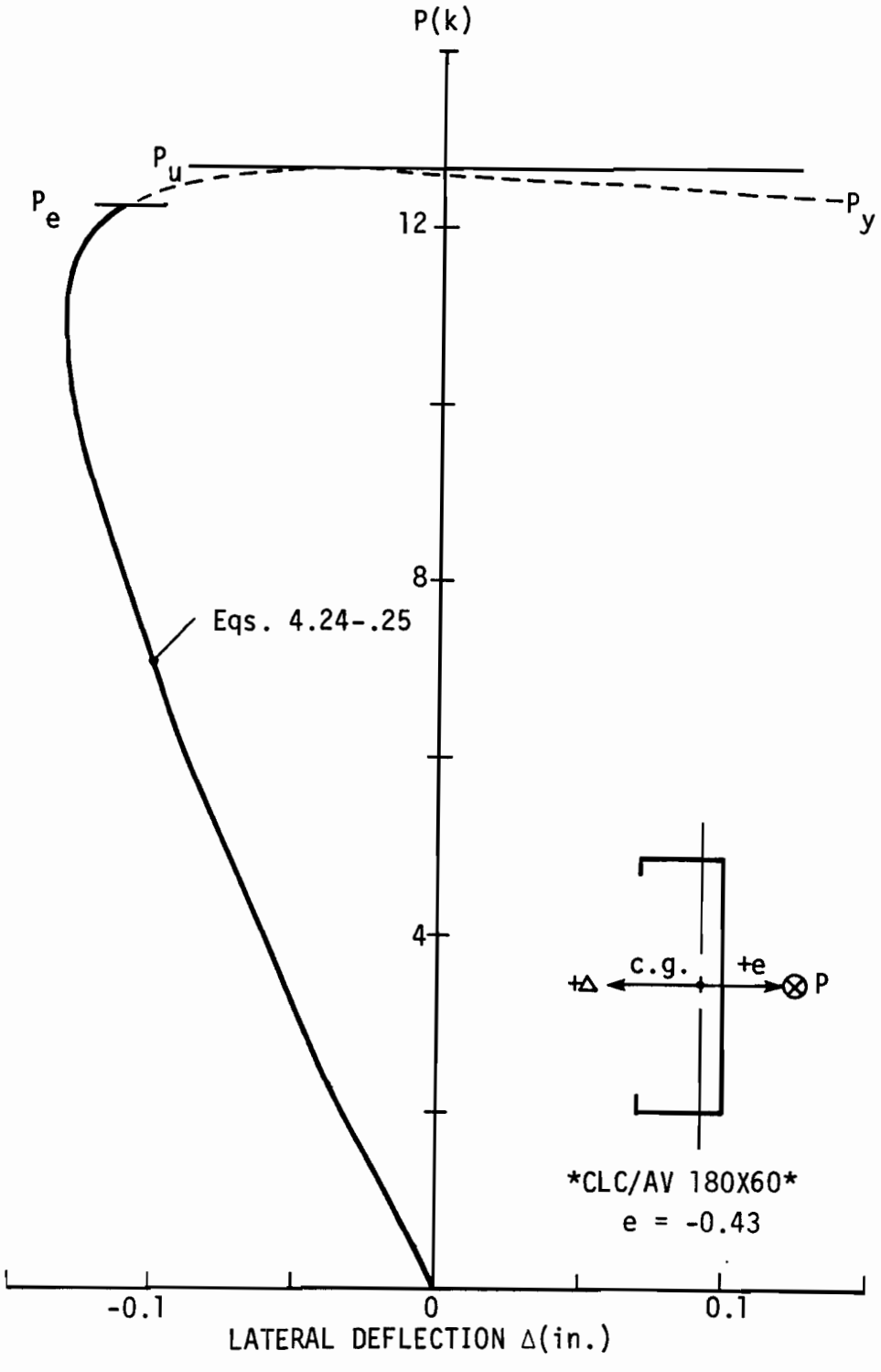

Figure 4.8 LOAD-DEFLECTION RESPONSE AND ELASTIC FAILURE

CHAPTER 5

EXPERIMENTAL INVESTIGATION

5.1 Introduction

The experimental investigation to study the influence of local buckling on the structural behavior and on the strength of cold-formed steel columns is discussed in this chapter. The investigation is divided into two major areas. One area deals with testing stub columns, which have small length-to-minimum radius of gyration ratios to preclude overall buckling effects. The primary objective of these tests is to provide quantitative information on local and post-local buckling interaction in structural sections. More specifically, lipped channels and (plain) channels are investigated, and the local buckling interaction is provided simply by varying, in a systematic manner, the cross-sectional dimensions of the sections.

The other area deals with long column tests. Typically the length is now increased to introduce overall modes and to allow interaction of local buckling and beam-column response. Singly-symmetric lipped channels of varying lengths are tested under concentric and eccentric loads.

5.2 Test Specimens

All test specimens were fabricated by press-braking thin sheets of 16 and 18 gage steel into the desired cross-sectional shapes (Yu [1973]). A local sheet metal shop was used for the fabrication, which was generally of good quality.

The cross sections and related parameters for the channel and lipped channel test specimens are defined in Figure 5.1. The web, flange, and lip are referenced by the subscripts 1, 2, and 3, respectively, and the flat widths and overall widths are labeled w_i and W_i ($i = 1,2,3$), respectively. Other information contained in this figure is discussed later.

The cross-sectional dimensions of the stub and long columns are reported in Tables 5.1 and 5.2, respectively. These were obtained from measurements taken at the two quarter-points, of the length, nearest the ends, and the results were then averaged. Thus, an effort was made to account for any lengthwise variation of the dimensions.

A special designation is used to identify each specimen, e.g., SLC/1 120x60. In this example, the "SLC" refers to a Stub (column) Lipped Channel, the "1" refers to an original cross section, and the "120x60" refers to the approximate web and flange width-to-thickness ratios, w_1/t and w_2/t, respectively. Other specimens use the following identifiers. "SC" and "CLC" refer to Stub (column) Channels and (long) Column Lipped Channels. A "2" refers to a duplicate specimen or to one having a different length.

All specimens with an integer designation are concentrically loaded, and those with a mixed number designation, e.g., "2.1", are eccentrically loaded about the y axis defined in Figure 5.1b. The specific eccentricities are presented later in this chapter.

Several different lipped channel cross sections were tested as stub columns. These included flange width-to-thickness ratios, w_2/t, ranging from 30 to about 90 and web width-to-thickness ratios, w_1/t, ranging from 60 to 360. Likewise, several channel cross sections were tested as stub

columns. Two specific w_2/t ratios of 30 and 60 were studied with w_1/t ratios ranging from 40 to 180.

Thus, a total of twelve (12) different lipped channel cross sections and eight (8) different channel cross sections were investigated, for a total of 36 stub columns, including duplicate specimens and those having a different length. This wide range of parameter variation was judged adequate for providing the quantitative information needed to study local buckling interaction in the specific structural sections under consideration.

For the long columns, which are set out in Table 5.2, five different lipped channel cross sections were investigated. The specific sections were chosen to match several of the stub columns under study. Various lengths and loading conditions, either concentric or eccentric, were considered for each section yielding a total of 22 long columns. Several sections employed braces or ties which were welded to the lips (see Figure 5.1 and Table 5.2). This extra support was provided to the flanges to study its influence on the behavior and strength of the section.

5.2.1 Test Specimen Design

The design of the stub columns consisted of choosing a length short enough to preclude the detrimental effects of overall buckling modes, but sufficiently long so as not to restrict the local buckling behavior. For this purpose the recommendations of Technical Memorandum No. 3 of the Structural Stability Research Council (SSRC), "Stub-Column Test Procedure," reprinted in Johnston [1976], were utilized. These stipulate a length less than twenty times the least radius of gyration, $L < 20r_{min}$, but greater than three times the largest dimension of the cross section,

$L > 3w_{max}$. In most cases, it was possible to choose a length to satisfy these requirements, e.g., see the L/w_{max} and L/r_{min} ratios in Table 5.6. However, in a few cases, a length of $3w_{max}$ proved larger than $20r_{min}$; therefore, two specimens were designed with lengths equal to approximately $20r_{min}$ and $3w_{max}$.

The design of the long columns consisted of choosing the cross-sectional dimensions and length such that weak axis flexural buckling was the governing overall mode. This involved preventing torsional-flexural buckling for the singly symmetric, open shaped sections. For these purposes, the procedures of Chapter 4 were employed, e.g., Equations 4.13 and 4.16.

Finally, the edge stiffeners or lips of the lipped channels were proportioned, in most cases, to meet the stiffener requirements proposed by Desmond [1978a,b] (see Section 3.4). Further discussion of the edge stiffeners is postponed until Chapter 6, where all experimental results are critically evaluated.

5.3 Material Properties

The material properties of the specimens were determined from standard tensile tests (ASTM [1975]) of at least three coupons. The coupons were cut from the virgin steel sheets, before fabrication of the specimens, and were aligned parallel to the rolling direction of the sheets. This direction was also parallel to the forming direction of the sections.

The average material properties are presented in Table 5.3. In most cases the material exhibited sharp yielding behavior; however, there were two exceptions to this. Material VII had a low proportional limit of approximately 0.6 times the yield stress but had an extended yield plateau.

And material XXII exhibited gradual yielding behavior. In both cases the 0.2% offset method was used to define the yield stress.

The modulus of elasticity, E, was determined graphically from load-strain plots for all tensile tests. These plots were automatically produced by an extensometer and chart recorder. The mean value of E for 59 sharp yielding tests is 29.29×10^3 ksi with a standard deviation of 3.65×10^3 ksi. This result is slightly lower than the mean value of $E = 30.0 \times 10^3$ ksi reported by Venkataramaiah et. al. [1980] for 63 tensile tests and the mean value of $E = 31.3 \times 10^3$ ksi reported by Thomasson [1978] for 36 tests. As a result, the comparable value of $E = 29.5 \times 10^3$ ksi recommended by the AISI Specification [1980] is assumed valid for use in this study.

Further, it is assumed that the tensile yield strength provides a conservative estimate of the compressive strength and that the cold working effects at the corners of the section are negligible when describing the material properties of the overall cross section.

5.4 Initial Imperfections

The behavior and strength of thin compression elements (plates) and columns are clearly influenced by the presence of initial imperfections (Yamaki [1959], Timoshenko and Gere [1961]). Therefore, in this study, the initial imperfections were measured systematically.

Two types of imperfection are of interest: local and overall. Local imperfections are defined as the deviations from flatness of the various plate elements and as the deviations from perfect cross-sectional geometry (fabrication type). Overall imperfections refer to the deviations from straightness of the column.

5.4.1 Local Initial Imperfection of Stub Columns

The devices used to measure local initial imperfection in stub columns are shown in Figure 5.2. The relatively simple device number one (1) determines the out-of-flatness of stiffened and edge-stiffened elements, as referenced to their longitudinal edges. It consists of a ground bar, and fixed and movable support points, where the latter are established at a constant distance from the top of the bar. The imperfection is calculated based on measurements taken with (see figure) and without the device using an independent 0.001-inch dial gage.

A slightly more complicated device number two (2), in Figure 5.2, is used to measure the fabrication type of local imperfection, which is specialized here to mean the deviations of the flange element from a right angle established off of the corners of the web. The major difference of this device is that it incorporates a perfectly square, ground bar. Again, the imperfection is calculated from 0.001-inch dial gage measurements taken with (see figure) and without the device.

The sources of error associated with the local initial imperfection measuring devices are an imperfection in the device itself, e.g., out-of-flatness of the ground bar; error in placement; and dial gage error. Therefore, the accuracy of measurement is of the order of a few thousandths of an inch.

It is mentioned that the devices of Figure 5.2 are not capable of detecting any overall twist of the section, which was observed visually in several of the specimens.

The maximum amplitudes of local initial imperfections, Δ^{max}, and associated imperfection-to-thickness ratios, Δ^{max}/t, are reported in Table 5.4 for a wide sampling of the specimens. These maximums were

determined from measurements taken at discrete points spaced typically about an inch apart along the length. The initial imperfection at the centerline of the web and flanges, Δ_{web} and $\Delta_{fl.}$, respectively, were obtained using imperfection measuring device one (1) and, therefore, refer to the out-of-flatness of the elements (see the figure at the bottom of Table 5.4). In contrast, the initial imperfections of the flange, at the flange-lip juncture, and of the lip, $\Delta_{fl.lip}$ and Δ_{lip}, respectively, were determined using imperfection measuring device two (2). Therefore these refer to the fabrication type described earlier (see the figure at the bottom of Table 5.4).

Generally, the out-of-flatness of the webs and flanges increases with increasing flat width-to-thickness ratio. This tendency in lipped channels is shown in Figure 5.3 where the maximum imperfection of the web and flanges, Δ_{web} and $\Delta_{fl.}$, is plotted as a function of their width-to-thickness ratios, w/t. The scattering of the imperfections about the best-fit (linear regression) line is typical for this type of data.

A similar correlation between the imperfection Δ_{web} for plain channels and the parameter w/t was not observed. Also, this imperfection is generally larger than the comparable imperfection for lipped channels (see Table 5.4). These differences are attributed to the larger torsional flexibility of the channel's cross section which makes such sections more susceptible to local imperfection. This hypothesis is reinforced when the fabrication imperfections $\Delta_{fl.lip}$ for the channels and lipped channels are compared; again, the channel imperfection is generally much larger.

Also, relatively large local initial imperfections are found in the lips of the specimens (see Δ_{lip} of Table 5.4). This is caused by fabrication difficulties associated with forming unstiffened elements having very small width-to-thickness ratios.

The typical longitudinal variation of local initial imperfection in stub columns is presented in Figures 5.4 through 5.10. In these figures, the imperfection Δ is plotted against the ratio of column station (longitudinal distance from one end) z to column length L. The sign convention associated with the imperfection is depicted in the figures.

In Figure 5.4 the longitudinal variation of local imperfection at the web's centerline ($\mathbb{C}$) is shown for a typical channel section, SC/1 120x60. It follows roughly a sinusoidal distribution, with large amplitudes occurring at the ends of the specimen.

The local imperfections (fabrication type) of the flanges for the same section are shown in Figure 5.5. Their variation resembles closely a half-wave of a cosine function. Because the imperfection for both flanges is in the same (common) direction, the section exhibits an asymmetry of imperfection about a plane parallel to the flanges and through the centerline of the web.

A different longitudinal variation of flange local imperfection (fabrication type) is observed in Figure 5.6 for another specimen, SC/1 60x60. This time it is linear along the length. In addition, the transverse variation of imperfection across the flanges is indicated from a comparison of the imperfection at the flange tip, Δ_2, and the value at the centerline of the flange, Δ_3, both at a constant z/L. The variation is nonlinear with the maximum amplitude occurring at the tip of the flange.

Similarly, for lipped channels, the longitudinal variation of local imperfection is shown in Figures 5.7 through 5.10. In Figure 5.7 the local imperfection of the web and flanges, obtained using measuring device one (1) of Figure 5.2a, is plotted for specimen SLC/2 120x60. Again the variation is sinusoidal, and the largest amplitude occurs in the element with the larger w/t ratio, i.e., in the web.

The transverse variation, at constant z/L, of web local imperfection for specimen SLC/2 180x60 is indicated in Figure 5.8, where Δ_1 and Δ_2 refer to the imperfection at the centerline and quarter point, respectively. From the magnitudes shown, the transverse variation increases quite rapidly from the web-flange juncture to the quarter point and then flattens out across the central quarter of the web.

The local imperfection in the flanges, at the flange-lip juncture, of specimen SLC/2 180x60 is shown in Figure 5.9. This is the fabrication type, obtained using imperfection measuring device two (2) of Figure 5.2b, and represents the deviations of the flange from a right angle established off of the web. Very large magnitudes are experienced near the ends of the specimen which is typical for this type of imperfection.

Lastly, the local imperfection (fabrication type) of the lips of specimen SLC/2 180x60 is given in Figure 5.10. Again the variation is sinusoidal along the length.

Other researchers have reported data on local initial imperfections. Thomasson [1978] presented probably the most interesting results for thin-walled, lipped channel, long columns. He included local imperfection contours for the webs, maximum amplitudes, and mean values. All reported data was obtained using an imperfection measuring device very similar to that shown in Figure 5.2a (device 1); therefore the imperfections were

referenced to the longitudinal edges of the web. For web w/t ratios of 468, 319, 319, and 214, the following maximum centerline web imperfections were reported: Δ^{max} of .087, .118, .098, and .028 (inches) and Δ^{max}/t of 3.44, 3.19, 2.60, and 0.49, respectively. This data reinforces and extends the conclusions based on Table 5.4 and Figure 5.3 (see associated discussions) that larger imperfections are expected with larger w/t ratios.

Another researcher, Kalyanaraman [1978], presented some limited data on local imperfections of flanges of thin-walled channels (see Figure 5.1a). From a random sampling, a maximum amplitude of 0.2t was reported. However, because the details of measurement, type of imperfection, and associated w/t ratios were not reported, the use of this data is questionable.

5.4.2 Local and Overall Initial Imperfections of Long Columns

Initial imperfections in long columns are addressed in this section. Both local and overall imperfections are obtained using the scheme presented in Figure 5.11a (Dat [1980]). First, the column is placed in a horizontal position, resting on welded end plates. Then the elevation, at a station z along the column, is determined by sighting through a surveyor's level to an optical tooling scale placed on the column. The level is mounted with a special optical micrometer which is capable of reading directly to 0.001 inches, and the verticality of the scale is maintained by means of a bubble level. After taking readings at stations 3 to 4 inches apart, a closure check is made to ensure that no movement occurred in the level or specimen. The error associated with this method is due to micrometer error and scale placement, and is estimated to be on the order of a few thousandths of an inch.

The elevations determined above must be reduced to correct for any out-of-levelness of the column. For this purpose, the following procedure is utilized where reference is made to the sloping imperfect column of Figure 5.11b. The initial and final elevations e_i and e_f are measured at the distances z_i and z_f along the column, and are not measured at the ends of the column due to the presence of welds. The reduction formula for the overall imperfection Δ_z at a distance z is derived as

$$\Delta_z = e_z - e_i - (e_f - e_i)(z - z_i)/(z_f - z_i) \qquad 5.1$$

where e_z is the associated elevation. A negative Δ_z is indicated in Figure 5.11b.

Because the column is resting on end plates, it is also necessary to account for the self-weight deflection d_z of the column. For this purpose the following correction is applied to Δ_z (Equation 5.1), e.g., Δ(corrected) = $\Delta_z - d_z$.

$$d_z = (\rho L^4/24Er^2)(\xi - 2\xi^3 + \xi^4) \qquad 5.2$$

where $\xi = z/L$, ρ = density of steel = 2.836×10^{-4} k/in.^{3}, and r is the radius of gyration about an axis perpendicular to the deflection. The above equation assumes simply supported ends.

The weak axis (y axis in Figure 5.1) overall imperfection Δ_w obtained from Equation 5.1, where the subscript $_z$ is implied, and the value corrected for self-weight deflection, Equation 5.2, are shown in Figure 5.12. The imperfection represents an average of two sets of measurements taken along the edges of the web. Edge measurements are employed to eliminate the effect of web local imperfections, and the average is employed to correct for twisting of the cross section. Some twisting occurs naturally

in the specimens, and additional twisting is introduced simply by resting the specimens on the two independent end plates. The latter is unavoidable due to the low torsional stiffness of the thin open sections.

The weak axis imperfection Δ_w varies roughly, in Figure 5.12, as a sine wave, and the maximum amplitude occurs just to one side of center. Due to the forming process, the web locates generally on the concave side of the deflected shape, which is indicated by the sign convention shown in the insert to the figure. Also, the self-weight deflection is seen to be too large to ignore.

The determination of the strong axis (x axis in Figure 5.1) overall imperfection, Δ_s, differs from that described above. It is based on two sets of measurements: one with the strong axis placed parallel with the horizontal (one flange upward) and one with the section rotated 180° (other flange upward). The individual imperfection for each set, Δ_1 and Δ_2, calculated from Equation 5.1 and uncorrected for self-weight, is shown in Figure 5.13. These differ in magnitude and deflect in the same common direction. The overall strong axis imperfection Δ_s is obtained by averaging the imperfections Δ_1 and Δ_2 which eliminates the need for a self-weight correction. The results are plotted in Figure 5.14 and are compared with the weak axis overall imperfection Δ_w, which is corrected for self-weight. Both imperfections Δ_w and Δ_s have a similar longitudinal variation and location of maximum amplitude, but the magnitude of Δ_w is larger due to the smaller bending resistance in the weak axis direction.

Local imperfections for the flanges are also determined using the measurement device of Figure 5.11. This imperfection is the fabrication type discussed earlier and represents approximately the deviations from a

right angle established off of the web. It is obtained by first positioning the web as close as possible to vertical, which proved difficult due to the unavoidable twisting of the section. Then the imperfection is calculated simply by subtracting the elevations of the flange at the flange-web juncture from those at the flange-lip juncture. Since the method is self-correcting for any out-of-levelness of the column, Equation 5.1 is unnecessary. Also, a relatively large error is expected for the above method due to errors in vertical placement of the web.

The local imperfection in the flanges of a representative column is presented in Figure 5.15. Typical of this imperfection is the large values that are exhibited at the ends of the specimen (see also Figure 5.9 for stub columns). Sharp peaks are also observed due to welding braces to the section (see Figure 5.1). It is not known what effect, if any, this welding induced distortion has on the behavior and strength.

A summary of maximum amplitudes for local and overall imperfections of several long columns is reported in Table 5.5. The maximum flange local imperfection $\Delta_{fl.lip}^{max}$ (fabrication type — see figure of Table 5.4) and associated Δ/t values are, in general, much larger than the comparable stub column imperfections of Table 5.4. Consequently, the length influences this type of imperfection.

The maximum amplitudes of overall initial imperfection and associated L/Δ values are reported in the remainder of Table 5.5. The weak axis overall imperfection Δ_w ranges from L/6871 to L/1227, and the strong axis overall imperfection Δ_s ranges from L/12000 to L/3159. A statistical analysis of the data is not appropriate due to the large scatter of values.

It is informative to compare the above maximum overall imperfections with existing specification recommendations. The AISC [1975] Specification, which is primarily intended for hot rolled steel shapes, stipulates that the overall imperfection in compression members should not exceed 1/1000 of the length between points of lateral support, or

$$\Delta < L/1000 \qquad 5.3$$

Likewise, the Swedish Code for Sheet Metal Construction StBK-N5 [1977], as reported by Thomasson [1978], places the following restrictions on maximum overall imperfections Δ

$$\Delta < 2 \times 10^{-5} L(L/r) \quad \text{for } L/r > 50 \qquad 5.4a$$

$$\Delta < L/1000 \quad \text{for } L/r \leq 50 \qquad 5.4b$$

where r is the radius of gyration. It is observed that the latter Swedish requirement, Equation 5.4b, is identical to the AISC Equation 5.3. Lastly, the analogous American specification for cold-formed steel members, AISI [1980], does not place restrictions on maximum overall imperfection.

All overall imperfections reported in Table 5.5 satisfy the above requirements. For the Swedish limitations, Equation 5.4a is applicable for the specimens whose L/r ratios range from about 60 to 100 (see Table 5.9 for specific L/r values).

Information on maximum overall initial imperfections has been reported by others. Dat [1980] presented results for 49 relatively stocky cold-formed steel specimens and described various methods of measurement to obtain overall imperfections. He reported maximum imperfections which varied from L/12200 to L/240, and the values for nine specimens exceeded L/1000. It is believed that these very large imperfections were not due to actual crookedness of the column and were, rather, due to inaccuracies

in the methods of measurement (especially Method 2 described by Dat [1980], page 282). If consideration is given to only the measurements obtained from the method which is similar to that used in the present study (see Figure 5.11a), the maximum overall imperfection of the twelve corresponding specimens varies between L/12200 and L/1205 and satisfies the requirement of Equation 5.3.

Thomasson [1978] investigated thin-walled sections, which had a constant L/r ratio of 70, and reported an absolute maximum overall imperfection of L/2500. Therefore, his results satisfy the above requirements, e.g., Equations 5.3 and 5.4a.

5.5 Experimental Procedures, Instrumentation, and Alignment

5.5.1 Stub Column Test Procedure

Technical Memorandum No. 3 of the SSRC, "Stub-Column Test Procedure," (Johnston [1976]) was employed, in part, for the tests. The ends of the stub columns were machine ground, hand filed, and lapped with a lapping compound and plate. A few specimens proved too flexible (large w/t) or too large to be machine ground; hence these were finished entirely by hand. The tolerance on end flatness was less than one thousandth of an inch. No special effort was made to ensure parallelism of the two ends. Then the specimen was set to bear on ground, cold-rolled steel, bearing plates, which were centered in either a Southwark-Emery (300,000-pound capacity) or a Baldwin (400,000-pound capacity) hydraulic testing machine. Hydrostone bedding was used between the bearing plates and fixed machine

heads in an effort to distribute the load and to correct for any out-of-parallelism of the specimen ends. The overall stub column test setup is shown in Figure 5.16.

After successful alignment was obtained (see Section 5.5.4), the specimens were tested using a static method where the load and strains were allowed to stabilize at each load increment. If any load shedding occurred, the load was increased to the original value and allowed to stabilize again before any readings were taken. Typical load increments of not more than 5% of the ultimate load were employed, and smaller increments were used once local instability or the ultimate load were approached.

5.5.2 Long Column Test Procedure

Technical Memorandum No. 4 of the SSRC, "Procedure for Testing Centrally Loaded Columns," (Johnston [1976]) was used, in part, for these tests. The ends of the specimens were only roughly prepared by hand filing. Then 3/4-inch hot-rolled steel plates were welded to the ends of the specimen. Sequential, intermittent welding, on both sides of the cross section, was employed in an effort to control weld-induced distortion (Salmon and Johnson [1971]).

Special end fixtures developed by Pekoz [1967] were used in the long column tests (see Figure 5.17). These provided a pinned-end condition (knife edge) about the weak axis and a fixed-end condition about the strong axis. Also, the fixtures were equipped with wedges and positioning screws which facilitated alignment. Hydrostone bedding was used between the end plates of the specimen and fixtures. Finally, it is noted that

these end fixtures have been employed successfully, in the past, by other Cornell University researchers (DeWolf [1973], Kalyanaraman [1978], and Dat [1980]).

An alternate procedure was used for test CLC/1.1 120x30 only. This consisted of using steel half-rounds between ground end plates and the testing machine. The ends of this specimen were prepared as described in Section 5.5.1 and were set to bear on the plates; no welding was used.

A Southwark-Emery (300,000-pound capacity) long column hydraulic testing machine was used for all column tests. The typical long column test setup is shown in Figure 5.18. A loading procedure identical to that described above for stub columns was employed.

5.5.3 Instrumentation

Typical experimental instrumentation consisted of several strain and dial gages placed at the midheight of the column. All strain gages were single wire type W64, Precision Measurement Company, with a gage length of 0.64 inches. The strain gage instrumentation, as shown in Figure 5.1, employed paired gages at all locations. These gages supplied information on alignment, local instability of the plate elements, and membrane strains.

The strains were monitored during the tests with a Hewlett Packard computer data acquisition system, which proved very useful in a couple of respects. First, the system provided real time displays of reduced data. This feature facilitated alignment and general monitoring of the test. Second, all data was stored on cassettes which allowed for easy processing at a later date; in fact, many of the figures in this and later chapters were computer generated.

The dial gage instrumentation consisted of several 0.001-inch gages, placed at the midheight of the column (see Figure 5.19). These gages were employed to measure local and overall (lateral) deflections. The axial deformation was measured for only stub columns, using a 0.0001-inch dial gage. During the initial stages of testing, the long columns were instrumented with dial gages to monitor the movement of the ends of the column, and end fixtures, relative to the testing machine heads. Since no movement was detected, the use of these gages was abandoned.

5.5.4 Alignment

The special alignment procedures used to ensure concentric or eccentric loading of stub and long columns are described in this section. All stub columns were loaded concentrically, but the loading conditions for the long columns varied.

Alignment for concentric loading was based on a uniform strain condition at the midheight of the column; thus the influences of initial imperfections were minimized. The alignment procedure consisted of monitoring the strains at load increments up to the minimum of 0.75 P_{crl} or 0.5 P_u. The load P_{crl} is the critical load, of the section, associated with the local buckling stress of a simply supported plate of width-to-thickness ratio equal to that of the largest element. The load P_u is the estimated ultimate load. Since small loads proved unsatisfactory, an absolute minimum alignment load of 0.15 P_u was established. If the relative error ER of the corner membrane strains, which is defined below, was less than about 15%, then alignment was considered satisfactory.

$$ER = (MAX - MIN)/MIN \qquad 5.5$$

where MAX and MIN are the maximum and minimum corner membrane strains at midheight, respectively. For only channel sections the "corner" strain of relatively small flanges ($w_2/t \approx 30$) was established from the strain gages located at the tip of the flanges, and for relatively large flanges ($w_2/t \approx 60$) the corner strain was established from the "optional" gages defined in Figure 5.1a, which were located at the center of the flange. For all other specimens the corner membrane strains were obtained from the gages located on the longitudinal edges of the flanges.

Initially, the concentrically loaded specimens were centered in the testing machine using geometrical alignment (SSRC Technical Memorandum No. 4, Johnston [1976]). Geometrical alignment consists of centering the specimen, in the testing machine, at its gross centroid. Rarely did this procedure result in proper alignment due to the unavoidable dimensional imperfections, initial imperfections, and slight out-of-flatness at the ends of the stub columns.

Improper alignment of the stub columns was corrected by the following method. First, the top machine head was separated from the hardened hydrostone bedding. Then, thin metal shims, typically 0.001 and 0.002 inches thick, were placed on the hydrostone to adjust the position of applied loading. Extra precautions must be exercised during this phase so as not to move the stub column. Next, the machine head was slowly lowered into contact, and alignment was again checked. This process was repeated as necessary. In general, alignment was a very time-consuming procedure which took typically several hours. Still, the method represents a considerable improvement over methods used in the past which consisted of physically moving the specimen and recasting the hydrostone

(see Dat [1980] and Desmond [1978a], to name a few). Once satisfactory alignment was obtained, a small load of 100 to 200 pounds was maintained on the specimen; from which point the test was started.

The eccentrically loaded long columns were aligned similarly using the longitudinal membrane strain distributions. However, this time actual and theoretical strains were compared (Figure 5.20). The corresponding load levels were identical to those described above for concentric alignment. Two separate comparisons were made, one each about the strong and weak axes. The strong axis alignment consisted of comparing the two actual corner strains along reference axis a, ε_{act1a} and ε_{act2a}, to those along reference axis b, ε_{act1b} and ε_{act2b}, respectively. A relative error ER estimate, defined below, was used for the comparison.

$$ER = |\varepsilon_{actia} - \varepsilon_{actib}|/\min(|\varepsilon_{actia}|,|\varepsilon_{actib}|) \quad . \; . \; . \; i = 1,2 \qquad 5.6$$

where | | indicates absolute value, min ( ) indicates minimum, and for i = 1,2 the alignment is defined along axes 1 and 2, respectively (see Figure 5.20). If the two errors defined by Equation 5.6 were less than 15%, strong axis alignment was considered satisfactory.

Weak axis alignment was determined from a comparison of actual strains ε_{act} against theoretically predicted strains ε_{th} (see Figure 5.20). The theoretical strains ε_{thi}, along axes one (i = 1) and two (i = 2) were defined by the approximate beam-column formulas (see Chapter 4)

$$\varepsilon_{thi} = P/EA \pm Pec_i/EI(1' - P/P_{cr}) \quad . \; . \; . \; i = 1,2 \qquad 5.7$$

where P is the axial load, e the alignment eccentricity relative to the gross centroid, A the area, I the weak axis moment of inertia, c_i the

distance from the gross centroid the appropriate strain gages, and a minus sign is associated with i = 2. The critical buckling load P_{cr} is given by

$$P_{cr} = \pi^2 EI/L^2 \qquad 5.8$$

The strains ε_{thi}, in Equation 5.7, were assumed small; thus local buckling effects were negligible, and all cross-sectional properties were based on the gross cross section. Again, a relative error estimate was used for the comparison. Thus,

$$ER = |\varepsilon_{thi} - \varepsilon_{actij}|/\varepsilon_{thi} \quad \ldots\ldots \; i = 1,2 \text{ and } j = a,b \qquad 5.9$$

If the four separate errors given by Equation 5.9 were less than 15%, weak axis alignment was considered satisfactory. It is noted that an error tolerance of less than 15% proved impractical.

Improper alignment of either the concentrically or eccentrically loaded long columns was corrected by using the positioning screws and/or wedges provided in the end fixtures. After alignment was obtained, a small load of 150 to 200 pounds was maintained on the specimen.

5.5.4.1 Summary of Column Alignment

All test specimens, except those noted below, satisfied the alignment criteria discussed in the previous section. Many specimens had error tolerances of less than 10%.

The specimens which did not satisfy the alignment criteria include: SLC/1 240x60, SLC/2 360x90, SC/1 60x60, and CLC/2 180x60. For one specimen, SLC/1 120x30, the alignment was close, and an error of approximately 20% was observed at the alignment load. For another specimen, CLC/2.2 180x60, alignment was satisfactory at loads less than, and equal to, the alignment load, but at slightly higher loads strong axis alignment deteriorated and proved unsatisfactory.

5.6 Experimental Results

The experimental results for the stub and long columns of the present study are reported in this section. Information on ultimate strengths, local buckling behavior (stub columns), sub-ultimate response (stub columns), loading eccentricity (long columns), and failure modes are included. However, because the information discussed in this section is intended to serve as an introduction to the subsequent chapter, reference is made to that chapter for a more comprehensive presentation, including comparisons with theoretical predictions.

5.6.1 Stub Columns

The experimental ultimate loads, P_{uexp}; associated length-to-minimum radius of gyration (gross section) ratios, L/r_{min}; and ratios of maximum longitudinal membrane edge-to-yield strain, $\varepsilon_u/\varepsilon_y$; are reported in Table 5.6. The maximum edge strains ε_u were obtained from strain gage readings on the flanges, closest to the flange-web junctures, at loads within 3% of ultimate. Typically, the $\varepsilon_u/\varepsilon_y$ ratios ranges from about 0.7 to greater than 1.0. The larger values of $\varepsilon_u/\varepsilon_y$ are generally experienced for the lipped channels with fully effective flanges, e.g., SLC/- -x30, and for the channel sections, SC. One test, SLC/2 360x90, exhibits a relatively low $\varepsilon_u/\varepsilon_y$ ratio of 0.56 which is caused by poor alignment (see Section 5.5.5).

As noted above, the maximum membrane edge strain ε_u failed, in general, to reach a yield condition. Since this condition (yielding) is assumed in a theoretical analysis (Chapter 2), it is important to establish possible reasons for this behavior. One reason is due to the small

tangent stiffness of a locally buckled plate near the ultimate load (see Figure 2.8). Thus, the edge strain, which is measured just prior to ultimate, increases dramatically with the small additional load that is necessary to reach ultimate. A second and related reason is that the maximum axial membrane strain may not be representative of the maximum principal membrane strain, which ultimately controls failure. Discussion of this reason is continued in Section 5.6.2. A third reason is that edge yielding may not be indicative of failure because of prior surface yielding on the crests of the buckles. In general, surface yielding occurred on the lips, flanges, and webs of the specimens with small w/t ratios. However, it is believed that surface yielding is not critical for the type of specimens under study here, but may control failure for specimens which have unstiffened plate elements with eccentric loading toward the free edges of these elements. A final reason is due to the physical positioning of the strain gages. For example, the edge strain at midheight of the column, where the gages were placed, may not coincide with the maximum edge strain. Also, the strain gages were necessarily placed at a small distance (transverse) from the edges of the elements and, therefore, were influenced by local buckling.

Ordinarily, the uniformly compressed lipped channel stub columns maintain a uniform strain condition across their cross section throughout the loading history. This behavior is illustrated in Figure 5.21a where the strains at reference axes one (1) and two (2) are nearly identical for all loads P. Another example is contained in Figure 5.21b where the strains begin to diverge from each other, by relatively small amounts, after local buckling of the flanges and web, which is indicated by the kink in the load-strain response.

In contrast, for lipped channels with relatively large web w_1/t ratios, the uniform strain condition is violated, and large strain gradients are experienced across the flanges. This behavior is illustrated in Figure 5.22 where there are now significant differences between the strains at the two reference axes. These differences occur after buckling of the web element which forces the flange-lip assembly to rotate about the web-flange juncture. In turn, this reduces the effectiveness of the flange and causes the strain gradient. It is noted that deflections, at the flange-lip juncture, in a direction perpendicular to the flange were observed experimentally for all lipped channels. Yet this deflection, which increased with increasing web-to-flange width ratios w_1/w_2, seemed to alter significantly the response of only the specimens with relatively large w_1/w_2 ratios.

Generally, the axial deformation is predicted better from strain gages than that predicted from dial gages (DeWolf [1973]). This is illustrated in Figure 5.23 where the axial load-deformation response is plotted for a typical lipped channel specimen. The curve labeled "dial gage" is obtained directly from the dial gage readings; whereas the curve labeled "strain gages" is obtained indirectly from the strain gage readings at the four corners of the section. Because the latter curve is in better correspondence, at low load levels, with the fully effective (gross cross section) curve, the strain gages are adopted in this study to calculate the axial deformation. The disagreement between the dial gage and fully effective curves at low load levels is apparently caused by the initial seating of the stub column ends, which are not perfectly flat due to small imperfections, against the base plates. It is noted that good agreement is obtained between the dial gage readings and deformation

calculated from the strain gage readings for specimens with small w/t ratios, but this agreement deteriorates as the w/t ratios are increased.

The common failure mode of the stub columns was by the formation of a kink in the section, usually near midheight (see Figure 5.24). The kink was observed to form at the location of the largest amplitude of the local buckling half-waves(s). In this respect the specimens with larger plate aspect ratios had several half-waves. Also, for the specimens with large web w_1/t ratios, equal to 240 and 360, the kink formed usually closer to the ends of the specimen. Stable load shedding, where the load decreased slightly and then stabilized, and small drift in the gages provided an indication that collapse was imminent.

5.6.1.1 Local Buckling Stresses

The major parameter for consideration in a local buckling study is the critical buckling stress f_{cr}. Yet this quantity is rather indefinite in nature due to local initial imperfections present in a real plate. Nevertheless, several approximate methods have been proposed for its experimental determination (Johnson [1966]). Of these, the modified strain reversal method is adopted in the present study due to the method's ease of instrumentation and interpretation of results. In this method, the compressed plate is instrumented with paired strain gages placed at the same location and on either side of the plate (see Figure 5.25). As the plate is initially compressed, the gages read essentially the same strain level. However, when the plate begins to buckle, the readings start to deviate from each other due to flexural waving. The resulting tensile strain on the convex side of the plate causes eventually a reversal

of the total strain (gage 10), i.e., it overcomes the strain component due to the axial load. The maximum strain level on the convex side is defined as the critical strain ε_{cr}.

The load-strain response indicated in Figure 5.25 was typical for plate elements with small w/t ratios but was not typical for elements with larger w/t ratios. This is exemplified in Figure 5.26 where the buckling response is indicated for a web with a w/t ratio three times that of the web in Figure 5.25. In the latter, only one strain reversal occurs; whereas in the former multiple strain reversals occur which is attributed to a constantly changing buckled shape. The critical strain is defined at the point of first strain reversal. Also, from Figure 5.26, the membrane strain is observed to remain relatively constant, after local buckling, but decreases as the ultimate load is approached.

The local buckling response for a complete section is illustrated in Figure 5.27. First, the web element buckles at the critical strain ε_{cr11}. Again, the strain histories for the web indicate that the buckled form changes as the load is increased. Next, the flange buckles at ε_{cr17} where the buckling mode is primarily local (Figure 3.5a). It is noted that buckling of the web and flange do not occur simultaneously. Eventually, the flange buckling switches to a local-torsional mode (Figure 3.5c) at the critical strain ε_{cr19}. Failure occurs soon after this stage is reached.

Not all specimens followed the exact behavior indicated in Figure 5.27. However, it demonstrates that the assumption of simultaneous buckling of all elements (Chapter 3) is violated for an actual thin-walled section.

The buckling strain histories, such as those contained in Figures 5.25 through 5.27, are used to calculate the associated elastic buckling coefficients K_i from

$$K_i = 12\varepsilon_{cr}(1 - \mu^2)(w_i/t)^2/\pi^2 \quad \ldots \quad i = 1,2,3 \qquad 5.10$$

where w_i is the flat width of the ith element. The results are reported in Table 5.7. Double values are indicated for K_2 and K_3 because the section has two flanges and two lips.

The experimental buckling coefficients of Table 5.7 are compared graphically, in Figures 5.28 and 5.29, to the theoretical values from Chapter 3 (Figures 3.1 and 3.2), for channels and lipped channels, respectively. It is recalled that the theoretical (numerical) analysis of Chapter 3 accounts for local buckling interaction between the plate elements of a section. For channels (Figure 5.28) there is fair correlation between the theoretical and experimental web buckling coefficients, K_1. But the theoretical buckling coefficients for the flanges, K_2, overestimate the experimental results, which lie closer to the simply supported value of $K_2 = 0.425$.

Similar results are observed in Figure 5.29 for the lipped channels. In this case, there is fair correlation between the theoretical and experimental buckling coefficients for the flanges, K_2, but the theoretical predictions of the web buckling coefficient, K_1, are unconservative.

It is important to discuss the factors which affect the experimental buckling coefficients. One obvious factor, which influences even the theoretical predictions, is the length of the section. Since this factor was considered in the design of the specimens (Section 5.2.1), it is

relatively unimportant. A second and most crucial factor is the uneveness across the ends of the specimens. This causes the affected element to buckle prematurely (belatedly) which is substantiated by the extremely low buckling coefficients reported in Table 5.7, e.g., for specimen SLC/2 360x90, $K_1 = 0$. It appears that this factor is especially critical for unstiffened elements (flanges of channels) and web elements with large flat width ratios, w_1/t. The last factor concerns positioning of the strain gages. If the gages happen to be located near a point of inflection in the buckled shape, they will give too high of an estimate of the buckling coefficient. It is recalled that the strain gages, used to obtain the buckling coefficients of Table 5.7, were generally positioned at the midheight of the stub column.

The last factor, discussed above, was investigated by instrumenting several lipped channels with additional pairs of buckling strain gages (Vann et. al. [1973]). These gages were placed at the same location on the cross section as those at the centerline (midheight) but were spaced at a distance z along the length. The distance z was taken equal to approximately one-half of the flat width of the appropriate plate element. The buckling coefficients, obtained from the additional strain gages, are compared in Table 5.8 against the values obtained from the gages at the centerline (℄). In short, the additional gages give mixed results which agrees with conclusions reached in another investigation (Mulligan [1979]).

5.6.2 Long Columns

The experimental results for the long columns are reported in Table 5.9. The ratios of test length to minimum radius of gyration,

$\bar{L}/r_{min}$, range from 40 to 100 which provides a broad data base. The test length $\bar{L}$ accounts for the offset in the center of rotation due to the end fixtures and base plates, and differs from the specimen length L, in Table 5.2, by 2 x 1.5 inches. Also, as discussed earlier, several columns are tested with braces (see Figure 5.1). For a given cross section, both concentric and eccentric loading conditions are studied. The experimental eccentricities e listed in Table 5.9 are defined as positive toward the shear center (see Figure 5.1). For reference the distance $\bar{x}$ which defines the location of the gross centroid relative to the web is also listed in this table.

Because the response is very sensitive to the position of the applied load (see Section 4.5.2), the experimental eccentricity is determined from actual test measurements and differs from the alignment eccentricity discussed in Section 5.5.4. More specifically, the experimental eccentricity is determined from

$$e = (\varepsilon_1 - \varepsilon_2)\, EI\, (1 - P/P_{cr})/P(c_1 + c_2) \qquad 5.11$$

where all notation is defined following Equation 5.7. The load P and the average strains ε_1 and ε_2 are obtained from test measurements, and Equation 5.11 is applied at several load levels, up to the alignment load (see Section 5.5.4). The results are then averaged to obtain the experimental eccentricities listed in Table 5.9. Generally, these eccentricities differed from the alignment values by less than 10%.

In addition, the ratios of maximum membrane edge strain, obtained within 8% of the ultimate load, to yield strain, $\varepsilon_u/\varepsilon_y$, are reported in Table 5.9. The reference axis, either one (1) or two (2), where the

maximum edge strain occurs is also indicated (see Figure 5.20). In most cases, the $\varepsilon_u/\varepsilon_y$ ratios for long columns with flange flat width ratios, w_2/t, equal to 60 exceed the corresponding values for equivalent stub columns (Table 5.6). However, for w_2/t equal to 90, the opposite is true, and the long column $\varepsilon_u/\varepsilon_y$ ratios are less.

For several tests the maximum edge strain, ε_u, failed to reach yielding. The reasons for this behavior were discussed in Section 5.6.1. However, in the present case, the effect noted earlier of low post-buckling plate stiffness, near ultimate, is exaggerated due to beam-column behavior (Timoshenko [1955]). Also, Thomasson [1978] investigated experimentally the appropriateness of using the maximum axial membrane strain to represent failure. He found this stress (strain) to be of the same order as both the principal stress, which was within 10° of the axial direction, and the effective stress of von Mises yield criterion (Timoshenko [1956]). Moreover, calculations of the maximum surface effective stress indicated yield had occurred. It is mentioned that Thomasson observed relatively low values of the maximum membrane edge strain (axial), e.g., see Section 5.7.2. A final reason for the low values of ε_u is the failure modes which are discussed next.

Typical failure modes for the concentrically loaded long columns, without braces, are shown in Figure 5.30. Collapse was initiated by the formation of a kink usually at the midheight of the column. And similar to the results for the stub columns, stable load shedding and drifting of the gages occurred just prior to collapse. Generally, failure was gradual.

The failure modes for two eccentrically loaded columns with and without braces, CLC/2.1 and CLC/2.2 180x90, respectively, are compared in Figure 5.31. For the column without braces, failure occurred near the end of the specimen and was gradual. Also note the relatively low value of $\varepsilon_u/\varepsilon_y$ that is observed for this test (Table 5.9). On the other hand, the column with braces failed suddenly, near the center, and displayed significant differences in lateral deflections at the two corners, i.e., the individual deflections obtained from dial gages A and B of Figure 5.19. This indicated twisting of the section and torsional-flexural buckling.

One column, CLC/1 90x90, without braces collapsed violently by an elastic local-torsional failure of the flanges (see Figure 5.32). The collapse of the individual flanges was shifted in phase and occurred away from the midheight of the specimen. Because difficulties were encountered when fabricating this square section ($w_1 \simeq w_2$), the flanges had large local initial imperfections* (fabrication type) which interacted adversely with local-torsional buckling of the flanges to produce premature failure.

The failure modes for the remaining specimens are briefly summarized below. For almost all specimens failure was gradual. An exception to this was test CLC/2.2 180x60 which failed violently. For this test failure occurred initially in only one flange due to improper strong axis alignment (Section 5.5.5). Also, the majority of specimens failed near the midheight. The exceptions to this include CLC/2.4 120x60 and CLC/3 180x90 which failed near the ends. Finally, significant twisting of the cross section was noted for tests CLC/2.1 180x60, CLC/2 180x90, and CLC/3 180x90.

*These imperfections were observed visually and were not actually measured.

From the above discussion, the braces are seen to significantly effect the strength and behavior of the specimens. A more direct evaluation consists of equating the ultimate strengths (Table 5.9) of the six sections which have comparable dimensions and loading conditions. Although not strictly applicable due to variations in the yield strength and dimensions, the mean ultimate loads for the braced and unbraced sections are 11.3 and 9.8k., respectively, which indicates the braces are quite effective. Equally important, braces were not used for several tests which experienced low maximum edge strains.

Finally, the local buckling stresses for the long columns are not reported because of the effect of the longitudinal stress gradient (see Section 3.3.2) which changes continually with increasing load (see Section 4.5.2). However, it is mentioned that the web buckling coefficients, K_1, followed generally the results discussed earlier for stub columns.

5.7 Other Experimental Research

In this section the experimental research of others is briefly reviewed. Reference is implied to previous discussions.

5.7.1 Stub Columns

In the early fifties, Chilver [1953] presented an interesting and widely referenced paper on the stability and strength of thin-walled steel struts (short columns). Results were reported for tests on channel and lipped channel sections, from which empirical methods of strength prediction were derived. Chilver's test results are reviewed in Table 5.10.

The yield strengths were obtained from compression tests of representative material. Also, for a constant cross section, several tests were conducted on specimens with different lengths, and the minimum ultimate load was reported. The associated lengths were not reported. Actually, Chilver reported ultimate (average) stresses, and not loads; hence the loads listed in Table 5.10 were obtained from independent calculations. Lastly, it is observed that a majority of Chilver's specimens had relatively small element w/t ratios.

More recently, Pekoz [1977] conducted exploratory research on cold-formed steel channel and lipped channel sections. In this study the ends of the specimens were hand filed to a plane, and in some cases, copper end pads were used to distribute the load. For the specimens listed in Table 5.11, Pekoz stated that the stub column length requirements discussed in Section 5.2.1 were satisfied, e.g., $L > 3xw_{max}$ and $L \leq 20r_{min}$. Since the lengths of the channel sections were not reported, this can not be verified. However, the lengths were reported for the lipped channel sections, and in general these sections satisfied the above requirements. Finally, the yield strengths associated with the thickness $t \approx 0.02$ and 0.06 inches were 43.77 and 32.92 ksi, respectively.

5.7.2 Long Columns

Thomasson [1978], in a comprehensive study, reported tests of concentrically loaded, lipped channel, steel columns (see Table 5.12). Geometrical alignment was used for these tests where the specimen was centered in roller bearing end fixtures (simple support about the weak axis). The specimens were held in the fixtures by locking guide bars, and

copper or neoprene shims were used between the specimen and top plate of the fixtures. Since the center of rotation of the fixture was not coincident with the ends of the specimen, a correction of 2 x 3.74 inches was added to the specimen length L = 98.4 inches to define the test length $\overline{L}$ = 105.9 inches. Also, thin braces (1.18" x 0.12" strips), spaced at 11.8 inches, were used between the lips, similar to the L brace of Figure 5.1. Because Thomasson failed to mention the manner of brace connection but discussed "holes" in the lips, it was assumed that the braces were attached by screws. Extensive experimental measurements were made using strain and dial gages. And in one test, A104, an attempt was even made to define the local buckling pattern by preloading the specimen before attaching the strain gages. However, when the specimen was actually tested, the buckling pattern shifted which negated the above procedure.

The ratios of maximum membrane edge strain (axial), at the midheight and at the web-flange juncture, to yield strain, $\varepsilon_u/\varepsilon_y$, are listed in Table 5.12. These values were obtained graphically from load-strain plots reported by Thomasson at loads within about 5% of ultimate. Generally, the maximum edge strain failed to reach yield, and reasons for this behavior were discussed in Section 5.6.2. The very low value of $\varepsilon_u/\varepsilon_y$ for test A155 was caused by misalignment about the strong axis.

Thomasson also tested lipped channel sections with one and two longitudinal (intermediate) stiffeners in the web. A review of these tests is not included here. However, it is noted that several sections failed prematurely in a local-torsional flange mode. Thomasson discussed this and reasoned that the intermediate stiffeners increased the stiffness

of the web which caused the lips to carry a higher stress level relative to a similar section without intermediate stiffeners. Thus, the risk of local-torsional flange failure was accentuated. Apparently the thin braces, which were relatively weak in compression, and their method of connection, with screws, were inadequate.

Another researcher (Loughlan [1979]) conducted an experimental study of thin-walled, lipped channel, steel columns. The specimens incorporated relatively large stiffeners and were subjected to both concentric and positive eccentric loading (see Table 5.13). Moreover, a simply supported boundary condition was provided about the weak and strong axes by special end fixtures. These consisted of a hardened and polished spherical support pin and loading block with a matching spherical recess. To facilitate alignment, special guide bars, situated on the fixtures, and calibrated positioning handles were used. Because the end fixtures affected the location of the center of rotation, the test length $\overline{L}$, in Table 5.13, was calculated assuming a correction of 2 x 1.52 inches. The yield strengths associated with the thicknesses, t, approximately equal to 0.03 and 0.06 inches were 35.10 and 33.79 ksi., respectively.

5.8 Summary

To sum up, the experimental investigation of the present study was reported in this chapter. The first phase concentrated on concentrically loaded (uniform compression), channel and lipped channel, stub columns. Extensive measurements of the specimens revealed large initial imperfections. And, to facilitate concentric alignment, special procedures were described, which proved very successful. Then the experimental results were discussed. Local buckling coefficients (stresses) for the individual

copper or neoprene shims were used between the specimen and top plate of the fixtures. Since the center of rotation of the fixture was not coincident with the ends of the specimen, a correction of 2 x 3.74 inches was added to the specimen length L = 98.4 inches to define the test length $\overline{L}$ = 105.9 inches. Also, thin braces (1.18" x 0.12" strips), spaced at 11.8 inches, were used between the lips, similar to the L brace of Figure 5.1. Because Thomasson failed to mention the manner of brace connection but discussed "holes" in the lips, it was assumed that the braces were attached by screws. Extensive experimental measurements were made using strain and dial gages. And in one test, A104, an attempt was even made to define the local buckling pattern by preloading the specimen before attaching the strain gages. However, when the specimen was actually tested, the buckling pattern shifted which negated the above procedure.

The ratios of maximum membrane edge strain (axial), at the midheight and at the web-flange juncture, to yield strain, $\varepsilon_u/\varepsilon_y$, are listed in Table 5.12. These values were obtained graphically from load-strain plots reported by Thomasson at loads within about 5% of ultimate. Generally, the maximum edge strain failed to reach yield, and reasons for this behavior were discussed in Section 5.6.2. The very low value of $\varepsilon_u/\varepsilon_y$ for test A155 was caused by misalignment about the strong axis.

Thomasson also tested lipped channel sections with one and two longitudinal (intermediate) stiffeners in the web. A review of these tests is not included here. However, it is noted that several sections failed prematurely in a local-torsional flange mode. Thomasson discussed this and reasoned that the intermediate stiffeners increased the stiffness

of the web which caused the lips to carry a higher stress level relative to a similar section without intermediate stiffeners. Thus, the risk of local-torsional flange failure was accentuated. Apparently the thin braces, which were relatively weak in compression, and their method of connection, with screws, were inadequate.

Another researcher (Loughlan [1979]) conducted an experimental study of thin-walled, lipped channel, steel columns. The specimens incorporated relatively large stiffeners and were subjected to both concentric and positive eccentric loading (see Table 5.13). Moreover, a simply supported boundary condition was provided about the weak and strong axes by special end fixtures. These consisted of a hardened and polished spherical support pin and loading block with a matching spherical recess. To facilitate alignment, special guide bars, situated on the fixtures, and calibrated positioning handles were used. Because the end fixtures affected the location of the center of rotation, the test length $\bar{L}$, in Table 5.13, was calculated assuming a correction of 2 x 1.52 inches. The yield strengths associated with the thicknesses, t, approximately equal to 0.03 and 0.06 inches were 35.10 and 33.79 ksi., respectively.

5.8 Summary

To sum up, the experimental investigation of the present study was reported in this chapter. The first phase concentrated on concentrically loaded (uniform compression), channel and lipped channel, stub columns. Extensive measurements of the specimens revealed large initial imperfections. And, to facilitate concentric alignment, special procedures were described, which proved very successful. Then the experimental results were discussed. Local buckling coefficients (stresses) for the individual

plate elements, obtained from strain gage measurements, were compared against the theoretical predictions of Chapter 3. Generally, the agreement between experimental and theoretical buckling coefficients was fair for channels but deteriorated for lipped channels. One reason for this poor correlation was that the plate elements of the test specimens buckled at different loads which contradicted the theoretical assumption of simultaneous buckling of all plate elements. Also, in several tests, the maximum membrane edge strain, at the web-flange juncture, failed to reach the yield strain. The reasons for this behavior were discussed at length in the text. Even though the specimens were uniformly compressed, a strain gradient across the flanges was observed for the lipped channels with relatively large webs. This response was caused by local buckling of the web which reduced the effectiveness of the flange.

The second phase of the investigation concentrated on concentrically and eccentrically loaded, lipped channel, long columns. Again extensive measurements revealed large local and overall initial imperfections. For the latter, the imperfection was less than one thousandth of the length. Also, an alignment procedure was described which employed comparisons of actual to predicted strains. Then the experimental results were discussed. Generally, the specimens failed gradually by flexural yielding. However, several specimens failed either by torsional-flexural buckling or local-torsional collapse of the flanges, and, in some cases, the failure mode was violent. Finally, the strength and behavior of some columns were significantly affected by the use of braces which tied the flanges together.

Discussion of the experimental results is continued in the next chapter where they are compared to theoretical predictions.

Table 5.1 DIMENSIONS OF STUB COLUMN SPECIMENS*

Specimen		W_1 (in.)	W_2	W_3	t	OR	L	Material†
SLC/1	60x30	3.252	1.639	0.388	.0482	0.150	11.95	XII
SLC/1	90x30	4.594	1.634	0.389	.0480	0.152	11.98	XII
SLC/1	120x30	6.070	1.656	0.380	.0482	0.170	10.96	XII
SLC/1	60x60	3.144	3.217	0.678	.0473	0.121	18.02	I
SLC/2	60x60	3.126	3.212	0.680	.0477	0.117	18.02	I
SLC/1	120x60	5.961	3.226	0.681	.0473	0.125	17.98	I
SLC/2	120x60	5.938	3.238	0.666	.0471	0.123	17.98	I
SLC/1	180x60	8.984	3.214	0.689	.0472	0.121	22.02	I
SLC/2	180x60	8.969	3.223	0.691	.0469	0.131	26.97	I
SLC/1	240x60	11.81	3.223	0.681	.0469	0.125	22.00	I
SLC/2	240x60	11.84	3.230	0.694	.0470	0.142	35.97	II
SLC/3	240x60	11.80	3.220	0.682	.0471	0.125	21.97	I
SLC/1	60x90	3.178	4.492	0.753	.0449	0.144	25.50	V
SLC/2	60x90	3.156	4.496	0.756	.0449	0.150	25.48	V
SLC/1	90x90	4.523	4.492	0.757	.0446	0.149	25.47	IV
SLC/2	90x90	4.508	4.488	0.758	.0450	0.146	25.48	IV
SLC/1	180x90	11.07	5.723	1.347	.0612	0.148	35.09	VI
SLC/2	180x90	11.08	5.754	1.315	.0610	0.156	35.10	VI
SLC/3	180x90	8.828	4.480	0.762	.0481	0.164	25.47	VII
SLC/4	180x90	8.805	4.531	0.746	.0502	0.166	25.50	X
SLC/5	180x90	8.789	4.523	0.768	.0508	0.172	25.51	X
SLC/1	270x90	13.06	4.523	0.750	.0501	0.166	30.00	X
SLC/2	270x90	13.02	4.543	0.750	.0502	0.166	38.24	XI
SLC/1	360x90	17.36	4.476	0.755	.0490	0.158	29.99	IX
SLC/2	360x90	17.38	4.476	0.752	.0493	0.150	50.99	VIII
SC/1	60x30	3.230	1.609	—	.0484	0.168	9.976	XII
SC/1	90x30	4.609	1.612	—	.0478	0.164	10.94	XII
SC/1	120x30	6.102	1.612	—	.0472	0.172	8.961	XII
SC/2	120x30	6.117	1.605	—	.0482	0.168	16.85	XII
SC/1	40x60	2.051	3.095	—	.0480	0.152	15.14	XXII
SC/2	40x60	2.095	3.093	—	.0481	0.152	15.14	XXII
SC/1	60x60	3.058	3.080	—	.0479	0.125	9.141	XXII
SC/1	100x60	5.070	3.077	—	.0481	0.125	15.14	XXII
SC/1	120x60	6.125	2.973	—	.0474	0.156	18.98	XII
SC/1	180x60	8.844	2.984	—	.0476	0.164	17.98	XII
SC/2	180x60	8.852	2.980	—	.0476	0.164	24.98	XII

*Refer to Fig. 5.1 for definition of cross-sectional parameters.

†Refer to Table 5.3 for definition of material properties.

Table 5.2 DIMENSIONS OF LONG COLUMN SPECIMENS*

Specimen		W_1 (in.)	W_2	W_3	t	OR	L	Material††
CLC/1.1	120x30	6.094	1.640	0.362	.0482	0.131	17.96	XII
CLC/1	120x60	6.164	3.193	0.713	.0447	0.154	60.00	V
CLC/2	120x60	6.141	3.192	0.671	.0450	0.152	72.02	III
CLC/2.1	120x60†	6.172	3.171	0.710	.0474	0.168	72.00	XV
CLC/2.2	120x60	6.156	3.182	0.728	.0484	0.166	72.72	XIV
CLC/2.3	120x60†	6.148	3.183	0.712	.0476	0.166	72.66	XIV
CLC/2.4	120x60†	6.140	3.191	0.714	.0476	0.164	72.00	XIII
CLC/3	120x60	6.180	3.192	0.671	.0455	0.154	118.1	III
CLC/4	120x60	6.117	3.197	0.694	.0454	0.156	118.0	III
CLC/5	120x60†	6.164	3.169	0.720	.0480	0.164	72.00	XIII
CLC/1	180x60	9.117	3.199	0.680	.0450	0.152	69.01	IV
CLC/2	180x60	9.133	3.194	0.688	.0448	0.156	92.12	V
CLC/2.1	180x60†	9.164	3.177	0.707	.0478	0.156	92.05	XXI
CLC/2.2	180x60	9.102	3.187	0.741	.0481	0.156	92.09	XX
CLC/3	180x60	9.141	3.194	0.684	.0442	0.150	115.0	V
CLC/4	180x60†	9.078	3.199	0.726	.0484	0.164	92.03	XVIII
CLC/1	90x90	4.516	4.480	0.778	.0484	0.166	96.16	XVI
CLC/1	180x90	8.742	4.496	0.785	.0478	0.162	72.07	XV
CLC/2	180x90	8.773	4.476	0.766	.0477	0.166	96.07	XVII
CLC/2.1	180x90†	8.719	4.484	0.766	.0475	0.152	96.03	XVIII
CLC/2.2	180x90	8.750	4.492	0.773	.0482	0.164	96.19	XVI
CLC/3	180x90†	8.766	4.488	0.753	.0481	0.166	96.16	XIX

*Refer to Fig. 5.1 for definition of cross-sectional parameters.

††Refer to Table 5.3 for definition of material properties.

†Braces used, refer to Fig. 5.1.

Table 5.3 TENSILE MATERIAL PROPERTIES

Material*	Yield Stress (ksi)	Ultimate Stress (ksi)	Percent Elongation
I	33.39	45.72	38
II	34.63	46.65	40
III	31.95	46.04	47
IV	32.59	46.66	46
V	32.41	46.43	44
VI	59.80	79.35	22
VII†	53.42	71.13	29
VIII	29.33	42.27	48
IX	29.20	42.15	49
X	28.83	42.10	47
XI	29.49	42.29	49
XII	32.79	43.58	41
XIII	32.47	45.11	41
XIV	31.82	45.03	43
XV	31.82	44.69	42
XVI	34.34	45.51	42
XVII	35.42	46.39	42
XVIII	33.06	44.55	42
XIX	33.85	45.17	42
XX	34.34	45.68	46
XXI	34.98	45.93	39
XXII††	51.62	64.08	22

*Unless noted otherwise, all sharp yielding.

†Low proportional limit, 0.2% offset used to define yield stress.

††Gradual yielding, 0.2% offset used to define yield stress.

Table 5.4 MAXIMUM AMPLITUDE OF LOCAL INITIAL IMPERFECTIONS IN STUB COLUMNS

Specimen	Web		Flange				Lip	
	Δ^{max}_{web}*	Δ^{max}_{web}/t	$\Delta^{max}_{fl.lip}$*	$\Delta^{max/t}_{fl.lip}$	$\Delta^{max}_{fl.}$*	$\Delta^{max}_{fl.}/t$	Δ^{max}_{lip}*	Δ^{max}_{lip}/t
SC/1 40x60	.020	0.42	.036	0.75		—†		—
			.128	2.67		—		—
SC/1 60x60	.016	0.33	.061	1.27		—		—
			.095	1.98		—		—
SC/1 100x60	.049	1.02	.132	2.74		—		—
			.122	2.54		—		—
SC/1 120x60	.011	0.23	.145	3.06		—		—
			.127	2.68		—		—
SC/1 180x60	.042	0.88	.192	4.03		—		—
			.091	1.91		—		—
SLC/2 60x60	.008	0.17	.026	0.54	.004	0.08	.008	0.17
			.020	0.42	.007	0.15	.011	0.23
SLC/2 120x60	.009	0.19	.013	0.28	.004	0.08	.004	0.08
			.005	0.11	.004	0.08	.008	0.17
SLC/2 180x60	.013	0.28	.044	0.94	.008	0.17	.012	0.26
			.056	1.19	.006	0.13	.008	0.17
SLC/2 240x60	.040	0.85	.019	0.40	.010	0.21	.009	0.19
			.049	1.04	.008	0.17	.006	0.13
SLC/1 60x90	.005	0.11		—	.012	0.27	.036	0.80
				—	.017	0.38	.043	0.96
SLC/1 90x90	.006	0.13		—	.013	0.29	.014	0.31
				—	.009	0.20	.014	0.31
SLC/5 180x90	.015	0.30		—	.005	0.10	.024	0.47
				—	.005	0.10	.019	0.37

†Not measured or not applicable.

*In inches, where:

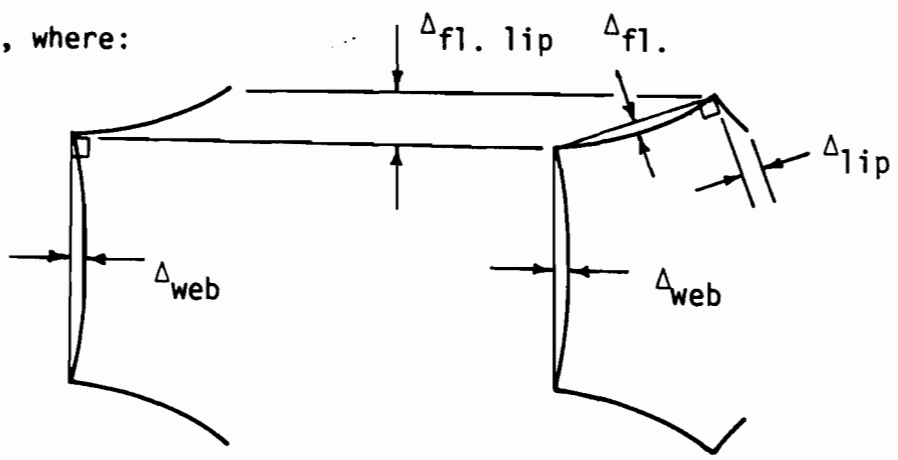

for SC. for SLC

Table 5.5 MAXIMUM AMPLITUDE OF LOCAL AND OVERALL INITIAL IMPERFECTIONS IN LONG COLUMNS

Specimen		Local		Overall			
		$\Delta_{fl.lip}^{max}$*	$\Delta_{fl.lip}^{max/t}$	Δ_{w}^{max}†	L/Δ_{w}^{max}	Δ_{s}^{max}†	L/Δ_{s}^{max}
CLC/2.1	120x60	.287	6.05	.042	1714.	.020	3600.
		.163	3.44				
CLC/2.2	120x60	.102	2.11	.012	6060.	.017	4278.
		.139	2.87				
CLC/2.3	120x60	.113	2.37	.038	1912.	.023	3159.
		.111	2.33				
CLC/2.4	120x60	.067	1.41	.045	1600.	.021	3428.
		.075	1.58				
CLC/4	120x60	.054	1.19	.063	1873.	.011	10727.
		.070	1.54				
CLC/5	120x60	.060	1.25	.045	1600.	.006	12000.
		.083	1.73				
CLC/2	180x60	.115	2.57	.038	2424.	.016	5758.
		.092	2.05				
CLC/2.1	180x60	.164	3.43	.068	1354.	.021	4383.
		.136	2.84				
CLC/2.2	180x60	.039	0.81	.034	2708.	.007	13156.
		.103	2.14				
CLC/4	180x60	.216	4.46	.075	1227.	.023	4001.
		.094	1.94				
CLC/2.1	180x90	.178	3.75	.071	1352.	.029	3311.
		.160	3.37				
CLC/2.2	180x90	.215	4.46	.014	6871.	.017	5658.
		.078	1.62				

*See figure at bottom of Table 5.4, in inches.

†See Fig. 5.14, in inches.

Table 5.6 EXPERIMENTAL RESULTS FOR STUB COLUMNS

Specimen		L/w_{max}	L/r_{min}**	P_{uexp}(k)	ϵ_u/ϵ_y*
SLC/1	60x30	4.0	20.0	10.40	1.06
SLC/1	90x30	2.8	20.8	10.05	0.89
SLC/1	120x30	1.9	19.7	10.15	1.43
SLC/1	60x60	6.1	15.0	13.20	0.78
SLC/2	60x60	6.1	15.1	13.60	0.78
SLC/1	120x60	3.1	15.0	13.00	0.74
SLC/2	120x60	3.2	15.0	13.60	0.79
SLC/1	180x60	2.5	19.1	12.80	0.72
SLC/2	180x60	3.1	23.4	12.80	0.81
SLC/1	240x60	1.9	19.9	12.80	0.84
SLC/2	240x60	3.1	32.4	12.00	0.72
SLC/3	240x60	1.9	19.9	12.60	0.88
SLC/1	60x90	6.1	18.2	11.50	0.75
SLC/2	60x90	6.1	18.3	11.80	0.97
SLC/1	90x90	6.0	15.4	11.90	0.96
SLC/2	90x90	6.0	15.4	12.00	1.03
SLC/1	180x90	3.3	16.3	31.15	0.85
SLC/2	180x90	3.3	16.2	31.40	0.90
SLC/3	180x90	3.0	15.7	15.20	1.18
SLC/4	180x90	3.0	15.6	13.80	0.70
SLC/5	180x90	3.0	15.6	14.60	0.73
SLC/1	270x90	2.4	19.1	13.60	0.81
SLC/2	270x90	3.0	24.2	14.00	0.90
SLC/1	360x90	1.8	20.2	12.50	0.70
SLC/2	360x90	3.0	34.4	11.20	0.56
SC/1	60x30	3.4	19.4	7.40	0.85
SC/1	90x30	2.6	22.3	7.35	0.77
SC/1	120x30	1.6	19.2	7.80	1.16
SC/2	120x30	2.9	36.4	7.10	1.53
SC/1	40x60	5.1	16.6	7.88	0.95
SC/2	40x60	5.1	16.2	7.89	0.94
SC/1	60x60	3.1	9.0	9.16	1.09
SC/1	100x60	2.6	15.1	9.20	1.02
SC/1	120x60	3.3	20.0	8.20	1.02
SC/1	180x60	2.1	19.8	8.52	0.85
SC/2	180x60	2.9	27.6	8.50	1.57

*ϵ_u = maximum membrane strain

ϵ_y = yield strain

**Based on gross cross section

Table 5.7 EXPERIMENTAL BUCKLING COEFFICIENTS FOR STUB COLUMNS

Specimen		Web	Flanges		Lips	
		K_1	K_2	K_2	K_3	K_3
SLC/1	60x30	3.32	*	0.81	†	†
SLC/1	90x30	3.46	†	†	†	†
SLC/1	120x30	1.53	†	†	†	†
SLC/1	60x60	3.09	3.08	3.40	*	0.145
SLC/2	60x60	2.96	3.05	3.11	0.119	0.120
SLC/1	120x60	2.74	2.40	2.51	*	*
SLC/2	120x60	2.81	2.95	3.09++	*	0.129
SLC/1	180x60	2.05	2.82	2.78++	0.064	0.040
SLC/2	180x60	2.82	*	2.92	*	0.027
SLC/1	240x60	4.70	*	*	*	*
SLC/2	240x60	3.34	1.60++	1.52++	*	*
SLC/3	240x60	1.80	*	1.69**	*	*
SLC/1	60x90	1.87	3.59	3.04	0.146	*
SLC/2	60x90	1.71	3.53	3.04++	0.085	0.086
SLC/1	90x90	2.94	2.77	3.34++	0.111	0.090
SLC/2	90x90	3.24	2.01	3.89++	0.067	0.086
SLC/1	180x90	3.15	1.48	1.55	0.112	0.070
SLC/2	180x90	3.03	2.47	2.21	0.116	0.120
SLC/3	180x90	3.01	1.97	1.82	0.048	0.064
SLC/4	180x90	3.12	3.49**	3.79++	0.030	0.061
SLC/5	180x90	2.03	1.44++	1.56	0.084	*
SLC/1	270x90	1.78	2.71	2.66	*	0.106
SLC/2	270x90	0.56	2.15++	1.67	*	0.066
SLC/1	360x90	0.	2.52**	2.74**	*	*
SLC/2	360x90	0.	2.12	2.19	0.080	0.032
SC/1	60x30	1.94	0.566	0.486	—	—
SC/1	90x30	2.94	0.332	0.426	—	—
SC/1	120x30	3.31	0.174	0.642	—	—
SC/2	120x30	2.13	0.195	0.138	—	—
SC/1	40x60	1.46	0.	0.050	—	—
SC/2	40x60	1.09	0.302	0.	—	—
SC/1	60x60	0.802	0.282	0.261	—	—
SC/1	100x60	2.93	0.317	0.271	—	—
SC/1	120x60	4.39	0.141	0.168	—	—
SC/1	180x60	4.71	0.032	0.151	—	—
SC/2	180x60	0.390	0.197	0.085	—	—

*Buckling not detected.

†Not measured.

**Flange buckling in local-torsional mode.

++Flange buckling in local mode with subsequent buckling in local-torsional mode.

Table 5.8 INFLUENCE OF STRAIN GAGE LOCATION ON BUCKLING COEFFICIENT

Specimen		Web			Flanges		
		K_1 @ ℄	z*	K_1 @ z	K_2 @ ℄	z	K_2 @ z
SLC/2	60x90	1.71	2.25	2.30	3.53	2.25	3.82
					3.14	2.25	3.04
SLC/1	90x90	2.94	2.25	3.33	2.77	2.25	3.14
					3.94	2.25	3.34
SLC/5	180x90	2.45	4.22	2.03	2.89	2.00	1.44
					3.11	2.00	1.56
SLC/2	270x90	0.71	6.34	0.56	2.54	2.00	2.15
					1.67	2.00	1.81
SLC/2	360x90	0.	8.50	0.40	2.12	2.00	3.60
					2.19	2.00	4.00

*z = distance from ℄, in inches.

Table 5.9 EXPERIMENTAL RESULTS FOR LONG COLUMNS

Specimen		$\bar{L}/r_{min}$ ††	e (in.)	$\bar{x}$ (in.)††	P_{uexp} (k)	$\varepsilon_u/\varepsilon_y$ (1,2)*
CLC/1.1	120x30	36.3	-0.203	0.380	8.00	1.14 (2)
CLC/1	120x60	53.1	0.	1.047	9.80	0.82 (1)
CLC/2	120x60	63.7	0.	1.035	10.40	0.96 (1)
CLC/2.1	120x60†	63.8	-0.536	1.036	10.30	1.14 (2)
CLC/2.2	120x60	64.0	-0.534	1.047	8.75	0.80 (2)
CLC/2.3	120x60†	64.1	0.982	1.043	6.75	0.80 (1)
CLC/2.4	120x60†	63.1	-0.212	1.048	12.40	0.65 (2)
CLC/3	120x60	102.8	0.	1.032	8.20	1.04 (1)
CLC/4	120x60	102.2	0.	1.046	8.40	1.14 (1)
CLC/5	120x60†	63.7	0.	1.039	11.80	0.83 (1)
CLC/1	180x60	63.2	0.	0.857	9.60	1.10 (1)
CLC/2	180x60	83.5	0.	0.856	8.75	0.85 (1)
CLC/2.1	180x60†	83.7	-0.424	0.854	10.40	0.80 (2)
CLC/2.2	180x60	82.9	-0.397	0.870	10.00	0.77 (2)
CLC/3	180x60	103.6	0.	0.855	7.60	0.94 (1)
CLC/4	180x60†	82.8	0.	0.871	10.80	0.72 (1)
CLC/1	90x90	60.1	0.	1.791	11.00	0.48 (1)
CLC/1	180x90	45.9	0.	1.403	12.30	0.89 (1)
CLC/2	180x90	61.0	0.	1.386	12.10	0.64 (1)
CLC/2.1	180x90†	60.8	-0.521	1.394	12.50	0.91 (2)
CLC/2.2	180x90	60.8	-0.515	1.396	8.75	0.65 (2)
CLC/3	180x90†	61.0	0.	1.387	11.80	0.71 (1)

*ε_y = yield strain

ε_u = maximum membrane strain

(1) " " " @ flange-web juncture.

(2) " " " @ flange-lip juncture.

†Braces used, refer to Fig. 5.1.

††Based on gross cross section.

Table 5.10 CHILVER'S [1953] STUB COLUMN TESTS*

Specimen	w_1/t	w_2/t	W_1 (in.)	W_2	W_3	t	Yield Stress (ksi)	P_{uexp} (k)
Channels								
C1	12	14	2.0	2.0	—	.128	49.28	35.5
C2	12	10	2.0	1.5	—	.128	54.21	29.0
C3	16	18	1.25	1.25	—	.064	41.66	8.68
C4	19	21	1.5	1.5	—	.064	46.59	9.22
C5	41	33	1.625	1.25	—	.036	44.58	4.07
C6	17	19	1.0	1.0	—	.048	48.83	4.98
C7	24	19	1.0	0.75	—	.036	43.23	2.88
C8	7	9	0.875	0.875	—	.080	59.58	10.7
C9	27	14	4.0	2.0	—	.128	47.49	41.7
C10	79	40	4.0	2.0	—	.048	26.66	5.28
C11	121	40	6.0	2.0	—	.048	26.66	5.56
C12	163	40	8.0	2.0	—	.048	29.12	5.54
Lipped Channels								
LC1	121	38	6.0	2.0	0.5	.048	42.56	12.4
LC2	46	18	5.75	2.5	1.0	.116	39.87	52.0
LC3	58	27	5.0	2.5	0.5	.080	42.56	25.5
LC4	46	24	4.0	2.25	0.375	.080	35.62	23.9
LC5	40	21	3.5	2.0	0.375	.080	44.13	24.6
LC6	27	10	4.0	1.75	0.625	.128	46.14	50.8
LC7	19	8	3.0	1.5	0.375	.128	47.04	35.9
LC8	39	12	2.75	1.0	0.5	.064	47.49	14.5
LC9	30	8	2.75	1.0	0.5	.080	47.94	19.4
LC10	35	14	1.875	0.875	0.25	.048	50.40	7.66
LC11	32	17	1.75	1.0	0.25	.048	54.66	9.22
LC12	204	69	10.0	3.5	0.75	.048	26.66	9.48
LC13	163	79	8.0	4.0	0.75	.048	27.10	10.2
LC14	121	79	6.0	4.0	0.75	.048	27.78	9.26
LC15	79	79	4.0	4.0	0.75	.048	26.66	9.43
LC16	38	38	2.0	2.0	0.375	.048	28.00	7.26

*Refer to Fig. 5.1 for definition of cross-sectional parameters. Assume OR = 2t.

Table 5.11 PEKOZ'S [1977] STUB COLUMN TESTS*

Specimen	w_1/t	w_2/t	W_1 (in.)	W_2	W_3	t	L	L/r_{min}	P_{uexp} (k)
Channels†									
P4	37	10	2.382	0.699	—	.059	**	<20	7.42
P6$	37	10	2.382	0.699	—	.059	**	<20	7.25
P8	37	10	2.382	0.699	—	.059	**	<20	7.64
P5$	75	10	4.665	0.699	—	.059	**	<20	8.49
P7$	75	10	4.665	0.699	—	.059	**	<20	8.15
P9	75	10	4.665	0.699	—	.059	**	<20	8.15
P2.14	96	15	5.945	1.181	—	.059	11.81	37.6	9.33
Lipped Channels††									
P2.1	149	45	3.307	1.063	0.295	.022	13.78	35.7	3.24
P2.2	146	44	3.228	1.043	0.226	.022	10.63	29.0	2.74
P2.3	50	46	1.157	1.071	0.323	.022	10.55	25.6	3.28
P2.4	51	46	1.185	1.087	0.220	.022	8.07	20.1	3.01
P2.6	97	98	6.012	6.031	1.417	.059	19.68	8.6	19.9
P2.7	97	97	6.016	6.020	2.146	.059	19.68	8.3	22.5
P2.8	97	97	6.016	6.020	0.772	.059	19.68	9.1	20.9
P2.9	97	38	6.004	2.508	1.224	.059	19.68	19.6	19.8
P2.10	97	38	6.004	2.508	0.394	.059	19.68	22.7	15.8
P2.11	97	38	6.004	2.508	0.654	.059	19.68	21.3	17.0
P2.12	96	16	5.945	1.212	0.394	.059	11.81	29.8	11.2
P2.13	96	16	5.945	1.212	0.169	.059	11.81	34.4	9.78

*Refer to Fig. 5.1 for definition of cross-sectional parameters. $Copper end pads used.

**Not reported.

†OR = 0.138 in.

††Assume for t = .022 in., OR = 0.041 in.
for t = .059 in., OR = 0.138 in.

Table 5.12 THOMASSON'S [1978] LONG COLUMN TESTS*

Specimen	w_1/t	w_2/t	W_1 (in.)	W_2	W_3	t	Yield Stress (ksi)	$\bar{L}/r_{min}$	$P_{u\,exp}$ (k)	$\varepsilon_u/\varepsilon_y$
A71	465	152	11.80	3.974	.784	.025	56.71	74.7	3.60	†
A74	466	153	11.82	3.990	.824	.025	57.29	74.0	3.64	0.84
A75	465	153	11.80	3.982	.800	.025	57.72	74.4	3.48	0.55
A76	449	146	11.84	3.970	.808	.026	41.77	74.6	3.26	†
A101	315	103	11.84	3.994	.814	.037	67.30	74.4	8.30	†
A102	315	103	11.84	3.994	.806	.037	66.72	74.5	7.87	0.61
A103	314	103	11.82	3.998	.790	.037	66.72	74.5	8.34	†
A104	305	99	11.78	3.959	.787	.038	68.89	75.3	7.76	0.56
A151	204	66	11.84	3.994	.828	.057	55.40	74.7	17.2	†
A152	208	67	11.87	3.993	.823	.056	54.97	74.8	15.7	†
A153	215	70	11.86	3.983	.846	.054	57.29	74.7	16.0	†
A154	212	69	11.89	4.007	.949	.055	57.00	73.1	16.4	†
A155	211	69	11.84	4.024	.957	.055	55.11	72.7	12.8	0.41
A156	211	68	11.84	3.984	.858	.055	55.26	74.5	15.5	†

*All had concentric loading; braces, 1.18" x 0.12" strips, spaced @ 11.8"; and OR = t + 0.059". Refer to Fig. 5.1 for definition of cross-sectional parameters.

†Strains not measured.

Table 5.13 LOUGHLAN'S [1979] LONG COLUMN TESTS*

Specimen	w_1/t	w_2/t	W_1 (in.)	W_2	W_3	t	L	$\bar{L}/r_{min}$	e	$\bar{x}$	P_{uexp} (k)
L1	120	58	4.030	2.023	0.758	.032	72.0	94.0	0.292	0.743	3.12
L2	124	59	4.012	2.019	0.773	.031	48.0	63.8	0.294	0.747	3.60
L3	126	75	4.076	2.502	1.017	.031	72.0	74.7	0.402	1.019	3.52
L4	121	73	4.046	2.504	1.016	.032	60.0	62.7	0.404	1.022	3.78
L5	124	75	4.032	2.511	1.029	.031	48.0	50.9	0.407	1.021	4.10
L6	158	59	5.065	2.023	0.751	.031	72.0	95.3	0.066	0.669	3.80
L7	156	59	5.007	2.018	0.758	.031	60.0	80.0	0.066	0.672	3.97
L8	156	59	5.011	2.022	0.769	.031	48.0	64.6	0.066	0.677	4.31
L9	158	75	5.062	2.500	1.016	.031	72.0	75.0	0.184	0.934	4.34
L10	157	75	5.046	2.512	1.020	.031	60.0	62.7	0.186	0.942	4.57
L11	151	73	5.022	2.509	1.023	.032	48.0	50.8	0.186	0.943	4.65
L12	182	58	6.013	2.030	0.762	.032	72.0	96.3	0.182	0.620	3.35
L13	183	58	6.024	2.024	0.790	.032	60.0	80.7	0.183	0.624	3.53
L14	182	57	6.006	2.019	0.765	.032	48.0	65.8	0.181	0.616	3.85
L15	191	75	6.092	2.503	1.014	.031	72.0	75.6	0.	0.861	4.90
L16	185	73	6.093	2.508	1.024	.032	60.0	63.4	0.	0.866	5.18
L17	188	75	6.016	2.511	1.022	.031	48.0	51.2	0.	0.872	5.31
L18	221	60	7.040	2.007	0.758	.031	72.0	99.3	0.220	0.560	3.13
L19	220	59	7.007	2.018	0.761	.031	60.0	82.9	0.222	0.566	3.39
L20	214	57	7.027	2.020	0.787	.032	48.0	66.7	0.224	0.572	3.67
L21	222	75	7.051	2.509	1.009	.031	72.0	76.4	0.159	0.804	3.86
L22	222	75	7.052	2.511	1.012	.031	60.0	64.1	0.159	0.805	4.42
L23	219	75	6.981	2.512	1.033	.031	48.0	51.7	0.161	0.815	4.14

Table continued on next page.

Table 5.13 continued

Specimen	w_1/t	w_2/t	W_1 (in.)	W_2	W_3	t	L	$\bar{L}/r_{min}$	e	$\bar{x}$	P_{uexp} (k)
L24	91	28	6.061	2.005	0.731	.064	72.0	100.1	0.	0.601	14.8
L25	89	35	6.059	2.495	1.000	.065	72.0	77.2	0.083	0.857	16.0
L26	88	34	6.052	2.494	1.007	.066	60.0	64.8	0.083	0.859	16.4
L27	89	35	6.025	2.499	1.011	.065	48.0	52.3	0.083	0.864	16.6
L28	107	28	7.074	2.004	0.740	.064	72.0	102.0	0.106	0.555	11.5
L29	105	27	7.063	2.009	0.740	.065	60.0	85.5	0.106	0.558	12.6
L30	104	27	6.998	1.998	0.745	.065	48.0	69.4	0.106	0.558	13.6
L31	107	35	7.081	2.499	1.001	.064	72.0	78.0	0.	0.797	17.0
L32	107	35	7.070	2.490	1.007	.064	60.0	65.7	0.	0.796	17.0
L33	106	35	7.022	2.505	1.044	.064	48.0	52.6	0.	0.813	18.0

*Refer to Fig. 5.1 for definition of cross-sectional parameters.
Assume OR = t + .059".

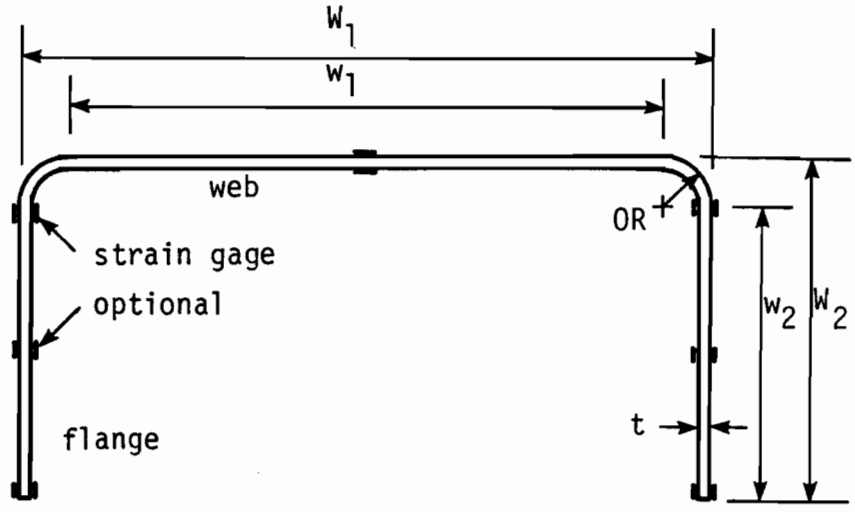

(a) Channel

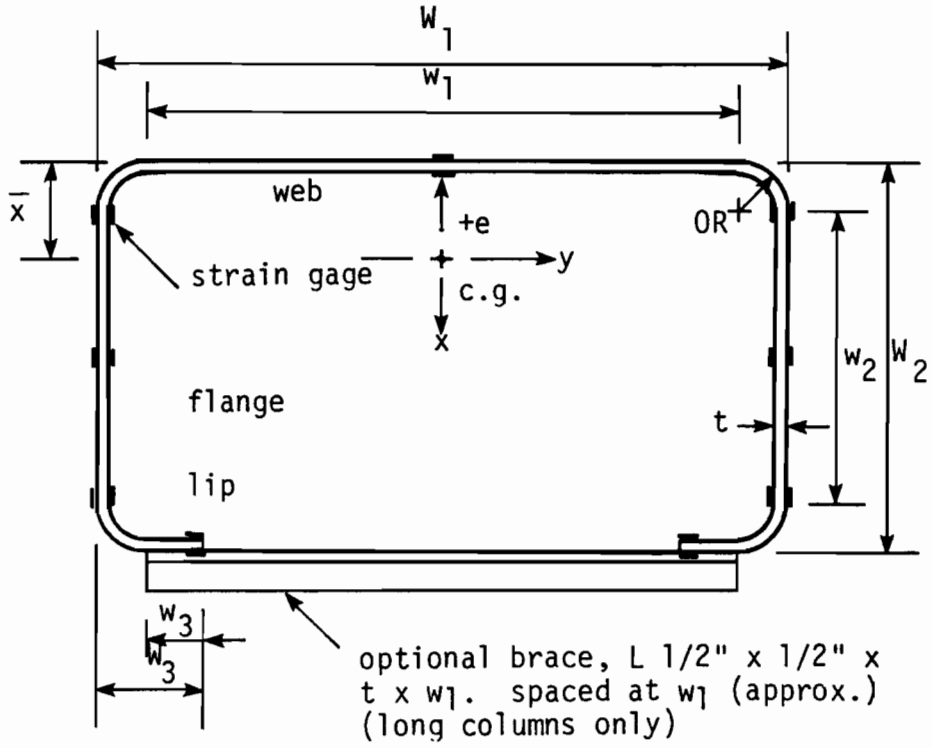

(b) Lipped Channel

Figure 5.1 TEST SPECIMEN CROSS SECTION AND TYPICAL STRAIN GAGE INSTRUMENTATION

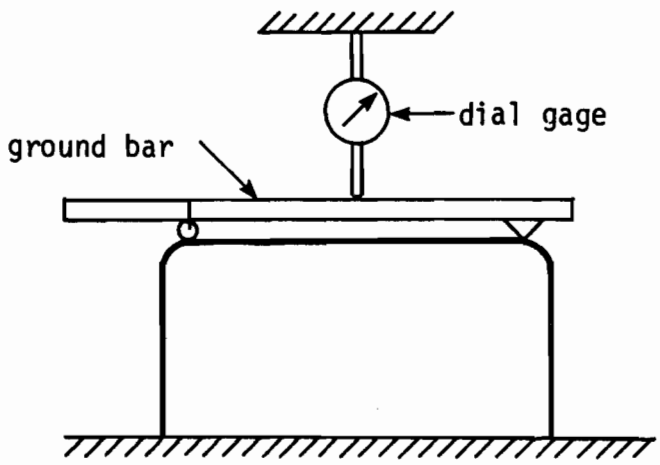

(a) Device 1

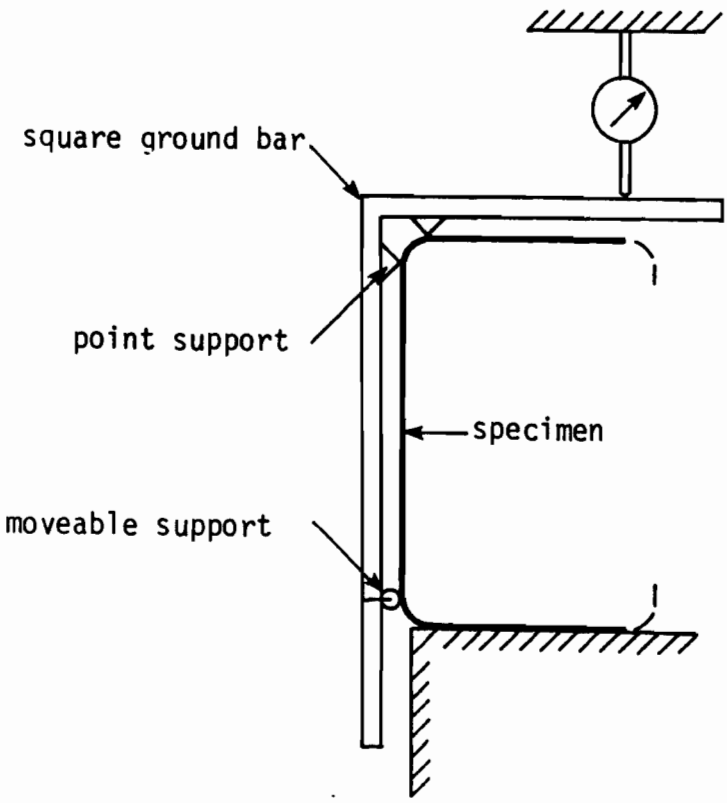

(b) Device 2

Figure 5.2 LOCAL INITIAL IMPERFECTION MEASURING DEVICES FOR STUB COLUMNS

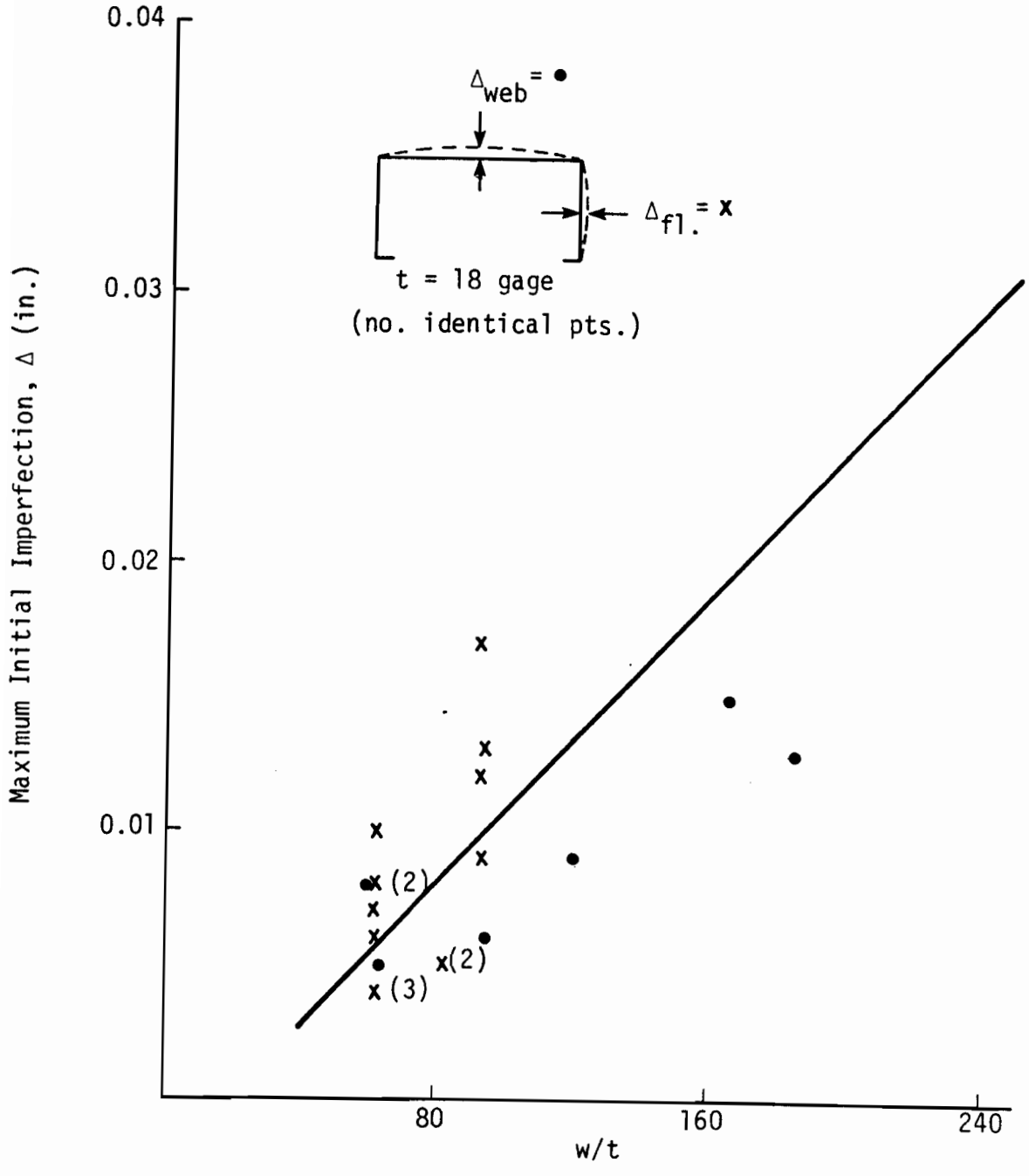

Figure 5.3 VARIATION OF MAXIMUM LOCAL INITIAL IMPERFECTION WITH FLAT WIDTH-TO-THICKNESS RATIO FOR LIPPED CHANNELS

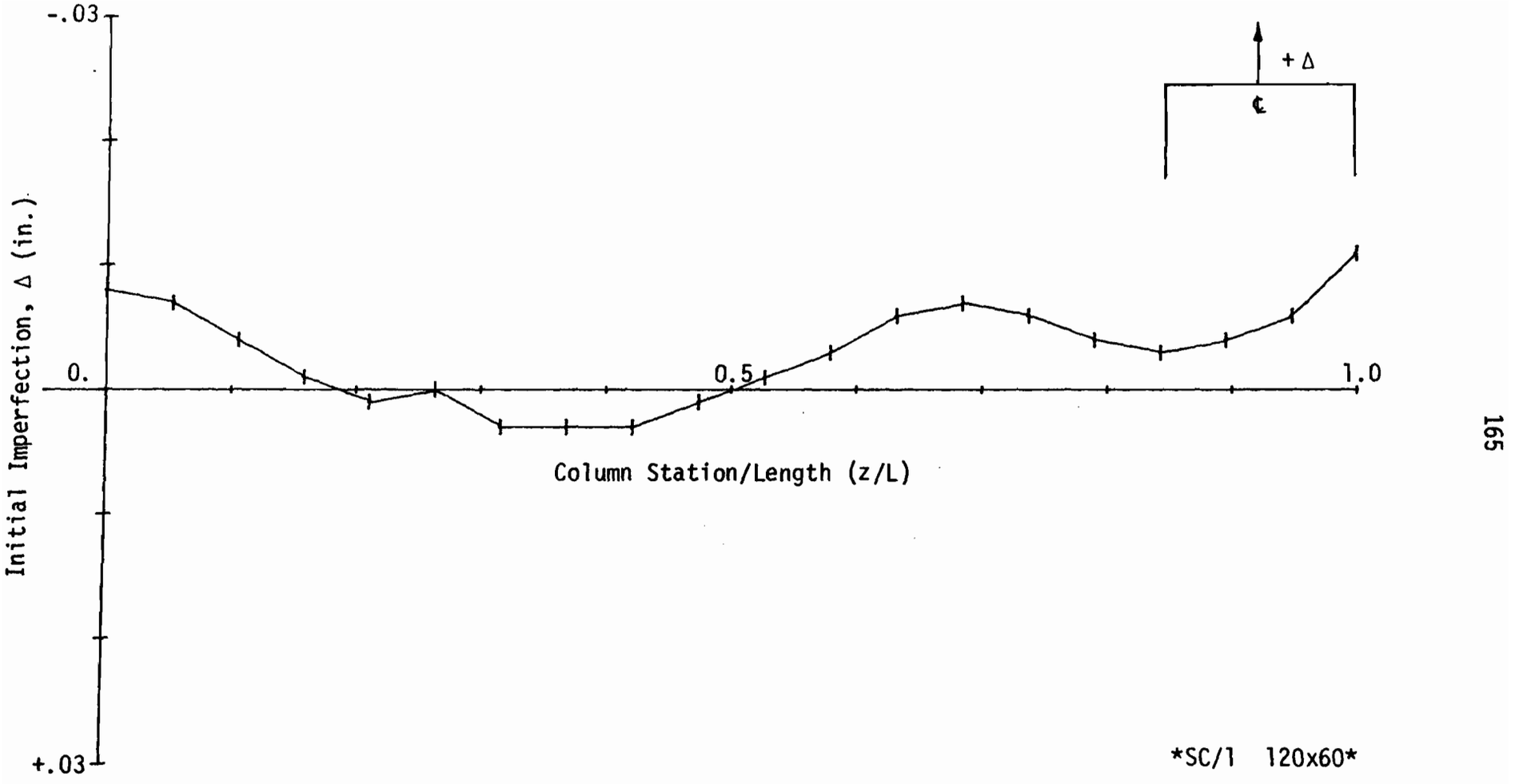

Figure 5.4 LOCAL INITIAL IMPERFECTION IN WEB OF CHANNEL STUB COLUMN SC/1 120x60

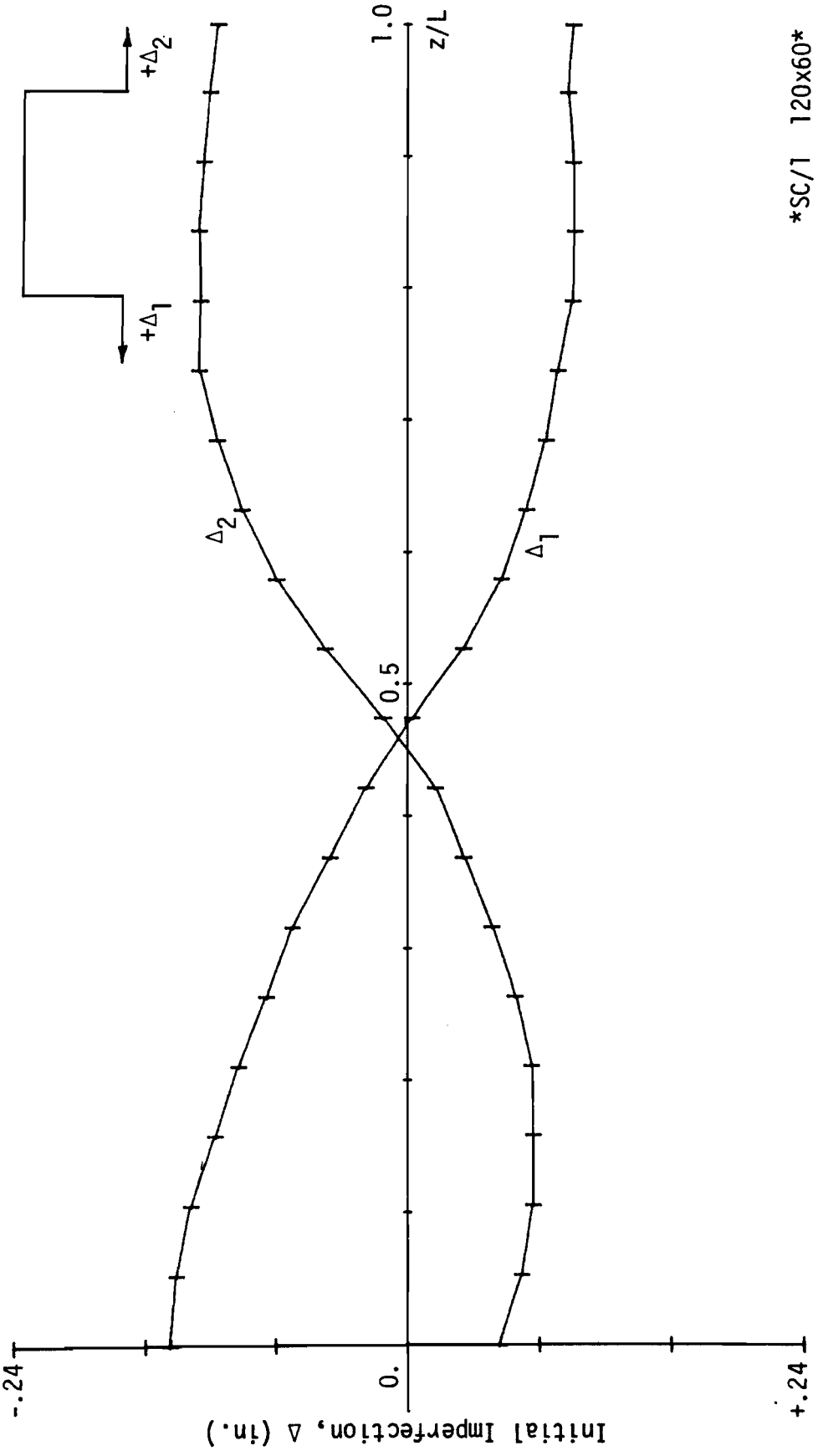

Figure 5.5 LOCAL INITIAL IMPERFECTION IN FLANGES OF CHANNEL STUB COLUMN SC/1 120x60

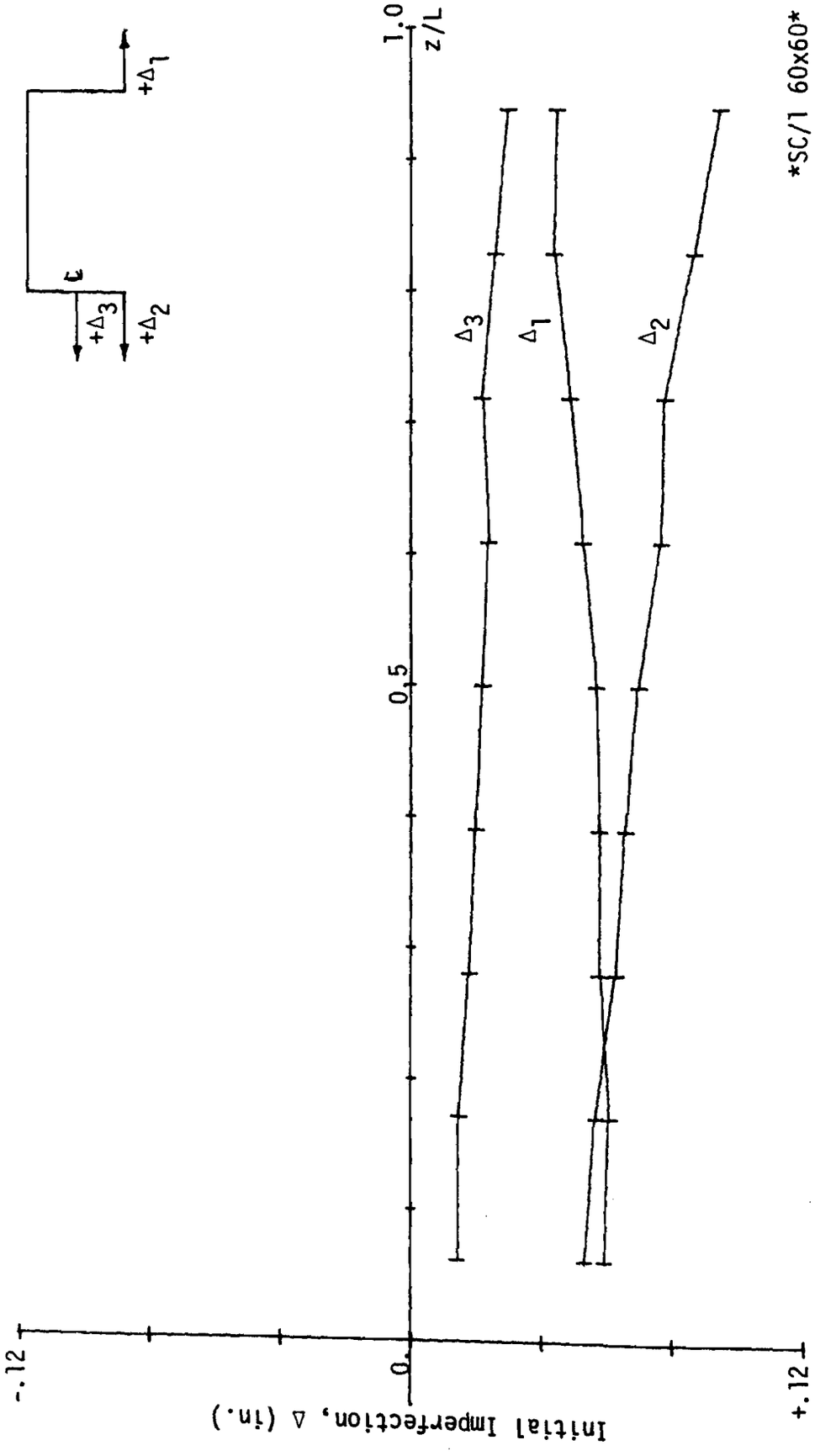

Figure 5.6 LOCAL INITIAL IMPERFECTION IN FLANGES OF CHANNEL STUB COLUMN SC/1 60x60

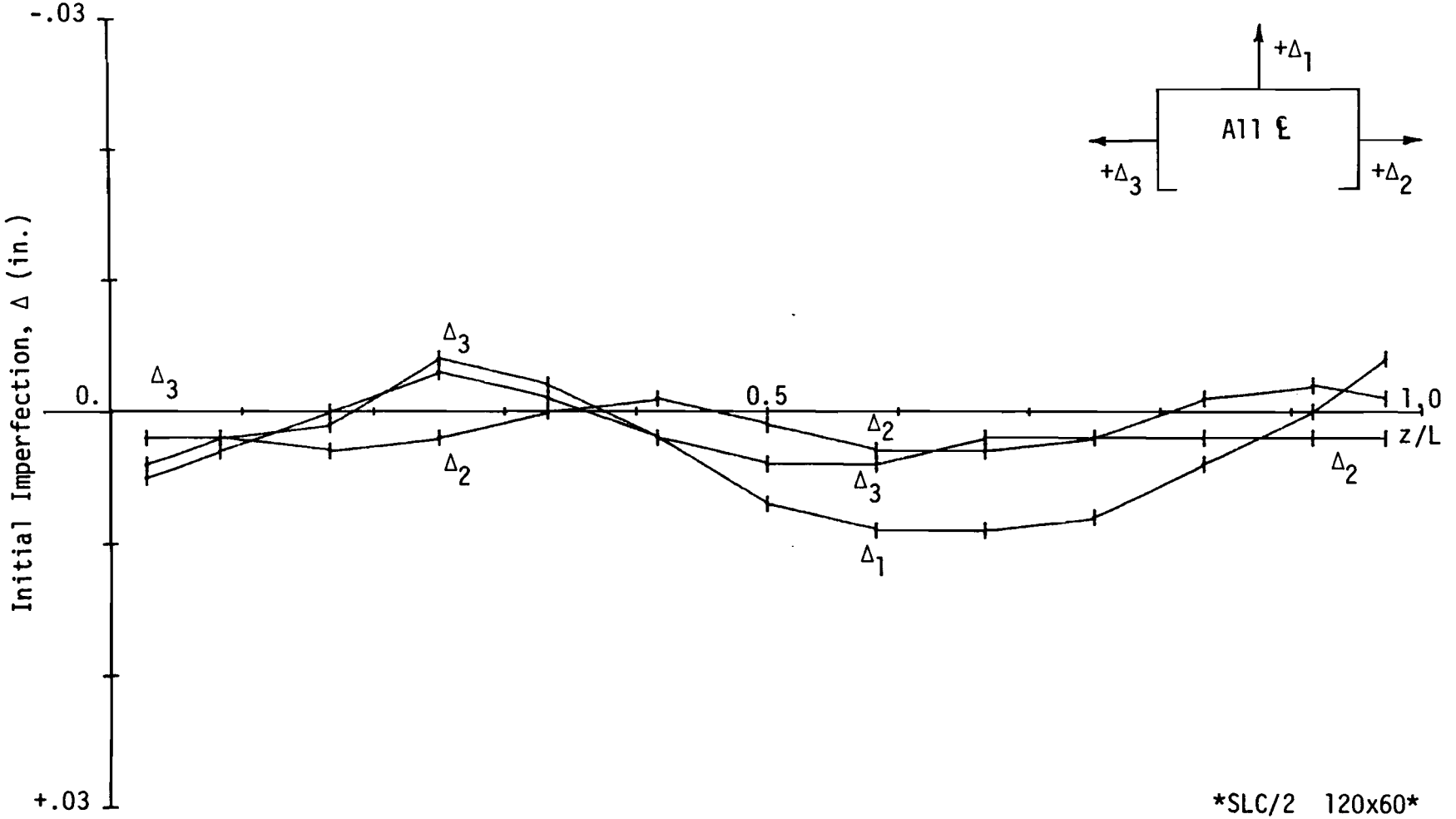

Figure 5.7 LOCAL INITIAL IMPERFECTION IN WEB AND FLANGES OF LIPPED CHANNEL STUB COLUMN SLC/2 120x60

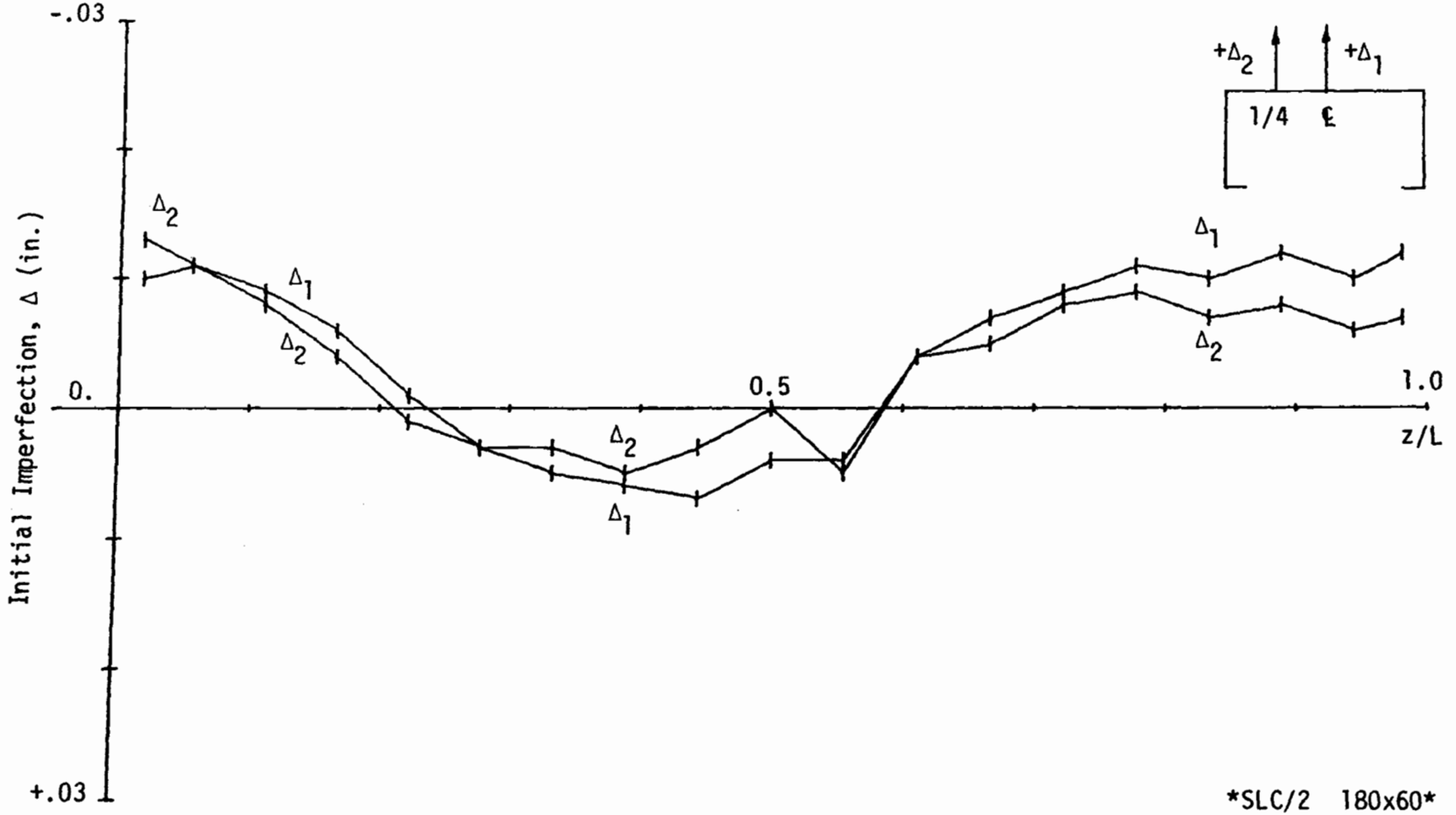

Figure 5.8 LOCAL INITIAL IMPERFECTION IN WEB OF LIPPED CHANNEL STUB COLUMN SLC/2 180x60

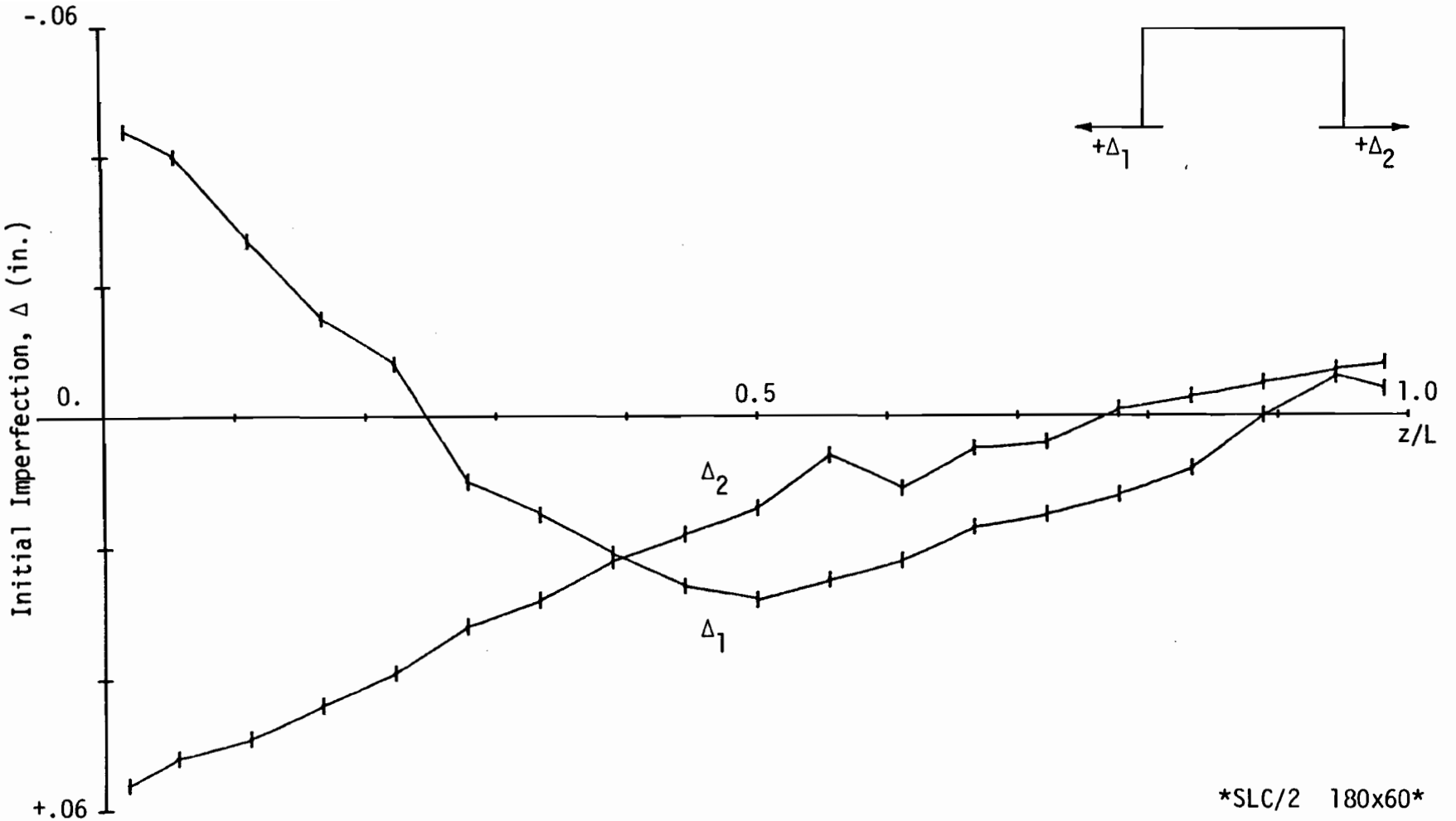

Figure 5.9 LOCAL INITIAL IMPERFECTION IN FLANGES, AT FLANGE-LIP JUNCTURE, IN LIPPED CHANNEL STUB COLUMN SLC/2 180x60

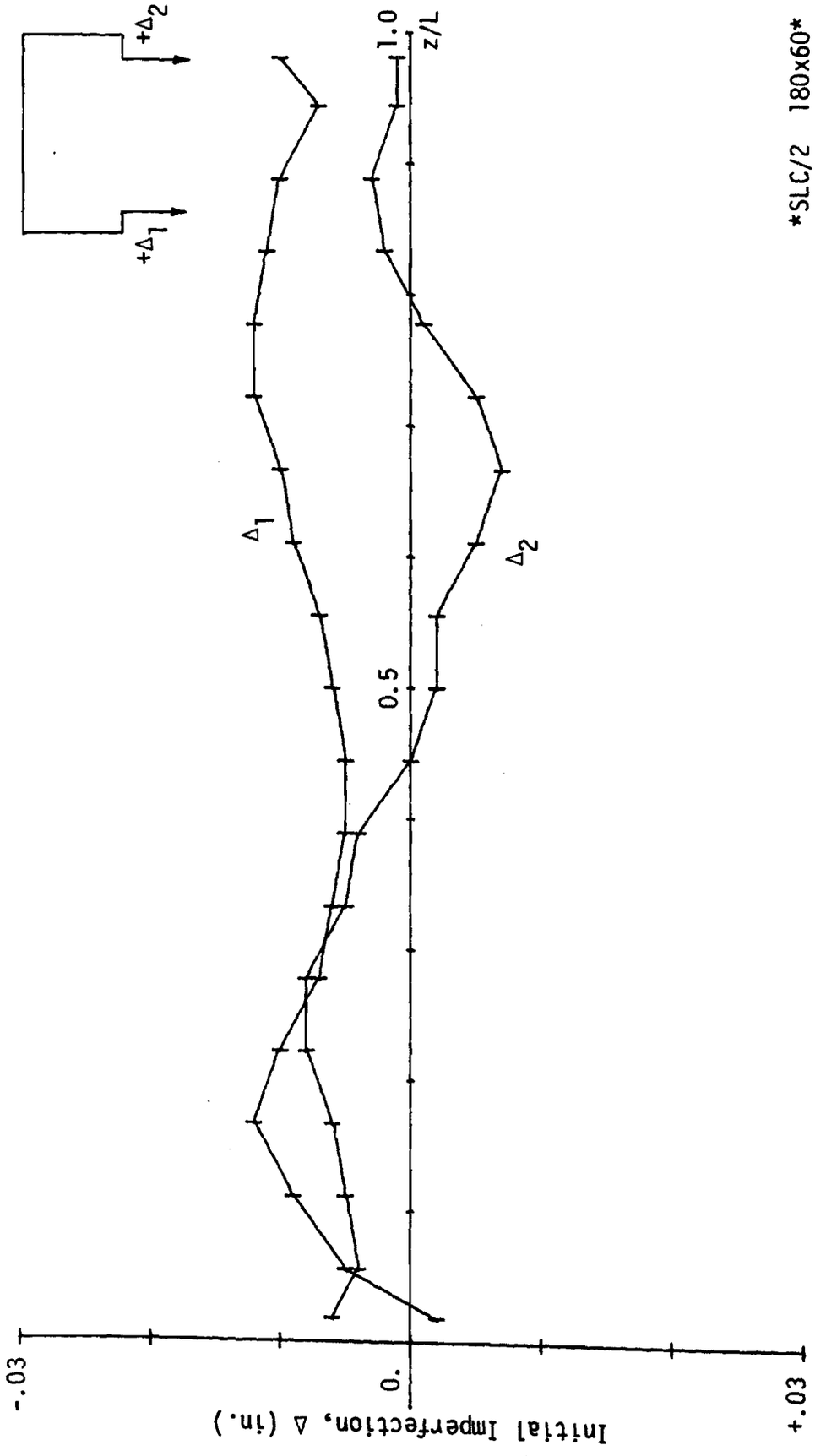

Figure 5.10 LOCAL INITIAL IMPERFECTION IN LIP OF LIPPED CHANNEL STUB COLUMN SLC/2 180x60

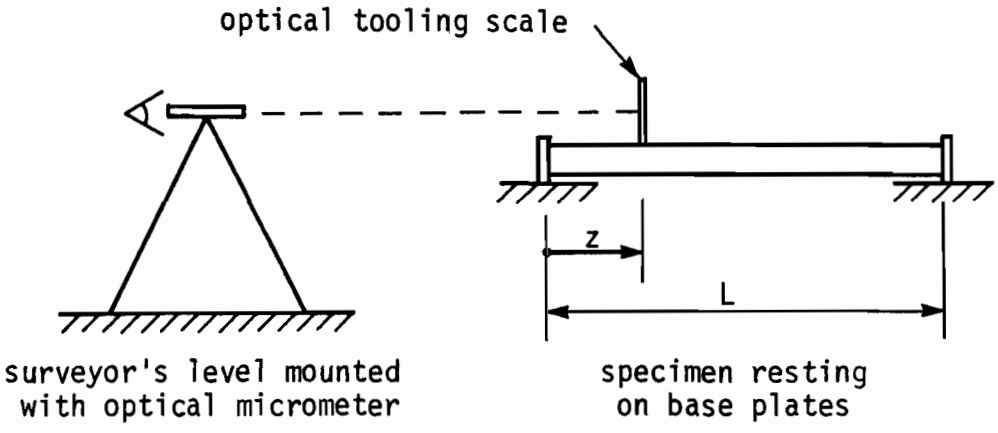

(a) Measurement (after Dat [1980])

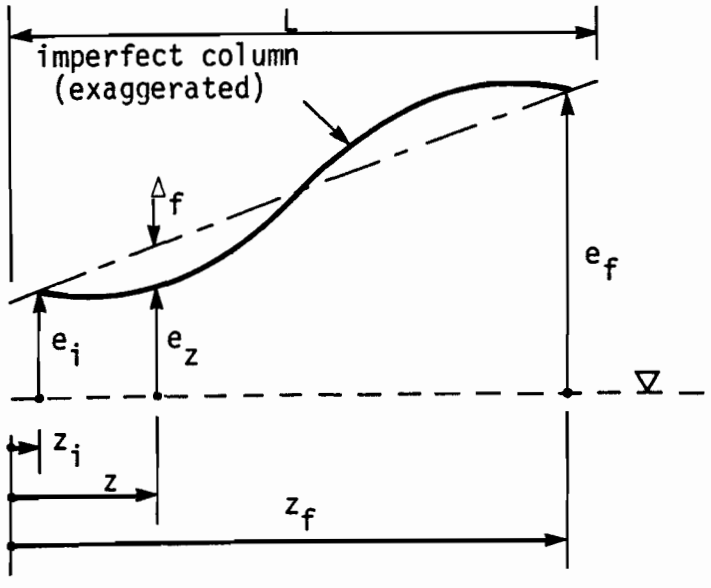

(b) Reduction

Figure 5.11 OVERALL INITIAL IMPERFECTION MEASUREMENT AND REDUCTION FOR LONG COLUMNS

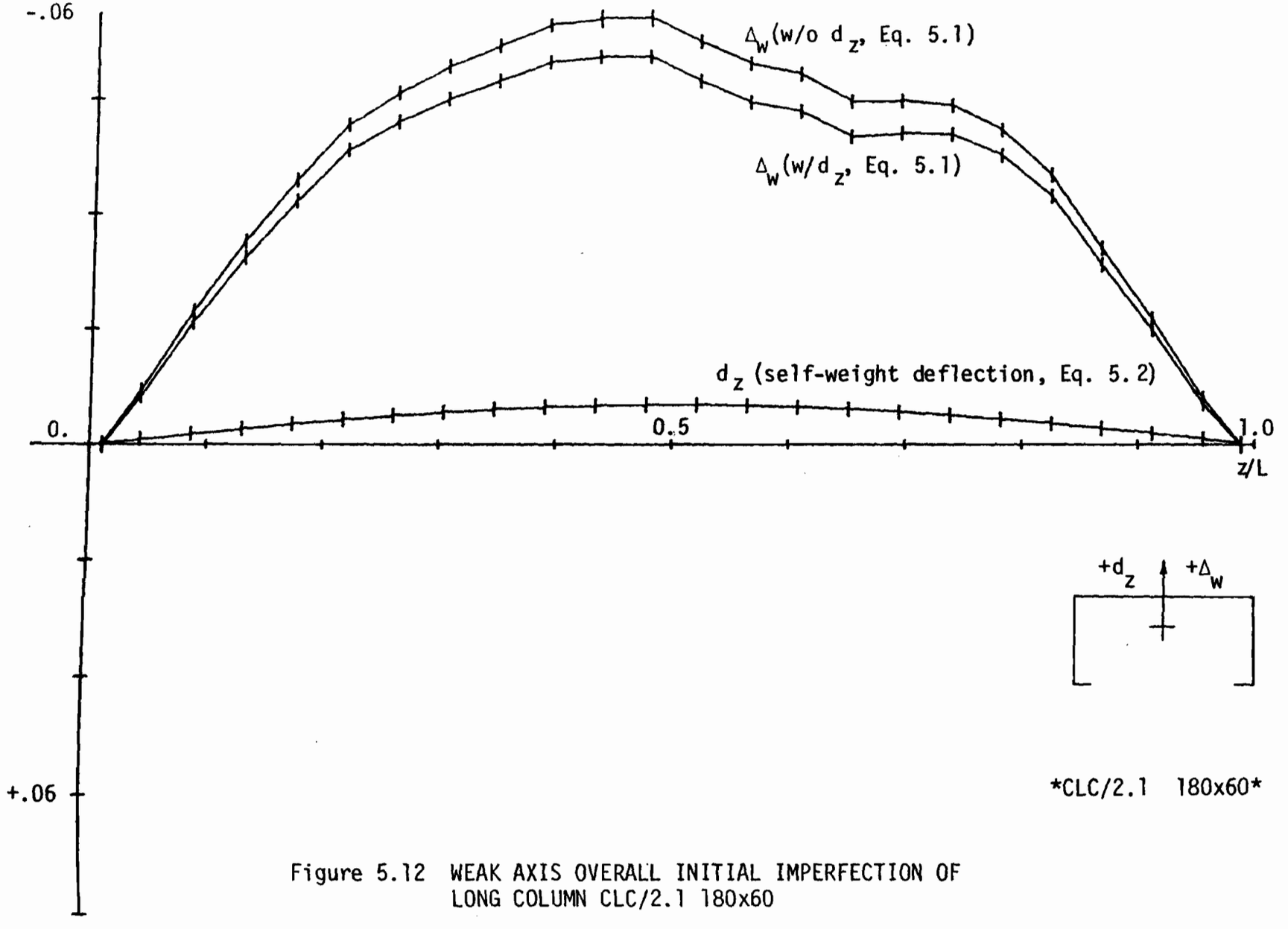

Figure 5.12 WEAK AXIS OVERALL INITIAL IMPERFECTION OF LONG COLUMN CLC/2.1 180x60

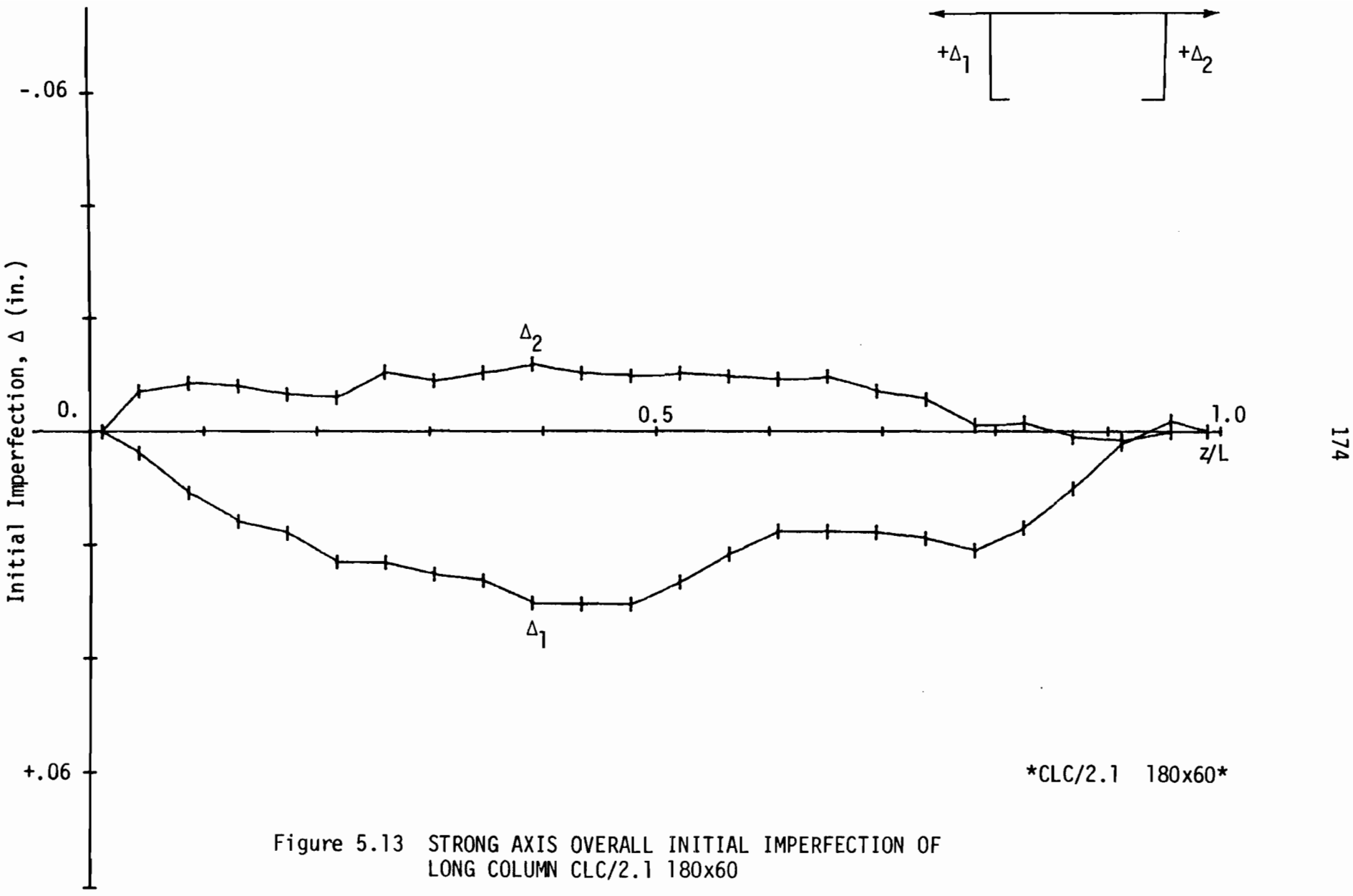

Figure 5.13 STRONG AXIS OVERALL INITIAL IMPERFECTION OF LONG COLUMN CLC/2.1 180x60

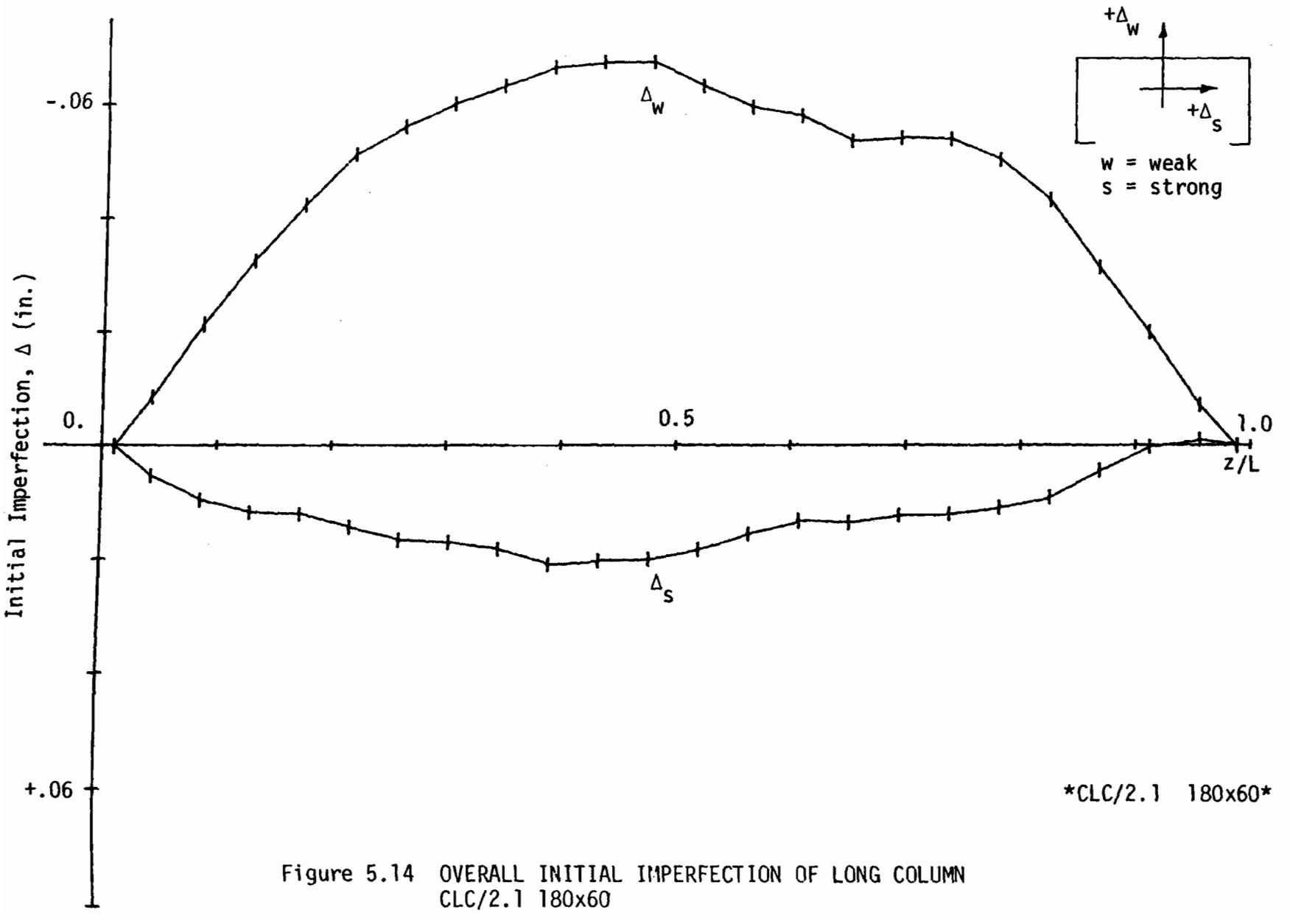

Figure 5.14 OVERALL INITIAL IMPERFECTION OF LONG COLUMN CLC/2.1 180x60

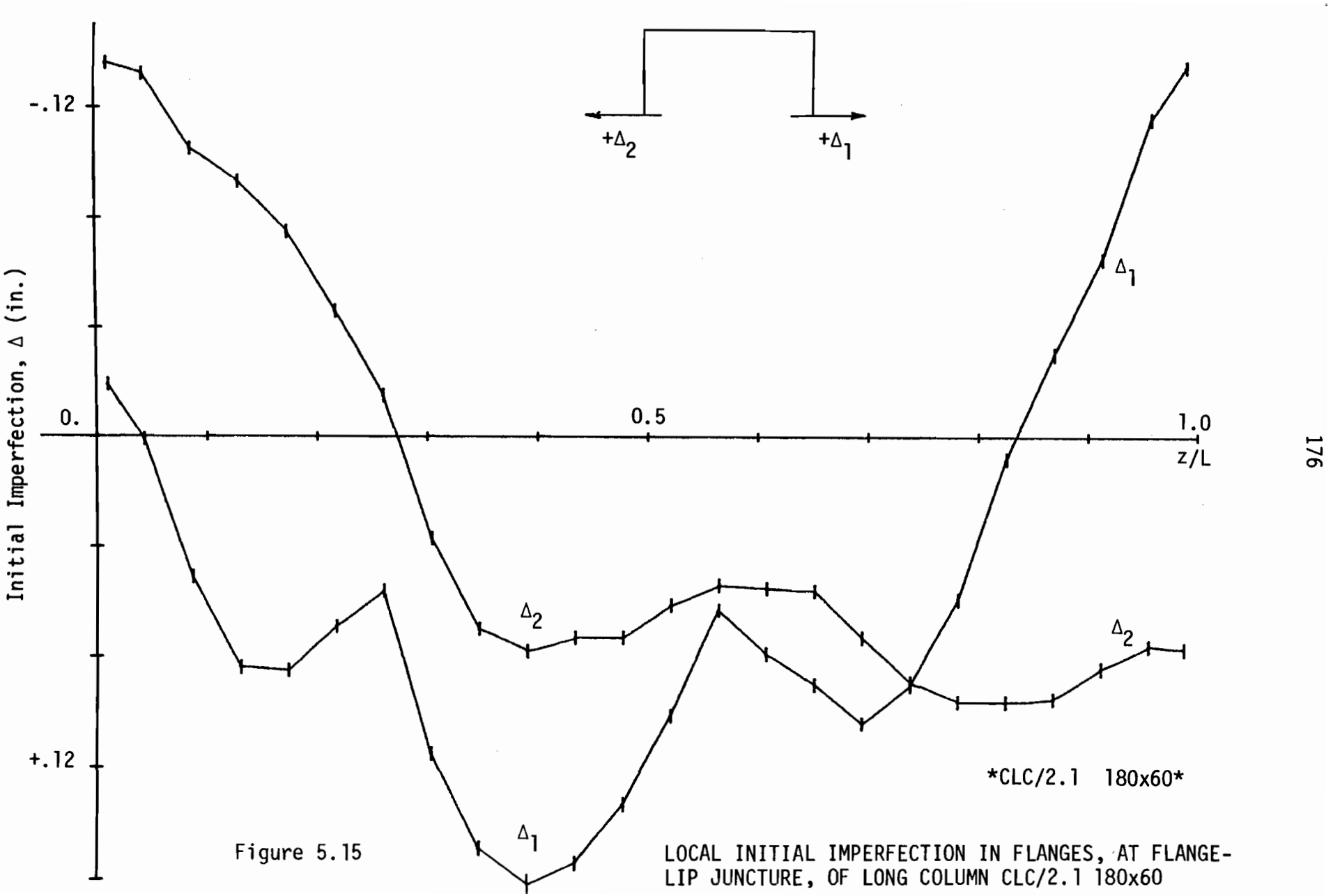

Figure 5.15 LOCAL INITIAL IMPERFECTION IN FLANGES, AT FLANGE-LIP JUNCTURE, OF LONG COLUMN CLC/2.1 180x60

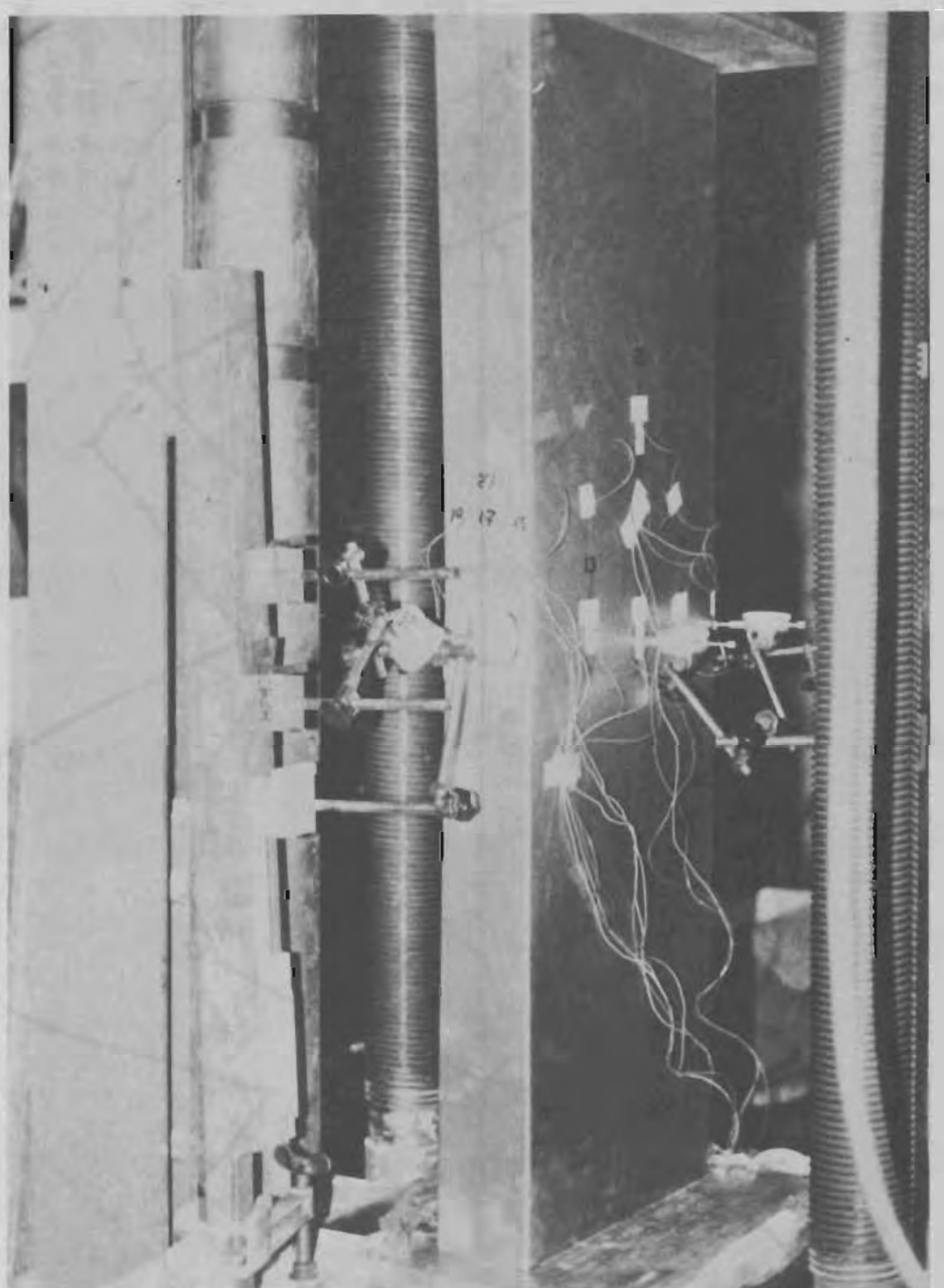

Figure 5.16 STUB COLUMN TEST SETUP

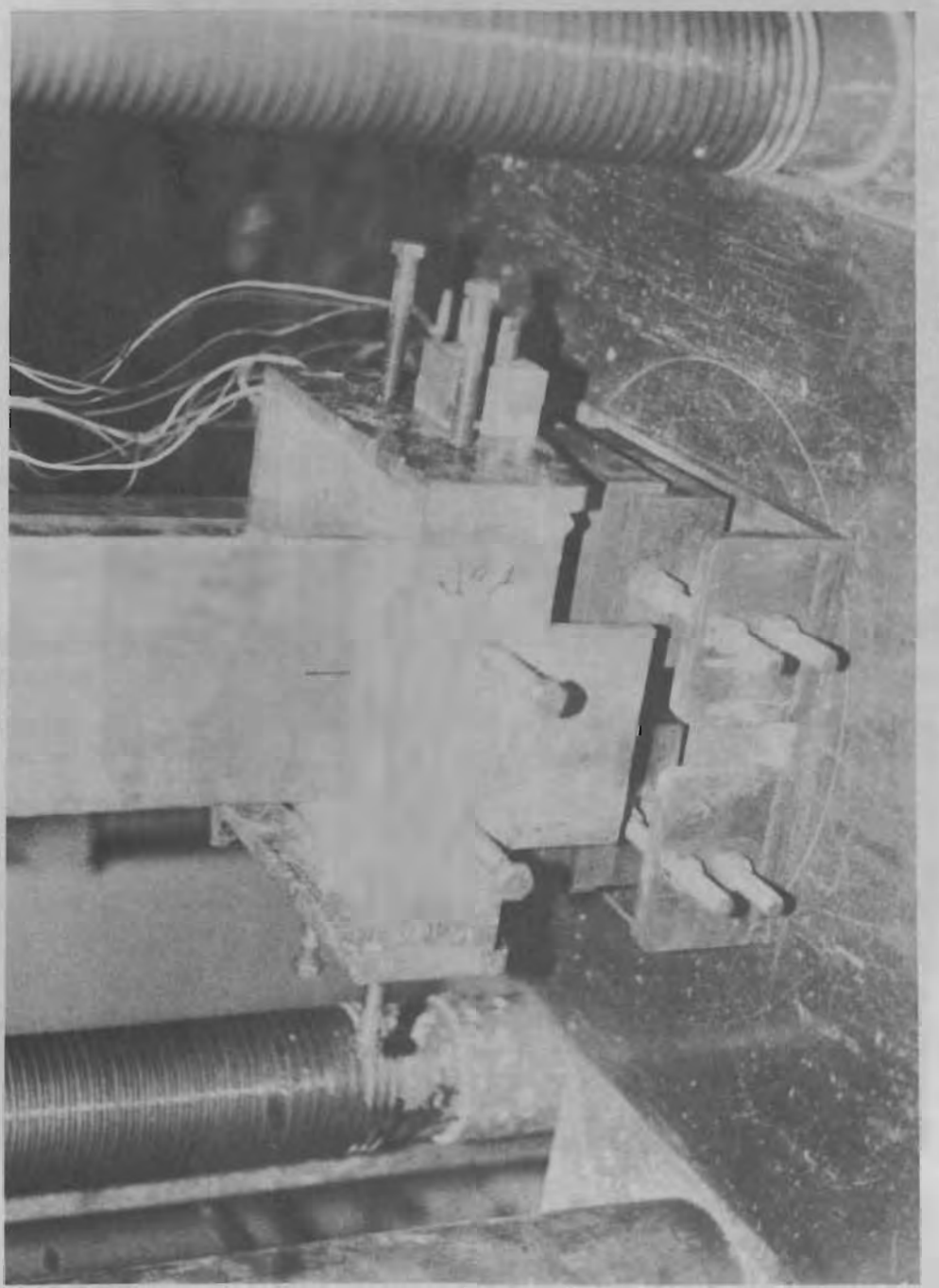

Figure 5.17 LONG COLUMN END FIXTURE

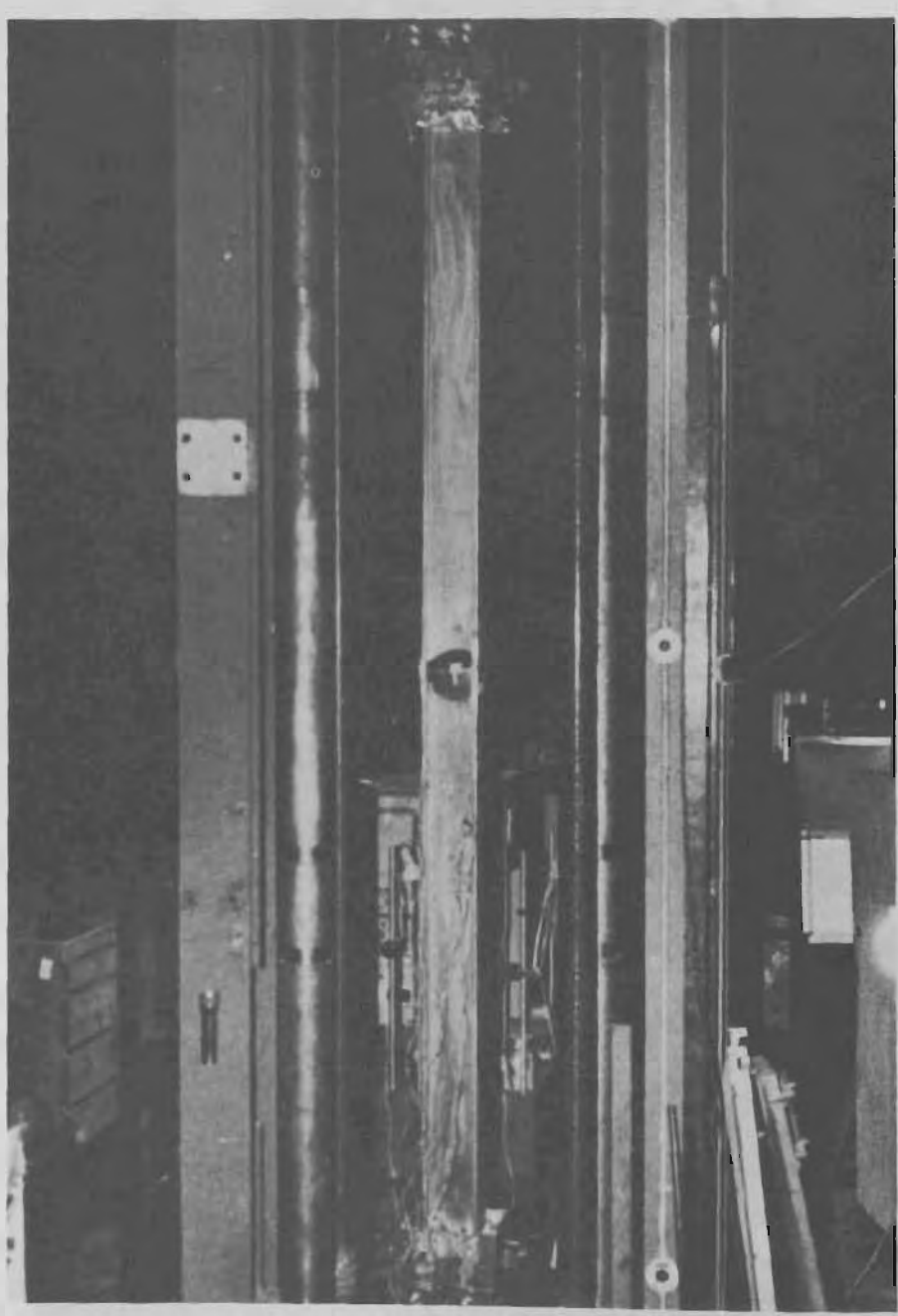

Figure 5.18 LONG COLUMN TEST SETUP

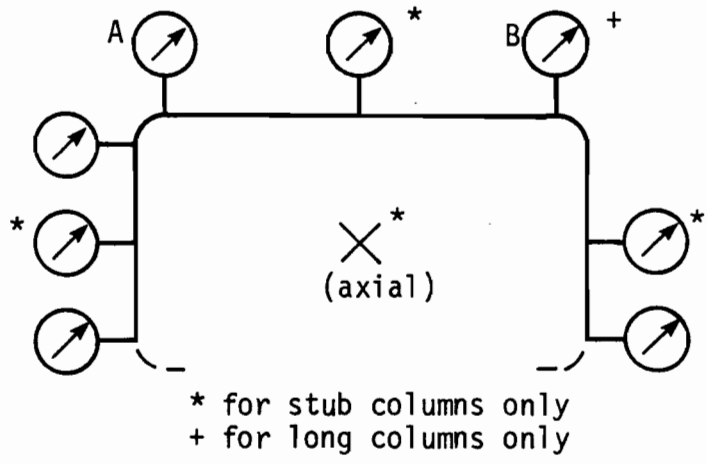

Figure 5.19 TYPICAL DIAL GAGE INSTRUMENTATION (at midheight)

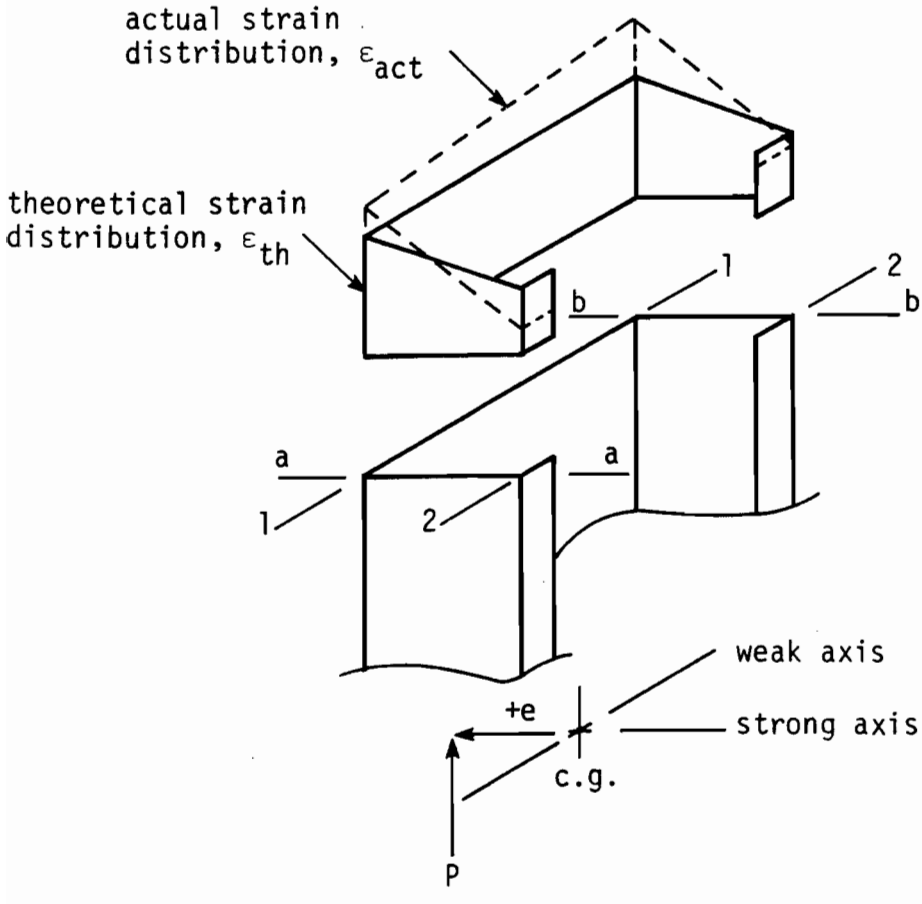

Figure 5.20 ECCENTRIC ALIGNMENT OF LONG COLUMNS
- LONGITUDINAL STRAIN DISTRIBUTIONS -

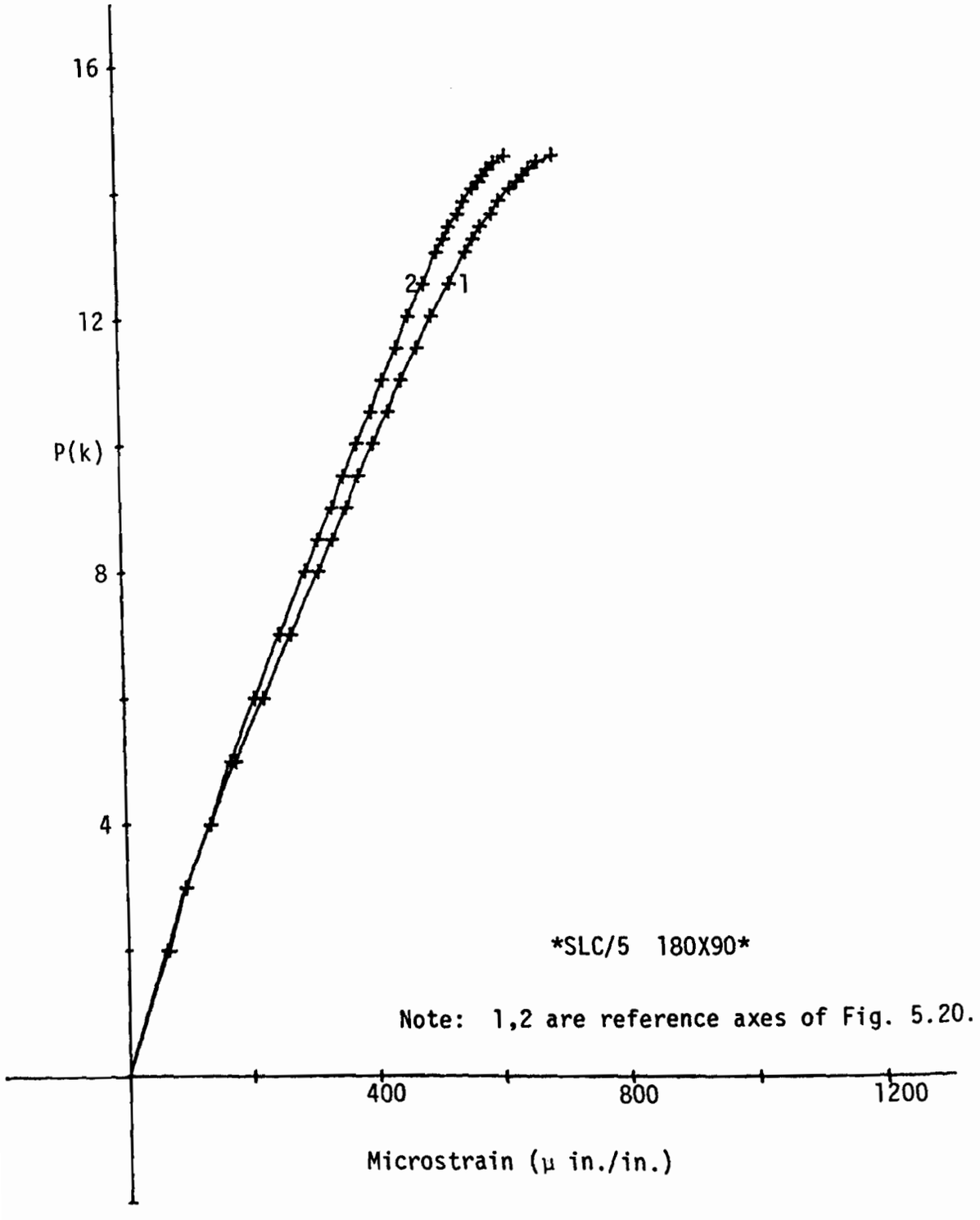

(a)

Figure 5.21 AXIAL LOAD-STRAIN RESPONSE FOR LIPPED CHANNEL STUB COLUMNS

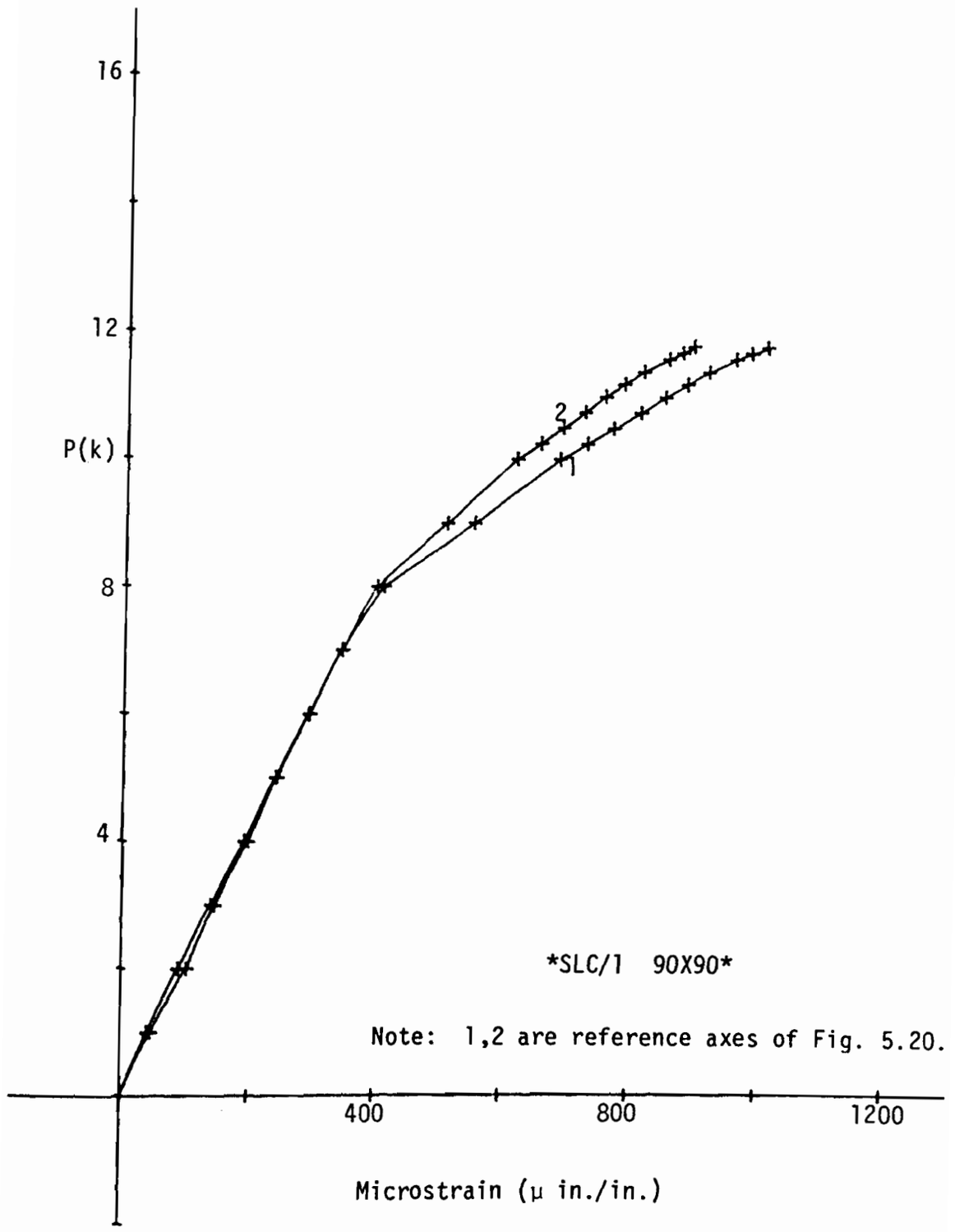
16
12
8
4
P(k)
2
1
400
800
1200
SLC/1 90X90
Note: 1,2 are reference axes of Fig. 5.20.
Microstrain (μ in./in.)

(b)

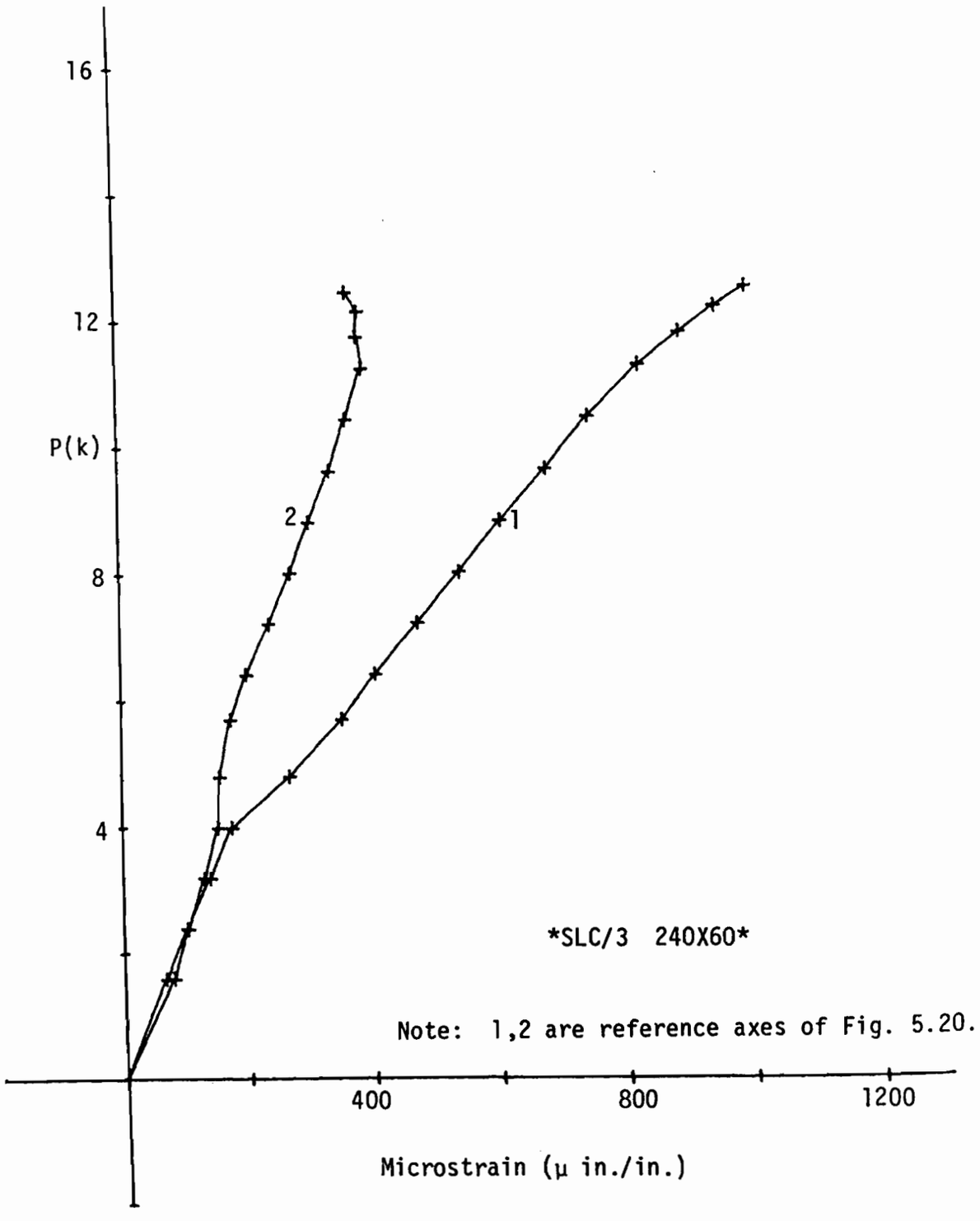

Figure 5.22 STRAIN GRADIENT IN LIPPED CHANNEL STUB COLUMNS
WITH LARGE WEB TO FLANGE

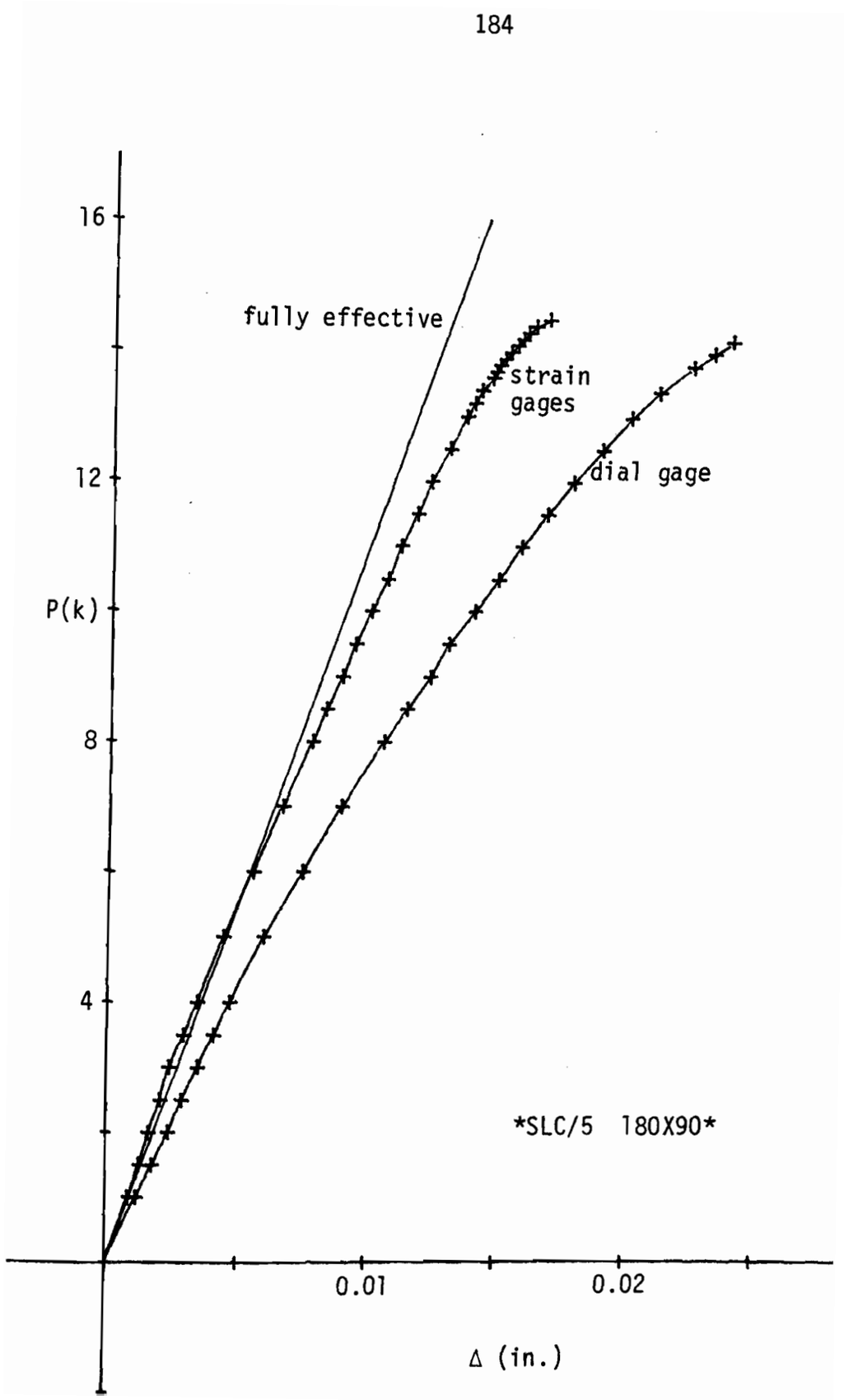
16
12
8
4
P(k)
fully effective
strain
gages
dial gage
SLC/5 180X90
0.01
0.02
Δ (in.)

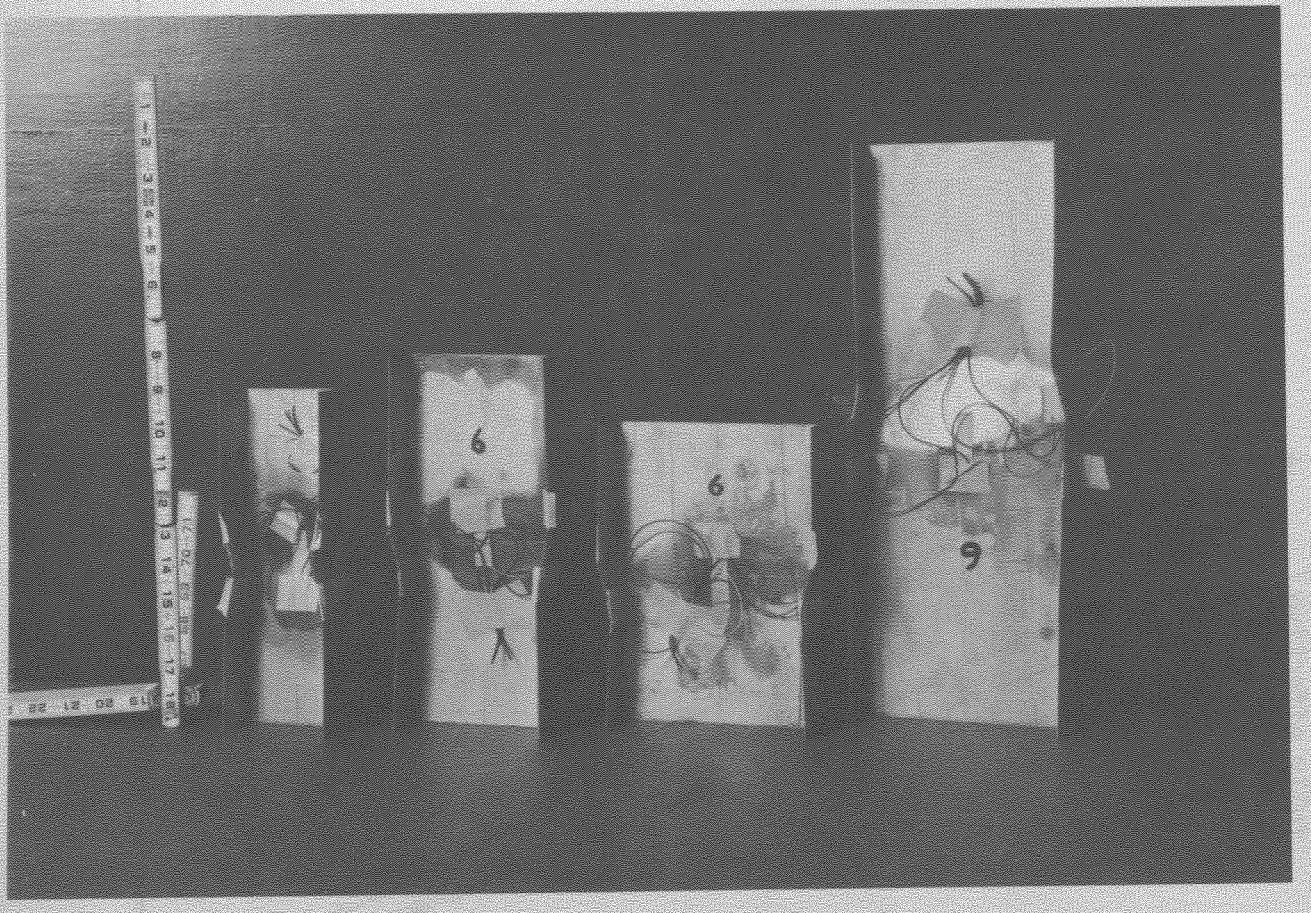

(a) Channels

Figure 5.24 STUB COLUMN FAILURE MODES

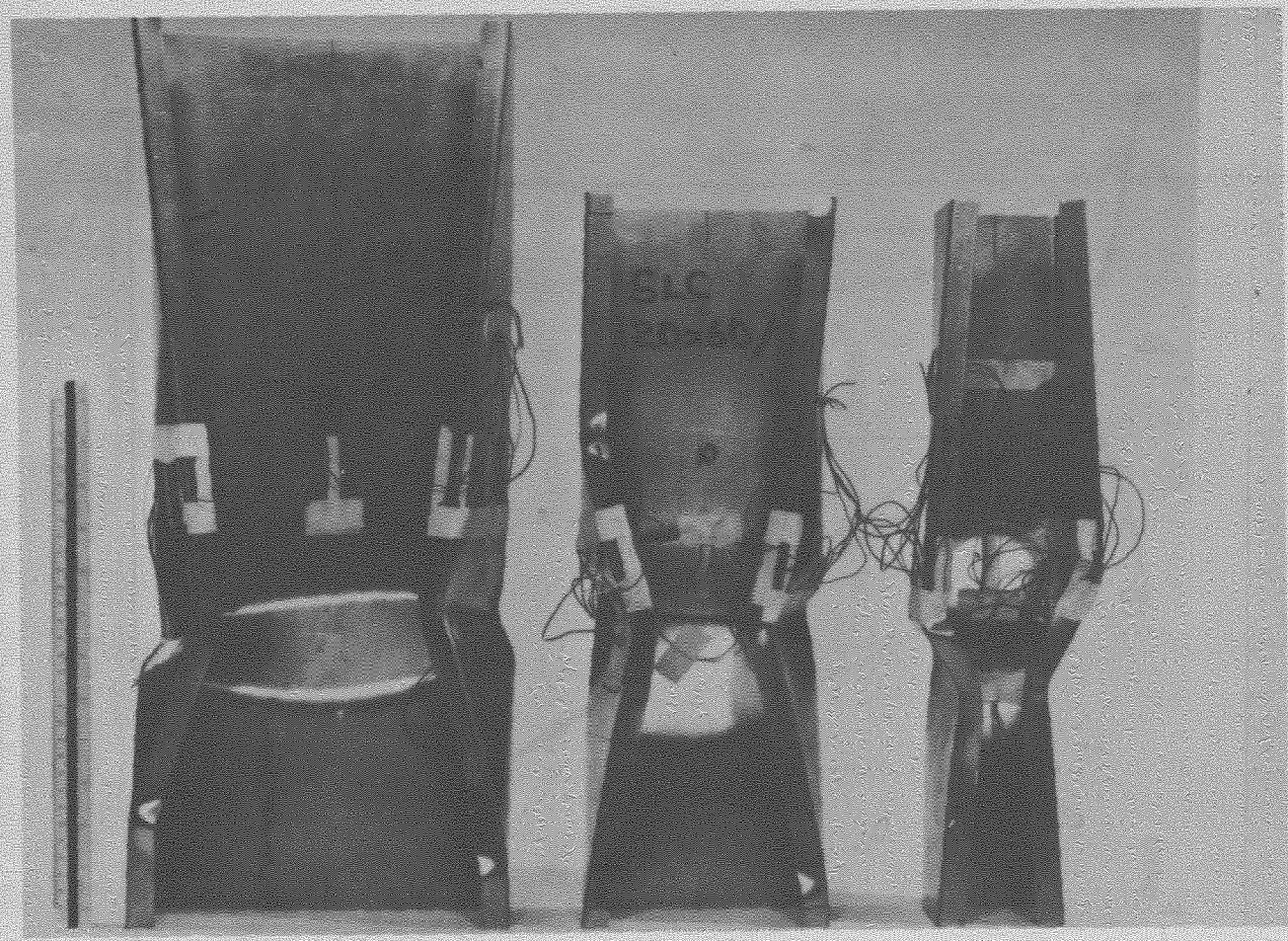

(b) Lipped Channels

Figure 5.24 Continued

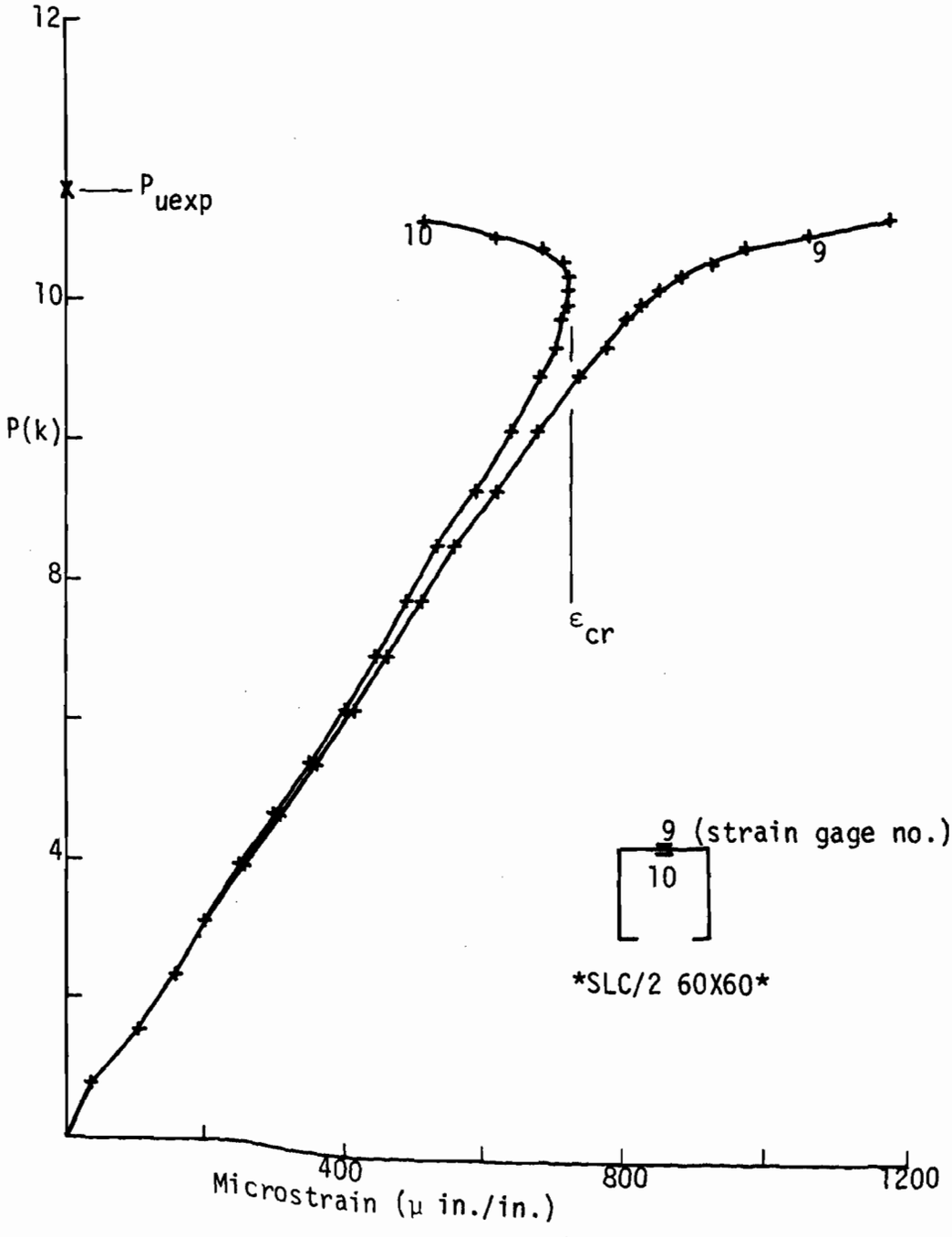

Figure 5.25 DETERMINATION OF CRITICAL BUCKLING STRESS

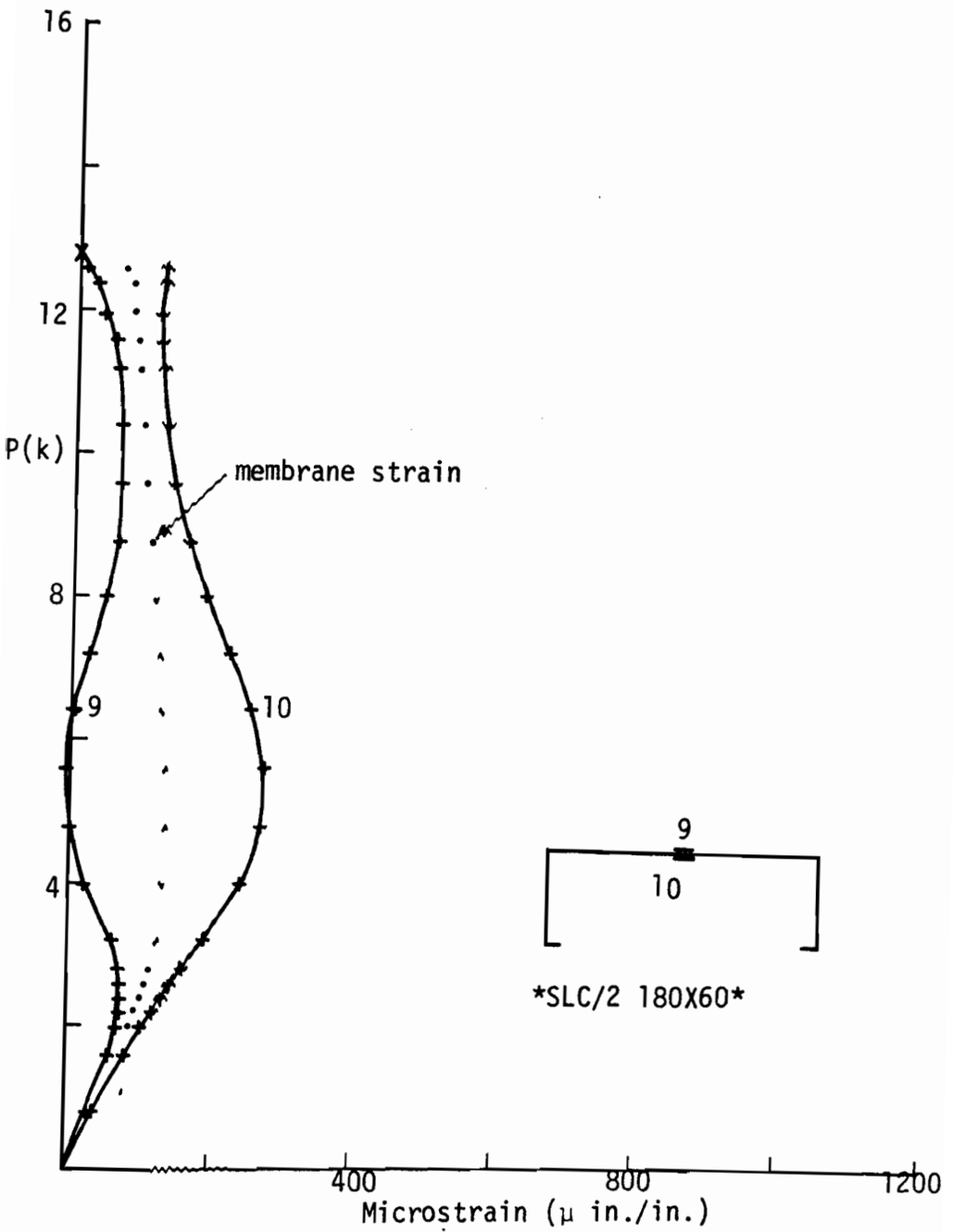

Figure 5.26 WEB LOCAL BUCKLING

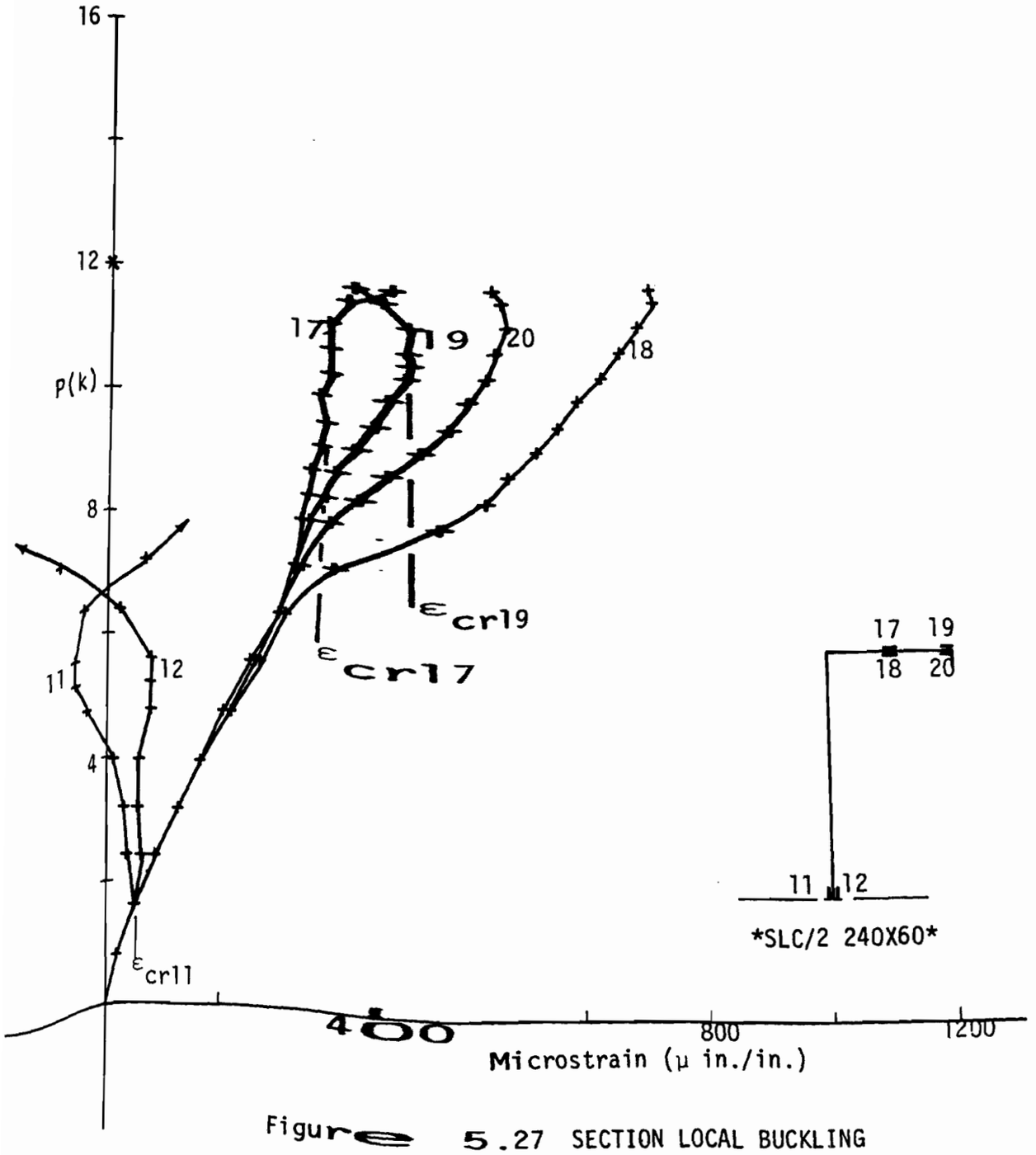

Figure 5.27 SECTION LOCAL BUCKLING

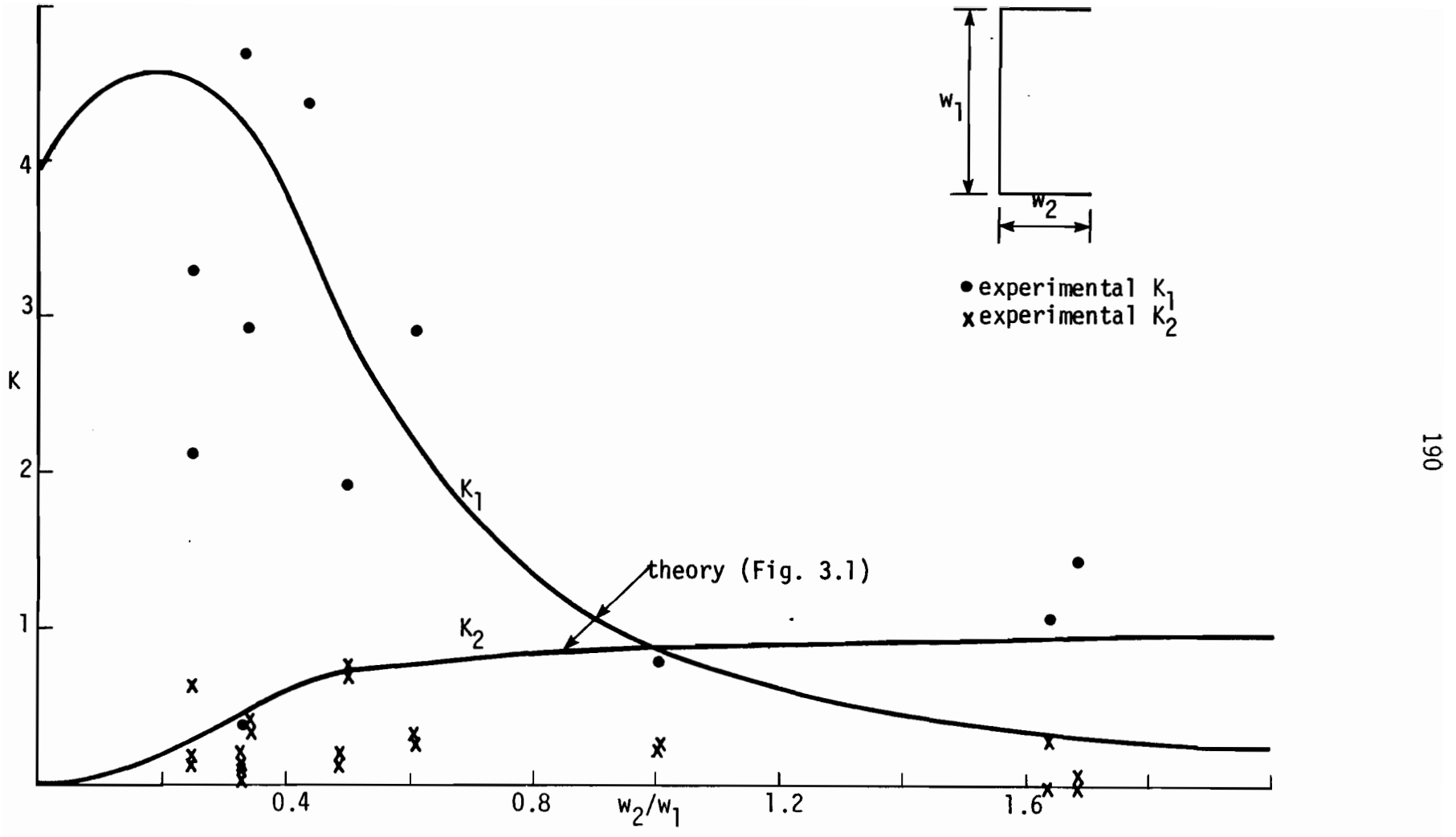

Figure 5.28 COMPARISON OF EXPERIMENTAL AND THEORETICAL BUCKLING COEFFICIENTS FOR CHANNELS

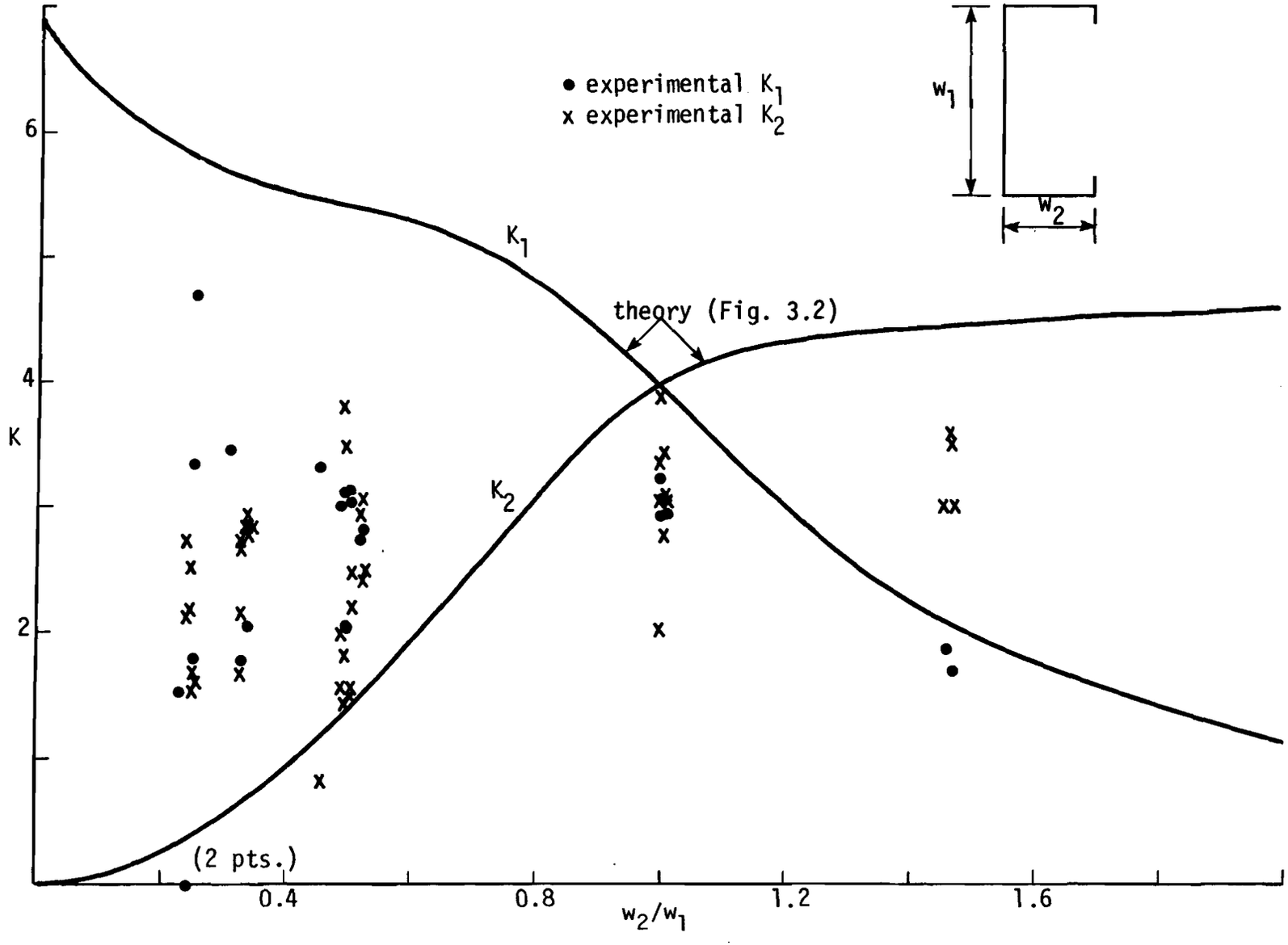

Figure 5.29 COMPARISON OF EXPERIMENTAL AND THEORETICAL BUCKLING COEFFICIENTS FOR LIPPED CHANNELS

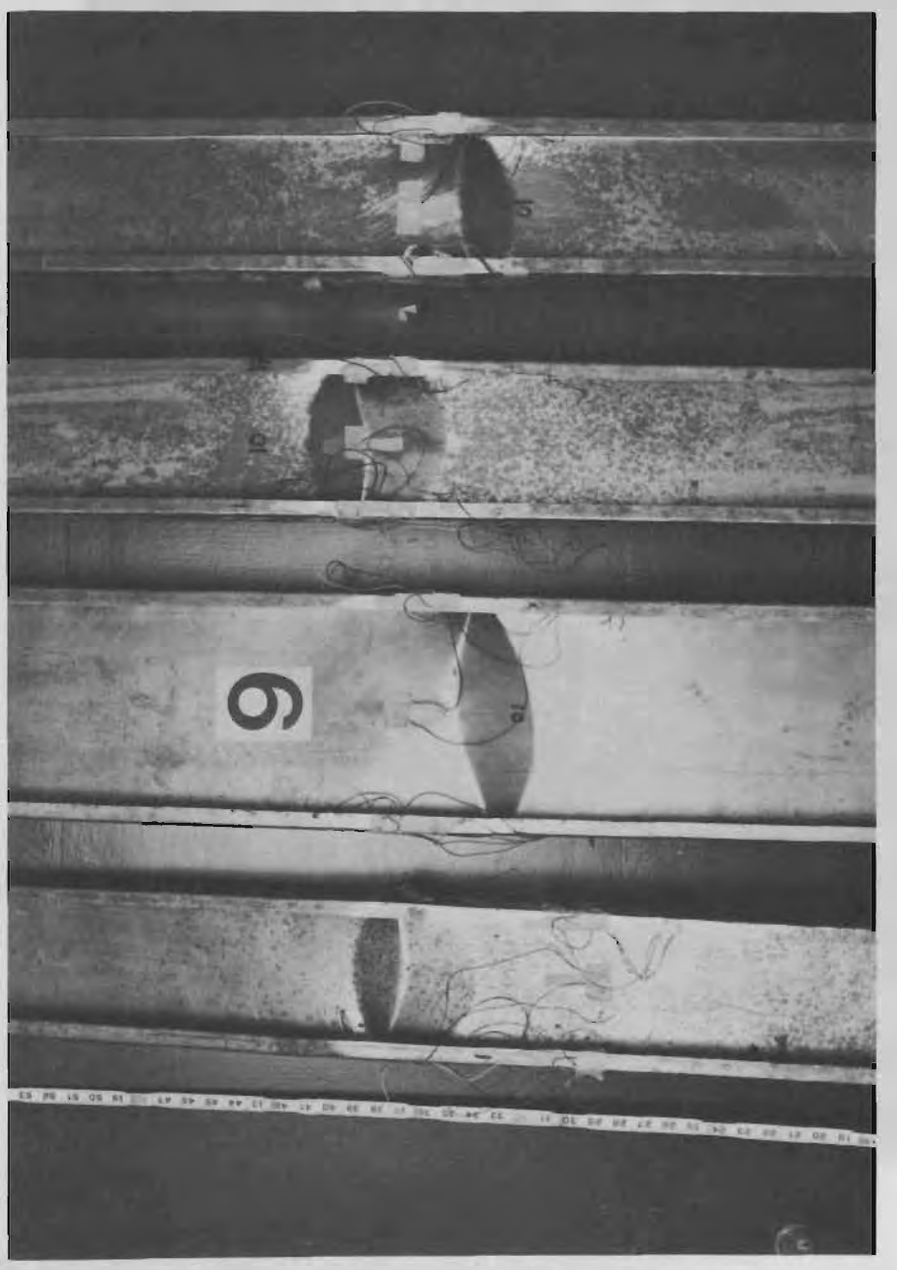

Figure 5.30 FAILURE MODES FOR CONCENTRICALLY LOADED LONG COLUMNS

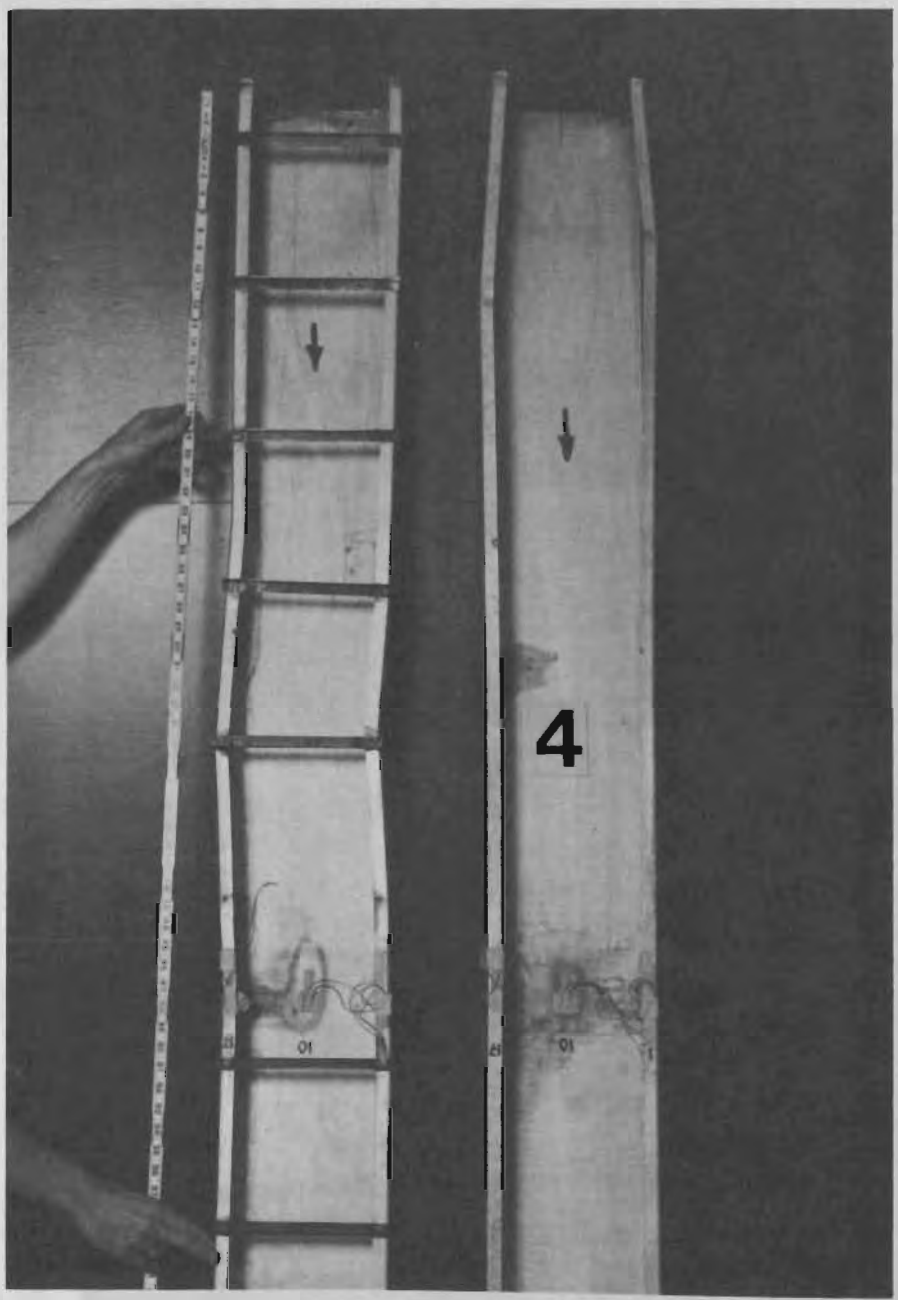

Figure 5.31 FAILURE MODES FOR ECCENTRICALLY LOADED LONG COLUMNS
– WITH AND WITHOUT BRACES –

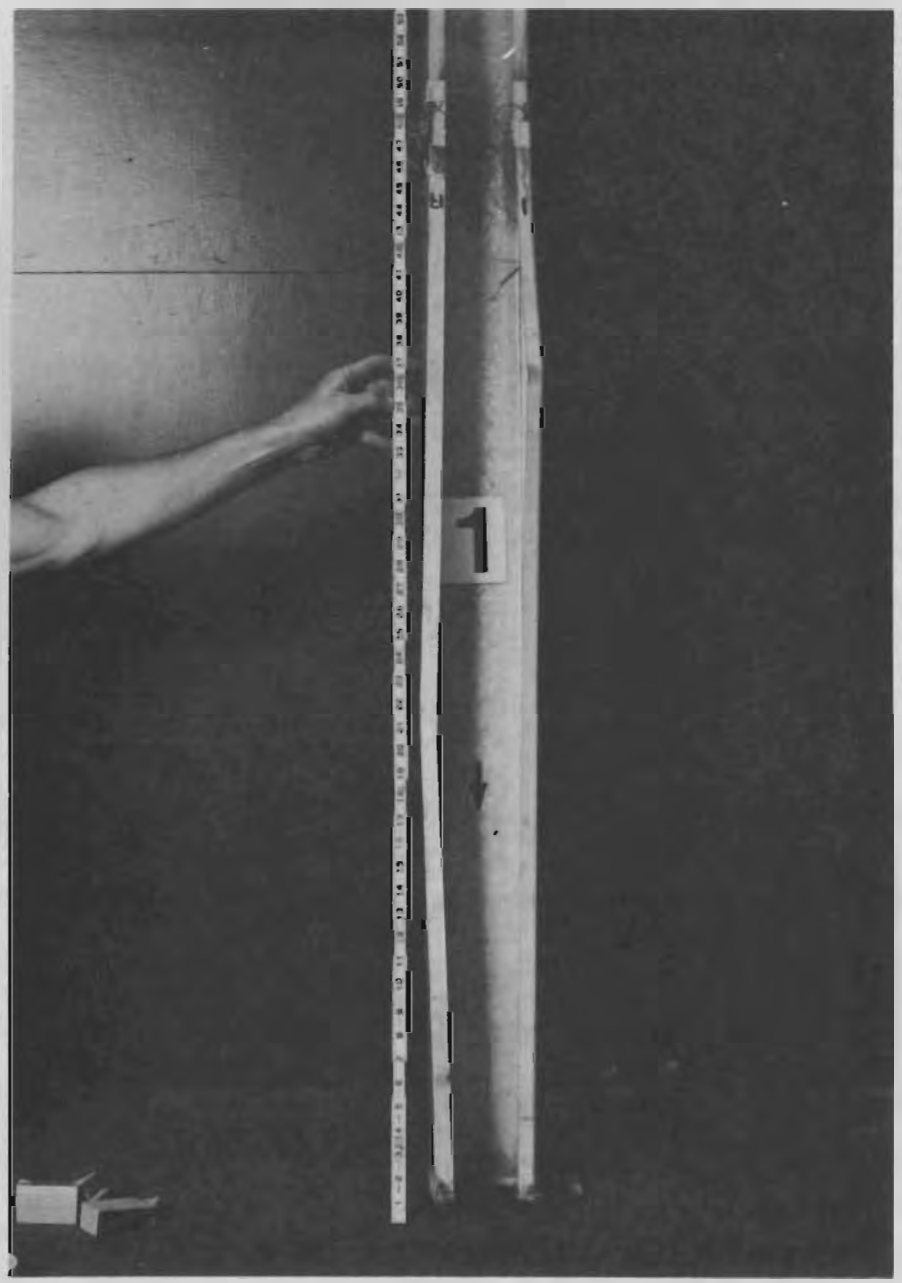

Figure 5.32 VIOLENT FAILURE MODE FOR TEST CLC/1 90x90

CHAPTER 6

COMPARISON OF EXPERIMENTAL AND THEORETICAL RESULTS

6.1 Introduction

In the present chapter the experimental results are compared with the theoretical predictions obtained from the methods of Chapters 2 through 4. The primary concern is an evaluation of the effective section method as applied to singly-symmetric stub and long columns, and beam-columns. However, comparisons with current, or proposed, design methods are also included. Finally, both ultimate strength and sub-ultimate response are considered.

6.2 Stub Column Evaluation

6.2.1 General

The stub columns test results are evaluated with respect to the effective section method of Section 3.5.1, where a loading condition of uniform compression is assumed. The response for all stub columns is predicted using two separate approaches to define the effective section. In one approach, Winter's stiffened plate effective width Equation 2.9 is applied to all component plate elements of the section. Thus

$$w_e/w = \sqrt{f_{cr}/f_e}\,(1.0 - 0.218\sqrt{f_{cr}/f_e}) \qquad 2.9$$

where the critical stress is calculated from

$$f_{cr} = K\pi^2E/12(1 - \mu^2)(w/t)^2 \qquad 2.4$$

The specific support conditions assumed to define the buckling coefficient K are defined subsequently. The second approach employs the sub-ultimate effective width Equation 2.48 for all component elements, or

$$w_e/w = A/\lambda^2 + B/\lambda + C + D\lambda \qquad 2.48$$

where $\lambda = (f_e/f_{cr})^{\frac{1}{2}}$ and the constants A-D are defined in Section 2.3.2. Also, in a few cases, Thomasson's [1978] equations of Section 2.3.1 are used to determine the effective widths of all component elements and are compared with the approaches defined above.

Once the effective area A_e is defined from the individual element contributions, the axial load P is simply calculated from

$$P = f_e A_e \qquad 3.26$$

At ultimate conditions the edge stress is set equal to the yield stress, i.e., $f_e = F_y$, and the effective width approaches of Equations 2.9 and 2.48 give identical results.

In addition, the influence of local buckling interaction between component plate elements is investigated by evaluating two different ultimate loads, P_{us} and P_{ui}. Only the strengths predicted via Equation 2.48, or equivalently Equation 2.9, are included in this evaluation. For the calculation of P_{us}, local buckling interaction is ignored; accordingly the buckling coefficient K, in Equation 2.4, is taken equal to the simply supported values of K = 0.425 for unstiffened elements and K = 4.0 for stiffened and edge stiffened elements. It is noted that these values are also employed in all sub-ultimate predictions, i.e., in Equations 2.9, 2.48, or Thomasson's equations, all with $f_e < F_y$. For the calculation of P_{ui}, local buckling interaction is presumed, and the buckling coefficients K are obtained from a finite strip local instability analysis of the

Moreover, the edge stiffeners of the lipped channels are evaluated against Desmond's [1978] requirements which are reviewed in Section 3.4. The adequate (required) stiffener centroidal moment of inertia is designated as I_{sa}, and the actual stiffener moment of inertia, I_s, is calculated using the approximation and effective area distribution of Figure 3.9b.

6.2.2 Ultimate Strength

The predicted ultimate loads P_{us} and P_{ui} defined above are compared, in Table 6.1, with the experimental values, P_{uexp}, for channel stub columns. Generally, the ultimate load P_{us}, which is calculated assuming simply supported boundary conditions between plate elements, provides slightly better overall correlation with experimental results. For the eleven tests, the mean strength ratio P_{uexp}/P_{us} of 1.079 is slightly conservative and deviates by 8.8% on the average. However, the other ultimate load P_{ui}, which accounts for local buckling interaction, yields approximately the same correlation; for example, the mean strength ratio P_{uexp}/P_{ui} and associated standard deviation are 1.102 and 5.6%, respectively.

While either of the predicted ultimate loads evaluated above provides acceptable correlation with experimental results for channel sections, their acceptability may actually be dictated by excessive waving of the unstiffened flanges. This aspect is examined in Figure 6.1 where the maximum out-of-plane deformation Δ_{max} at the free edge of the flange, obtained just prior to failure, is plotted against the web-to-flange width ratio, w_1/w_2. The positive slope of the best-fit lines, which are obtained from a linear regression analysis of the data points for each

flange width-to-thickness ratio, w_2/t, indicates that local buckling interaction affects the waving of the flanges. More important though are the magnitudes of the deformation. These increase with increasing w_2/t ratio and for large w_2/t ratios, equal to 60, exceed four times the thickness of the element. In contrast to this, Kalyanaraman [1978] reported deformations for comparable flanges of only about one-half those measured in the present study. This difference is due to the restraint provided, to the flanges, by the relatively compact webs of the built-up "I" sections tested by Kalyanaraman. Since this type of support is normally unavailable in all construction applications, it appears that the limitations placed on unstiffened compression elements (flanges) by the AISI Specification [1980] may be warranted, e.g., noticeable deformations are expected for $w_2/t > 30$, and the maximum allowable w_2/t ratio is limited to 60.

Next, the predicted ultimate loads P_{us} and P_{ui} are compared, in Table 6.2, with the experimental results for lipped channel stub columns. In all but one case, the edge stiffeners satisfy Desmond's requirements, i.e., $I_s > I_{sa}$ which are defined in the preceding section. The exception, SLC/3 180x90, is eliminated from consideration. The first three specimens, with $w_2/t \approx 30$, fall in Desmond's fully effective (flange) range, and the rest fall in the post-buckling range. Moreover, most stiffeners are fully effective, e.g., see Equation 2.9 in Section 3.4.

Two other sections, SLC/2 240x60 and SLC/2 360x90, are also eliminated from consideration because of improper alignment and/or because of their large length-to-minimum radius of gyration ratios (see Section 5.5.4.1 and Table 5.6). Also large, overall, lateral deflections occurred for these tests, which were not observed for comparable but

shorter specimens. It is noted that improper alignment of SLC/1 120x30 and SLC/1 240x60 did not seem to affect their strength; therefore these tests are included in the following evaluation.

From the statistical evaluations of the remaining twenty-two lipped channels presented in Table 6.2, it is seen that the predicted ultimate load P_{us}, which disregards local buckling interaction between plate elements, provides the better correlation when compared with the experimental results. A mean strength ratio, P_{uexp}/P_{us}, of 0.968 is obtained which deviates by about 4% on the average. Further, this strength ratio shows a general tendency of decreasing with increasing web-to-flange width ratio, w_1/w_2. Yet the largest discrepancy which occurs for test SLC/2 360x90 is unconservative by only 12%.

The other ultimate load P_{ui}, which accounts for local buckling interaction, provides more conservative predictions of strength. In this case, the mean strength ratio P_{uexp}/P_{ui} and associated standard deviation are 1.126 and 10.6%, respectively. Also, the conservatism of this predicted load is especially evident for lipped channels with large w_1/w_2 ratios.

Better agreement with experimental results is obtained when local buckling interaction is ignored; therefore the corresponding ultimate load P_{us} is examined in more detail below. The diminishing correlation, noted earlier, of this load with increasing w_1/w_2 ratio is shown in Figure 6.2a. (Note the exaggerated and broken scale that is used for the vertical axis.) The best-fit lines are obtained from a linear regression analysis of the data points for each flange w_2/t ratio. As discussed in Section 5.6.1, one reason for this behavior, for large w_1/w_2 ratios, is local buckling interaction which is not recognized in the method that is

used to calculate P_{us}. Although this is true, the flange w_2/t ratio has about the same effect, and as this parameter is increased, the strength ratio P_{uexp}/P_{us} decreases. The effect of w_2/t is particularly clear when local buckling interaction is absent, i.e., when $w_1/w_2 \simeq 1.0$. In this case increasing the w_2/t ratio from 60 to 90 causes approximately a 10% decrease in the strength ratio.

The above findings suggest that the method used to calculate the ultimate load P_{us} for lipped channels has limited applicability and that extrapolating this method to sections with large flange w_2/t ratios (greater than 90) in combination with large w_1/w_2 ratios (greater than three) may lead to unconservative predictions of strength.

For completeness, the influence of the web-to-flange width ratio, w_1/w_2, on the predicted ultimate load P_{ui}, which accounts for local buckling interaction, is investigated in Figure 6.2b. In this figure the strength ratio P_{uexp}/P_{ui} is plotted as a function of the w_1/w_2 ratio, and best fit lines are drawn through the data points for each flange w_2/t ratio. It is observed from Figure 6.2b that the correlation between predicted and experimental ultimate strengths are again influenced by the w_1/w_2 ratio (compare Figures 6.2a and b). Moreover, the method used to calculate P_{ui} is excessively conservative for lipped channels with large flange w_2/t ratios in combination with large w_1/w_2 ratios.

6.2.3 Sub-Ultimate Response

Next the sub-ultimate response of the stub columns is evaluated. As discussed in Section 6.2.1, various effective width approaches are used to define the effective section. For each approach the predicted axial load-deformation (shortening) response is compared with experimental

results. Because the predicted ultimate strengths are in general agreement with the experimental results when local buckling interaction is ignored, all sub-ultimate calculations are performed assuming simply supported boundary conditions between plate elements. Also, unless noted otherwise, the experimental axial deformation is based on the average of the membrane strains near the flange-web junctures for channels and near the flange-web and flange-lip junctures for lipped channels. Only representative results for a limited number of stub columns are presented here, and the evaluation of the remaining specimens is contained in Appendix D, Figures D.1 through D-26.

First, the sub-ultimate response for channel stub columns is evaluated. Figure 6.3 compares the experimental axial load-deformation for test SC/1 90x30 against that predicted from the two effective section methods which are defined from either Equation 2.9 or 2.48. While both these equations yield conservative predictions of deformation, the sub-ultimate approach of the present study, Equation 2.48, is in better agreement with the experimental results. Of course, both equations, 2.9 and 2.48, give identical results at ultimate (yielding) which is indicated by the intersection of the two corresponding curves.

The axial response for a channel section, SC/1 100x60, with a flange width-to-thickness ratio equal to twice that considered above is evaluated in Figure 6.4. For this test the axial shortening predicted via Equation 2.48 is in excellent accord with experimental results over the full load range.

Other channel stub columns are considered in Appendix D, Figures D.1 through D.9. Generally, the sub-ultimate deformation predicted from

Equation 2.48 agrees well with experimental results and leads to unconservative predictions in only one case, e.g., test SC/2 180x60 of Figure D.9. Since good correlation is obtained for a nearly identical but shorter test, SC/1 180x60 of Figure D.8, the unconservatism noted above for SC/2 180x60 is probably caused by its relatively large length (see Section 5.2.1 and L/r_{min} ratio of Table 5.6).

Second, the sub-ultimate response for lipped channel stub columns is evaluated in Figures 6.5 through 6.9. In the first figure, 6.5, the experimental axial load-deformation response for SLC/2 120x60 is compared with the results predicted from Equations 2.9 and 2.48. Again, both these equations give conservative predictions of deformation, and the response predicted from Equation 2.48 is in better correspondence with the experimental results. Only when the predicted ultimate load is approached does the response predicted from Equation 2.48 deviate from the experimental results. This disagreement is caused by the use of Equation 2.9 as a boundary condition when deriving the sub-ultimate Equation 2.48 in Chapter 2 (see Equation 2.41).

Another lipped channel, SLC/2 180x60, is evaluated in Figure 6.6. This time even better correlation, as compared with that of Figure 6.5, is obtained between Equation 2.48 and the experimental results. Also, shown in Figure 6.6 is the response predicted from Thomasson's [1978] effective width approach, e.g., Equations 2.33 through 2.37. Generally, his approach predicts slightly more conservative deflections than those predicted from the sub-ultimate approach of the present study, i.e., than Equation 2.48. A case where there is a larger discrepancy between the response predicted from these two approaches is shown in Figure 6.7.

Up to this point it has been entirely satisfactory to base the experimental axial deformation, for lipped channels, on the average of the membrane strains at the flange-lip and flange-web junctures (corners). However, for sections with relatively large web-to-flange ratios, w_1/w_2, this basis is affected by local buckling interaction and leads to an unconservative approximation of the actual deformation. Buckling of the web element has an adverse effect on the flange-lip assembly and produces effectively a concentration of axial stiffness around the flange-web junctures. Therefore, a more accurate representation of the actual deformation is obtained by basing the experimental deformation on the strains at the flange-web junctures only.

The above response is illustrated in Figure 6.8 for test SLC/1 120x30 which has fully effective flanges (no local buckling) and has $w_1/w_2 \simeq 4$. Both the aforementioned experimental deformations are included for comparison, where the label ". . .4 corner strains" refers to the membrane strains at the flange-lip and flange-web junctures. Although the experimental response for this section is affected by local buckling interaction, the deformation predicted from Equation 2.48 and by ignoring any interaction correlates well with the experimental values (based on the flange-web strains).

The axial response for test SLC/1 270x90, shown in Figure 6.9, is also affected by local buckling interaction. Again, the experimental deformation which is based on the flange-web strains is more representative of the actual response, and the experimental deformation which is based on the "4 corner strains" (see above discussion) is shown only to indicate that there is an interactional effect. For this test, the deformation predicted from Equation 2.48 is slightly unconservative in the

lower half of the load range but develops improved correlation as the load is increased. Finally, test SLC/1 270x90 is particularly interesting since it exhibits the stiffening action that is usually associated with post-buckled plates.

All remaining lipped channel stub columns are evaluated in Appendix D, Figures D.10 through D.26. In most cases, good correlation is observed between the sub-ultimate predictions of Equation 2.48 and the experimental results. However, because several sections are affected by local buckling interaction, the limitations stated at the end of the ultimate strength evaluation (in Section 6.2.2), seem equally applicable to sub-ultimate predictions.

6.3 Long Column Evaluation

6.3.1 General

The response predicted with the effective section method of Section 4.5.2 is compared below against the experimental results for long columns and beam-columns. The effective section is defined in Figure 4.2, and the effective widths are determined from:

for the web (element number 1 of Figure 4.2),

$$w_{1e}/w_1 = A/\lambda^2 + B/\lambda + C + D\lambda \qquad 4.20$$

where $\lambda = (f_1/f_{cr1})^{\frac{1}{2}}$ and A-D are constants defined in Section 4.5.2.

for the flanges (element number 2),

$$w_{2ei} = w_{2e}/2 \qquad 4.21$$

where $$w_{2e}/w_2 = \sqrt{f_{cr2}/f_i}\,(1.0 - 0.218\sqrt{f_{cr2}/f_i}) \qquad 6.1$$

and for $f_j > 0$,

$$w_{2ej} = w_{2ei}(1.5 - 0.5f_j/f_i) \qquad 4.22$$

or for $f_j < 0$,

$$w_{2ej} = 1.5w_{2ei} + w_o \qquad 4.23$$

where if $f_1 > f_2$ then $i = 1$ and $j = 2$, or

if $f_1 < f_2$ then $i = 2$ and $j = 1$

and for the lips (element number 3),

$$w_{3e}/w_3 = \sqrt{f_{cr3}/f_2}\ (1.0 - 0.218\sqrt{f_{cr3}/f_2}) \qquad 6.2$$

where the general critical buckling stress f_{crn} is defined as

$$f_{crn} = K_n\pi^2E/12(1 - \mu^2)(w_n/t)^2 \ . \ . \ . \ . \ n = 1,2,3 \qquad 6.3$$

and the buckling coefficients K_n are taken as $K_1 = K_2 = 4.0$ and $K_3 = 0.425$.

The edge stresses f_1 and f_2 along reference axes one (1) and two (2) in Figure 4.2 are calculated from

$$f_k = P/A_e \pm (Pe_ec_k/I_e)\ \sec\ (pL/2) \ . \ . \ . \ . \ k = 1,2 \qquad 4.24$$

where $p = (P/EI_e)^{\frac{1}{2}}$ and the section properties A_e, I_e, e_e, and c_k are referenced to the effective section. The associated lateral deflection Δ at the midheight of the column is given by

$$\Delta = e_e[1 - \cos(pL/2)]/\cos(pL/2) \qquad 4.25$$

Reference is made to Chapter 4 for the definition of all variables that are not defined above. Finally, the ultimate load which is calculated from the effective section method is designated as P_u.

As discussed in Section 4.5.2, the ultimate load may actually be limited by either flexural buckling or torsional-flexural buckling. The load associated with the former is calculated from the modified SSRC approach of Equation 4.13 and is designated as P_e, and the latter is

calculated from the Q-factor method of Equation 4.16 and is designated as P_{tf}. (See Section 4.5.2 for the details of these calculations.)

An alternate effective section approach is also investigated where Winter's stiffened plate effective width equation is applied to the web, e.g.,

$$w_{1e}/w_1 = \sqrt{f_{cr1}/f_1}\,(1.0 - 0.218\sqrt{f_{cr1}/f_1}) \qquad 6.4$$

In all other respects this approach is identical to the effective section method described above. Generally both these methods give identical predictions of ultimate strength, and the major difference arises in the predictions of sub-ultimate response.

For the concentrically loaded long columns, a comparison is made between the experimental ultimate loads, P_{uexp}, and an approach where the flexural buckling strength is used to define ultimate conditions. The buckling strength is calculated from the modified SSRC load, defined previously, and from the Q-factor load, P_f, which is based on Equation 4.7.

Also, the edge stiffeners (lips) are evaluated with respect to Desmond's requirements of Section 3.4.

6.3.2 Ultimate Strength

The predicted ultimate strengths described above are compared in Table 6.3 against the experimental results for the concentrically loaded long columns. All specimens have edge stiffeners which satisfy Desmond's requirements. Further, one specimen, CLC/1 180x60, had improper alignment, and two others, CLC/2&3 180x90, failed in a torsional-flexural mode. Because these factors did not detract significantly from the strengths of

these columns, they are included in the comparison. Also, specimen CLC/1 90x90 and the last column of Table 6.3 are excluded from the present comparison and are discussed subsequently.

First, the flexural buckling loads, P_f and P_e, are evaluated against the experiment results. This evaluation is included to determine the accuracy of the current Q-factor method (P_f) of the AISI Specification [1980] and the modified SSRC method (P_e), which was proposed recently for specification adoption, as applied to concentrically loaded, singly-symmetric, lipped channels. From the statistical evaluation presented at the bottom of Table 6.3, it is apparent that the predicted loads P_f and P_e are nearly identical and that both give unconservative (15%) predictions of ultimate strength. The reason for this unconservatism is that the Q-factor and modified SSRC methods, on which the respective loads P_f and P_e are based, do not recognize the actual beam-column behavior exhibited by the locally buckled columns.

On the other hand, the actual behavior of the columns is recognized by the effective section method of Section 4.5.2, which is based on beam-column theory. From Table 6.3, the associated ultimate loads P_u are slightly conservative; a mean strength ratio P_{uexp}/P_u of 1.136 is obtained which deviates on the average by about 4%. It is noted for two slender columns, CLC/3&4 120x60, an elastic failure is predicted. The cause of this behavior is discussed in Section 4.5.2. Also, when the alternate effective section is employed, i.e., when Equation 6.4 is applied to the web; slightly different ultimate loads, noted at the bottom of Table 6.3, are predicted for only the two columns noted above. Calculations of the torsional-flexural buckling load, P_{tf}, which are not presented here, show

that this mode of failure is not critical for any of the concentrically loaded columns.

The effect of lateral support for the edge stiffened elements (flanges) can be assessed in Table 6.3 by comparing the strength ratios P_{uexp}/P_u of "duplicate" columns which were tested with and without braces, e.g., the pairs CLC/5&2 120x60, CLC/4&2 180x60, and CLC/3&2 180x90. Although this effect is dependent on the dimensions of the section, the specific columns noted above are proportioned such that they are not appreciably influenced by the use of braces. (Recall that the results for CLC/2 180x60 are affected by poor alignment. Also, a comparison of strength ratios, and not the experimental ultimate loads, is appropriate because of small differences in dimensions and material for the "duplicate" columns.)

While the concentrically loaded columns are evaluated above in a straightforward manner, a corresponding evaluation for the eccentrically loaded columns is more complicated. Several of these columns are loaded eccentrically such that the load carrying capacity is maximized; consequently the possibility of flexural or torsional-flexural buckling is increased.

Moreover, eccentric loading on the side of the gross centroid opposite the shear center, negative eccentricity in Figure 4.2, causes a larger proportion of the load to be carried by the edge stiffener and exaggerates the problem with edge stiffened elements that was alluded to in Chapters 2, 4, and 5. For example, LaBoube's effective width approach for beam webs was discussed in Section 2.2.2 where a reduction factor was employed to account for the inadequate support provided, to the web, by

unstiffened compression elements; the effective section method of Section 4.5.2 was restricted to edge stiffened elements which were constrained externally against local-torsional buckling, e.g., by braces; and the sometimes sudden nature of local-torsional buckling of unbraced edge stiffened elements (flanges) was illustrated in Section 5.6.2. Basically, the problem with unbraced edge stiffened elements is that, when the aspect ratio is large, the ever present initial imperfections (fabrication type) interact with the overall modes of action and degrade their structural strength.

A related problem was investigated by Douty [1962] for laterally unbraced webs of thin-walled beams of open section, where bending was about the major axis, e.g., lipped channels with bending about the y axis in Figure 5.1a ($e = -\infty$, pure moment). The strength of the webs was determined by treating a portion of the compression flange and web as a column on an elastic foundation subject to torsional-flexural buckling. A rather complex design method was formulated and was verified experimentally. Douty's method was never adopted directly by the AISI Specification [1980], probably because of its complexity; instead his method was relegated to a related publication (AISI [1971]).

A similar approach is taken here for sections with unbraced edge stiffened elements where the strength is limited by instability of the unbraced element. If the edge stiffener (lip) is designed according to Desmond's requirements and if local buckling interaction, with the web, is ignored, then the local and local-torsional buckling modes for the edge stiffened element are synonymous. This serves to define the buckling stress of the latter mode which is critical for failure of the unbraced element. In order to prevent this mode it is necessary to limit the edge

stress f_2, at the flange-lip juncture, to values less than the buckling stress, e.g.,

$$f_2 \leq f_{cr2} \qquad 6.5$$

where f_{cr2} is defined by Equation 6.3 with n = 2 and K_2 = 4.0. The above equation is employed in conjunction with the effective section method of Section 4.5.2 (or the alternate effective section discussed in the preliminaries), and when the stress f_2 reaches the equality given in Equation 6.5, the limiting stress ultimate load, P_{ul}, is attained. Equation 6.5 applies, of course, to only sections with unbraced edge stiffened elements. Now, with an approach for unbraced elements defined, it is possible to proceed with the evaluation of the long columns.

The eccentrically loaded long columns (beam-columns) are evaluated in Table 6.4, which is quite complicated due to the nature of the problem. For reference, the notation used to identify the various predicted ultimate loads is reviewed at the bottom of the table. Also, the symbol x indicates that the predicted ultimate load does not control, and the load which does control is underlined. Further, two sections, CLC/2.1&2.2 180x60, are eliminated from this evaluation. For the first section, poor agreement is obtained between the predicted flexural buckling load, P_e, and the experimental strength. This does not invalidate the method used to predict the load P_e; in fact, because of the experimental torsional-flexural failure mode, it suggests that the method used to predict the torsional-flexural buckling load, P_{tf}, is inadequate when Q < 1 (partially effective), as discussed at the end of Section 4.5.1. For the second section, CLC/2.2 180x60, the response is affected by poor lateral alignment.

As is evidenced in Table 6.4, good correlation is obtained between predicted and experimental strengths for the remaining beam-columns. Flexural yielding is predicted quite well by the effective section method of Section 4.5.2; for example, the mean of the strength ratios P_{uexp}/P_u (numbers without parentheses) equals 1.046 which has a standard deviation of 0.103.* It is noted that a slightly unconservative result (9%) is obtained for CLC/1.1 120x30 because of its large web-to-flange width ratio. Torsional-flexural buckling is predicted for only CLC/2.1 180x90, and the associated strength ratio P_{uexp}/P_{tf} equals 0.924. Finally, local-torsional buckling of the unbraced flanges is predicted, from Equation 6.5 and the effective section method of Section 4.5.2, for three sections, including CLC/1 90x90 of Table 6.3. The corresponding mean strength ratio P_{uexp}/P_{ul} (of the numbers without parentheses) and standard deviation are 1.132 and 0.180, respectively.* The wide spread of the results for this last predicted load is caused by variances in the local imperfection. Also, the load P_{ul} predicted for CLC/1 90x90 is somewhat conservative (27%); however this degree of conservatism seems warranted in view of the sudden failure mode that is associated with this specimen.

Overall, the mean ratio of experimental to predicted ultimate strength for the twenty concentrically and eccentrically loaded long columns of Tables 6.3 and 6.4 is 1.107 which has a standard deviation of about 9%.

*Because of the limited number of tests, these statistical analyses may not be meaningful.

Again, the ultimate loads predicted using the alternate effective section approach, i.e., applying Equation 6.4 to the web, are listed in Table 6.4 (numbers in parentheses) for comparison purposes. The differences between these loads and those predicted when Equation 4.20 is applied to the web are small, and the major difference arises in sub-ultimate predictions.

6.3.3 Sub-Ultimate Response

Next, the sub-ultimate response of the long columns is evaluated. The theoretical response is predicted using both the effective section method of Section 4.5.2 and, for comparison, the alternate effective section approach where Equation 6.4 is applied to the web, defined in Figure 4.2. Both these methods are reviewed in Section 6.3.1. The predicted response is compared against two independent experimental measurements. One is the axial load-membrane strain history where the strains at reference axes (1) and (2) in Figure 4.2 are obtained by extrapolating the readings from the strain gages located near the flange-web and flange-lip junctures (see Figure 5.1b). Actually, two sets of membrane strains are obtained, one for each flange, and the results are averaged. The other measurement is the axial load-lateral deflection where the deflection is determined from the average of dial gages A and B in Figure 5.19.

Only representative columns are evaluated in this section. For example, the relative response for nearly identical (geometry and material properties) columns with varying load eccentricities are compared in Figures 6.10 through 6.13; the response for a slender column is presented in Figure 6.14; and the effects of local-torsional flange failure and

torsional-flexural buckling are illustrated in Figures 6.15 through 6.16 and Figure 6.17, respectively. An evaluation of the remaining specimens is contained in Appendix E, Figures E.1 through E.12.

The predicted and experimental strain histories for the concentrically loaded test CLC/2 120x60 are compared in Figure 6.10a, where a positive strain indicates compression. Generally, good correlation is obtained when the effective section method of Section 4.5.2 is employed. For comparison with this, the correlation with experimental results deteriorates when the alternate effective section is used. This is especially noticeable for the strain at reference axis (1) where the majority of load resistance is provided. The corresponding axial load versus lateral deflection response is presented in Figure 6.10b, where a positive deflection is in the direction opposite to the shear center (see Figure 4.2). As expected, the deflection is predicted better with the method of Section 4.5.2, and excessively conservative predictions are obtained using the alternate method. Also, the behavior of this column is interesting because it illustrates the inadequacies of the flexural buckling strength approach which was evaluated in Table 6.3. At low load levels the response is purely axial, without any lateral deflection. But at higher load levels it changes due to the effects of local buckling, and lateral deflections occur. Ultimately the transformed (partially effective) beam-column fails by flexural yielding.

The beam-column effects are exaggerated for the response shown in Figure 6.11 for test CLC/2.3 120x60, which has a positive eccentricity, e, of 0.982.* (The eccentricity is defined as positive for values on the shear center side of the gross centroid, see Figure 4.2.) The effective section method of Section 4.5.2 tracks the strain history (Figure 6.11a)

*inches.

quite well and provides excellent predictions of lateral deflection (Figure 6.11b).

The maximum load resistance for the CLC/2- 120x60 series of tests is acquired when the eccentricity equals -0.212*, i.e., for test CLC/2.4 120x60 of Figure 6.12. For this test a state of nearly uniform compression is obtained at ultimate (see Figure 6.12a). The effective section method of Section 4.5.2 provides better agreement with sub-ultimate strains, and any discrepancies are caused by the sensitivity to eccentricities which are discussed in Section 4.5.2. The corresponding lateral deflections are set out in Figure 6.12b. In this case, the lateral deflections predicted with the alternate effective section are extremely unconservative.

A larger eccentricity, e = -0.536*, is considered in Figure 6.13 for test CLC/2.1 120x60. For this test excellent correlation with experimental strains (Figure 6.13a) is provided by the effective section method of Section 4.5.2. In addition, this method predicts slightly different ultimate loads than those predicted with the alternate effective section because failure is controlled by yielding along reference axis (2). Finally, the sub-ultimate lateral deflections predicted with the method of Section 4.5.2 are in very good correspondence with the experimental results (Figure 6.13b), and the deflections predicted with the alternate method are again unconservative.

The response for a slender, concentrically loaded column (CLC/3 120x60) is illustrated in Figure 6.14. Although hardly perceptible in this figure, an elastic failure is predicted with the effective section method of Section 4.5.2 due to the interaction between local and overall buckling. Nevertheless, this method provides good correlation with

*inches.

experimental strains (Figure 6.14a) and deflections (Figure 6.14b). Also, the kink in the response (Figure 6.14) predicted with the above method is caused by the different flange effective width equations employed for compression and tension, e.g., Equations 4.22 and 4.23.

For the tests previously evaluated, the possibility of an elastic local-torsional failure of the flange was excluded due either to the use of lateral braces (Figure 5.1) or the low strain levels that were experienced along reference axis (2). A case where this mode of failure occurs violently is considered in Figure 6.15 for the unbraced, concentrically loaded test CLC/1 90x90. In this instance, the predicted response is limited by the ultimate load P_{u1} which is defined from the limiting critical strain ε_{cr_2} (or stress) obtained from Equation 6.5, e.g., see Figure 6.15a. Slightly different loads P_{u1} are obtained depending on whether the effective section method of Section 4.5.2 or the alternate effective section are employed. Reasonable agreement with experimental results is obtained with the former method for sub-ultimate strains (Figure 6.15a) and lateral deflections (Figure 6.15b).

Another case where local-torsional flange failure limits the response is presented in Figure 6.16. For this test (CLC/2.2 180x90) which has eccentric loading towards the unsupported side of the flange, e.g., e = -0.515*, the effective section method of Section 4.5.2 provides good correlation with the experimental results.

The response considered in Figure 6.16 is drastically changed when a nearly identical section (geometry, material properties, and loading) is furnished with braces, e.g., test CLC/2.1 180x90 of Figure 6.17. In this case, torsional-flexural buckling limits the response, which is indicated experimentally, in Figure 6.17b, by twisting of the section. (The "dots"

*inches.

shown in this figure represent the individual lateral deflections that are associated with the dial gages A and B of Figure 5.19, and the "plus signs" represent the average values.) Again, the effective section method of Section 4.5.2, which ignores torsional-flexural action, provides good correspondence with the experimental sub-ultimate strains (Figure 6.17a) and deflections (Figure 6.17b), and the alternate effective section provides unconservative predictions because the effective (actual) eccentricity is misjudged. Ultimate conditions for this column are defined at the torsional-flexural buckling load, P_{tf}.

6.4 Evaluation of Other Experimental Research

The experimental research of others, discussed in Section 5.7, is evaluated here. This research is important because it extends the data base on which the effective section method is founded. Discussions are kept to a minimum, and reference is implied to previous sections where all notation is defined.

6.4.1 Stub Columns

Chilver's [1953] stub columns are evaluated in Table 6.5. For the channel sections, the ultimate load P_{us}, which is based on the effective section method and on the assumption of simply supported plate boundary conditions, produces very satisfactory results when compared to the experimental strengths. The associated mean strength ratio P_{uexp}/P_{us} and standard deviation for the twelve channels are 0.970 and 0.074, respectively. In contrast to this unsatisfactory comparisons of experimental and predicted strengths, which contradict the findings of the present study, are obtained for the lipped channels, particularly for LC10 and LC12

through LC15. Note that only the lipped channels with adequate edge stiffeners, i.e., with $I_s > I_{sa}$, are evaluated in Table 6.5.

As noted earlier, Chilver failed to report the lengths that were associated with his specimens. Also, alignment procedures were not discussed. Because these two factors — length and alignment — were found, in the present study, to affect the strength of stub columns; it is entirely plausible to assume that they affected Chilver's results also and contributed to premature failure of the specimens noted above.

The stub columns investigated by Pekoz [1977] are evaluated in Table 6.6. Again, for the channels, entirely satisfactory agreement is obtained between predicted and experimental strengths; for example, the mean strength ratio P_{uexp}/P_{us} and standard deviation for the seven tests are 1.026 and 0.044, respectively.

A corresponding evaluation of the adequately stiffened ($I_s > I_{sa}$) lipped channels of Table 6.6 is complicated by the fact that several of the specimens do not satisfy the requirement of Equation 3.23. This requirement, rewritten below, was established by Desmond [1978] to preclude the detrimental effect of stiffener buckling on edge stiffened elements.

$$D_s \leq 0.25w_2 \qquad 6.6$$

where $D_s = w_3 + r$ (see Figure 3.9a). For the specimens which do not satisfy Equation 6.6, it is necessary to employ the following equation, proposed by Desmond, for calculation of the flange buckling coefficient, K_2.

$$K_2 = 5.25 - 5D_s/w_2 \qquad 6.7$$

All other aspects of the method used to predict the ultimate load P_{us} remain unchanged.

The predicted strengths P_{us}, where Equation 6.7 is employed as necessary, are compared, in Table 6.6, with the experimental results of the lipped channels tested by Pekoz. In brief, good correlation is obtained, and the mean strength ratio P_{uexp}/P_{us} for the seven tests equals 1.014.

6.4.2 Long Columns

The concentrically loaded, lipped channel, long columns investigated by Thomasson [1978] are evaluated in Table 6.7. It is recalled from Chapter 5 that braces were used to support the flanges and that the columns had extremely large plate flat width-to-thickness ratios. Also, one column, A155, is excluded from the evaluation due to improper alignment. For the remaining thirteen columns, the ultimate load P_u which is based on the effective section method of Section 4.5.2 is in good accord with the experimental results. Overall, a mean strength ratio P_{uexp}/P_u of 1.076 is predicted which deviates on the average by about 5%.

Similarly, the thirty-three long columns of Loughlan [1979] are evaluated in Table 6.8. In this case, both concentrically and eccentrically loaded columns were tested, and large edge stiffeners were employed. From this table, good correspondence between predicted and experimental strengths is observed; the mean strength ratio P_{uexp}/P_u and associated standard deviation are 1.099 and 0.086, respectively.

6.5 Summary

The effective section method which was developed for analyzing uniformly compressed, thin-walled, stub columns was evaluated with respect to the experimental results for channel and lipped channel sections. In

brief, the predicted ultimate strengths were in excellent correspondence with the experimental values when local buckling interaction between component plate elements was ignored. On the other hand, occounting for local buckling interaction through the critical buckling stress parameter of the effective width equation (2.48 or 2.9) provided somewhat conservative predictions of strength. This was especially noticeable of lipped channels with large web-to-flange width ratios, $w_1/w_2 > 2$.

The effective section method which ignored local buckling interaction was also evaluated for predicting the sub-ultimate response for stub columns. When the sub-ultimate effective width equation (2.48) was employed, the predicted axial deformation correlated well with experimental results; however, when the stiffened plate effective width equation (2.9) was employed, the predicted deformation was too conservative.

Overall, the effective section method which employed the sub-ultimate effective width Equation 2.48 and which ignored local buckling interaction produced good correlation with both experimental sub-ultimate response and strength. Still it proved necessary to place limitations on this method. For channel sections, excessive out-of-plane deformations, exceeding four times the thickness, were observed at ultimate for flanges (unstiffened element) with large flat width-to-thickness ratios, $w_2/t \approx 60$, which may prove unacceptable. Also, for lipped channels, the correlation between predicted and experimental results deteriorated for sections with large web-to-flange ratios, $w_1/w_2 \geq 3$, in combination with large flange width-to-thickness ratios, $w_2/t \approx 90$.

Next, the long columns were evaluated. A comparison of the expermental results for concentrically loaded lipped channels and the Q-factor and modified SSRC methods for predicting flexural buckling showed that

these methods overestimated the strength. In contrast to this, the effective section and beam-colun analysis method, which was developed in Chapter 4, provided good predictions of the actual flexural yielding strength.

To prevent local-torsional failure of the long columns with laterally unbraced flanges (edge stiffened element), it proved necessary to limit the stress, in the flange, to its local buckling value. This mode of failure was especially critical for eccentric loading toward the lip (edge stiffener) but was not restricted to this situation. Satisfactory agreement with experimental ultimate loads was obtained with this limiting stress approach provided that it was used in conjunction with the effective section analysis method.

An evaluation of the remaining eccentrically loaded long columns demonstrated good correlation between the experimental strengths and the values predicted with the effective section analysis method. However, mixed results were obtained with the Q-factor method for predicting torsional-flexural buckling.

The effective section analysis method was also compared with the experimental sub-ultimate response for long columns. Comparison with the independent measurements of longitudinal edge strains and lateral deflections showed good agreement with the predicted values when the sub-ultimate effective width equation (2.48) was employed for the web (stiffened element) But when the stiffened plate effective width equation (2.9) was employed, the predicted sub-ultimate response was unsatisfactory, and, in some cases, was unconservative.

Finally, the effective section method for stub and long columns was evaluated with respect to the experimental research of others. In brief, this evaluation reinforced the findings discussed above.

Table 6.1 EVALUATION OF CHANNEL STUB COLUMNS

Specimen		P_{uexp} (k)	$\frac{P_{uexp}}{P_{us}}$ †	$\frac{P_{uexp}}{P_{ui}}$ †
All SC/				
1	60x30	7.40	1.113	1.079
1	90x30	7.35	1.084	1.056
1	120x30	7.80	1.144	1.173
2	120x30	7.10	1.006	1.032
1	40x60	7.88	0.953	1.075
2	40x60	7.89	0.947	1.072
1	60x60	9.16	1.068	1.173
1	100x60	9.20	1.019	1.022
1	120x60	8.20	1.176	1.142
1	180x60	8.52	1.183	1.148
2	180x60	8.50	1.180	1.146
	Mean (N = 11)		1.079	1.102
	Standard deviation		0.088	0.056

† P_{us} determined using simply supported buckling coefficients.

P_{ui} determined using interactional buckling coefficients.

Table 6.2 EVALUATION OF LIPPED CHANNEL STUB COLUMNS

Specimen		I_s/t^4	I_s/I_{sa}	P_{uexp} (k)	$\frac{P_{uexp}}{P_{us}}$ †	$\frac{P_{uexp}}{P_{ui}}$ †
All SLC/						
1	60x30	35.92§	1.493	10.40	1.072	1.106
1	90x30	36.64§	1.544	10.05	1.014	1.123
1	120x30	33.60§	1.538	10.15	0.999	1.151
1	60x60	220.6§	1.137	13.20	1.024	1.024
2	60x60	216.9§	1.126	13.60	1.043	1.043
1	120x60	223.7§	1.153	13.00	0.974	1.121
2	120x60	211.5§	1.080	13.60	1.030	1.187
1	180x60	233.5§	1.202	12.80	0.952	1.221
2	180x60	240.3§	1.234	12.80	0.957	1.226
1	240x60	229.7§	1.175	12.80	0.957	1.301
2	240x60	241.9§	1.229	12.00	0.863*	1.167*
3	240x60	227.7§	1.171	12.60	0.935	1.270
1	60x90	346.3	1.227	11.50	0.932	0.963
2	60x90	351.6	1.248	11.80	0.953	0.984
1	90x90	358.0	1.260	11.90	0.951	0.951
2	90x90	350.1	1.242	12.00	0.946	0.946
1	180x90	434.7	1.202	31.15	0.920	1.090
2	180x90	427.2	1.174	31.40	0.929	1.099
3	180x90	264.5	0.794	15.20	0.762*	0.897*
4	180x90	246.8§	1.034	13.80	0.954	1.123
5	180x90	260.3§	1.109	14.60	0.983	1.155
1	270x90	252.5§	1.058	13.60	0.935	1.221
2	270x90	250.9§	1.037	14.00	0.945	1.234
1	360x90	276.1§	1.134	12.50	0.884	1.230
2	360x90	267.6§	1.099	11.20	0.784*	1.094*
			Mean (N = 22)		0.968	1.126
			Standard deviation		0.045	0.106

§Fully effective stiffener.

†P_{us} determined using simply supported buckling coefficients.

P_{ui} determined using interactional buckling coefficients.

*Not included in statistical evaluation, see text.

Table 6.3 EVALUATION OF CONCENTRICALLY§ LOADED LONG COLUMNS

	Specimen	I_s/t^4	I_s/I_{sa}	P_{uexp} (k)	$\frac{P_{uexp}}{P_f^*}$	$\frac{P_{uexp}}{P_e^*}$	$\frac{P_{uexp}}{P_u^*}$	$\frac{P_{uexp}}{P_{ul}^*}$
All CLC/								
1	120x60	307.0	1.566	9.80	0.846	0.845	1.057	x
2	120x60	249.4	1.288	10.40	0.928	0.925	1.162	x
3	120x60	240.4	1.257	8.20	0.816	0.822	1.108°	x
4	120x60+	269.9	1.407	8.40	0.832	0.837	1.124°	x
5	120x60+	254.1	1.408	11.80	0.929	0.926	1.157	x
1	180x60	259.9	1.326	9.60	0.823	0.827	1.162	x
2	180x60'	273.0	1.397	8.75	0.792	0.801	1.148	x
3	180x60+	273.0	1.397	7.60	0.748	0.768	1.160	x
4	180x60+	254.5	1.396	10.80	0.847	0.855	1.223	x
1	90x90	316.9"	1.191	11.00	0.783**	0.775**	0.838**	1.274°°
1	180x90	332.3"	1.273	12.30++	0.886	0.884	1.135	x
2	180x90	307.3"	1.122	12.10++	0.838	0.840	1.108	x
3	180x90+	287.8	1.080	11.80++	0.830	0.833	1.088	x
		Mean (N = 12)			0.843	0.847	1.136	
		Standard deviation			0.052	0.046	0.043	

" Partially effective stiffener, all others fully effective.
+ Braces used, refer to Figure 5.1.
++ Experimentally observed torsional-flexural failure.
' Poor alignment.
* P_f = flexural buckling load - Q-factor method.
P^f = flexural buckling load - modified SSRC method.
P^e_u = flexural yielding ultimate load - effective section method of Section 4.5.2. For P_{uexp}/P_{ul} column of table, refer to Table 6.4.
° Elastic failure predicted.
When Eq. 6.4 is applied to web, P_{uexp}/P_u = 1.110, 1.126 for CLC/3&4, respectively.
°° When Eq. 6.4 is applied to web, P_{uexp}/P_{ul} = 1.207.
Refer to Table 6.4.
** Not included in statistical evaluation, see text.
§ Concentric with respect to gross section.

Table 6.4 EVALUATION OF ECCENTRICALLY LOADED LONG COLUMNS

Specimen		e	I_s/t^4	I_s/I_{sa}	P_{uexp} (k)	$\frac{P_{uexp}}{P_u^*}$	$\frac{P_{uexp}}{P_e^*}$	$\frac{P_{uexp}}{P_{tf}^*}$	$\frac{P_{uexp}}{P_{ul}^*}$
All CLC/									
1.1	120x30	-0.203	28.76	1.024	8.00	0.911 (0.851)	x	x	x
2.1	120x60+	-0.536	180.4	1.404	10.30	1.109 (1.087)	x	x	x
2.2	120x60	-0.534	177.7	1.444	8.75	0.908x (0.891)	x	x	0.929 (0.913)
2.3	120x60+	0.982	180.7	1.392	6.75	1.142 -#	x	x	x
2.4	120x60+	-0.212	183.2	1.384	12.40	1.024 -	x	x	x
2.1	180x60+	-0.424	189.3	1.283	10.40++	0.808°x (0.828)	0.821**	0.820x	x
2.2	180x60'	-0.397	187.1	1.475	10.00	0.809° (0.815)**	x	x	x
2.1	180x90+	-0.521	268.1"	1.164	12.50++	0.879x -	x	0.924	x
2.2	180x90	-0.515	266.4"	1.161	8.75	0.586x -	x	0.613x	1.192 (1.150)
			Mean			1.046			1.132
			Standard Deviation			0.103			0.180
			N			4			3°°

Refer to following page for footnotes.

Table 6.4 - Continued

" Partially effective stiffener, all others fully effective.
+ Braces used, refer to Figure 5.1.
++ Experimentally observed torsional-flexural failure.
x Predicted load does not control or not applicable.
' Poor alignment.
* P_u = flexural yielding ultimate load - effective section method: no. without parentheses indicates Eq. 4.20 applied to web, as in Section 4.5.2, no. with parentheses indicates Eq. 6.4 applied to web.
P_e = flexural buckling load - modified SSRC method.
P_{tf} = torsional-flexural buckling load - Q-factor method.
P_{ul} = limiting stress ultimate load, refer to above description of P_u.
$P_u^{ul} = (P_u)$, refer to above description of P_u.
° Elastic failure predicted.
°° Includes CLC/1 90x90 of Table 6.3.
** Not included in statistical evaluation, see text.

Table 6.5 EVALUATION OF CHILVER'S [1953] STUB COLUMNS

Specimen	I_s/t^4	I_s/I_{sa}	P_{uexp} (k)	$\frac{P_{uexp}}{P_{us}}$
Channels				
C1	—	—	35.5	1.121
C2	—	—	29.0	0.913
C3	—	—	8.68	1.096
C4	—	—	9.22	0.959
C5	—	—	4.07	1.018
C6	—	—	4.98	0.950
C7	—	—	2.88	0.941
C8	—	—	10.7	0.948
C9	—	—	41.7	0.972
C10	—	—	5.28	0.920
C11	—	—	5.56	0.931
C12	—	—	5.54	0.866
		Mean (N = 12)		0.970
		Standard deviation		0.074
Lipped Channels				
LC2	44.63	20.66	52.0	1.004
LC6	7.016	*	50.8	1.087
LC7	1.195	*	35.7	1.010
LC8	32.58	*	14.5	0.944
LC9	15.84	*	19.4	0.967
LC10	8.698	*	7.66	0.856
LC11	8.698	1.644	9.22	0.910
LC12	288.3	1.517	9.48	0.785
LC13	288.3	1.312	10.2	0.826
LC14	288.3	1.296	9.26	0.744
LC15	288.3	1.323	9.43	0.795
		Mean (N = 11)		0.902
		Standard deviation		0.110

* Stiffener not required.

Table 6.6 EVALUATION OF PEKOZ'S [1977] STUB COLUMNS

Specimen	I_s/t^4	I_s/I_{sa}	P_{uexp} (k)	$\frac{P_{uexp}}{P_{us}}$
Channels				
P4	—	—	7.42	1.063
P6	—	—	7.25	0.039
P8	—	—	7.64	1.094
P5	—	—	8.49	1.033
P7	—	—	8.15	0.991
P9	—	—	8.15	0.991
P2.14	—	—	9.33	0.972
			Mean (N = 7)	1.026
			Standard deviation	0.044
Lipped Channels				
P2.1	182.7	1.134	3.24	1.047+
P2.3	227.7	1.402	3.28	1.113+
P2.6	721.6	2.437	19.9	0.913
P2.7	1198.	4.054	22.5	1.051+
P2.9	538.1	4.848	19.8	1.095+
P2.12	19.60	74.8	11.2	0.966+
P2.13	1.094	4.176	9.78	0.910
			Mean (N = 7)	1.014
			Standard deviation	0.084

+ Equation 6.7 employed.

Table 6.7 EVALUATION OF THOMASSON'S [1978] LONG COLUMNS

Specimen	I_s/t^4	I_s/I_{sa}	P_{uexp} (k)	$\frac{P_{uexp}}{P_u}$
A71	667.2	1.110	3.60	1.061
A74	671.1	1.106	3.64	1.062
A75	658.6	1.084	3.48	1.016
A76	929.6	1.874	3.26	1.009
A101	404.2	0.912	8.30	1.120
A012	401.9	0.910	7.87	1.065
A103	391.4	0.886	8.34	1.130
A104	365.2	0.844	7.76	0.998
A151	197.8	0.759	17.2	1.124
A152	203.9	0.772	15.7	1.065
A153	232.0	0.832	16.0	1.142
A154	284.2	1.034	16.4	1.118
A155	293.6	1.082	12.8	0.880*
A156	232.9	0.886	15.5	1.081
		Mean (N = 13)		1.076
		Standard deviation		0.048

* Not included in statistical evaluation.

Table 6.8 EVALUATION OF LOUGHLAN'S [1979] LONG COLUMNS

Specimen	e (in.)	I_s/t^4	I_s/I_{sa}	P_{uexp} (k)	$\frac{P_{uexp}}{P_u}$
L1	0.292	701.4	3.849	3.12	1.012
L2	0.294	772.8	4.116	3.60	1.012
L3	0.402	1116.	4.736	3.52	0.980
L4	0.404	1081.	4.728	3.78	0.951
L5	0.407	1126.	4.789	4.10	1.049
L6	0.066	733.8	3.900	3.80	1.121
L7	0.066	746.3	3.977	3.97	1.060
L8	0.066	765.8	4.072	4.31	1.066
L9	0.184	1116.	4.736	4.34	1.116
L10	0.186	1119.	4.726	4.57	1.104
L11	0.186	1087.	4.748	4.65	1.011
L12	0.182	708.4	3.873	3.35	1.071
L13	0.183	756.5	4.149	3.53	1.017
L14	0.181	713.5	3.924	3.85	1.025
L15	0.	1114.	4.723	4.90	1.152
L16	0.	1088.	4.754	5.18	1.079
L17	0.	1120.	4.735	5.31	1.109
L18	0.220	746.3	4.000	3.13	1.129
L19	0.222	751.6	4.005	3.39	1.101
L20	0.224	751.3	4.129	3.67	1.040
L21	0.159	1109.	4.693	3.86	1.035
L22	0.159	1112.	4.700	4.42	1.133
L23	0.161	1129.	4.767	4.14	1.008
L24	0.	108.6	4.409	14.8	1.361+
L25	0.083	262.6	3.374	16.0	1.179
L26	0.083	257.2	3.570	16.4	1.105
L27	0.083	269.8	3.437	16.6	1.086
L28	0.106	112.8	4.595	11.5	1.245+
L29	0.106	107.5	4.721	12.6	1.195+
L30	0.106	109.8	4.991	13.6	1.172
L31	0.	273.7	3.231	17.0	1.235
L32	0.	277.7	3.340	17.0	1.164
L33	0.	303.1	3.535	18.0	1.158
				Mean (N = 33)	1.099
				Standard deviation	0.086

+ Elastic failure predicted.

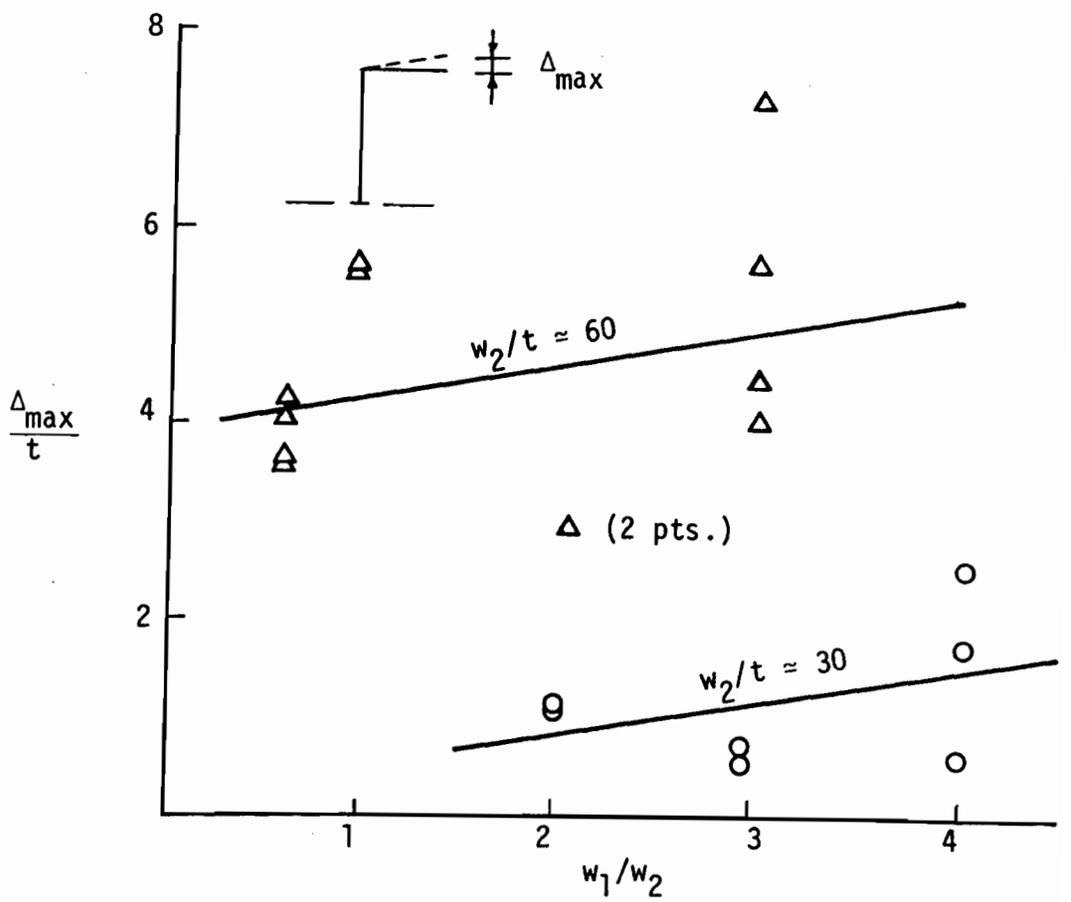

Figure 6.1 MAXIMUM FLANGE OUT-OF-PLANE DEFORMATION FOR CHANNEL SECTIONS

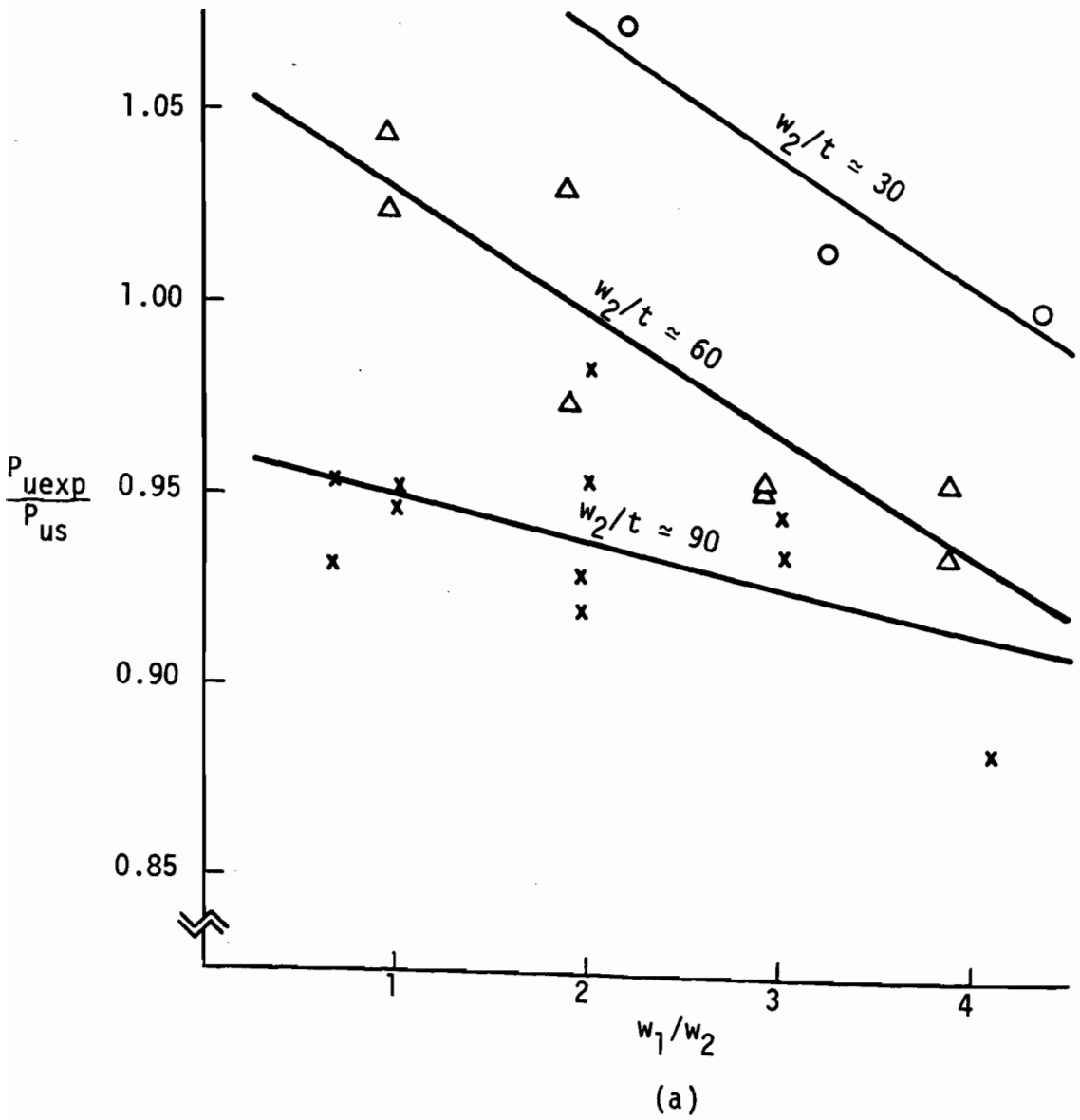

Figure 6.2 INFLUENCE OF LOCAL BUCKLING INTERACTION ON ULTIMATE STRENGTH FOR LIPPED CHANNEL SECTIONS

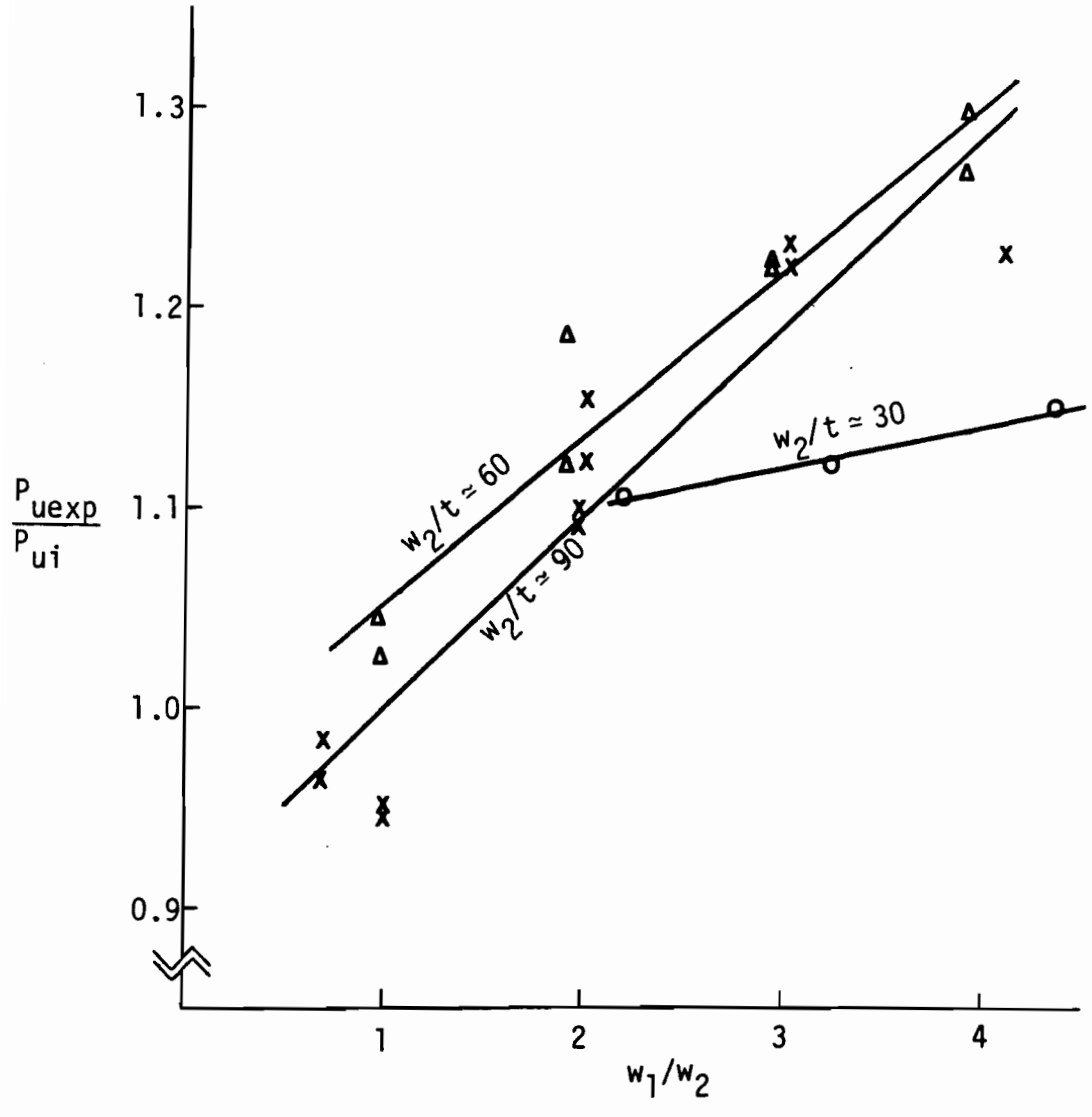

(b)

Figure 6.2 - Continued

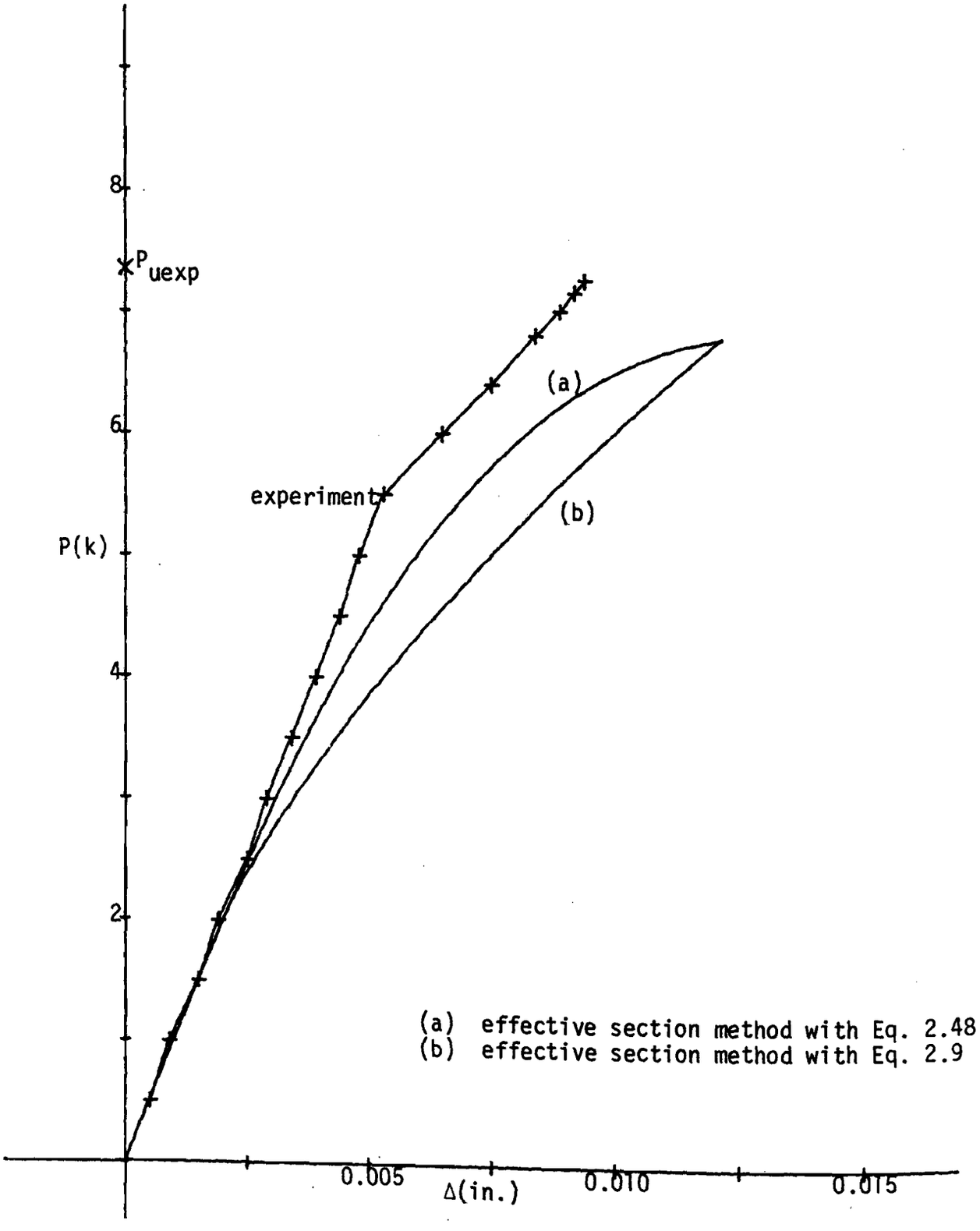

Figure 6.3 AXIAL LOAD-DEFORMATION RESPONSE FOR CHANNEL SC/1 90X30

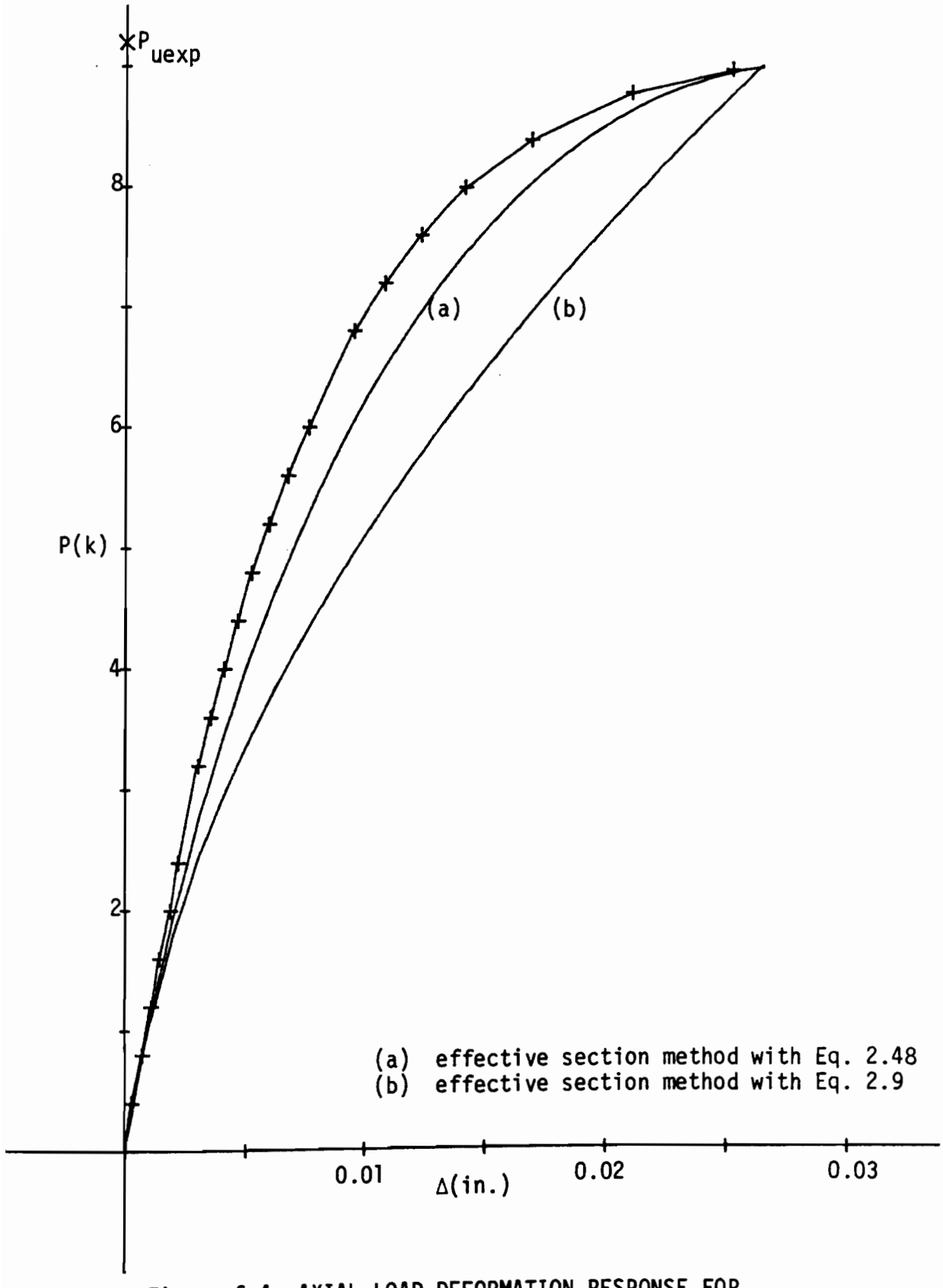

Figure 6.4 AXIAL LOAD-DEFORMATION RESPONSE FOR CHANNEL SC/1 100X60

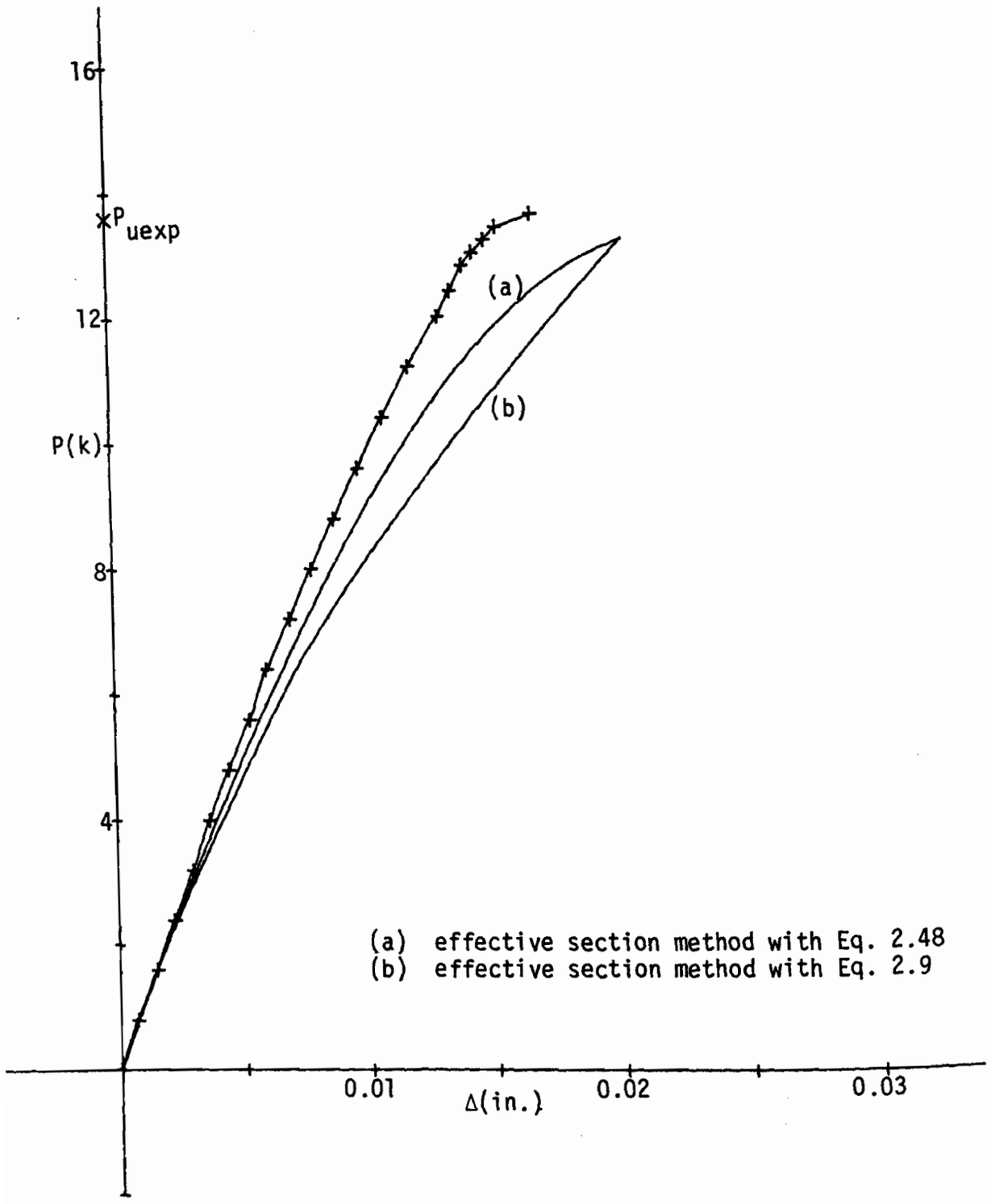

Figure 6.5 AXIAL LOAD-DEFORMATION RESPONSE FOR LIPPED CHANNEL SLC/2 120X60

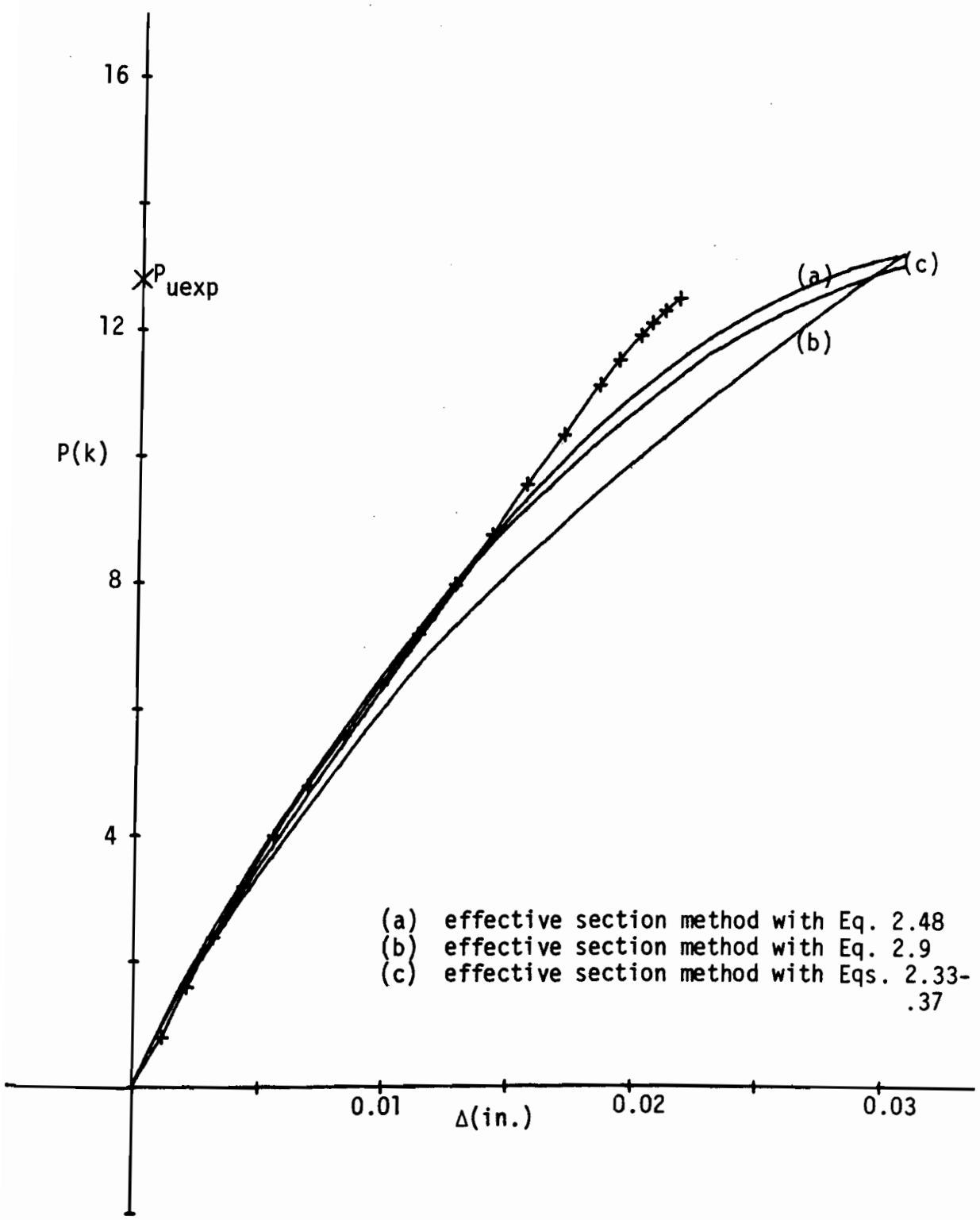

Figure 6.6 AXIAL LOAD-DEFORMATION RESPONSE FOR LIPPED CHANNEL SLC/2 180X60

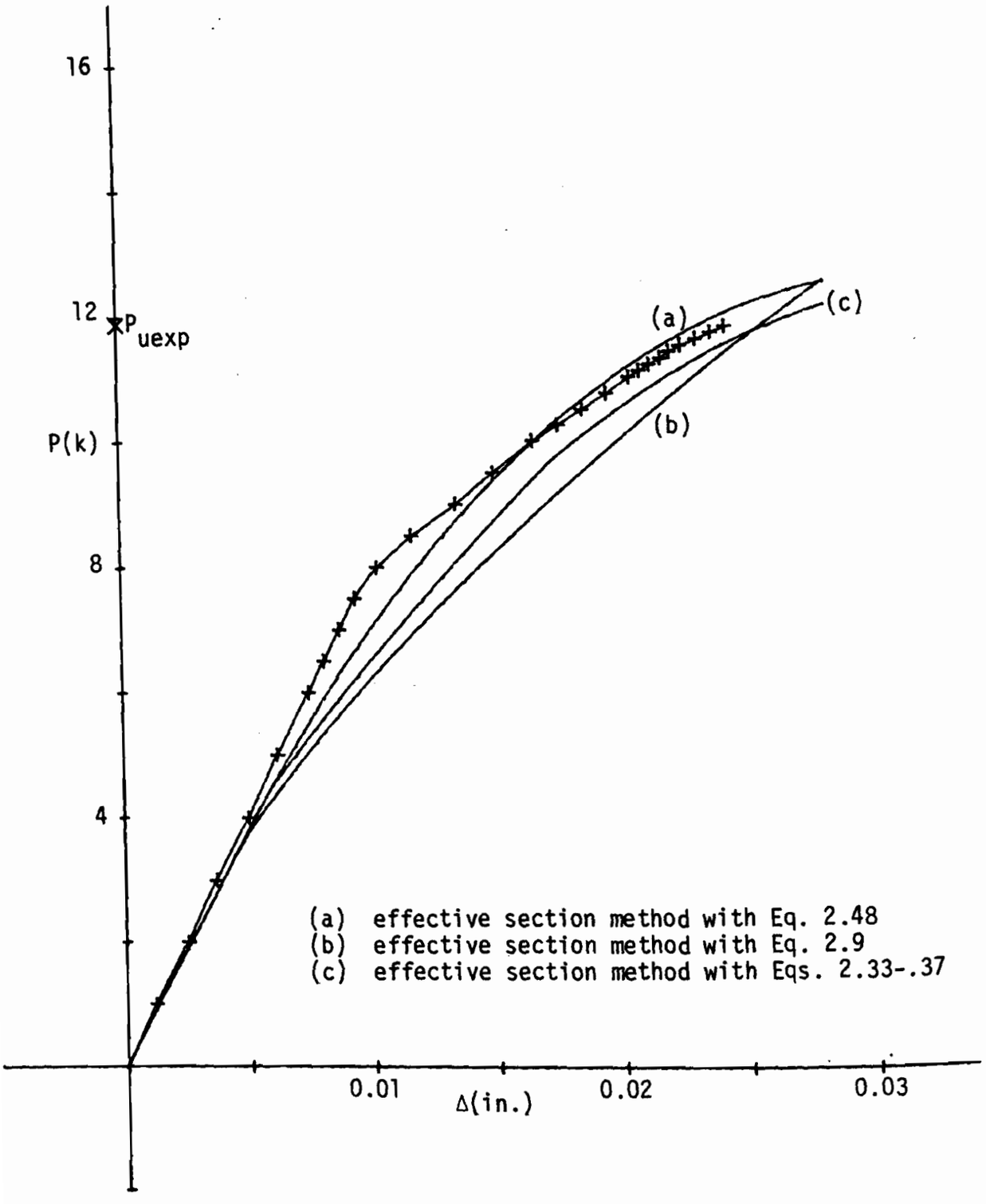

Figure 6.7 AXIAL LOAD-DEFORMATION RESPONSE FOR LIPPED CHANNEL SLC/1 90X90

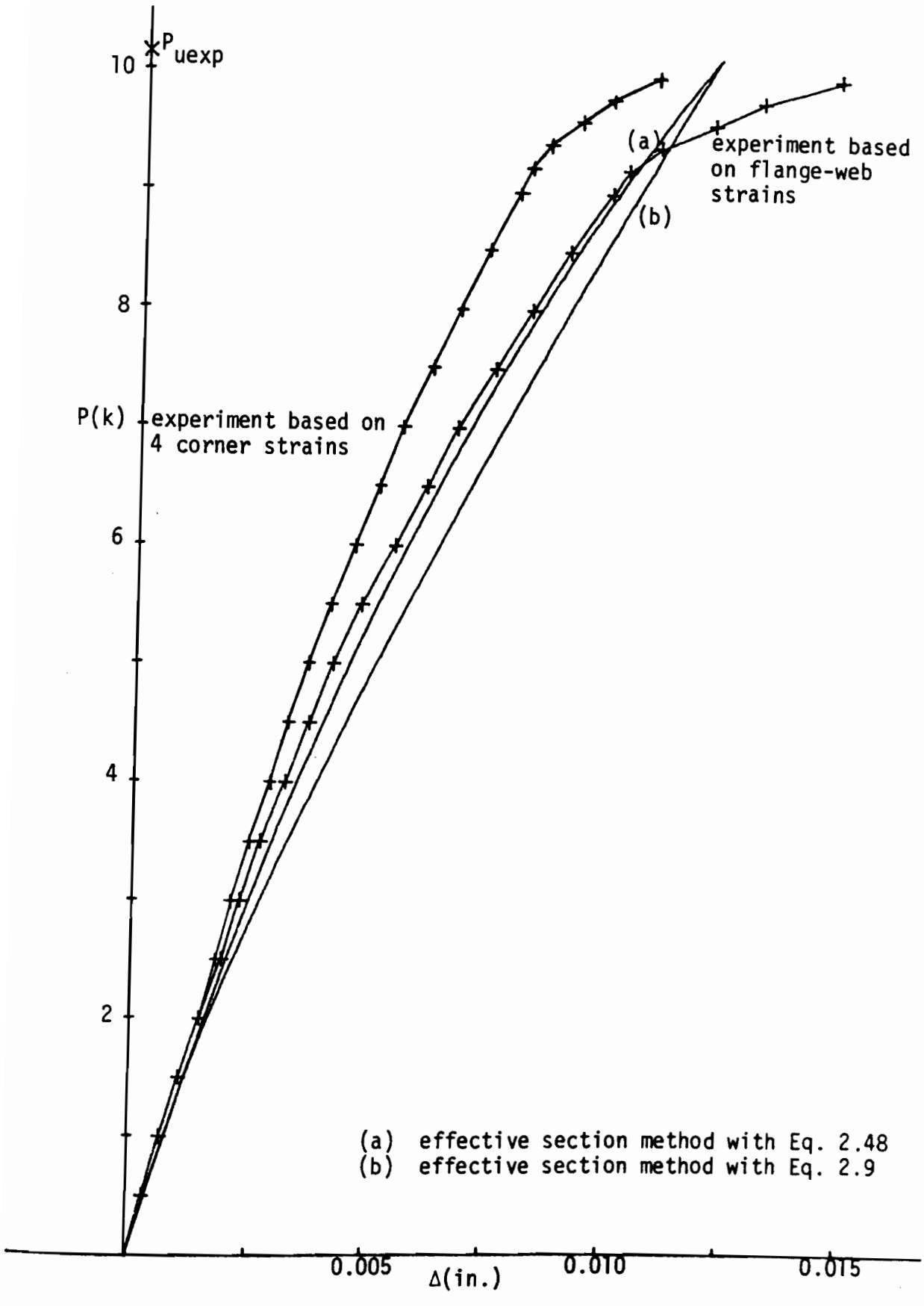

Figure 6.8 AXIAL LOAD-DEFORMATION RESPONSE FOR LIPPED CHANNEL SLC/1 120X30

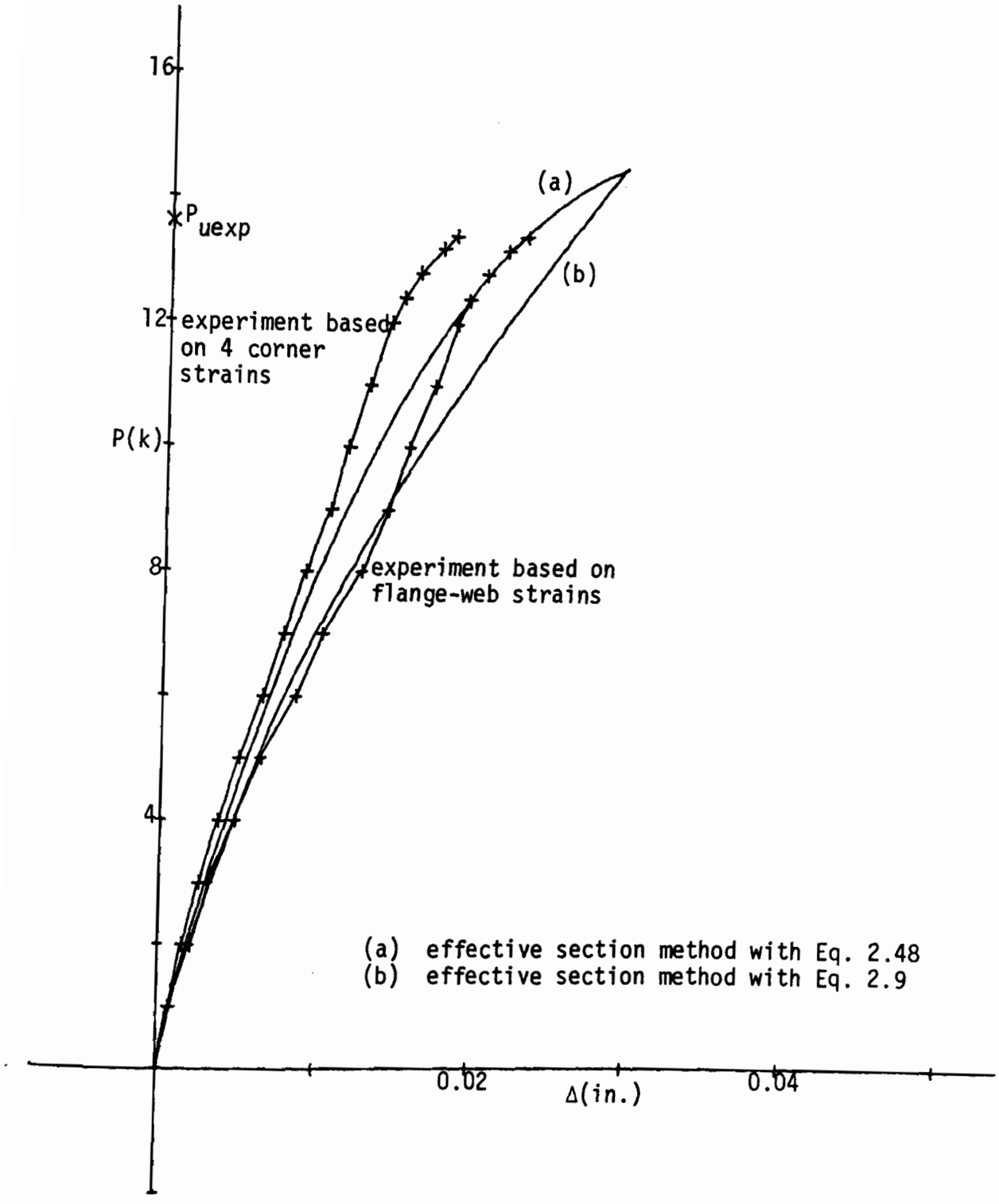

Figure 6.9 AXIAL LOAD-DEFORMATION RESPONSE FOR LIPPED CHANNEL SLC/1 270X90

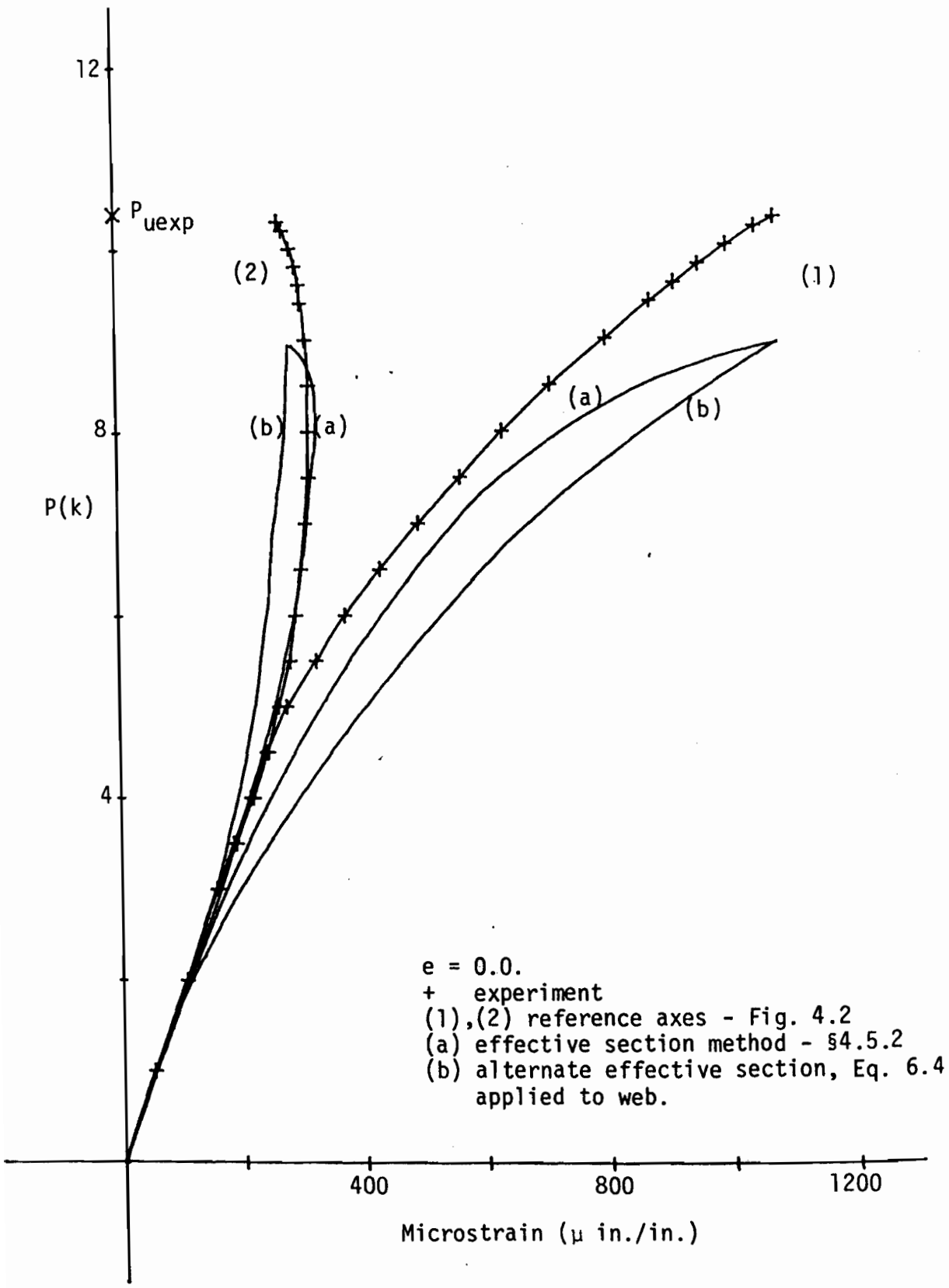

(a) Axial Load-Strain

Figure 6.10 SUB-ULTIMATE RESPONSE FOR CLC/2 120X60

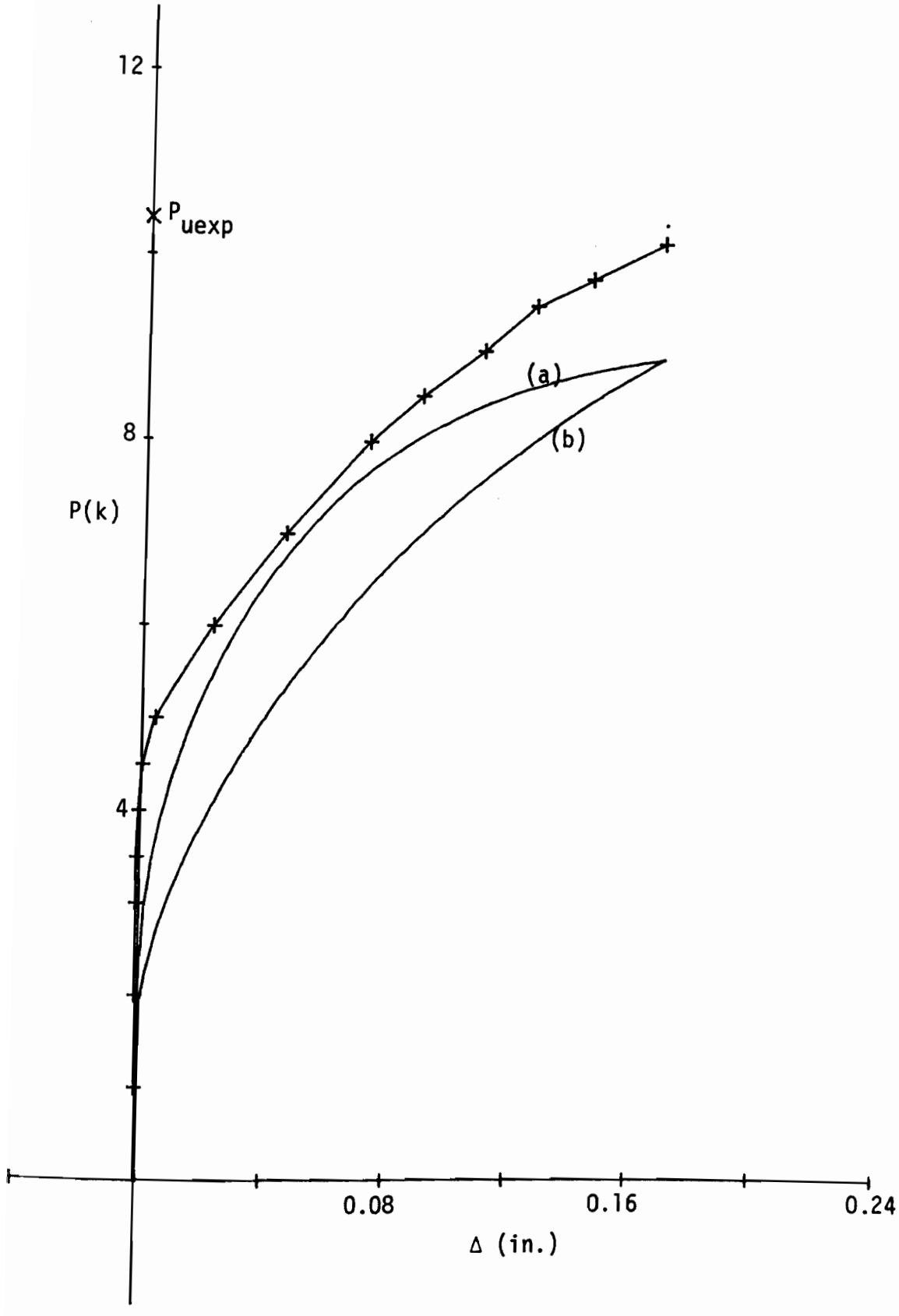

(b) Axial Load-Lateral Deflection

Figure 6.10 CLC/2 120X60 - continued

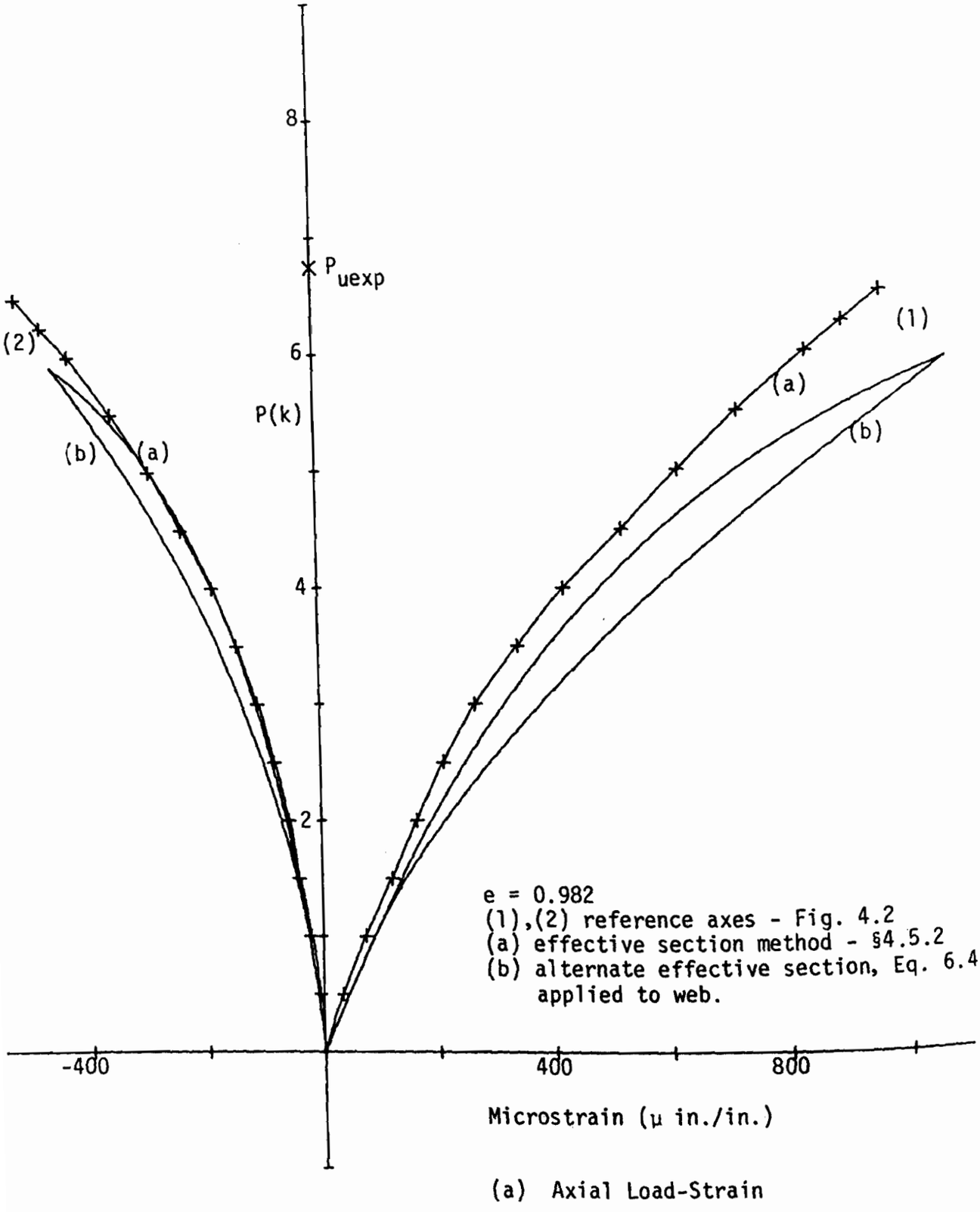

(a) Axial Load-Strain

Figure 6.11 SUB-ULTIMATE RESPONSE FOR CLC/2.3 120X60

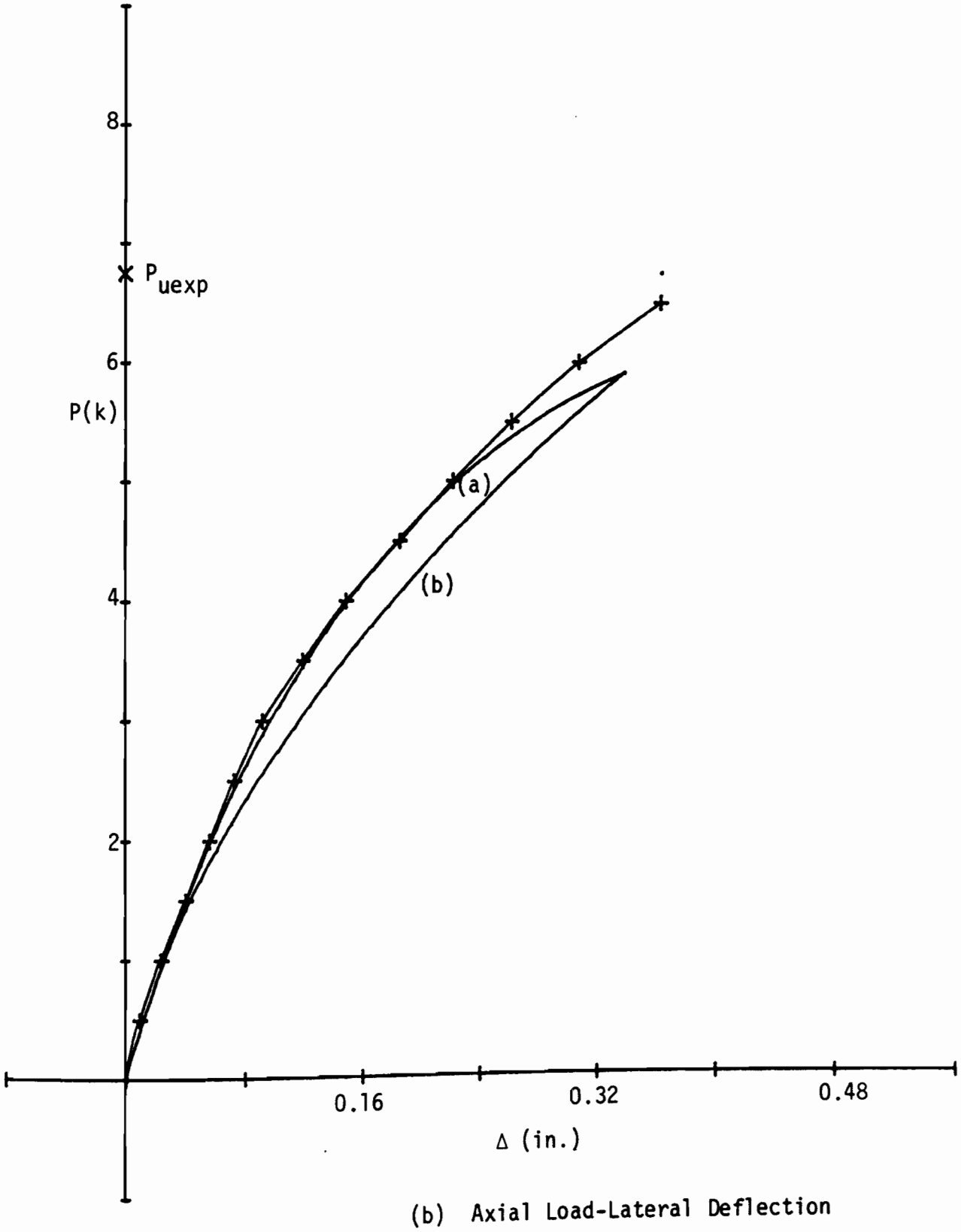

(b) Axial Load-Lateral Deflection

Figure 6.11 CLC/2.3 120X60 - Continued

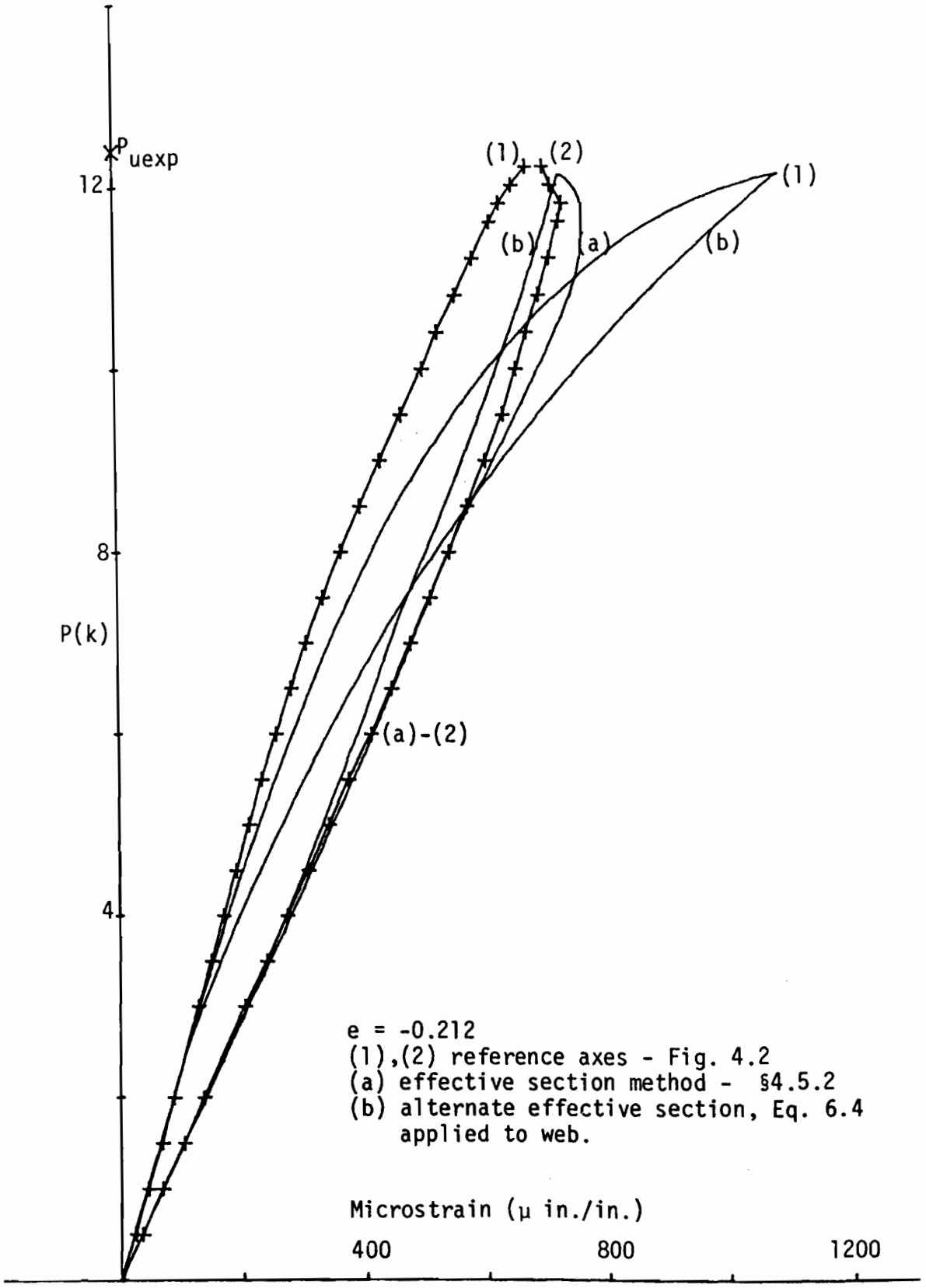

(a) Axial Load-Strain

Figure 6.12 SUB-ULTIMATE RESPONSE FOR CLC/2.4 120X60

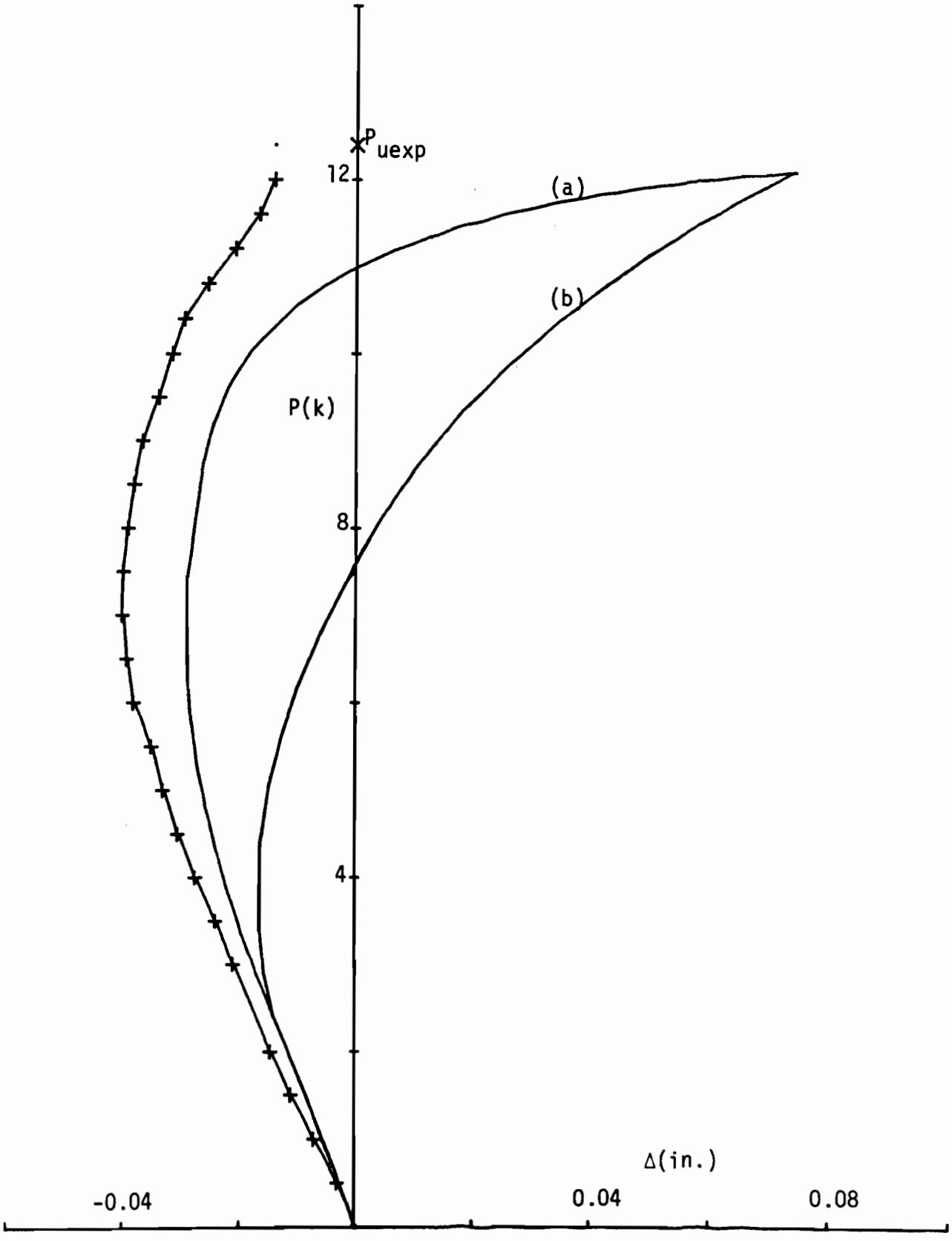

(b) Axial Load-Lateral Deflection

Figure 6.12 CLC/2.4 120X60 - Continued

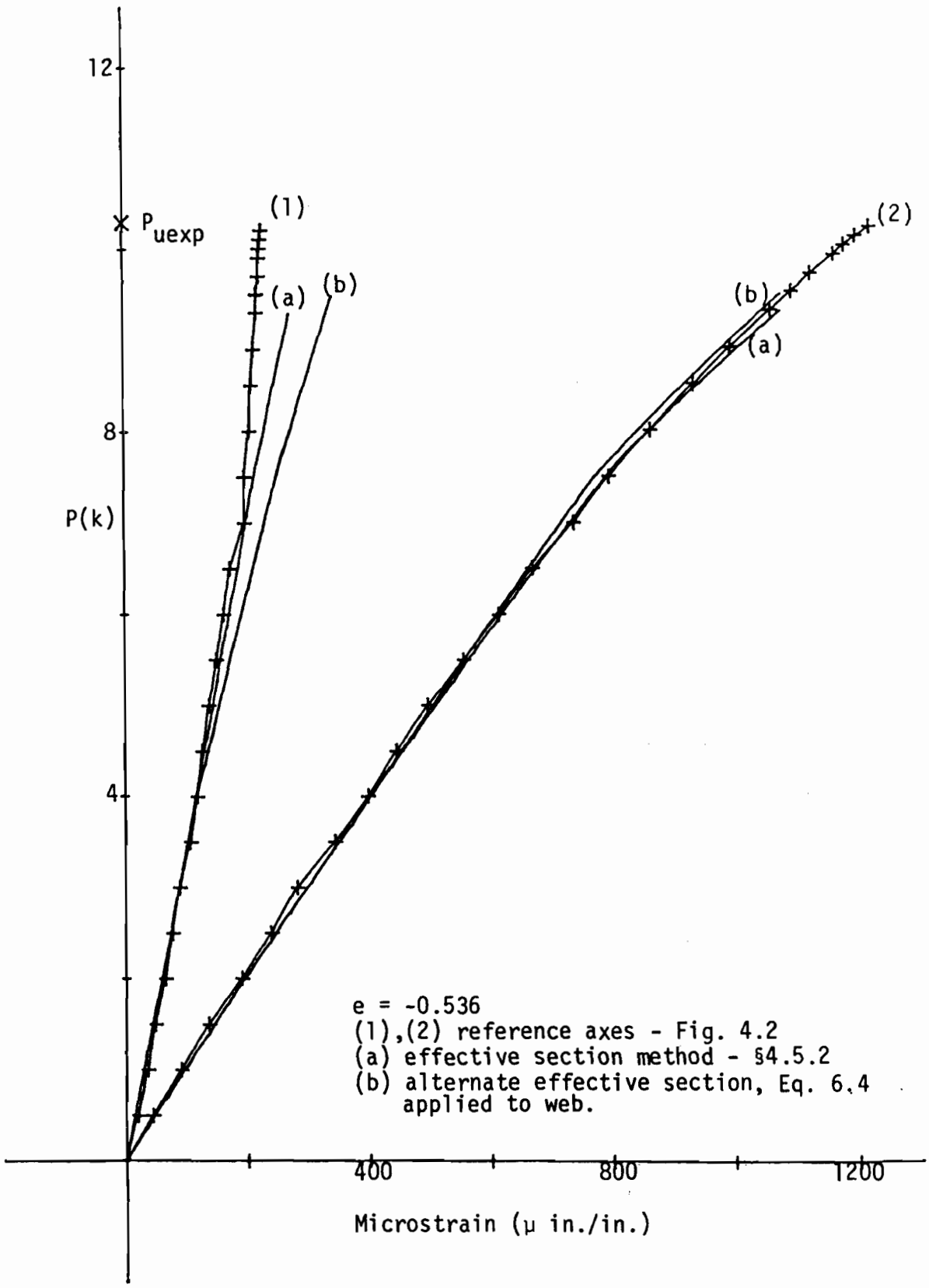

(a) Axial Load-Strain

Figure 6.13 SUB-ULTIMATE RESPONSE FOR CLC/2.1 120X60

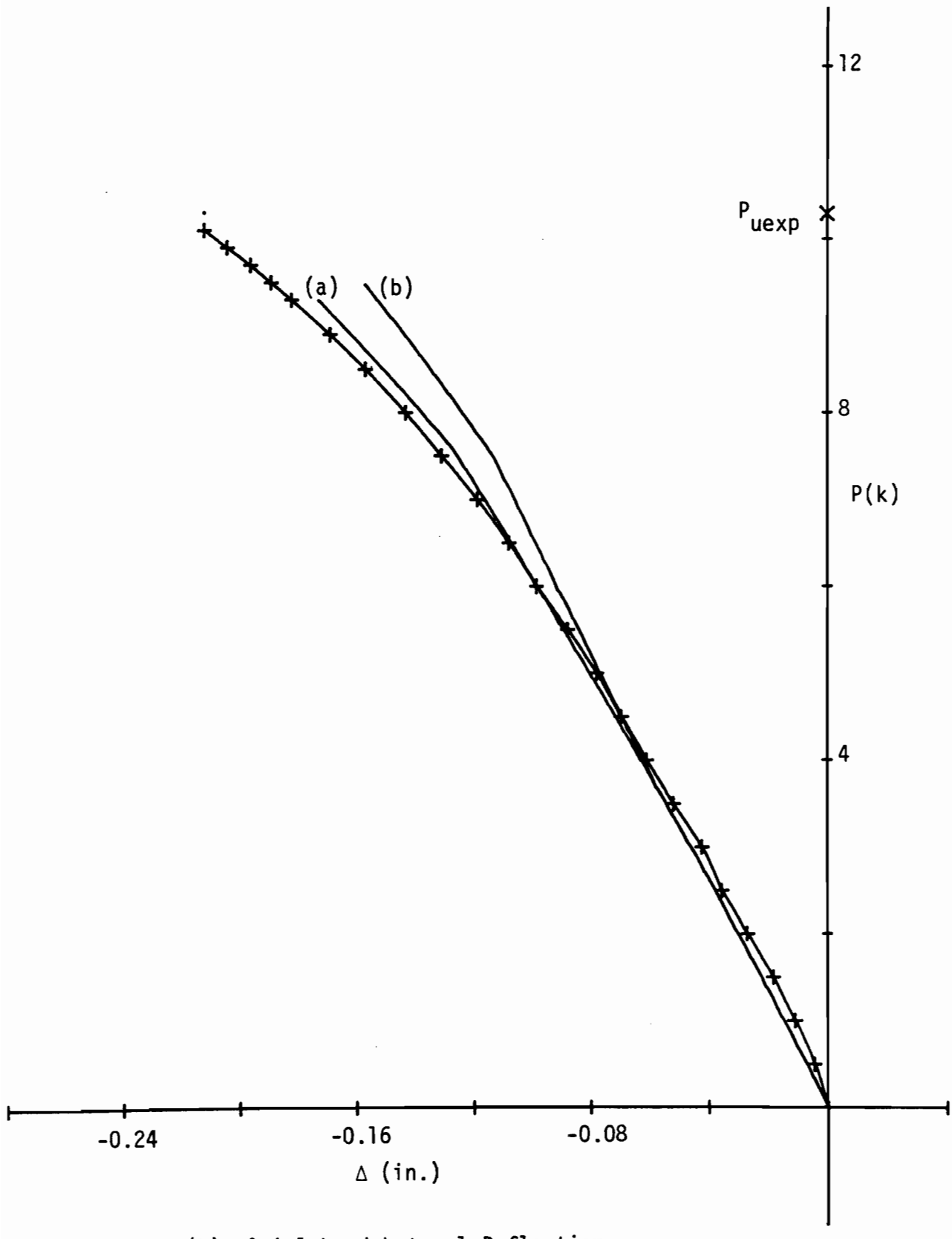

(b) Axial Load-Lateral Deflection

Figure 6.13 CLC/2.1 120X60 - Continued

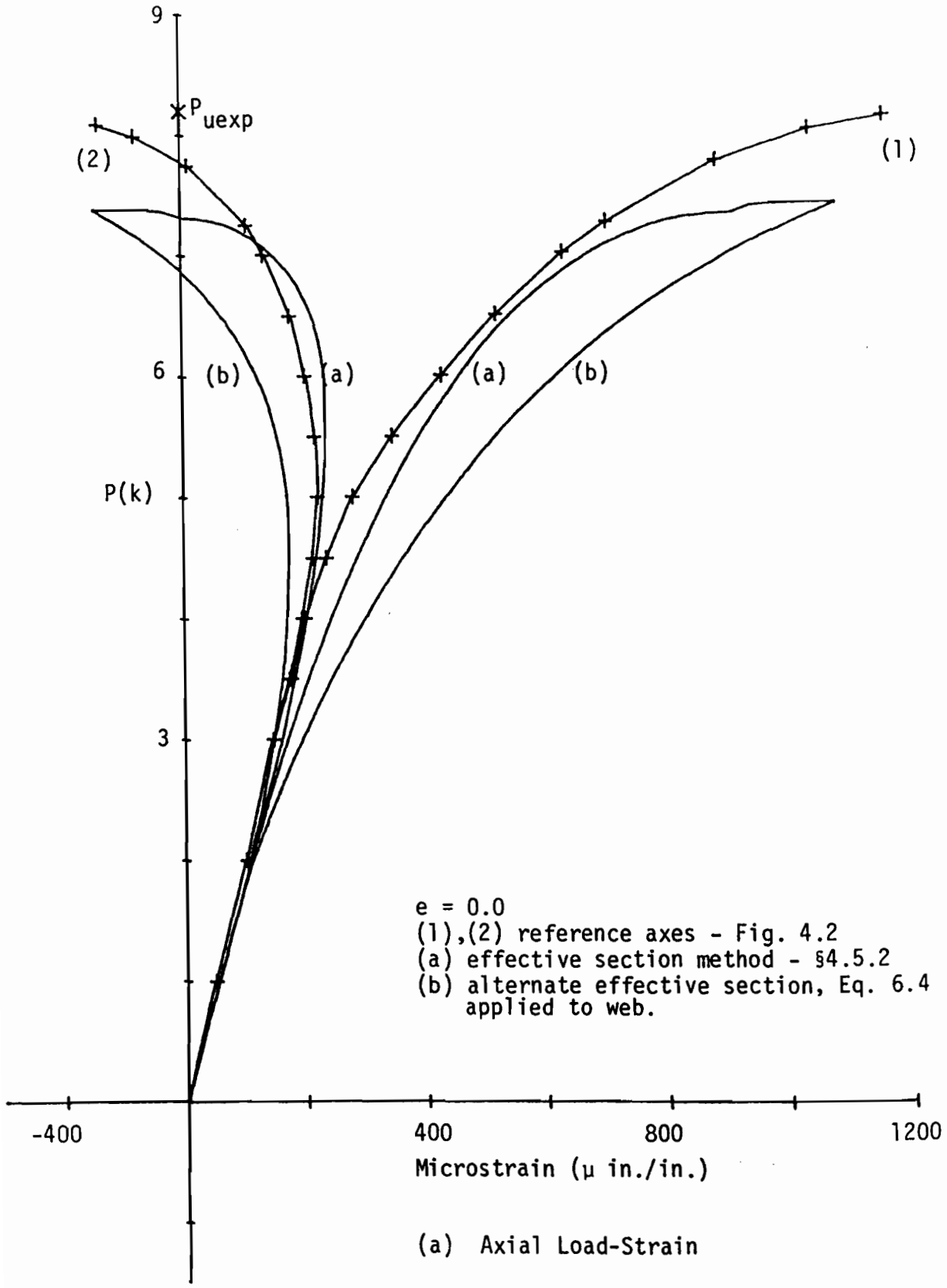

Figure 6.14 SUB-ULTIMATE RESPONSE FOR CLC/3 120X60

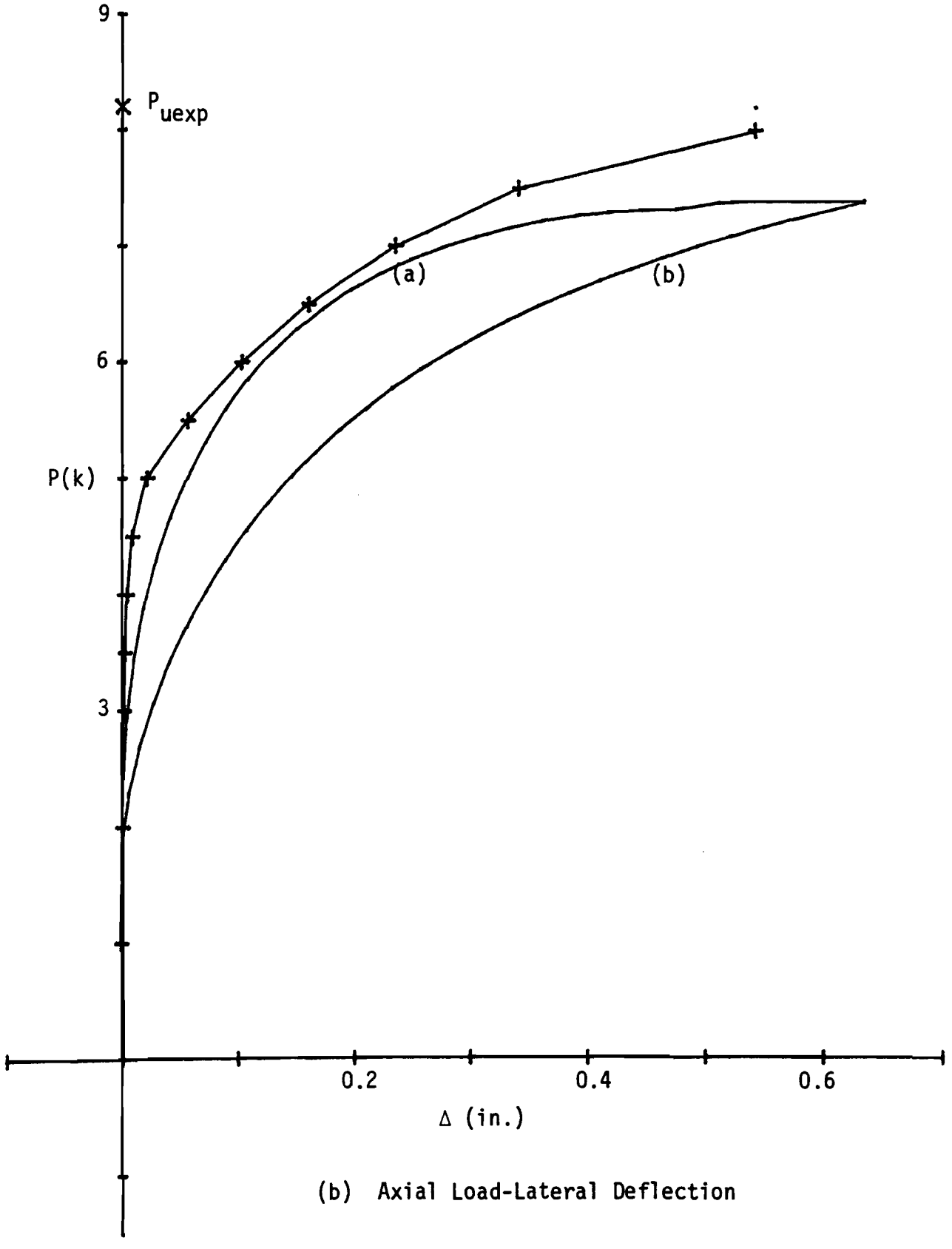

(b) Axial Load-Lateral Deflection

Figure 6.14 CLC/3 120X60 - Continued

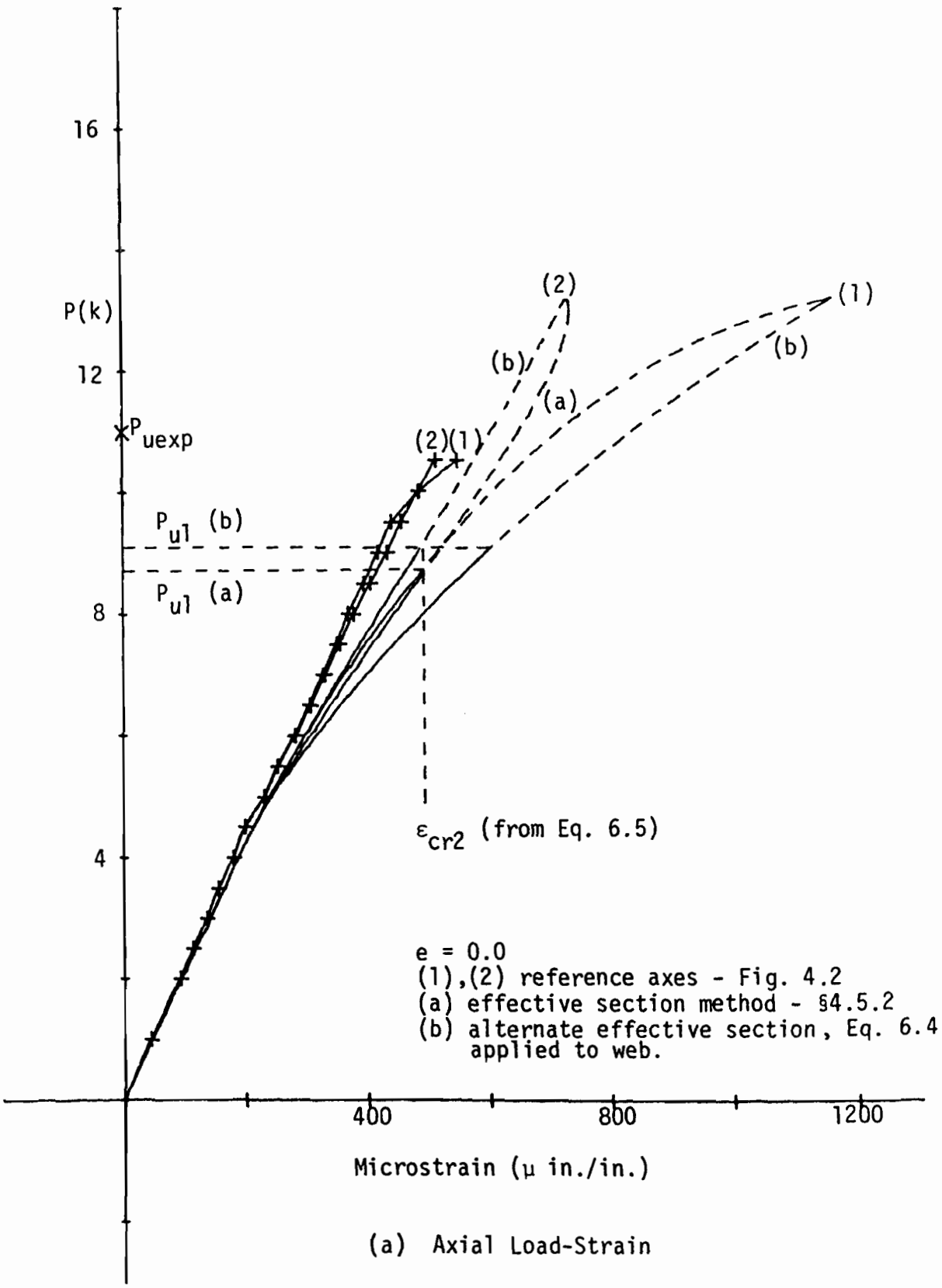

Figure 6.15 SUB-ULTIMATE RESPONSE FOR CLC/1 90X90

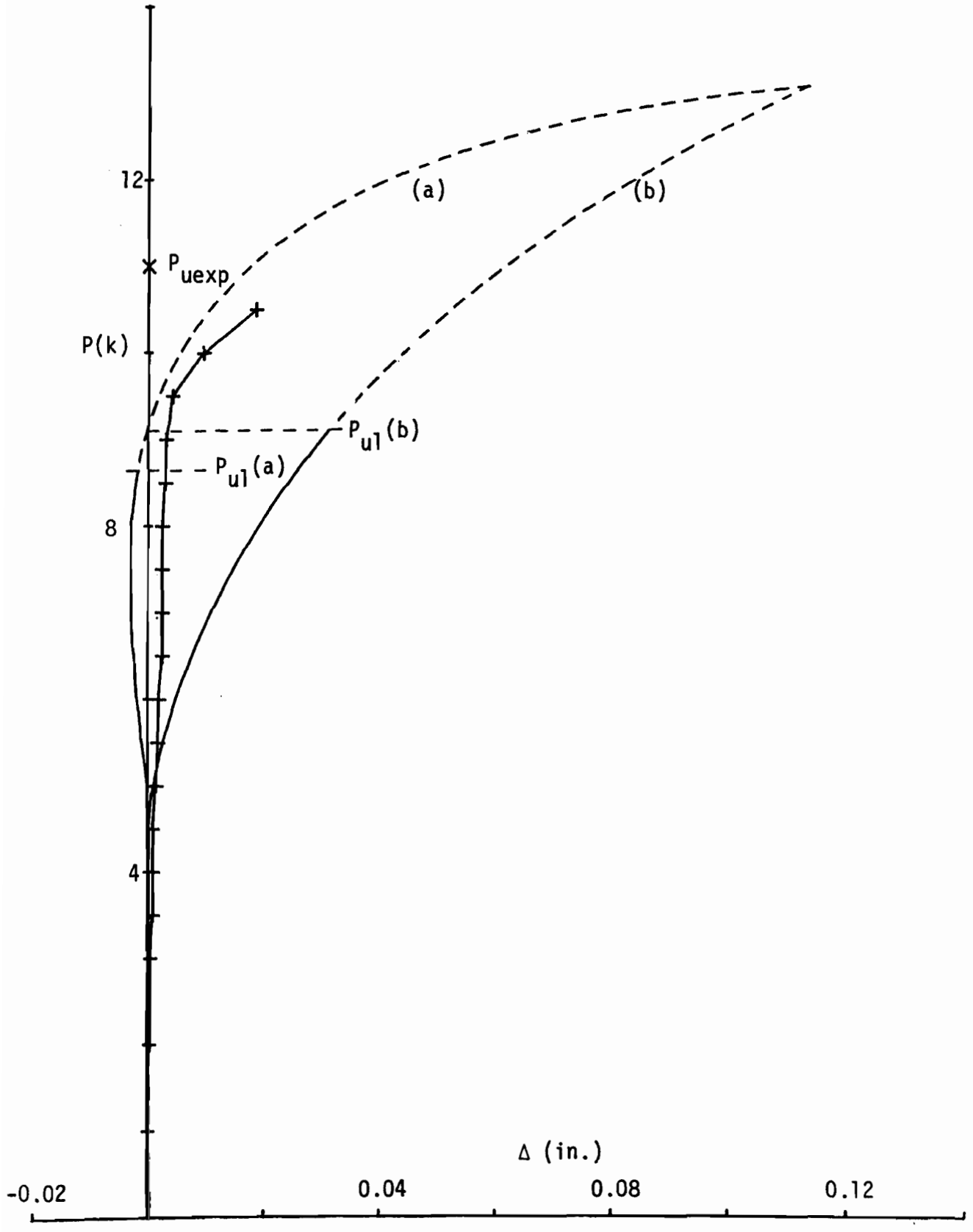

(b) Axial Load-Lateral Deflection

Figure 6.15 CLC/1 90X90 - Continued

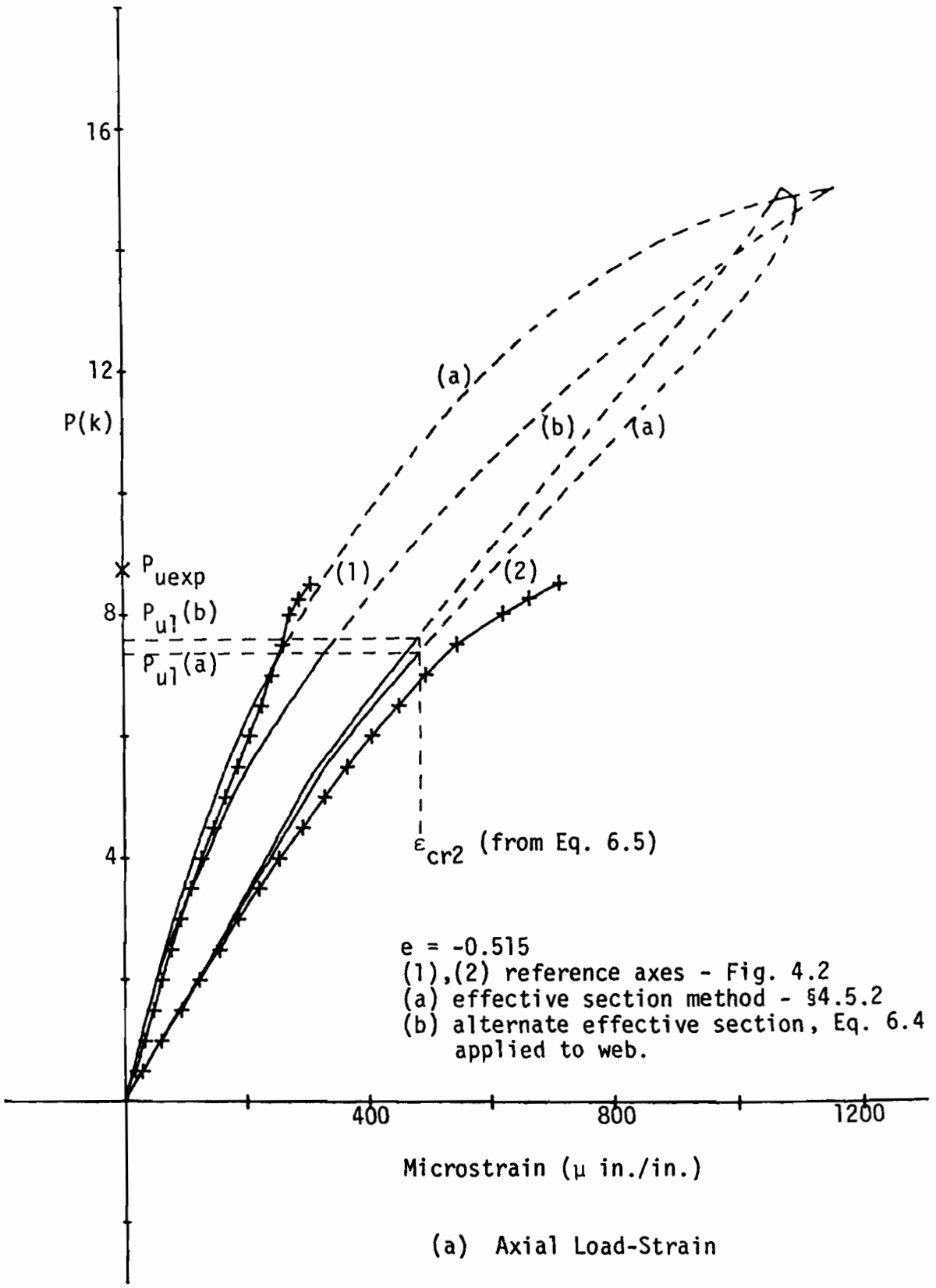

Figure 6.16 SUB-ULTIMATE RESPONSE FOR CLC/2.2 180X90

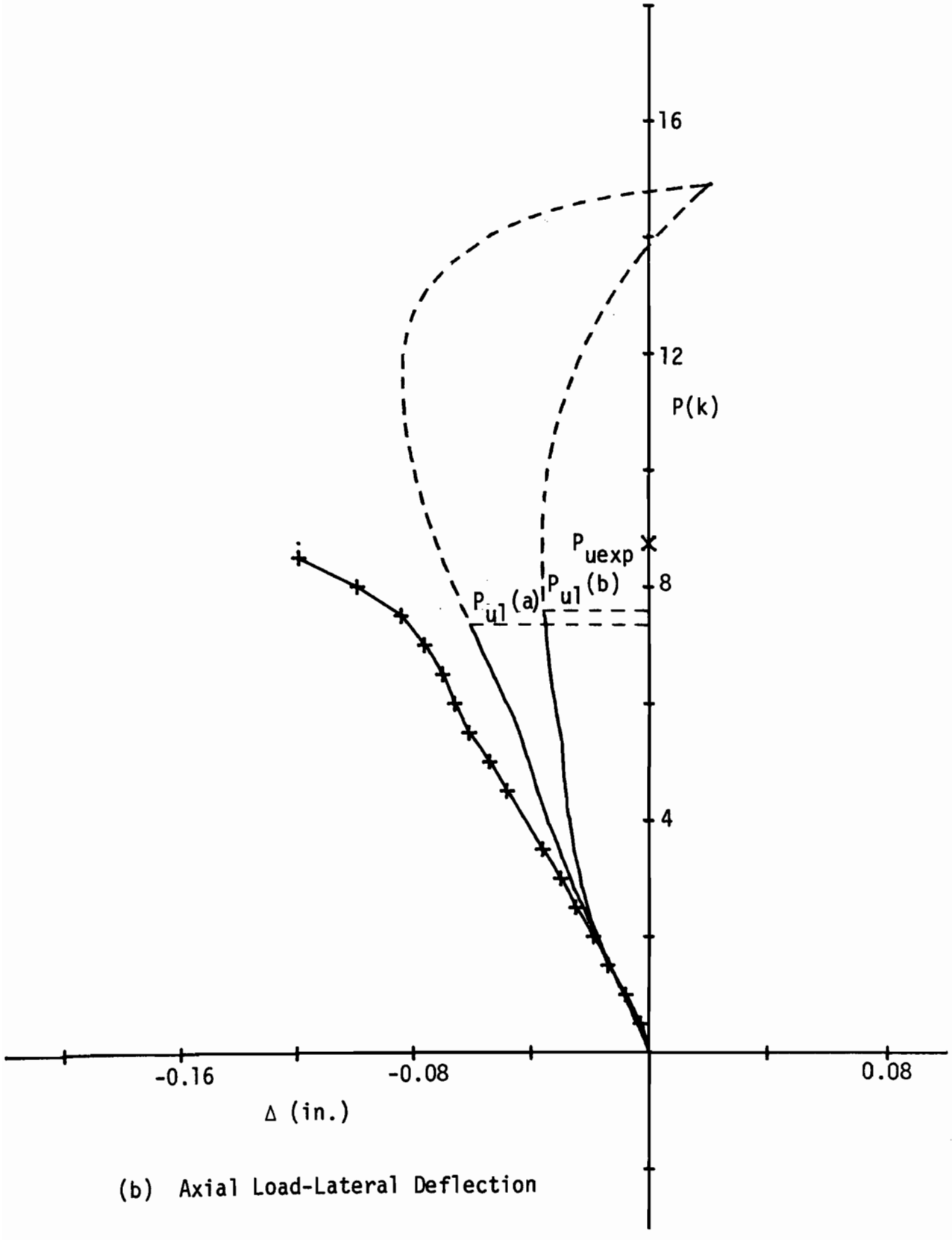

(b) Axial Load-Lateral Deflection

Figure 6.16 CLC/2.2 180X90 - Continued

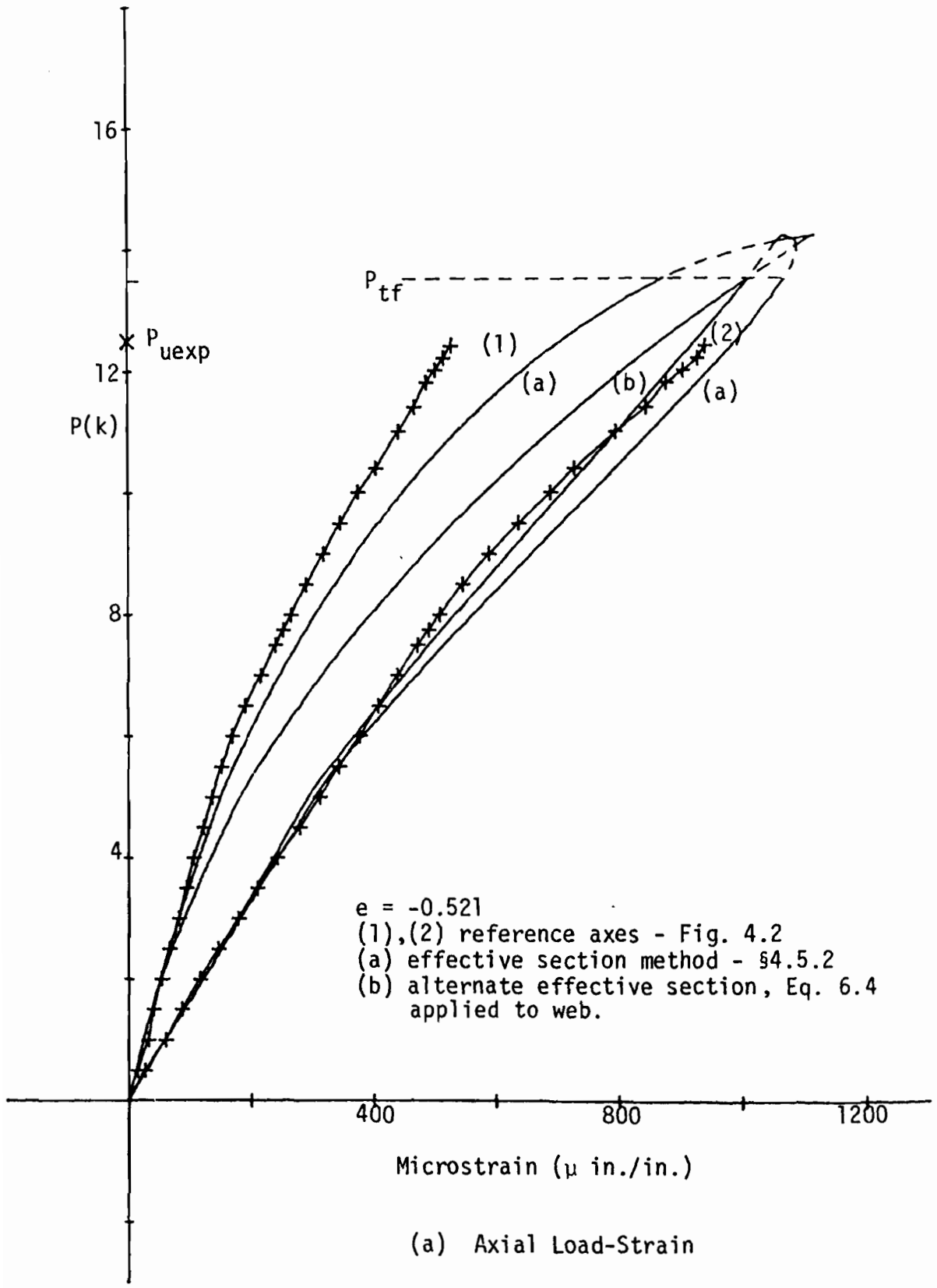

(a) Axial Load-Strain

Figure 6.17 SUB-ULTIMATE RESPONSE FOR CLC/2.1 180X90

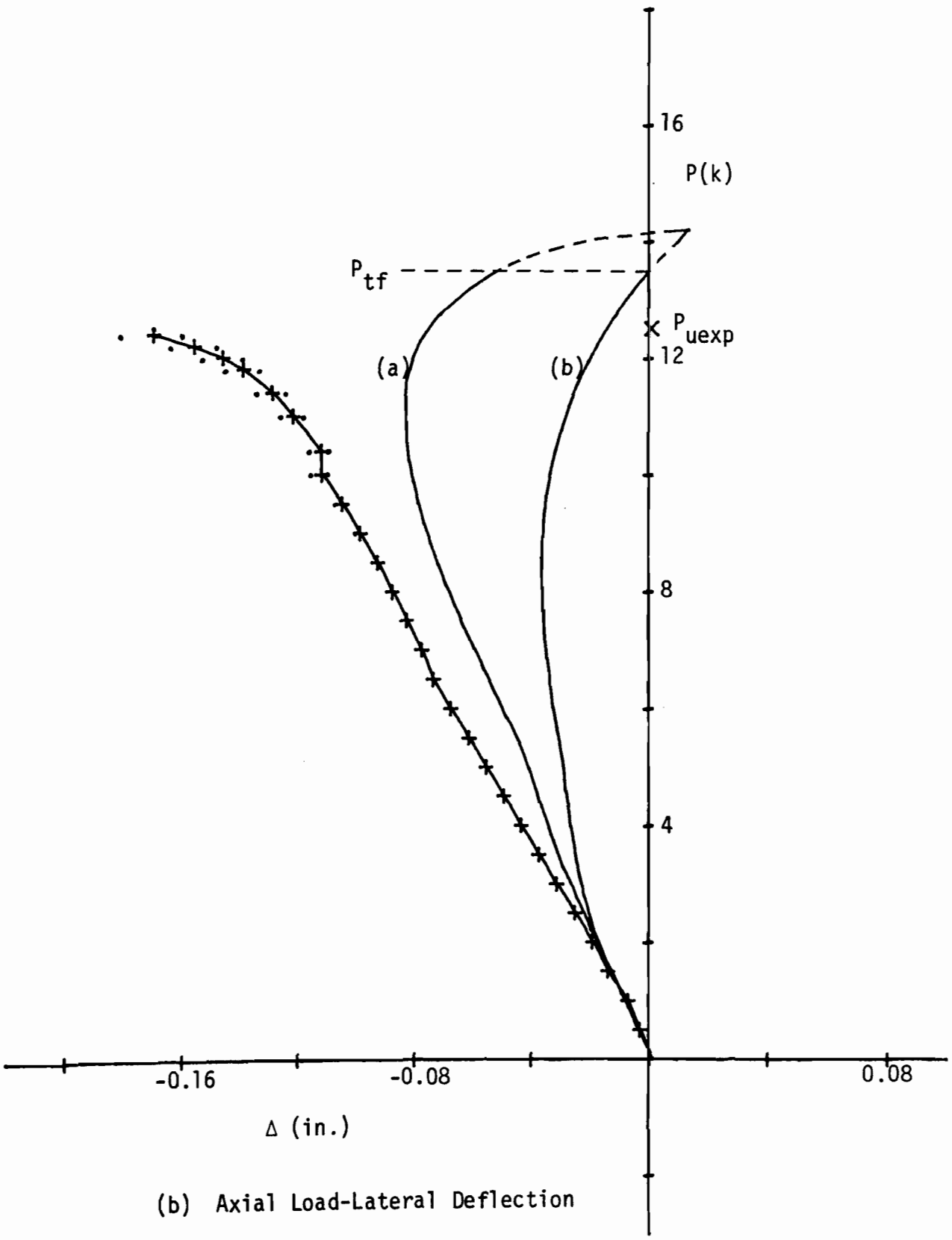

(b) Axial Load-Lateral Deflection

Figure 6.17 CLC/2.1 180X90 - Continued

CHAPTER 7

CONCLUSION

7.1 Summary and Conclusions of Research

The influence of local buckling on the structural behavior and strength of cold-formed steel columns was studied in the research described herein. Specifically, the study was concerned with singly-symmetric shapes where local buckling interaction occurred between the component plate elements and where local buckling interacted with overall modes of action. For these situations analysis methods were derived which correlated well with the results of an experimental investigation. An effective section approach was followed throughout the study in an effort to unify existing and proposed methods for treating the effects of local buckling.

CHAPTER 2 dealt with the post-buckling behavior of isolated thin plates. Eccentrically compressed stiffened elements (plates) were investigated, and an effective width approach was proposed which was consistent with current design specifications. This approach was a modification to empirical Swedish research.

The sub-ultimate response of uniformly compressed, post-buckled plates was also treated. For this case an effective width approach was derived which simulated theoretical solutions and behavior. While the purpose of this approach was to provide a means of accurately predicting

service load (sub-ultimate) deflections, it was equally applicable to ultimate conditions. In the latter instance the approach was again consistent with current design specifications.

Finally, uniformly compressed stiffened and unstiffened elements were addressed, and the unified effective width approach for these elements was reestablished.

CHAPTER 3 studied the more practical application of local buckling in structural sections where interaction occurred between the component plate elements. Generally this work precluded overall modes of action.

The finite strip method was employed to formulate the equations which governed the linearized elastic instability of thin-walled structures. Special numerical procedures and algorithms were developed to enable computer generation and solution of the resulting system of equations. The specifics of the formulation, solution methods, and program verification were considered in Appendices A-C, respectively. Overall, the methods which were developed proved very effective for analyzing the instability of the type of structure under study.

Next, the finite strip method was applied to uniformly compressed thin-walled channel and lipped channel sections which established the characteristics of local buckling interaction. For the latter section, the effects of non-uniform compression and of edge stiffeners were also investigated and found to significantly affect the response.

Then edge stiffeners were discussed in greater detail, and current and proposed stiffener requirements were reviewed. In addition, an idealized flange-stiffener model was analyzed to study the influence of

stiffener radius on instability. The results showed that an arc shaped stiffener was less effective in resisting buckling than an equivalent (equal moment of inertia) right angled lip.

Finally, an effective section method was defined to account for post-local buckling interaction in uniformly compressed stub columns. The interactional effect was reflected thorough the critical buckling stress term of an effective width equation from Chapter 2. A simpler method was also suggested wherein local buckling interaction was ignored. Based on a comparison of the ultimate strengths predicted by these methods for short channel and lipped channel sections, it was observed that, at least theoretically, the interactional effect was more important for the latter section.

CHAPTER 4 treated the interaction between local and overall buckling in long columns. This chapter was prefaced with an illustrative example of local and flexural buckling interaction for a channel section. Then current analysis (design) methods for locally buckled columns and beam-columns were reviewed. This included the Q-factor method for flexural and torsional-flexural buckling, the modified SSRC method for flexural buckling, and a "mixed" method for flexural yielding.

Next, an analysis method was derived to predict the sub-ultimate response and strength of singly-symmetric, lipped channel columns and beam-columns. Local buckling effects were taken into account directly by an effective section which was defined with the methods of Chapter 2. The usual beam-column formulas supplanted with the effective section properties formed the basis of the analysis method. Because the effective

section was dependent on the stress, and vice versa, an iterative solution procedure proved necessary. The effective section analysis method was then applied to representative long columns. These analyses demonstrated that for a certain range of loading eccentricities it was possible to increase the strength of singly-symmetric lipped channel columns over that associated with concentric loading conditions.

CHAPTER 5 reviewed the experimental investigation, which was separated into two areas. The first dealt with the stub column tests (uniform compression) of cold-formed steel channels and lipped channels. The required local buckling interaction between component plate elements was provided by systematically varying the cross-sectional dimensions of the sections. The second area dealt with the long column tests of concentrically and eccentrically loaded lipped channels. Several "duplicate" long columns were equipped with intermittent lateral braces (lip to lip) to support the flanges (edge stiffened elements). The objective of the long column tests was to study the influence of local buckling on the overall modes of behavior. Extensive measurements of local and overall initial imperfections were reported, and special alignment procedures were discussed, for both the stub and long column tests.

For the stub columns, poor correlation was obtained between the experimental local buckling stresses and the theoretical values from Chapter 3. This behavior was especially noticeable for the buckling stresses that were associated with the flanges (unstiffened elements) of channels and webs (stiffened elements) of lipped channels. Also, the theoretical assumption of simultaneous buckling of all component plate

elements was, in general, violated experimentally. Finally, a strain gradient was observed, across the flanges, for lipped channels with relatively large web-to-flange ratios.

For the long columns, a comparison of the ultimate strengths of the "duplicate" sections which were tested with and without braces revealed that this extra support increased the load resistance. In addition, some columns, without braces, failed suddenly by a local-torsional collapse of the flanges, even though the edge stiffeners were designed to meet the requirements that were reviewed in Chapter 3.

CHAPTER 6 compared the theoretical and experimental results. The effective section method developed in Chapter 3 was evaluated for predicting the sub-ultimate response and strength of the channel and lipped channel stub columns. The sub-ultimate predictions included the sub-ultimate approach from Chapter 2.

The effection section method which ignored local buckling interaction of the component plate elements provided good correlation with the experimental strengths of channel and lipped channel stub columns (N = 33, M = 1.005, S = 0.081).* Also, the stiffened plate effective width approach (Equation 2.9) was found to predict sub-ultimate deflections which were excessively conservative when compared with actual test measurements. In contrast to this, good correlation with sub-ultimate response was obtained with the sub-ultimate effective width approach (Equation 2.48) which was proposed in this study.

*N = number of tests, M = mean of experimental to predicted strength ratios, and S = standard deviation.

For the long columns, the experimental results were compared to the values predicted with the methods of Chapter 4. Again, both strength and sub-ultimate response were considered. Also, a method was developed for analyzing lipped channels with laterally unsupported flanges (edge stiffened elements).

The effective section and beam-column analysis method developed in Section 4.5.2 provided good correlation with the strengths (N = 16, M = 1.114, S = 0.071) and sub-ultimate response of the concentrically and eccentrically loaded, long column, lipped channels. Moreover, the analysis approach developed to predict the strength associated with local-torsional failure of the columns with laterally unsupported flanges agreed with limited experimental results (N = 3, M = 1.132, S = 0.180).

In contrast to the above, current analysis methods, e.g., the Q-factor and modified SSRC methods for flexural buckling, were found to produce unconservative estimates of the actual strength for the concentrically loaded long columns (N = 12; M = 0.843,0.847; S = 0.052,0.046; respectively). Also, the sub-ultimate response predicted with the stiffened plate effective width equation (2.9) proved unsatisfactory and, in some cases, was unconservative when compared to the experimental results.

Finally, the experimental results reported by other researches were evaluated with respect to the effective section methods of Chapters 3 and 4. This included tests of channel and lipped channel stub columns and lipped channel long columns. In brief, this evaluation reinforced the findings discussed above.

7.2 Future Research

As a result of this study, the following areas for future research have been identified.

1. Local Buckling Interaction — While the present study addressed this quite thoroughly, the experimental program was necessarily limited in scope. For example, the maximum flange width-to-thickness ratios, w_2/t, were limited to 60 (unstiffened elements) for channels and to 90 (edge stiffened element) for lipped channels. Also the correlation of the methods developed for analyzing stub columns showed a tendency of decreasing when compared to the experimental results for lipped channel sections with large flange w_2/t ratios in combination with large web-to-flange width ratios, w_1/w_2. Therefore, additional research of these areas is warranted.

Likewise, in long column applications, the behavior of lipped channels with large w_2/t and w_1/w_2 ratios needs to be investigated. Research in this area should include additional testing of eccentrically loaded lipped channel columns with laterally unsupported flanges.

2. Eccentrically Compressed Unstiffened Elements — A thorough investigation of this area is needed. Present effective width approaches for uniformly compressed unstiffened elements are inadequate because they assume that the maximum stress occurs along the supported edge which is incorrect when the loading is applied eccentrically toward the free edge. Also, it is expected that these elements will be sensitive to initial imperfections and local-torsional failure, similar to that observed in the present study for edge stiffened elements. An experimental program is recommended which includes stub and long column and beam-column tests of channel sections.

3. Torsional-Flexural Buckling — Little, if any, experimental evidence exists to support the Q-factor method for torsional-flexural buckling when the section is buckled locally, i.e., when $Q < 1$. Moreover, in the present study, mixed results were obtained with this method when failure occurred in a torsional-flexural mode. The research on biaxially loaded open sections which is currently underway at Cornell University could be expanded to include the above area.

4. Beam-Columns — The present investigation concentrated on thin-walled lipped channel beam-columns where the loading was applied eccentrically about the minor axis (y axis of Figure 5.1b). A corresponding investigation is needed where bending is applied about the major axis. The effective width approach developed for eccentrically compressed stiffened elements seems applicable, but requires verification.

5. Stiffeners — Arc shaped edge stiffeners were found theoretically, in the present study, to be less effective in resisting local buckling of the supported plate than right angled lip stiffeners of equal moment of inertia. Because certain economies are realized in forming arc shaped stiffeners, it is recommended to conduct further research on this stiffener shape. It is noted that the recently proposed edge stiffener requirements, which were reviewed in Chapter 3, were based on tests of sections with right angled lip edge stiffeners. Research in this area could also include a study of plate elements with more than one stiffener, e.g., multiple intermediate (longitudinal) stiffeners and intermediate stiffeners used in conjunction with edge stiffeners. To the author's knowledge, no experimental investigation has been conducted in these areas.

APPENDIX A

FINITE STRIP INSTABILITY FORMULATION

A.1 Introduction

Explicit forms of the finite strip discretization and instability formulation discussed in Chapter 3 are derived here. The specific formulation combines a second-order plate bending finite strip and a linear plane stress strip (Cheung [1968,1969]). Since these discretizations are complete and continuous, a convergent solution is expected (Zienkiewicz [1977]).

A.2 Finite Strip Formulation

A typical plate bending-membrane finite strip is shown in Figure A.1. A displacement formulation is adopted where the field variable $\underset{\sim}{u}$; consisting of the in-plane displacements u and v, and the out-of-plane displacement w; is related to the local degrees of freedom (nodal displacements) $\underset{\sim}{\Delta}$ by

$$\underset{\sim}{u} = \lfloor u \; v \; w \rfloor^T = \underset{\sim\sim}{N}\underset{\sim}{\Delta} = \begin{bmatrix} \underset{\sim}{N}_m^p & \underset{\sim}{0} \\ \underset{\sim}{0} & \underset{\sim}{N}_m^b \end{bmatrix} \begin{Bmatrix} \underset{\sim}{\Delta}_m^p \\ \underset{\sim}{\Delta}_m^b \end{Bmatrix} \qquad \text{A.1}$$

where the superscripts b and p refer to (plate) bending and plane stress, respectively, and $\underset{\sim}{0}$ represents an appropriate matrix of zeros. Four degrees of freedom are employed along each nodal line (side) of the strip, e.g.,

$$\underset{\sim}{\Delta}_m^p = \lfloor u_1 \; v_1 \; u_2 \; v_2 \rfloor^T \qquad \text{A.2}$$

$$\underset{\sim}{\Delta}_m^b = \lfloor w_1 \ \theta_1 \ w_2 \ \theta_2 \rfloor^T \qquad \text{A.3}$$

The shape functions $\underset{\sim}{N}_m^p$ are derived from a linear polynomial in the transverse direction and harmonic functions in the longitudinal direction,

$$\underset{\sim}{N}_m^p = \begin{bmatrix} (1 - \xi)\sin\alpha_m y & 0 & \xi\sin\alpha_m y & 0 \\ 0 & (1 - \xi)\cos\alpha_m y & 0 & \xi\cos\alpha_m y \end{bmatrix} \qquad \text{A.4}$$

where $\xi = x/b$ and $\alpha_m = m\pi/L$.

On the other hand, the shape functions $\underset{\sim}{N}_m^b$ are chosen as the product of a beam function in the transverse direction and a harmonic function Y_m in the longitudinal direction

$$\underset{\sim}{N}_m^b = Y_m \lfloor (1 - 3\xi^2 + 2\xi^3) \ b\xi(1 - 2\xi + \xi^2) \ (3\xi^2 - 2\xi^3) \ b\xi(\xi^2 - \xi) \rfloor \qquad \text{A.5}$$

where $Y_m = \sin\alpha_m y$. A.6

It is noted that the discretization of Equation A.1 satisfies the boundary conditions associated with a rigid diaphragm at the ends of the strip. Furthermore, only one harmonic m of the general finite strip discretization given by*

$$\underset{\sim}{u} = \sum_m^M \underset{\sim m}{N} \underset{\sim m}{\Delta} \qquad \text{A.7}$$

is considered in Equation A.1. This restriction is equivalent to assuming that there is no interaction between the various local buckling modes represented by the M harmonics. Actually, for the specific boundary and loading conditions to be considered here, the various harmonics do uncouple, and the one harmonic discretization of Equation A.1 is sufficient. Thus, the subscript m will be dropped for convenience only but is implicitly assumed in the development which follows.

*Equation A.7 is equivalent to Equation 3.4 with the Y_m included in $\underset{\sim}{N}$.

Next, the infinitesimal strain-displacement relations are introduced as

$$\underset{\sim}{\varepsilon}_o^p = \lfloor \partial u/\partial x \quad \partial v/\partial y \quad \partial u/\partial y + \partial v/\partial x \rfloor^T \qquad A.8$$

for plane stress and

$$\underset{\sim}{\varepsilon}_o^b = \lfloor -\partial^2 w/\partial x^2 \quad -\partial^2 w/\partial y^2 \quad 2\partial^2 w/\partial x \partial y \rfloor^T \qquad A.9$$

for linearized plate bending where the strains are defined as the plate curvatures. Combining the above strain-displacement relations with the non-linear contributions allows the total strain vector $\underset{\sim}{\varepsilon}$, Equation 3.7, to be written as

$$\underset{\sim}{\varepsilon} = \begin{Bmatrix} \underset{\sim}{\varepsilon}^p \\ \underset{\sim}{\varepsilon}^b \end{Bmatrix} = \begin{Bmatrix} \underset{\sim}{\varepsilon}_o^p \\ \underset{\sim}{\varepsilon}_o^b \end{Bmatrix} + \begin{Bmatrix} \underset{\sim}{\varepsilon}_L^p \\ \underset{\sim}{0} \end{Bmatrix} \qquad A.10$$

A typical term of the nonlinear strain $\underset{\sim}{\varepsilon}_L^p$, which accounts for the coupling of in-plane and out-of-plane action, is given by

$$\tfrac{1}{2}[(\partial u/\partial x)^2 + (\partial v/\partial x)^2 + (\partial w/\partial x)^2] \qquad A.11$$

Thus, it is seen that all the terms of Green's strain are retained, where the terms in w model the local buckling modes and those in u and v model the overall modes (Graves Smith and Sridharan [1978a]).

Further, a vector of displacement gradients is introduced as

$$\underset{\sim}{\Theta} = \lfloor \underset{\sim}{\Theta}_x \quad \underset{\sim}{\Theta}_y \rfloor^T \qquad A.12$$

where

$$\underset{\sim}{\Theta}_x = \lfloor \partial u/\partial x \quad \partial v/\partial x \quad \partial w/\partial x \rfloor^T$$

$$\underset{\sim}{\Theta}_y = \lfloor \partial u/\partial y \quad \partial v/\partial y \quad \partial w/\partial y \rfloor^T$$

This equation allows the nonlinear strain $\underset{\sim}{\varepsilon}_L^p$ to be conveniently expressed as

$$\underset{\sim}{\varepsilon}_L^p = \tfrac{1}{2}\underset{\sim\sim}{A}\underset{\sim}{\Theta} \qquad A.13$$

where the matrix $\underset{\sim}{A}$ is defined by

$$\underset{\sim}{A} = \begin{bmatrix} \underset{\sim}{\Theta}_x^T & \underset{\sim}{0} \\ \underset{\sim}{0} & \underset{\sim}{\Theta}_y^T \\ \underset{\sim}{\Theta}_y^T & \underset{\sim}{\Theta}_x^T \end{bmatrix}$$

Introducing the finite strip discretization of Equation A.1 into Equation A.13 allows the nonlinear strains to be written in terms of nodal displacements as

$$\underset{\sim}{\varepsilon}_L^p = \tfrac{1}{2}\underset{\sim}{A}\underset{\sim}{G}\underset{\sim}{\Delta} \qquad \text{A.14}$$

From a comparison of the above equation and the second term on the right-hand-side of Equation 3.8,

$$\underset{\sim}{\varepsilon} = \underset{\sim}{B}_o\underset{\sim}{\Delta} + \tfrac{1}{2}\underset{\sim}{B}_L\underset{\sim}{\Delta} \qquad 3.8$$

the linear strain matrix $\underset{\sim}{B}_L$ is identified as

$$\underset{\sim}{B}_L = \underset{\sim}{A}\underset{\sim}{G} \qquad \text{A.15}$$

Moreover, if the discretization of Equation A.1 is also introduced into the infinitesimal strains, Equations A.8 and A.9, the total strain $\underset{\sim}{\varepsilon}$ of Equation A.10 follows as

$$\underset{\sim}{\varepsilon} = \begin{bmatrix} \underset{\sim}{B}_o^p & \underset{\sim}{0} \\ \underset{\sim}{0} & \underset{\sim}{B}_o^b \end{bmatrix} \begin{bmatrix} \underset{\sim}{\Delta}^p \\ \underset{\sim}{\Delta}^b \end{bmatrix} + \tfrac{1}{2} \begin{bmatrix} \underset{\sim}{B}_L^p & \underset{\sim}{B}_L^b \\ 0 & 0 \end{bmatrix} \begin{bmatrix} \underset{\sim}{\Delta}^p \\ \underset{\sim}{\Delta}^b \end{bmatrix} \qquad \text{A.16}$$

where the small displacement strain matrix $\underset{\sim}{B}_o$ and the linear strain matrix $\underset{\sim}{B}_L$ of Equation 3.8 are separated into their plane stress and bending components.

Next, the stresses $\underset{\sim}{\sigma}$, defined below

$$\underset{\sim}{\sigma} = \left\lfloor \sigma_x \; \sigma_y \; \sigma_{xy} \; \vdots \; M_x \; M_y \; M_{xy} \right\rfloor^T = \left\lfloor \underset{\sim}{\sigma}^p \quad \underset{\sim}{\sigma}^b \right\rfloor^T \qquad \text{A.17}$$

are related to the strains by the following isotropic, elastic constitutive law

$\underset{\sim}{I}$ is a diagonal identity matrix, and the T_x, etc., are membrane loads. The form of the initial stress matrix given above verifies its symmetric nature. Moreover, in the present formulation, only a longitudinal membrane loading, T_y, is considered. For this loading a consistent representation is followed where the same shape functions that are used in the v displacement discretization, Equation A.4, are employed, i.e.,

$$T_y = (1 - \xi)T_{y1} + \xi T_{y2} \qquad \text{A.25}$$

where $\xi = x/b$ and the T_{y1} and T_{y2} are the magnitudes of the membrane loading along sides one (1) and two (2), respectively (Figure A.1). Again, $\underset{\sim}{K}_\sigma$ is broken down into its plane stress and bending components as

$$\underset{\sim}{K}_\sigma = \begin{bmatrix} \underset{\sim}{K}^p_\sigma & \underset{\sim}{0} \\ \underset{\sim}{0} & \underset{\sim}{K}^b_\sigma \end{bmatrix} \qquad \text{A.26}$$

An explicit form of the above equation is listed in Table A.3. In this table, it is noted that the coefficients of $\underset{\sim}{K}_\sigma$ are dependent on stress levels and geometric properties. Due to the latter dependence, $\underset{\sim}{K}_\sigma$ is alternately described as a geometric stiffness matrix.

It is informative at this point to consider the effect of including several terms in the finite strip discretization, e.g., employing Equation A.7 instead of the one term discretization of Equation A.1. It is not necessary to differentiate between plane stress or bending by the superscripts p and b, respectively, because the result is the same for both. First, Equation A.7 is written in expanded form as

$$\underset{\sim}{u} = \left\lfloor \underset{\sim}{N}_1 \; \underset{\sim}{N}_2 \; \cdots \; \underset{\sim}{N}_m \; \cdots \; \underset{\sim}{N}_M \right\rfloor \left\lfloor \underset{\sim}{\Delta}_1 \; \underset{\sim}{\Delta}_2 \; \cdots \; \underset{\sim}{\Delta}_m \; \cdots \; \underset{\sim}{\Delta}_M \right\rfloor^T \qquad \text{A.27}$$

where the series is terminated at the Mth term. For this discretization the small displacement stiffness matrix, $\underset{\sim}{K}_o$, can be shown to take the following form (Cheung [1976]).

$$\underset{\sim}{K}_o = \begin{bmatrix} \underset{\sim}{K}_{11} & \underset{\sim}{K}_{12} & \cdots & \underset{\sim}{K}_{1M} \\ \underset{\sim}{K}_{21} & \underset{\sim}{K}_{22} & \cdots & \cdots \\ \cdots & \cdots & \cdots & \cdots \\ \underset{\sim}{K}_{M1} & \cdots & \cdots & \underset{\sim}{K}_{MM} \end{bmatrix} \qquad \text{A.28}$$

$$\text{with } \underset{\sim}{K}_{mn} = \int_v \underset{\sim}{B}_{om}^T (\underset{\sim}{C}\underset{\sim}{D}) \underset{\sim}{B}_{on} dV \qquad \text{A.29}$$

And if the expressions for the strain matrix $\underset{\sim}{B}_o$ are derived from expansions of the type in Equations A.1, A.4, and A.5, the general stiffness matrix of Equation A.29 is found to include the following two harmonic integrals

$$\int_0^L \sin(m\pi y/L)\sin(n\pi y/L)dy$$

$$\int_0^L \cos(m\pi y/L)\cos(n\pi y/L)dy \qquad \text{A.30}$$

which are zero for all $m \neq n$ due to the orthogonality of the harmonic functions. Therefore, only the diagonal stiffness matricies, with $m = n$, of Equation A.28 survive the integration.

An entirely similar situation arises for the initial stress matrix $\underset{\sim}{K}_\sigma$. The several termed discretization of Equation A.27 gives rise to a general stiffness matrix of the form of Equation A.28 which includes the two harmonic integrals of Equation A.30. Again only the matricies with $m = n$ survive the integration.

When the above results for $\underset{\sim}{K}_o$ and $\underset{\sim}{K}_\sigma$ are combined, the total system

$$(\underset{\sim}{K}_o + \lambda \underset{\sim}{K}_\sigma)\delta\underset{\sim}{\Delta} \qquad 3.15$$

uncouples, and the original assumption pertaining to a one harmonic discretization is justified (see Equation A.1 and related discussions). Physically, for each harmonic m, the solution of Equation 3.15 yields the corresponding buckling mode, e.g., with $m = 1$, the buckling mode has only

one longitudinal wave. The matricies given in Tables A.1 through A.3 are general and include the harmonic parameter m.

A.3 Global Formulation

The equations governing the instability of an entire structure are obtained by "summing" the stiffness contributions of the various finite strips. Symbolically this is written as

$$\underset{\sim}{K} = \sum_{s} \underset{\sim}{K}_{s} \qquad \text{A.31}$$

where the summation is over all strips s. One point worth noting is that, in the transformation from local to global coordinates implied by Equation A.31, the "extra degree of freedom" complication sometimes encountered in a finite element formulation (see Chapter 13 of Zienkiewicz [1977]) does not arise in a finite strip formulation. This is due to the unique representation of the u and w displacements in the longitudinal direction (see Equations A.4 and A.5).

Table A.1 LINEAR PLANE STRESS FINITE STRIP STIFFNESS MATRIX

$$\underset{\sim}{K}_o^p = ELt/2(1 - \mu^2) \begin{bmatrix} K1 & K2 & K4 & -K5 \\ & K3 & K5 & K6 \\ \text{symm.} & & K1 & -K2 \\ & & & K3 \end{bmatrix}$$

$$K1 = (1/b + (1 - \mu)b\alpha_m^2/6)$$

$$K2 = (3\mu - 1)\alpha_m/4$$

$$K3 = (b\alpha_m^2/3 + (1 - \mu)/2b)$$

$$K4 = (-1/b + (1 - \mu)b\alpha_m^2/12)$$

$$K5 = -(\mu + 1)\alpha_m/4$$

$$K6 = (b\alpha_m^2/6 + (\mu - 1)/2b)$$

$$\alpha_m = m\pi/L$$

Table A.2 SECOND-ORDER PLATE BENDING FINITE STRIP STIFFNESS MATRIX

$$\underset{\sim}{K}_o^b = ELt^3/12(1-\mu^2)\begin{bmatrix} K1 & K2 & K4 & -K5 \\ & K3 & K5 & K6 \\ \text{symm.} & & K1 & -K2 \\ & & & K3 \end{bmatrix}$$

$$K1 = (6/b^3 + 6\alpha_m^2/5b + 13\alpha_m^4/70)$$

$$K2 = (3/b^2 + (\mu/2 + 1/10)\alpha_m^2 + 11b^2\alpha_m^4/420)$$

$$K3 = (2/b + 2b\alpha_m^2/15 + b^3\alpha_m^4/210)$$

$$K4 = (-6/b^3 - 6\alpha_m^2/5b + 9b\alpha_m^4/140)$$

$$K5 = (-3/b^3 - \alpha_m^2/10 + 13b^2\alpha_m^4/840)$$

$$K6 = (1/b - b\alpha_m^2/30 - b^3\alpha_m^4/280)$$

$$\alpha_m = m\pi/L$$

Table A.3 CONSISTENT INITIAL STRESS FINITE STRIP STIFFNESS MATRIX FOR LONGITUDINAL MEMBRANE LOADING (SEE FIGURE A.1)

$$\underset{\sim}{K}_{\sigma} = C \begin{bmatrix} K1 & 0 & K2 & 0 & & & & \\ & K1 & 0 & K2 & & \multicolumn{3}{c}{\underset{\sim}{0}} & \\ & & K3 & 0 & & & & \\ & & & K3 & & & & \\ & & & & K4 & K5 & K7 & K10 \\ & \text{symmetric} & & & & K6 & K8 & K11 \\ & & & & & & K9 & K12 \\ & & & & & & & K13 \end{bmatrix}$$

$C = b(m\pi)^2/1680L$

$K1 = 70(3T_{y1} + T_{y2})$

$K2 = 70(T_{y1} + T_{y2})$

$K3 = 70(T_{y1} + 3T_{y2})$

$K4 = 8(30T_{y1} + 9T_{y2})$

$K5 = 2b(15T_{y1} + 7T_{y2})$

$K6 = b(5T_{y1} + 3T_{y2})$

$K7 = 54(T_{y1} + T_{y2})$

$K8 = 2b(6T_{y1} + 7T_{y2})$

$K9 = 24(3T_{y1} + 10T_{y2})$

$K10 = -2b(7T_{y1} + 6T_{y2})$

$K11 = -3b(T_{y1} + T_{y2})$

$K12 = -2b(7T_{y1} + 15T_{y2})$

$K13 = b^2(3T_{y1} + 5T_{y2})$

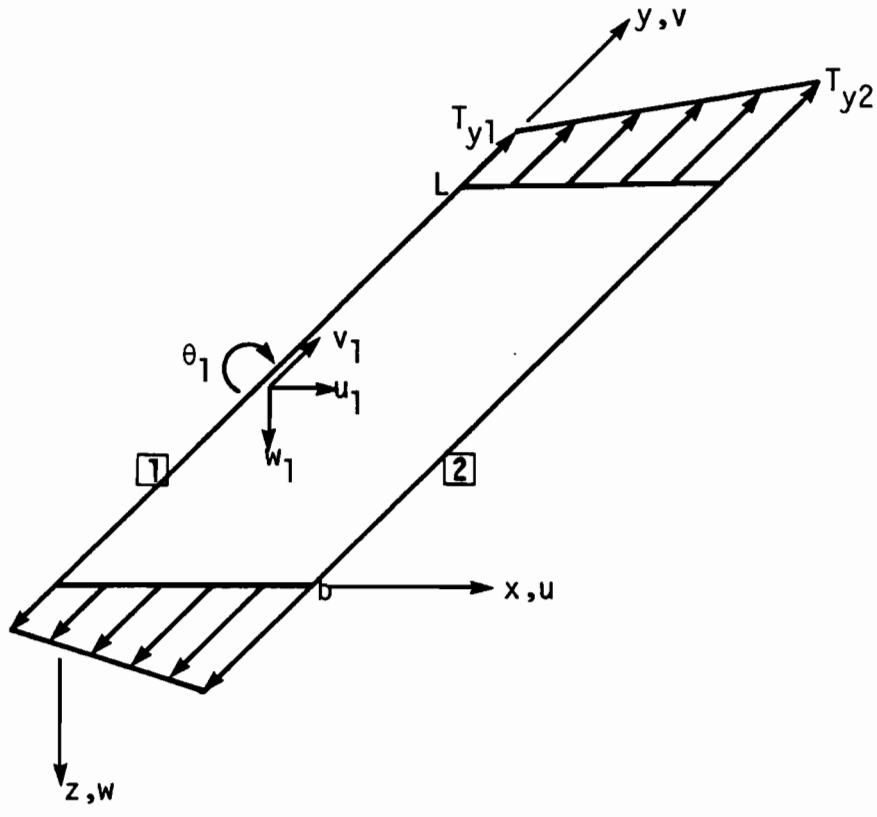

Figure A.1 MEMBRANE AND BENDING FINITE STRIP SUBJECTED TO A LINEARLY VARYING LONGITUDINAL EDGE LOAD

APPENDIX B

NUMERICAL SOLUTION OF THE INSTABILITY PROBLEM

B.1 Introduction

In the preceding appendix all the ingredients necessary for the formulation of the equations governing the instability problem were defined, but the method of solution was not established. The present appendix addresses this aspect, and the specific solution method and corresponding computer program are discussed.

B.2 The Eigenproblem and Its Solution

The basic problem is to obtain an eigensolution of the global instability equations given in Equation 3.15 which is rewritten in the following form

$$\underset{\sim}{K}\underset{\sim}{v} = \lambda \underset{\sim}{K}_{\sigma}\underset{\sim}{v} \qquad \text{B.1}$$

where $\underset{\sim}{K}$ is the small displacement stiffness matrix, $\underset{\sim}{K}_{\sigma}$ the initial stress stiffness matrix, and λ and $\underset{\sim}{v}$ are the eigenvalue and corresponding eigenvector. Since only the smallest buckling load is of interest in an instability analysis, the solution method outlined here is concerned with obtaining the smallest positive eigenvalue of Equation B.1. Alternately, the following inverse system may be formed

$$\underset{\sim}{K}_{\sigma}\underset{\sim}{v} = \mu \underset{\sim}{K}\underset{\sim}{v} \qquad \text{B.2}$$

where the eigenvalue $\mu = 1/\lambda$. In this case, the largest positive eigenvalue is required.

The choice of which of the above systems to solve depends on the specific solution method being utilized. For example, some methods require the matricies $\underset{\sim}{K}$ and $\underset{\sim}{K}_\sigma$ to possess certain properties. Therefore, the properties of these matricies need to be established before selecting the solution method.

The matricies of the systems B.1 or B.2 are both symmetric and banded. Further, $\underset{\sim}{K}$ is positive definite and $\underset{\sim}{K}_\sigma$ is, in general, indefinite. In the two systems, only real eigenvalues are defined, but these may be negative as well as positive. Negative eigenvalues occur when the structure can buckle with the primary loading reversed (Jennings [1977]). Thus, the possibility of negative eigenvalues must be recognized in the development of a solution process. Finally, the order of the instability equations defining a specific problem will generally be small. This is due to the use of the FSM.

Based on the small system size, it might at first be thought that one of the more standard methods, such as forward iteration applied to Equation B.2, is applicable for the eigensolution. However, convergence of the power method (forward iteration) depends on the selection of the initial starting vector and the properties of the eigensystem. For example, if the system B.2 has two dominant eigenvalues which are equal in magnitude but of opposite sign, the method converges to two alternating eigenvectors (Jennings [1977]). This case was actually encountered in the present study when, in the early stages of program development, the power method of eigensolution was under investigation. It is noted that for this case the eigenvalue converged to an incorrect result. Therefore, a more reliable solution method was sought adopting the philosophy that such an algorithm was worth some trade off in solution cost.

In the present study the determinant search method (Bathe and Wilson [1976], Bathe [1971]) was employed for the eigensolution. This method, which proved very successful, combines several of the more standard techniques of eigensolution in an effective and efficient way. First, an implicit polynomial iteration scheme is used to obtain an approximation to the desired eigenvalue. In using this scheme, it is recognized that convergence may be slow and that the cost of solution may be high because a factorization is performed at each iteration. Thus, at this stage, the desired eigenvalue is obtained to some relatively high tolerance. Next, the system is shifted at the approximate eigenvalue obtained from polynomial iteration, and inverse iteration is used to obtain the eigenvalue to the final desired accuracy. The purpose of the above shifting is to accelerate the convergence characteristics of inverse iteration. The two basic methods, i.e., polynomial and inverse iteration, that make up the determinant search technique are described in the next section, along with another useful eigenproperty.

B.2.1 Inverse Iteration, Polynomial Iteration, and the Sturm Sequence Property

Inverse iteration (Bathe and Wilson [1976]) is used to obtain the smallest eigenvalue λ_1 and associated eigenvector $\underset{\sim}{v}_1$ of the system

$$\underset{\sim}{K}\underset{\sim}{v} = \lambda \underset{\sim}{K}_\sigma \underset{\sim}{v} \qquad \text{B.1}$$

where $\underset{\sim}{K}$ is assumed positive definite. The first step of the solution process is to obtain a factorization of $\underset{\sim}{K}$. In this study, a LDL^T factorization is adopted, e.g.,

$$\underset{\sim}{K} = \underset{\sim}{L}\underset{\sim}{D}\underset{\sim}{L}^T \qquad \text{B.3}$$

where $\underset{\sim}{L}$ is a lower triangular matrix having unit diagonals and $\underset{\sim}{D}$ is a diagonal matrix. Next, an initial iteration vector $\underset{\sim}{x}_1$ is assumed, usually equal to a unit vector, and assuming $y_1 = \underset{\sim}{K}_\sigma \underset{\sim}{x}_1$ the iteration proceeds as follows for k = 1,2, . . .

$$\underset{\sim}{K}\bar{\underset{\sim}{x}}_{k+1} = \underset{\sim}{y}_k \qquad \text{B.4a}$$

$$\bar{\underset{\sim}{y}}_{k+1} = \underset{\sim}{K}_\sigma \bar{\underset{\sim}{x}}_{k+1} \qquad \text{B.4b}$$

$$\rho(\bar{x}_{k+1}) = \frac{\bar{\underset{\sim}{x}}^T_{k+1}\, \underset{\sim}{y}_k}{\bar{\underset{\sim}{x}}^T_{k+1}\, \bar{\underset{\sim}{y}}_{k+1}} \qquad \text{B.4c}$$

$$\underset{\sim}{y}_{k+1} = \frac{\bar{\underset{\sim}{y}}_{k+1}}{(\bar{\underset{\sim}{x}}^T_{k+1}\, \bar{\underset{\sim}{y}}_{k+1})^{\frac{1}{2}}} \qquad \text{B.4d}$$

where $\rho(\bar{\underset{\sim}{x}}_{k+1})$ is the Rayleigh quotient. In the above algorithm a Euclidean normalization is adopted. The iteration step given by Equation B.4a is solved for $\bar{\underset{\sim}{x}}_{k+1}$ using the factorization of Equation B.3 and the well-known processes of forward elimination and back-substitution. As $k \to \infty$, the Rayleigh quotient and iteration vector $\underset{\sim}{x}_{k+1}$, which is defined below, converge to λ_1 and $\underset{\sim}{v}_1$, respectively.

$$\underset{\sim}{x}_{k+1} = \frac{\bar{\underset{\sim}{x}}_{k+1}}{(\bar{\underset{\sim}{x}}_{k+1}\, \bar{\underset{\sim}{y}}_{k+1})^{\frac{1}{2}}} \qquad \text{B.5}$$

In practice the iteration is terminated once some error criterion is satisfied, e.g.,

$$ER \leq TOL \qquad \text{B.6}$$

where ER is the error estimate and TOL the specified tolerance. If a relative error estimate is chosen, then ER is given by

$$ER = \left| \frac{\lambda_1^{k+1} - \lambda_1^k}{\lambda_1^{k+1}} \right| \qquad \text{B.7}$$

where the current and previous approximations of the λ_1 are given by λ_1^{k+1} and λ_1^k, respectively. For 2s-digit accuracy in the eigenvalue, the tolerance TOL is taken as 10^{-2s}. The corresponding eigenvector is then accurate to about s-digits.

In polynomial iteration (Bathe et al. [1976]), it is chosen to solve for the roots of the characteristic polynomial $p(\lambda)$ of Equation B.1, i.e.,

$$p(\lambda) = \det(\underset{\sim}{K} - \lambda \underset{\sim}{K}_\sigma) = 0 \qquad \text{B.8}$$

Given that an approximation to λ_1 has been obtained and that the factorization of $(\underset{\sim}{K} - \lambda \underset{\sim}{K}_\sigma)$ exists as

$$(\underset{\sim}{K} - \lambda \underset{\sim}{K}_\sigma) = \underset{\sim}{L}\underset{\sim}{D}\underset{\sim}{L}^T \qquad \text{B.9}$$

the value of $p(\lambda)$ is effectively calculated by

$$p(\lambda) = \prod_i d_{ii} \qquad \text{B.10}$$

where d_{ii} are elements of $\underset{\sim}{D}$.

Now, assuming that at the k^{th} stage of iteration there are two approximations α_{k-1} and α_k to λ_1, such that $\alpha_{k-1} < \alpha_k$, the next approximation is calculated using

$$\alpha_{k+1} = \alpha_k - \eta \frac{p(\alpha_k)}{p(\alpha_k) - p(\alpha_{k-1})} (\alpha_k - \alpha_{k-1}) \qquad \text{B.11}$$

If the variable $\eta = 1$, the above equation reduces to normal secant iteration, in which $\alpha_{k+1} \leq \lambda_1$, and as $k \to \infty$, $\alpha_{k+1} \to \lambda_1$. However, convergence may be slow for this case. To accelerate convergence the variable η is taken greater than one, and the method is now identified as accelerated secant iteration. Caution is advised when using $\eta > 1$ since the method may now jump over one or more roots. However, for $\eta = 2$, the iteration scheme can jump over only one root (Bathe [1976]). Satisfactory convergence is obtained when the second term on the right-hand-side of Equation B.11 is less than one-half the final tolerance.

One final attribute of an eigensystem is the Sturm sequence property. First, it is assumed that at some shift equal to α the LDL^T factorization of $(\underset{\sim}{K} - \alpha\underset{\sim}{K}_\sigma)$ can be accomplished. The Sturm property then states that " . . . the number of negative elements $\underset{\sim}{D}$ is equal to the number of eigenvalues smaller than α." (Bathe [1976], page 375) This very important property is used extensively in the determinant search algorithm described in the next section.

B.2.2 Determinant Search Algorithm

The in-core determinant search algorithm developed for this study is discussed here. Since the algorithm is based on work by Bathe [1971,1976], his work is appropriately acknowledged.

The algorithm consists of three phases. In the first phase, inverse iteration and the Sturm sequence property are used to obtain a lower bound for λ_1 of the system B.1. The next phase involves employing Secant iteration and the Sturm sequence property to obtain a closer lower bound of λ_1. Assuming the current estimate of λ_1 to be given by $\overline{\lambda}$, the inverse system B.2 is now shifted at $1/\overline{\lambda}$ such that all its eigenvalues are negative. In the last phase, inverse iteration is applied to the shifted system from which the final eigenvalue and eigenvector are ultimately obtained.

A flow chart of the complete algorithm is shown in Figure B.1 where the notation used requires explanation. The variables IT and NITE refer to the number of iterations and maximum number of iterations, respectively. The variable $\overline{\lambda}$ refers to the current estimate of λ_1, and η is the constant of Equation B.11. Finally, a Sturm sequency check is indicated

by the variable NSC which is equal to the number of negative diagonal elements of $\underset{\sim}{D}$ at the current shift.

As mentioned earlier, the first phase of the algorithm uses inverse iteration to find a lower bound on the smallest positive eigenvalue λ_1 of the system B.1. Once the error criterion is satisfied (see Equations B.6 and B.7), a conservative estimate of λ_1 is taken as (1 - .01) times the value obtained from inverse iteration. However, since the tolerance used to terminate the iteration is relatively high, the algorithm may have accepted convergence to some other eigenvalue λ_i where $\lambda_i > \lambda_1$. Therefore, the Sturm sequence property is used to ensure that the algorithm returns a conservative estimate of λ_1. If there exists NSC (>0) negative diagonal elements in the factorization at the current shift $\bar{\lambda}$, the next estimate for $\bar{\lambda}$ is taken as the previous value divided by (NSC + 1). This process is repeated until NSC = 0. It is noted that the algorithm recognizes possible failure of inverse iteration in which case the Sturm loop is utilized to recover $\bar{\lambda} < \lambda_1$.

At this stage there exists only one starting value for polynomial iteration, and two are needed. Therefore, $\bar{\lambda}/2$ is selected for the other starting value. Initially accelerated secant iteration, Equation B.11 with $n = 2$, is used to accelerate convergence. However, since the objective of this phase is to obtain a lower bound, the algorithm switches to normal secant iteration once it is detected that the iteration has jumped over λ_1. Secant iteration is terminated when the error criterion is satisfied (see Section B.2.1) or when it proves uneconomical to obtain a shift in the vicinity of λ_1, i.e., IT $\geq$ NITE. The final phase of the

algorithm is entered with the latest estimate of λ_1 equal to $\bar{\lambda}$. A shift of $1/\bar{\lambda}$ is now imposed on the system B.2 as

$$(\underset{\sim}{K}_\sigma - 1/\bar{\lambda}\ \underset{\sim}{K})\underset{\sim}{v} = \omega \underset{\sim}{\underset{\sim}{K}}\underset{\sim}{v} \qquad \text{B.12}$$

where ω is the eigenvalue of the shifted system. Inverse iteration is used to obtain the smallest negative eigenvalue ω_1 of this system to about 8-digit accuracy. The largest eigenvalue, μ_n, of the original system B.2 is then calculated from

$$\mu_n = 1/\bar{\lambda} + \omega_1 \qquad \text{B.13}$$

Finally, the smallest eigenvalue of the system is determined by

$$\lambda_1 = 1/\mu_n \qquad \text{B.14}$$

B.3 The Equation Solver

The equation solver that is used in conjunction with the determinant search algorithm of the previous section must possess special features for the total algorithm to run successfully. These features and the equation solver developed in this study are discussed here.

Probably the most important requirement placed on the equation solver is that it must be efficient. Therefore, an in-core skyline solver is implemented. The skyline solver proves efficient because no reduction operations are performed on zero elements outside the skyline of a matrix. In addition, storage requirements are reduced since it is necessary to store only the elements within the skyline. More information on the skyline method of solution is given by Bathe [1976].

The special features of the equation solver are now discussed. One obvious feature is that the solver must be able to factorize indefinite

systems, i.e., negative elements of $\underset{\sim}{D}$ in the LDL^T factorization must be allowed. Such systems arise primarily in the polynomial iteration phase of th eigenvalue routine. Also in this phase, it is assumed that a LDL^T factorization exists, and since the factorization is performed by Gaussian elimination without pivoting; the factorization cannot be guaranteed. The reason for this is that multiplier growth (Bathe [1976]) can occur. However, this is easily detected, and in the present solver a flag is returned to indicate its occurrence. Once multiplier growth is encountered, the current shift is changed slightly, and the factorization is reattempted. The ability to proceed in this manner follows from the fact that the specific shift obtained from polynomial iteration does not affect the final accuracy of the eigenvalues (Bathe [1976]).

Two final points deserve mentioning. One is that the Sturm sequence count is incorporated in the LDL^T factorization portion of the solver which eliminates the need for an extra loop on $\underset{\sim}{D}$. Secondly, the calculation of the determinant is also included in the solver. In this calculation, scaling factors are incorporated because the magnitude of the determinant can easily overflow the largest number allowed on the computer.

B.4 Variable Length and Minimum Buckling Load Analysis

The local buckling behavior of simple plates is well-known (Timoshenko and Gere [1961]). Typically this behavior is represented in the form of plate buckling curves such as that shown in Figure C.1, where the buckling coefficient K (stress) is plotted against the plate aspect ratio α. In this figure it is seen that the buckling coefficient acquires a

minimum value at some specific aspect ratio. This behavior is similar for other thin plates and thin-walled structures. Therefore, it is advantageous to have an automatic way of generating curves such as that described above, i.e., through a "variable length analysis," and, if necessary, to have an automatic way of obtaining the minimum buckling stress, i.e., through a "minimum buckling load analysis." In this section the procedures developed for these analyses are discussed.

In a variable length analysis it is assumed that some initial length, final length, and length increment are given. Thus an effective scheme would consist merely of a simple loop on the length over the range of interest. However, the necessity of reformulating the global stiffness matricies governing the problem, Equation B.1, for each length may be eliminated by recognizing the dependence of $\underset{\sim}{K}$ and $\underset{\sim}{K}_\sigma$ on the length. For example, the small displacement matrix $\underset{\sim}{K}$ is assembled as a sum of the following matricies

$$\underset{\sim}{K} = \underset{\sim}{K}_1(c) + \underset{\sim}{K}_2(L) + \underset{\sim}{K}_3(1/L) + \underset{\sim}{K}_4(1/L^3) \qquad \text{B.15}$$

where ( ) indicates dependence and c is a constant. A similar breakdown of the initial stress matrix is not necessary since $\underset{\sim}{K}_\sigma = \underset{\sim}{K}_\sigma(1/L)$. In the computer implementation of Equation B.15, each of the matricies $\underset{\sim}{K}_i$ are stored separately. Thus, for a given length the matricies $\underset{\sim}{K}$ and $\underset{\sim}{K}_\sigma$ are obtained simply by multiplying each of the $\underset{\sim}{K}_i$ and $\underset{\sim}{K}_\sigma$ by a length factor and using Equation B.15.

The minimum buckling load analysis assumes the existence of a smooth curve, $\lambda_1(L)$, which relates the smallest eigenvalue, λ_1, of the system of Equation B.1 to the length, L. Further three known starting values $({}_i\lambda_1, L_i)$; i = 1,2,3; are assumed to exist which bracket the required

minimum eigenvalue, λ_{1min}, such that ${}_1\lambda_1 > {}_2\lambda_1 < {}_3\lambda_1$. Since the length associated with λ_{1min} is generally unknown, it is necessary to use the variable length analysis, say with a rather large length increment, to bracket its location. Once this location is bracketed, quadratic interpolation is employed to estimate the length $\bar{L}$ that is associated with λ_{1min}. Then the actual eigenvalue $\bar{\lambda}$ associated with the length $\bar{L}$ is determined by updating the stiffness matricies, e.g., through Equation B.15, and resolving Equation B.1. At stage this stage there are four sets $({}_i\lambda_1, L_i)$ of points describing the $\lambda_1(L)$ curve. One of these sets is eliminated by a complicated procedure, which is not described here, leaving three sets with ${}_1\lambda_1 > {}_2\lambda_1 < {}_3\lambda_1$. The above process is repeated until the difference between the current minimum, $\bar{\lambda}$, and the previous minimum, ${}_2\lambda_1$, is less than some specified tolerance. Also in the actual computer implementation of the above algorithm, it was found necessary to monitor the differences $|{}_i\lambda_1 - {}_{i+1}\lambda_1|$ for i = 1,2 to preserve numerical stability.

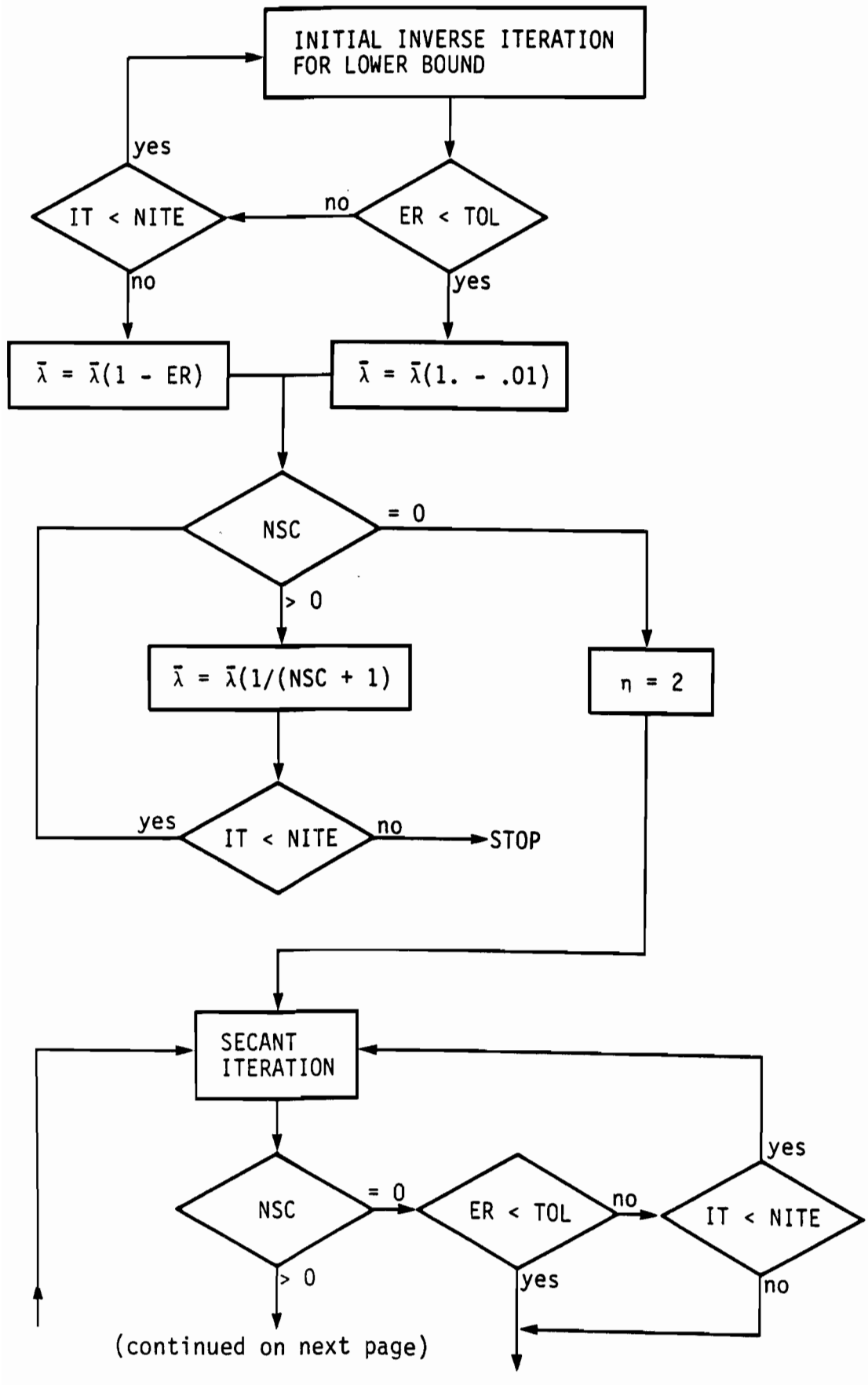

FIGURE B.1. DETERMINANT SEARCH ALGORITHM

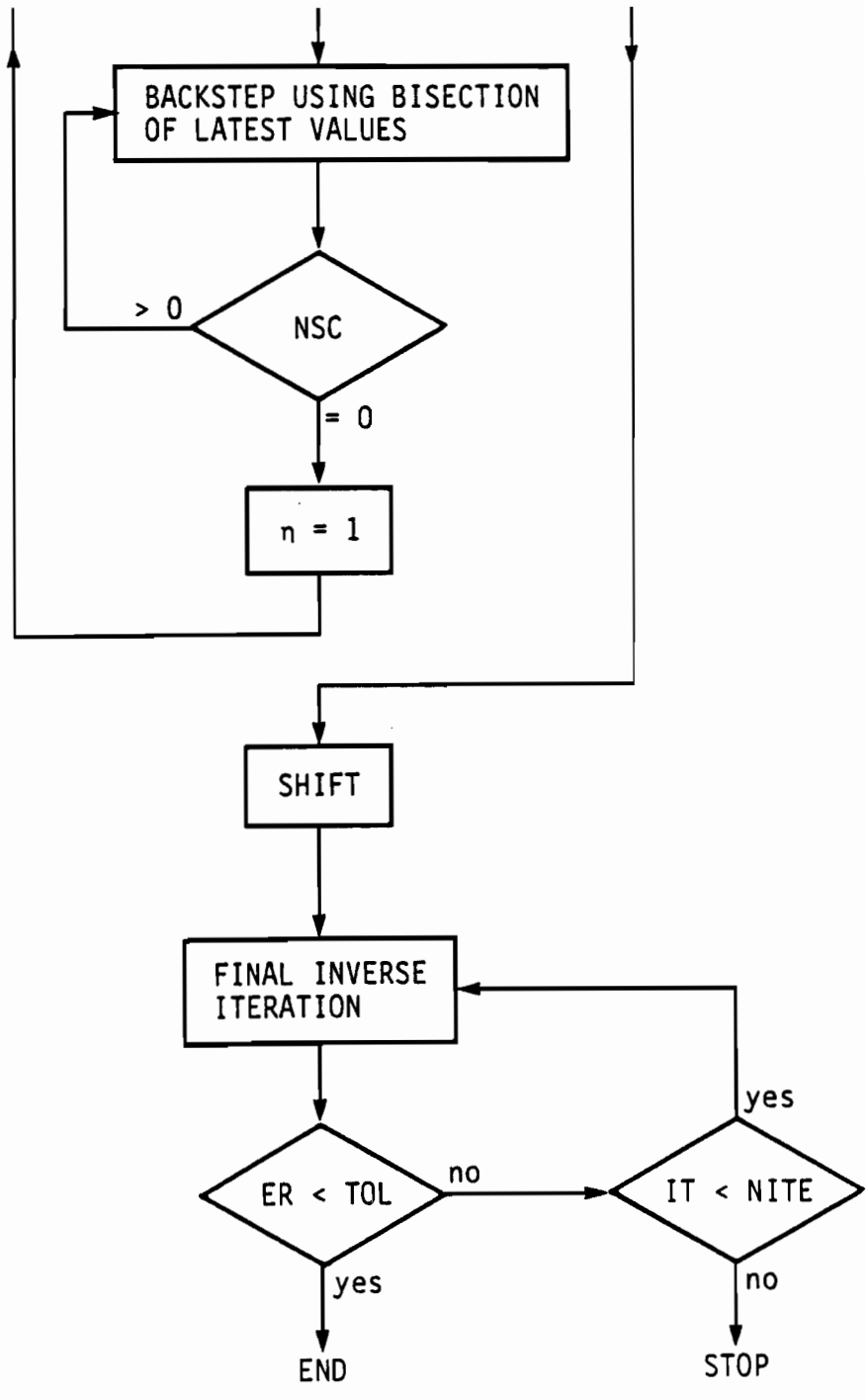

FIGURE B.1. continued

APPENDIX C

VERIFICATION OF FINITE STRIP INSTABILITY ANALYSIS PROGRAM

C.1 Introduction

The finite strip, instability analysis, computer program and underlying theory are verified in the present appendix by analyzing several simple plates for local and overall instability. Accordingly, the results obtained from these analyses are compared against known solutions. Also, a comparison is made with results obtained using the finite element method.

C.2 Local Buckling

Local buckling of single plates with various support and loading conditions are treated first. The analyses are performed at the wavelength which corresponds to the known minimum buckling solution. Because the response is limited to local buckling, all in-plane degrees of freedom are restrained.

The results offered in the following examples are given in terms of the buckling coefficient K which is related to the buckling stress f_{cr} by the well-known expression

$$f_{cr} = K\pi^2 E/(12(1 - \mu^2)(w/t)^2) \qquad C.1$$

where w is the total width of the plate. Further, a Poisson ratio μ of 0.3 is assumed in all analyses discussed here.

First, the classic example of the buckling of a simply supported plate under uniform axial compression is considered. For this case it is known that the minimum buckling coefficient occurs for a square plate.

This information and symmetry are employed in the analysis. The results obtained using several finite strip idealizations are listed in Table C.1. All results are excellent.

The above case was also investigated by Kapur and Hartz [1966] using the finite element method. Their results are presented in Table C.2 where it is seen that the buckling coefficient approaches the exact value from below. This is due to the use of a non-conforming plate bending element in the analysis. A comparison of the FSM and the FEM may be made by examining Tables C.1 and C.2. Because Kapur did not take advantage of symmetry, the number of equations NEQ listed in Table C.1 should be multiplied by two when making this comparison. The economy and accuracy of the finite strip method are clearly demonstrated.

Another example considered here is the buckling of a simply supported plate subjected to in-plane bending. This is an important practical problem in the design of webs for wide flange sections. In addition, this problem has unique eigenvalue characteristics, e.g., the smallest two eigenvalues (buckling loads) are equal in absolute value but of opposite sign. Although there is no exact solution for this problem, Timoshenko [1961] has obtained an approximate solution using an energy method. The results generated by the FSM are listed in Table C.3. Again, the results are excellent.

Finally, a uniformly compressed simply supported plate with "variable" length is analyzed to test the variable length and minimum buckling load solution algorithms (see Section B.4). Four strips and symmetry are used for the calculations. The results are shown in the plate buckling curve of Figure C.1, where the buckling coefficient K is plotted as a function of plate aspect ratio α. At the minimum point of the curve, the

buckling coefficient differs from the exact value by 0.001%, and the associated length differs from its exact value by about 0.03%.

C.3 Overall Buckling

In this section, the overall buckling of a single plate is investigated. The term overall buckling is defined here to include flexural, torsional, lateral, or combination buckling modes.

First, strong axis (z-axis, see Figure A.1) flexural buckling of a uniformly compressed plate is studied. Hence, all out-of-plane degrees of freedom were restrained. The exact results for this case are derived from the usual Euler column buckling formula written here in terms of a critical line load $(T_y)_{cr}$

$$(T_y)_{cr} = \pi^2 EI/wL^2 \qquad C.2$$

where I is the moment of inertia and w the total plate width. Next, the strong axis $I = tw^3/12$ is substituted into the above formula which yields

$$(T_y)_{cr} = \pi^2 Etw^2/12L^2 \qquad C.3$$

The results obtained using the FSM are listed in Table C.4. The differences from the exact values, Equation C.3, are attributed to the lateral expansion of the plate (a Poisson effect) which is not accounted for in the one-dimensional theory of column buckling. However, these differences tend to disappear as more strips are employed in the analysis.

Flexural buckling about the weak axis (x-axis, see Figure A.1) is now examined. The exact solution is obtained by substituting $I = wt^3/12$ into the Euler Equation C.2, e.g.,

$$(T_y)_{cr} = \pi^2 Et^3/12L^2 \qquad C.4$$

For this case all degrees of freedom are freed and one finite strip proves satisfactory. The finite strip results differ from the exact value, Equation C.4, by 0.001%.

Representation of the other buckling modes, such as torsional, is not possible using a single plate. The reason for this is that, in the formulation, there is no coupling between bending and membrane behavior for flat structures. However, for a thin-walled structure that is made up of a series of plates, interconnecting at angles, these other overall modes are possible since the coupling is now represented.

Table C.1 BUCKLING COEFFICIENTS K FOR A SIMPLY SUPPORTED PLATE UNDER UNIFORM AXIAL COMPRESSION

No. of strips	NEQ*	K	% Error
1	2	4.0086	0.216
2	4	4.0005	0.013
4	8	4.0000	0.001
exact results (Timoshenko [1961])		4.0	

*NEQ = no. of equations

Table C.2 BUCKLING COEFFICIENTS K FOR THE STRUCTURE OF TABLE C.1 USING THE FINITE ELEMENT METHOD (AFTER KAPUR AND HARTZ [1966])

No. of elements	NEQ	K	% Error
9	20	3.645	-8.88
16	39	3.77	-5.75
36	95	3.887	-2.80
64	175	3.933	-1.68
100	279	3.96	-1.00
144	407	3.977	-0.58

Table C.3 BUCKLING COEFFICIENTS K FOR A SIMPLY SUPPORTED PLATE SUBJECTED TO PURE IN-PLANE BENDING

No. of strips	NEQ	K	% Error
2	4	25.455	6.506
4	8	23.965	0.273
6	12	23.897	-0.013
known solution (Timoshenko [1961])		23.9	

Table C.4 STRONG AXIS FLEXURAL BUCKLING OF A SINGLE PLATE*

No. of strips	NEQ	$(T_y)_{cr}$	% Error
1	4	2.7106	9.855
2	6	2.5276	2.442
3	8	2.4937	1.067
4	10	2.4819	0.586
6	14	2.4734	0.242

*L = 1000.0, b = 10.0, t = 1.0, E = 30000.0, μ = 0.3
Exact results = Equation C.3

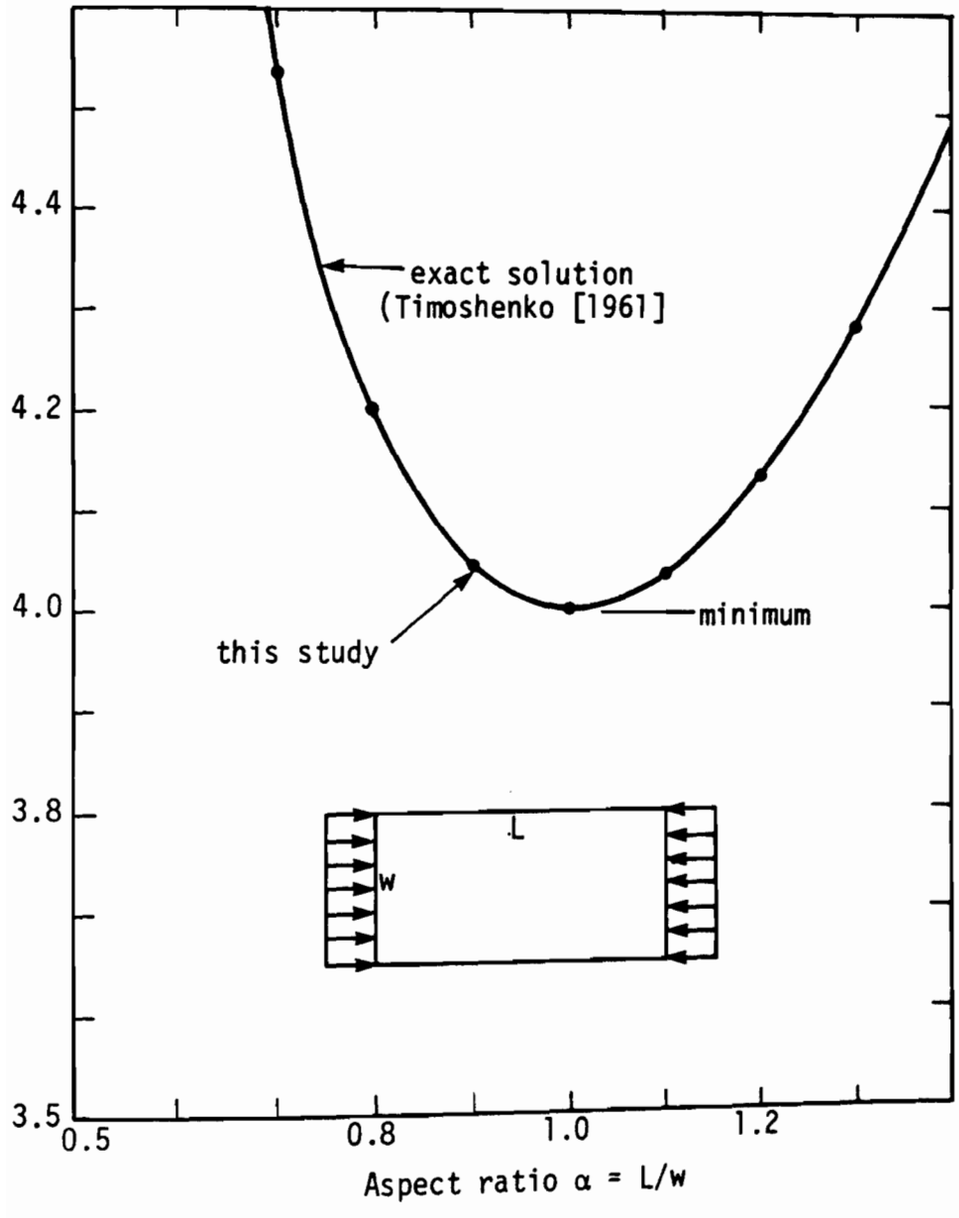

Figure C.1 PLATE BUCKLING CURVE FOR A SIMPLY SUPPORTED PLATE IN UNIFORM COMPRESSION

APPENDIX D

SUB-ULTIMATE RESPONSE FOR STUB COLUMNS

Note: This appendix contains graphs of the axial load-deformation response for channel and lipped channel stub columns which are not presented in Chapter 6. Reference is made to Section 6.2 for relevant discussions. Also, the following notation is employed:

(a) refers to the effective section method with Equation 2.48 and

(b) refers to the effective section method with Equation 2.9.

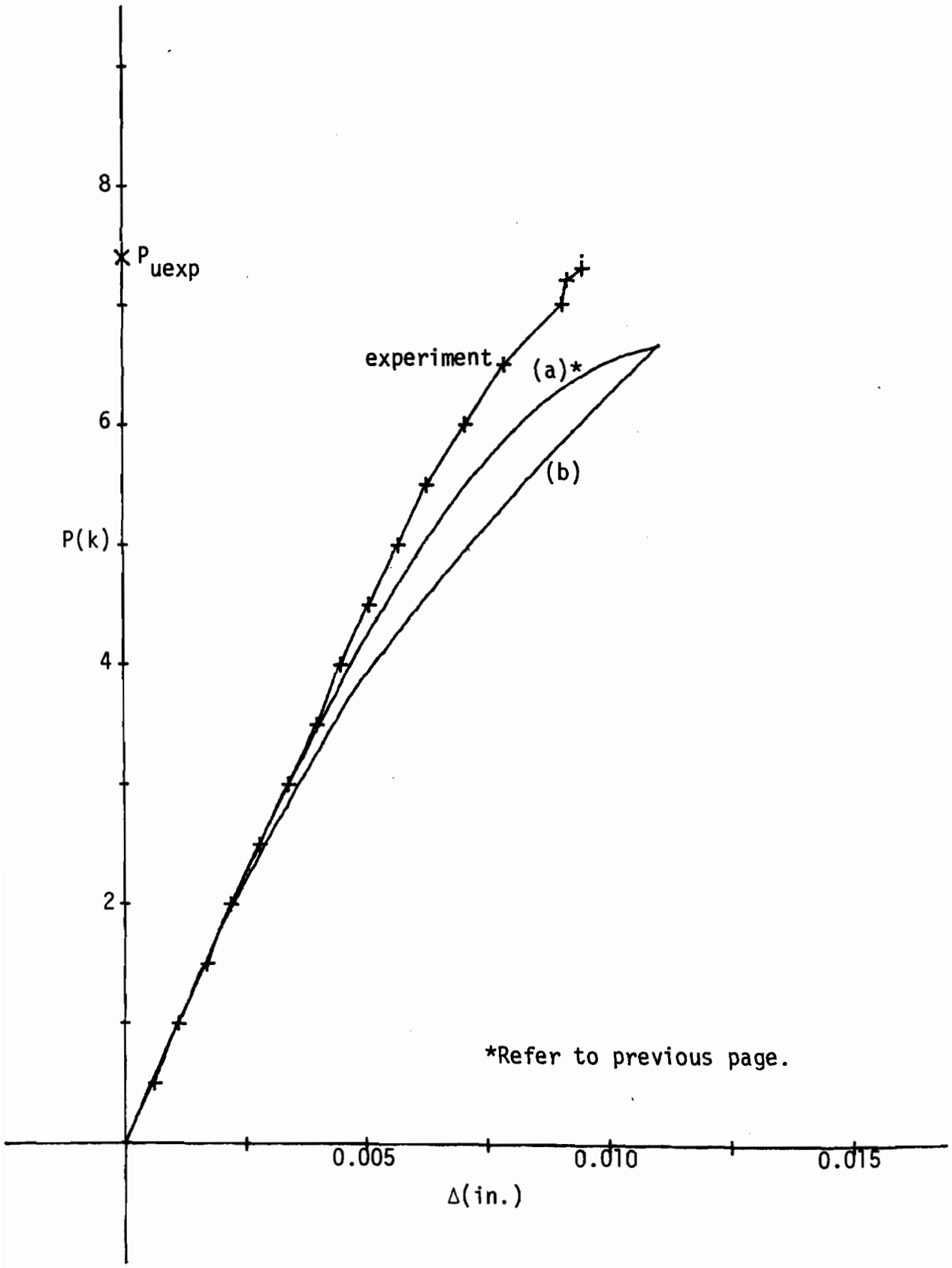

Figure D.1 SC/1 60X30

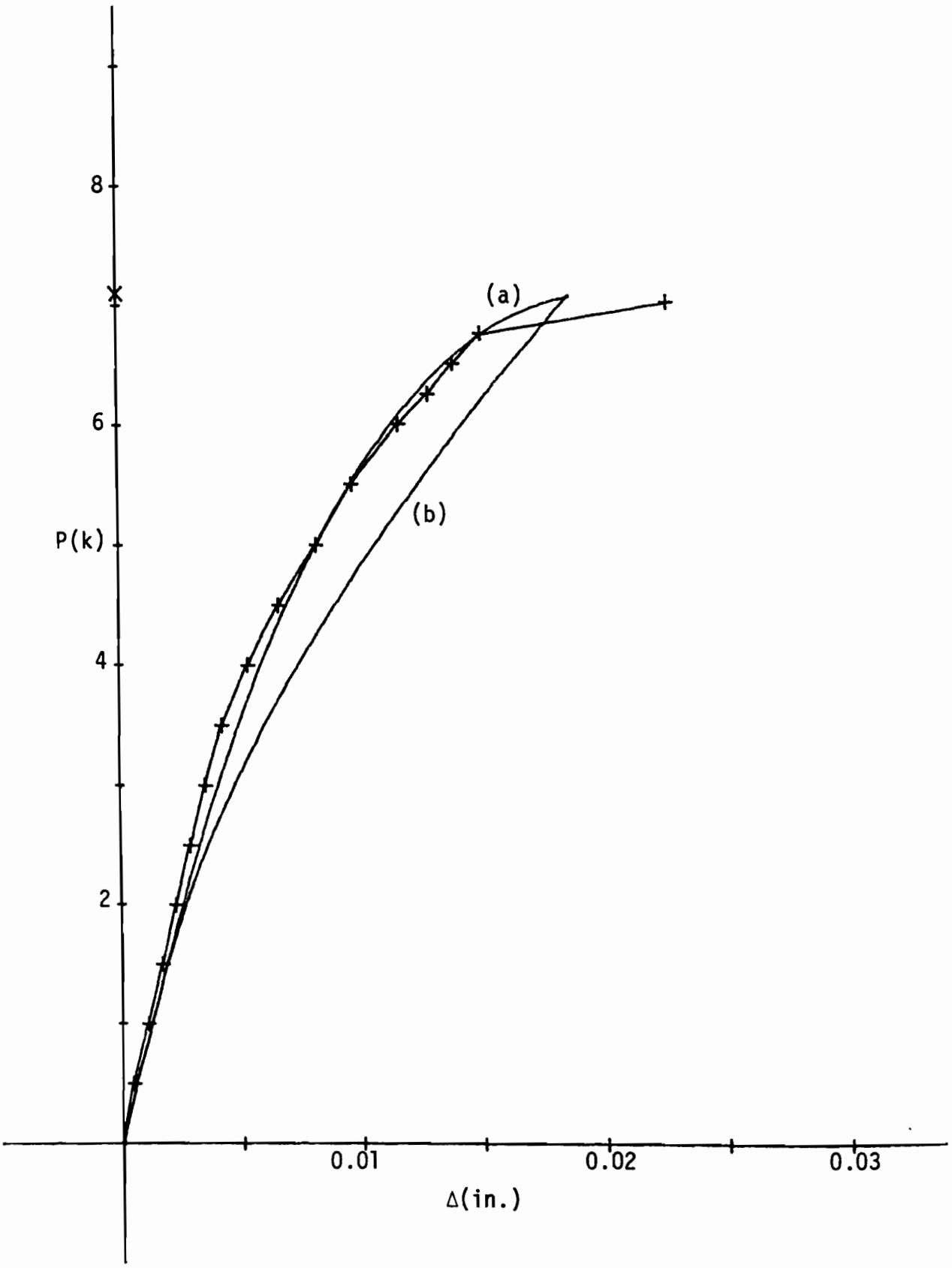

Figure D.3 SC/2 120X30

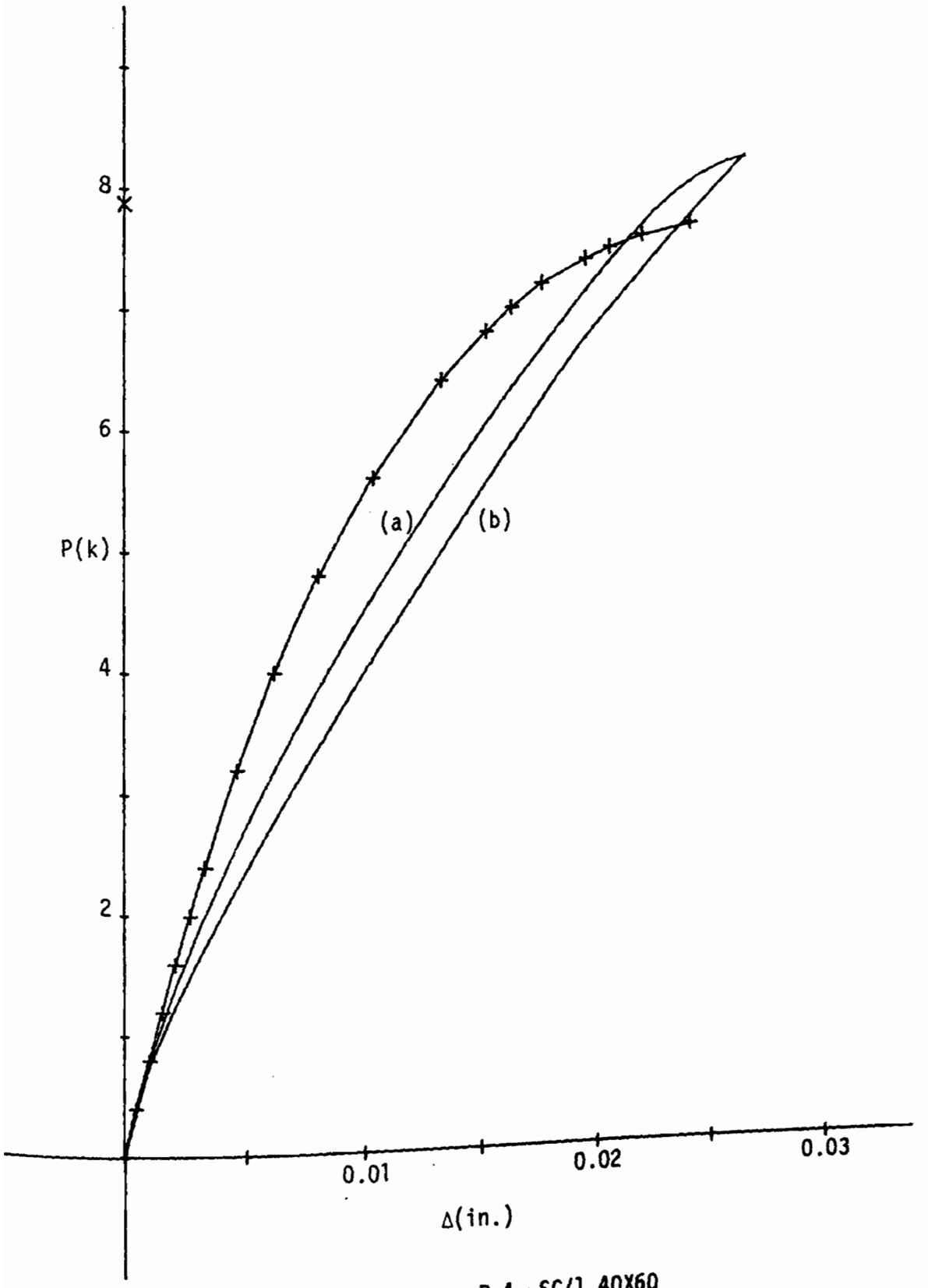

Figure D.4 SC/1 40X60

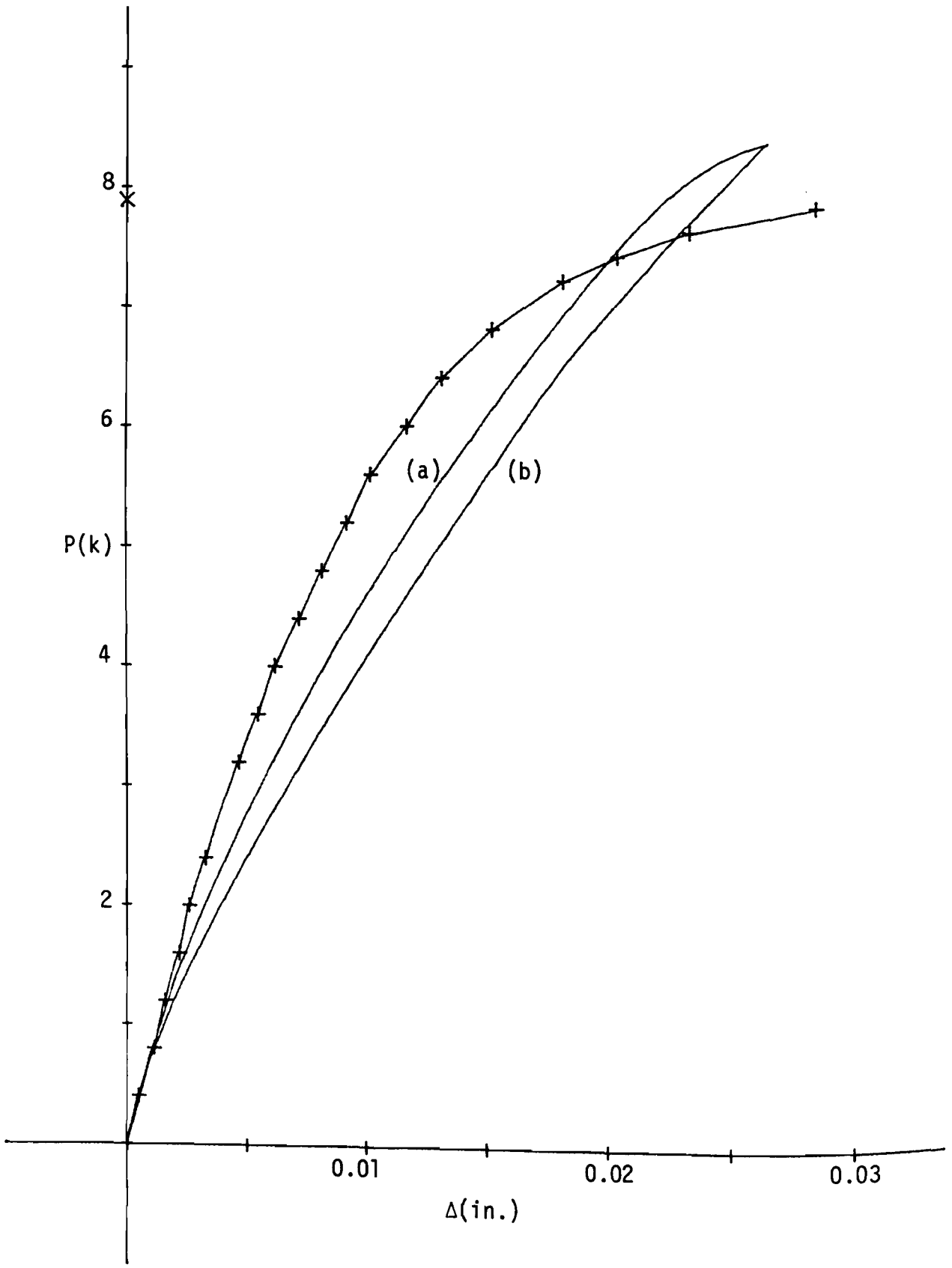

Figure D.5 SC/2 40X60

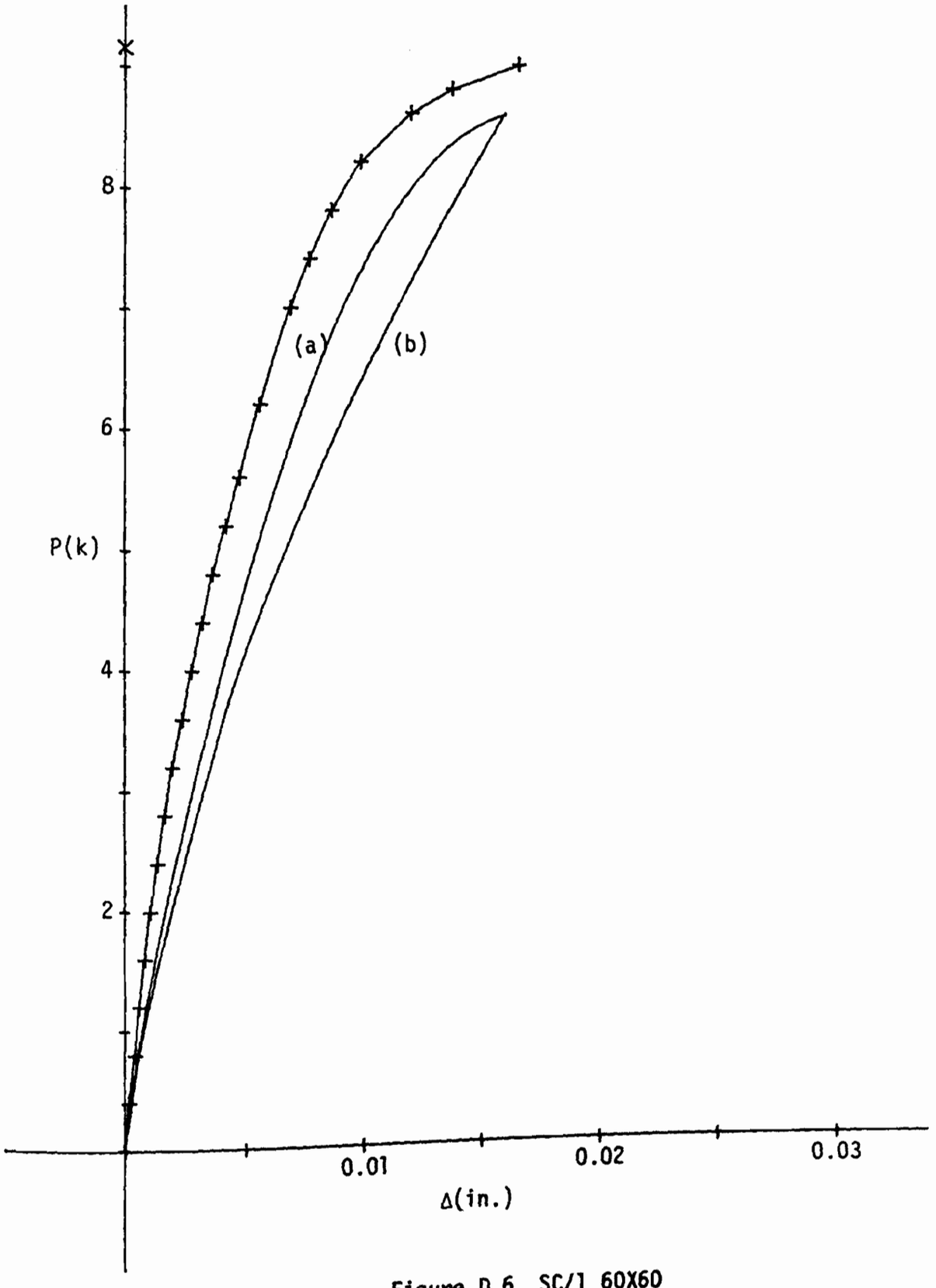

Figure D.6 SC/1 60X60

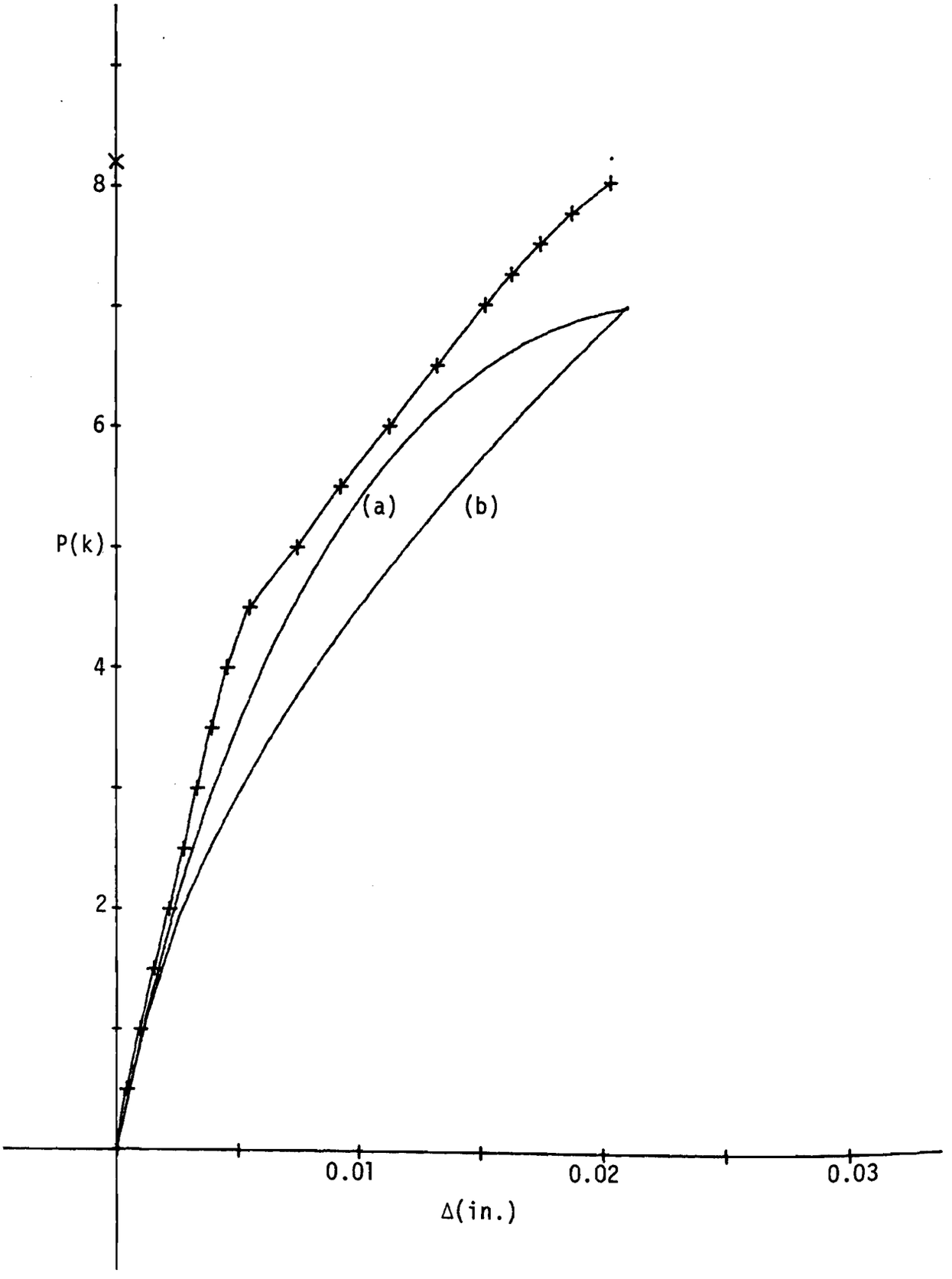

Figure D.7 SC/1 120X60

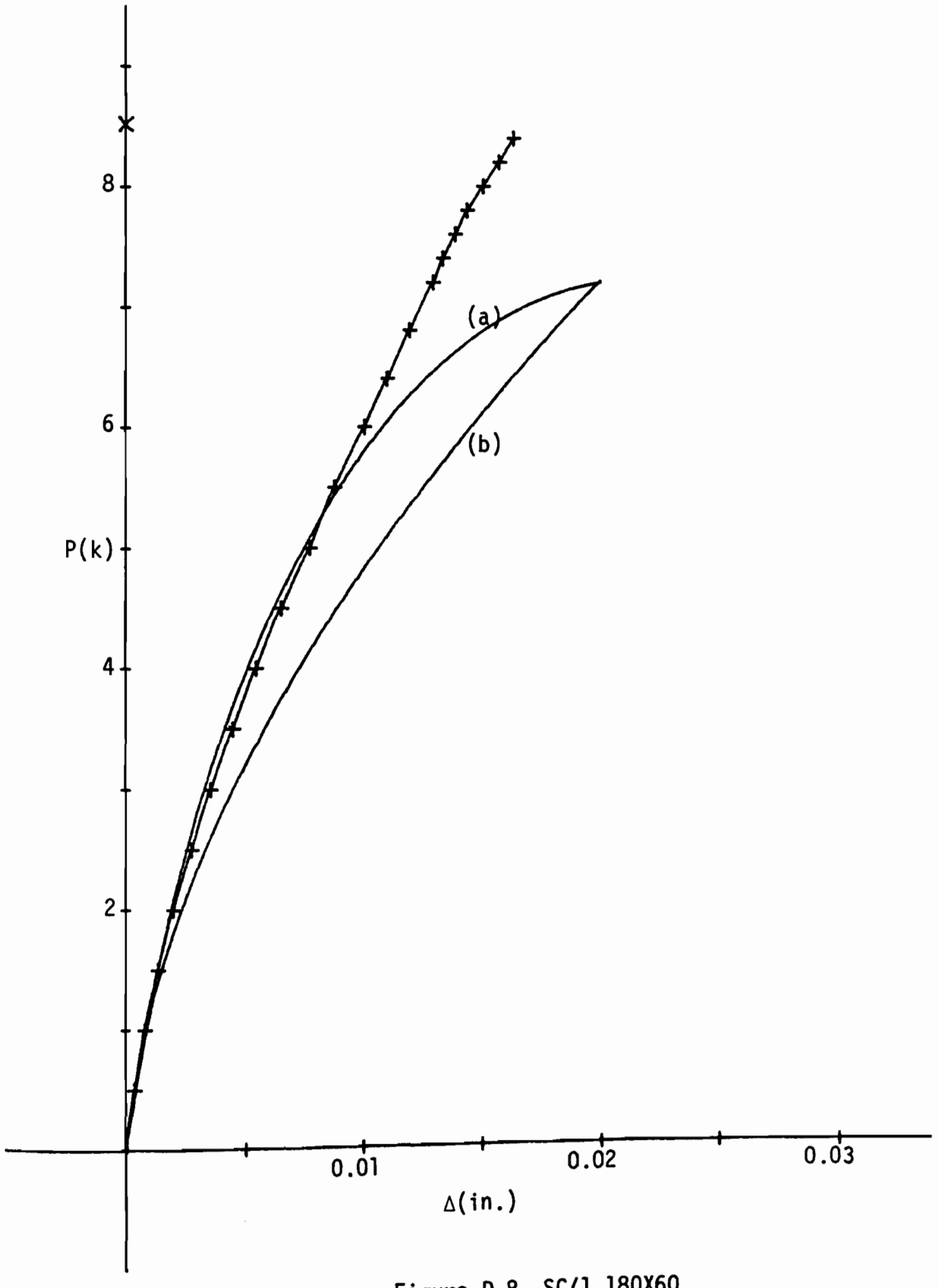

Figure D.8 SC/1 180X60

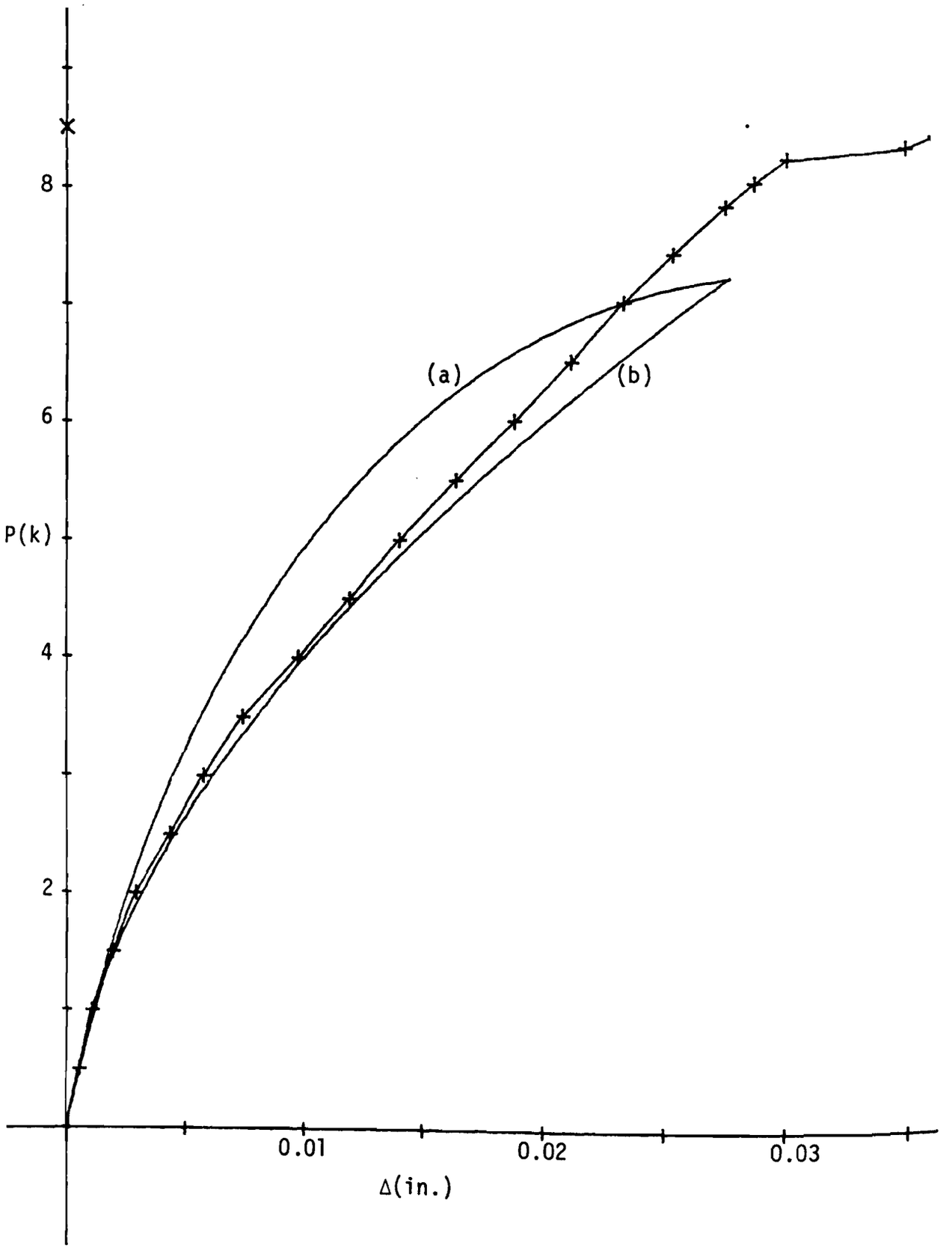

Figure D.9 SC/2 180X60

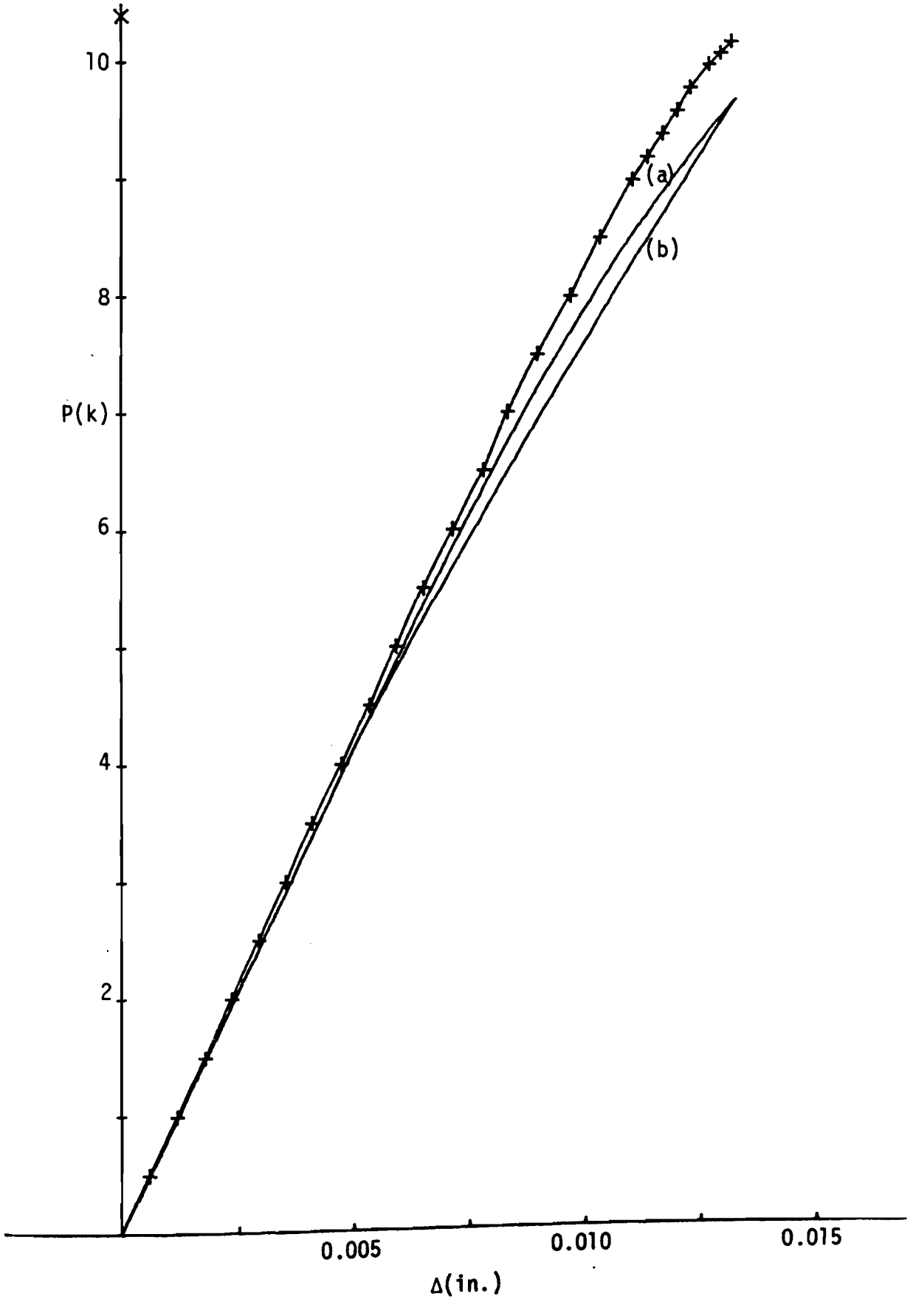

Figure D.10 SLC/1 60X30

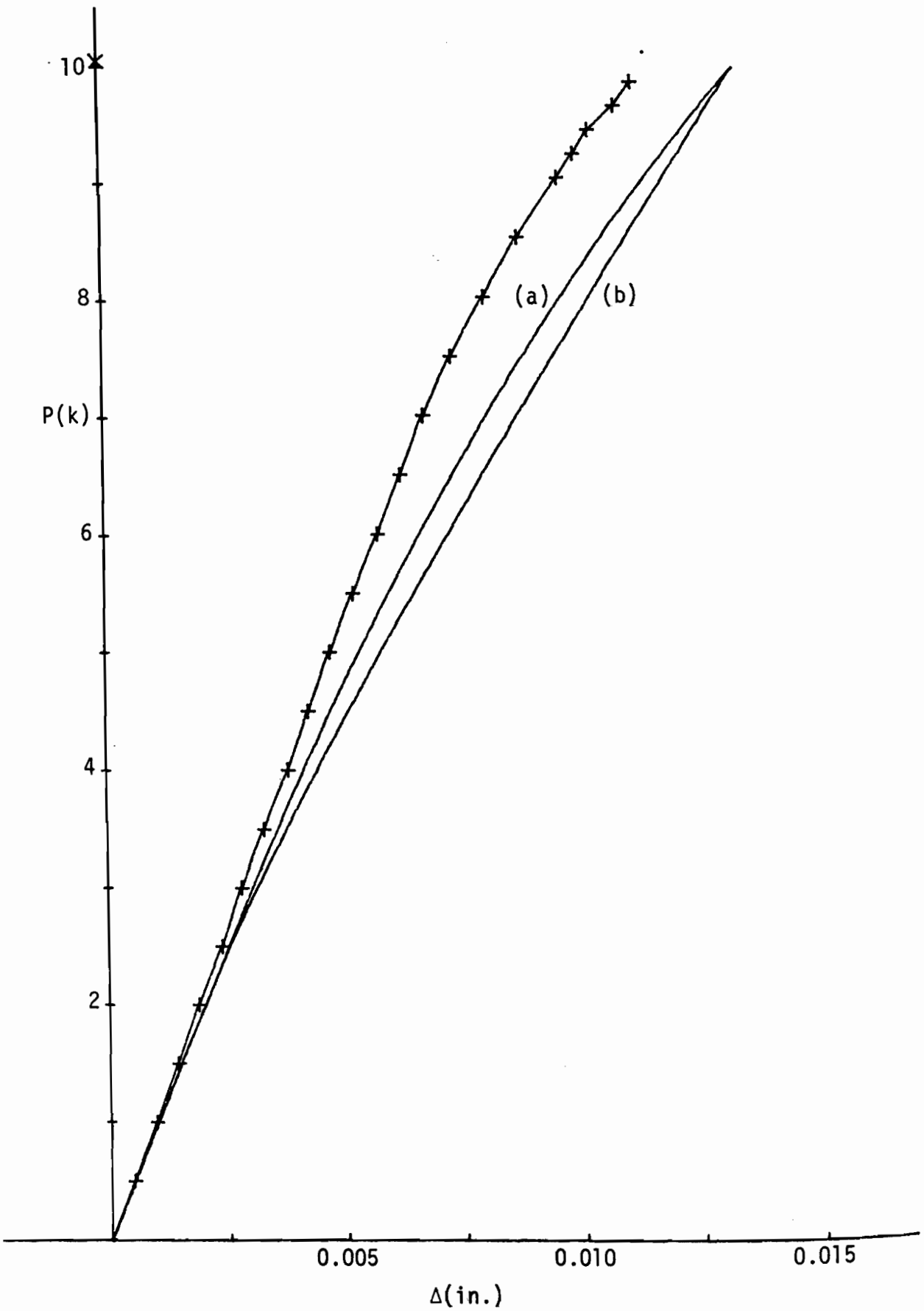

Figure D.11 SLC/1 90X30

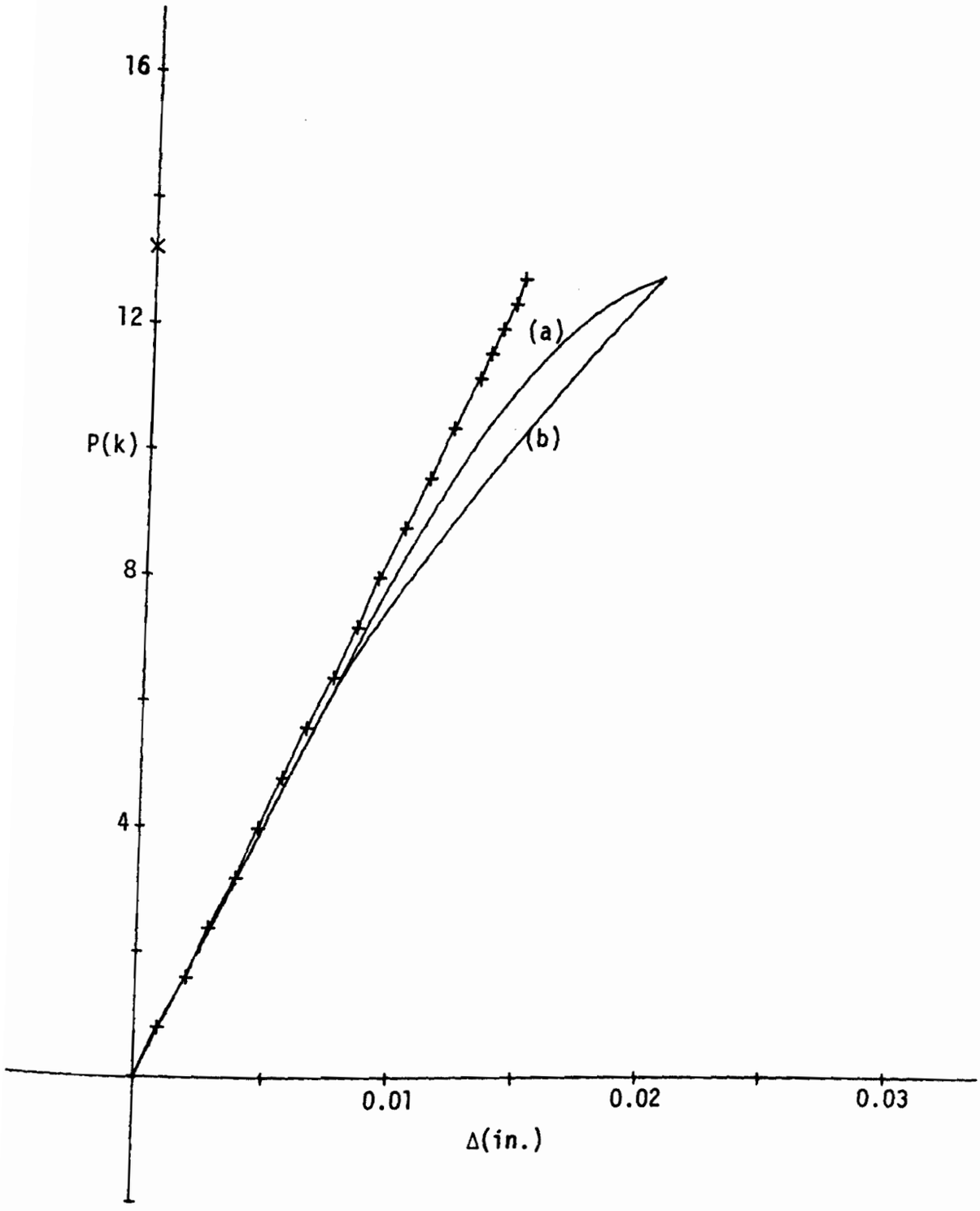

Figure D.12 SLC/1 60X60

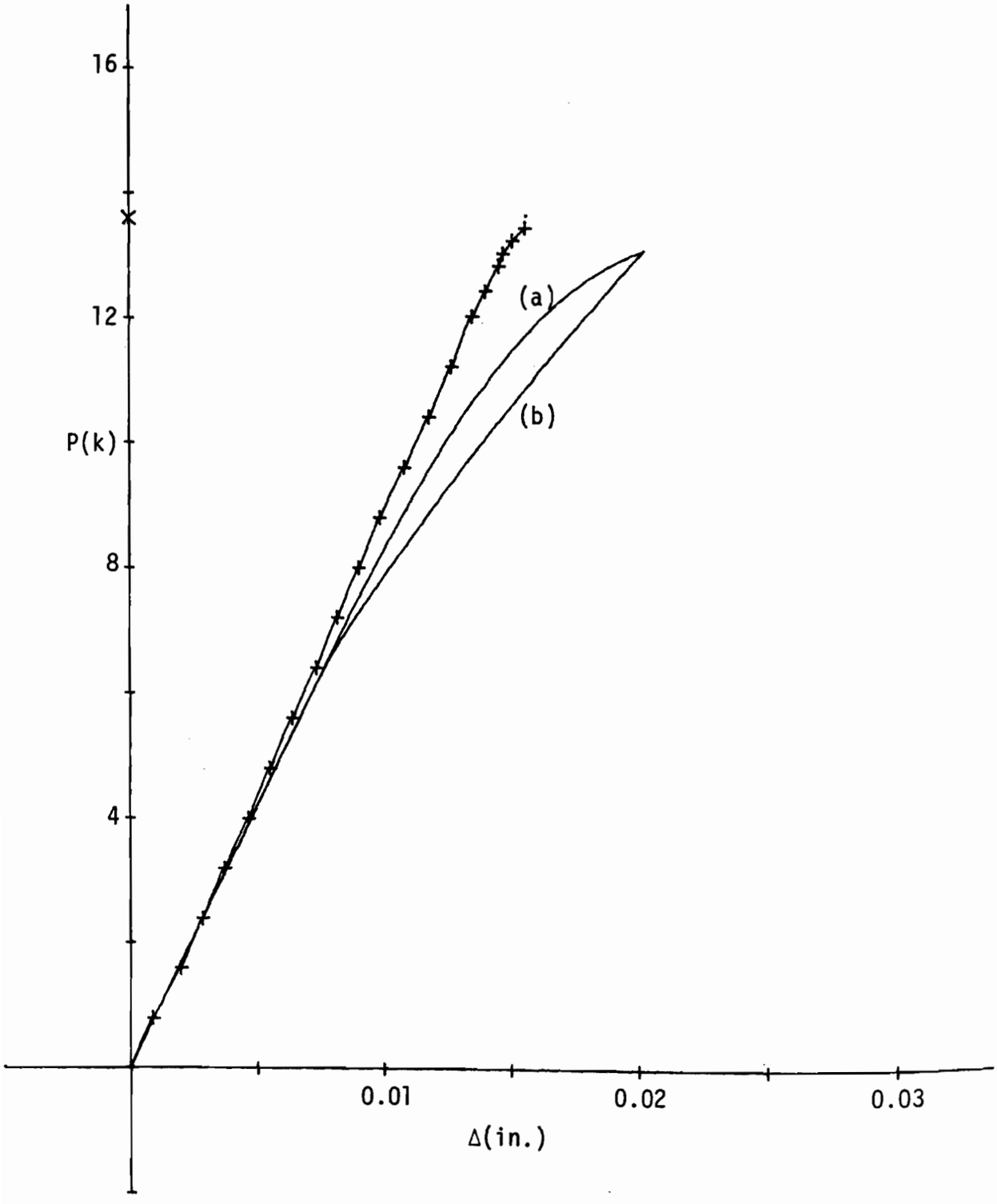

Figure D.13 SLC/2 60X60

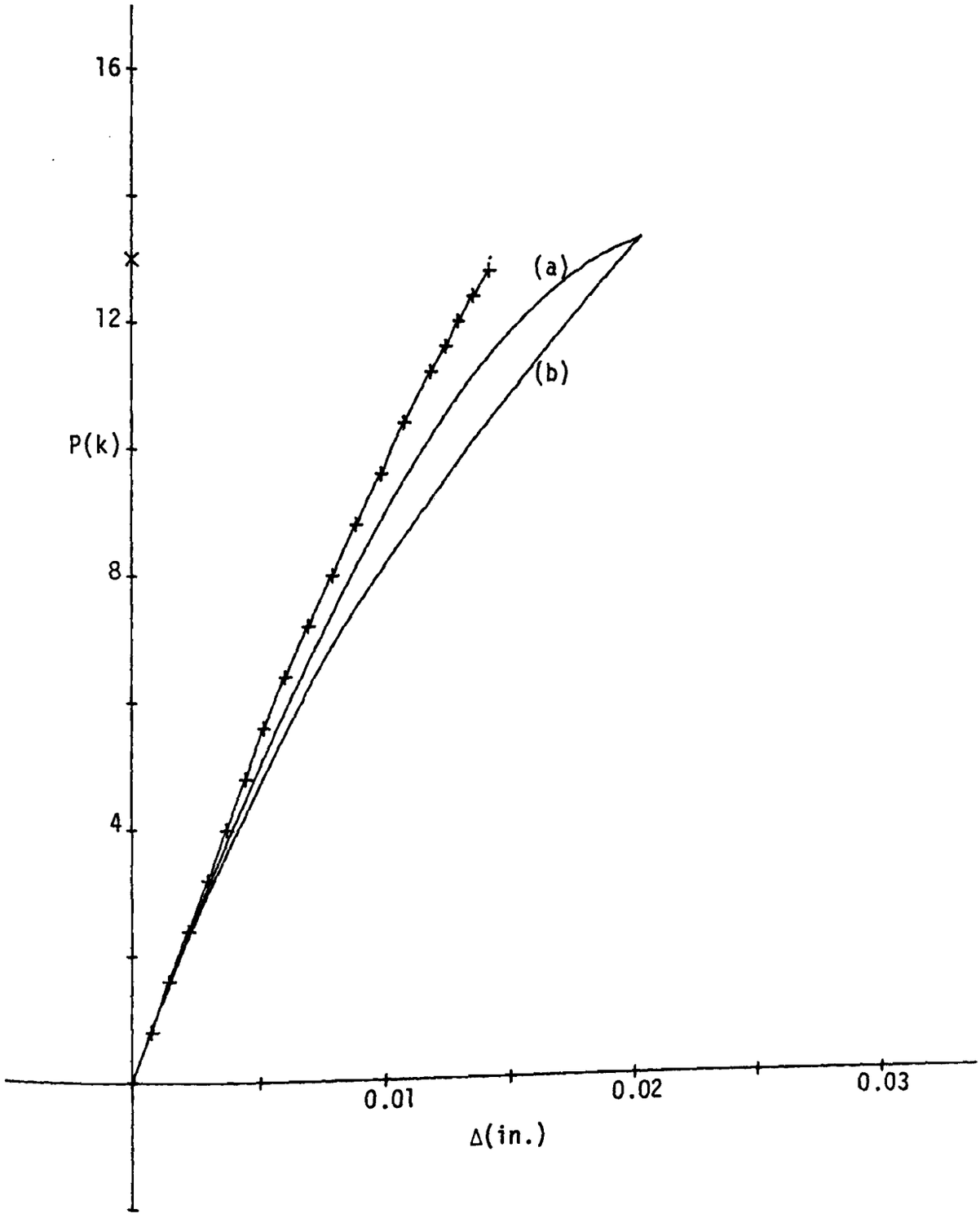

Figure D.14 SLC/1 120X60

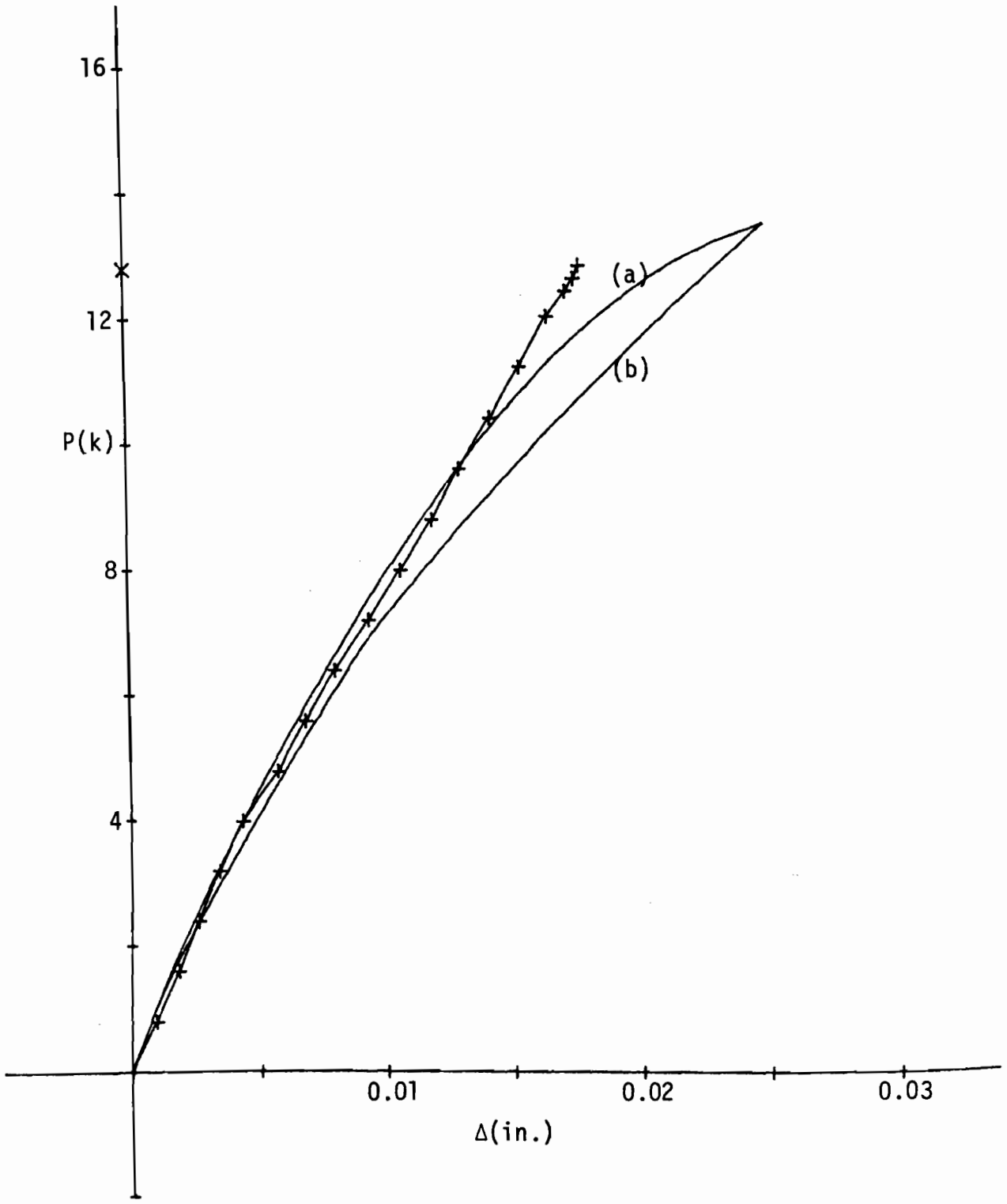

Figure D.15 SLC/1 180X60

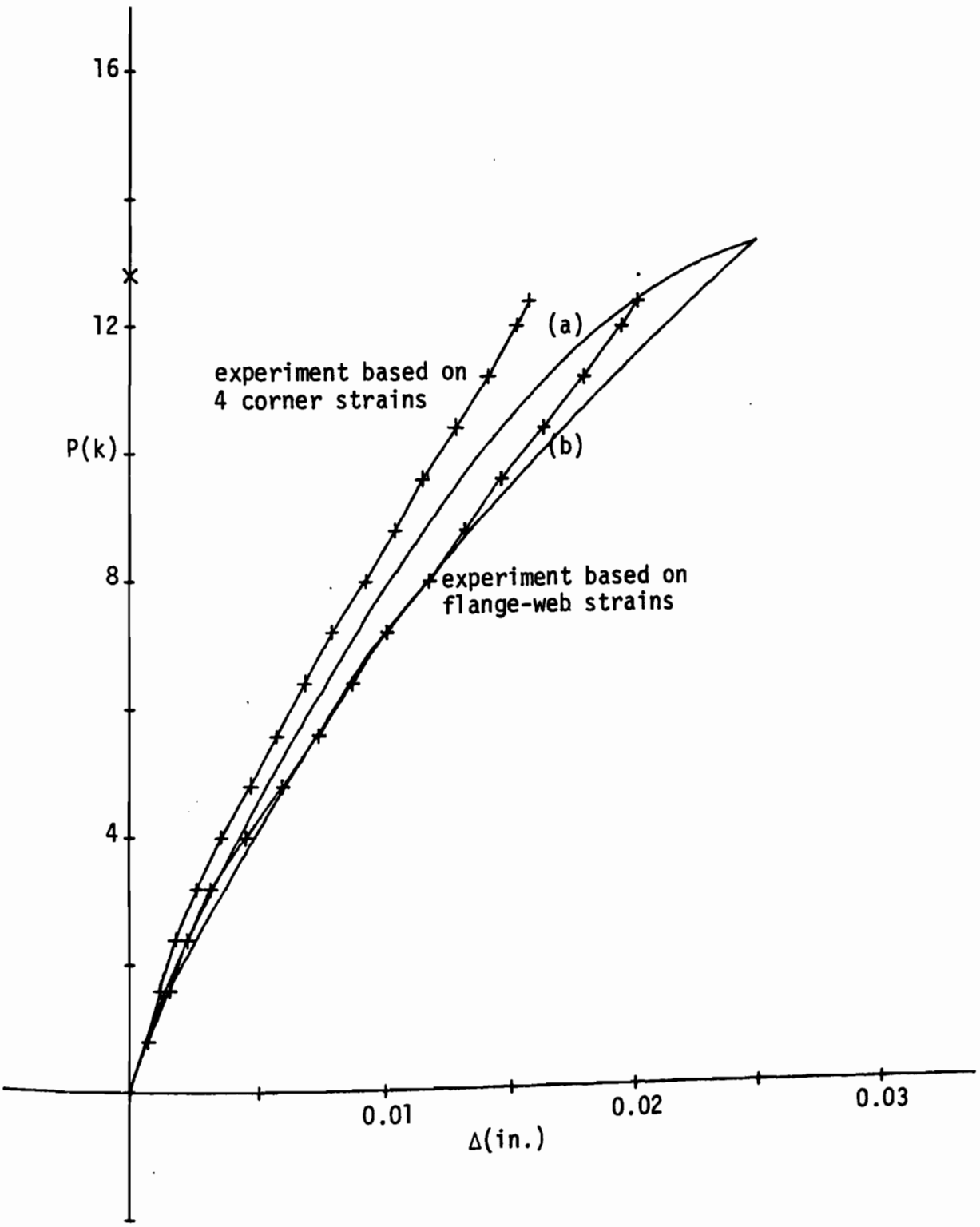

Figure D.16 SLC/1 240X60

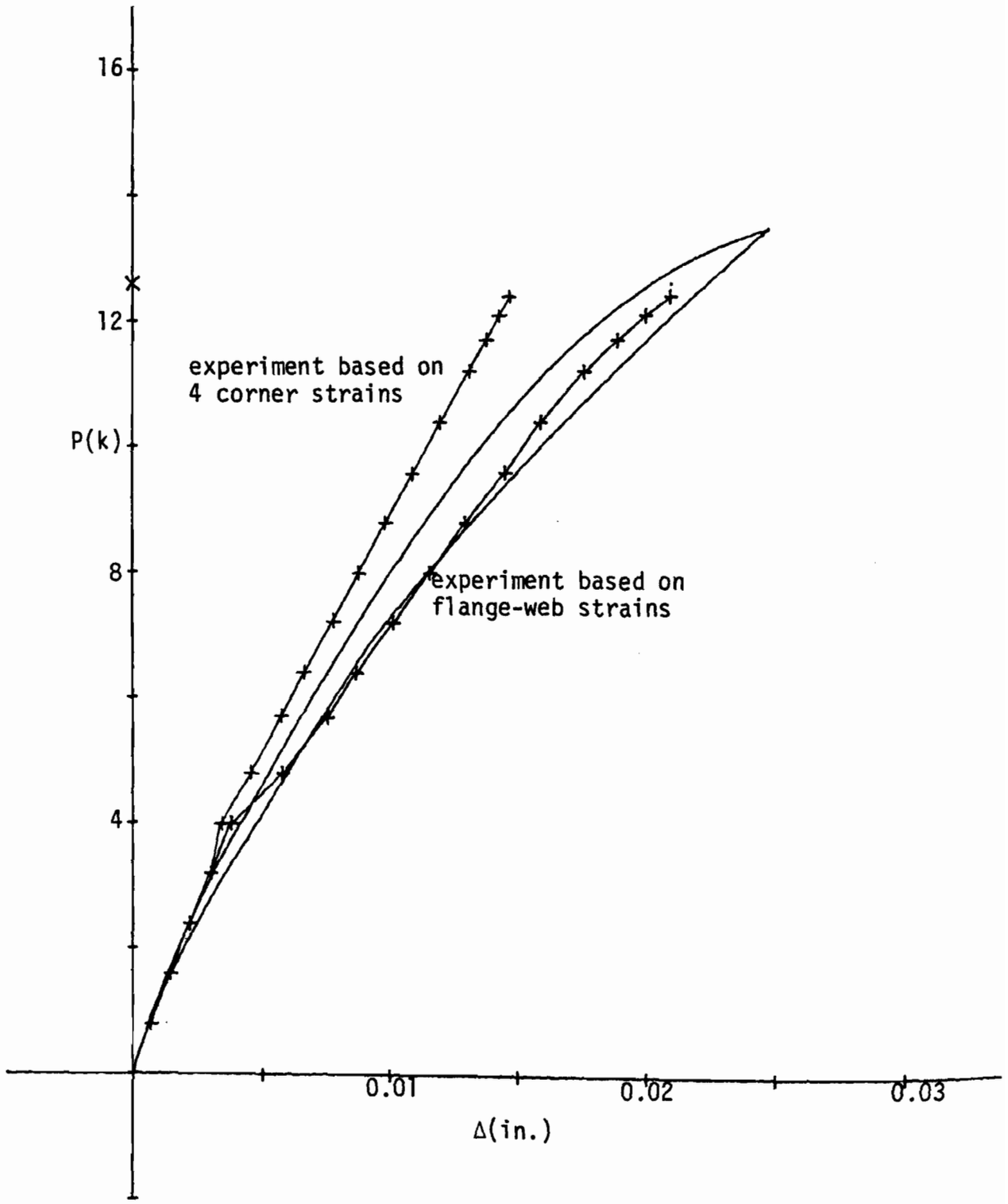

Figure D.17 SLC/3 240X60

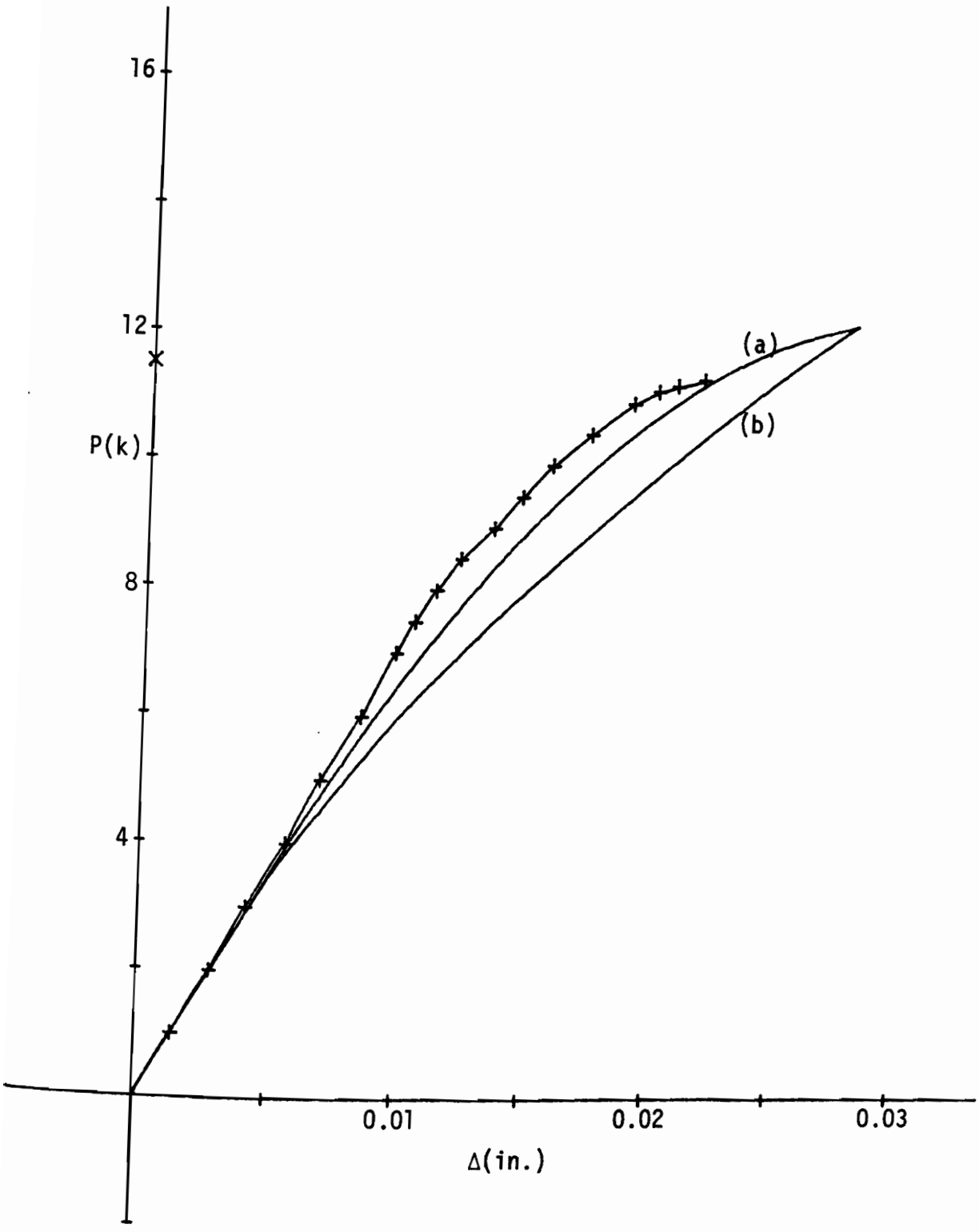

Figure D.18 SLC/1 60X90

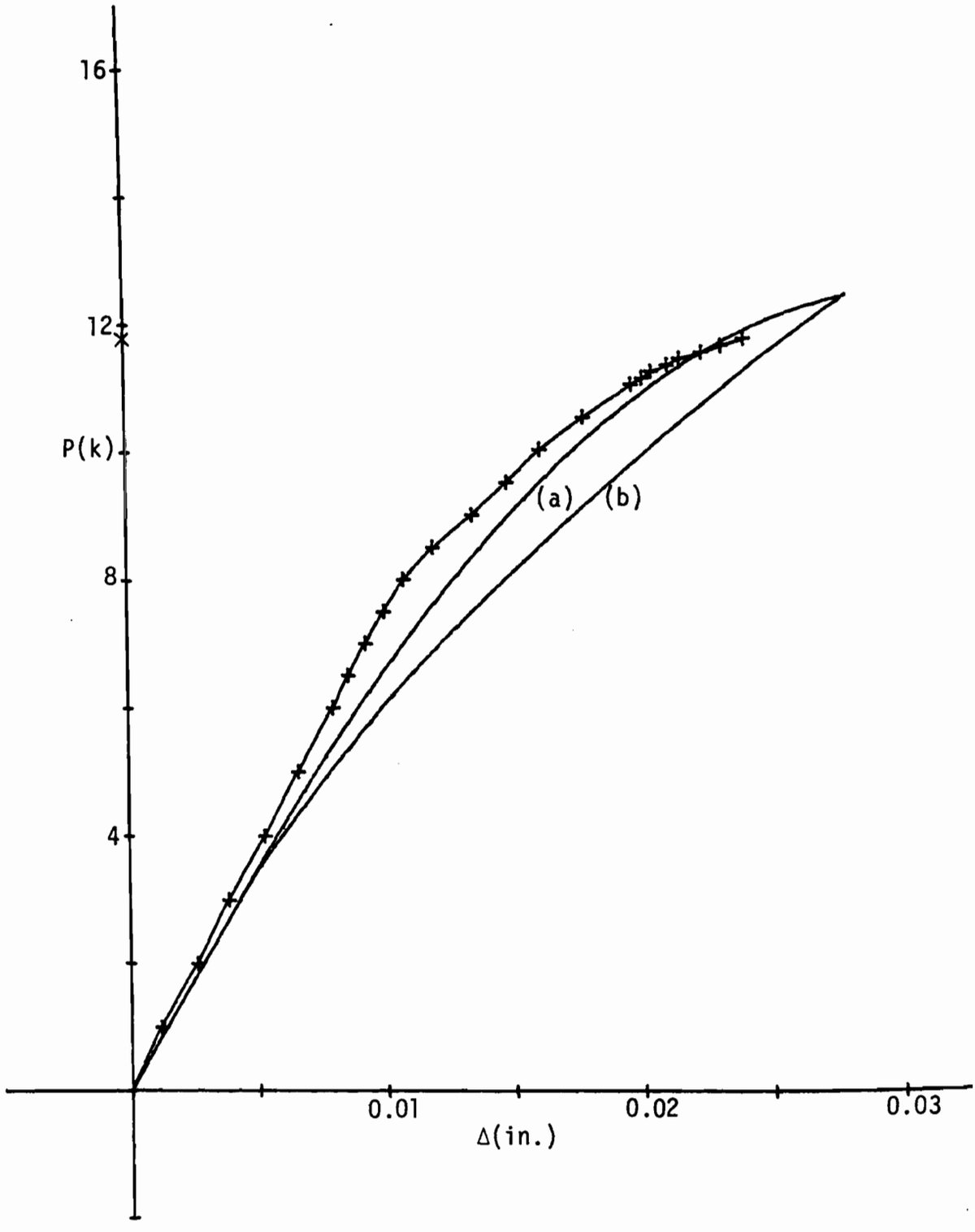

Figure D.19 SLC/2 60X90

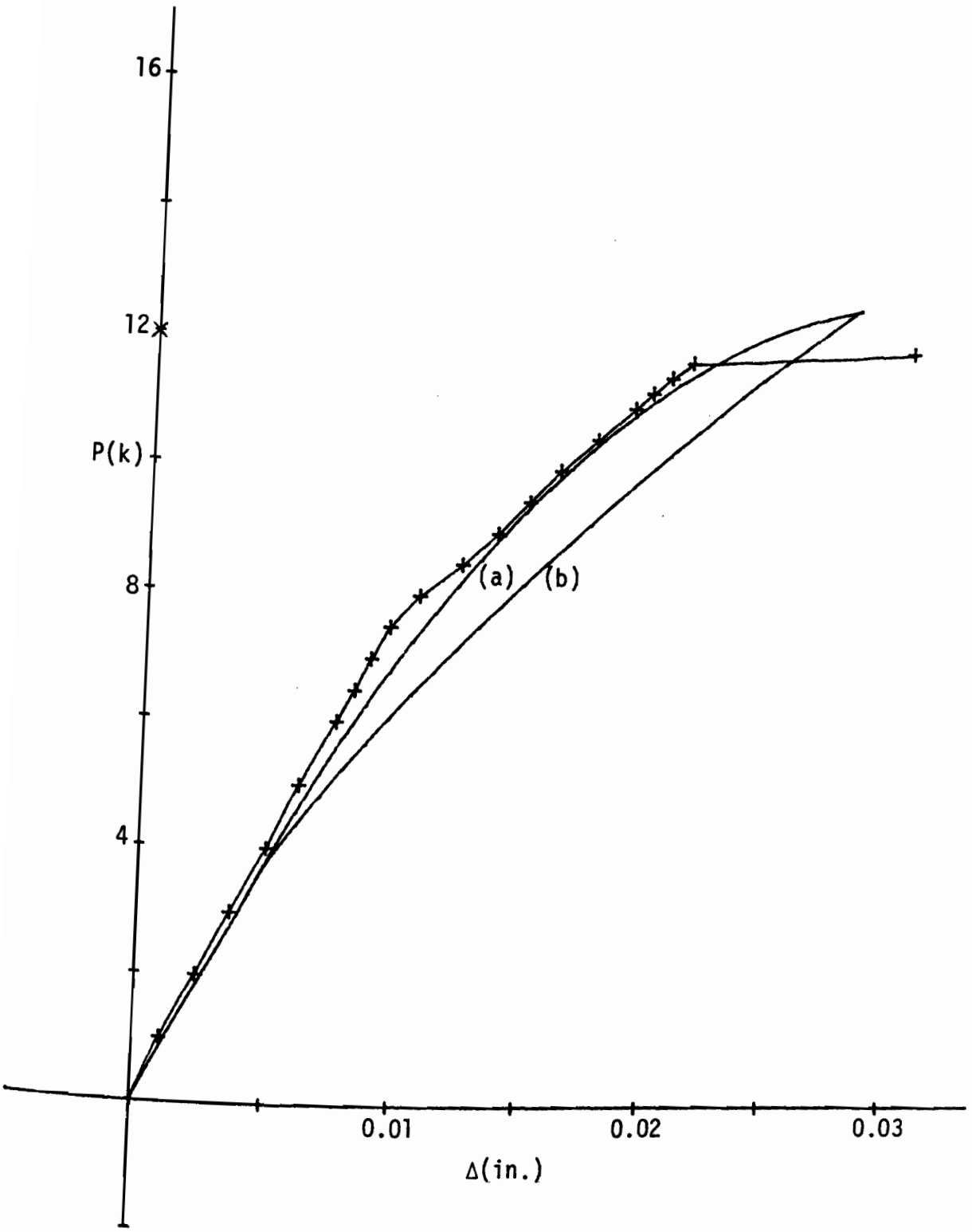

Figure D.20 SLC/2 90X90

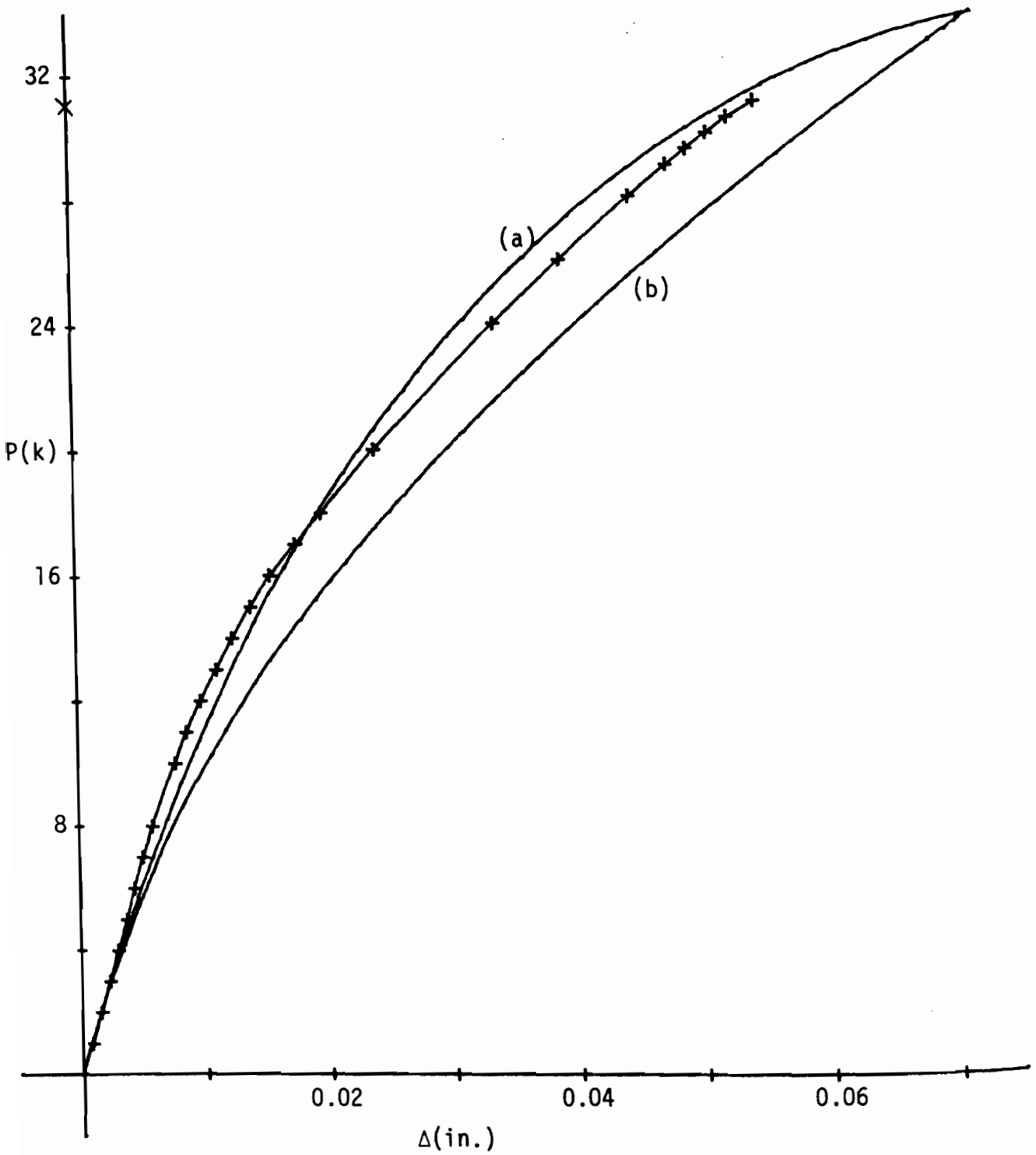

Figure D.21 SLC/1 180X90

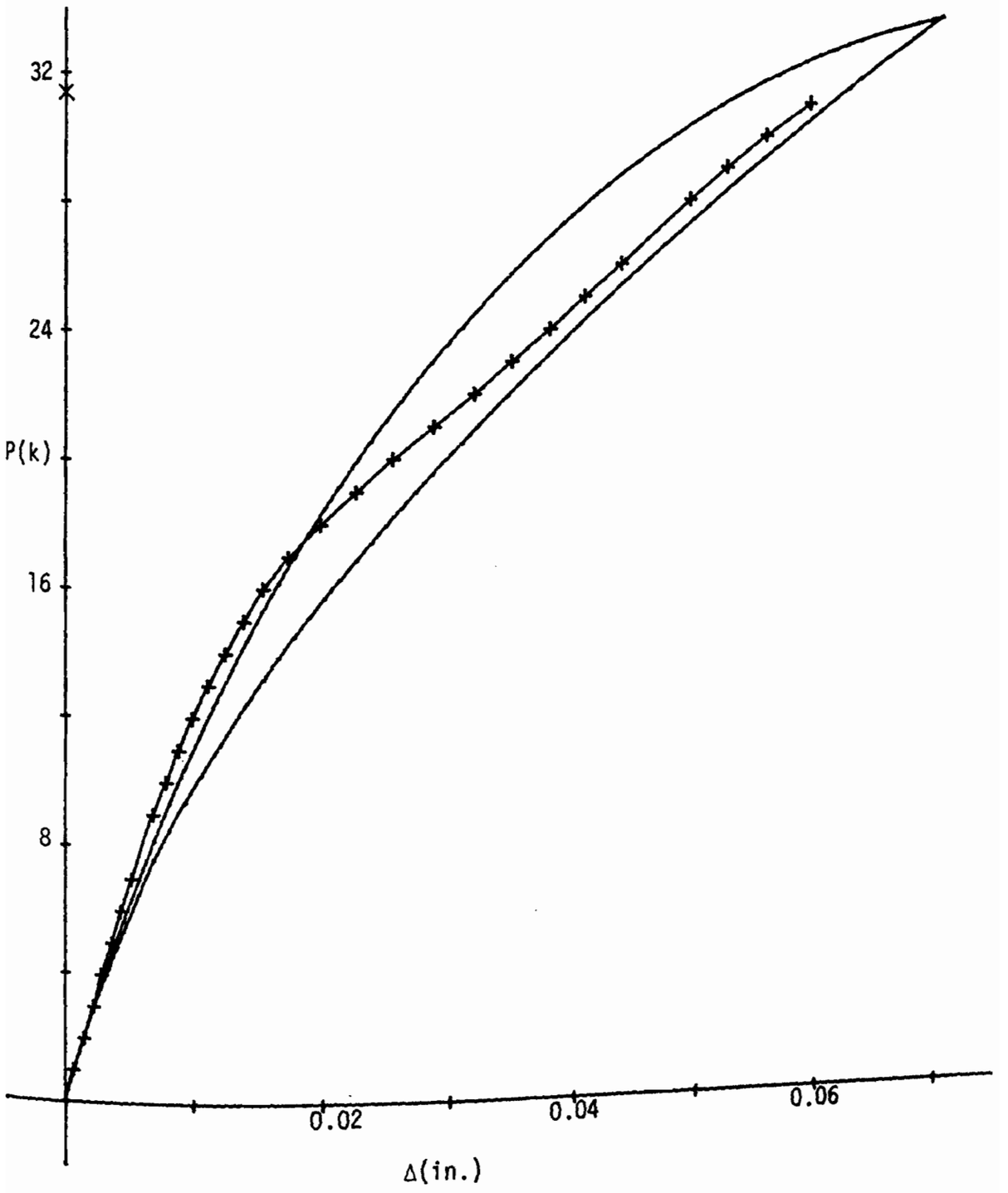

Figure D.22 SLC/2 180X90

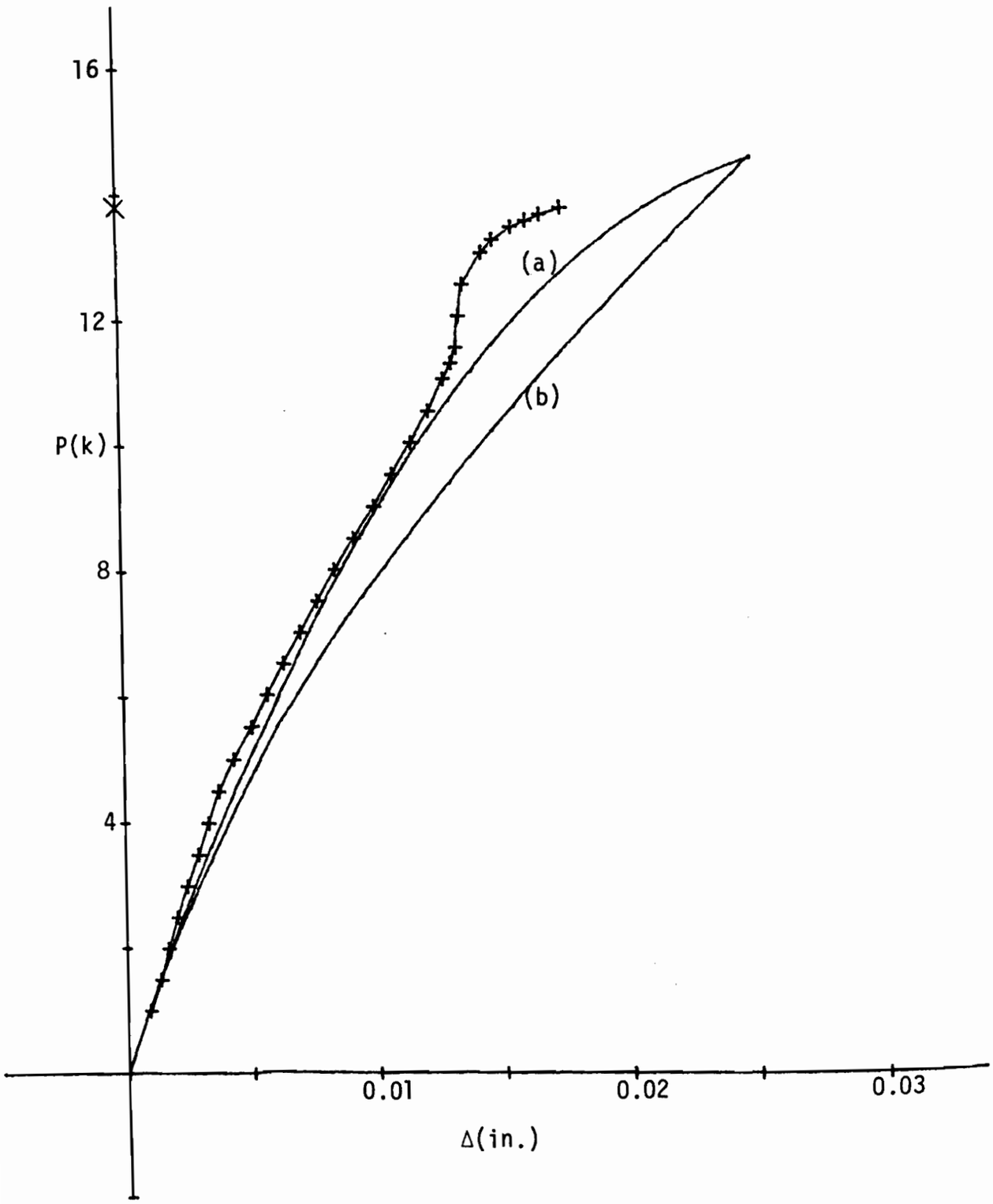

Figure D.23 SLC/4 180X90

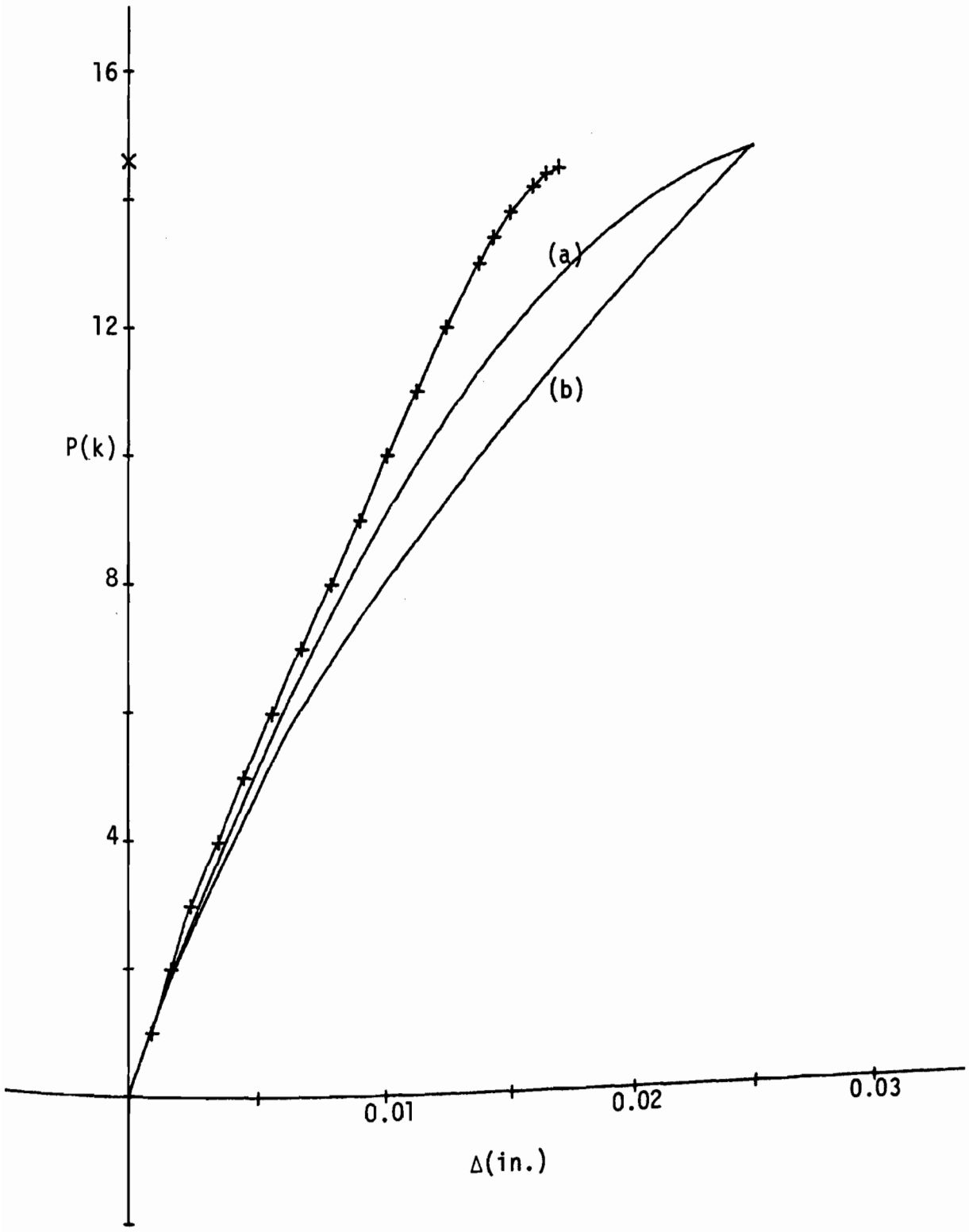

Figure D.24 SLC/5 180X90

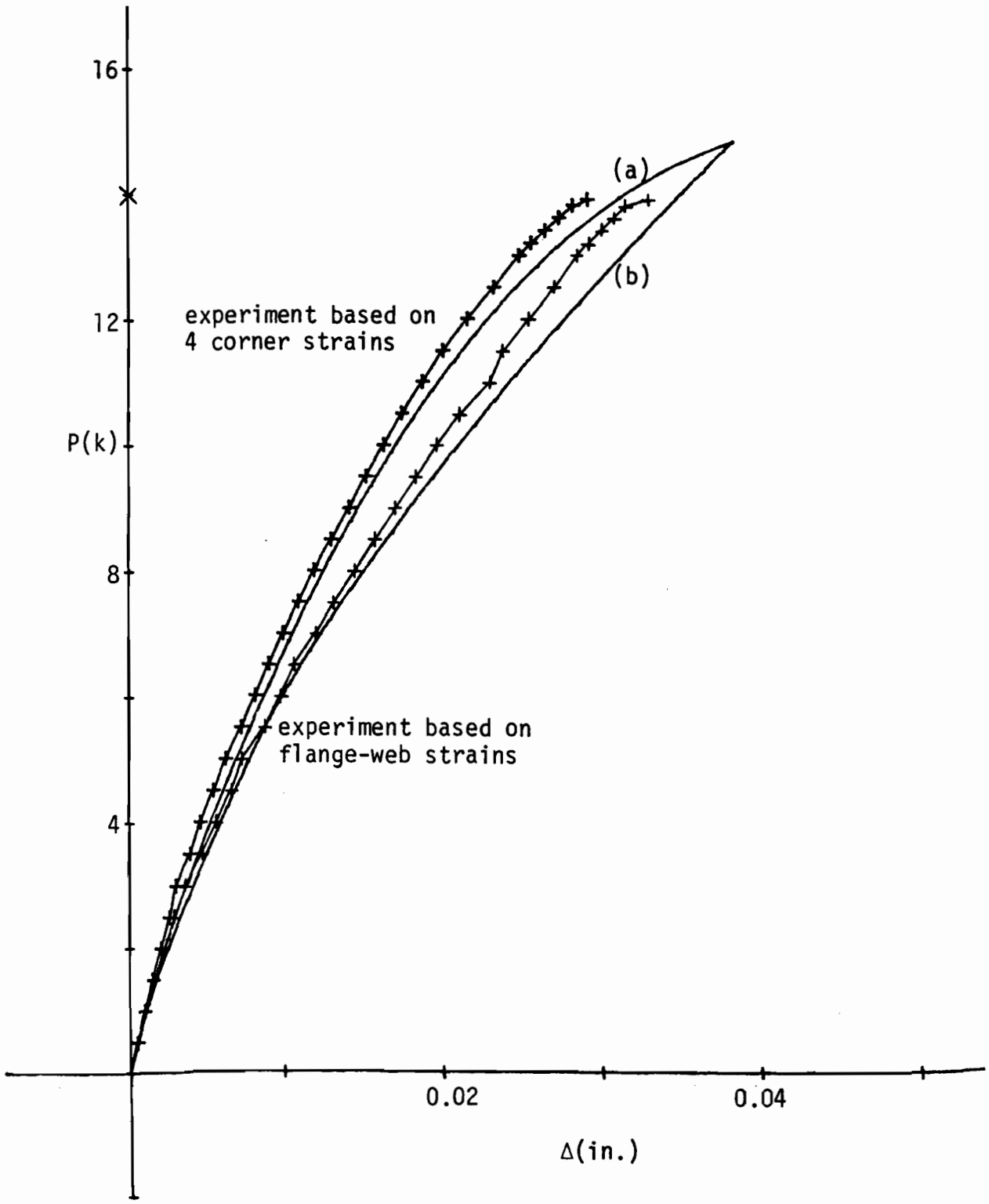

Figure D.25 SLC/2 270X90

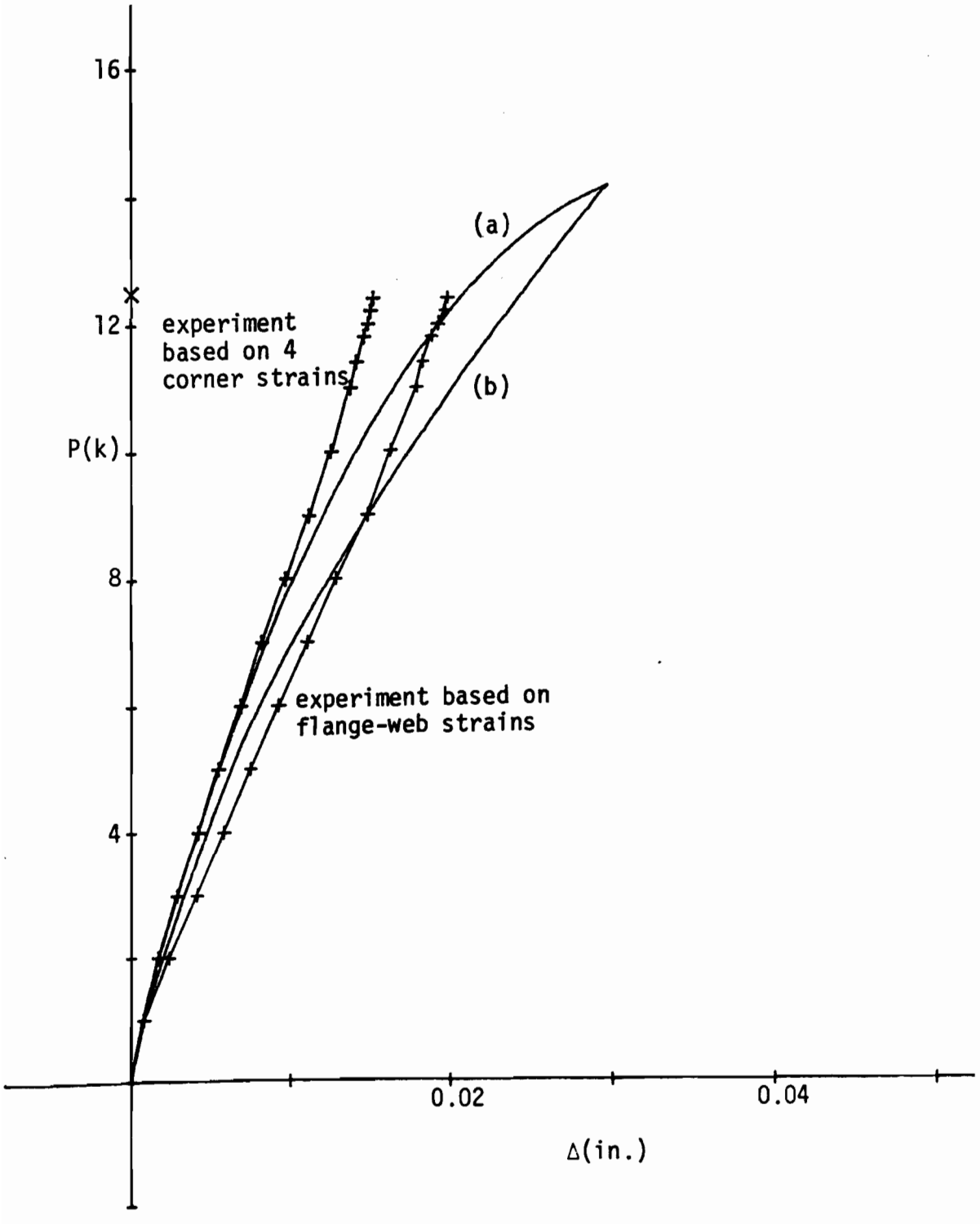

Figure D.26 SLC/1 360X90

APPENDIX E

SUB-ULTIMATE RESPONSE FOR LONG COLUMNS

Note: This appendix contains graphs of the axial load-strain and the axial load - lateral deflection responses for the columns and beam-columns which are not presented in Chapter 6. Reference is made to Section 6.3 for relevant discussions. Also, the following notation is employed:

(1), (2) refer to the reference axes of Figure 4.2,

(a) refers to the effective section method of paragraph 4.5.2, and

(b) refers to the alternate effective section method discussed in paragraph 6.3.1.

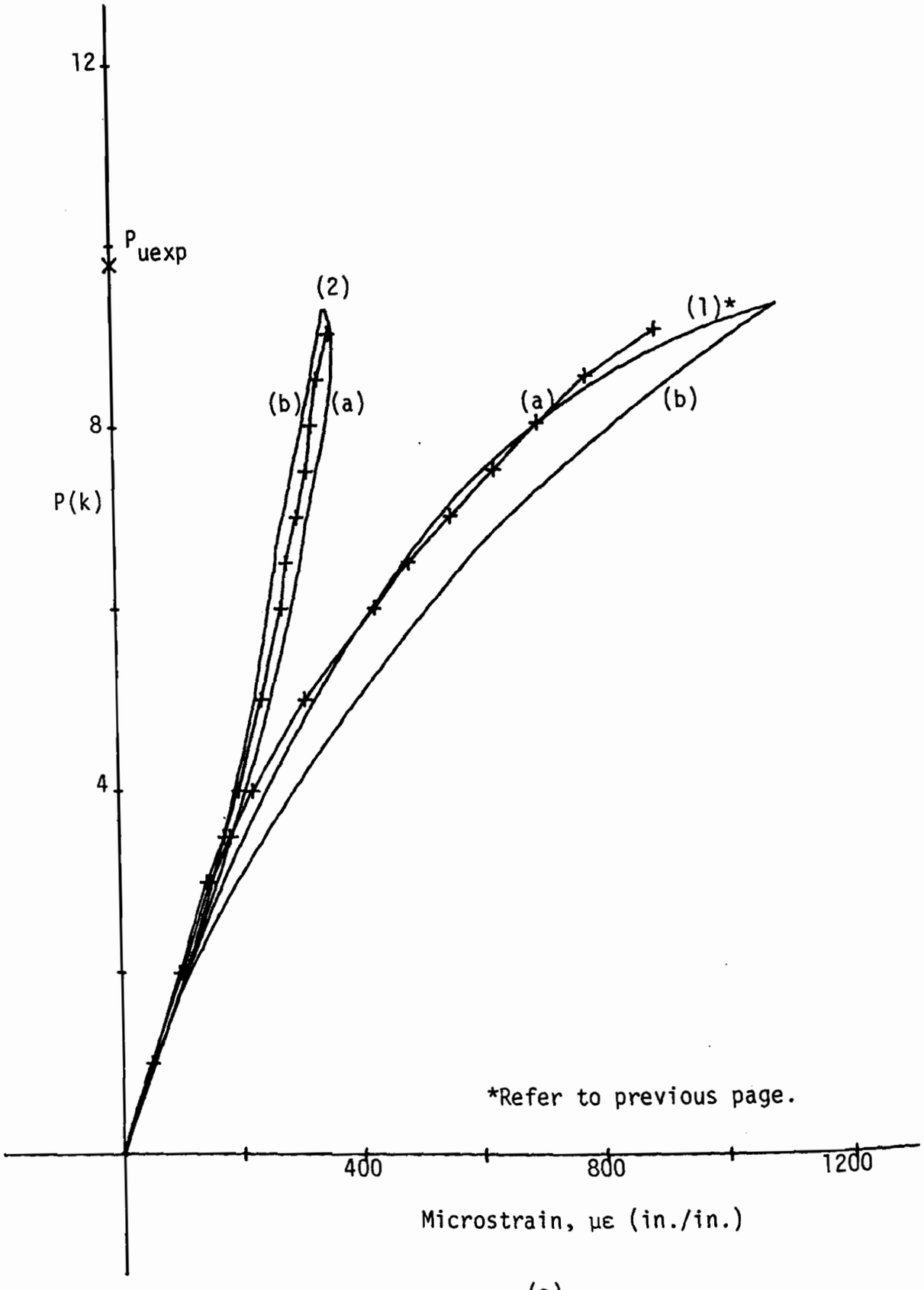

*Refer to previous page.

(a)

Figure E.1 CLC/1 120X60

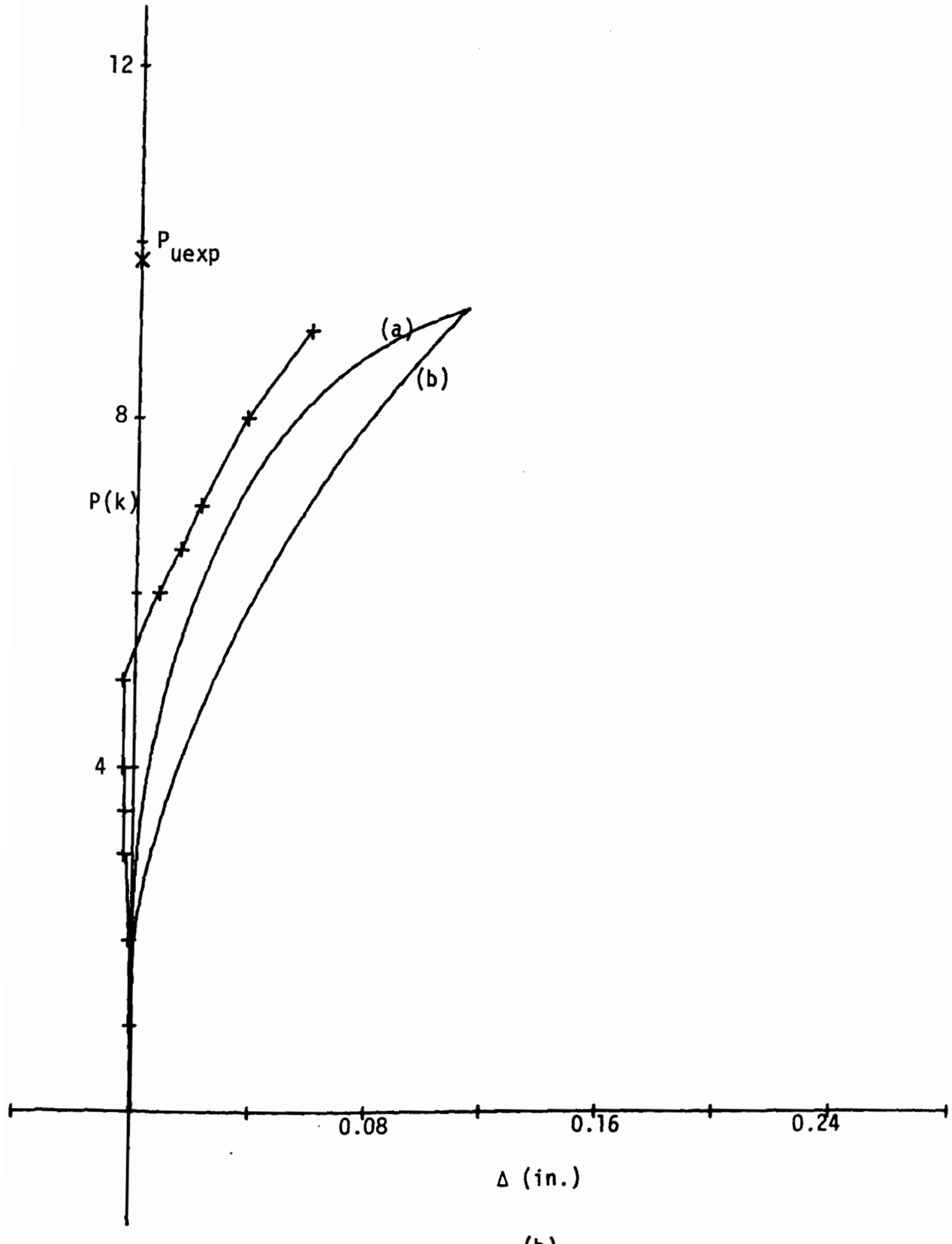

(b)

Figure E.1 CLC/1 120X60 - continued

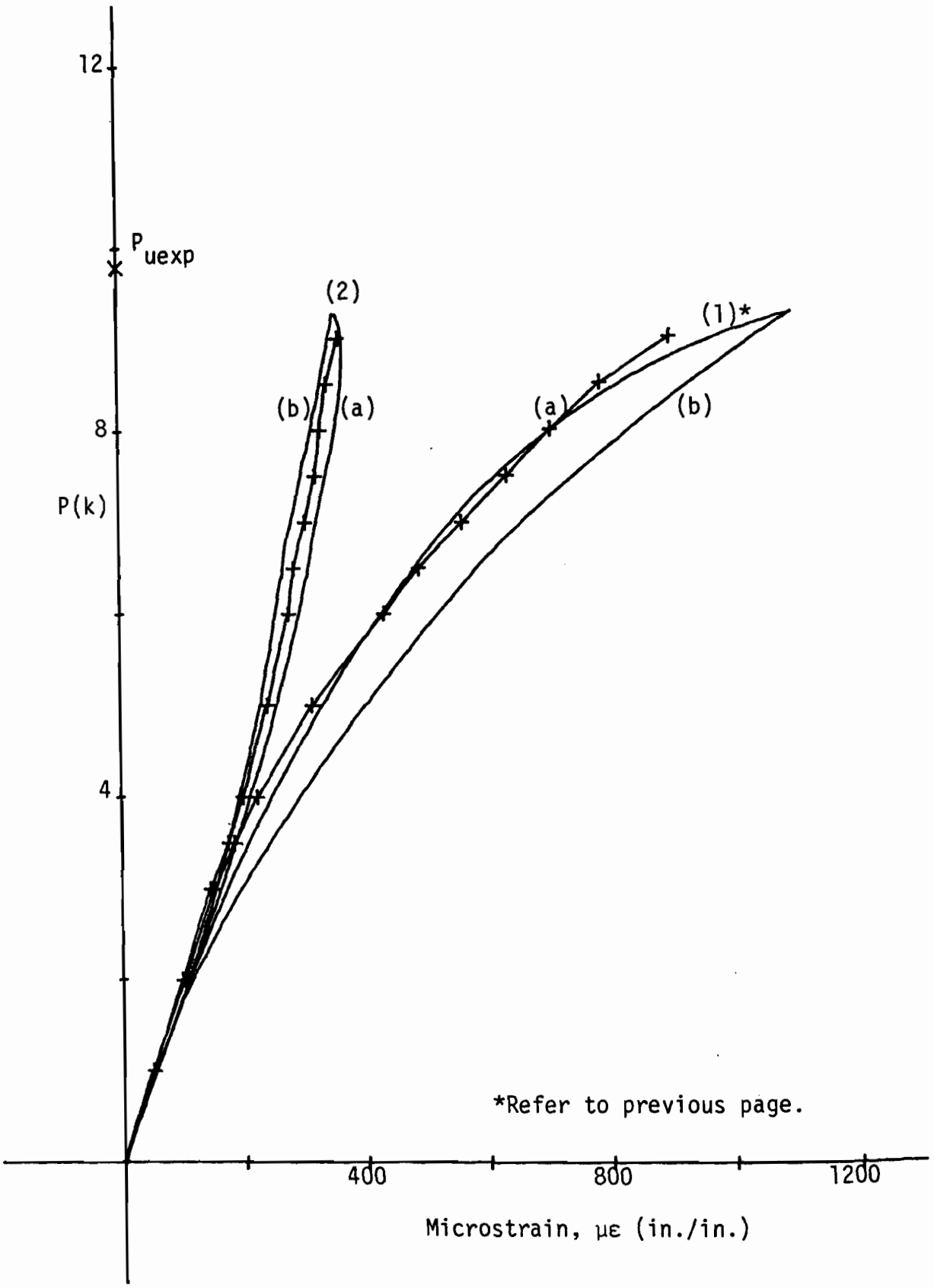

*Refer to previous page.

(a)

Figure E.1 CLC/1 120X60

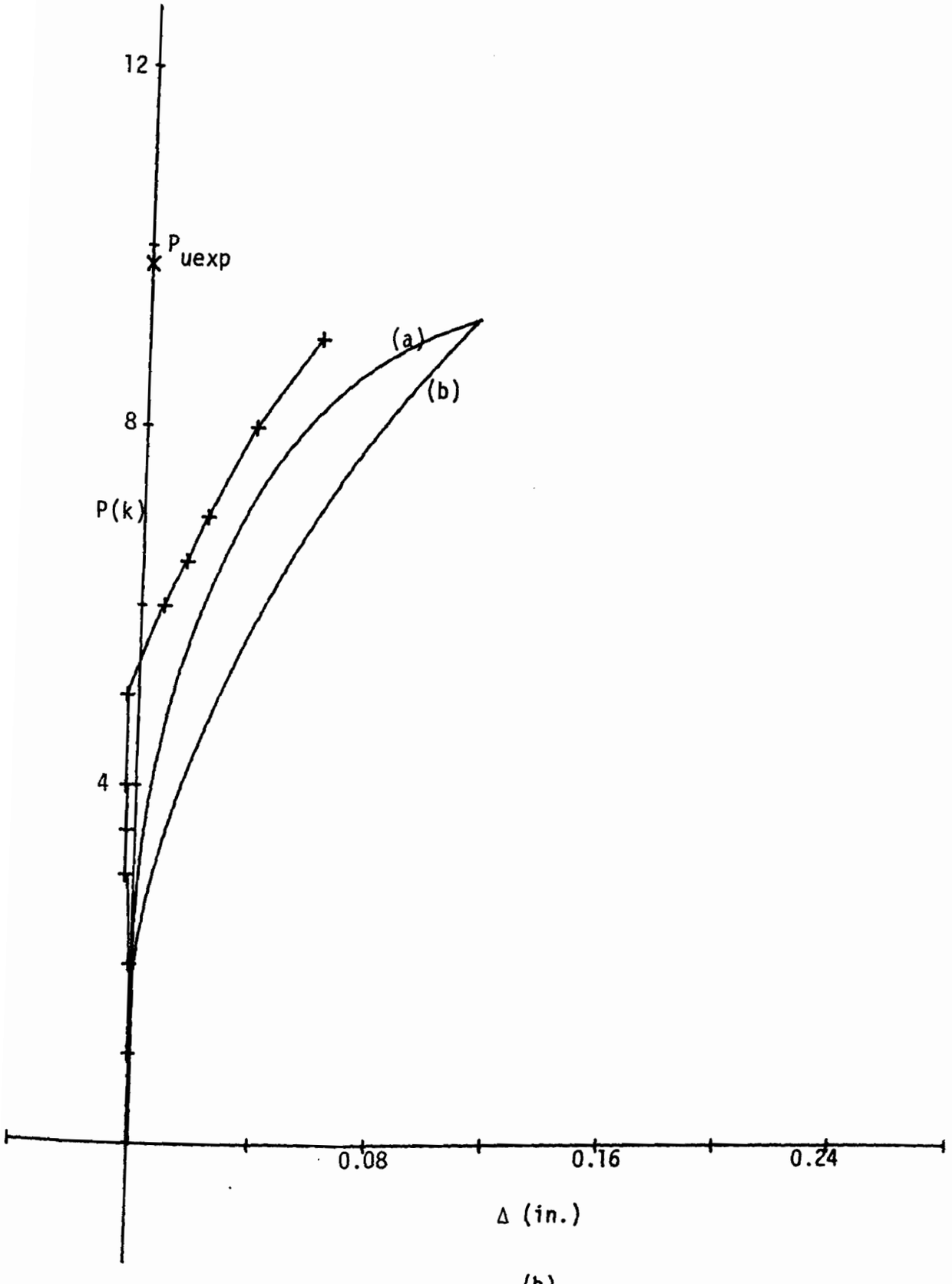

(b)

Figure E.1 CLC/1 120X60 - continued

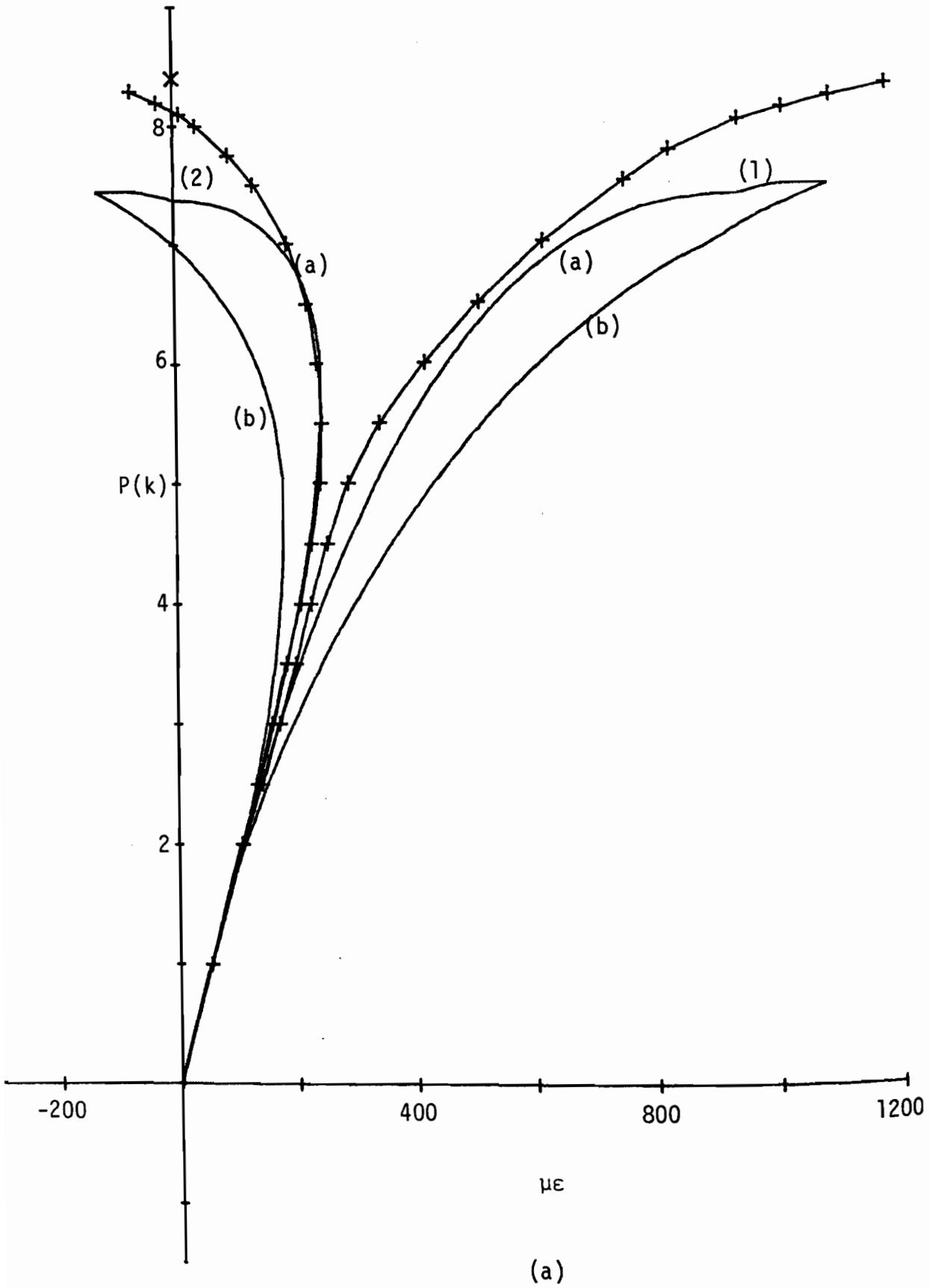

(a)

Figure E.2 CLC/4 120X60

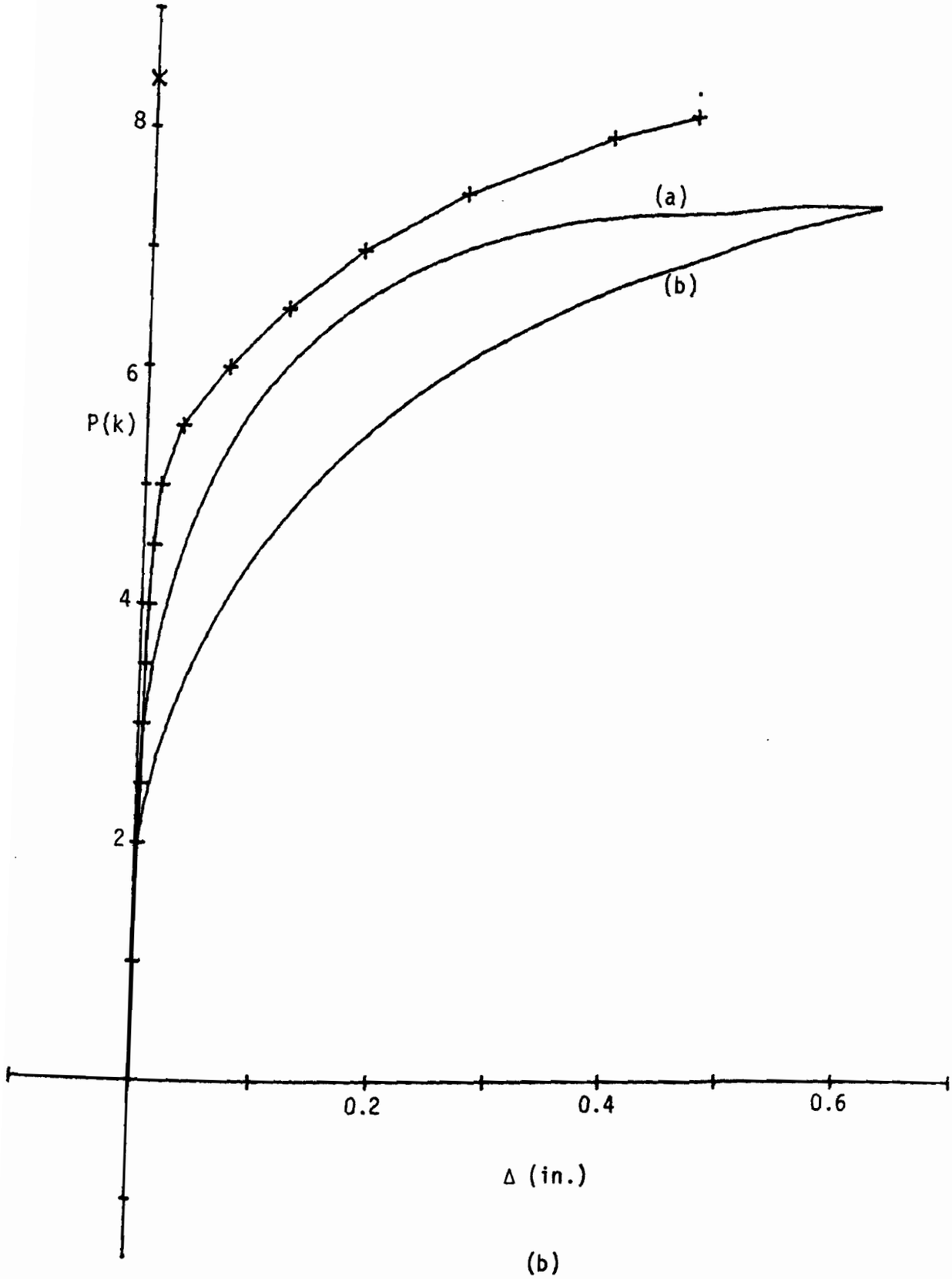

(b)

Figure E.2 CLC/4 120X60 - continued

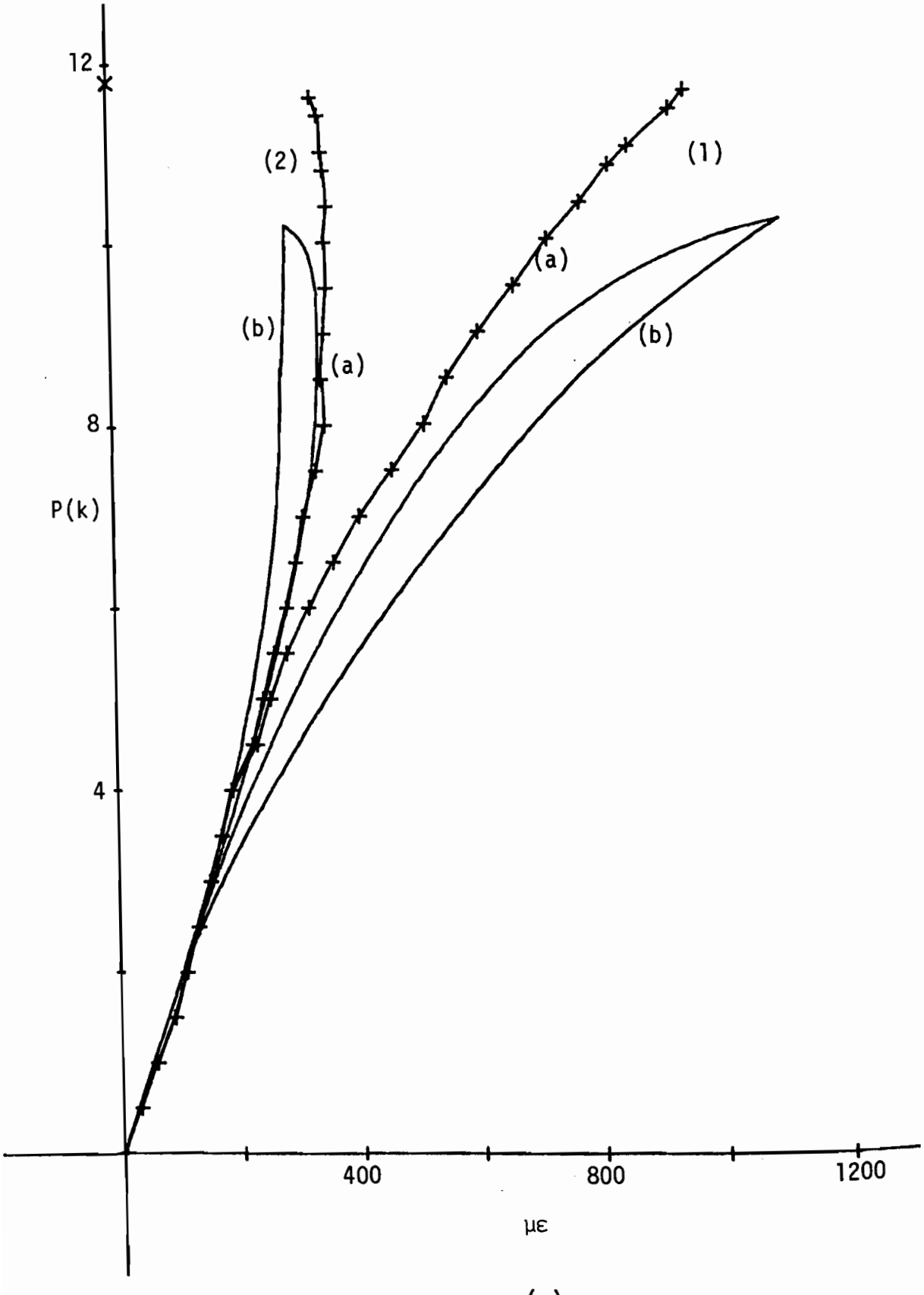

(a)

Figure E.3 CLC/5 120X60

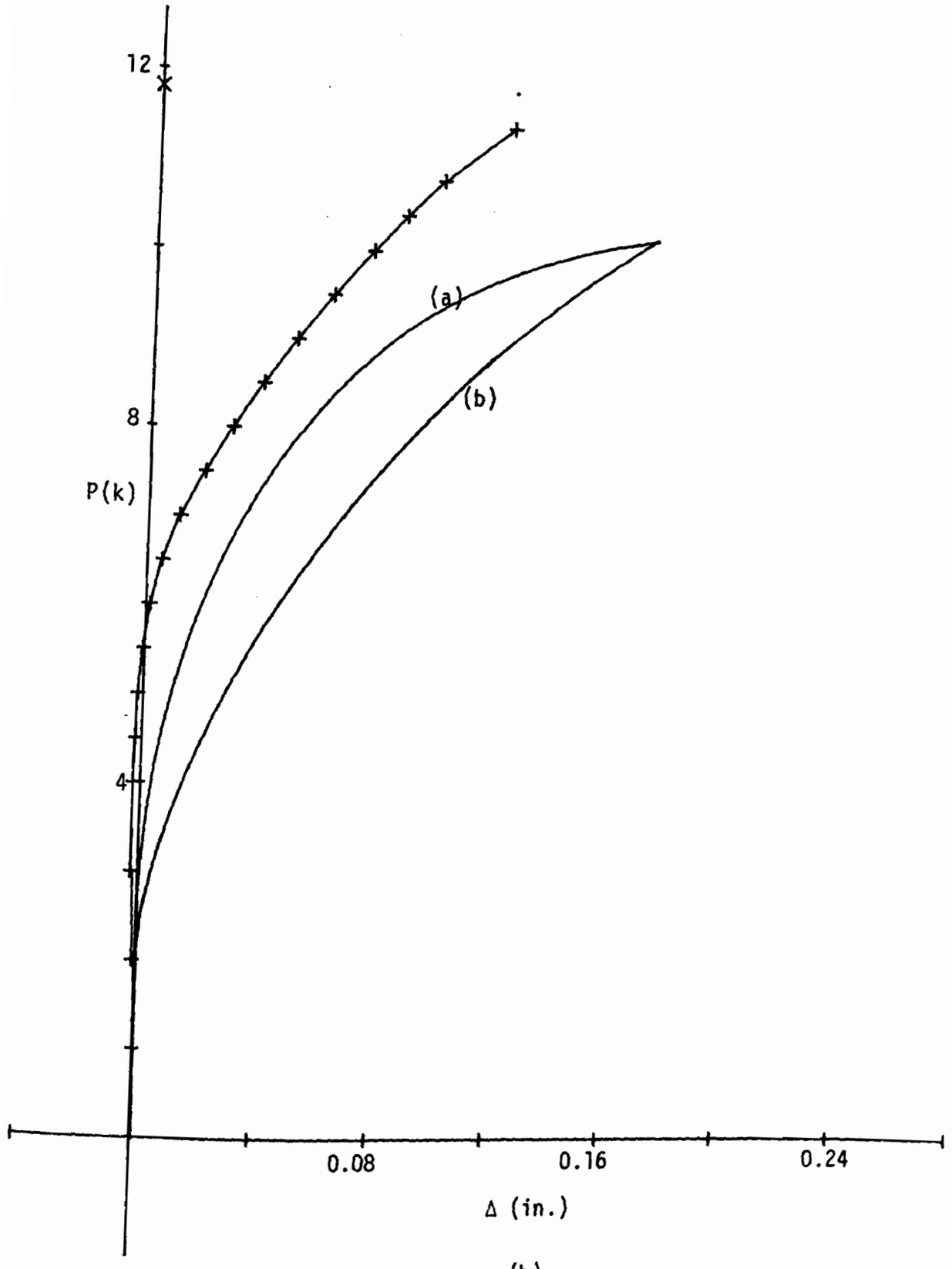

(b)

Figure E.3 CLC/5 120X60 - continued

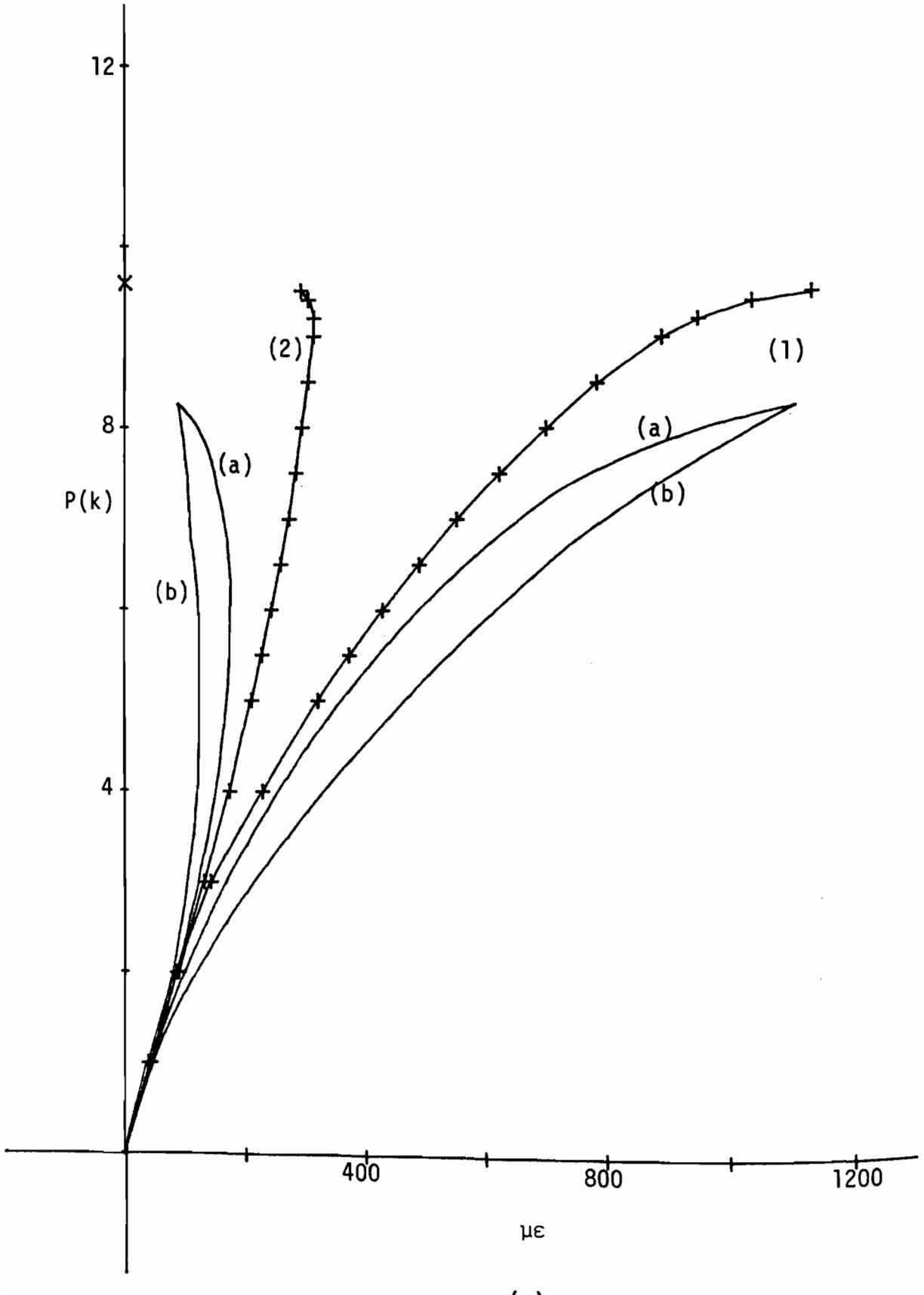

(a)

Figure E.4 CLC/1 180X60

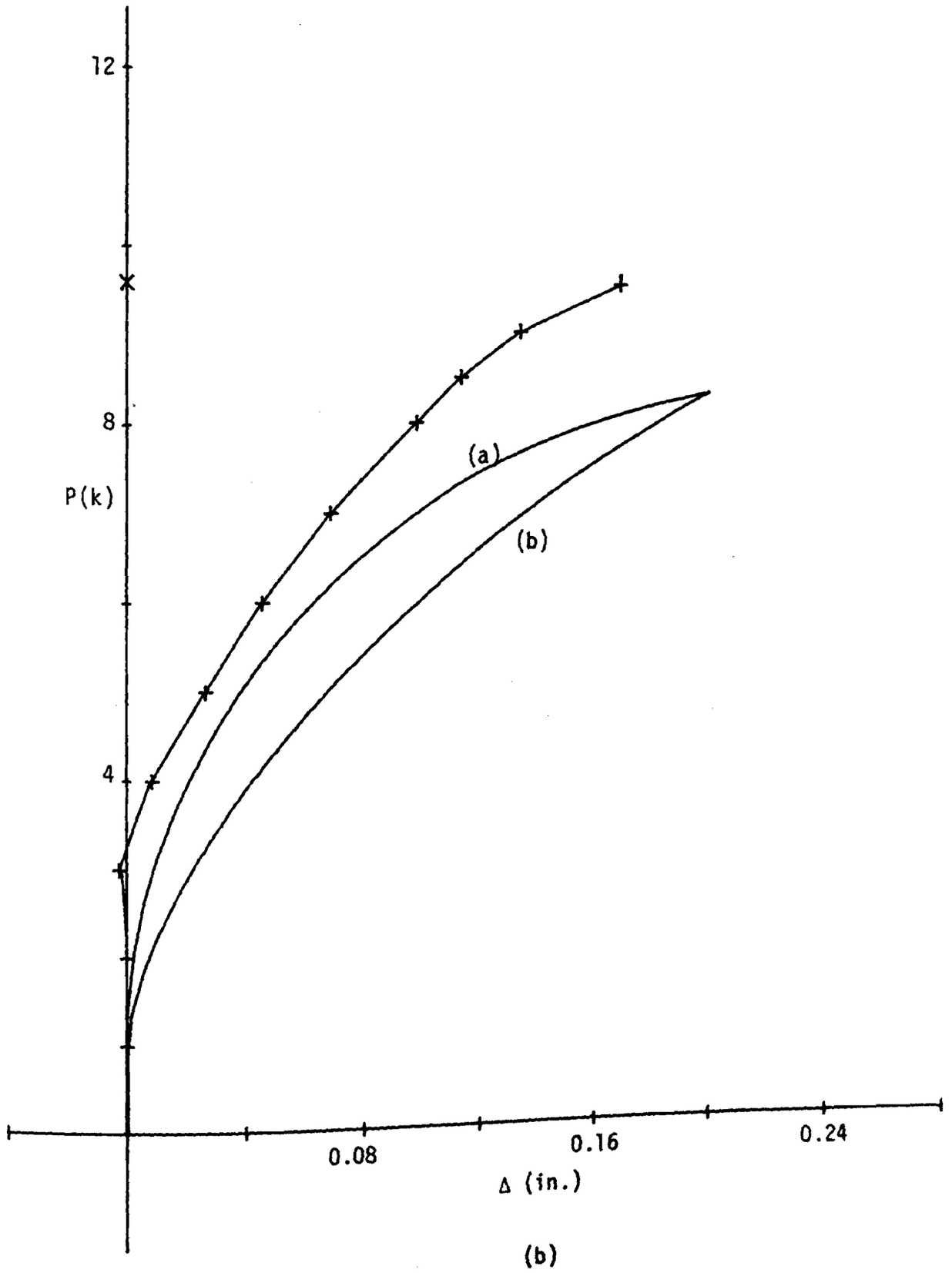

(b)

Figure E.4 CLC/1 180X60 - continued

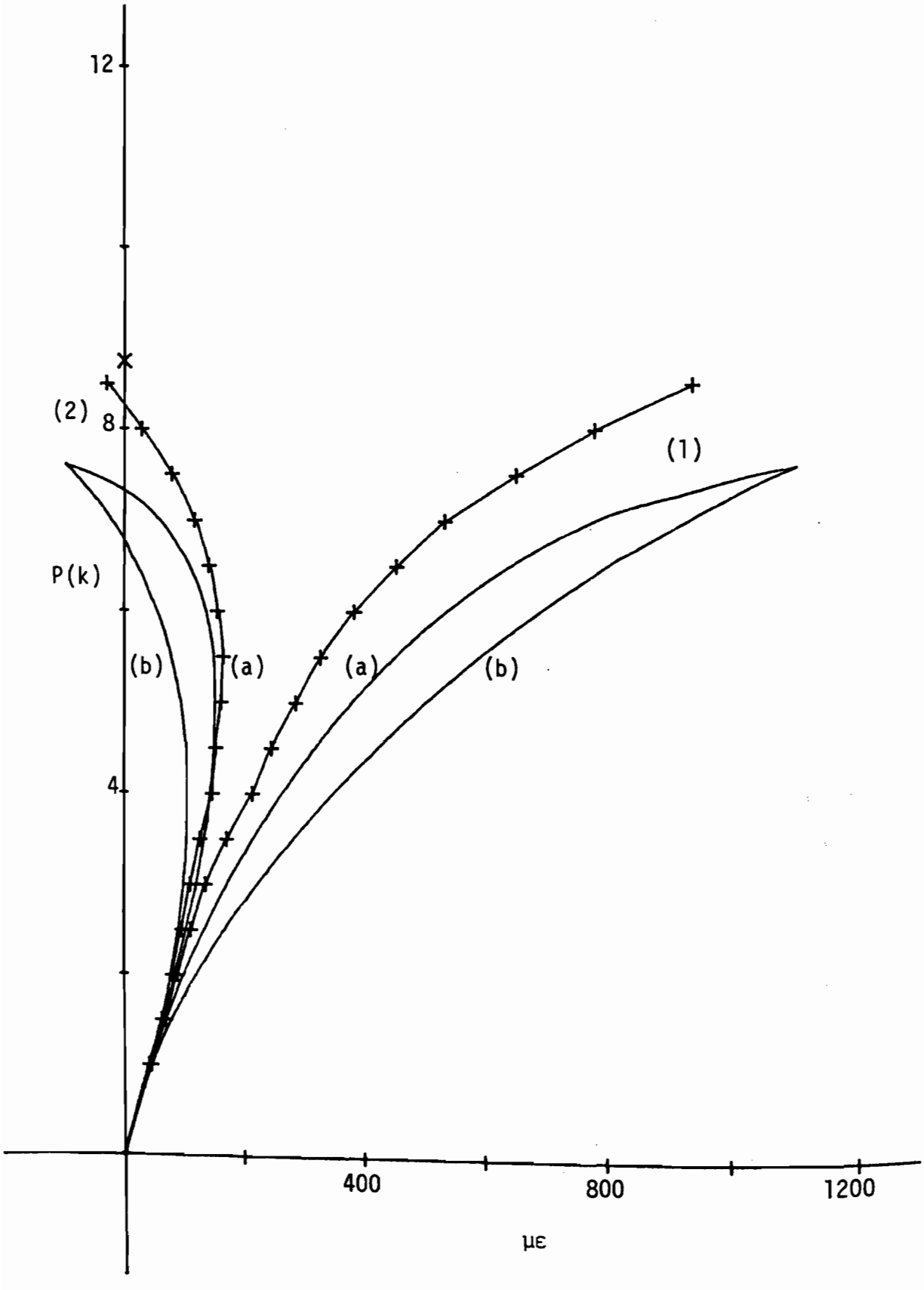

Figure E.5 CLC/2 180X60

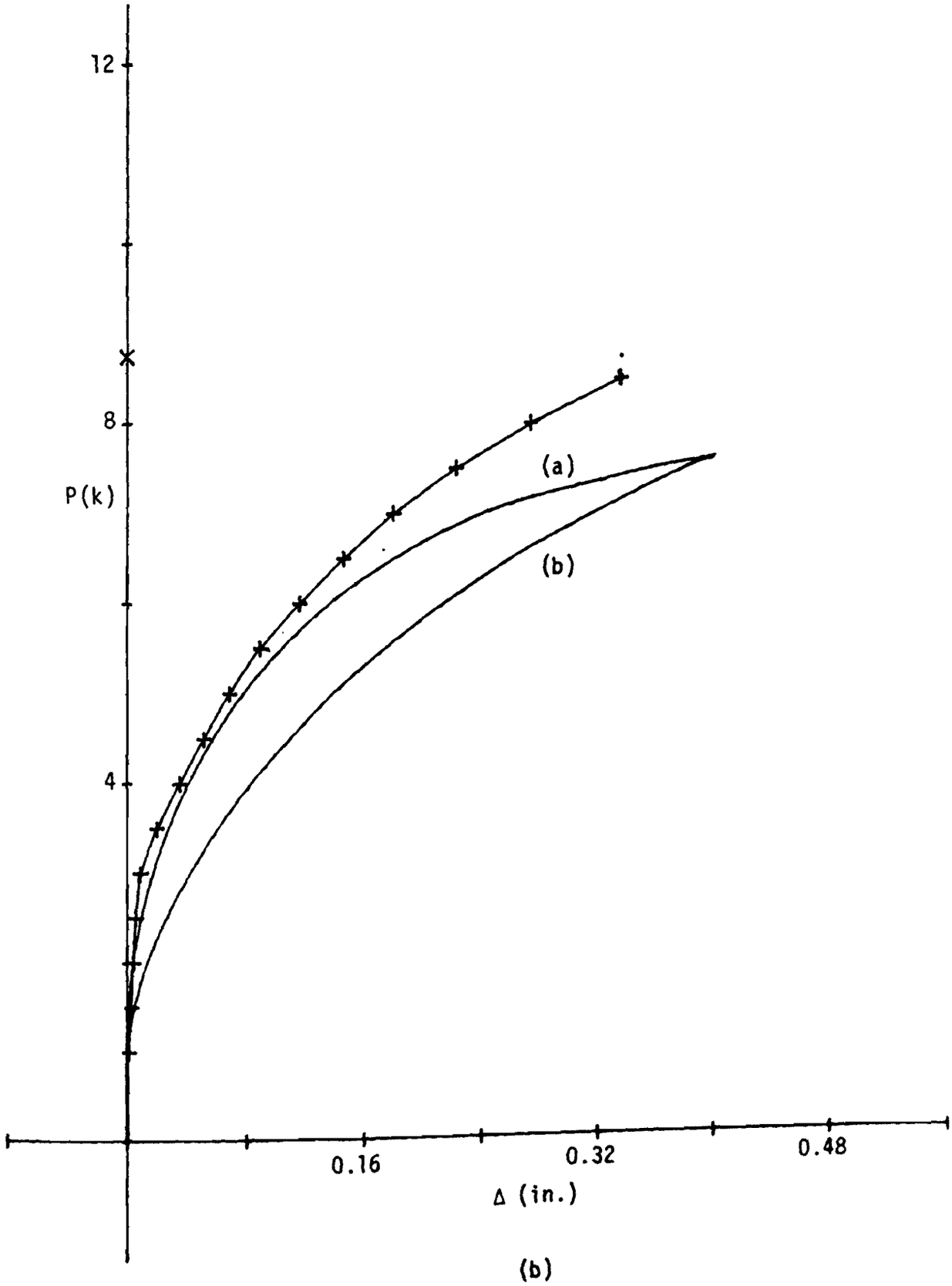

(b)

Figure E.5 CLC/2 180X60 - continued

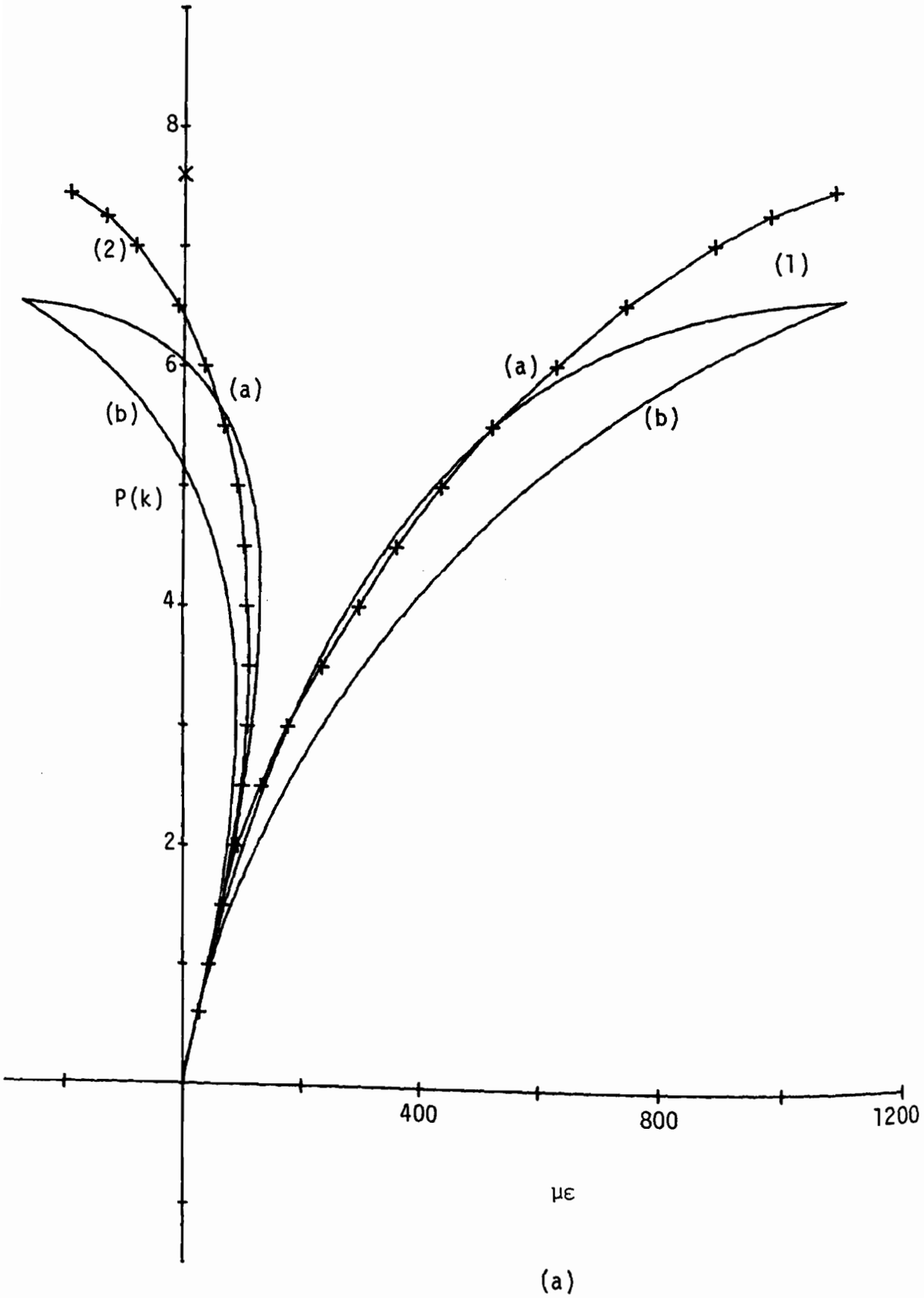

(a)

Figure E.6 CLC/3 180X60

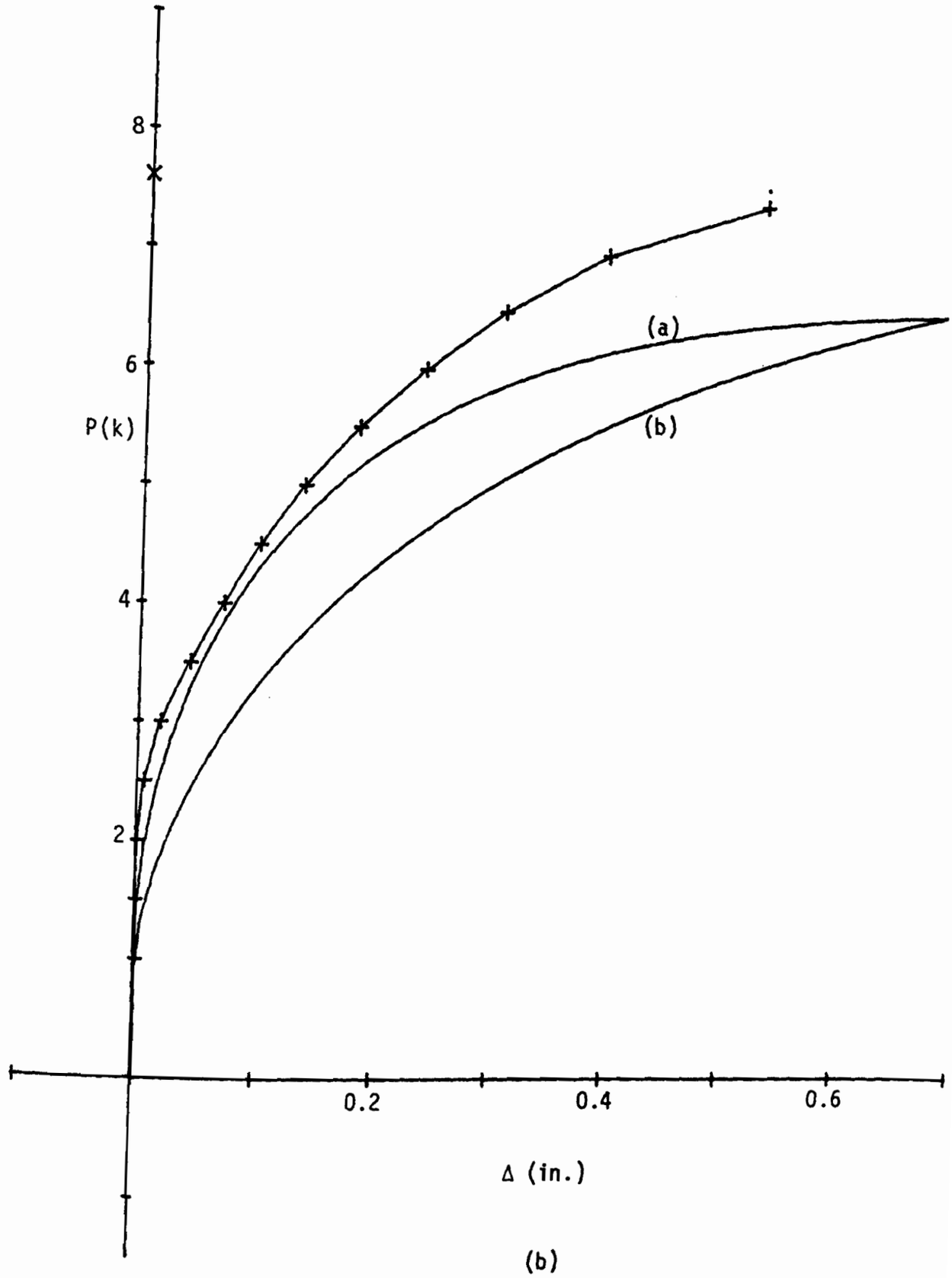

(b)

Figure E.6 CLC/3 180X60 - continued

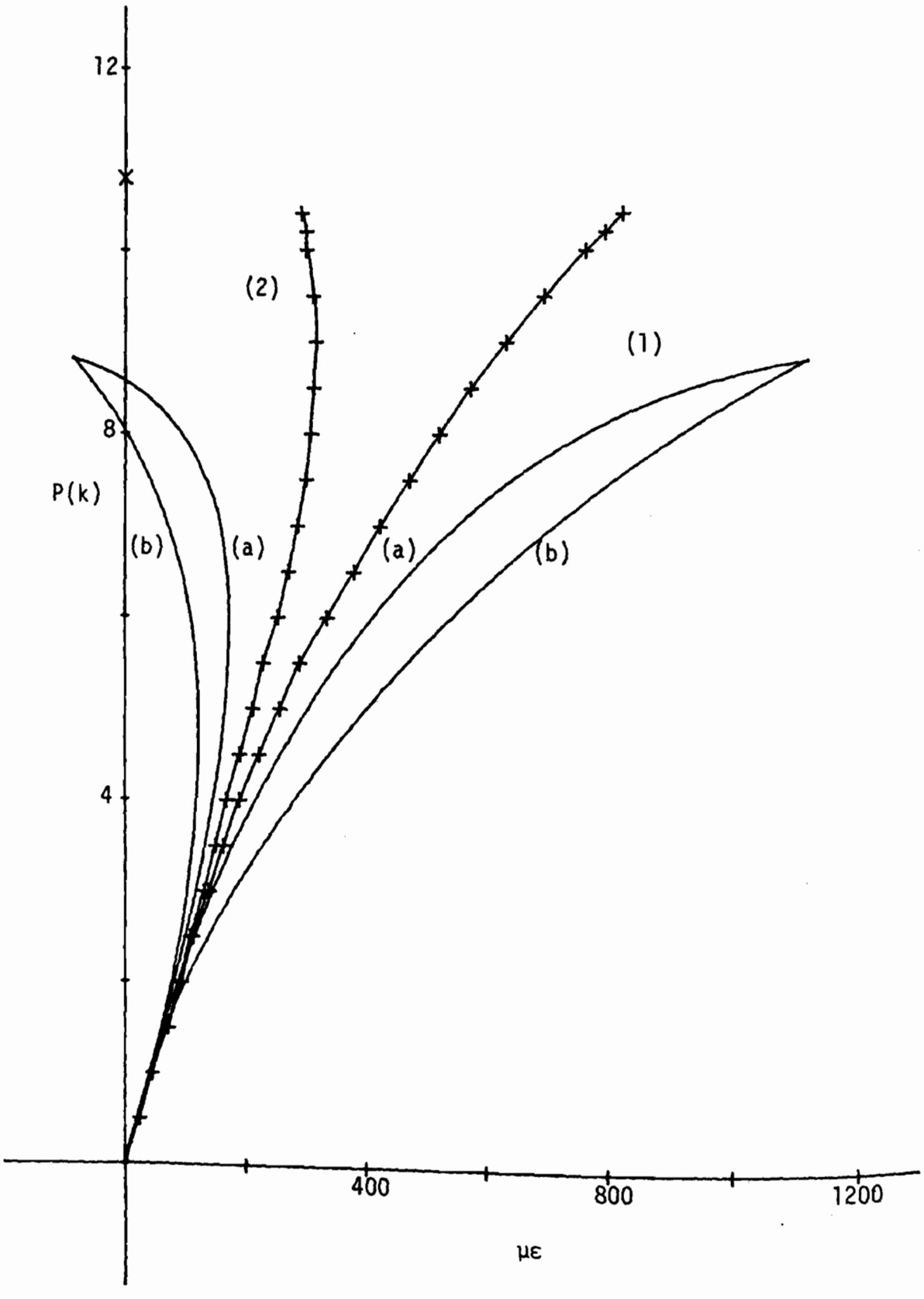

(a)

Figure E.7 CLC/4 180X60

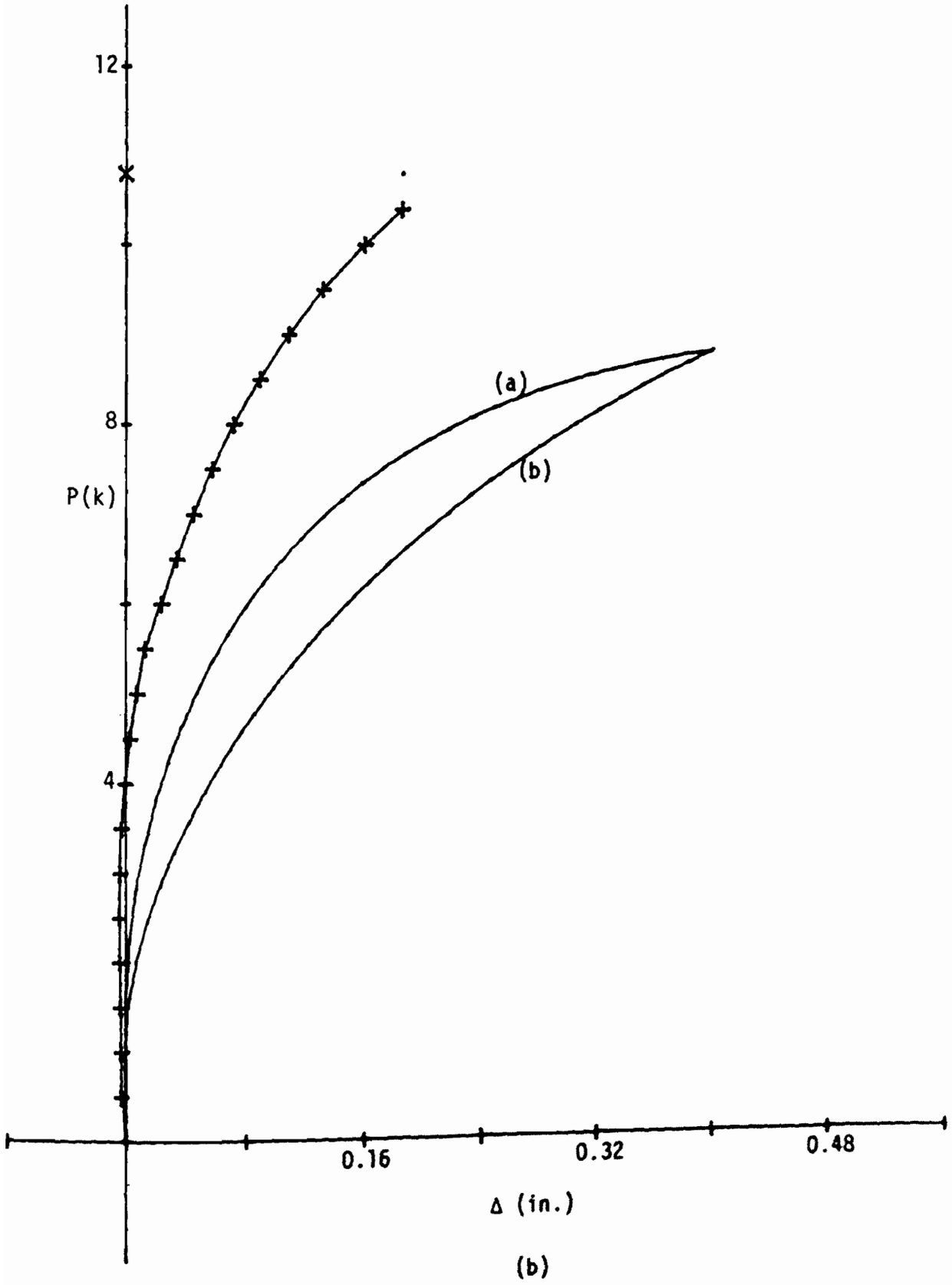

(b)

Figure E.7 CLC/4 180X60 - continued

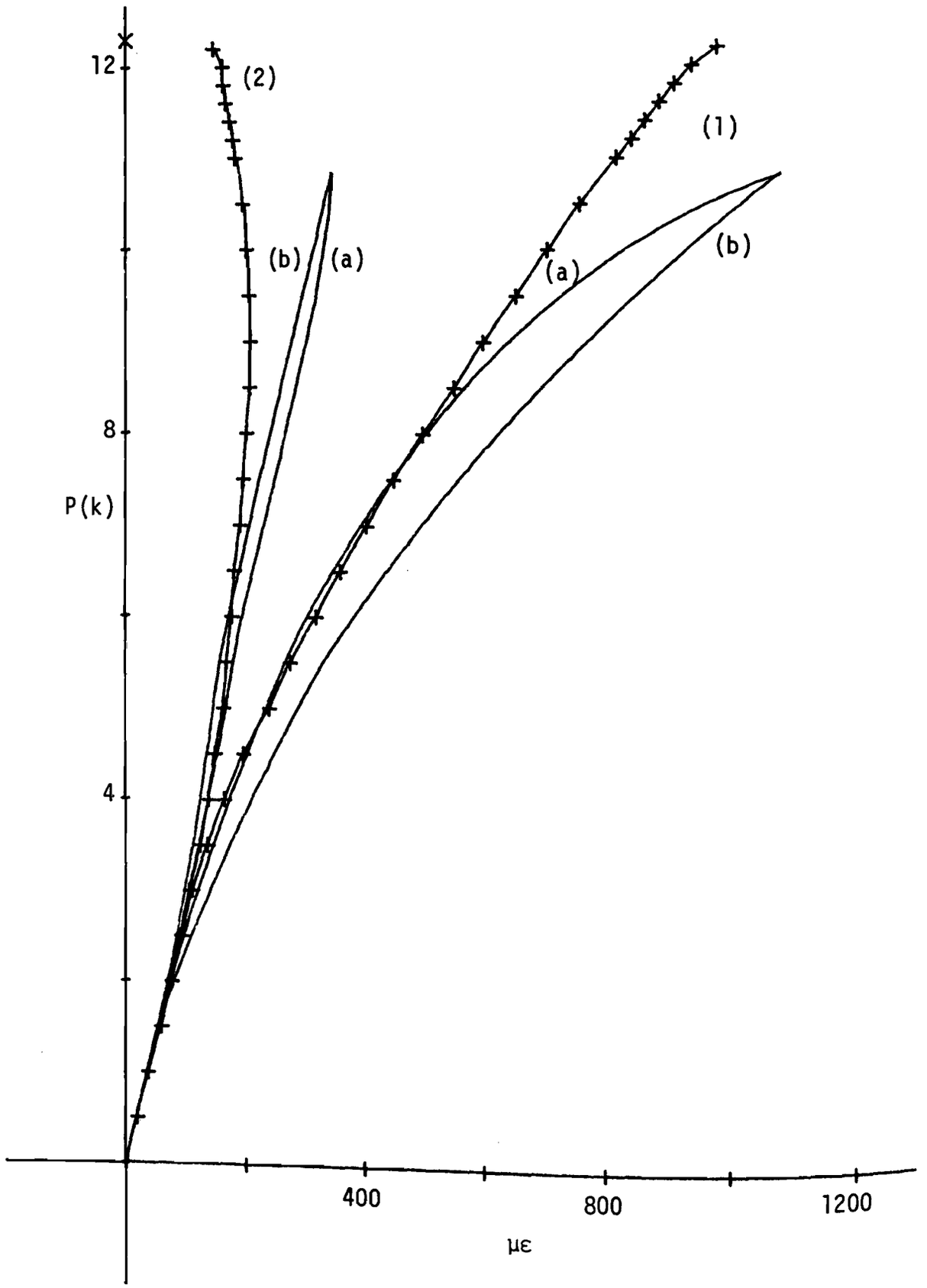

(a)

Figure E.8 CLC/1 180X90

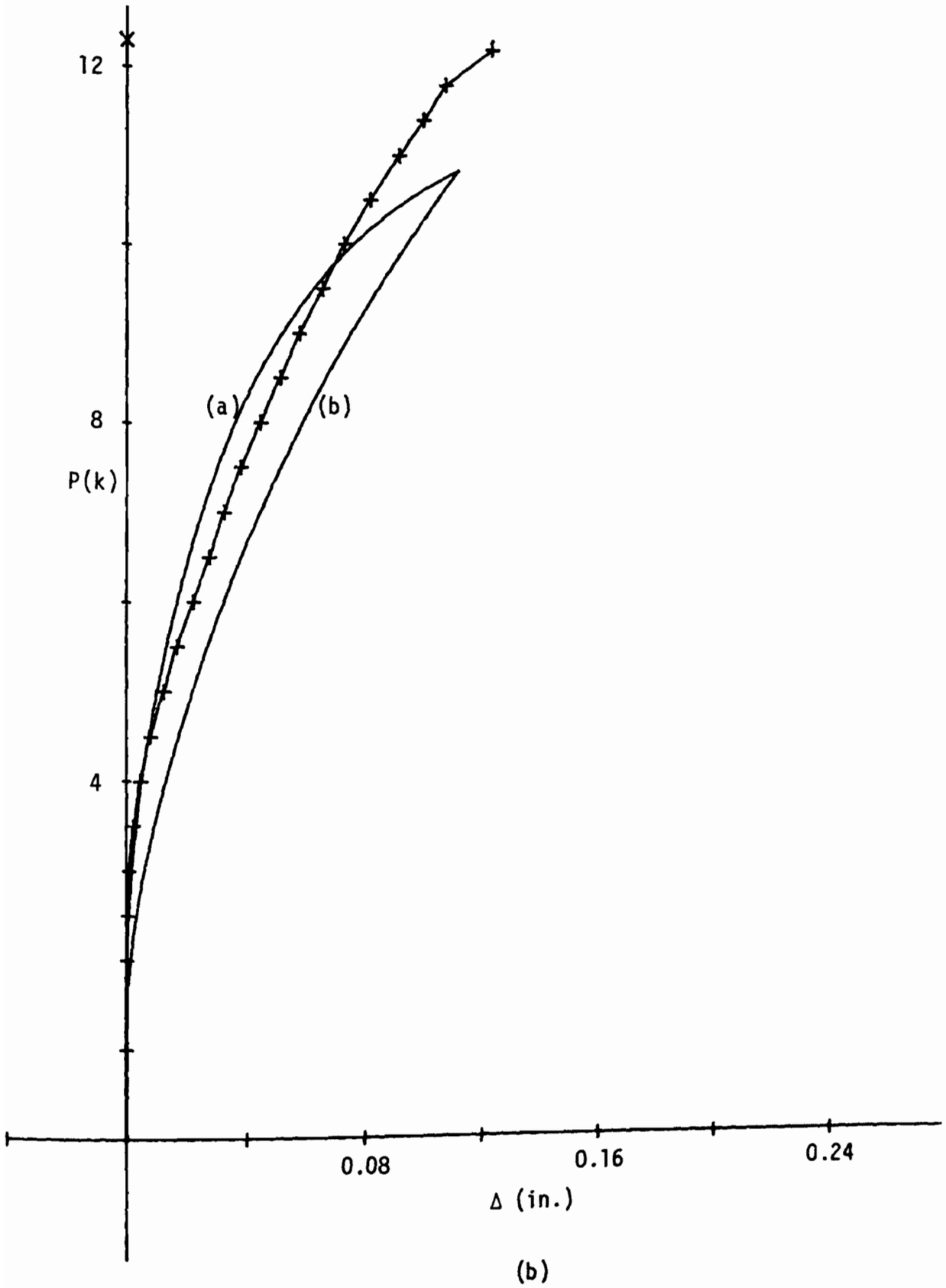

(b)

Figure E.8 CLC/1 180X90 - continued

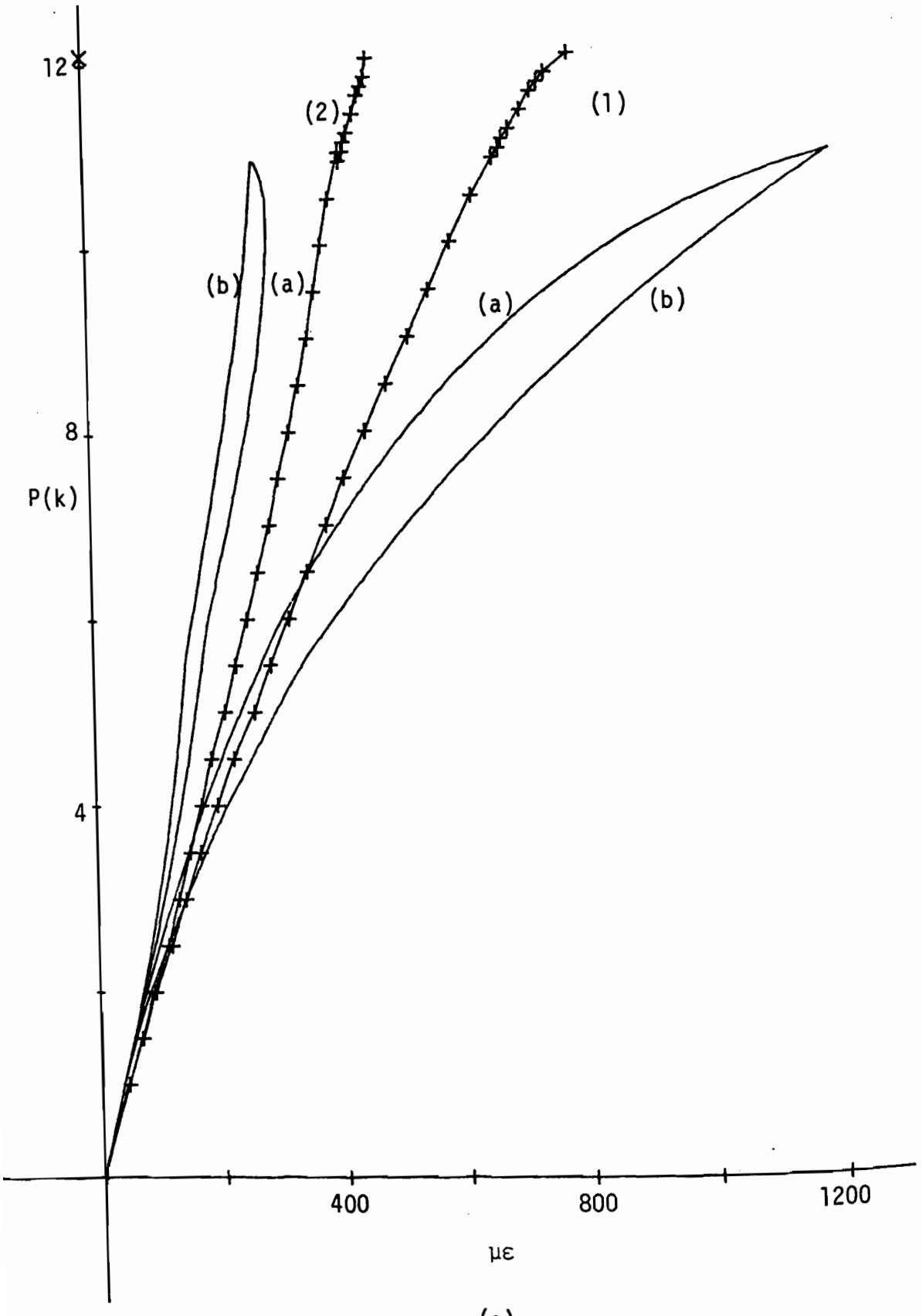

Figure E.9 CLC/2 180X90

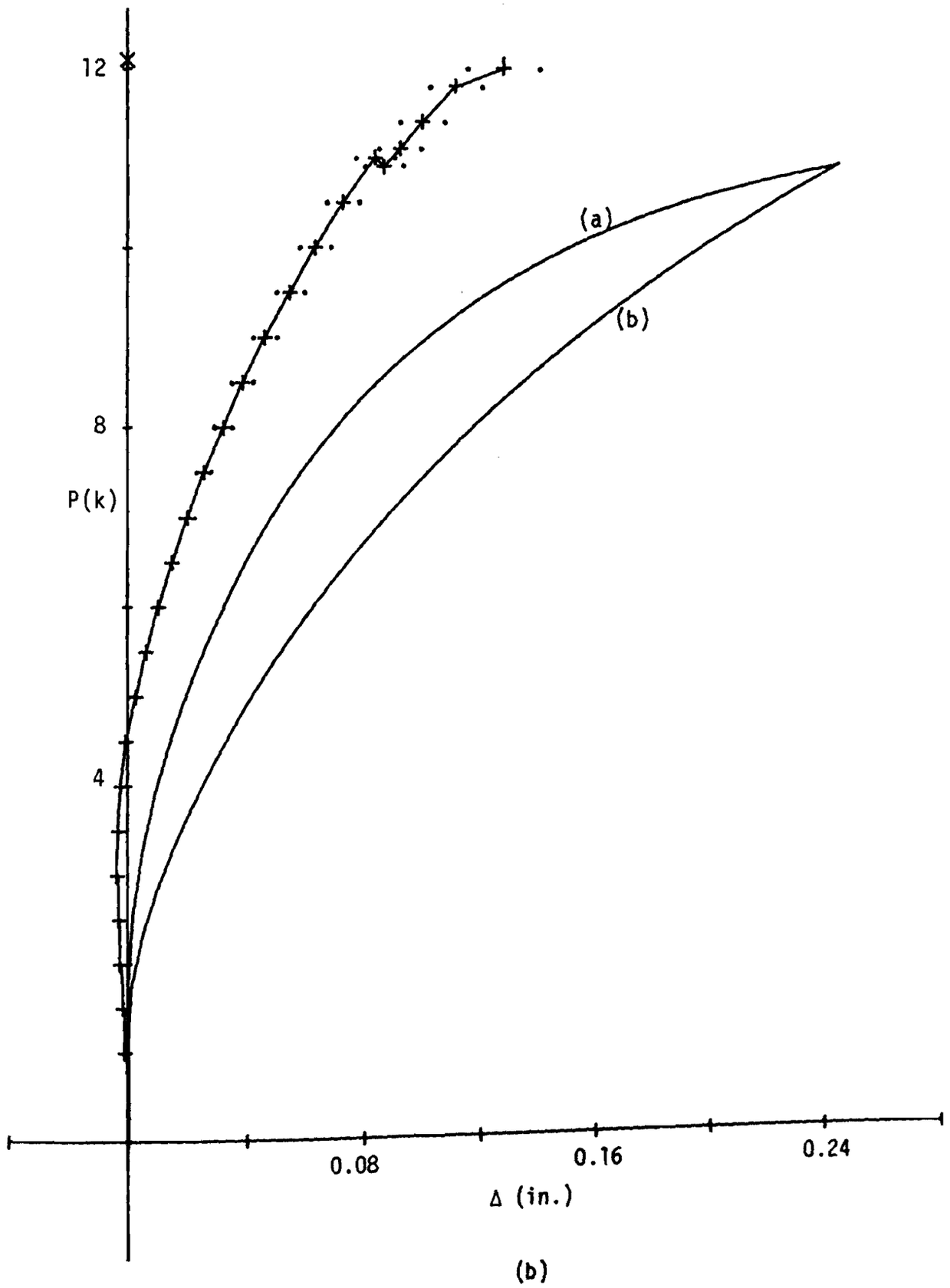

(b)

Figure E.9 CLC/2 180X90 - continued

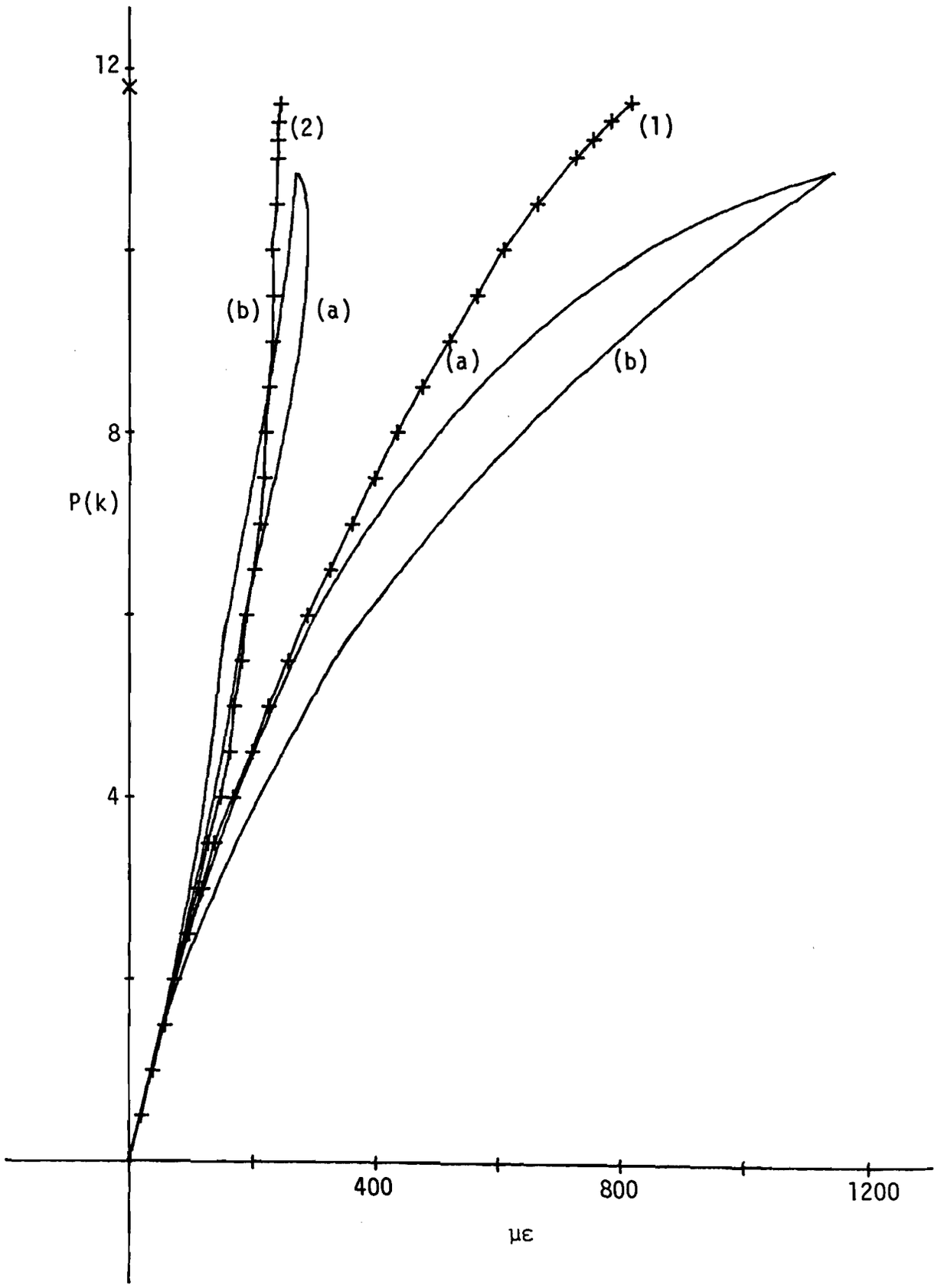

Figure E.10 CLC/3 180X90

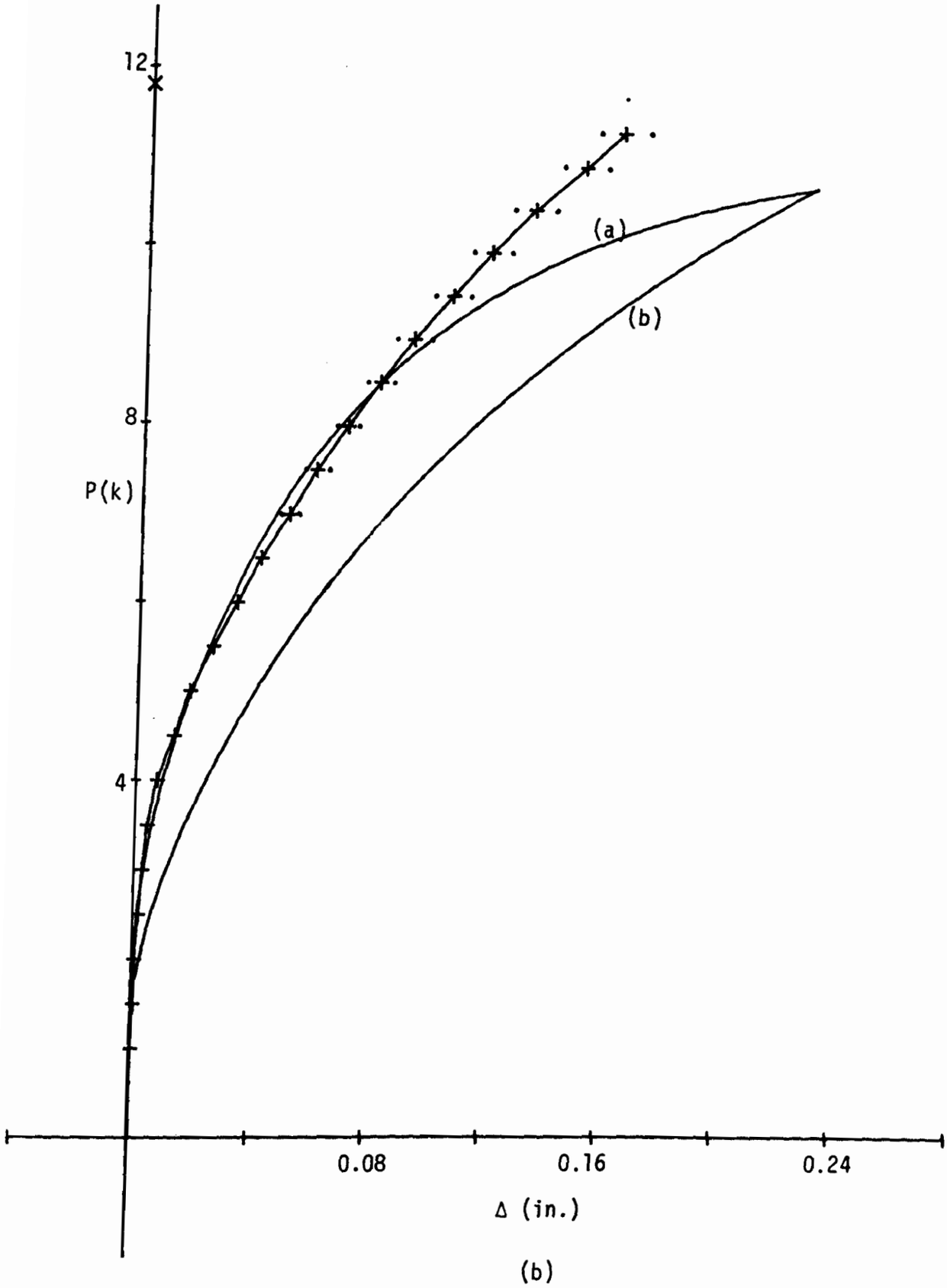

(b)

Figure E.10 CLC/3 180X90 - continued

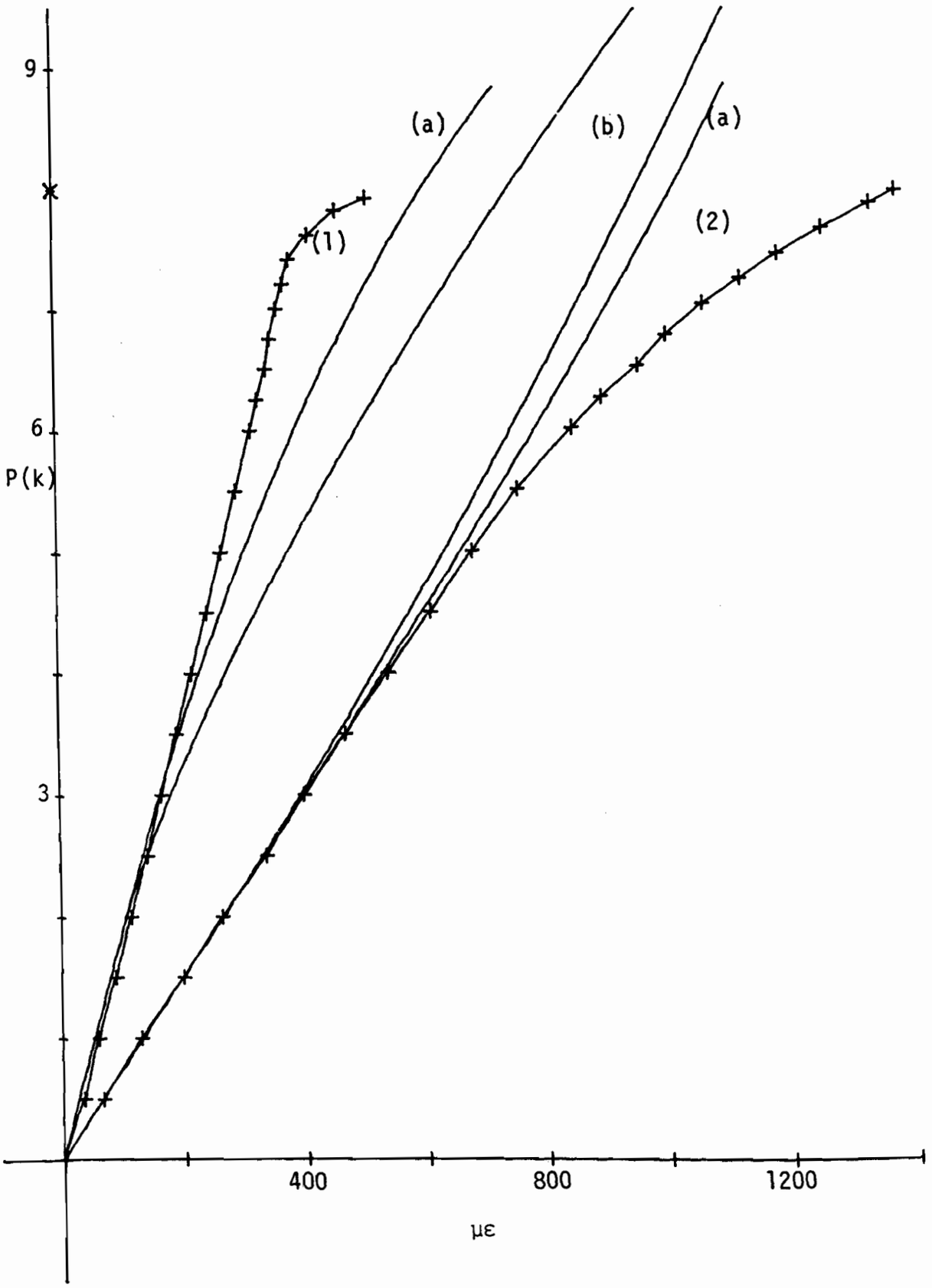

(a)

Figure E.11 CLC/1.1 120X30

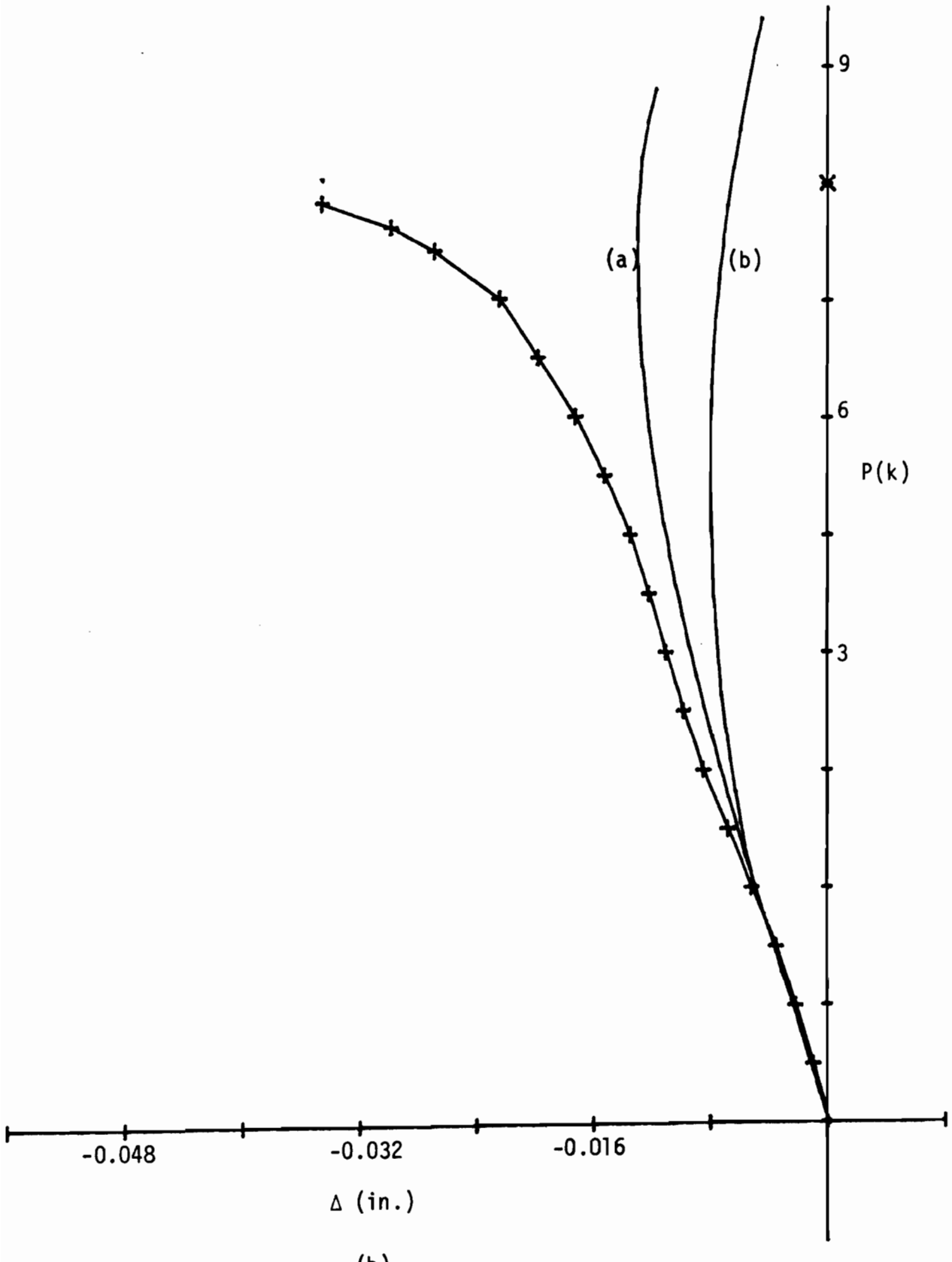

(b)

Figure E.11 CLC/1.1 120X30 - continued

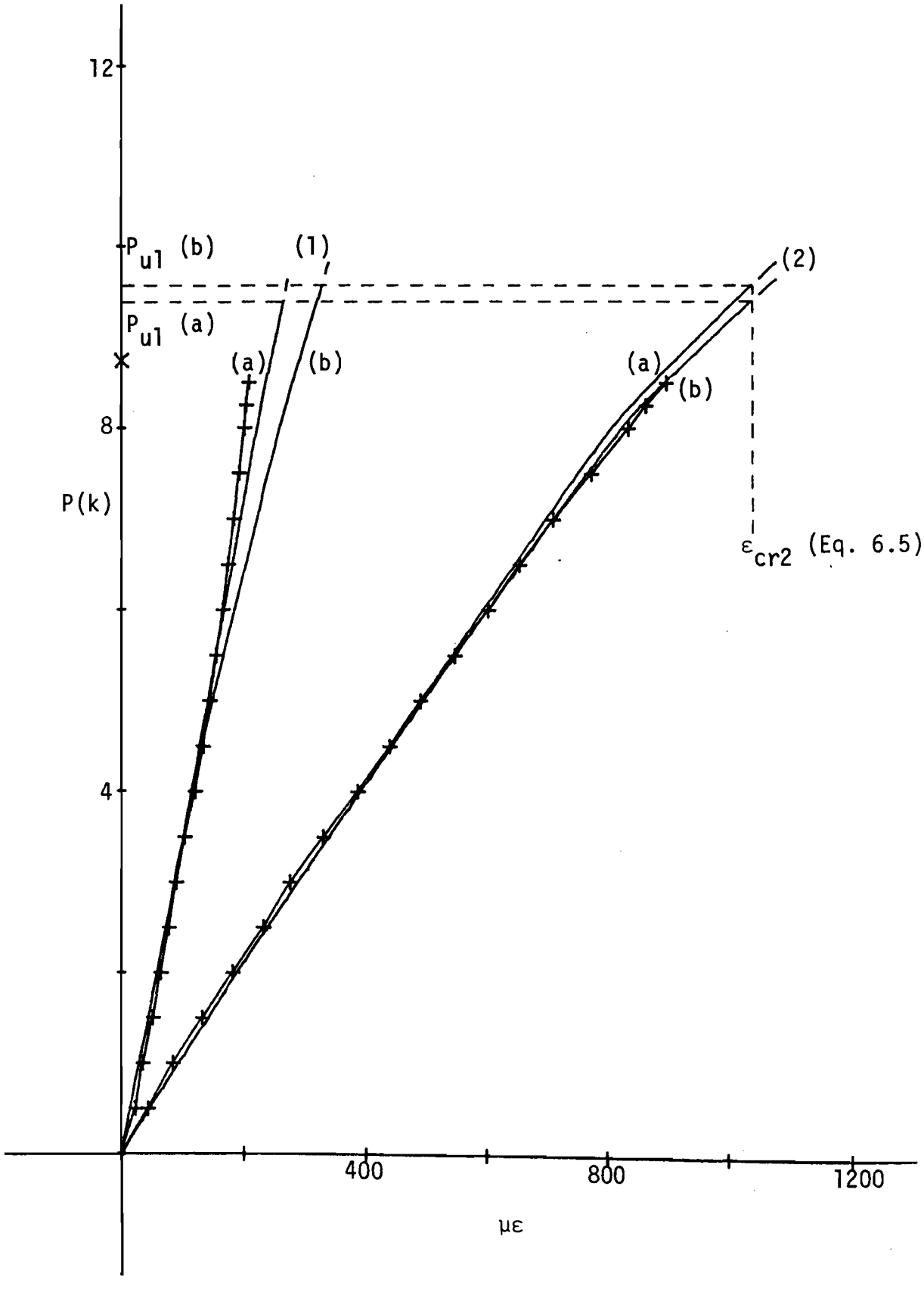

(a)

Figure E.12 CLC/2.2 120X60

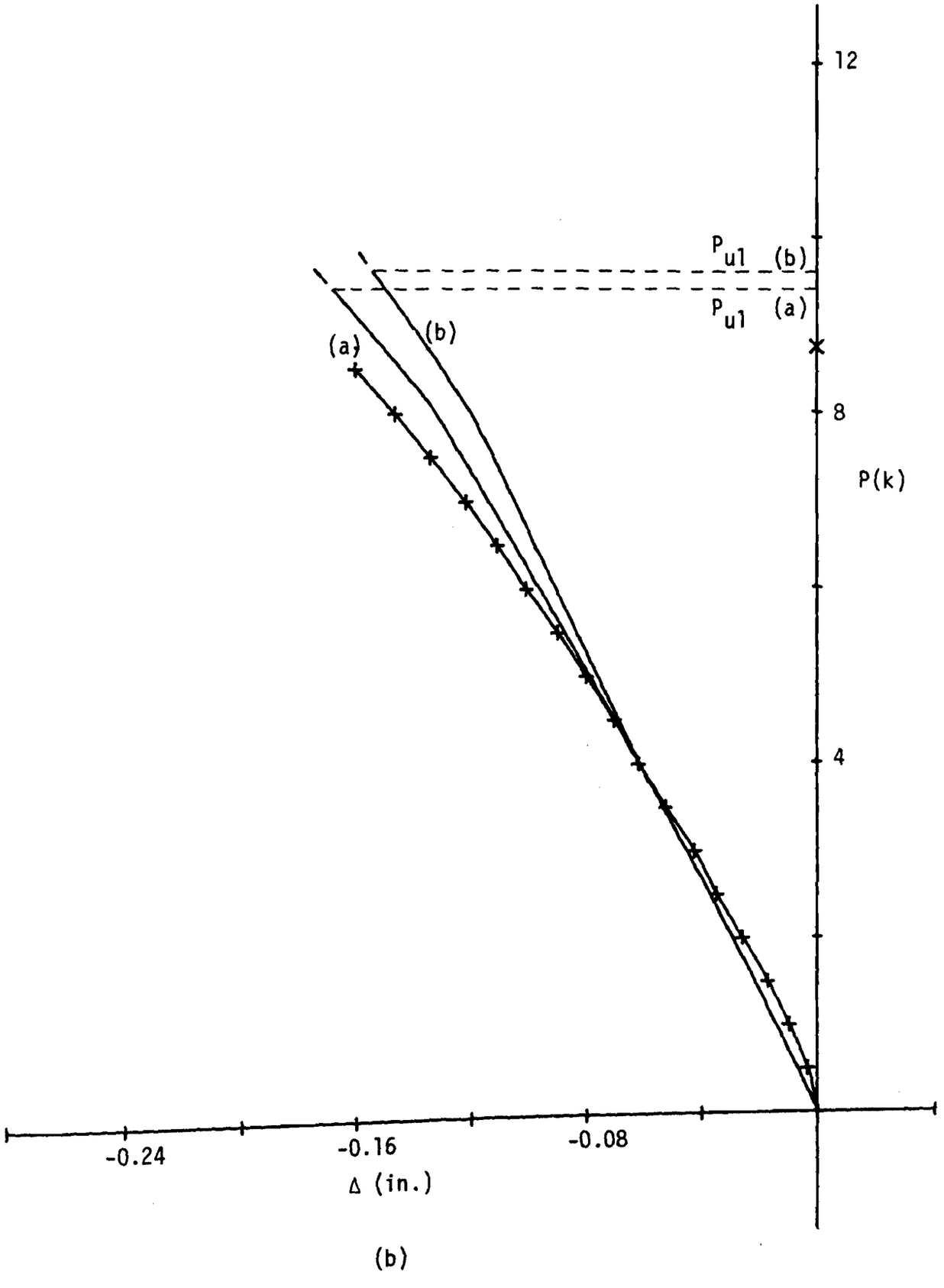

(b)

Figure E.12 CLC/2.2 120X60 - continued

REFERENCES

AISC, American Institute of Steel Construction [1975], "Specification for the Design, Fabrication, and Erection of Structural Steel for Buildings," New York.

AISI, American Iron and Steel Institute [1980], "Specification for the Design of Cold-Formed Steel Structural Members," Washington, D.C., September.

AISI [1980a], "The New and the Old Specification for the Design of Cold-Formed Steel Structural Members," Research Report SG 80-1, Committee of Sheet Steel Producers, Washington, D.C., September.

AISI [1971], "Supplementary Information on the 1968 Edition of the Specification for the Design of Cold-Formed Steel Structural Members," Washington, D.C.

ASTM, American Society for Testing and Materials [1975], "Standard Methods of Tension Testing of Metallic Materials," ASTM Designation: E8-69, Part 10, 90-109.

BS 449 [1974], British Standard Specification, Addendum No. 1 (PD4064).

Bathe, K.J. [1971], "Solution Methods for Large Generalized Eigenvalue Problems in Structural Engineering," Report UC SESM 71-20, Civil Engineering Department, University of California, Berkeley.

Bathe, K.J. and Wilson, E.L. [1976], Numerical Methods in Finite Element Analysis, Prentice-Hall, Inc., New Jersey.

Bijlaard, P.P. and Fisher, G.P. [1952], "Interaction of Column and Local Buckling in Compression Members," NACA Technical Note 2640, Washington, D.C.

Bijlaard, P.P. and Fisher, G.P. [1953], "Column Strength of H-Sections and Square Tubes in Postbuckling Range of Component Plates," NACA Technical Note 2994, Washington, D.C.

Bulson, P.S. [1969], The Stability of Flat Plates, American Elsevier, New York.

Chajes, A. [1974], Principles of Structural Stability Theory, Prentice-Hall, Inc., New Jersey.

Chajes, A., Fang, P.J., and Winter, G. [1966], "Torsional Flexural Buckling, Elastic and Inelastic, of Cold-Formed Thin Walled Columns," Engineering Research Bulletin No. 66-1, Cornell University, Ithaca, New York, August.

Cheung, Y.C. [1968], "Finite Strip Method Analysis of Elastic Slabs," J. of the Engineering Mechanics Div., ASCE, V. 94, EM6, 1365-1378.

Cheung, Y.C. [1969], "Folded Plate Structures by Finite Strip Method," J. of the Structural Div., ASCE, V. 95, ST12, 2963-2979.

Cheung, Y.C. [1976], Finite Strip Method in Structural Analysis, Pergamon Press, New York.

Chilver, A.H. [1953], "The Stability and Strength of Thin-Walled Steel Struts," The Engineer, Vol. 196, August, 180-183.

Cook, R.D. [1974], Concepts and Applications of Finite Element Analysis, John Wiley and Sons, Inc., New York.

Crandall, S.H. [1956], Engineering Analysis, McGraw Hill Book Co., New York.

Dat, D.T. [1980], "The Strength of Cold-Formed Steel Columns," Ph.D. Thesis, Cornell University, Ithaca, New York, January.

Dawson, R.G. and Walker, A.C. [1972], "Post-Buckling of Geometrically Imperfect Plates," J. of the Structural Div., ASCE, Vol. 98, No. ST1, January, 75-94.

Desmond, T.P. [1978a], "The Behavior and Strength of Thin-Walled Compression Elements with Longitudinal Stiffeners," Report No. 369, Department of Structural Engineering, Cornell University, Ithaca, New York, September.

Desmond, T.P., Pekoz, T., and Winter, G. [1978b], "Edge Stiffeners for Cold-Formed Steel Members," Fourth International Specialty Conference on Cold-Formed Steel Structures, St. Louis, Missouri, Vol. 1, 120-156.

DeWolf, J.T. [1973], "Local and Overall Buckling of Cold-Formed Compression Members," Report No. 354, Department of Structural Engineering, Cornell University, Ithaca, New York, November.

DeWolf, J.T., Pekoz, T., and Winter, G. [1974], "Local and Overall Buckling of Cold-Formed Members," J. of the Structure Div., ASCE, Vol. 100, No. ST10, October, 2017-2036.

Douty, R.T. [1962], "A Design Approach to the Strength of Laterally Unbraced Compression Flanges," Bulletin No. 37, Cornell University Engineering Experiment Station, Ithaca, New York.

Dym, C.L. [1974], Stability Theory and Its Applications to Structural Mechanics, Noordhoff International Publishing, the Netherlands.

Fok, W.C., Rhodes, J., and Walker, A.C. [1976], "Local Buckling of Outstands in Stiffened Plates," Aeronautical Quarterly, Vol. 27, May, 277-291.

Frieze, P.A. [1978], "Elasto-Plastic Buckling in Short Thin-Walled Beams and Columns," Proceedings, Institution of Civil Engineers, Part 2, Vol. 65, December, 857-874.

Gallagher, R.H. [1975], Finite Element Analysis Fundamentals, Prentice-Hall, Inc., New Jersey.

Gerard, G. [1957], "Handbook of Structural Stability Part IV - Failure of Plates and Composite Elements," NACA Technical Note 3784, Washington, D.C.

Gilbert, R.B. and Calladine, C.R. [1974], "Interaction Between the Effects of Local and Overall Imperfections on the Buckling of Elastic Columns," J. Mech. Phys. Solids, Vol. 22, 519-540.

Graves Smith, T.R. [1969], "The Ultimate Strength of Locally Buckled Columns of Arbitrary Length," Thin Walled Steel Structures, Rockey, K.C. and Hill, H.V. eds., Crosby Lockwood, London, 35-60.

Graves Smith, T.R. and Sridharan, S. [1978a], "A Finite Strip Method for the Buckling of Plate Structures Under Arbitrary Loading," Int. J. Mech. Sci., Vol. 20, 685-693.

Graves Smith, T.R. and Sridharan, S. [1978b], "A Finite Strip Method for the Post-Locally-Buckled Analysis of Plate Structures," Int. J. Mech. Sci., Vol. 20, 883-842.

Hancock, G.J. [1979], "Nonlinear Analysis of Thin Sections in Compression," Research Report No. R355, School of Civil Engineering, University of Sydney, Sydney, November.

Hornbeck, R.W. [1975], Numerical Methods, Quantum Publishers Inc., New York.

Jennings, A. [1977], Matrix Computation for Engineers and Scientists, John Wiley and Sons, Ltd., London.

Johnson, A.L. [1966], "The Structural Performance of Austenitic Stainless Steel Members," Report No. 327, Department of Structural Engineering, Cornell University, Ithaca, New York.

Johnston, B.G., ed. [1976], Guide to Stability Design Criteria for Metal Structures, Third Edition, John Wiley and Sons, New York.

Jombock, J.R. and Clark, J.W. [1961], "Postbuckling Behavior of Flat Plates," J. of the Structural Div., ASCE, Vol. 87, No. ST5, June, 17-33.

Kalyanaraman, V., Pekoz, T., and Winter, G. [1977], "Unstiffened Compression Elements," J. of the Structural Div., ASCE, Vol. 103, No. ST9, Proc. Paper 13197, September, 1833-1848.

Kalyanaraman, V. [1978], "Performance of Unstiffened Compression Elements," Report No. 362, Department of Structural Engineering, Cornell University, Ithaca, New York, February.

Kapur, K.K. and Hartz, B.J. [1966], "Stability of Plates Using the Finite Element Method," J. of the Engineering Mechanics Div., ASCE, Vol. 92, EM2, 177-195.

Konig, J. and Thomasson, P-O. [1980], "Thin-Walled C-Shaped Panels Subject to Axial Compression or to Pure Bending," Thin-Walled Structures - Recent Technical Advances and Trends in Design, Research and Construction, Proceedings of the International Conference on Thin-Walled Structures held at the University of Strathclyde, Glasgow, April 1979, Rhodes, J. and Walker, A.C., eds., Granada, London.

Kroll, W.D., Fisher, G.P, and Heimerl, G.J. [1943], "Charts for Calculation of the Critical Stress for Local Instability of Columns with I, Z, Channel, and Rectangular-Tube Section," NACA Wartime Report L-429, Washington, D.C.

LaBoube, R.A. [1978], "Webs for Cold-Formed Steel Flexural Members - Structural Behavior of Beam Webs Subjected to Bending Stress," Civil Engineering Study 78-1, Structural Series, University of Missouri - Rolla.

Levy, S. [1942], "Bending of Rectangular Plates with Large Deflections," NACA Technical Note 846, Washington, D.C.

Loughlan, J. [1979], "Mode Interaction in Lipped Channel Columns Under Concentric or Eccentric Loading," Ph.D. Thesis, Department of Mechanics of Materials, University of Strathclyde, Glasgow.

Loughlan, J. and Rhodes, J. [1980], "The Interactive Buckling of Lipped Channel Columns Under Concentric or Eccentric Loading," Thin-Walled Structures – Recent Technical Advances and Trends in Design, Research and Construction, Proceedings of the International Conference on Thin-Walled Structures held at the University of Strathclyde, Glasgow, April 1979, Rhodes, J. and Walker, A.C., eds., Granada, London.

Marguerre, K. [1937] "The Apparent Width of the Plate in Compression," NACA Technical Note No. 833, Washington, D.C. (Translation of "Die mittragende Breite der gedruckten Platte," Luftfahrtforschung, Vol. 14, No. 3, 121-128).

McGuire, W. [1968], Steel Structures, Prentice-Hall, Inc., New Jersey.

Miller, E.A. [1943], "A Study of the Strength of Short, Thin Walled Steel Studs," M.S. Thesis, Cornell University, Ithaca, New York.

Mulligan, G.P. [1979], "Performance of Trapezoidal Intermediate Stiffeners for Cold-Formed Steel Compression Elements," Report No. 79-2, Department of Structural Engineering, Cornell University, Ithaca, New York, September.

Pekoz, T.B. [1967], "Torsional-Flexural Buckling of Thin-Walled Open Sections Under Eccentric Axial Loading," Ph.D. Thesis, Cornell University, Ithaca, New York.

Pekoz, T.B. [1969], "Torsional Flexural Buckling of Thin-Walled Sections Under Eccentric Load," Cornell Engineering Research Bulletin 69-1, Department of Structural Engineering, Cornell University, Ithaca, New York, September.

Pekoz, T. [1977], "Post-Buckling Interaction of Plate Elements," Progress Report to Swedish Building Research Council, Department of Structural Engineering, Cornell University, Ithaca, New York.

Plank, R.J. and Wittrick, N.H. [1974], "Buckling Under Combined Loading of Thin Flat-Walled Structures by a Complex Finite Strip Method," Int. J. Num. Meth. Eng., Vol. 8, 323-339.

Przemieniecki, J.S. [1973], Finite Element Structural Analysis of Local Instability, AIAA Journal, Vol. 11, No. 1, 33-39.

Rhodes, J. and Harvey, J. [1971a], "Plates in Uniaxial Compression with Various Support Conditions at the Unloaded Boundaries," Int. J. Mech. Sci., Vol. 13, 787-802.

Rhodes, J. and Harvey, J. [1971b], "Effects of Eccentricity of Load or Compression on the Buckling and Post-Buckling Behavior of Flat Plates," Int. J. Mech. Sci., Vol. 13, 867-879.

Rhodes, J., Harvey, J., and Fok, W. [1975], "The Load-Carrying Capacity of Initially Imperfect Eccentrically Loaded Plates," Int. J. Mech. Sci., Vol. 17, 161-175.

Rhodes, J. and Harvey, J.M. [1976], "Plain Channel Section Struts in Compression and Bending Beyond the Local Buckling Load," Int. J. Mech. Sci., Vol. 8, 511-519.

Rhodes, J. and Harvey, J.M. [1977], "Examination of Plate Post-Buckling Behavior," J. of the Engineering Mechanics Div., ASCE, Vol. 103, No. EM3, June, 461-478.

Rhodes, J. [1978], "Secondary Local Buckling in Thin-Walled Sections," ACTA Technica Academiae Scientiarum Hangaricae, Tomus 87 (1-2), 143-153.

Rhodes, J. and Loughlan, J. [1980], "Simple Design Analysis of Lipped Channel Columns," Fifth International Specialty Conference on Cold-Formed Steel Structures, St. Louis, Missouri.

Salmon, C.G. and Johnson, J.E. [1971], Steel Structures-Design and Behavior, Intext, New York.

Seaburg, P.A. [1981], "The ABC's (and Q) of Cold-Formed Steel Design," Civil Engineering, ASCE, Vol. 51, No. 1, January, 52-56.

StBK-N5 [1977], "Tunnplatsnorm," Forslag 1977-06-10 (Draft Swedish Code for Sheet Metal Construction) Statens stalbyggnadskommittes tunnplatsgrupp, Stockholm.

Thomasson, P-O [1973], "The Influence of Web Buckling on the Load-Carrying Capacity of Trapezoidal Steel Sheet Sections," (in Swedish), Nordiske Forskningsdager for Stalkonstruksjoner, Oslo, August.

Thomasson, P-O [1978], "Thin-Walled C-Shaped Panels in Axial Compression," Document D1: 1978, Swedish Council for Building Research, Stockholm.

Timoshenko, S. [1955], Strength of Materials - Part I Elementary Theory and Problems, Third Ed., D. Van Nostrand Company, Princeton, New Jersey.

Timoshenko, S. [1956], Strength of Materials - Part II Advanced Theory and Problems, Third ed., D. Van Nostrand Company, Princeton, New Jersey.

Timoshenko, S.P. and Gere, J.M. [1961], Theory of Elastic Stability, McGraw-Hill Book Co., New York.

Tulk, J.D. and Walker, A.C. [1976], "Model Studies of the Elastic Buckling of a Stiffened Plate," J. of Strain Analysis, Vol. 11, No. 3, 137-143.

Tvergaard, V. [1973a], "Imperfection-Sensitivity of a Wide Integrally Stiffened Panel Under Compression," Int. J. Solids Structures, Vol. 9, 177-192.

Tvergaard, V. [1973b], "Influence of Post-Buckling Behavior on Optimum Design of Stiffened Panels," Int. J. Solids Structures, Vol. 9, 1519-1534.

Usami, T. [1982], "Post-Buckling of Plates in Compression and Bending," J. of the Structural Div., ASCE, Vol. 108, No. ST3, March, 591-609.

van der Neut, A. [1969], "The Interaction of Local Buckling and Column Failure of Thin-Walled Compression Members," Proceedings of the Twelfth International Congress of Applied Mechanics, Stanford University, August 1968, Hetenyi, M. and Vincenti, W.G., eds., Springer-Verlag, Berlin, 389-399.

van der Neut, A. [1973], "The Sensitivity of Thin-Walled Compression Members to Column Axis Imperfection," Int. J. Solids Structures, Vol. 9, 999-1011.

Vann, W. and Sehested, J. [1973], "Experimental Techniques for Plate Buckling," Second International Specialty Conference on Cold-Formed Steel Structures, St. Louis, Missouri.

Venkataramaiah, K.R., Roorda, J., and Srinivasaiah, K.R. [1980], "Elastic Modulus of Cold-Formed Sheet Steel," Fifth International Specialty Conference on Cold-Formed Steel Structures, St. Louis, Missouri, 703-725.

von Karman, T., Sechler, E.E., and Donnell, L.H. [1932], "The Strength of Thin Plates in Compression," Transactions ASME, Vol. 54, 53.

Walker, A.C. [1964], "Thin-Walled Structural Forms under Eccentric Compressive Load Actions," Ph.D. Thesis, University of Glasgow, Scotland.

Walker, A.C. [1975], Design and Analysis of Cold-Formed Sections, Halsted Press, New York.

Wang, S.T. and Pao, H.Y. [1980], "Stability Analysis of Locally Buckled Singly Symmetric Columns," Thin-Walled Structures - Recent Technical Advances and Trends in Design, Research and Construction, Proceedings of the International Conference on Thin-Walled Structures held at the University of Strathclyde, Glasgow, April 1979, Rhodes, J. and Walker, A.C., eds., Granada, London.

Winter, G. [1947], "Strength of Thin Compression Flanges," Transactions ASCE, Vol. 112, 527-554. (Reprinted in Bulletin No. 35/3 with additional appendix, Cornell University Engineering Experiment Station, Ithaca, New York, 1947).

Winter, G. [1948], "Performance of Thin Steel Compression Flanges," Preliminary Publication, Third Congress, IABSE, Liege, 137-148. (Reprinted in "Four Papers on the Performance of Thin Walled Steel Structures," Reprint No. 33, Cornell University Engineering Experiment Station, Ithaca, New York, November 1950).

Winter, G. [1970], "Commentary on the 1968 Edition of the Specification for the Design of Cold-Formed Steel Structural Members," American Iron and Steel Institute, Washington, D.C.

Wittrick, W.H. and Williams, F.W. [1971], "Initial Buckling of Channels in Compression," J. of the Engineering Mechanics Div., ASCE, Vol. 97, EM3, 711-726.

Wood, W.D. and Schrefler, B. [1978], "Geometrically Non-Linear Analysis - A Correlation of Finite Element Notations," Int. J. Num. Meth. Eng., Vol. 12, 635-642.

Yamaki, N. [1959], "Postbuckling Behavior of Rectangular Plates with Small Initial Curvature Loaded in Edge Compression," Journal of Applied Mechanics, Vol. 26, September, 407-414.

Yu, W. [1973], Cold-Formed Steel Structures, McGraw Hill Book Company, New York.

Zienkiewicz, O.C. and Nayak, G.C. [1971], "A General Approach to Problems of Plasticity and Large Deformation Using Isoparametric Elements," Proc. Conf. on Matrix Methods in Structural Mechanics, Wright-Patterson Air Force Base, Ohio, 881-928.

Zienkiewicz, O.C. [1977], The Finite Element Method, McGraw-Hill Book Company (UK) Limited, London.